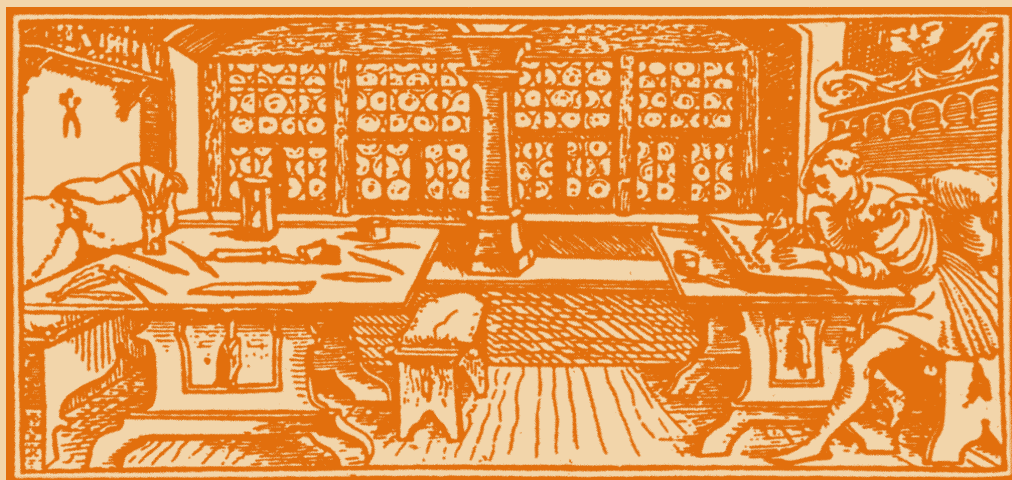


STUDIA

UNIVERSITATIS
BABEȘ-BOLYAI

C h e m i a

C L U J - N A P O C A 2 0 0 0



S T U D I A
UNIVERSITATIS BABEȘ-BOLYAI
CHEMIA
1-2

EDITORIAL OFFICE: Gh. Bîlășcu no. 24, 3400 Cluj-Napoca ♦ Phone 064-40.53.52

SUMAR - SOMMAIRE - CONTENTS - INHALT

ZITA FAZAKAS, STEFAN HOBAL, JANOS ZSAKO, Spectrophotometric and Rectangular Diffusion Study of Solubilizing Egg Yolk Lecithin Liposomes with Detergents Under Titrimetric and Equilibrium Condition	3
MIHAELA DRAGAN, SIMION DRAGAN, ION SIMINICEANU, Characterisation of Mellapak 750Y Structured Packing Determining the Effective Mass Transfer Area	11
FLORIN DAN IRIMIE, CSABA PAISZ, MONICA TOSA, CORNELIA MAJDIK, PAULA MOLDOVAN, RADU MISCA, MIHAELA CAPRIOARA, MADALINA NEACSU, Bioorganic Reduction of Some 5-Phenyl-furan-2-carbaldehydes Mediated by Bakers' Yeast	23
FLORIN DAN IRIMIE, CSABA PAISZ, MONICA TOSA, CORNELIA MAJDIK, MIHAELA CAPRIOARA, MADALINA NEACSU, PETER VEGH, Mass Spectrometry of Some New 10-Pentyl-10 H-Phenothiazine Derivatives	29
FLORIN DAN IRIMIE, CSABA PAISZ, MONICA TOSA, CORNELIA MAJDIK, PAULA MOLDOVAN, MIHAELA CAPRIOARA, MADALINA NEACSU, Cannizzaro Reaction in the Phenothiazine Series	39
LUMINITA MUNTEAN, TUROS GYORGY, CRINA SOCACI, ION GROSU, SORIN MAGER, ALIN MIHIS, Stereochemistry and NMR Spectra of Some New 5-Methyl-2,2-substituted-1,3-dioxanes	47
LUMINITA MUNTEAN, EUGEN MESAROS, GERARD PLE, ION GROSU, SORIN MAGER, Synthesis and Stereochemistry of Some New 2,5-Polysubstituted-1,3-dioxanes	55
CLAUDIA MURESANU, IOAN BALDEA, The Oxidation of Toluene by Potassium Permanganate in Perchloric Acid Medium	61
ERNESTO ESTRADA, NICOLAIS GUEVARA, ANTON A. KISS, FLORIN MOTOC, MIRCEA V. DIUDEA, Connectivity Indices of Dendrimers	71
MARCELA ARDELEAN, GABRIEL KATONA, IONEL HOPARTEAN, MIRCEA V. DIUDEA, Cluj and Szeged Indices in Property Modeling	81
ANTON A. KISS, GABRIEL TURCU, MIRCEA V. DIUDEA, Correlating Studies by Cluj and Szeged Indices	99
ALEXANDRA RUSTOIU-CSAVDARI, IOAN BALDEA, The Effect of Copper, Lead and Iron Ions on the Oxidation of Mercaptosuccinic Acid by Chromate	107

ALEXANDRA RUSTOIU-CSAVDARI, IOAN BALDEA, LUCIAN COPOLOVICI, DANA MIHAI, The Hydrogen Peroxide – Iodide Reaction in Kinetic Analysis, an Attempt for Multicomponent Calibration.....	119
DAN RUSU, CRISTINA ROSU, MARIANA RUSU, GHEORGHE MARCU, Spectrophotometric and Paper Electrophoretic Studies of the Copper (II) Polyoxotungstobismuthate Complexes	139
ADRIAN MARIUS HAIDUC, ANCA GABRIELA HAIDUC, IOVANCA HAIDUC, Waters Sampling of Waste Waters	147
LILIANA CRACIUN, JAMES JACKSON, Heats of Formation of Medium-Ring Strained Cyclo- and Polycycloalkanes: Comparison of AB INITIO Group Equivalent Schemes with the PM3 and MMX Methods	157
MARIA CURTUI, LOREDANA SORAN, Extraction of Zirconium (IV) with Tritolylphosphate	169
JANOS ZSAKO, MARIA TOMOAI-COTISEL, AURORA MOCANU, Interaction of Procaine with Biomembranes.....	175
RODICA MICU-SEMIUC, IONEL HAIDUC, RADU SEMIUC, ONUC COZAR, Spectroscopic Studies of Some Metallic Bis-Dithiophosphonates, M(DTP) ₂ , and of Some Adducts	185
LIVIU ONICIU, CLAUDIA G. MURESANU, CRISTINA G. BUCSA, Mediated Anodic Oxidation of Toluene with the Ce (IV) / Ce (III) System in Sulphuric Acid Medium...	199
VICTOR BOCOS-BINTINTAN, EMIL CORDOS, MUSATA BOCOS-BINTINTAN, Analytical Applications of Ion Mobility Spectrometry.....	209
VICTOR BOCOS-BINTINTAN, Ion Mobility Spectrometry – Theory and Instrumentation.....	219
ANA-MARIA RUSU, KATALIN BARTOK, WILLIAM PURVIS, WILLIAM DUBBIN, Pilot Assessment of Contaminant Elements in Soils and Cryptogam Plants from Emissions from an Ore Processing Plant, Zlatna Region, Romania.....	239
ANA-MARIA RUSU, KATALIN BARTOK, VICTOR DIN, WILLIAM PURVIS, WILLIAM DUBBIN, Trace Element Measurement by ICP-AES for the Routine Multi-Element Analysis of Lichen and Soil Samples for Environmental Pollutant Studies.....	249
IOAN CRISTEA, ERIKA KOZMA, ANAMARIA RITIU, The Acid Catalysed Hydration of 1-Isopropyl-4-Methylenbicyclo[3.1.0] Hexane (Sabinene). The Synthesis of the Terpinen-4-ol	257
LADISLAU KEKEDY-NAGY, EMIL A. CORDOS, Flame Atomic Emission Determination of Potassium in Natural Waters with the Methane-Air Flame as Excitation Source.....	263
LADISLAU KEKEDY-NAGY, EMIL CORDOS, Flame Atomic Absorption Determination of Zinc in Natural Waters Using the Methane-Air Flame	273
GABRIELA OPREA, CRISTINA MIHALI, Investigation of Adsorption Products of Oxyne Onto Blende and Smithsonite by IR Spectroscopy.....	281
GABRIELA OPREA, CRISTINA MIHALI, Reagents with Chelant Action for Zn (II) and the Possibility of Using Them in Flotation.....	289
OSSI HOROVITZ, ELENA MARIA PICA, GHEORGHE NIAC, Thermodynamic Evaluation of Coal Reactivity.....	299
LORENTZ JANTSCHI, SIMONA MUREȘAN and MIRCEA V. DIUDEA, Modeling Molar Refraction and Chromatographic Retention by Szedged Indices	313

SPECTROPHOTOMETRIC AND RECTANGULAR DIFFUSION STUDY OF SOLUBILIZING EGG YOLK LECITHIN LIPOSOMES WITH DETERGENTS UNDER TITRIMETRIC AND EQUILIBRIUM CONDITION

ZITA FAZAKAS¹, ȘTEFAN HOBAI¹ and JÁNOS ZSAKÓ²

1. *Department of Biochemistry, University of Medicine and Pharmacy, 38 G.Marinescu st., Tg.Mures, Romania.*

2. *Department of Physical Chemistry, Babes-Bolyai University, 11 Arany János st., Cluj, Romania.*

ABSTRACT. The interaction of the liposomes with detergents helps to understand the solubilization of biological membranes for protein separation and reconstitution.

After evaporation of an organic solvent from a solution of egg yolk lecithin, the lipid was hydrated and sonicated resulting a SUV suspension. The suspension was titrated with detergent solutions (Triton X-100, sodium deoxycholate) and the optical transmissions and diffusions were recorded. At the same time these optical values were measured for samples at equilibrium. The differences between these values were interpreted in terms of thermodynamics.

INTRODUCTION

Liposomes are models of cellular membrane, due to lipid arrangement in their membrane and their electrochemical properties. They can be used as drug vectors with controllable pharmacokinetics. They are biodegradable, having a small intrinsic toxicity and a reduced antigenic potential.

This study concerning the interaction of phospholipid liposomes with non-ionic and ionic detergents is determined by the fact that biological membrane solubilization for separation or membrane protein reconstitution is achieved by this procedure [1,2].

It integrates in actual interest in founding some procedures for isolation of membrane proteins or their integration in phospholipid anulus into membranes. The solubilization of vesicle membranes is frequently studied by measuring turbidity, optical diffusion and absorption, as well as fluorescence [3-9].

I. Materials

1. Devices: Rotary evaporator Buchi type 350. Sonicator with titanium probe type Ultrasonics A180G. Spectrophotometer Specol with zv amplifier and FR optical diffusion system and photocells. Microtitrator TiMi. Recorders K-200. Automatic microburette Radelkis OP-930.

2. Substances: Egg yolk lecithine, SIGMA type X-E (cat.no.P5394/1996) purified by us by neutral alumina column chromatography, verified by thin layer chromatography (silicagel). The mobile phase was a mixture $\text{CHCl}_3:\text{CH}_3\text{OH}:\text{H}_2\text{O}$ (65:30:4,vol). The identification of the phospholipid was made with iodine and shows a single spot. Sodium deoxycholate (DOCNa)(Merck). TRITON X-100 (TX-100) (Sigma). Tris(hydroxymethyl)aminomethane-HCl (TRIS-Cl) (Austranal).

3. Solvents: CHCl_3 purified by distillation on P_2O_5 . CH_3OH redistilled. Solvent mixture $\text{CHCl}_3:\text{CH}_3\text{OH}$ (9:1,vol).

4. Solutions: Buffer TRIS-Cl, 0.05M, pH=7.2. DOCNa 20 mM in buffer TRIS-Cl. TX-100 20 mM in buffer TRIS-Cl.

II. Methods

A. Liposome preparation

The suspension of small unilamellar vesicles (SUV) was prepared by sonication of a suspension of multilamellar vesicles (MLV) obtained by film hydration [10].

1 ml lecithin solution in a solvent mixture, 18.6 mmol, was evaporated under methane current for 15 minutes, at 52 °C. The lipid film formed on the wall of a 100 ml flask attached to the rotary evaporator, was dried at a low pressure ($p < 0.01$ Torr) for 4 hours at room temperature. Taking into account the mass of the lipid film and phosphate content of it (mineralized with nitroperchloric mixture, and assayed by Briggs method), we determined the mean molecular weight of the lecithin as being 766 Da.

We mention that this molecular weight is almost identical with the value of the lecithin supplied by Avanti Polar Lipids Inc. (USA).

The lipid film was hydrated at the room temperature with 16.5 ml buffer TRIS-Cl, under methane, for 20 minutes in the flask.

Taking into account that transition temperature of the lecithin is between -15° C and -7°C, all the operations took place over the shown temperature interval. Aliquots of 4 ml from MLV suspension were sonicated for 30 minutes, with some pauses for cooling. The ultrasound generator was adjusted at the power level 2, tuning 3.

After sonication, the aliquotes containing SUV were centrifugated for 20 min at 3000 rpm, in order to remove particles of titanium released from the sample.

B. Optical measurements

Optical transmission was measured on 1 cm path and diffusion measurements were made on a perpendicular direction on the incident beam, using the TiMi microtitrator, the transmitted and diffused light being repected by identical photocells, conected to K-200 recorders.

B1. Titration curves

1.5 ml SUV suspension was introduced from microburette into a cuvette with X-Y transparence, in the microtitrator. The detergent solution (20 mM) was added into the cuvette, under agitation produced by a magnetic stirrer with constant angular speed. The rate of microtitration was 4 $\mu\text{l}/\text{sec}$.

SPECTROPHOTOMETRIC AND RECTANGULAR DIFFUSION STUDY

The recording of the optical transmissions (T) and diffusions (D) were made with two photocells, connected to the two recorders.

The titration curve of optical transmission had a sygmoidal shape (fig.1).

The diffusion curves had a hyperbolic shape between the initial point and the upper end of the hyperbola there was an increase of optical diffusion, wich had a maximum, situated about at the point which corresponds to the molar ratio phospholipid/detergent = 1.

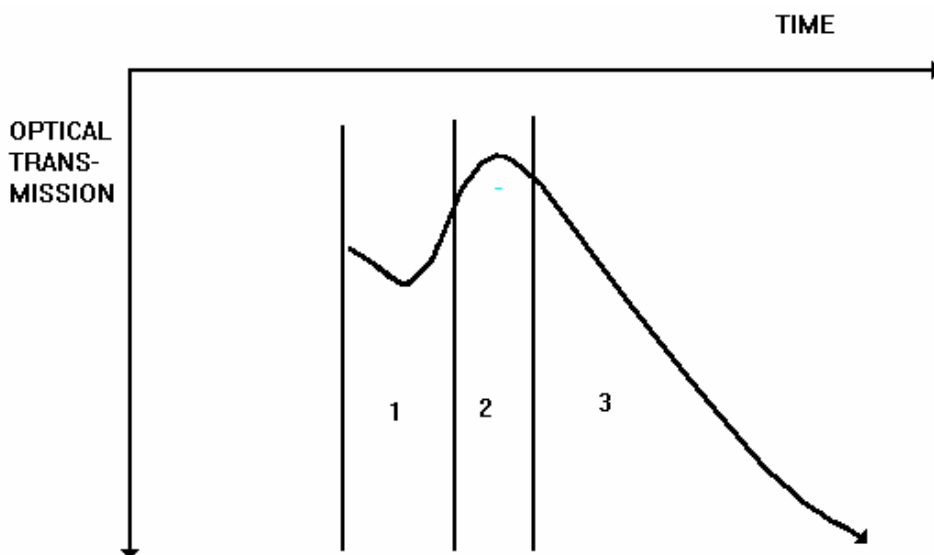


Figure 1. Optical transmission during the titration.

B2. Transmission and diffusion measurements under equilibrium conditions

Aliquotes of 1.5 ml SUV were treated with different volumes of detergent solution and after 2 hours were measured the optical transmissions and diffusions still under agitation.

RESULTS

It were taken into account some detergent volumes, added under dynamic (titrimetric) and equilibrium conditions, and for the resulted solutions, there were measured their percentage transmissions (T%) and diffusions (D%).

For transmission measurement the compensator was calibrated so that the maximum of recording width to be between 0-100% optical transmission. For optical diffusion the compensator was calibrated so that the difference between abscissa of the start and the abscissa towards reach the recorder pen at end of titration to be between 0-100%.

In Table 1 appear the values of percentage transmissions of samples titrated with TX-100 and of those being under equilibrium conditions.

Table 1.

Percentage transmissions (T%) of the suspensions treated with TX-100.

Detergent total conc.(mM)	0.52	1.01	1.48	1.93	2.35	2.76
Dynamic system (T%)	28.50	29.00	38.00	50.00	70.00	89.50
Equilibrium system (T%)	29.50	34.75	42.25	54.25	86.00	96.75

In Table 2 appear the values of percentage diffusions of samples titrated with TX-100 and of those being under equilibrium conditions.

Tabel 2

Percentage diffusions (D%) of the suspensions treated with TX-100.

Detergent total conc.(mM)	0.52	1.01	1.48	1.93	2.35	2.76
Dynamic system (D%)	104.60	85.90	47.90	24.30	10.60	3.50
Equilibrium system (D%)	98.90	84.50	47.90	29.20	8.50	2.50

In Table 3 appear the same data as in Table 1, using DOCNa instead of TX-100 and the differences Δv , expressed in μmol , necessary to equalize the transmission of the titrated samples with equilibrium ones.

Table. 3

Percentage transmission (T%) of the suspensions treated with DOCNa

Detergent total conc.(mM)	0.52	1.01	1.48	1.93	2.35	2.76
Dynamic system (T%)	-	36.50	-	50.00	80.00	-
Equilibrium system (T%)	-	41.50	-	60.25	84.75	-
Δv (μmol)	-	0.100	-	0.205	0.095	-

In Table 4 appear the same data as in Table 2 using DOCNa instead of TX-100 and the values necessary to equalize in the histograms the diffusions under the two conditions.

Table 4**Percentage diffusions of the suspensions treated with DOCNa.**

Detergent total conc.(mM)	0.52	1.01	1.48	1.93	2.35	2.76
Dynamic system (D%)	-	87.30	-	42.90	16.90	-
Equilibrium system (D%)	-	59.90	-	36.90	18.70	-
Δv (μmol)	-	0.548	-	0.12	-0.036	-

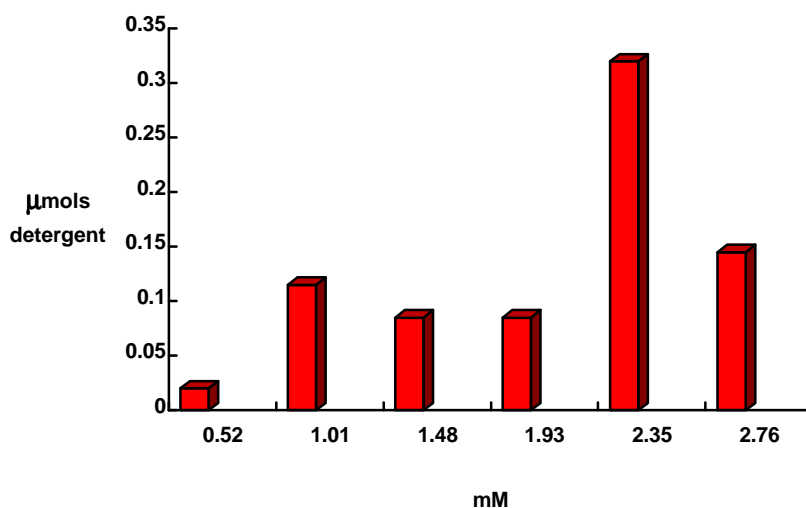


Figure 2. The values of the differences (Δv) for titration with TX-100 and for equilibrium conditions.

(Δv) which equalize transmission of titrated samples with of those in equilibrium conditions, calculated at some total detergent concentrations. This Figure corresponds to data from Table 1.

In Figure 3 there are the histograms of the detergent (TX-100) amounts (Δv) which equalize diffusions of titrated samples with of those being under equilibrium conditions, calculated at some total detergent concentrations. This Figure corresponds to data from Table 2.

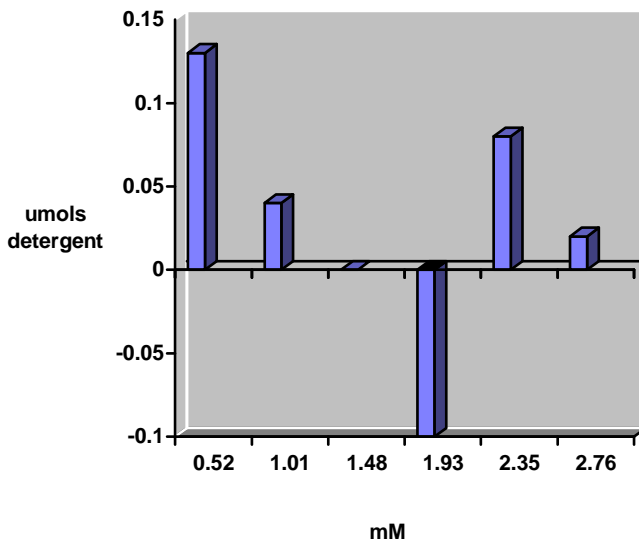


Figure 3. The values of the differences (Δv) for titration with TX-100 and for equilibrium conditions.

DISCUSSIONS AND CONCLUSIONS

Experimental data indicate that the transmissions of the samples in equilibrium conditions are higher than those titrated in the concentration interval 0-2.76 mM. This fact indicates that the solubilization process with TX-100 has a determined kinetics on the whole area of detergent concentration, the measurements being made at total detergent concentrations higher than his CMC. This difference reaches a maximum at the molar ratio lipid:detergent=1:2.37. It is situated at total detergent concentration of 2.35 mM (tab.1). The difference of the transmissions can be compensate by addition at the sample, which is in dynamic conditions, of 0.135 μmol of TX-100. The transmission of samples titrated with DOCNa (tab.3) evaluates similar with ones titrated with TX-100. The difference between the two evolutions consists in the fact that the maximum of the values of Δv for titration with DOCNa, is not situated at molar ratio corresponding to TX-100, but at ratio 1:1.89 (phosfolipid-detergent), that is at a total concentration of detergent smaller than in the case shown at titration with TX-100.

The diffusions in dynamic conditions are higher than under equilibrium conditions in the concentration interval 0.52-1.01 mM TX-100 (tab.2). At 1.48 mM detergent, diffusions are identical in both conditions. At 1.93 mM the diffusion under equilibrium conditions is higher than under dynamic conditions. Between 2.35-2.76 mM there is the same situation as in the interval 0.52-1.01 mM TX-100.

There is a difference between transmission and diffusion evolution, that is not on the whole interval of detergent concentration, solubilization under dynamic conditions remains after solubilization under equilibrium conditions. As well, at 1.93 mM TX-100 the apparent solubilizant effect of detergent it is more increased in dynamic system, than in equilibrium system. Taking into account that vesicles population is heterogeneous from the dimensional point of view, just a part of them being SUV, it is to be expected a difference between the transmission variation and the diffusion variation with the increase of detergent concentration.

The interaction of liposomes with anionic and ionic detergents, graphically represented by the relationship $T=f(\text{time})$ (fig.1), has two stages:

I. Passive tritonization

Under both conditions (dynamic and equilibrium ones), the solubilization process [11] starts with the charging of the vesicles with detergent (portion 1 on the transmission curve), called "vesicular charging". This charging produces the increase of the vesicles volume, therefore a decrease of transmission and an increase of diffusion. On the portion 2 begins the transition: *liposomes (charged)* --- > *mixed micelles* and the charging continuously of a part of liposomes, which maintains the transmission approximately constant. This portion contains the point at which molar ratio lipid-detergent =1:1.

II. Active tritonization

Under both conditions, in the following stage it is produced the accelerate transformation *liposomes*---> *mixed micelles*, which determines the rapid increase of transmission and decrease of diffusion. Finally, the mixed micelles grow richer with detergent molecules, tending towards "pure micelles".

It was found that at 2.35 mM TX-100, which is a solubilizing concentration, the differences between optical values for dynamic and equilibrium conditions reach a maximum. This is explained by taking into account that, in spite of the pronounced increase of the entropy in the course of solubilization, this process has a greater enthalpy than the process of liposome charging with detergent molecules at sub-solubilizing concentrations.

REFERENCES

1. A.de la Maza, and J.L. Parra, Biophys.J.,1997, **72**,1668.
2. A.de la Maza, and J.L. Parra, Chem. Phys.Lipids, 1995, **77**,79.
3. M.D.Jackson, C.F.Schmidt, D.Lichtenberg, B.J.Litman, A.D.Albert, Biochemistry, 1982, **21**, 4576.
4. A.Alonso, M.A.Urbaneja, F.M.Goni, F.G.Carmona, F.G.Canovas, C.G.Fernandey, Biochim. Biophys. Acta, 1987, **902**, 237.
5. M.Ollivon, O.Eidelman, R.Blumenthal, A.Walter, Biochemistry, 1988, **27**,4576.
6. M.M. da Graca, O.Eidelman, M.Ollivon, A.Walter, Biochemistry, 1989, **28**,8921.

7. J.Lasch, J.Hoffmann, W.G.Omelyanenko, A.A.Klibanov, V.P.Torchilin, H.Binder, K.Gawrisch, *Biochim. Biophys. Acta*, 1990, **1022**,171.
8. M.A. Partearroyo, M.A.Urbaneja, F.M.Goni, *FEBS.Lett.*, 1992, **302**, 138.
9. Șt.Hobai, Z.Fazakas, E. Molnár, I.Antofie, *Rev.Med.Farm.Tg.Mureș*, 1999, **45**, 207.
10. R.R.C. New, *Liposomes. A practical approach*, IRL Press at Oxford University Press, 1990, p.36.
11. J. Lasch, *Biochim.Biophys. Acta*, 1995, **1241**, 269.

CHARACTERISATION OF MELLAPAK 750Y STRUCTURED PACKING DETERMINING THE EFFECTIVE MASS TRANSFER AREA

MIHAELA DRAGAN¹, S. DRAGAN¹, AND I. SIMINICEANU²

¹University "Babes-Bolyai" of Cluj- Napoca, 11 Arony Janos, 3400 Cluj-Napoca, Romania

²Technical University of Iasi, Faculty of Industrial Chemistry, 71 Bd. Mangeron, 6600 Iasi

ABSTRACT. The effective mass transfer area of a Mellapak 750 Y structured packing was measured in a bench- scale plant with a column having an internal diameter of 100mm, and a packing height of 518 mm, using a broad range of gas and liquid flow rates. The absorption of carbon dioxide into sodium hydroxide aqueous solutions of 0.5 and 1.0 mol/L has been employed as test reaction. The validity of data obtained was tested by checking the two conditions of fast pseudo first order irreversible reaction. The data have been correlated by a criterial equation giving the ratio between the effective and the geometric areas versus the Reynolds number of the liquid phase. The coefficients of the equation have been identified by regression.

Keywords: absorption rate, absorption column, chemical method, criterial equation.

INTRODUCTION

Increased attention has been devoted in the last few years to optimize the absorption process. This was partly due to the severity of the legislation imposed in industrial countries on the prevention of air and water pollution [1]. The conventional beds of random packing caused difficulties in large diameter industrial separation columns. A frequent difficulty has been to attain uniform distribution of the liquid over the entire cross section and to assure that the packing was adequately wetted. The risk of maldistribution also existed in the region on packing close to the wall. Therefore, researchers and manufacturers have studied and developed new types of column interiors. Among these interiors, corrugated packings of the regular type, also called *structured packing*, have received the greatest attention owing to their favorable performance [2,3]. It is recognized that

structured packing makes possible reduction in exergy consumption by minimizing pressure drop per theoretical stage [3,4]. Structured packing can be made of plastic or metallic materials, depending on the application. They are made of corrugated sheets arranged in parallel, successive layers having an opposite angle of corrugation as shown in Figure 1. Flow channels resulting from this arrangement are inclined at an angle of 60 or 45 degrees to the horizontal. The particular form of the packings makes it possible to obtain a high geometric specific area, from 150 m^2/m^3 with Mellapak 150 Y to 750 m^2/m^3 Mellapak 750 Y.

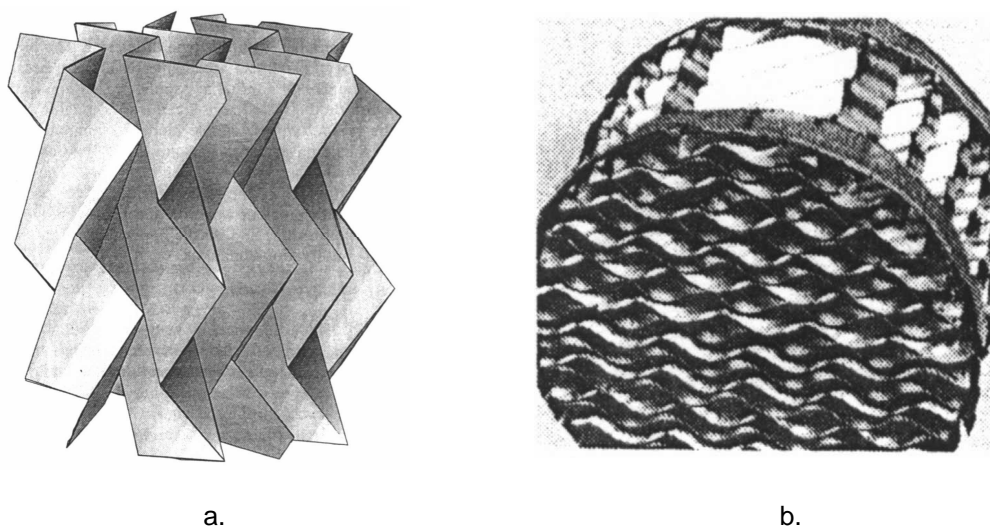


Figure 1. Structured packing of Mellapak 750 Y type. a- corrugated sheets, b- element of structured packing.

The present paper is devoted to the effective mass transfer area measurement of the Mellapak 750Y packing. The *effective* mass transfer area (a_e) is not identical neither to the *geometric* area (a) nor to the *wetted* area of the packing (a_w). The measurement of the specific geometric area of packing is straight forward but it is not a design parameter. The wetted area is that part of geometric area over which there is a liquid film. It depends on the surface tension interaction between the liquid and the solid packing, and can be measured by the dye technique. The effective mass transfer area may differ from the wetted area because of packets of almost stagnant liquid formed in contact points of packings. This liquid can account for the large wetted area but is practically useless for absorption because it comes quickly to equilibrium with the gas.

The effective mass transfer area is determined by chemical methods using a gas-liquid process as "model reaction" of known kinetics. The sulphite method, employing the oxidation of NaSO_3 , has been frequently used as test reaction [5,6,7]. Although there is controversy regarding the reaction order with respect to

oxygen and the reproductibility of the reaction kinetics is almost impossible [3,6]. Therefore, the absorption of CO₂ diluted with air into NaOH solutions has been chosen as model reaction in this work.

1. EXPERIMENTAL

The Mellapak structured metal sheet packing has been purchased from Sulzer Brothers Limited (Winterthur, Switserland). The corrugations of the metal sheets were inclined by an angle with respect to the vertical axis. For the Mellapak Y types this angle is always of 45⁰. The sheets are arranged vertically and parallel to each other (Figure 1). These corrugations define straight inclined channels of triangular cross section through which the gas flows. The liquid flows down the corrugated sheets approximately in countercurrent fashion to the gas. The Mellapak type used in this study was 750 Y, with a geometric specific area of 750 m²/m³ and a void fraction of 0.95. Measurements were also carried out with column packed with Raschig rings of 10 x8 x10 mm, made of glass , with the geometric area of 570 m²/m³ and a void fraction of 0.8. The flow chart of the bench- scale plant used for the absorption rate and pressure drop measurements is reproduced in the Fig 2.

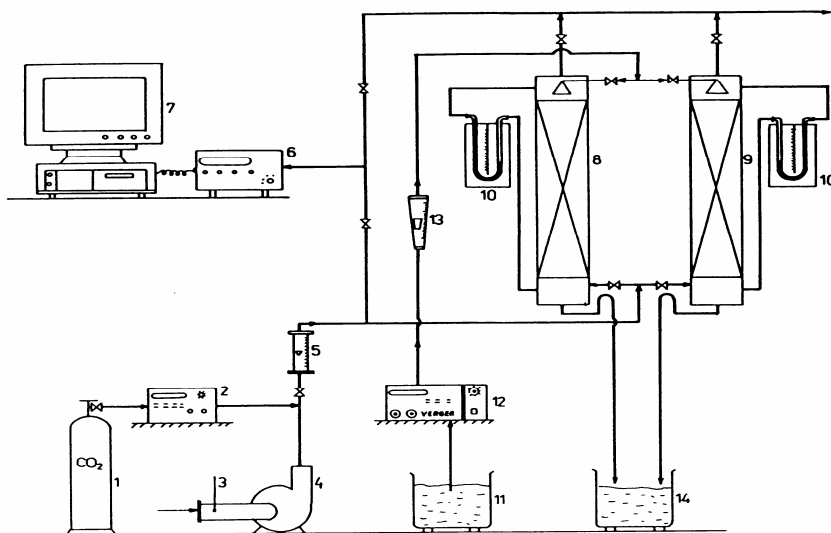


Figure 2. The experimental bench-scale plant

1- carbon dioxide cylinder, 2- carbon dioxide mass-flow meter, 3- air temperature controller, 4- air blower, 5- rotameter, 6- gas analyzer , 7- IBM compatible personal computer, 8/9- absorption columns, 10- manometer (mm WG), 11/14- solution tanks, 12- liquid pump, 13- liquid rotameter.

The first absorption column was equipped with a bed of 4.3175 liters of conventional packing. The second column contained 4.0663 liters of Mellapak 750 Y structured packing. To simulate the carbon dioxide absorption into the aqueous

NaOH solutions, three types of gas mixtures containing 5 %, 8 %, and 10 % vol. CO₂ have been used. The gas mixtures have been prepared from purified air and CO₂ of 99.99 purity from the cylinder. The aqueous NaOH solutions containing 0.5 , and 1.0 mol/L have been prepared from distilled water and NaOH of 99.99 purity from Merck GmbH. The solution has been analyzed by pH metric titration. The inlet and the outlet CO₂ concentrations in the gas mixture have been determined by BINOS 120 gas analyzer. The absorption rate has been calculated from the measured inlet (Y⁰_{CO2}) and outlet (Y_{CO2}) concentrations of the CO₂ in the gas by the equation (1):

$$V_{ab} = K V_G \left(\frac{Y^0_{CO_2} - Y_{CO_2}}{1 - Y_{CO_2}} \right) \text{ kmol/m}^3\text{s} \quad (1)$$

where : K = 10.0577 for the Mellapak , and K = 9.4725 for the Raschig rings.

The investigated systems and the variable factors (type of packing included) are listed in the Table 1.

Table 1.

The experimental conditions (T = 298 K, P= 1 bar)

Packing	Mellapak 750Y	Raschig rings
Column diameter, m	0.100	0.100
Height of the bed, m	0.518	0.550
Packing volume, L	4.0663	4.3175
Nominal size of the packing , mm	-	10 x 8 x 10
Equivalent diameter, mm	0.400	2.105
Void fraction of the bed	0.95	0.80
Geometric surface area, m ² /m ³	750	570
Concentration of NaOH solution, mol/L	0.50 ; 1.00	
CO ₂ mole fraction in the gas mixture	0.05 ; 0.08 ; 0.10	
Gas flow rate, m ³ /h	3.0 ; 5.0 ; 10.0	
Liquid flow rate, L/h	100 ; 120 ; 160 ; 200 ; 250.	

By combining the five variable factors a number of 240 pairs of input – output concentrations had to be measured in order to determine the corresponding absorption rates.

2. RESULTS

The tables 2 and 3 presented in this paper are only two of the sixteen tables containing all measured and calculated data.

Table 2.

Measured concentrations and calculated absorption rates in the two columns at C⁰_{NaOH} = 0.5 mol/L, and V_G = 10 m³/h.

No	Y ⁰ _{CO2}	V _L , L/h	Mellapak 750 Y		Raschig rings	
			Y _{CO2}	V _{ab, 10} ⁴ kmol/m ³ s	Y _{CO2}	V _{ab, 10} ⁴ kmol/m ³ s
1	0.05	100	0.035	4.343	0.035	4.093
2	0.05	120	0.034	4.627	0.033	4.629

CHARACTERISATION OF MELLAPAK 750Y STRUCTURED PACKING...

3	0.05	160	0.031	5.478	0.031	5.163
4	0.05	200	0.028	6.323	0.027	6.224
5	0.05	250	0.025	7.163	0.024	7.015
6	0.08	100	0.059	6.235	0.059	5.876
7	0.08	120	0.058	6.525	0.058	6.149
8	0.08	160	0.056	7.103	0.055	6.966
9	0.08	200	0.050	8.822	0.049	8.583
10	0.08	250	0.046	9.957	0.045	9.653
11	0.10	100	0.075	7.551	0.073	7.669
12	0.10	120	0.074	7.844	0.072	7.945
13	0.10	160	0.071	8.721	0.068	9.041
14	0.10	200	0.066	10.168	0.062	10.667
15	0.10	250	0.060	11.888	0.058	11.740

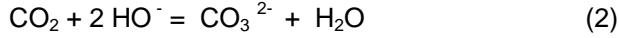
Table 3.
Measured concentrations and calculated absorption rates in the two columns at $C_{NaOH}^0 = 1.0 \text{ mol/L}$, and $V_G = 10 \text{ m}^3/\text{h}$.

No	$Y_{CO_2}^0$	$V_L, \text{ L/h}$	Mellapak 750 Y		Raschig rings	
			Y_{CO_2}	$V_{ab, 10^4} \text{ kmol/m}^3\text{s}$	Y_{CO_2}	$V_{ab, 10^4} \text{ kmol/m}^3\text{s}$
1	0.05	100	0.031	5.478	0.030	5.429
2	0.05	120	0.030	5.761	0.029	5.695
3.	0.05	160	0.027	6.604	0.026	6.488
4	0.05	200	0.024	7.443	0.022	7.538
5	0.05	250	0.022	7.199	0.020	8.061
6	0.08	100	0.050	8.823	0.050	8.315
7	0.08	120	0.049	9.107	0.049	8.583
8	0.08	160	0.047	9.675	0.046	9.384
9	0.08	200	0.042	11.082	0.041	10.707
10	0.08	250	0.040	11.642	0.039	11.244
11	0.10	100	0.065	10.458	0.066	9.585
12	0.10	120	0.064	10.746	0.064	10.127
13	0.10	160	0.060	11.889	0.059	11.473
14	0.10	200	0.054	13.586	0.052	13.332
15	0.10	250	0.049	14.983	0.047	14.644

As one can see from the two tables, the absorption rate in the column equipped with Mellapak 750Y is equal and frequently superior to that in the column with Raschig rings. To achieve the same and even a superior absorption rate with a pressure drop twenty folds lower [4] is obviously an important economic advantage of the structured packing. The next section is devoted to the effective mass transfer area determining.

3. EFFECTIVE MASS TRANSFER AREA

The absorption process carried out in the two experimental columns was accompanied by an irreversible second order reaction between the dissolved CO_2 and the NaOH in solution:



The concentration profiles of the two reactants in the liquid film are described by the differential equations (3) and (4):

$$D_{\text{CO}_2} \frac{d^2 C_{\text{CO}_2}}{dx^2} + k_2 C_{\text{CO}_2} C_{\text{HO}^-} = 0 \quad (3)$$

$$D_{\text{HO}^-} \frac{d^2 C_{\text{HO}^-}}{dx^2} + 2k_2 C_{\text{CO}_2} C_{\text{HO}^-} = 0 \quad (4)$$

with:

$$\begin{aligned} x = 0 ; C_{\text{CO}_2} &= C_{\text{CO}_2}^i ; \quad \frac{dC_{\text{HO}^-}}{dx} = 0 \\ x = \delta ; C_{\text{CO}_2} &= C_{\text{CO}_2}^0 ; \quad C_{\text{HO}^-} = C_{\text{HO}^-}^0 \end{aligned} \quad (5)$$

The analytical solution of the system (3) – (5) leads to the enhancement factor concept (E). This solution is available only if the reaction is considered to be pseudo -first order, i.e. the concentration of NaOH is undepleted in the liquid film [8,9.,10]: $C_{\text{HO}^-} = C_{\text{HO}^-}^0$. The solution is of the implicate form:

$$E = \frac{Ha \left(1 - \frac{E-1}{\beta} \right)}{\tanh \left[Ha \left(1 - \frac{E-1}{\beta} \right)^{1/2} \right]} \quad (6)$$

where:

$$Ha = \frac{(k_2 C_{\text{HO}^-}^0 D_{\text{CO}_2})^{1/2}}{k_L^0} \quad (7)$$

$$\beta = \frac{D_{\text{HO}^-} C_{\text{HO}^-}^0}{2D_{\text{CO}_2} C_{\text{CO}_2}^i} \quad (8)$$

$$\alpha = \frac{C_{\text{CO}_2}^0}{C_{\text{CO}_2}^i} = 0 \quad (9)$$

In the *fast reaction regim*, defined by $Ha > 5$, the enhancement factor equals the Hatta number and the absorption rate becomes:

$$V_{ab} = a_e C^i_{CO_2} (k_2 C^0_{HO} - D_{CO_2})^{1/2} \quad (10)$$

with: $E = Ha > 5 \quad (11)$

The condition (11) is necessary but not sufficient because at $Ha > 5$ the reaction may become spontaneous, too [10]. Therefore, a second condition must be fulfilled [9]:

$$\frac{Ha}{1 + \beta} < 0.5 \quad (12)$$

By representing the experimental absorption rate versus $X = C^i_{CO_2} (k_2 C^0_{CO_2} D_{CO_2})^{1/2}$, the effective mass transfer area can be obtained, as a slope of the straight line passing through the origin (Figs. 2 and 3).

Table 4.

The X coordinate of Figs. 2 and 4. $X = C^i_{CO_2} (k_2 C^0_{CO_2} D_{CO_2})^{1/2} \times 10^6, \text{ kmol/m}^2 \text{ s}$

$C^0_{HO} / Y^0_{CO_2}$	0.05	0.08	0.10
0.5	4.4180	7.0690	8.8360
1.0	5.7686	9.2995	11.5373

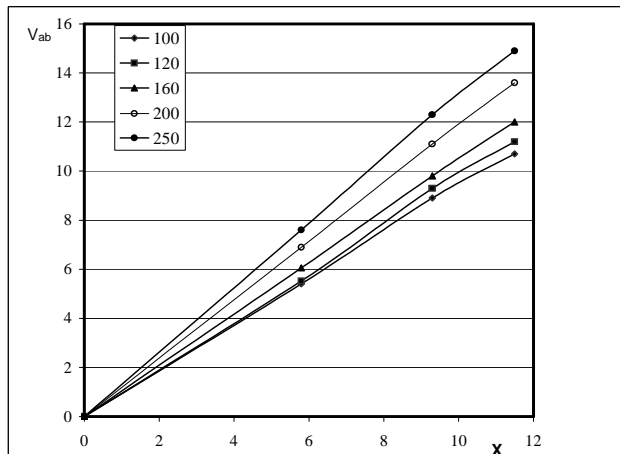


Figure 3. Absorption rate ($10^4 \text{ kmol/m}^3 \text{ s}$) versus X, at $C^0_{HO}=1.0 \text{ mol/L}$, $V_G=10 \text{ m}^3/\text{h}$, $T = 298 \text{ K}$, Mellapak 750Y (V_L in L/h as parameter)

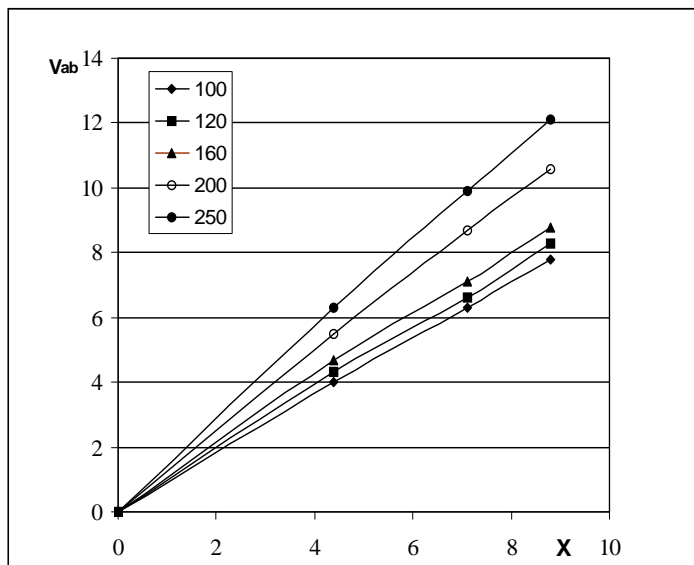


Figure 4. Absorption rate ($10^4 \text{ kmol/m}^3\text{s}$) versus X , at $C_{\text{HO}_2}^0=0.5 \text{ mol/L}$, $V_G=10 \text{ m}^3/\text{h}$, $T = 298 \text{ K}$, Mellapak 750Y (V_L in L/h as parameter)

The numerical values of the determined effective area from Figs. 3 and 4 are gathered in the Table 5.

Table 5.

Effective mass transfer area ($a_e, \text{m}^2/\text{m}^3$) of the Mellapak 750Y packing

$C_{\text{HO}_2}^0 / V_L, \text{L/h}$	100	120	160	200	250
0.5 mol/L	90.589	95.257	107.722	127.726	145.840
1.0 mol/L	93.504	97.001	107.199	122.996	135.326
Average	92.046	96.127	107.460	125.361	140.583

4. DATA VALIDATION AND CORRELATION

The values of the effective area in Table 5, determined by the equation (10) are valid only if the conditions (11) and (12) have been satisfied during the experiments. The Tables 6 and 7 present the numerical values of Hatta and $\frac{Ha}{1+\beta}$, respectively.

Table 6.

Hatta number for the experimental conditions ($T = 298 \text{ K}$, and $k_L^0 = 6.09 \cdot 10^5 \text{ m/s}$)

$C_{\text{HO}_2}^0, \text{mol/L}$	0.10	0.50	1.0	2.0
$k_2 \cdot 10^4, \text{L/mol s}$	0.838764	1.019060	1.278497	1.904145
$D_{\text{CO}_2} \cdot 10^9, \text{m}^2/\text{s}$	1.9627	1.8727	1.7479	1.6010
Ha	21.062	50.707	77.600	128.137

Table 7.

The ratio $Ha/1+\beta$ for the experimental conditions.

$Y^0_{CO_2} / C^0_{HO-}$	0.10	0.50	1.00	2.00
0.05	0.3817	0.1644	0.1072	0.0650
0.08	0.6042	0.2623	0.1717	0.1040
0.10	0.7498	0.3716	0.2146	0.1293

The necessary equations for the calculations of the parameters included in the relations (11) and (12) are listed in the **Appendix** [9,11-14]. As one can see from Tables 6 and 7, both conditions have been satisfied during the measurements.

Another way to validate the numerical values of the effective area obtained in this work could be the comparison with the existing data for similar packings. Unfortunately, such data for Mellapak 750 Y are lacking. The equation of Onda et al., cited by Danckwerts [9], predicts the wetted area of the conventional packings while the equation of Rizzuti and Brucato, cited by De Brito et al. [3], was established for effective area but also for random packed beds.

The data in Table 5 obtained in this work have been correlated by the criterial equation of the form:

$$\frac{a_e}{a} = 0.1245 \left(\frac{\rho_L d_p v_L}{\mu_L} \right)^{0.4} \quad (13)$$

where:
$$d_p = \frac{6(1-\varepsilon)}{a} \quad (14)$$

The constant and the exponent of the equation (13) have been identified by regression.

5. CONCLUSIONS

The effective mass transfer area of a Mellapak 750 Y structured packing and of 10 x 8 x10 glass Raschig rings has been determined by measuring. The absorption rates in two columns under identical operating conditions. The absorption of carbon dioxide diluted with air into aqueous NaOH solutions was employed as model reaction of known kinetics.

The new determined values for Mellapak 750Y have been correlated by a criterial equation. New measurements have to be done in broader intervals of fluid flow rates, at larger scale.

NOTATION

a , geometric specific area of the packing, m^2/m^3 ;
 a_e , effective mass transfer area, m^2/m^3 ;
 a_w , wetted area of the packing, m^2/m^3 ;
 C_{CO_2} , C_{HO-} , molar concentration in the liquid film of the carbon dioxide and natrium hydroxide, respectively, mol/L;
 $C^0_{CO_2}$, concentration of dissolved CO_2 at the interface, mol/L;

$C_{CO_2}^0$, $C_{HO^-}^0$, concentration in the liquid bulk of the CO_2 and HO^- respectively, mol/L;
 d_p , equivalent diameter of the packing, m;
 D_{CO_2} , D_{HO^-} , diffusivity in the liquid phase of CO_2 and HO^- , m^2/s ;
 E , enhancement factor;
 Ha , Hatta number;
 H , Henry constant, mol/L bar;
 H_0 , Henry constant of CO_2 in water, mol/L bar;
 K , constant in the equation (1);
 k_2 , second- order reaction rate constant, mol/L s;
 k_L^0 , physical mass transfer coefficient of CO_2 in the liquid phase, m/s;
 P , total pressure, bar;
 p_{CO_2} , partial pressure of CO_2 , bar;
 T , temperature, K;
 \tanh , hyperbolic tangent;
 V_{ab} , absorption rate, kmol/ m^3s ;
 V_G , gas flow rate, m^3/s ;
 V_L , liquid flow rate, m^3/s ;
 v_L , liquid rate, m^3/m^2s ;
 X , coordinate in the figs. 3 and 4, kmol/ m^2s ;
 α , the ratio $C_{CO_2}^0/C_{CO_2}^i$;
 β , non dimensional group defined by the equation (8);
 δ , liquid film thickness, m;
 ε , void fraction of the packing bed;
 μ_{HO_2} , μ_L , viscosity of the water and the solution, respectively, Pa s;
 ρ_L , liquid density, kg/m^3 .

REFERENCES

1. A.K. C o k e r, *Understand the Basics of Packed- Column Design*, Chem.Eng.Progr.vol.11(1991), 93-99.
2. E.Brunazzi, and A. Paglianti, *Mechanistic Pressure Drop Model for Columns Containing Structured Packings*, A.I.Ch.E. Journal, vol.43 (1997), 317-327.
3. H. De Britto, U. von Stockar, A. M. Bangerter, and M. Laso, *Effective Mass-Transfer Area in a Pilot Plant Column*, Ind.Eng. Chem. Res., vol.33 (1994), 647-656.
4. M. Dragan, A. Fridl, M. Harasek, S. Dragan, and I. Siminiceanu, *Hydrodynamics of a New Type of Structured Packing*, Studia Univ. Babeş- Bolyai, Chem., vol. 43(1998), 52-61.
5. M. M. Sharma, and P.V. Danckwerts, *Chemical Methods of Measuring Interfacial Area and Mass Transfer Coefficients in Two Fluid Systems*, Brit. Chem 15 (1970), 522-527.
6. Siminiceanu I., and M. Ivaniciuc, *Measuring of the Mass Transfer Parameters in Gas-Liquid Contactors by Chemical Methods*, Analele Stiint.Univ. Al.I. Cuza Iasi, vol.5 (1997), 145-150.

7. J.P. Euzen, P. Trambouze, and J.P. Waquier, *Scale-Up Methodology for Chemical Processes*, Editions Technip, Paris, 1993.
8. Siminicéanu, and M. Ivaniću, *Modeling of Gas Treating with Chemical Solvents*, Science and Technol. Environ. Prot., vol. 5 (1998), 25-33.
9. P.V. Danckwerts, *Gas-Liquid Reactions*, Mc Graw Hill, New York, 1970.
10. Siminicéanu, C. Petrila, and C. German, *Acceleration Factor Determining for Gas Absorption in Chemical Solvents*, Rev. Chim. (Bucharest), vol.47 (1996), 265-169.
11. Siminicéanu I., *Carbon Dioxide Absorption into Promoted Potash Solutions. I. Enhancement Factor Determining*, Studia Univ. Babes- Bolyai, Chem., vol. 36 (1991), 71-77.
12. R. Zarzycki, and A. Chacu, *Absorption*, Pergamon Press, Oxford, 1993.
13. D. Herskovits, V. Herskovits, K. Stephan, and A. Tamir, *Characterization of a Two Phase Impinging Jet Absorber*, Chem. Eng. Sci., vol. 43 (1990), 1281-1287.
14. Mihaela Dragana, *Transfer Characteristics of the Mellapak 750 Y Structured Packing*, Ph.D. Thesis, Technical University of Iasi, 1999.

APPENDIX

The concentration of dissolved CO₂ at the interface can be predicted by the system (A₁-A₃):

$$C^i_{CO_2} = H \cdot p_{CO_2} \quad (A_1)$$

$$\log \frac{H}{H_0} = -0.138 C^0_{NaOH} \quad (A_2)$$

$$\log H_0 = \frac{1140}{T} - 5.30 \quad (A_3)$$

The CO₂ diffusivity in pure water depends on the temperature as follows:

$$\log D^0_{CO_2} = -8.1764 + \frac{712.5}{T} - \frac{2.591 \times 10^5}{T^2} \quad (A_4)$$

while the diffusivity of the CO₂ in the NaOH aqueous solution was calculated by the relation:

$$D_{CO_2} = D^0_{CO_2} \left(\frac{\mu_{H_2O}}{\mu_L} \right)^{0.637} \quad (A_5)$$

The second -order reaction constant k₂ depends both on the temperature and on the ionic strength in a non- linear manner:

$$\log k_2 = 11.895 - \frac{2382}{T} + 0.221 C^0_{NaOH} - 0.016 (C^0_{NaOH})^2 \quad (A_6)$$

The physical mass transfer coefficient (k_L^0) has been evaluated by the equation of Onda et all [9]:

$$\frac{k_L^0}{aD_{CO_2}} = 0.0051(ad_p)^{0.4} \left(\frac{v_L \rho_L}{a\mu_L} \right)^{4/3} \left(\frac{av^2_L}{g} \right)^{-1/3} \left(\frac{\mu_L}{\rho_L D_{CO_2}} \right)^{1/2} \quad (A_7)$$

The ratio D_{H_2O}/D_{CO_2} is generally between 1.67 and 2.1. A value of 1.70 has been adopted.

BIOORGANIC REDUCTION OF SOME 5-PHENYL-FURAN-2-CARBALDEHYDES MEDIATED BY BAKERS' YEAST

F. D. IRIMIE¹, CS. PAIZS, MONICA TOȘA¹, CORNELIA MAJDIK¹, PAULA MOLDOVAN¹, R. MIȘCA¹, MIHAELA CĂPRIOARĂ¹, MĂDĂLINA NEACȘU²

¹Department of Biochemistry and Biochemical Engineering,
"Babeș-Bolyai" University of Cluj-Napoca, ROMANIA

²"Bios" Center of development and production", Cluj-Napoca, ROMANIA

ABSTRACT. Eight 5-phenyl-furyl-2-carbaldehydes variously substituted with halogenes atoms at the phenyl rings, were reduced to the corresponding alcohols with Bakers' Yeast (under mild conditions), with good yields.

INTRODUCTION

Bakers' yeast (*Saccharomyces cerevisiae*) may be an easily available "reagent" in every laboratory of organic chemistry. Its biocatalytical activity has been reported in two exhaustive reports [1,2].

Bakers' yeast is able to reduce variously substituted carbonyl groups, activated carbon-carbon double bonds and nitrocompounds. Unlike ketones, little attention has been paid to the reduction of heterocyclic aldehydes with *Saccharomyces cerevisiae*.

Bakers' yeast mediated reduction of some 5-phenyl-furan-2-carbaldehydes was already reported. In case of unsubstituted, 5-(4-methyl-phenyl)-furan-2-carbaldehyde and 5-(4-methoxy-phenyl)-furan-2-carbaldehyde, a large amounts of yeast was used (yeast/substrate = 50/5 (g/mmol)) and reactions were completed in six hours [3]. When 5-(2-,3- or 4-carbetoxy-phenyl)furan-2-carbaldehyde was used as substrate, bioreduction undergoes in same conditions with those presented previously, however it must be mentioned the chemoselectivity of the process, reduction undergoes without the enzymatic hydrolysis of the esteric function [4].

For investigate how the nature of substituents at the phenylic ring influence the bioreduction process, in this paper we presented the synthesis and Bakers' yeast mediated reduction of eight 5-aryl-furan-2-carbaldehydes substituted with halogen atoms.

The general procedure of synthesis and reduction of these furancarbaldehydes were presented in scheme 1.

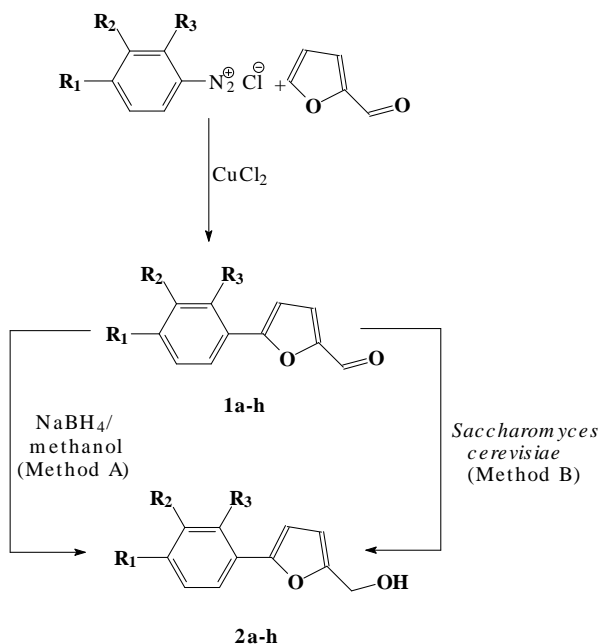
EXPERIMENTAL

The 5-phenyl-furan-2-carbaldehydes **1a-h** were prepared from the diazonium salts of the halogeneanilines and furan-2-carbaldehyde [5]. The known 5-phenyl-furan-2-carbaldehydes **1a-g** had identical physical and spectral data as described previously (Table 1).

Reagent and solvents were standard grade commercial products and used without further purification.

The elemental analysis for C, H and halogen were within $\pm 0,4\%$ of the theoretical values for **1g** and **2a-h**. The reagents were products of Aldrich.

The $^1\text{H-NMR}$ spectra were recorded on a Varian Gemini 300 spectrometer operating at 300 MHz. All spectra were taken in CDCl_3 solution and chemical shifts are expressed in ppm values from TMS as internal standard on δ scale. IR spectra were obtained in KBr pellets on a Nicolet FT 205 spectrometer and are reported in wavenumbers (cm^{-1}). The mass spectra were recorded on double focusing Varian Mat 311 spectrometer, with an electronic impact source at 70 eV and 300 mA.



Scheme 1. Synthesis and reduction of 5-aryl-furan-2-carbaldehydes **1a-h** to the corresponding alcohols **2a-h**

Thin layer chromatography was carried out using Merck Kieselgel 60 F₂₅₄ alumina sheets. Spots were visualized by treatment with 5% ethanolic phosphomolybdic acid solution and heating of the dried plates.

Assymetric nitrocellulose membrane with 0.33 μm media pore diameter was produced in accord with Loeb-Sourirjean method [6].

Preparative chromatographic separations were performed using vacuumchromatography on Merck Kieselgel 60 (0.063-0.200 nm). Melting points are uncorrected. All solvents were purified and dried by standard methods as required.

General procedure for synthesis of aldehydes 1a-h

To a solution of corresponding diazonium salt (0.1 mol) in water furan-2-carbaldehyde (0.1 mol) and CuCl_2 solution (6 g in 40 ml water) was added. The mixture was heated at 40°C, six hours. The organic layer was extracted with chloroform and dried on anhydrous magnezium sulphate. The chloroform was evaporated and the crude product was distilled *in vacuo*. Yields and melting points were given in Table 1.

General procedure for reduction of carbaldehyde 1a-h with NaBH_4 (Method A)

NaBH_4 (0.1 g) was added in isopropanol (7 ml). The mixture was stirred for 1.5 hours, while adding the substrate **1a-h** (0.2 g) in small amounts. The solution was allowed to stand over night, than diluted HCl (5%) was added until no more gas evolution was observed. The organic compounds were extracted with CHCl_3 (five times), than the solvent was removed *in vacuo* affording the hydroxy-derivatives, which were purified by column chromaatography and finally recrystalised from ethanol:acetone (1:1, v:v). Yields and melting points were given in Table 2.

General procedure for bioreduction of carbaldehyde 1a-h (Method B)

Substrates **1a-h** (5 mmol) were dissolved in ethanol (5 ml) and added at room temperature into a suspension of fresh bakers' yeast (5 g) in water (50 ml) with glucose (5 g). After time indicated in Table 2 the products were extracted from suspension with benzene-ethylacetate (1:1, v:v) (100 ml). After extraction assymetric nitrocellulose membrane was used to removed Bakers' yeast cells. Further work up was carried out as described in Method A.

RESULTS AND DISCUSSION

Table 1. Synthesis of 5-aryl-furan-2-carbaldehydes **1a-g**

1	R₁	R₂	R₃	Yield (lit.) [%]	m.p. (lit.) [°C]
a	F	H	H	53 (48)	69 (73-74 ^f)
b	Cl	H	H	62 (61)	128-129 (128-129 ^g)
c	Br	H	H	65 (66)	153 (154 ^g)
d	I	H	H	64 (66)	144 (145-146 ¹⁰)
e	H	Br	H	70 (67)	107(107 ¹⁰)
f	H	H	Cl	55 (56)	77 (76.5-77.5 ¹¹)
g	H	H	Br	60 (56)	57 (57-58 ¹⁰)

h	H	H	I	43	64
----------	---	---	---	----	----

Table 2. Reduction of 5-aryl-furan-2-carbaldehydes **1a-g**

2	Yield [%]		Time [h]	b.p. / p m.p. (lit.) [°C]
	Method A (lit.)	Method B		
a	90 (80)	70	4	41 (41 ¹)
b	85 (80)	80	5	81-82 (82-83 ⁸)
c	85 (80)	85	5	96-97 (97 ¹)
d	75	75	6	99
e	75 (70)	75	5	81 (81 ¹³)
f	84 (70)	64	5	63 (64-5 ¹³)
g	82	72	5	65
h	88	68	5	71

5-(2-iodophenyl)-furan-2-carbaldehyde (1h)

IR: 1675(CHO); ¹*H*-RMN: 6.87 (d,1H), 7.34 (d,1H), 7.55-7.93 (m,4H), 9.65 (s,1H); *MS*: 298(100)M, 270(13), 241(32), 171(2)

(5-(4-fluorophenyl)-furan-2-yl)methanol 2a

IR: 1060, 3180 (l.b)(-CH₂-OH); ¹*H*-NMR: 2.63 (OH), 4.69 (s,2H), 6.20 (d, 1H), 6.55 (d,1H), 7.55(d,2H), 7.96 (d,2H); *MS*: 192(100)M,193(10)M+1, 190(11)M-2, 175(95)M-17, 163(17), 146(34), 133(56)

(5-(4-chlorophenyl)-furan-2-yl)methanol 2b

IR: 1050, 3200 (l.b)(-CH₂-OH); ¹*H*-NMR: 2.43 (OH), 4.65 (s,2H), 6.21 (d, 1H), 6.50 (d,1H), 7.39(d,2H), 7.55 (d,2H); *MS*: 208(100)M, 210(33)M, 191(80)M-17, 193(26)M-17, 178(3), 180(1), 149(37), 139(42)

(5-(4-bromoophenyl)-furan-2-yl)methanol 2c

IR: 1040, 3190 (l.b)(-CH₂-OH); ¹*H*-NMR: 2.58 (OH), 4.67 (s,2H), 6.39 (d, 1H), 6.61 (d,1H), 7.18 (d,2H), 7.51 (d,2H); *MS*: 252, 254(100)M, 253, 255(11)M+1, 250, 252(11)M-2, 235, 237(71)M-17, 224, 226(10), 193, 195(40)

(5-(4-iodophenyl)-furan-2-yl)methanol 2d

IR: 1080, 3300 (l.b)(-CH₂-OH); ¹*H*-NMR: 2.54 (OH), 4.51 (d,1H), 6.20 (d, 1H), 6.43 (d,1H), 7.18 (d,2H), 7.41 (d,2H); *MS*: 300(100)M, 301(9)M+1, 298(70)M-2, 283(90)M-17, 270(13), 241(32)

(5-(3-bromophenyl)-furan-2-yl)methanol 2e

IR: 1060, 3250 (l.b)(-CH₂-OH); ¹*H*-NMR: 2.61 (OH), 4.68 (s,2H), 6.40 (d, 1H), 6.63 (d,1H),7.31-7.70 (m,3H), 7.82 (s,1H); *MS*: 252, 254(100)M, 253, 255(11)M+1, 250, 252(11)M-2, 235, 237(71)M-17, 224, 226(10), 193, 195(40)

(5-(2-chlorophenyl)-furan-2-yl)methanol 2f

IR: 1050, 3310 (l.b) (-CH₂-OH); ¹*H-NMR*: 2.58 (OH), 4.61 (s,2H), 6.29 (d,1H), 6.52 (d,1H), 7.30-7.87 (m,4H); *MS*: 208(100)M, 210(33)M, 191(80)M-17, 193(26)M-17, 178(3), 180(1), 149(37), 139(42)

(5-(2-bromophenyl)-furan-2-yl)methanol 2g

IR: 1060, 3190 (l.b) (-CH₂-OH); ¹*H-NMR*: 2.61 (OH), 4.60 (s,2H), 6.30 (d,1H), 6.50 (d,1H), 7.30-7.80 (m,4H); *MS*: 252, 254(100)M, 253, 255(11)M+1, 250, 252(11)M-2, 235, 237(71)M-17, 224, 226(10), 193, 195(40)

(5-(2-iodophenyl)-furan-2-yl)methanol 2h

IR: 1050, 3200 (l.b)(-CH₂-OH); ¹*H-NMR*: 2.59 (OH), 4.60 (s,2H), 6.49 (d,1H), 6.70 (d,1H), 7.3-7.6 (m,4H); *MS*: 300(100)M, 301(9)M+1, 298(70)M-2, 283(90)M-17, 270(13), 241(32)

The elemental analysis and the spectral data of **2a-h** showed identical values with those obtained through reduction with sodium borohydride.

The *IR*, *MS* and ¹*H-NMR* spectra and the elemental analysis of the isolated products confirmed the structures of compounds **2 a-h**. In *IR* spectra the presence of bands at 1040-90 cm⁻¹ and at the 3180-3350 cm⁻¹ and the absence of bands at 1670-1680 cm⁻¹ (which are observed in the *IR* spectra of aldehydes **1a-h**), confirmed the presence of an primary benzylic type alcohol, in the structures of compounds **2 a-h**.

Molecular peaks for **2 a-h** are clear, the characteristic fragment for benzylic type alcohols (M-17) were observed.

In case of **2 a-h**, the presence of the singlet at δ=4,6-4,8 corresponding for two protons, indicated the transformation of the aldehydic group.

The sufficient amount of yeast was ten times lower (yeast/substrate) =5/5 g/mmol) in comparison with those used in cases described in introductory section, moreover reaction times were comparable. These facts could be explained with the withdrawing character of halogen atom reducing electron density at the carbonyl group, which facilitate the hydride transfer from oxidoreductases cofactors (NADH, H⁺, FADH₂), however reaction time probably was influenced by diffusion process too.

In case of biocatalytic reduction, secondary products were not appeared, the substrates were totally transformed. The reaction mass was simply worked up, the purification of products was simple.

CONCLUSION

Biocatalytical reduction of halogenated 5-phenyl-furyl-2-carbaldehydes is an alternative and a new synthetic procedure. The main advantages are the mild conditions, good yields and the simplicity of the method.

REFERENCES

1. Csuk, R., Glantzer, B.I. *Chem.Rev.* 1991, **91**, 49, (1991).
2. Santinello, E., Ferraboschi, P., Grisente, P., Manzocchi, A. *Chem.Rev.*, 1992, **92**, 1071.
3. Irimie, F.D., Paizs, Cs., Silaghi–Dumitrescu, R., Toșa, M., Majdik, C.
1. *Roum. Biotechnol. Lett.* 1999, **4**(1), 71.
4. Irimie, F.D., Paizs, Cs., Silaghi–Dumitrescu, R., Toșa, M., Majdik, C. *Progrss in catalysis* 1999, **8**, 70.
5. Ryohei, O. *Mem.Fac. Eng.Kyoto.Univ.* 1952, **14**, 195; *Chem. Abstr.* **48**, 1935f.
6. Liteanu, C., Rădulescu, Gh. *Bazele membranologiei*, București, 1983.
7. Oleinik, T. *Pharm. Chem. J. (Engl. Transl.)* 1971, **5**(7), 401.
8. Akashi, Oda, *Kogyo Kagaku Zasshi* 1950, **53**, 81; *Chem. Abstr.* 1953, 2164.
9. Chadwich, R., Jhonson, T. *J. Chem. Soc. Perkin Trans.1* 1973, 2327.
10. Obushak, N., Ganushchak, N. I., Zavalii, P.Yu *J. Org. Chem. Engl. Transl.* 1986, **22**(11), 2093.
11. Krutsikova, N. *Chem. Zvesti* 1971, **25**, 142.
12. Frimm, *Chem. Zvesti* 1972, **26**, 55114.
13. Schwarzer P h., *Handbook of Separations, Technoques for Chemical Engineers* 1988, 2-20, 2^{end} Ed., McGraw Hill Book Co., New-York, St. Louis, San Francisco.

MASS SPECTROMETRY OF SOME NEW 10-PENTYL- 10H-PHENOTHIAZINE DERIVATES

FLORIN IRIMIE¹, CSABA PAIZS¹, MONICA TOȘA¹, CORNELIA MAJDIK¹,
MIHAELA CĂPRIOARĂ¹, MĂDĂLINA NEACȘU², PETER VEGH³

¹*Department of Biochemistry and Biochemical Engineering,
"Babeș-Bolyai" University of Cluj-Napoca, ROMANIA*

²*"Bios" Center of development and production", Cluj-Napoca, ROMANIA*

³*"ITIM" Research Center", Cluj-Napoca, ROMANIA*

ABSTRACT. The fragmentation processes of ten new phenothiazine derivatives **1-10** have been investigated. The main decomposition routes consist of losses of small neutral groups (O, OH, SO, SO₂, CO, CH₂=CO) and/or fragments of the alkyl substituent.

INTRODUCTION

The importance and widespread use of different phenothiazine derivatives in medical practice gave rise to a continuous interest in their mass spectromeric behaviour, resulting a well-documented mass spectrometry of these compounds [1-5]. However, the same is not true for phenothiazine S-oxides and S,S-dioxides, although the significance of these derivatives is now also evident: the metabolic oxidation of phenothiazine drugs to cyclic S-oxides has been postulated repeatedly [6] and the metabolic formation of sulfone derivatives from chlorpromazine has been shown recently in man [7].

These facts prompted us to study the details of the electron-impact induced fragmentation of some phenothiazine derivatives.

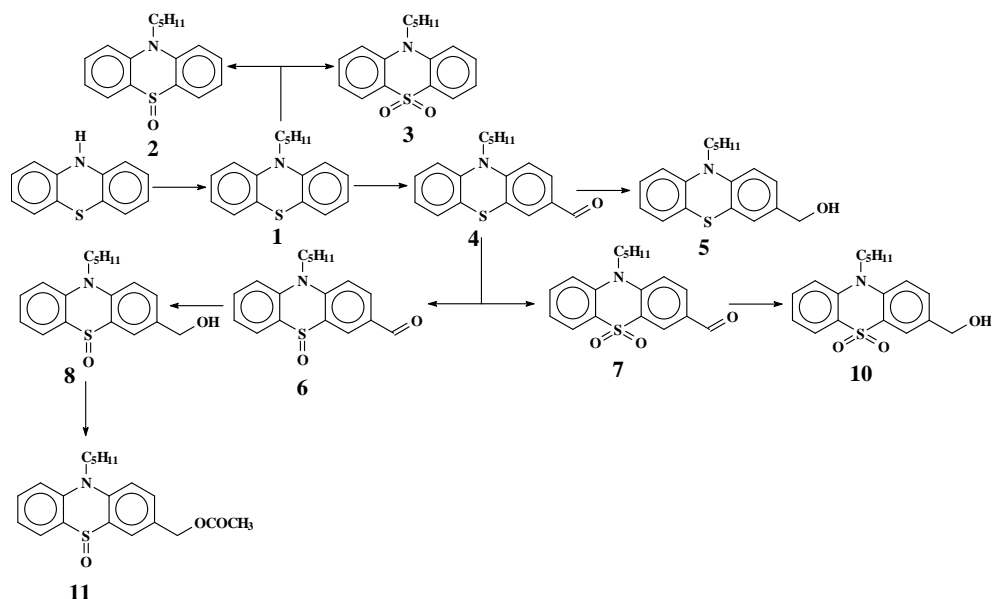
In this paper is presented the mass spectral behaviour of ten new phenothiazine based structures **1-11**. 10-Pentyl-10H-phenothiazine was recently synthesized [8] and functionalized at C-3 atom (Scheme 1) as reported previously [9-12].

EXPERIMENTAL

The mass spectra were recorded on double focussing Varian Matt 312 mass spectrometer, with electron impact source at 70 eV and 300 mA. The source temperature was 170 °C.

10-Pentyl-phenothiazine **1** was prepared by alkylation of phenothiazine with pentylbromide in the presence of sodium amide [8]. 10-Pentyl-10*H*-phenothiazine-3-carbaldehyde **4** was obtained by Vilsmeier-Haack formylation from **1** [9]. Sulfoxides (**2**, **6**) and sulfones (**3**, **9**) were prepared using selective oxidative methods [8]. 3-Hydroxymethyl compounds (**5**, **8**, **10**) were synthesised from the corresponding carbaldehydes by Baker's yeast mediated reductions [9], ester **11** was obtained by enzymatic esterification of the appropriate alcohol **8** [10,11].

Scheme 1. Reaction pathway for synthesis of compounds **1-11**

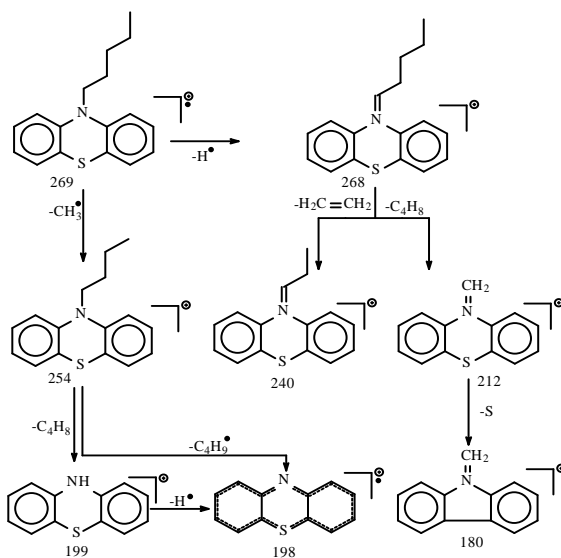


RESULTS AND DISCUSSION

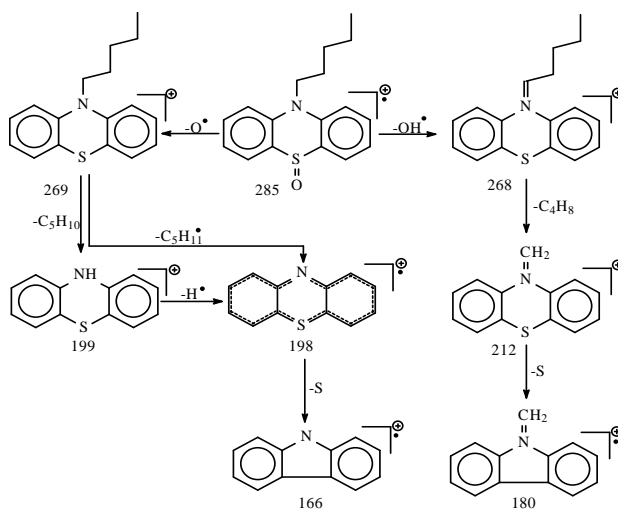
In mass spectrum of 10-Pentyl-10*H*-phenothiazine **1** (scheme 2), the base peak corresponds to the elimination of the alkyl substituent by formation of phenazathionium cation as fragment. Molecular peak was relatively stable, with 60% abundance.

α , β and δ -cleavages in the alkyl substituent appeared, but only α -cleavage conduct to the formation of a $m/z=212$ fragment with high relative intensity (58%).

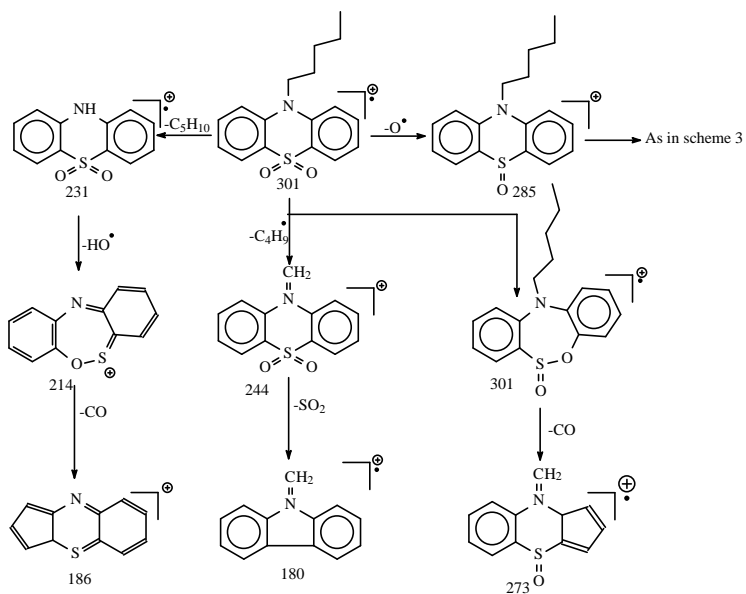
The mass spectral behaviour of 10-pentyl-10*H*-phenothiazine-5-oxide is very dissimilar to that of phenothiazine sulfoxide [5], which gives the $m/z=269$ base peak fragment (Scheme 3). Any further fragmentation of the $(M-OH)^+$ ions has been found almost negligible. Elimination of an O atom from the molecular ion resulted in low abundant $(M-O)^+$ peaks, their main further fragmentation, consisting of the loss of the alkylic substituent, leading to abundant $(M-O-C_5H_{11})^+$ peak.



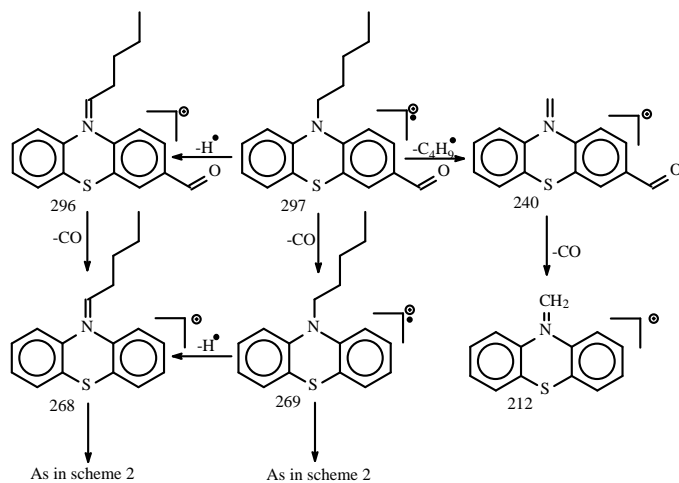
Scheme 2. Fragmentation scheme of 10-Pentyl-10H-phenothiazine 1



Scheme 3. Fragmentation scheme of 10-Pentyl-10H-phenothiazine-5-oxide 2



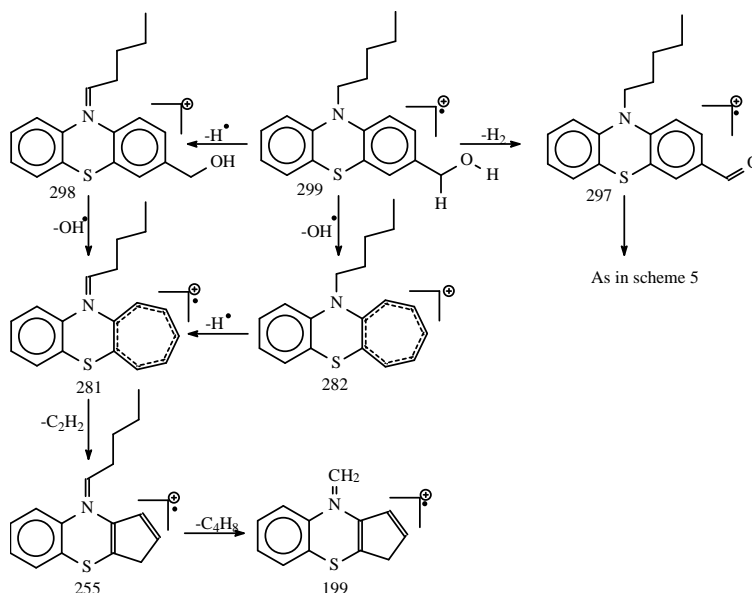
Scheme 4. Competing routes in fragmentation of 10-Pentyl-10*H*-phenothiazine-5,5-dioxide **3**



Scheme 5. Fragmentation routes in the case of 10-pentyl-10*H*-phenothiazine-3-carbaldehyde **4**

The molecular ion of 10-Pentyl-10*H*-phenothiazine-5,5-dioxide **3** form the base peak of the spectrum and decompose in competing routes. Molecular ion undergoes rearrangement [14], with the formation of C-O bond. Elimination of an O atom gives the corresponding sulfoxidie fragment. Expulsion of SO₂ from the fragment generated by the α -cleavage of the alkyl-substituent ($m/z=244$) was also appeared. Base peak fragment ($m/z=231$) was formed by elimination of C₅H₁₀. Further elimination of O atom produced rearrangement which gives the possibility of elimination of an CO molecule.

In case of 10-pentyl-10*H*-phenothiazine-3-carbaldehyde **4**, molecular ion was the base ion. Its fragmentation undergoes predominantly in two ways: *via* α -cleavage of the pentyl substituent or *via* elimination of an CO molecule characteristic for aromatic and heteroaromatic compounds. β,γ,δ -cleavage of the alkyl substituent generated fragments with low stability which were not mentioned in the fragmentation scheme 5.

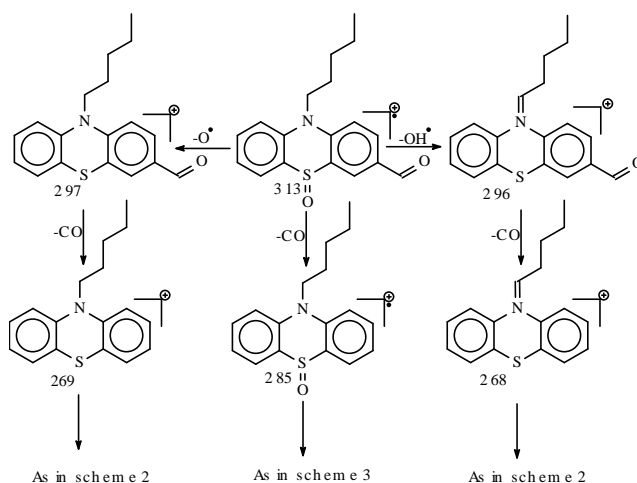


Scheme 6. Fragmentation of (10-Pentyl-10*H*-phenothiazine-3-yl)methanol **5**

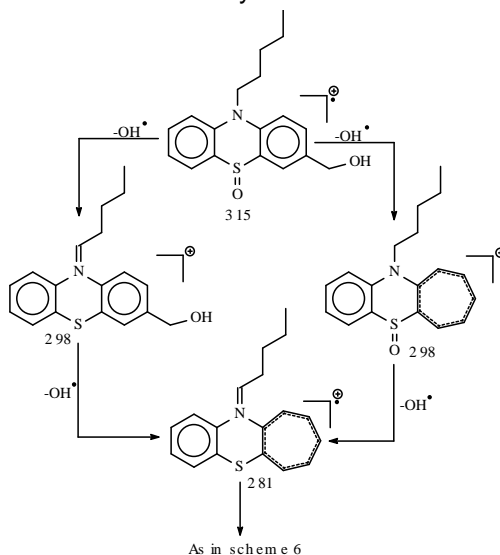
Fragmentation of (10-Pentyl-10*H*-phenothiazine-3-yl) methanol **5** undergoes in two ways: elimination of a H₂ molecule generating the aldehyde fragment, or elimination of an OH fragment which conducts by a ring rearrangement to the $m/z=282$ fragment. Fragmentation of molecular ion by cleavage of the alkyl substituent was not observed.

Fragmentation of 10-Pentyl-10*H*-phenothiazine-3-carbaldehyde-5-oxide **6** undergoes by elimination of characteristic fragments for phenothiazine-5-oxides and aromatic aldehydes. M-O-CO, M-OH-CO, M-CO-OH peaks appeared in the mass spectrum of **6** (Scheme 7), together with the fragmentation of molecular ion *via* cleavage of the alkyl group.

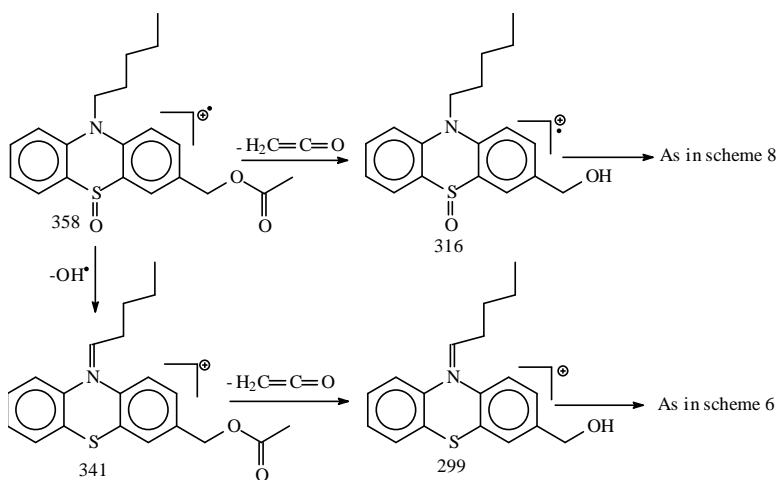
Fragmentation of (10-Pentyl-10*H*-phenothiazine-3-yl)-methanol-5-oxide **7** (Scheme 8) undergoes only by elimination of OH, which is characteristic for benzyl type alcohols and phenothiazine-sulfoxides too, any other peaks on the spectra appeared from the cleavage of the fragment with $m/z=282$. No other path for fragmentation was observed. The corresponding acetate **8** (Scheme 9), by elimination of cetene, generated the alcohol-sulfoxid fragment. No M-29 or M-43 peaks which are characteristic for ester appeared.



Scheme 7. Fragmentation routes in the case of 10-pentyl-10*H*-phenothiazine-3-carbaldehyde-5-oxide **6**

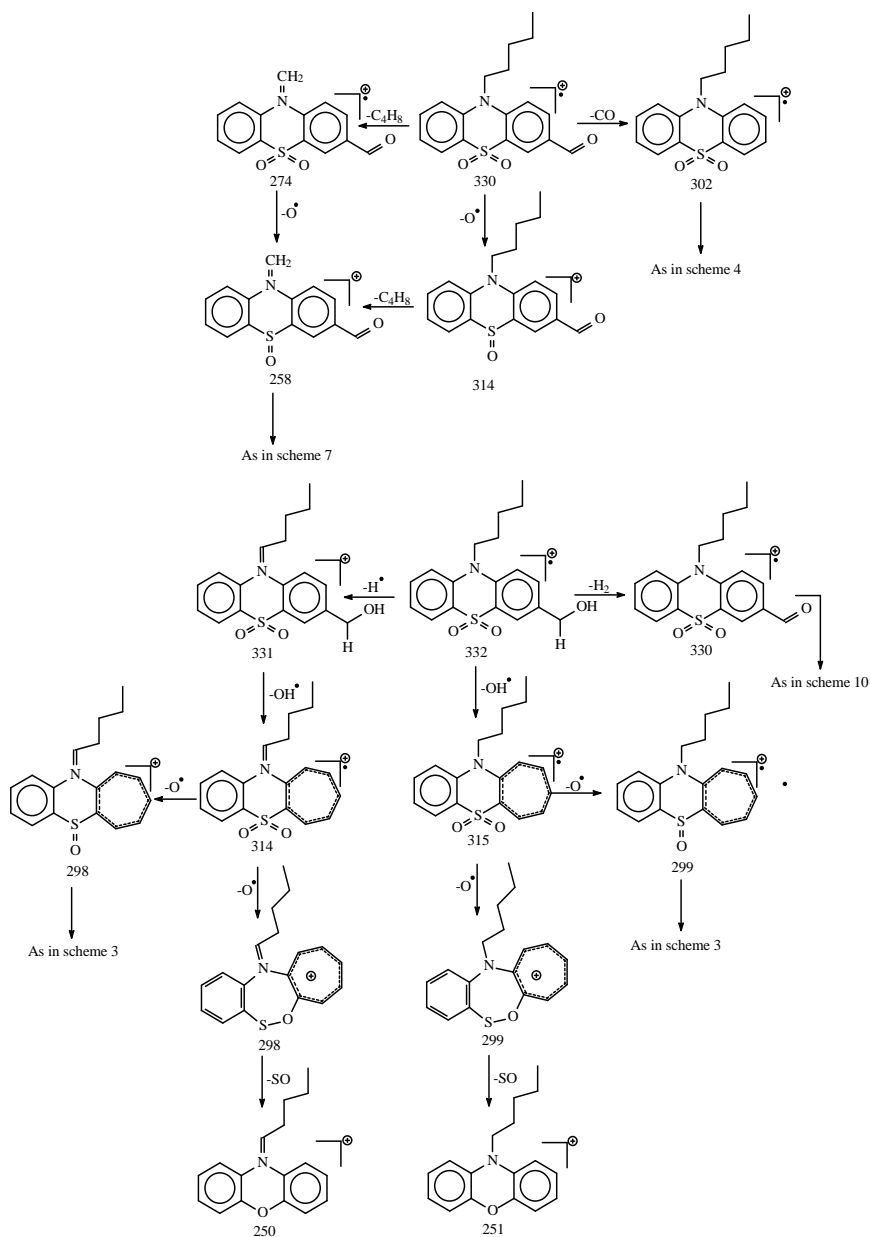


Scheme 8. Fragmentation routes in the case of (10-pentyl-10*H*-phenothiazine-3-yl)-methanol-5-oxide **7**



Scheme 9. Fragmentation routes in the case of (10-pentyl-10*H*-phenothiazine-3-yl)methyl acetate **8**

Decomposition processes of sulfonealdehyde **9** and sulfonealcohol **10** (Scheme 10) were in agreement with those presented for 10-alkyl-10*H*-phenothiazine-5,5-sulfone (**3**), 10-alkyl-10*H*-phenothiazine-3-carbaldehyde (**4**), respectively (10-alkyl-10*H*-phenothiazine-3-yl)methanol (**5**), the observed fragmentation processes lead to stable ionic structures *via* heteroaromatization, or by extension of the π -conjugation.



Scheme 10. Fragmentation routes in case of 10-pentyl-10H-phenothiazine-3-carbaldehyde-5,5-dioxide **9** and (10-pentyl-10H-phenothiazine-3-yl)-methanol-5,5-dioxide **10**

CONCLUSION

Fragmentation scheme of ten new phenothiazine compounds were presented. Molecular peaks were clear, the characteristic fragments in each case were observed. For sulfoxides and sulfones, ring rearrangement paths were proposed in according with literature data.

REFERENCES

1. Duffield, A. M., Craig, J.C., Kray, L.R. *Tetrahedron* 1968, **24**, 7267.
2. Audier, L., Cambon, A., Guedi, R., Azzaro, M. *J. Het. Chem* 1968, **5**, 393.
3. Audier, L., Azzaro, M., Cambon, A., Guedi, R. *Bull. Soc. Chim. Fr.*1968, **3**, 1013.
4. Guedi, R., Cambon, A., Audier, L., Azzaro, M. *Bull. Soc. Chim. Fr.*1968, **3**, 1021.
5. Heiss, J., Zeller, K.P. *Org. Mass Spectrom.* 1969, **2**, 17.
6. Chetty, M.; Pillay, V. L.; Moodley, S. V., Miller, R. *Eur. Neuropsychopharmacol.* 1996, **6**, 85.
7. Aravagiri, M., Marder, S. R., Yuwiler, A., Midha, K.K., Kula, N.S., Baldessarini, R.I. *Neuropsychopharmacology* 1995, **13**, 235.
8. Tosa, M., Paizs, Cs., Majdik, C., Poppe, L., Silberg, I.A.I., Irimie, F.D., Novak, L. *Heterocyclic Commun.* (in press).
9. Tosa, M., Paizs, Cs, Majdik, C., Poppe, L, Kolonits, P, Irimie, F.D., Novak, L. *Synthesis* (in press).
10. Irimie, F.D., Tosa, M., Paizs, Cs., Majdik, Moldovan, P., *Roum. Biotechnol. Lett.* (in press).
11. Tosa, M., Paizs, Cs., Majdik, C., P., Irimie, F.D., *Roum. Biotechnol. Lett.* (in press).
12. Tosa, M., Paizs, Cs., Majdik, C., P., Irimie, F.D., *Tetrahedron. Assym.* (in press).
13. Taulov, I., Tamas, J., Hegedus-Vajda, J., Simov, D. *Acta Chim. Sci. Hung.* 1980, **105(2)**, 109.
14. Taulov, I., Tamas, J., Hegedus-Vajda, J., Simov, D. *Acta Chim. Sci. Hung.* 1980, **105(2)**, 117.
15. Bornschein, M. *Pharmazie* 1971, **27**, 188.
16. Spreizer, H., Scholz, M. *Liebigs Ann. Bioorg. Chem.* 1996, **12**, 2069.
17. Taulov, I., Simov, D. *Org. Mass. Spectrom.* 1971, **5**, 1133.

CANNIZARRO REACTION IN THE PHENOTHIAZINE SERIES

FLORIN-DAN IRIMIE¹, CSABA PAIZS¹, MONICA TOȘA¹, CORNELIA MAJDIK¹,
PAULA MOLDOVAN¹, MIHAELA CĂPRIOARĂ¹, MĂDĂLINA NEACȘU²

¹*Department of Biochemistry and Biochemical Engineering,
"Babeș-Bolyai" University of Cluj-Napoca, ROMANIA*

²*"Bios" Center of development and production", Cluj-Napoca, ROMANIA*

ABSTRACT. Cannizarro reaction in the phenothiazine series was extended with the aim at preparing the 10-alkyl-10*H*-phenothiazine-3-carboxylic acids and 10-alkyl-10*H*-phenothiazine-3-methanols.

INTRODUCTION

10-Alkylphenothiazines were used to enhance the reaction rate of different oxidative enzymes, such peroxidase [1,2]. To investigate the influence of different substituents upon these enzyme mediated reactions, various substituted phenothiazines were needed.

Starting from substituted diphenylamines, by cyclisation with sulfur, different C-1, C-2 and C-3 substituted phenothiazines can be prepared [3,4].

N-Alkylphenothiazines could be converted in the corresponding 3-substituted compounds, but in some cases the 3,7-disubstituted derivatives can also appear [5].

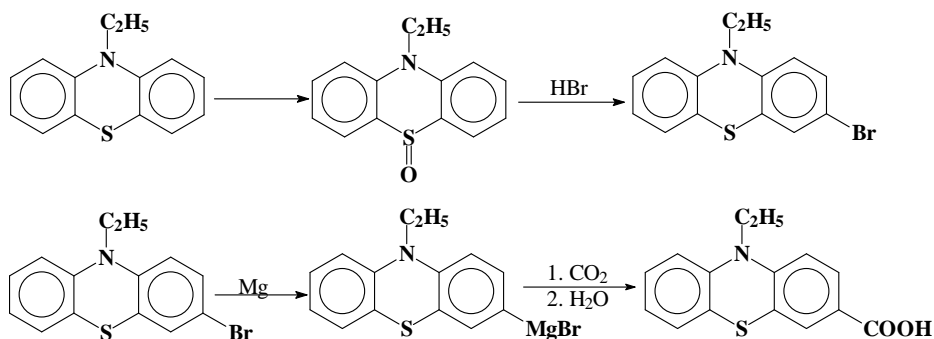
3-Bromophenothiazines were found to be authentic intermediates in order to access some phenothiazine derivatives, mostly *via* Grignard reaction [3] or *via* organolytic intermediates [7]; both methods were used for synthesis of N-alkylphenothiazine-3-carboxylic acids.

10-Ethylphenothiazine-3-carboxylic acid was firstly synthesised from 10-ethyl-phenothiazine by a five step procedure [6] (Scheme 1).

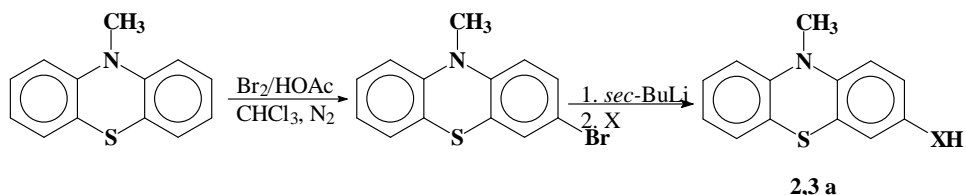
Gilman and Eisch [3] described the synthesis of the some 3-substituted compounds starting from 3-bromo-10-ethylphenothiazine *via* the Grignard reagent and subsequent carboxylation.

Recently, Ebdrup described the introduction of carboxy- and hydroxymethylene groups in position 3 of 10-methylphenothiazine by a bromine-lithium exchange reaction [7] with improved yields (Scheme 2).

10-Metyl-, respectively 10-ethyl-10*H*-phenothiazine-3-carboxylic acids were prepared starting from the corresponding 10-Alkyl-10*H*-phenothiazine-3-carbaldehyde by oxidation with alkaline hydroxides or silver oxide [4], or by Cannizarro reaction [8].



Scheme 1

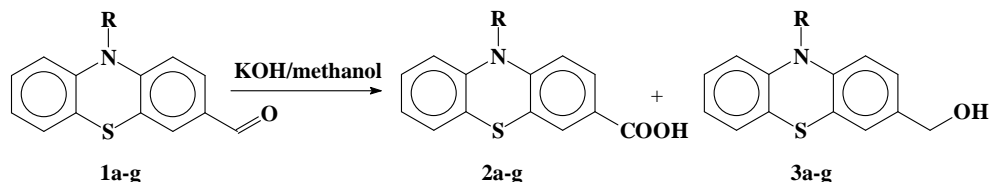


X	Comp.	Yield [%]
CO ₂	2 a	85
(CH ₂ O) _n	3 a	38

Scheme 2

In alkaline media was performed the concomitant oxidation of the carbonyl group and of the sulfur bridge [9] with potassium permanganate to the corresponding S,S-dioxide compound.

In this paper is described an improved procedure of Cannizarro reaction for the synthesis of 10-alkyl-10*H*-phenothiazine-3-carboxylic acids **2a-g** and the corresponding (10-alkyl-10*H*-phenothiazin-3-yl)methanols **3a-g** starting from the 3-formyl-derivatives **1a-g** in methanolic solutions (Scheme 3). Five new compounds **2c-g** were prepared in this way.



Scheme 3

For comparison, the 10-alkyl-10*H*-phenothiazine-3-carboxylic acids **2a-g** were prepared by oxidation of 10-alkyl-10*H*-phenothiazine-3-carbaldehydes **1a-g** with silver oxide as described [4] and the (10-alkyl-10*H*-phenothiazine-3-yl)methanols **3a-g** by reduction with sodium tetrahydroborate [10].

EXPERIMENTAL

Reagents and solvents were purchased from Aldrich or Fluka. The 10-alkyl-10*H*-phenothiazine-3-carbaldehydes **1a-g** were synthesized as previously described [10].

The ¹H-NMR and ¹³C-NMR spectra were recorded on a Varian Gemini 300 spectrometer operating at 300 and 75 MHz, in CDCl₃. Chemical shifts are expressed in ppm values (TMS internal standard) on δ scale. The IR spectra were recorded on a FT-IR Nicolet 205 spectrophotometer, in KBr pellets. Wave numbers are expressed in cm⁻¹.

The elemental analysis for C, H, N and S were within +/- 0.2% of the theoretical values for all derivatives.

TLC was carried out using Merck Kieselgel 60 F₂₅₄ alumina sheets. Spots were visualized by treatment with 5% ethanolic phosphomolybdic acid solution and heating of the dried plates. Preparative chromatographic separations were performed using vacuum-chromatography on a Merck Kieselgel 60 (0.063-0.200 mm) silica-gel.

Melting points are uncorrected.

General procedure for synthesis of 10-alkyl-10*H*-phenothiazine-3-carboxylic acids **2a-g** and (10-alkyl-10*H*-phenothiazine-3-yl)methanols **3a-g** by Cannizarro reaction (Method A)

In a solution of KOH (10 g) in methanol (50 ml), a solution of 10-alkyl-10*H*-phenothiazine-3-carbaldehydes **1a-g** (20 mmol) in methanol (5 ml) was added and the reaction was kept 3-4 hours at reflux (TLC control). The solvent was distilled *in vacuo* and from the resulting mixture (alcohols **3a-g**, sodium salts of acid **2a-g**) the alcohols were separated by column chromatography using dichloromethane as eluent and recrystallized from ethanol. The silica gel was dried and sodium salts of acids were desorbed in boiling water (2x100 ml). The combined water solutions were treated with 32% hydrochloric acid, the precipitate filtered off and the desired products **2a-g** recrystallized from hexane. The yields and the melting points are given in Table 1.

General procedure for synthesis of 10-alkyl-10*H*-phenothiazine-3-carboxylic acids **2a-g** by oxidation with silver oxide (Method B)

Silver nitrate (2.4 g, 0.014 mol) was dissolved in water (14 ml) and 10% NaOH solution (6 ml, cca 0.015 mol) was added. After five minutes the formed precipitate was filtered, washed with water and suspended in 10% NaOH solution (30 ml, cca 0.065 mol). The mixture was heated at 80 °C and the substrate **1a-g**

(0.01 mol) was added with stirring. The reaction was perfected at 80 °C 2-4 hours (TLC control). After cooling, the mixture was diluted with water (100 ml). The unsolved products were filtered off and washed with water (2x25 ml). From the filtrate, the desired products **2a-g** were precipitated with 32% hydrochloric acid, filtered, washed with water, dried and recrystallized from ethanol.

The yields and the melting points are given in table 1.

General procedure for synthesis of (10-alkyl-10*H*-phenothiazine-3-yl)methanols **3a-g** by chemical reduction (Method C)

The substrates **2a-g** (0.2 g) were dissolved in absolute methanol (5 ml) and NaBH₄ was added in small portions under stirring at room temperature; when the solution was decolorated, HCl soln. 2N was added dropwise, the resulting mixture was evaporated to dryness and the crude residue was extracted with water-toluene (1:2). The organic layer was dried over anhydrous magnesium sulfate and the solvent was removed. The residual crude (10-Alkyl-10*H*-phenothiazin-3-yl)methanols **3a-g** were purified by column chromatography on silica gel using toluene-acetone (9:1) as eluent.

10-Methyl-10*H*-phenothiazine-3-carboxylic acid **2a**

¹H-NMR: 3.28 (3H, s), 6.67 (2H, m), 6.89 (1H, t), 7.01 (1H, dd), 7.08 (1H, m), 7.49 (1H, d), 7.56 (1H, dd); ¹³C-NMR: 35.7, 113.6, 114.7, 122.4, 123.6, 125.8, 127.1, 127.6, 127.7, 130.3, 131.1, 143.9, 150.8, 171.5; IR: 3052, 2988, 2868, 1678, 1532, 1584, 1448, 1434, 1417, 1342, 1332, 1299, 1262, 1248, 1152, 1125, 1111; Anal. Calc. for C₁₄H₁₃NO₂S: C, 65.35, H, 4.31, N, 5.44, S, 12.46; Found: C, 65.32, H, 4.38, N, 5.41, S, 12.51

10-Ethyl-10*H*-phenothiazine-3-carboxylic acid **2b**

¹H-NMR: 1.45 (3H, t), 3.98 (2H, q), 6.86 (2H, m), 6.96 (1H, t), 7.11-7.20 (2H, m), 7.78 (1H, d), 7.87 (1H, dd); ¹³C-NMR: 12.7, 42.4, 114.4, 115.8, 122.9, 123.5, 124.9, 127.3, 127.4, 127.6, 129.4, 130.3, 143.3, 150.5, 171.5; IR: 3060, 2983, 2860, 1671, 1598, 1574, 1443, 1424, 1407, 1399, 1328, 1297, 1267, 1252, 1162, 1135, 1109; Anal. Calc. for C₁₅H₁₃NO₂S: C, 66.40, H, 4.83, N, 5.16, S, 11.82; Found: C, 66.32, H, 4.78, N, 5.11, S, 11.91

10-Propyl-10*H*-phenothiazine-3-carboxylic acid **2c**

¹H-NMR: 1.02 (3H, t), 1.84 (2H, m), 3.86 (2H, t), 6.85 (2H, m), 6.95 (1H, t), 7.14 (1H, d), 7.18 (1H, t), 7.81 (1H, d), 7.88 (1H, dd); ¹³C-NMR: 11.2, 20.1, 49.7, 114.5, 115.9, 122.9, 123.4, 124.8, 127.4, 127.5, 127.6, 129.3, 130.3, 143.2, 150.5, 171.6; IR: 3061, 2983, 2860, 1673, 1600, 1575, 1472, 1422, 1407, 1399, 1364, 1277, 1241, 1252, 1168, 1142, 1112; Anal. Calc. for C₁₆H₁₅NO₂S: C, 67.34, H, 5.30, N, 5.11, S, 11.91; Found: C, 67.32, H, 5.38, N, 5.21, S, 11.89;

10-Butyl-10*H*-phenothiazine-3-carboxylic acid **2d**

¹H-NMR: 0.96 (3H, t), 1.48 (2H, m), 1.79 (2H, m), 3.90 (2H, t), 6.86 (3H, m), 7.13 (2H, m), 7.82 (1H, t), 7.86 (1H, dd); ¹³C-NMR: 13.8, 20.1, 28.7, 47.6, 114.5, 115.8, 122.9, 123.4, 124.8, 127.3, 127.4, 127.4, 129.3, 130.1, 143.3, 150.4, 171.5;

IR: 3060, 2932, 2872, 1687, 1601, 1574, 1470, 1420, 1407, 1399, 1328, 1297, 1270, 1214, 1159, 1140, 1112; *Anal. calculated for* C₁₇H₁₇NO₂S: C, 68.20, H, 5.72, N, 5.72, S, 10.71; *Found*: C, 68.32, H, 5.68, N, 5.81, S, 10.78.

10-(2-Methylpropyl)-10H-phenothiazine-3-carboxylic acid 2e

¹H-NMR: 0.94 (6H, d), 2.14 (1H, m), 3.84 (2H, d), 6.82 (2H, m), 6.94 (1H, t), 7.09 (H, dd), 7.15 (H, m), 7.51 (H, d), 7.61 (H, dd); ¹³C-NMR: 19.9, 25.6, 55.4, 115.8, 116.6, 123.4, 124.9, 125.9, 127.4, 127.4, 128.8, 129.3, 130.9, 143.2, 151.2, 171.6; *IR*: 3062, 2938, 2878, 1677, 1609, 1578, 1472, 1428, 1401, 1392, 1322, 1292, 1274, 1216, 1161, 1138, 1114; *Anal. calculated for* C₁₇H₁₇NO₂S: C, 68.20, H, 5.72, N, 5.72, S, 10.71; *Found*: C, 68.22, H, 5.66, N, 5.81, S, 10.72.

10-(3-Methylbutyl)-10H-phenothiazine-3-carboxylic acid 2f

¹H-NMR: 0.96 (6H, d), 1.68-1.76 (2H, m), 1.78-1.83 (1H, m), 3.91 (2H, t), 6.87 (2H, m), 6.95 (1H, t), 7.11-7.19 (2H, m), 7.83 (1H, d), 7.89 (1H, dd); ¹³C-NMR: 22.6, 26.4, 35.6, 46.2, 114.5, 115.8, 122.9, 123.4, 124.9, 127.3, 127.4, 127.5, 129.3, 130.2, 143.3, 150.4, 171.6; *IR*: 3060, 2932, 2872, 1687, 1601, 1574, 1470, 1420, 1407, 1399, 1328, 1297, 1270, 1214, 1159, 1140, 1112; *Anal. calculated for* C₁₈H₁₉NO₂S: C, 68.98, H, 6.11, N, 4.47, S, 10.23; *Found*: C, 68.82, H, 6.18, N, 4.38, S, 10.27.

10-Pentyl-10H-phenothiazine-3-carboxylic acid 2g

¹H-NMR: 0.86 (3H, t), 1.25-1.42 (4H, m), 1.75 (2H, m), 3.78 (2H, t), 6.82 (H, d), 6.93 (H, t), 7.03 (H, d), 7.11 (H, t), 7.48 (H, d), 7.48 (H, dd); ¹³C-NMR: 13.9, 22.2, 26.3, 28.8, 47.7, 114.7, 115.9, 123.5, 123.6, 124.9, 127.4, 127.6, 128.3, 130.1, 130.9, 143.3, 171.6; *IR*: 3056, 2932, 2868, 1682, 1611, 1578, 1472, 1420, 1417, 1392, 1338, 1292, 1268, 1214, 1159, 1140, 1112; *Anal. calculated for* C₁₈H₁₉NO₂S: C, 68.98, H, 6.11, N, 4.47, S, 10.23; *Found*: C, 68.88, H, 6.28, N, 4.42, S, 10.22.

(10-Methyl-10H-phenothiazine-3-yl)methanol 3a

¹H-NMR: 3.33 (3H, s), 4.54 (2H, s), 6.73-6.78 (2H, m), 6.90 (1H, t), 7.11-7.15 (4H, m); ¹³C-NMR: 35.4, 64.7, 113.9, 114.1, 122.5, 123.3, 126.1, 126.4, 127.2, 127.5, 127.5, 135.3, 145.8, 145.4; *IR*: 3432, 2984, 1464, 1332, 1288, 1260, 1200, 1144, 1076, 1048, 760; *MS*: 245, 244, 243, 242, 232, 231, 230, 229, 226, 214, 212, 211, 201, 200, 199; *Anal. Calc. for* C₁₄H₁₃NOS: C, 69.11, H, 5.39, N, 5.76, S, 13.18; *Found*: C, 69.14, H, 5.31, N, 5.77, S, 13.23

(10-Ethyl-10H-phenothiazine-3-yl)methanol 3b

¹H-NMR: 1.38 (3H, t), 3.88 (2H, q), 4.51 (2H, s), 6.78-6.83 (2H, m), 6.87 (1H, t), 7.09-7.13 (4H, m); ¹³C-NMR: 13.1, 41.9, 64.6, 114.9, 115.1, 122.4, 124.3, 124.8, 126.2, 127.2, 127.3, 127.4, 135.1, 144.5, 144.5; *IR*: 3320, 2984, 1464, 1328, 1288, 1240, 1216, 1132, 1120, 1112, 1064, 1040, 1024, 1008, 756; *MS*: 259, 258, 257, 256, 242, 240, 231, 230, 229, 228, 213, 212, 211, 200, 199; *Anal. Calc. for* C₁₅H₁₅NOS: C, 70.01, H, 5.87, N, 5.44, S, 12.46; *Found*: C, 69.97, H, 5.81, N, 5.47, S, 13.43.

(10-Propyl-10H-phenothiazine-3-yl)methanol 3c

¹H-NMR: 0.95 (3H, t), 1.76 (2H, m), 3.74 (2H, t), 4.45 (2H, s), 6.74 (1H, d), 6.79 (1H, d), 6.86 (1H, t), 7.02-7.16 (4H, m); ¹³C-NMR: 11.3, 20.1, 49.1, 64.4, 115.2, 115.2, 115.4, 122.3, 124.6, 124.9, 127.1, 127.2, 127.4, 132.2, 134.9, 144.7, 145.2; *IR*: 3352, 2960, 1496, 1468, 1336, 1288, 1248, 1232, 1136, 1120, 1112, 1092, 1040, 1028, 1008, 748; *MS*: 273, 272, 271, 270, 255, 254, 244, 243, 242, 231, 230, 229, 228, 213, 212, 210; *Anal. Calc. for* C₁₆H₁₇NOS: C, 70.82, H, 6.31, N, 5.16, S, 11.81; *Found*: C, 70.84, H, 6.37, N, 5.25, S, 11.73.

(10-Butyl-10H-phenothiazine-3-yl)methanol 3d

¹H-NMR: 0.91 (3H, t), 1.45 (2H, m), 1.74 (2H, m), 3.80 (2H, t), 4.48 (2H, s), 6.78 (1H, d), 6.82 (1H, d), 6.87 (1H, m), 7.09-7.13 (4H, m); ¹³C-NMR: 13.8, 20.2, 28.9, 47.1, 64.5, 115.2, 115.3, 115.4, 122.4, 124.6, 125.1, 126.2, 126.3, 127.1, 127.2, 127.4, 134.9; IR: 3352, 2960, 1496, 1468, 1332, 1288, 1244, 1216, 1136, 1120, 1108, 1084, 1040, 748; MS: 287, 286, 285, 284, 269, 268, 244, 243, 242, 231, 230, 229, 228, 213, 212, 210, 200, 199; Anal. Calc. for: C₁₇H₁₉NOS: C, 71.54, H, 6.71, N, 4.91, S, 11.23; Found: C, 71.64, H, 6.77, N, 4.85, S, 11.32.

(10-(2-Methylpropyl)-10H-phenothiazine-3-yl)methanol 3e

¹H-NMR: 0.97 (6H, d), 2.16 (1H, m), 3.65 (2H, d), 4.78 (2H, s), 6.78 (1H, d), 6.82 (1H, d), 6.87 (1H, m), 7.11-7.13 (4H, m); ¹³C-NMR: 20.2, 45.9, 55.3, 64.6, 115.7, 115.9, 122.5, 122.7, 125.3, 125.9, 126.2, 126.8, 126.9, 127.2, 127.5, 127.8; IR: 3400, 2952, 1496, 1464, 1336, 1288, 1244, 1232, 1144, 1116, 1104, 1068, 1012, 736; Anal. Calc. for C₁₇H₁₉NOS: C, 71.54, H, 6.71, N, 4.91, S, 11.23; Found: C, 71.61, H, 6.74, N, 4.89, S, 11.29

(10-(2-Methylbutyl)-10H-phenothiazine-3-yl)methanol 3f

¹H-NMR: 0.94 (6H, d), 1.68 (2H, m), 1.72 (1H, m), 3.84 (2H, t), 4.52 (2H, s), 6.85 (3H, t), 7.11 (4H, m); ¹³C-NMR: 22.6, 26.4, 35.9, 45.9, 64.8, 115.4, 115.4, 115.5, 122.4, 124.9, 125.5, 126.2, 126.4, 127.3, 127.5, 127.7, 135.1; IR: 3344, 2952, 1488, 1468, 1328, 1288, 1248, 1216, 1136, 1116, 1104, 1084, 1040, 748; Anal. Calc. pt. C₁₈H₂₁NOS: C, 72.20, H, 7.07, N, 4.68, S, 10.71; Determinat: C, 72.28, H, 7.11, N, 4.62, S, 10.67

(10-Pentyl-10H-phenothiazine-3-yl)methanol 3g

¹H-NMR: 0.87 (3H, t), 1.27-1.40 (4H, m), 1.77 (2H, m), 3.79 (2H, t), 4.37 (2H, s), 6.77-6.82 (2H, m), 6.86 (1H, t), 7.09-7.12 (4H, m); ¹³C-NMR: 14.1, 22.4, 29.2, 4.5, 49.2, 64.5, 115.2, 122.3, 124.8, 125.1, 126.2, 126.6, 126.9, 127.2, 127.6, 132.4, 144.9, 145.4; IR: 3400, 2952, 1488, 1468, 1316, 1288, 1252, 1220, 1136, 1124, 1104, 984, 748. Anal. Calc. for C₁₈H₂₁NOS: C, 72.20, H, 7.07, N, 4.68, S, 10.71; Found: C, 72.28, H, 7.04, N, 4.69, S, 10.69.

RESULTS AND DISCUSSION

The IR and NMR spectra and the elemental analysis confirmed the structures of compounds **1a-g** and **3a-g**.

The yields and melting points of synthesized derivatives **2a-g** and **3a-g** were given in Table 1, in comparison with those described in literature in the case of methyl- and ethyl derivatives.

Sodium salts of **2a-g** had better solubility in organic solvents than in water. For this reason the work up of the reaction mass from Cannizzaro reaction could not be performed by selective extraction in water-organic heterogeneous system. This property of the carboxylates **2a-g** made them potential phase transfer catalysts.

Methanol as solvent in Cannizzaro reaction rises the yields in comparison with the method when the reaction was performed in a two-phase system, however the reaction time was longer.

Table 1.

Yields and melting points

Compd.	Yield [%]		m.p.(lit.) [°C]
	Method A	Method B	
2a	39	58	245(240-244 ¹)
2b	32	55	204(200 ³)
2c	30	55	179
2d	29	56	143
2e	31	58	124
2f	28	52	188
2g	29	54	167
3a	48	82	132(133 ¹)
3b	42	68	99(98 ⁹)
3c	39	72	-
3d	44	75	-
3e	31	78	-
3f	33	73	-
3g	34	71	-

CONCLUSIONS

Cannizarro reaction performed in methanol as solvent is a convenient method for concomitant synthesis of (10-alkyl-phenothiazine)-3-carboxylic acids **2a-g** and (10-alkyl-phenothiazine-3-yl)methanols **3a-g**. Structures of **2a-g** and **3a-g** were confirmed by elemental analysis and spectral data and were the same with those obtained with silver oxide (for acids) and with sodium tetrahydroborate (for alcohols).

REFERENCES

- Schneider, P., Ebdrup, S., Spane, L. *PCT Int. Appl.* **1994**, 94/12619; *Chem. Abstr.* 121, 128770k.
- Schneider, P., Ebdrup, S. *PCT Int. Appl.* **1994**, 94/12621; *Chem. Abstr.* 121, 128769s.
- Gilman, H., Shirley, D. A. *J. Am. Chem. Soc.* **1955**, 77, 888.
- Cauquil, G., Casadevall, M.A. *Compt. Rend.* **1955**, 240, 1784.
- Gilman, H.; Eisch, J. *J. Am. Chem. Soc.* **1955**, 77, 3862.
- Gilman, H., Ess, R.P., Shirley, D. A.: *J. Am. Chem. Soc.* **1944**, 66, 1214.
- Ebdrup, S. *J. Chem. Soc. Perkin Trans. 1* **1998**, 6, 1147.
- Burger, Schmalz, *J. Org. Chem.* **1954**, 19, 1841.
- Bodea, C., Farcasan, V., Oprean, I. *Rev. Roumaine de Chim.* **1965**, 10, 1103.
- Toşa, M., Paizs, C.s., Majdik, C., Irimie, F.D., Szabo, E., Poppe, L., Novak, L., *Synthesis*, in press.

SYNTHESIS AND STEREOCHEMISTRY OF SOME NEW 2,5-POLYSUBSTITUTED -1,3-DIOXANES

LUMINITA MUNTEAN^a, EUGEN MESAROS^a, GERARD PLE^b, ION GROSU^a,
SORIN MAGER^a

*a "Babeș-Bolyai" University, Department of Chemistry, 11 Arany Janos Str.,
Cluj-Napoca, RO-3400, Romania*
*b Université de Rouen, IRCOF, UMR 6014, Faculté des Sciences,
76821 Mont Saint - Aignan, Cedex, France*

ABSTRACT. The synthesis and the stereochemistry of some new 1,3-dioxanes bearing aliphatic, aromatic and heteroaromatic substituents in the acetal part of the dioxanic heterocycle are reported.

INTRODUCTION

In previous works, the stereochemistry of 2,5-substituted-1,3-dioxanes, exhibiting anancomeric or flipping structure, in correlation with the nature of the substituents, has been reported¹⁻¹¹.

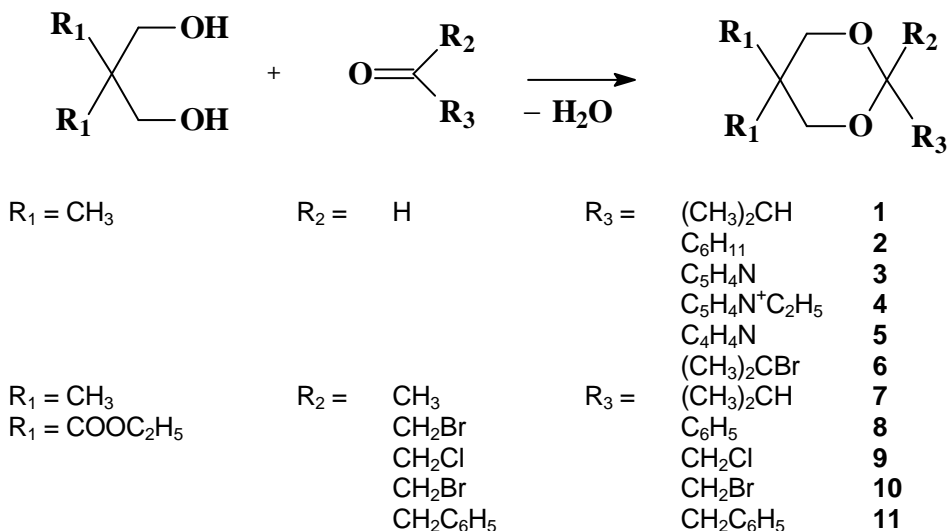
The compounds displaying identical geminal substituents or geminal substituents with very close conformational free enthalpies, show flipping structures. Their ¹H- and ¹³C-NMR spectra exhibit unique signals (at mean values of the chemical shifts) for the equatorial and axial positions of the protons of the heterocycle and for the axial and equatorial positions of the protons and carbon atoms of the homomorphic groups located at positions 2 and 5.

In the case of compounds having different substituents located at the same position, the conformational equilibria are shifted towards the conformation with the group exhibiting the largest conformational free enthalpy in equatorial position. For these compounds (with anancomeric structure), the NMR spectra show different signals for the axial and equatorial protons of the ring and for the protons and carbon atoms of the similar groups located in it.

It was considered of interest to study by means of NMR spectra, the stereochemistry of some new 1,3-dioxane derivatives, bearing many types of substituents at the positions 2- and 5.

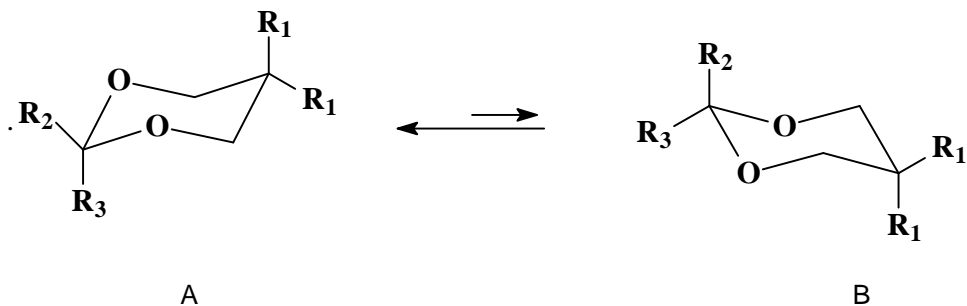
RESULTS AND DISCUSSION

New 2,5-substituted-1,3-dioxanes have been obtained (Scheme 1) by the condensation reaction of 2,2-substituted-1,3-propanediols with aldehydes and ketones:

**Scheme 1**

These compounds exhibit anancomeric or flipping structures, in correlation with the nature of the substituents.

Thus, the conformational analysis for compounds **1-8** shows anancomeric structures. At room temperature, the conformational equilibria are shifted towards the conformation A, in which the substituent with the largest conformational enthalpy (R_2) is in the equatorial position (Scheme 2):

**Scheme 2**

The NMR spectra of these compounds exhibit different signals for the axial and equatorial protons at the 4,6-positions of the heterocyclic ring as well as for the protons and for the carbon atoms of axial and equatorial methyl and ethyloxycarbonyl groups located at position 5.

The ^1H and ^{13}C -NMR data for compounds **1-8** are illustrated in Tables 1 and 2.

Table 1 ^1H -NMR data for compounds **1-8**

Compound	^1H -NMR			
	4,6- H_{eq}	4,6- H_{ax}	5- $\text{CH}_{3\text{eq}}$	5- $\text{CH}_{3\text{ax}}$
1	3.43	3.12	0.33	1.12
2	3.45	3.13	0.32	1.14
3	3.50	3.29	0.28	1.21
4	3.87	3.78	0.80	1.18
5	3.44	3.18	0.33	1.14
6	3.37	3.03	0.22	1.05
7	3.48	3.24	0.54	0.97
8	4.84	4.04	-	-

Table 2 ^{13}C -NMR data for compounds **1-8**

Compound	^{13}C -NMR				
	C^2	$\text{C}^{4,6}$	C^5	5- $\text{CH}_{3\text{ax}}$	5- $\text{CH}_{3\text{eq}}$
1	105.38	76.78	29.68	22.71	21.27
2	104.93	76.84	29.76	22.71	21.30
3	103.03	77.12	29.71	22.84	21.21
4	94.95	77.59	30.45	23.03	21.47
6	105.02	77.06	29.88	22.94	21.18
7	100.75	70.18	29.28	23.06	22.42
8	99.43	64.33	23.06	-	-

As an example, the ^1H -NMR spectrum of compound **8** (Figure 1) shows two doublets for the protons at positions 4 and 6 ($\delta_{4,6 \text{ eq}} = 4.84$ and $\delta_{4,6 \text{ ax}} = 4.04$ ppm), two quartets ($\delta_{\text{eq}} = 4.16$ and $\delta_{\text{ax}} = 3.60$ ppm) belonging to the protons of the methylene groups and also two triplets ($\delta_{\text{eq}} = 1.05$, $\delta_{\text{ax}} = 0.55$ ppm) for the methyl groups belonging to the axial and equatorial ester groups of 5-position. The spectrum also exhibits a singlet ($\delta = 3.30$ ppm) associated with the methylene protons of the CH_2Br substituent and a complex signal at 7-7.34 ppm belonging to the protons of the phenyl group.

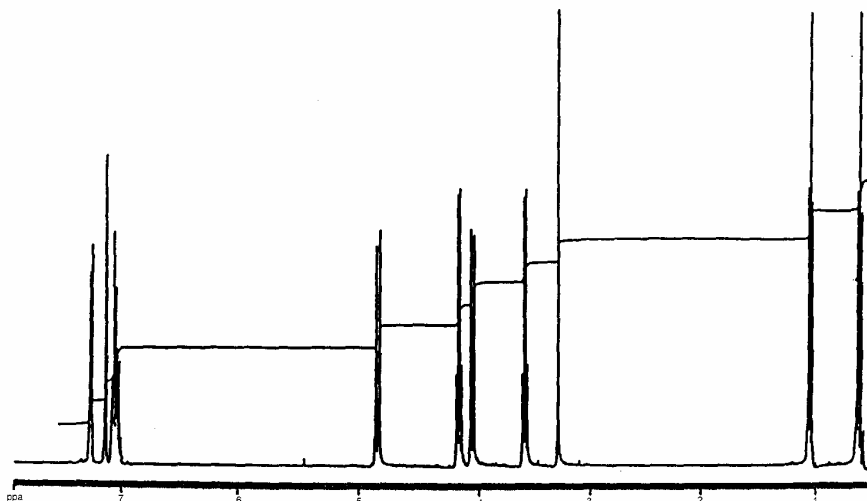
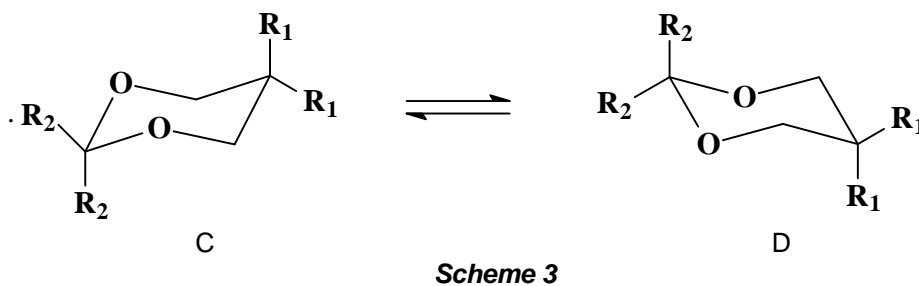


Fig.1. $^1\text{H-NMR}$ Spectrum of compound **8**

The conformational analysis shows flipping structures for compounds **9-11**. These compounds exhibit, at room temperature, a rapid inversion of the six membered ring (C D; Scheme 3):



The NMR spectra of these compounds exhibit unique signals (at the mean values of the chemical shifts) for the axial and equatorial positions of the protons of the ring and of the similar groups located in it (Table 3).

Table 3

Compound	$^1\text{H-NMR}$			
	4,6-H	CH_2Cl	CH_2Br	CH_2Ph
9	4.14	3.66	-	-
10	4.10	-	3.52	-
11	4.50	-	-	2.89

The $^1\text{H-NMR}$ spectrum of compound **11** (Figure 2) shows a singlet at $\delta = 4.50$ ppm corresponding to the protons at the positions 4 and 6 of the heterocycle, a quartet ($\delta = 3.81$ ppm) for the methylene group and a triplet ($\delta = 0.83$ ppm) for the protons of the methyl group of the ester groups located at the 5-position. In the spectrum also appears a complex signal ($\delta = 7-7.25$ ppm) due to the aromatic protons and a singlet at $\delta = 2.89$ ppm for the methylene protons of the benzyl groups.

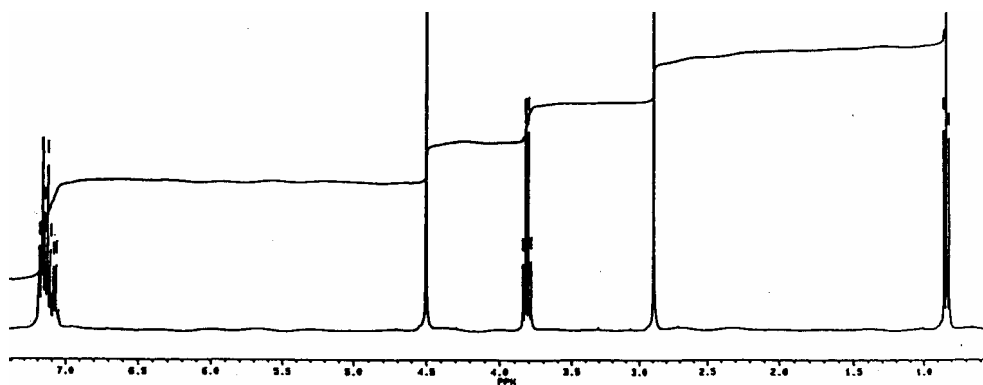


Fig.2. $^1\text{H-NMR}$ Spectrum of compound **9**

CONCLUSIONS

The stereochemistry of 1,3-dioxane derivatives have been determined by NMR investigations. The flipping or the anancomeric structure of the compounds has been deduced from the complexity of NMR spectra. The presence in the spectra of distinct signals for axial and equatorial positions have been associated with anancomeric structures, whereas the spectra with unique signals correspond to flipping structures.

EXPERIMENTAL

^1H - and ^{13}C -NMR spectra were recorded at room temperature, using C_6D_6 as solvent, in 5 mm tubes, on a Bruker AM 400 spectrometer, operating at 400 MHz for protons and at 100 MHz for carbon atoms. Melting points were measured with Electrothermal melting point apparatus and are uncorrected.

New compounds 1-11, general procedure:

Equimolecular amounts of 1,3-diol (0.1 mol) and carbonyl compound, with catalytic amount (0.1 g) of *p*-toluenesulphonic acid were solved in 200 ml of benzene. The mixture was refluxed and the water was removed using a Dean-Stark trap. When 80% of the theoretical amount of water was separated, the mixture was cooled at room temperature and then was neutralized with CH_3COONa powder in excess (0.2 g). The mixture was wash twice with 100 ml of water. After drying (with Na_2SO_4) the benzene was removed and the 1,3-dioxanic compound was purified by vacuum distillation (1-2 mm col. Hg) or by crystallisation from ethanol.

2-*i*-Propyl-5,5-dimethyl-1,3-dioxane 1

Liquid, b.p. = 49-50 °C (1 mm col. Hg). Yield 80%. C₉H₁₈O₂, found: C 69.02, H 11.19; required: C 68.35, H 11.39%

¹H-NMR (C₆D₆): δ 0.33 [3H, s, 5-CH_{3eq}], 1.05 [6H, d, J = 6.8 Hz, 2-CH(CH₃)₂], 1.12 [3H, s, 5-CH_{3ax}], 1.93 [H, dh, J = 4.5 Hz, J' = 6.8 Hz, 2-CH(CH₃)₂], 3.12 [2H, d, J = 11.0 Hz, 4,6-H_{ax}], 3.43 [2H, d, J = 11.0 Hz, 4,6-H_{eq}], 4.05 [H, d, J = 4.5 Hz, 2-H_{ax}]

¹³C-NMR (C₆D₆): δ 16.84 [2-CH(CH₃)₂], 21.27 (5-CH_{3eq}), 22.71 (5-CH_{3ax}), 29.68 (C⁵), 32.75 [2-CH(CH₃)₂], 76.78 (C^{4,6}), 105.38 (C²)

2-Cyclohexyl-5,5-dimethyl-1,3-dioxane 2

Liquid, b.p. = 90-92 °C (1 mm col. Hg). Yield 69%. C₁₂H₂₂O₂, found: C 71.92, H 11.22; required: C 72.72, H 11.11%

¹H-NMR (C₆D₆): δ 0.32 [3H, s, 5-CH_{3eq}], 1.14 [3H, s, 5-CH_{3ax}], 1.18-1.27 [11H, m, overlapped peaks], 3.13 [2H, d, J = 11.0 Hz, 4,6-H_{ax}], 3.45 [2H, d, J = 11.0 Hz, 4,6-H_{eq}], 4.10 [H, d, J = 4.8 Hz, 2-H_{ax}]

¹³C-NMR (C₆D₆): δ 21.30 (5-CH_{3eq}), 22.71 (5-CH_{3ax}), 26.01, 26.69, 27.41, 42.51 (cyclohexanic ring), 29.76 (C⁵), 76.84 (C^{4,6}), 104.93 (C²)

2-Pyridyl-5,5-dimethyl-1,3-dioxane 3

Liquid, b.p. = 95-96 °C . Yield %. C₁₂H₁₅O₂N, found: C 69.21, H 7.61, N 7.06; required: C 68.39, H 7.77, N 7.25%

¹H-NMR (C₆D₆): δ 0.28 [3H, s, 5-CH_{3eq}], 1.21 [3H, s, 5-CH_{3ax}], 3.29 [2H, d, J = 11.5 Hz, 4,6-H_{ax}], 3.50 [2H, d, J = 11.5 Hz, 4,6-H_{eq}], 5.65 [H, s, 2-H_{ax}], 6.62, 7.15, 7.75, 8.44 (4H, overlapped peaks, aromatic protons)

¹³C-NMR (C₆D₆): δ 21.20 (5-CH_{3eq}), 22.84 (5-CH_{3ax}), 29.71 (C⁵), 77.12 (C^{4,6}), 103.03 (C²), 120.78, 123.32, 135.87, 148.57, 158.04 (aromatic carbon atoms)

N-Ethyl, 2-(5,5-dimethyl-1,3-dioxane-2-yl) pyridinium iodine 4

Solid, m.p. = .138 °C. Yield 48%. C₁₃H₂₀O₂NJ, found: C 43.88, H 5.89, N 3.96, J 37.23 required: C 44.69, H 5.73, N 4.01, J 36.39%

¹H-NMR (C₆D₆): δ 0.80 [3H, s, 5-CH_{3eq}], 1.18 [3H, s, 5-CH_{3ax}], 1.65 [3H, t, J = 7.2 Hz, N-CH₂-CH₃], 3.78 [2H, d, J = 11.2 Hz, 4,6-H_{ax}], 3.87 [2H, d, J = 11.2 Hz, 4,6-H_{eq}], 5.00 [2H, q, J = 7.2 Hz, N-CH₂-CH₃], 6.16 [H, s, 2-H_{ax}], 8.15, 8.28, 8.48, 9.66 (4H, m, overlapped peaks, aromatic protons)

¹³C-NMR (C₆D₆): δ 17.43 (N-CH₂-CH₃), 21.47 (5-CH_{3eq}), 23.03 (5-CH_{3ax}), 30.45 (C⁵), 54.79 (N-CH₂-CH₃), 77.59 (C^{4,6}), 94.95 (C²)

2-Pyridyl-5,5-dimethyl-1,3-dioxane 5

Liquid, b.p. = 84-86 °C . Yield 40%. C₁₀H₁₅O₂N, found: C 67.96, H 8.10, N 7.91; required: C 66.63, H 8.28, N 7.73%

¹H-NMR (C₆D₆): δ 0.33 [3H, s, 5-CH_{3eq}], 1.14 [3H, s, 5-CH_{3ax}], 3.18 [2H, d, J = 11.8 Hz, 4,6-H_{ax}], 3.44 [2H, d, J = 11.8 Hz, 4,6-H_{eq}], 5.29 [H, s, 2-H_{ax}], 6.26, 6.36, 6.49 (3H, m, aromatic protons)

2-(2-Bromo-2-propyl)-5,5-dimethyl-1,3-dioxane 6

Solid, m.p. = 110-112 °C . Yield 70%. C₉H₁₇O₂Br, found: C 44.69, H 7.34, Br 34.71; required: C 45.37, H 7.14, Br 34.03%

¹H-NMR (C₆D₆): δ 0.22 [3H, s, 5-CH_{3eq}], 1.05 [3H, s, 5-CH_{3ax}], 1.77 [6H, s, (CH₃)₂CBr], 3.03 [2H, d, J = 11.0 Hz, 4,6-H_{ax}], 3.37 [2H, d, J = 11.0 Hz, 4,6-H_{eq}], 4.22 [H, s, 2-H_{ax}]

$^{13}\text{C-NMR}$ (C_6D_6): δ 21.18 (5- $\text{CH}_{3\text{eq}}$), 22.94 (5- $\text{CH}_{3\text{ax}}$), 28.88 [$(\text{CH}_3)_2\text{CBr}$], 29.88 (C^5), 63.39 , [$(\text{CH}_3)_2\text{CBr}$], 77.06 ($\text{C}^{4,6}$), 105.02 (C^2)

2,5,5-Trimethyl-2-*i*-Propyl-1,3-dioxane 7

Liquid, b.p. = 68 $^\circ\text{C}$ Yield 55%. $\text{C}_{10}\text{H}_{20}\text{O}_2$, found: C 71.03, H 11.51; required: C 69.76, H 11.63%

$^1\text{H-NMR}$ (C_6D_6): δ 0.54 [3H, s, 5- $\text{CH}_{3\text{eq}}$], 0.97 [3H, s, 5- $\text{CH}_{3\text{ax}}$], 1.06 [6H, d, $J = 6.5$ Hz, 2- $\text{CH}(\text{CH}_3)_2$], 1.20 [3H, s, 2- $\text{CH}_{3\text{ax}}$], 2.08 [H, h, $J = 6.5$ Hz, 2- $\text{CH}(\text{CH}_3)_2$], 3.24 [2H, d, $J = 11.0$ Hz, 4,6- H_{ax}], 3.38 [2H, d, $J = 11.0$ Hz, 4,6- H_{eq}]

$^{13}\text{C-NMR}$ (C_6D_6): δ 15.42 [2- $\text{CH}_{3\text{ax}}$], 17.10 [2- $\text{CH}(\text{CH}_3)_2$], 22.42 (5- $\text{CH}_{3\text{eq}}$), 23.06 (5- $\text{CH}_{3\text{ax}}$), 29.98 (C^5), 36.21 [2- $\text{CH}(\text{CH}_3)_2$], 70.18 ($\text{C}^{4,6}$), 100.75 (C^2)

2-Bromomethyl-5,5-di(ethyloxycarbonyl)-2-phenyl-1,3-dioxane 8

Liquid, b.p. = 181 $^\circ\text{C}$. Yield 62% $\text{C}_{17}\text{H}_{21}\text{O}_6\text{Br}$, found: C 50.93, H 5.16, Br 20.54; required: C 50.74, H 5.22, Br 20.15%

$^1\text{H-NMR}$ (C_6D_6): δ 0.55 [3H, t, $J = 7.1$ Hz, 5- $\text{COOCH}_2\text{CH}_{3\text{ax}}$], 1.05 [3H, t, $J = 7.1$ Hz, 5- $\text{COOCH}_2\text{CH}_{3\text{eq}}$], 3.30 [2H, s, 2- CH_2Br], 3.60 [2H, q, $J = 7.1$ Hz, 5- $\text{COOCH}_2\text{CH}_{3\text{ax}}$], 4.04 [2H, d, $J = 11.3$ Hz, 4,6- H_{ax}], 4.16 [2H, q, $J = 7.1$ Hz, 5- $\text{COOCH}_2\text{CH}_{3\text{eq}}$], 4.84 [2H, d, $J = 11.3$ Hz, 4,6- H_{eq}], 7-7.34 [5H, m]

$^{13}\text{C-NMR}$ (C_6D_6): δ 13.58 (5- $\text{COOCH}_2\text{CH}_{3\text{ax}}$), 14.11 (5- $\text{COOCH}_2\text{CH}_{3\text{eq}}$), 39.96 (CH_2Br), 53.37 (C^5), 61.66 (5- $\text{COOCH}_2\text{CH}_{3\text{ax}}$), 62.12 (5- $\text{COOCH}_2\text{CH}_{3\text{eq}}$), 64.33 ($\text{C}^{4,6}$), 99.43(C^2), 128.66, 129.11, 129.19, 135.94 (aromatic carbon atoms)

2,2-Di(chloromethyl)-5,5-di(ethyloxycarbonyl)-1,3-dioxane 9

Liquid, b.p. = 147-148 $^\circ\text{C}$. Yield 64%. $\text{C}_{12}\text{H}_{18}\text{O}_6\text{Cl}_2$, found: C 44.59, H 5.62, Cl 21.13; required: C 43.77, H 5.47, Cl 21.58%

$^1\text{H-NMR}$ (CDCl_3): δ 1.15 [6H, t, $J = 7.0$ Hz, 5- $\text{COOCH}_2\text{CH}_3$], 3.66 [4H, s, 2- CH_2Cl], 4.14 (4H, s, 4,6-H), 4.20 [4H, q, $J = 7.0$ Hz, 5- $\text{COOCH}_2\text{CH}_3$]

2,2-Di(bromomethyl)-5,5-di(ethyloxycarbonyl)-1,3-dioxane 10

Liquid, b.p. = 180-181 $^\circ\text{C}$. Yield 64%. $\text{C}_{12}\text{H}_{18}\text{O}_6\text{Br}_2$, found: C 35.17, H 4.22, Br 38.04; required: C 34.28, H 4.28, Br 38.57%

$^1\text{H-NMR}$ (CCl_4): δ 1.15 [3H, t, $J = 7.0$ Hz, 5- $\text{COOCH}_2\text{CH}_3$], 3.52 [4H, s, 2- CH_2Br], 4.10 (4H, s, 4,6-H), 4.12 [2H, q, $J = 7.0$ Hz, 5- $\text{COOCH}_2\text{CH}_3$]

2,2-Dibenzyl-5,5-di(ethyloxycarbonyl)-1,3-dioxane 11

Solid, m.p. = 61-62 $^\circ\text{C}$. Yield 72%. $\text{C}_{24}\text{H}_{28}\text{O}_6$, found: C 71.30, H 6.67; required: C 69.90, H 6.79%

$^1\text{H-NMR}$ (CCl_4): δ 0.86 [3H, t, $J = 7.1$ Hz, 5- $\text{COOCH}_2\text{CH}_3$], 2.89 [4H, s, 2- CH_2Ph], 3.81 [4H, q, $J = 7.0$ Hz, 5- $\text{COOCH}_2\text{CH}_3$], 4.50 (4H, s, 4,6-H), 7-7.25 (10H, overlapped peaks)

$^{13}\text{C-NMR}$ (CCl_4): δ 13.81 ($\text{COOCH}_2\text{CH}_3$), 54.03 (C^5), 61.66 ($\text{COOCH}_2\text{CH}_3$), 62.58 ($\text{C}^{4,6}$), 101.04(C^2), 126.47, 128.01, 131.12, 135.59 (aromatic carbon atoms), 167.69 ($\text{COOCH}_2\text{CH}_3$)

REFERENCES

1. M. J. O. Anteunis, D. Tavernier, F. Borreman, *Heterocycles*, 4, **1976**, 293.
2. S.Mager, I. Hopartean, M. Horn, I. Grosu, *Studia Univ."Babeş-Bolyai", Chemia*, 24, **1979**, 32.
3. S. Mager, I. Grosu, *Studia Univ."Babeş-Bolyai", Chemia*, 33, **1988**, 47.
4. I. Grosu, M. Horn, D. Kovacs, S. Mager, *Studia Univ."Babeş-Bolyai", Chemia*, 37, **1992**, 7.
5. I. Grosu, S. Mager, E. Mesaroş, L. Muntean, C. Socaci, *Studia Univ."Babeş-Bolyai", Chemia*, 42, **1997**, 85.
6. S. Mager, I. Grosu, M. Horn, I. Hopârtean, M. Dărăbanţu, C. Puşcaş, D. Kovacs, G. Plé, *Roumanian Chemical Quarterly Reviews*, 3, **1995**, 201.
7. I. Grosu, S. Mager, G. Plé, *Rev.Roum.Chim.*, 43, **1998**, 725.
8. I. Grosu, S. Mager, G. Plé, R. Martinez, L. Muntean, E. Mesaroş, *Heterocycles*, 41, **1995**, 2233.
9. I. Grosu, S. Mager, G. Plé, L. Muntean, I. Schirger, *Heterocyclic Commun.*, 2, **1996**, 423.
10. I. Grosu, S. Mager, G. Plé, N. Plé, A. Toscano, E. Mesaroş, R.Martinez, *Liebigs Annalen / Recueil*, **1997**, 2371.
11. I. Grosu, S. Mager, L. Toupet, G. Plé, E. Mesaroş, A. Mihiş, *Acta Chem.Scand.*, 52, **1998**, 366.

STEREOCHEMISTRY AND NMR SPECTRA OF SOME NEW 5-METHYL-2,2-SUBSTITUTED-1,3-DIOXANES

LUMINITA MUNTEAN, TUROS GYORGY, CRINA SOCACI, ION GROSU,
SORIN MAGER, ALIN MIHIS

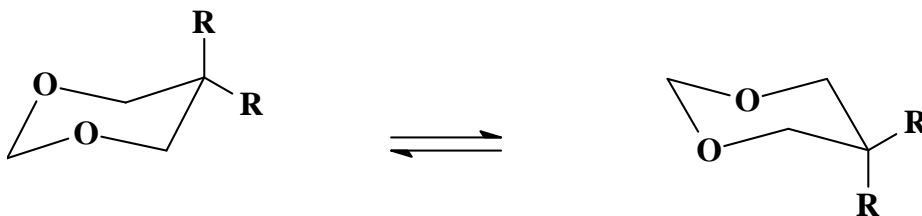
*"Babeș-Bolyai" University, Department of Chemistry, 11 Arany Janos Str.,
Cluj-Napoca, RO-3400, Romania*

ABSTRACT. The synthesis, stereochemistry and NMR spectra of some new 2,2- substituted-5-methyl-1,3-dioxanes are reported.

INTRODUCTION

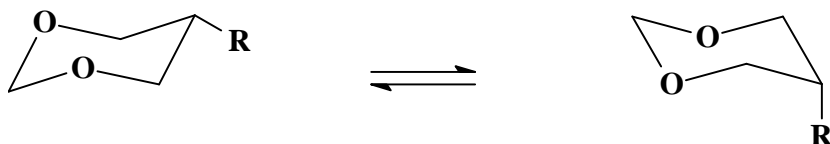
The 2 and/or 5-substituted-1,3-dioxanes display flipping or anancomeric structures, in correlation with the nature of the substituents. The compounds bearing identical substituents in the 5-position, exhibit flipping structure, with a rapid inversion of the heterocycle (Scheme1)¹⁻¹²

Scheme 1



Their NMR spectra exhibit unique signals for the axial and equatorial positions of the protons of the heterocycle and for the axial and equatorial positions of the protons and carbon atoms of the similar substituents.

For the monosubstituted 5-alkyl-1,3-dioxane derivatives, the conformational analysis revealed anancomeric structures, despite the fact that the value of the conformational free enthalpy is quite small (in comparison with the largest value for the alkyl groups located at the 2-position, e.g. $\Delta G^0_{\text{Me(position 2)}} = 3,98\text{kcal/mol}^{12}$, $\Delta G^0_{\text{Me(position 5)}} = 0,83\text{kcal/mol}^{13}$). The conformational equilibria are shifted towards the conformer having the alkyl substituent equatorially placed (Scheme 2)

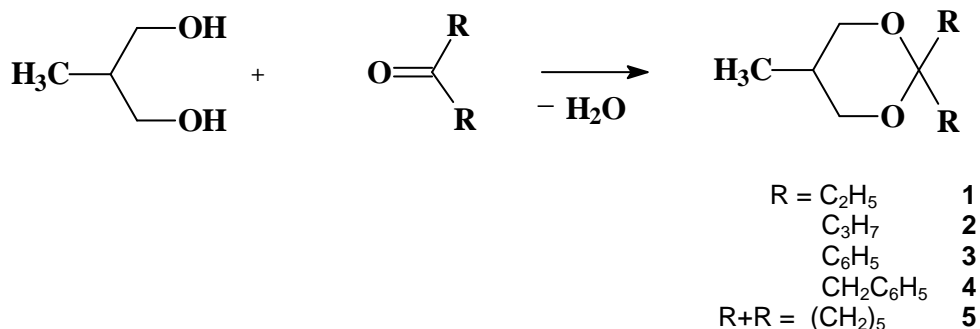
**Scheme 2**

The NMR spectra of these compounds exhibit different signals for the axial and equatorial protons of the 1,3-dioxanic ring and for the protons and the carbon atoms of the equatorial and axial identical groups located in it.

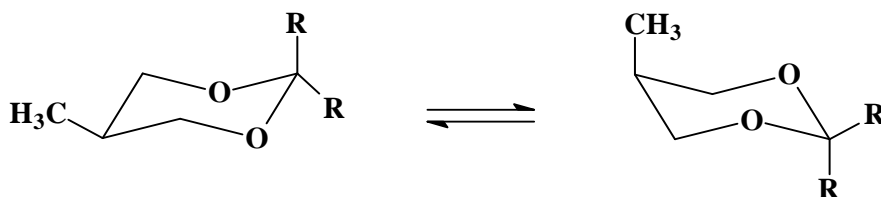
It was considered of interest to study by means of NMR spectra the stereochemistry of some new 5-methyl-1,3-dioxanes bearing homomorphic groups in the position 2.

RESULTS AND DISCUSSION

New 1,3-dioxane compounds (**1-5**) have been obtained by the condensation reaction between 2-methyl-1,3-propanediol and symmetric ketones (Scheme 3):

**Scheme 3**

All the investigated compounds exhibit anancomeric structures, the conformational equilibria being shifted towards the conformations that display the 5-methyl group in equatorial orientation (Scheme 4):

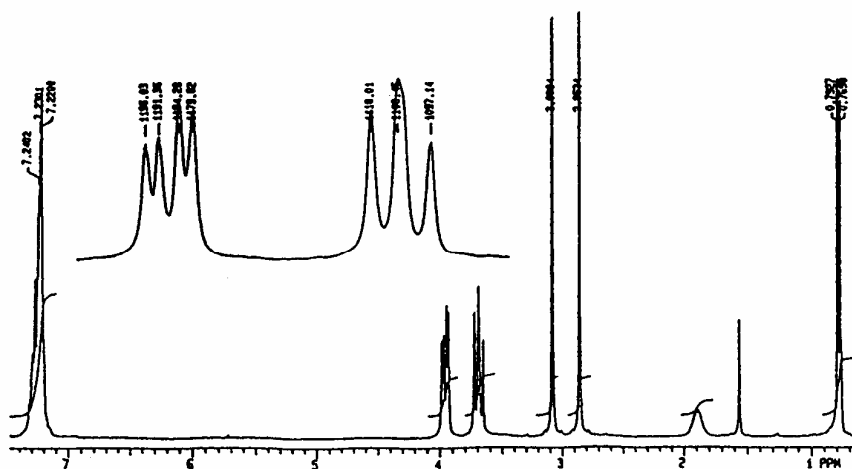
**Scheme 4**

The spectra of all these compounds exhibit different signals for the axial and equatorial orientations of the protons of the 1,3-dioxane ring and of the protons and carbon atoms of the identical alkyl groups located at the position 2 (Table 1).

Table 1 ^1H and ^{13}C -NMR data for compounds 1-5

Comp.	$^1\text{H-NMR}$			$^{13}\text{C-NMR}$			
	4,6- H_{ax}	4,6- H_{eq}	5- CH_3	C^2	$\text{C}^{4,6}$	C^5	5- CH_3
1	3.22	3.58	0.44	100.59	65.56	23.18	13.28
2	3.28	3.60	0.47	100.16	65.61	29.43	13.35
3	3.42	3.77	0.31	-	67.72	29.57	13.01
4	3.69	3.95	0.78	100.17	66.01	28.94	13.27
5	3.59	3.25	0.44	97.12	64.96	29.32	12.88

As an example, the $^1\text{H-NMR}$ spectrum for compound 4 (Figure 1) displays different signals for the axial and equatorial protons at positions 4 and 6. The equatorial protons exhibit a doublet of doublet ($\delta_{4,6 \text{ eq}} = 3.95 \text{ ppm}$) due to a large geminal coupling constant ($J = 11.7 \text{ Hz}$) and to a smaller coupling with the vicinal axial proton at position 5 ($^3J = 4.6 \text{ Hz}$). The axial protons exhibit an overlapped doublet of doublet that gives a triplet ($\delta_{4,6 \text{ ax}} = 3.69 \text{ ppm}$; $^2J = ^3J = 11.7 \text{ Hz}$). The spectrum also exhibits two singlets ($\delta = 2.85$ and $\delta = 3.08 \text{ ppm}$) corresponding to the axial, respectively equatorial methylene protons of the benzyl groups, a multiplet ($\delta = 1.88 \text{ ppm}$) for the axial proton at the position 5, a doublet ($\delta = 0.78 \text{ ppm}$) for the protons of the equatorial methyl group and a multiplet ($\delta = 7.23 \text{ ppm}$) for the aromatic protons.

**Fig.1.** $^1\text{H-NMR}$ Spectrum of compound 4

CONCLUSIONS

The NMR investigations of compounds **1-5** bearing similar substituents at position 2 and a methyl group at the position 5 of the 1,3-dioxane ring revealed anancomeric structures despite the smaller A values of the alkyl groups located in the aliphatic part of the heterocycle.

EXPERIMENTAL

¹H- and ¹³C-NMR spectra were recorded at room temperature, using C₆D₆ as solvent, in 5 mm tubes, on a Varian Gemini spectrometer, operating at 300 MHz for protons and at 75 MHz for carbon atoms. Melting points were measured with Electrothermal apparatus and are uncorrected.

New compounds 1-5, general procedure

Equimolecular amounts of 1,3-diol and carbonyl compound (0.1 mol) with catalytic amounts of *p*-toluenesulphonic acid (0.1 g) were solved in 200 ml of benzene. The mixture was refluxed and the resulted water was removed using a Dean-Stark trap. When 80% of the theoretical water was separated, after cooling at room temperature, the catalyst was neutralized (under stirring 0.5 h) with CH₃COONa powder in excess (0.2 g). The reaction mixture was washed twice with 100 ml water. The benzene was removed (after drying with Na₂SO₄) and the 1,3-dioxanic compounds were purified by crystallisation from ethanol or by vacuum distillation.

2,2-Diethyl-5-methyl-1,3-dioxane 1

Liquid, b.p.=186^oC. Yield 54%. C₉H₁₈O₂, found C 69.33, H 11.07; required C 68.35, H 11.39%

¹H-NMR (C₆D₆): δ 0.44 (3H, d, J = 6.7 Hz, 5-CH₃_{eq}), 0.86 (3H, t, J = 7.5 Hz, 2-CH₂CH₃_{ax}), 1.05 (3H, t, J = 7.5 Hz, 2-CH₂CH₃_{eq}), 1.62 (2H, q, J = 7.5 Hz, 2-CH₂CH₃_{ax}), 1.77 (2H, q, 2-CH₂CH₃_{eq}), 1.84-1.97 (H, m, 5-H_{ax}), 3.22 (2H, t, overlapped dd, J = J' = 11.8 Hz, 4,6-H_{ax}), 3.61 (2H, dd, J = 11.8 Hz, J' = 4.7 Hz, 4,6-H_{eq})

¹³C-NMR (C₆D₆): δ 7.65 (2-CH₂CH₃_{ax}), 8.17 (2-CH₂CH₃_{eq}), 13.28 (5-CH₃), 23.18 (C⁵), 29.39 (2-CH₂CH₃_{ax}), 29.52 (2-CH₂CH₃_{eq}), 65.61 (C^{4,6}), 100.59 (C²)

5-Methyl-2,2-dipropyl-1,3-dioxane 2

Liquid, b.p.=206^oC. Yield 61%. C₁₁H₂₂O₂, found C 70.28, H 11.96; required C 70.96, H 11.82%

¹H-NMR (C₆D₆): δ 0.47 (3H, d, J = 6.8 Hz, 5-CH₃_{eq}), 0.88-0.97 (6H, overlapped peaks, 2-CH₂CH₂CH₃_(ax+eq)), 1.30-1.80 (9H, overlapped peaks, 2-CH₂CH₂CH₃_(ax+eq) + 5-H_{ax}), 3.28 (2H, t, overlapped dd, J = J' = 11.8 Hz, 4,6-H_{ax}), 3.60 (2H, dd, J = 11.8 Hz, J' = 4.6 Hz, 4,6-H_{eq})

¹³C-NMR (C₆D₆): δ 13.35 (5-CH₃), 14.74 (2-CH₂CH₂CH₃_{ax}), 14.82 (2-CH₂CH₂CH₃_{eq}), 16.76 (2-CH₂CH₂CH₃_{ax}), 17.34 (2-CH₂CH₂CH₃_{eq}), 29.43 (C⁵), 33.57 (2-CH₂CH₂CH₃_{ax}), 39.69 (2-CH₂CH₂CH₃_{eq}), 65.61 (C^{4,6}), 100.16 (C²)

5-Methyl-2,2-diphenyl-1,3-dioxane 3

Solid, m.p. = 150⁰C. Yield 66%. C₁₇H₂₂O₂, found C 81.03, H 6.82; required C 80.31, H 6.82%

¹H-NMR (C₆D₆): δ 0.31 (3H, d, J = 6.6 Hz, 5-CH_{3eq}), 1.81 (H, m, 5-H_{ax}), 3.42 (2H, t, overlapped dd, J = J' = 11.3 Hz, 4,6-H_{ax}), 3.77 (2H, dd, J = 11.3 Hz, J' = 4.2 Hz, 4,6-H_{eq}), 7.0-7.80 (10H, m)

¹³C-NMR (C₆D₆): δ 13.01 (5-CH₃), 29.57 (C⁵), 67.72 (C^{4,6}), 126.48, 128.08, 128.39, 128.92 (aromatic carbon atoms)

2,2-Dibenzyl-5-methyl-1,3-dioxane 4

Solid, m.p.=58⁰C. Yield 76%. C₁₉H₂₂O₂, found C 81.40, H 7.63; required C 80.85, H 7.80%

¹H-NMR (C₆D₆): δ 0.78 (3H, d, J = 6.9 Hz, 5-CH_{3eq}), 1.88 (H, m, 5-H_{ax}), 2.85 (2H, s, CH_{2ax}), 3.08 (2H, s, CH_{2eq}), 3.69 (2H, t, overlapped dd, J = J'=11.7 Hz, 4,6-H_{ax}), 3.95 (2H, dd, J = 11.7 Hz, J'=4.6 Hz, 4,6-H_{eq}), 7.23 (10H, m)

¹³C-NMR (C₆D₆): δ 13.27 (5-CH₃), 28.94 (C⁵), 38.17 (CH₂Ph_{ax}), 43.22 (CH₂Ph_{eq}), 66.01 (C^{4,6}), 100.17 (C²), 126.36, 126.48, 127.86, 128.20, 130.86, 131.41, 137.31, 137.54 (aromatic carbon atoms)

3- Methyl-1,5-dioxa-spiro[5.5]undecane 5

Solid, m.p.=66⁰C. Yield 57%. C₁₀H₁₈O₂, found C 70.01, H 10.86; required C 70.59, H 10.60 %

¹H-NMR (C₆D₆): δ 0.44 (3H, d, J = 6.8 Hz, 3-CH_{3eq}), 1.30 (2H, m, H⁹), 1.43 (2H, m, H⁸), 1.59 (2H, m, H¹⁰), 1.73 (3H, m, overlapped peaks, H⁷, H³), 1.78 (2H, m, H¹¹), 3.25 (2H, t, overlapped dd, J = J' = 11.9 Hz, 2,4-H_{ax}), 3.59 (2H, dd, J = 11.9 Hz, J' = 4.8 Hz, 2,4-H_{eq})

¹³C-NMR (C₆D₆): δ 12.88 (3-CH₃), 22.52, 22.64 (C^{8,10}), 25.89 (C⁹), 29.10 (C^{7,11}), 29.32 (C³), 64.96 (C^{2,4}), 97.12 (C⁶)

REFERENCES

1. M. J. O. Anteunis, D. Tavernier, F. Borreman, *Heterocycles*, 4, **1976**, 293.
2. S. Mager, I. Hopartean, M. Horn, I. Grosu, *Studia Univ. "Babeş-Bolyai", Chemia*, 24, **1979**, 32.
3. S. Mager, I. Grosu, *Studia Univ. "Babeş-Bolyai", Chemia*, 33, **1988**, 47.
4. I. Grosu, M. Horn, D. Kovacs, S. Mager, *Studia Univ. "Babeş-Bolyai", Chemia*, 37, **1992**, 7.
5. I. Grosu, S. Mager, E. Mesaroş, L. Muntean, C. Socaci, *Studia Univ. "Babeş-Bolyai", Chemia*, 42, **1997**, 85.
6. S. Mager, I. Grosu, M. Horn, I. Hopartean, M. Dărăbanţu, C. Puşcaş, D. Kovacs, G. Plé, *Roumanian Chemical Quarterly Reviews*, 3, **1995**, 201.
7. I. Grosu, S. Mager, G. Plé, *Rev.Roum.Chim.*, 43, **1998**, 725.

8. I. Grosu, S. Mager, G. Plé, R. Martinez, L. Muntean, E. Mesaroş, *Heterocycles*, 41, **1995**, 2233.
9. I. Grosu, S. Mager, G. Plé, L. Muntean, I. Schirger, *Heterocyclic Commun.*, 2, **1996**, 423.
10. I. Grosu, S. Mager, G. Plé, N. Plé, A. Toscano, E. Mesaroş, R. Martinez, *Liebigs Annalen / Recueil*, **1997**, 2371.
11. I. Grosu, S. Mager, L. Toupet, G. Plé, E. Mesaroş, A. Mihiş, *Acta Chem.Scand.*, 52, **1998**, 366.
12. K. Pihlaja, P. Ayras, *Suomen Kemistilehti*, B42, **1969**, 4265.
13. F. W. Nader, E. L. Eliel, *J.Am.Chem.Soc.*, 92, **1970**, 3050.

THE OXIDATION OF TOLUENE BY POTASSIUM PERMANGANATE IN PERCHLORIC ACID MEDIUM

CLAUDIA MUREȘANU¹, IOAN BÂLDEA²

*Department of Physical Chemistry, Faculty of Chemistry and Chemical Engineering,
"Babeș-Bolyai" University of Cluj-Napoca, 11 Arany Janos Str., 3400-Romania;*

ABSTRACT. The reaction of potassium permanganate with toluene, catalyzed by Mn^{2+} , was studied spectrophotometrically. Permanganate ion is consumed mainly by two reaction routes: one is the direct oxidation of toluene and the other the reduction by the manganous ion. Both pathways exhibit a first - order dependence with respect to permanganate ion. Our kinetic study includes also the influence of toluene, hydrogen ion and manganous ion concentration upon reaction rate. The rate laws for the two reaction routes and for the global reaction were established. Several possible reaction mechanisms are discussed for C – H bond breaking in the case of direct oxidation of toluene by permanganate and for Mn^{3+} generation by reduction of MnO_4^- with Mn^{2+} .

Keywords: toluene, potassium permanganate, catalyze, redox reactions, kinetics.

Potassium permanganate is a well-known oxidant for various organic compounds, in acidic and basic media. We mention here only a few examples, like the oxidation of olefins¹, oxalic^{2 - 4} and formic acid⁵, 2,6-dinitrophenols⁶, toluene⁷, substituted toluenes⁸ and ethylbenzene⁹.

Related to the subject of our paper are the earlier works of Cullis and Ladbury⁷⁻⁹. They studied the oxidation of aromatic hydrocarbons with potassium permanganate, in a 50% aqueous acetic acid medium, by means of an iodometrical method. The main product was the corresponding aldehyde, for toluene and substituted toluenes oxidation and acetophenone in the case of ethylbenzene oxidation, when a stoichiometric ratio of initial concentrations of reactants was used. Besides side chain oxidation aromatic ring disruption was also observed, especially for the oxidation of xylenes. The results of the kinetic studies about the oxidation of aromatic hydrocarbons mentioned above⁷⁻⁹ revealed that, all reactions are first-order with respect to MnO_4^- concentration. Toluene, chlorotoluene and ethylbenzene oxidations are first order with respect to the organic compound, while for m- and p-xylene this order was less than one. A clear autocatalytic effect of Mn(II), involving the Mn(III) intermediate, could not be

¹muresanu@chem.ubbcluj.ro; ²ibaldea@chem.ubbcluj.ro

proved. It seemed rather that the mechanism of these reactions has two pathways, one in which Mn(III) is implied and one independent of this species⁷⁻⁹. The recent papers of Gardner and Kuehnert deal with the oxidation of alkylbenzenes in aqueous buffer¹⁰ and in neat toluene¹¹. They developed a hydride transfer mechanism for toluene oxidation in aqueous buffer and a radical mechanism if the reaction was performed in organic solvent. Benzyl alcohol¹²⁻¹⁴ and benzaldehyde¹⁵⁻¹⁷ oxidation with MnO_4^- were studied in acid medium while for toluene oxidation no recent kinetic are available in this medium. That is why we considered it interesting to devote this paper to a more detailed investigation of toluene oxidation by potassium permanganate in perchloric acid medium.

EXPERIMENTAL

The chemicals used in this study were of reagent grade purity and were acquired from commercial sources (Reactivul Bucuresti and Merck).

Kinetic measurements were performed by means of a Zeiss Spekol spectrophotometer, provided with a temperature jacket surrounding the cell holder. The jacket was connected to a Wobser U-10 recirculatory water bath. Reaction mixtures were prepared directly into the spectrophotometer glass cell, of 5-cm path length. The reaction was started by adding a measured amount of KMnO_4 stock solution over the mixture of toluene, HClO_4 , MnSO_4 , NaClO_4 in twice distilled water. Absorbance was measured at 520 nm, where KMnO_4 UV/VIS spectrum exhibits a maximum.

RESULTS AND DISCUSSIONS

Kinetic runs were performed in the presence of toluene and Mn(II) excess. Absorbance readings were processed according to the integrated form of a first-order rate law:

$$\ln(A - A_\infty) = \ln(A_0 - A_\infty) - k_{\text{obsd}} \cdot t \quad (1)$$

where: A_0 , A_∞ and A are the measured values of absorbance at the beginning, the end and at different time moments of the reaction ;

k_{obsd} is the observed first-order rate constant.

Semilogarithmic plots $\ln(A - A_\infty)$ versus t , at several excess concentrations of toluene were linear (**Fig.1**) up to 90 % of completion, so that it is obvious that reaction order with respect to MnO_4^- is one. If the reaction was approaching its end a slight downward curvature was noticed.

Observed rate constants were determined from the slopes of linear plots, of eq. (1), using a least square method. Two to four replicate kinetic runs were carried out for each set of conditions.

It is considered that the depletion of MnO_4^- , in the presence of Mn^{2+} , occurs by two pathways:

Pathway 1, which means the direct oxidation of toluene by permanganate;

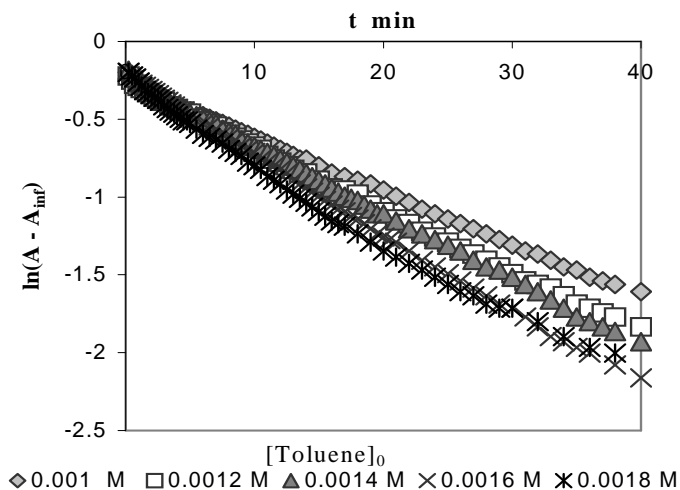


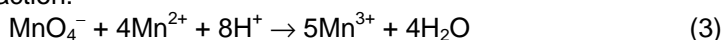
Fig.1 First order semilogarithmic plots at several excess concentrations of toluene; $[\text{MnO}_4^-] = 7 \cdot 10^{-5}$; $[\text{HClO}_4] = 1.4$; $[\text{MnSO}_4] = 10^{-2} \text{ mol} \cdot \text{dm}^{-3}$ and $\mu = 1.5 \text{ mol} \cdot \text{dm}^{-3}$ at 45°C .

Pathway 2, which is the autocatalytic, first order reduction of MnO_4^- by the manganous ion.

Our results, summarized in **Table 1**, revealed that enlarged concentrations of toluene lead to increased values of first-order rate constants according to:

$$k_{\text{obsd}} = (2.4 \pm 0.5) \cdot 10^{-4} + (0.34 \pm 0.04) \cdot [\text{Toluene}]_0 \quad \text{at } 45^\circ\text{C} \quad (2)$$

where the term of zero-order with respect to toluene represents the consumption of MnO_4^- due to the reaction:



The rate constant determined in the absence of toluene, $k_0 = 3.9 \pm 0.2 \text{ s}^{-1}$ at $[\text{H}^+] = 1.4$, $\mu = 1.5 \text{ mol} \cdot \text{dm}^{-3}$ and 45°C , is a close value to the intercept of eq.(3).

Table 1.

The dependence of first-order rate constants for toluene oxidation on the excess concentration of toluene; $[\text{MnO}_4^-] = 7 \cdot 10^{-5}$; $[\text{HClO}_4] = 1.4$; $[\text{MnSO}_4] = 10^{-2} \text{ mol} \cdot \text{dm}^{-3}$ and $\mu = 1.5 \text{ mol} \cdot \text{dm}^{-3}$ at 45°C .

$10^3 \cdot [\text{Toluene}]_0$ ($\text{mol} \cdot \text{dm}^{-3}$)	1.0	1.2	1.4	1.6	1.8
$10^4 \cdot \bar{k}_{\text{obsd}} \text{ (s}^{-1}\text{)}$	5.8 ± 0.6	6.5 ± 0.3	7.2 ± 0.2	7.9 ± 0.3	8.6 ± 0.2
$10^4 \cdot \bar{k}_{\text{obsd}}^* \text{ (s}^{-1}\text{)}$	3.4 ± 0.4	4.1 ± 0.3	4.8 ± 0.3	5.5 ± 0.2	6.4 ± 0.3

The values of first – order rate constants corrected for reduction of permanganate by manganous ion, $k^*_{\text{obsd}} = k_{\text{obsd}} - 2.4 \cdot 10^{-4}$, exhibited a first – order influence with respect to toluene concentration:

$$k^*_{\text{obsd}} = (1.5 \pm 0.5) \cdot 10^{-6} + (0.34 \pm 0.04) [\text{Toluene}]_0 \quad \text{at } 45^\circ\text{C} \quad (4)$$

$$k^*_{\text{obsd}} \approx (0.34 \pm 0.04) [\text{Toluene}]_0$$

The influence exerted by hydrogen ion concentration was investigated in the limits of 1 to 1.5 mol·dm⁻³ at constant toluene and Mn(II) concentration. The results presented in **Table 2** prove a linear dependence of the rate constant on the [H⁺], of the form:

$$k_{\text{obsd}} = (2.7 \pm 0.8) \cdot 10^{-4} + (2.7 \pm 0.2) \cdot 10^{-4} \cdot [\text{H}^+] \quad \text{at } 45^\circ\text{C} \quad (5)$$

A similar correction procedure, as for the influence of organic substrate, was used also in this case: $k^*_{\text{obsd}} = k_{\text{obsd}} - k_0$ where k_0 are the rate constants of pathway 2 obtained from kinetic runs in the absence of toluene (**Table 2**)

$$k_0 = (2.7 \pm 1.1) \cdot 10^{-5} + (1.7 \pm 0.1) \cdot 10^{-4} \cdot [\text{H}^+] \quad \text{at } 45^\circ\text{C} \quad (6)$$

$$k^*_{\text{obsd}} = (2.4 \pm 0.1) \cdot 10^{-4} + (9.34 \pm 0.6) \cdot 10^{-5} \cdot [\text{H}^+] \quad \text{at } 45^\circ\text{C} \quad (7)$$

This relationship is valid in strong acid media. At low acid concentration it is to expect a downward curvature of the $k_{\text{obsd}} = f(t)$ dependence, tending to a constant value, like that obtained by Cullis and Ladbury⁷, because KMnO₄ keeps it oxidizing effect upon organic substrates also in low acidic, neutral media and alkaline media.

Table 2.

The dependence of first-order rate constants for toluene oxidation on [H⁺];
[Toluene]₀ = 1.2 · 10⁻³; [MnO₄⁻] = 7 · 10⁻⁵; [MnSO₄] = 10⁻² mol·dm⁻³ and
μ = 1.5 mol·dm⁻³ at 45^oC.

[H ⁺] (mol·dm ⁻³)	1	1.1	1.2	1.3	1.4	1.5
10 ⁴ · \bar{k}_{obsd} (s ⁻¹)	5.4 ± 0.1	5.7 ± 0.1	6.0 ± 0.2	6.2 ± 0.2	6.5 ± 0.1	6.8 ± 0.1
10 ⁴ · \bar{k}_0 (s ⁻¹)	2.0 ± 0.1	2.2 ± 0.2	2.4 ± 0.1	2.5 ± 0.2	2.7 ± 0.1	2.9 ± 0.2
10 ⁴ · \bar{k}^*_{obsd} (s ⁻¹)	3.4 ± 0.1	3.6 ± 0.1	3.8 ± 0.2	3.8 ± 0.2	3.4 ± 0.1	3.9 ± 0.2

Because several autocatalytic oxidations of organic compounds by KMnO₄ are mentioned in literature²⁻⁶, we have studied the influence of Mn(II) upon the reaction rate. But, as it can be seen (**Fig.2**) no sigmoid curve was obtained for the change of absorbance with time, in the absence of Mn(II). Although we couldn't identify any autocatalytic effect, the reaction evolves much faster in the presence of Mn(II), proving the catalytic influence of manganous ion. A similar situation has been observed by other authors⁷⁻⁹ in the case of toluene, xylenes, chlorotoluene and ethylbenzene.

The first-order rate constant exhibits a second - order dependence on manganous ion concentration, with a small intercept:

$$k_{\text{obsd}} = (3.2 \pm 0.3) \cdot 10^{-4} + (3.08 \pm 0.13) \cdot [\text{Mn(II)}]^2 \quad \text{at } 45^\circ\text{C} \quad (8)$$

where the first term corresponds to the rate constant of toluene oxidation in the absence of Mn(II).

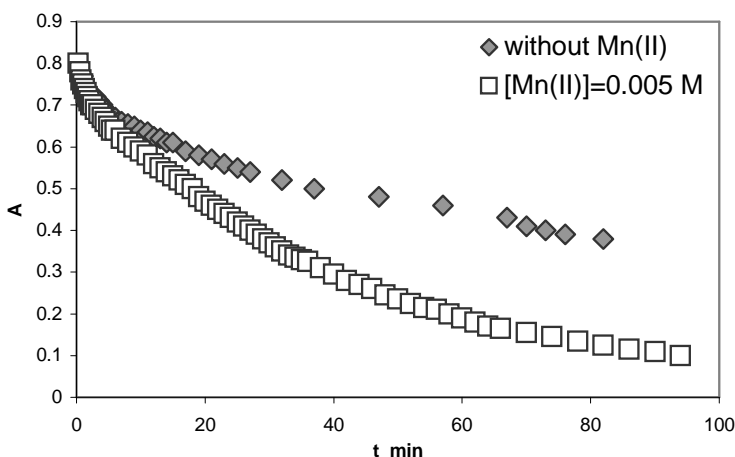


Fig. 2 The variation of absorbance with time in the absence and in the presence of Mn(II) catalysator; $[\text{Toluene}]_0 = 1.2 \cdot 10^{-3}$; $[\text{MnO}_4^-] = 7 \cdot 10^{-5}$; $[\text{HClO}_4] = 1.4 \text{ mol} \cdot \text{dm}^{-3}$ and $\mu = 1.5 \text{ mol} \cdot \text{dm}^{-3}$ at 45°C .

A similar dependence is obtained by processing data from kinetic runs in the absence of toluene:

$$k_0 = (6.65 \pm 0.06) \cdot 10^{-5} + (3.23 \pm 0.11) \cdot [\text{Mn}^{2+}]^2 \quad 45^\circ\text{C} \quad (9)$$

where the intercept represents the rate constant for solvent oxidation by permanganate ion. The manganous ion influences only the second pathway, this is why the dependence of the rate constants eq. (6) and (7) exhibits approximately the same slope.

Table 3.

The dependence of first-order rate constants for toluene oxidation on $[\text{Mn}^{2+}]$; $[\text{Toluene}]_0 = 1.2 \cdot 10^{-3}$; $[\text{MnO}_4^-] = 7 \cdot 10^{-5}$; $[\text{H}^+] = 1.4$ and $\mu = 1.5 \text{ mol} \cdot \text{dm}^{-3}$ at 45°C .

$10^2 \cdot [\text{Mn}^{2+}] \text{ (mol} \cdot \text{dm}^{-3}\text{)}$	0.5	1	1.5	2
$10^4 \cdot \bar{k}_{\text{obsd}} \text{ (s}^{-1}\text{)}$	3.5 ± 0.7	6.4 ± 0.1	10.4 ± 0.1	15.5 ± 0.4
$10^4 \cdot \bar{k}_0 \text{ (s}^{-1}\text{)}$	1.4 ± 0.1	3.9 ± 0.2	7.9 ± 0.1	13.6 ± 0.2

The rate law represents the sum of the rates for the two pathways:

$$r = -\frac{d[\text{MnO}_4^-]}{dt} = (k_0 \cdot [\text{Mn(II)}^2] + k \cdot [\text{Toluen}]_0)[\text{H}^+][\text{MnO}_4^-] \quad (10)$$

CONCLUSIONS

The oxidation of toluene by Mn(VII) yields benzaldehyde and benzoic acid, for reactions performed in aqueous acetic acid⁷, aqueous buffer¹⁰ and in neat toluene¹¹.

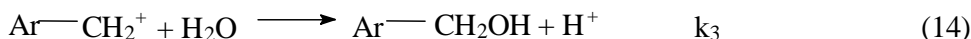
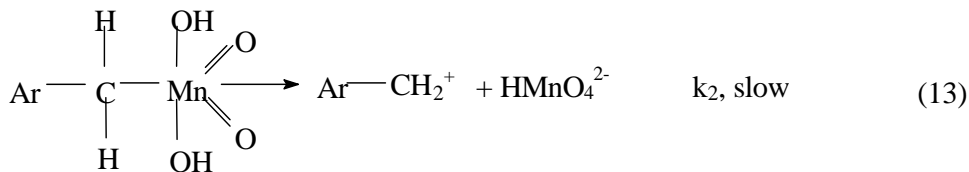
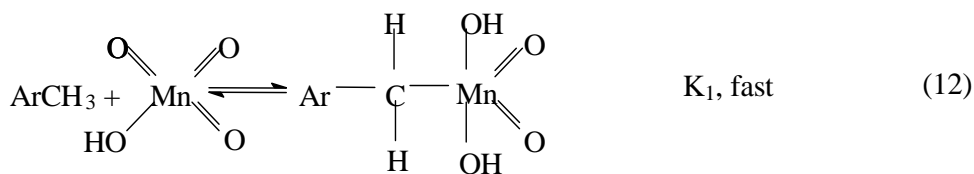
Therefore it is reasonable to consider the formation of same products if the reaction takes place in aqueous HClO₄ solution.

Many kinetic studies underline the large isotopic effect observed for the oxidation of organic compounds, like toluene, benzyl alcohol, tolylvaleric acids and for substituted mandelate ions^{10, 13, 18, 19, 20} with permanganate. Such a behavior indicates the C – H bond cleavage is the rate determining step. The oxidation of the C – H bond by KMnO₄ may proceed by:

A. proton transfer abstraction^{11,12}; **B.** hydrogen atom abstraction²⁰; **C.** hydride abstraction¹⁰; **D.** a [2 + 2] addition of a reactive C – H bond^{18, 19} to an Mn = O bond; **D.** formation of a manganese ester^{17, 21}.

Literature information, together with the experimental rate law, eq. (10) are to be accommodate by the reaction mechanism. In our opinion these requests are satisfied by three of the above mentioned reaction mechanisms, considering that oxidation proceeds by permanganate ion (pathway 1).

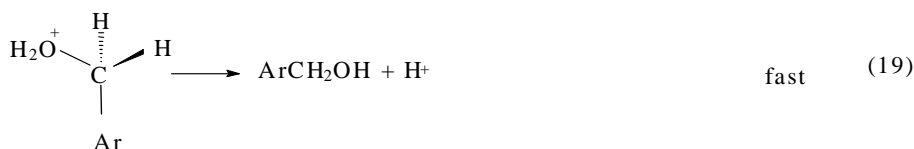
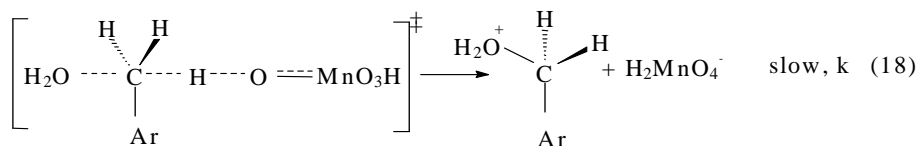
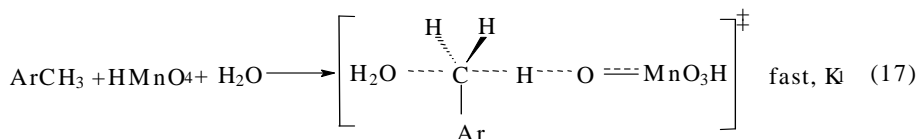
❖ A [2+2] addition of a C – H bond to the Mn = O bond, continued by homolytic or heterolytic bond cleavage in the rate determining step and subsequent reaction of the intermediate with the solvent.



THE OXIDATION OF TOLUENE BY POTASSIUM PERMANGANATE IN PERCHLORIC ACID MEDIUM

A free radical intermediate was excluded because experiments undertaken with toluene and benzylic alcohol in aqueous medium ruled out this possibility^{10, 13}. The resulting rate law will depend on permanganate, reductant and hydrogen ion concentration according to:

$$r = k_2 K_1 K [\text{ArCH}_3][\text{MnO}_4^-][\text{H}^+] \quad (15)$$

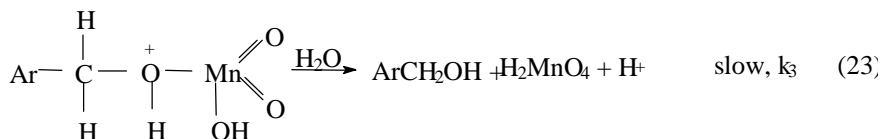
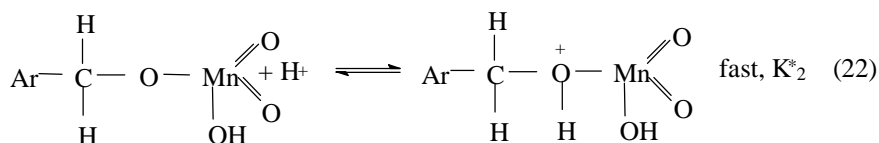
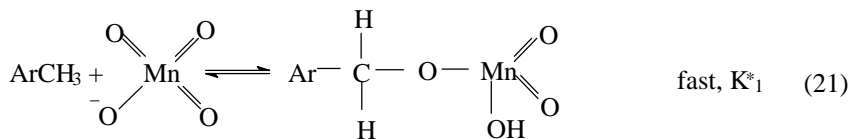


Hydride abstraction which in this case occurs similar to a $\text{S}_{\text{N}}2$ mechanism:
With the rate law:

$$r = k K K_1 [\text{ArCH}_3][\text{H}^+][\text{H}_2\text{O}][\text{MnO}_4^-] \quad (20)$$

Although the association constant for HMnO_4 is very low¹⁷ ($K = 2.99 \cdot 10^{-3}$) there are cases for which a greater reactivity of HMnO_4 compared to MnO_4^- is mentioned^{22, 23}

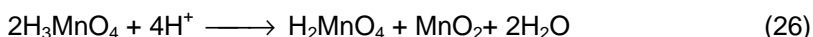
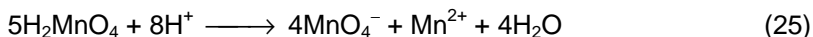
- ❖ The formation of an ester between permanganate ion and toluene, followed by the acid catalyzed hydrolysis of the ester.



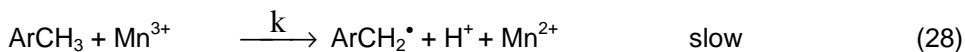
This mechanism will lead to a rate law similar to that deduced above:

$$r_1 = k_3 K_1^* K_2^* [\text{ArCH}_3][\text{MnO}_4^-][\text{H}^+][\text{H}_2\text{O}] \quad (24)$$

All these three mechanisms lead to a rate law of first order with respect to MnO_4^- , H^+ and toluene, similar to that obtained by us for the first pathway. In high acidic medium several redox and dismutation reactions between manganese species might occur, which explains why no MnO_2 formation was observed:

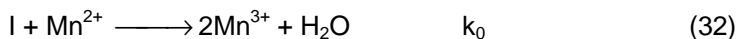


Hydrogen ion abstraction will be the rate determining step^{24, 25, 26-28}, when Mn^{3+} is the oxidizing species (pathway 2), followed by other reactions of the formed intermediate:



Recent literature on this subject, suggests for the generation of the Mn^{3+} intermediate, the formation of a monomeric and a dimeric Mn^{2+} complex (I), with a bridging ligand⁴, or the formation of a dinuclear complex between MnO_4^- and Mn^{2+} with oxo bridge²², followed by the reduction of the complex by Mn^{2+} to Mn^{3+} . Our reaction mixtures contained only ClO_4^- and SO_4^{2-} anions, which are weak in

complexing Mn^{2+} , that is why we considered the formation of the $MnO_4^- - Mn^{2+}$ complex:



The influence of hydrogen ion may be explained in two ways: if it is considered that the permanganic acid forms the binuclear complex with Mn^{2+} , or if it is considered that the hydrogen ion is involved in reduction of the complex. The formation of Mn^{3+} was considered as the rate-determining step, and the deduced rate law came to the form:

$$r_2 = k_0[MnO_4^-][Mn^{2+}]^2[H^+] \quad (33)$$

Although the rate law is quite similar to our experimental rate law eq.(10), we will continue the experimental investigations to come to a better understanding of the overall mechanism.

REFERENCES

1. Lee D. G. and Chen T., *J. Am. Chem. Soc.*, **1989**, *111*, 7534-7538.
2. Wawrezenczic E. M. and Vronska M., *Z. Phys. Chem.(Leipzig)*, **1980**, *261(2)*, 306-312.
3. Powell R. T. Oskin, T. and Ganapatshubramanian N., *J. Phys. Chem.*, **1989**, *93*, 2718-2721.
4. Pimienta V., Lavabre D., Levy G. and Micheau J. C., *J. Phys. Chem.*, **1994**, *98*, 13294-13299.
5. Mann D. R. and Tompkins F. C., *Trans. Faraday Soc.*, **1941**, *37*, 201-209.
6. Alexander E. A. and Tompkins F. C., *Trans. Faraday Soc.*, **1939**, *35*, 1156-1165.
7. Cullis C. F. and Ladbury J. W., *J. Chem. Soc.*, **1955**, 555-560.
8. Cullis C. F. and Ladbury J. W., *J. Chem. Soc.*, **1955**, 1407-1412.
9. Cullis C. F. and Ladbury J. W., *J. Chem. Soc.*, **1955**, 2851-2854.
10. Gardner K. A. and Mayer J. M., *Science*, **1995**, *269*, 1849 – 1851.
11. Gardner K. A. , Kuehnert L. L. and Mayer J. M., *Inorg. Chem.*, **1997**, *36*, 2069 – 2078.
12. Corma A. , Lambies V., Melo F. V. and Palou J., *Anal. Quim.*, **1980**, *76*, 304-310.
13. Banerji K. K., *J.C.S. Perkin 2*, **1973**, 435 – 437.
14. Mathur S., Gupta A. and Banerji K., *Ind. J. Chem.*, **1988**, *27A*, 581 – 583.
15. Tompkins F. C., *Trans. Faraday Soc.*, **1943**, *39*, 280 – 287.
16. Wiberg K. B. and Stewart R., *J. Am. Chem. Soc.*, **1955**, *77*, 1786 – 1795.

17. Sen Gupta K. K., Sen P. K. and Mukhopadhyay G., *Trans. Met. Chem.*, **1993**, 18, 369 – 371.
18. Lee D. G. and Chen T., *J. Org. Chem.*, **1991**, 56, 5341 – 5345.
19. Lee D. G. and Chen T., *J. Am. Chem. Soc.*, **1993**, 115, 11231 – 11236.
20. Braumann J. I. and Pandell A. J., *J. Am. Chem. Soc.*, **1970**, 92, 329 – 335.
21. Wiberg K. and Fox A. S., *J. Am. Chem. Soc.*, **1963**, 85, 3487 – 3491.
22. Simoyi R. H., DeKepper P., Epstein I. R. and Kustin K., *Inorg. Chem.*, **1986**, 25, 538 – 542.
23. Bhatia I., Banerji K. K.: *J.C.S. Perkin Trans. 2*, **1983**, 1577 – 1580.
24. Venkatachalapathy M. S., Ramaswamy R. and Udupa H. V. K., *Bull. Acad. Pol. Scien. (Ser. Chim.)*, **1959**, 7, 629 – 631.
25. Venkatachalapathy M. S., Ramaswamy R. and Udupa H. V. K., *Bull. Acad. Pol. Scien. (Ser. Chim.)*, **1958**, 6, 487 – 489
26. Heiba E. I., Dessau R. M. and Koehl W. J., *J. Am. Chem. Soc.*, **1969**, 91, 138 – 145.
27. Hanotier J., Hanotier–Bridoux M. and Radzetzky P., *J.C.S. Perkin 2*, **1973**, 4, 381 – 386.
28. Andrulic P., Dewaer M. J. S, Dietz R. and. Hunt R. L., *J. Am. Chem. Soc.*, **1966**, 88, 5473 – 5478.

CONNECTIVITY INDICES OF DENDRIMERS

ERNESTO ESTRADA^A, NICOLAIS GUEVARA^B, ANTON A. KISS^C, FLORIN MOTOC^C AND MIRCEA V. DIUDEA^C

^aDepartment of Drug Design. Centro de Bioactivos Químicos; ^bDepartment of Physics. Universidad Central de Las Villas. Santa Clara 54830. Villa Clara. Cuba; ^cUniversitatea "Babeș-Bolyai" Arany Janos 11, 3400 Cluj, Romania

ABSTRACT. Formulas for calculating connectivity-based indices Randi \equiv -type index calculated on vertices, χ , and on edges, ε , Zagreb index, M_2 , and Bertz index, B in regular homogeneous dendrimers are established. Values of the above topological indices for families of dendrimers, with up to 10 orbits, are calculated. Mutual intercorrelation of these indices, in the considered dendrimers, is evaluated.

INTRODUCTION

Dendrimers are hyperbranched molecules, synthesised basically by two procedures: (i) by "divergent growth", [1-3] when branched blocks are added around a central core, thus obtaining a new, larger orbit or generation and (ii) or by "convergent growth" [4-7] when large branched blocks, previously built up starting from the periphery, are attached to the core. These structures show spherical shape, which can be functionalized [8-11], thus modifying their physico-chemical or biological properties. Reviews in the field are available. [12-14]

Some particular definitions in dendrimers are needed :

Vertices in a dendrimer, except the external endpoints, are considered as branching points. The number of edges incident in a branching point is called degree, δ .

A regular dendrimer has all the branching points with the same degree, otherwise it is irregular [15-17].

A dendrimer is called *homogeneous* if all its radial chains (i.e., the chains starting from the core and ending in an external point) have the same length [12]. In graph theory, they correspond to the Bethe lattices [18].

A tree has either a monocenter or a dicenter [19] (i.e. two points joined by an edge). Accordingly, a dendrimer is called *monocentric* and *dicentric*, respectively. Examples are given in the Figure. The numbering of orbits (generations [12]) starts with zero for the core and ends with r , which is the radius

of the dendrimer (i.e., the number of edges along a radial chain, starting from the core and ending to an external node).

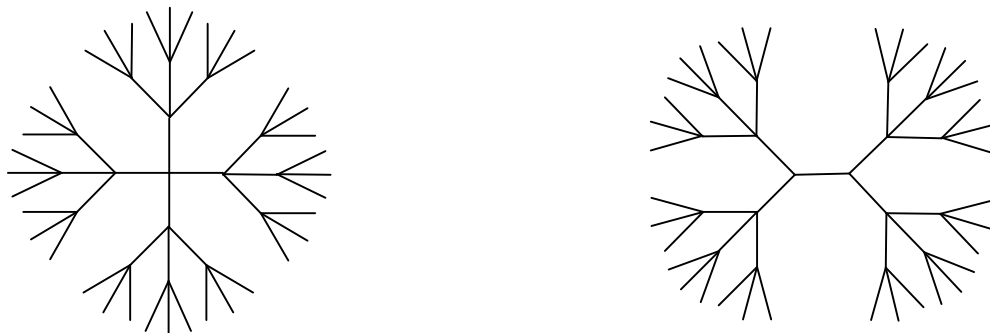


Figure. Monocentric and dicentric regular dendrimers

ATOM (VERTEX) CONNECTIVITY INDEX

The atom (vertex) connectivity index was introduced by Randić [20] as a measurement of the molecular branching in alkanes. It was subsequently extended by Kier and Hall to account for heteroatoms differentiation and it was renamed as molecular connectivity index [21]. The Randić original index is calculated from the following expression

$$\chi = \sum_{t=1}^m (\delta_i \delta_j)_t^{-0.5} \quad (1)$$

where the summation is carried out over all pairs of adjacent vertices, that is over all edges m , in the molecular graph. The index was later extended by Altenburg to include exponents other than -0.5 in the expression (1). The generalized vertex connectivity index is then calculated as

$$\chi = \sum_{t=1}^m (\delta_i \delta_j)_t^g \quad (2)$$

Several exponents have been investigated by Altenburg, Randić and very recently a mathematical justification of the necessity of use exponent different to -0.5 to avoid “accidental” degeneration of isomers was pointed out.

In order to calculate the vertex connectivity index for regular dendrimers we need to introduce some mathematical results that will be given below.

Let G be a regular dendrimer graph, then if G is a monocentric tree, the number of vertices in the s^{th} orbit or generation $n(s)$ is given by:

$$\mathbf{n(s) = \delta(\delta - 1)^{s-1} \quad ; \quad s \neq 0} \quad (3)$$

In case that the dendrimer be dicentric $n(s)$ is obtained as follows:

$$\mathbf{n(s) = 2(\delta - 1)^s \quad ; \quad s \neq 0} \quad (4)$$

A general expression to calculate the number of vertices in the s^{th} orbit of a regular dendrimer can be obtained from the combination of expressions (3) and (4):

$$\mathbf{n(s) = (k + 1) \cdot (\delta - k) \cdot (\delta - 1)^{s-1} \quad ; \quad s \neq 0} \quad (5)$$

where $k = 0$ for monocentric dendrimers and $k = 1$ for dicentric ones.

The total number of vertices, N , in the dendrimer can be obtained as follows:

$$\mathbf{N = (k + 1) + \sum_{s=1}^r n(s)} \quad (6)$$

where r is the number of orbits in the dendrimer. By combining (5) and (6) we obtain the following expression for the total number of vertices in G :

$$\mathbf{N = (k + 1) + (1 + \sum_{s=1}^r (\delta - k)(\delta - 1)^{s-1})} \quad (7)$$

and developing the geometrical progression given in (7) we have:

$$\mathbf{N = (k + 1) \left[\frac{(\delta - 1)^k (\delta - k) + k - 2}{\delta - 2} \right]} \quad (8)$$

In order to calculate the Randić χ index we can consider it as a combination of two χ indices, one of them χ_{ii} calculated from contributions coming from internal vertices in the dendrimer, i.e., those different from the end points, and the other χ_{ie} calculated from the end points contributions

$$\mathbf{\chi = \chi_{ii} + \chi_{ie}} \quad (9)$$

The χ_{ii} index is calculated as:

$$\chi_{ii} = \sum_{i=1}^{m_i} (\delta_i \delta_i)^g = m_i \cdot \delta^{2g} \quad (10)$$

where m_i is the number of internal vertices, i.e. those inside the r -1 orbit, having degree δ . The number of internal vertices m_i is obtained from the total number of vertices and the number of end points in G :

$$m_i = N - n(r) - 1 \quad (11)$$

where $n(r)$ is the number of vertices in the r th orbit, that is the number of end points. This number can be obtained from expression (5) to give:

$$m_i = N - (k+1) \cdot \delta^{1-k} \cdot (\delta-1)^{r+k-1} - 1 \quad (12)$$

and the internal vertex connectivity index is obtained as follows:

$$\chi_{ii} = (N-1)\delta^{2g} - (k+1)(\delta-1)^{(r+k-1)}\delta^{(2g-k+1)} \quad (13)$$

Following a similar procedure for χ_{ie} we obtain:

$$\chi_{ie} = (k+1)(\delta-1)^{(r+k-1)}\delta^{(g-k+1)} \quad (14)$$

and

$$\chi = \delta^{2g}(N-1) + (k+1)(\delta-1)^{(r+k-1)}\delta^{(g-k+1)}(1-\delta^g) \quad (15)$$

When, as in the original definition of Randić, $g = -1/2$, we have:

$$\chi_{-1/2} = \frac{N-1}{\delta} + \frac{(k+1)(\sqrt{\delta}-1)(\delta-1)^{(r+k-1)}}{\delta^k} \quad (16)$$

If we consider the case in which all the end points of a regular dendrimer are heteroatoms, i.e., atoms different from carbon and hydrogen, it is necessary to calculate a valence molecular connectivity index as defined by Kier and Hall [21]. This index will be obtained as follows:

$$\chi_{-1/2}^v = \frac{N-1}{\delta} + \frac{(k+1)(\delta-1)^{(r+k-1)}[(\delta^v)^{-0.5}\delta^{0.5}-1]}{\delta^k} \quad (17)$$

where δ^v is the valence degree for the heteroatom in the end point and δ is the degree of internal vertices in the dendrimer.

BOND (EDGE) ADJACENCY INDEX

The bond (edge) connectivity ε index [22] was introduced by Estrada as a measurement of molecular volume in alkanes. It was subsequently extended to molecules containing heteroatoms [23] and to account for spatial (3D) features [24] of organic molecules. The ε index is calculated by using the Randic graph theoretical invariant in which the vertex degrees is substituted by edge degrees. Mathematically, the index is obtained as follows

$$\varepsilon = \sum_{l=1}^S (\delta e_i \delta e_j)_l^g \quad (18)$$

where δe_i is the degree of edge i , S is the number of pairs of adjacent edges in the graph and g is an exponent which generally takes the value of -0.5 . It has been pointed out elsewhere that the edge degree can be expressed in terms of vertex degrees through the following expression:

$$\delta e_p = \delta_i + \delta_j - 2 \quad (19)$$

in which δ_i and δ_j are the degrees of vertices i and j incident to the edge e_p .

In regular dendrimers we can consider the ε index as the sum of three index accounting for contributions coming from pairs internal-internal adjacent edges ε_{ii} , pairs of internal-external adjacent edges ε_{ie} , and pairs of external-external adjacent edges ε_{ee} . One edge will be called internal if it is inside the $(r-2)$ th orbit or generation and external if it is outside this orbit, that is if it is incident to an external vertex (end point). It is straightforward to realize that the internal edges of the regular dendrimer have the same degree, $\delta e_i = 2\delta - 2$, and the external ones have degree $\delta e_e = \delta - 1$. Now, the expression for edge connectivity index can be written as:

$$\varepsilon = \varepsilon_{ii} + \varepsilon_{ie} + \varepsilon_{ee} \quad (20)$$

The ε_{ii} index can be calculated by adapting the expression (18) to consider internal edges only:

$$\varepsilon_{ii} = \sum_{l=1}^{S_{ii}} (\delta e_i)_k^{2g} = S_{ii} (2\delta - 2)^{2g} \quad (21)$$

where S_{ii} is the number of pairs of internal-internal edges, which can be obtained as follows:

$$S_{ii} = \binom{\delta}{2} N(r-2) \quad r \geq 2 \quad (22)$$

where $N(r-2)$ is the total number of vertices inside the $(r-2)^{\text{th}}$ orbit (including it):

$$S_{ii} = \frac{\delta(\delta-1)}{2} \left\{ (k+1) + (k+1)\delta^{1-k} \left[\frac{(\delta-1)^k - (\delta-1)^{r+k-2}}{2-\delta} \right] \right\}; \quad r \geq 2 \quad (23)$$

The internal edge connectivity index is then calculated as follows:

$$\varepsilon_{ii} = \frac{\delta}{4} (k+1)(2\delta-2)^{2g+1} \left\{ 1 + \delta^{1-k} \left[\frac{(\delta-1)^k - (\delta-1)^{r+k-2}}{2-\delta} \right] \right\}; \quad r \geq 2 \quad (24)$$

The internal-external edge connectivity index ε_{ie} can be calculated from the expression (18) by considering the number of pairs of internal-external adjacent edges S_{ie} in the dendrimer:

$$\varepsilon_{ie} = S_{ie} [(\delta-1)(2\delta-2)]^g \quad (25)$$

$$S_{ie} = (\delta-1) [(k+1)\delta^{1-k}(\delta-1)^{r+k-2}]; \quad r \geq 2 \quad (26)$$

The ε_{ie} index is then obtained from the following expression:

$$\varepsilon_{ie} = (k+1)(2\delta-2)^g \delta^{1-k} (\delta-1)^{g+r+k-1}; \quad r \geq 2 \quad (27)$$

In order to calculate the external-external edge connectivity index ε_{ee} we use the number of pairs of external-external adjacent edges S_{ee} , which is calculated as:

$$S_{ee} = \binom{\delta-1}{2} [(k+1)\delta^{1-k}(\delta-1)^{r+k-2}] \quad ; \quad r \geq 2 \quad (28)$$

The ε_{ee} index is calculated as follows

$$\varepsilon_{ee} = S_{ee} (\delta-1)^{2g} \quad (29)$$

$$\varepsilon_{ee} = \frac{\delta - 2}{2} (\delta - 1)^{2g+r+k-1} (k + 1) \delta^{1-k} \quad r \geq 2 \quad (30)$$

The edge connectivity index of regular dendrimers can be obtained by combining expressions (24), (27) and (30) in expression (20).

OTHER VERTEX CONNECTIVITY INDICES

As the equations for calculating the Rand≡ vertex index were established, it is easily to derive formulas for other two indices based on the connectivity in graph:

Zagreb Group index, M₂ [25]

$$M_2 = (N - n_r - 1) \delta^2 + n_r \delta \quad (31)$$

$$M_2 = \frac{\delta}{(\delta - 2)} [4(\delta - 1)^{(r+1)} - \delta^2 + k(k - 3)(\delta - 1)^r (\delta - 2)] \quad (32)$$

Bertz index, B [26]

$$B = (N - n_r) \binom{\delta}{2} \quad (33)$$

$$B = \left[\frac{2(\delta - 1)^{(r+1)} - 1}{(\delta - 2)} - (\delta - 1)^r k - (2 - k)(\delta - 1 + k)(\delta - 1)^{(r-1)} \right] \frac{(\delta - 1) \delta}{2} \quad (34)$$

Bertz index equals the number of connected pairs of edges in a regular dendrimer. Values of the above discussed indices are listed in Tables 1 and 2, for dendrimers having δ = 3 and 4 and generations up to ten.

Table 1.

Vertex and Edge Connectivity Indices for Regular Dendrimers Having δ = 3 and 4, and generations up to 10 Orbits

	N	$\chi_{-1/2}$ k = 0	$\varepsilon_{-1/2}$	N	$\chi_{-1/2}$ k = 1	$\varepsilon_{-1/2}$
δ = 3						
1	4	1.732	1.500	6	2.643	2.414
2	10	4.464	4.371	14	6.285	6.328
3	22	9.928	10.243	30	13.571	14.157
4	46	20.856	21.985	62	28.142	29.814
5	94	42.713	45.471	126	57.284	61.127
6	190	86.426	92.441	254	115.568	123.755
7	382	173.851	186.382	510	232.135	249.010

8	766	348.703	374.265	1022	465.270	499.519
9	1534	698.405	750.029	2046	931.540	1000.539
10	3070	1397.810	1501.558	4094	1864.080	2002.577
$\delta = 4$						
1	5	2	2.000	8	3.25	3.414
2	17	7	7.828	26	10.75	12.243
3	53	22	25.485	80	33.25	38.728
4	161	67	78.456	242	100.75	118.184
5	485	202	235.368	728	303.25	356.551
6	1457	607	714.103	2186	910.75	1071.654
7	4373	1822	2144.308	6560	2733.25	3216.962
8	13120	5467	6434.923	19680	8200.75	9652.885
9	39370	16400	19306.770	59050	24603.25	28960.655
10	118100	49210	57922.310	177100	73810.75	86883.966

Table 2.

Bertz and Zagreb Group Indices for Regular Dendrimers
Having $\delta = 3$ and 4, and generations up to 10 Orbits.

	N	B	M_2	N	B	M_2
r	k = 0			k = 1		
$\delta = 3$						
1	4	3	9	6	6	21
2	10	12	45	14	18	69
3	22	30	117	30	42	165
4	46	66	261	62	90	357
5	94	138	549	126	186	741
6	190	282	1125	254	378	1509
7	382	570	2277	510	762	3045
8	766	1146	4581	1022	1530	6117
9	1534	2298	9189	2046	3066	12261
10	3070	4602	18405	4094	6138	24549
$\delta = 4$						
1	5	6	16	8	12	40
2	17	30	112	26	48	184
3	53	102	400	80	156	616
4	161	318	1264	242	480	1912
5	485	966	3856	728	1452	5800
6	1457	2910	11632	2186	4368	17464
7	4373	8742	34960	6560	13116	52456
8	13120	26238	104944	19680	39360	157432
9	39370	78726	314896	59050	118092	472360
10	118100	236190	944752	177100	354288	1417144

Connectivity-type indices are highly intercorelated (correlating coefficient, $r > 0.9999$) in the set of homogeneous dendrimers with the degree 3 and 4 and generation up to ten.

The same correlation is shown vs. the number of vertices (i.e., the number of carbon atoms) in the dendrimer. It suggests that the connectivity-based indices are quite "amorphous" descriptors.

REFERENCES

1. G.R. Newkome, G.R. Baker, M.J. Saunders, P.S. Russo, V.K. Gupta.
2. Z.Q. Yao, J.E. Miller, K. Bouillon, *J.Chem.Soc., Chem.Comm.* (1986) 752.
3. A.M. Naylor, W.A. Goddard, G.E. Keifer, D.A. Tomalia, *J. Am.Chem.Soc.* **111** (1989) 2339.
4. A.B. Padies, H.K. Hall, D.A. Tomalia, J.R. McConnell, *J. Org.Chem.* **52** (1989) 5305.
5. C.J. Hawker, J.M. Frechet, *J. Am. Chem. Soc.* **112** (1990) 7638.
6. C.J. Hawker, R. Lee, J.M. Frechet, *J. Am. Chem. Soc.* **113** (1991) 4583.
7. K.L. Wooley, C.J. Hawker, J.M. Frechet, *J. Am. Chem. Soc.* **113** (1991) 4252; *Angew. Chem.* **106** (1994) 123.
8. D. Seebach, J.-M. Lapierre, K. Skobridis, G. Greiveldinger, *Angew. Chem.* **106** (1994) 457.
9. Z. Xu, J.S. Moore, *Angew. Chem.* **105** (1993) 261; 1394.
10. C. Worner, R. Mulhaupt, *Angew. Chem.* **105** (1993) 1367.
11. N. Launay, A.-M. Caminade, R. Lahana, J.-P. Majoral, *Angew.Chem.* **106** (1994) 1682.
12. M.R. Bruce, W. Devonport, A.J. Moore, *Angew. Chem.* **106** (1994) 1862.
13. D.A. Tomalia, A.M. Naylor, W.A. Goddard, *Angew.Chem., Int. Ed. Engl.*, **29** (1990) 138.
14. H.B. Melkburger, W. Jaworek, F. Vogtle, *Angew.Chem. Int. Ed. Engl.* **31** (1992) 1571.
15. F. Zeng, S.C. Zimmerman, *Chem. Rev.* **97** (1997) 1681.
16. M.V. Diudea, *Commun. Math. Comput. Chem. (MATCH)*, **32** (1995) 71.
17. M.V. Diudea, B. Parv, *J. Chem. Inf. Comput. Sci.* **35** (1995) 1015.
18. M.V. Diudea, G. Katona, B. Parv, *Croat. Chem. Acta*, **70** (1997) 509.
19. K. Balasubramanian, *J. Math. Chem.* **4** (1990) 89.
20. F. Harary, *Graph Theory*, Addison-Wesley, Reading, 1969.
21. M. Randić, *J. Am. Chem. Soc.* **97** (1975) 6609.
22. L.B. Kier, L.H. Hall, *Molecular Connectivity in Chemistry and Drug Research*, Acad. Press, N.Y. 1976.
23. E. Estrada, *J. Chem. Inf. Comput. Sci.* **35** (1995) 31.
24. E. Estrada, *J. Chem. Inf. Comput. Sci.* **35** (1995) 701.
25. E. Estrada, *J. Chem. Inf. Comput. Sci.* **35** (1995) 708.

26. I. Gutman, N. Trinajstić, *Chem. Phys. Lett.* **17** (1972) 535;
27. I. Gutman, B. Rušić, N. Trinajstić, C.F. Wilcox, Jr., *J. Chem. Phys.* **62** (1975) 3399.
28. S.H. Bertz, *Discr. Appl. Math.* **19** (1988) 65.

CLUJ AND SZEGED INDICES IN PROPERTY MODELING

M. ARDELEAN^A; G. KATONA^B; I. HOPARTEAN^A; M. V. DIUDEA^A

^a*Faculty of Chemistry and Chemical Engineering,
"Babeș-Bolyai" University, 3400 Cluj, Romania*

^b*"BIOS" Research and Production Centre, 3400 Cluj Napoca, Romania*

ABSTRACT. The novel Cluj and Szeged property indices are used for modeling biological and physico-chemical properties of a set of pirazolidin-diones (synthesised in our laboratory). These indices take into account the chemical nature of atoms (mass, electronegativity and partial charge), various kinds of interactions between the fragments of molecules as generated by Cluj and Szeged criteria and the 3D geometry of molecular structures as well. They offer good description for the antimicrobial and antifungal activity, surface tension ϵ and TLC Rf index of the compounds belonging to this class and some insight in the nature of intra- and intermolecular interactions governing the investigated molecular properties.

INTRODUCTION

A recent trend in structure-activity relationship (QSAR) and structure - property relationship (QSPR) is the use of topological and geometric parameters in evaluating and predicting the biological and physico-chemical properties of organic molecules. Topological indices (TIs) are single number descriptors of molecular topology and encode information regarding the size, shape, branching or centrality of molecular graphs. Geometric descriptors, such as the Euclidean distance between chemical substructures, total surface area and volume will complement the information supplied by TIs.¹⁻³

Several molecular properties, of which numerical value vary with changes in the molecular structure, such as the normal boiling point, critical temperature and pressure, viscosity, solubility, retention chromatographic index, are often used for characterizing chemicals in databases. It happens that a certain property is not available in tables or other reference sources, or it is dangerous to determine (e.g. because the substance is too toxic or explosive). Some novel compounds, with an

assumed structure, are rather instable in given experimental conditions, or simply, a compound is not available. In such cases, methods of evaluating physico-chemical properties from the structural features of organic molecules are welcome.²⁻⁶

Another interesting field of research in biochemistry and pharmacology is the rationalization of the action of classes of chemicals with specialized modes of action. Specificity in enzymology, immunology and toxicity arises out of specific structural features which lead to particular types of interaction, within the complex effector-receptor. Topological and geometric descriptors were used in many QSAR studies in the above domain.^{7,8}

The present paper reports an attempt to model the biological (antibiotic and antimycotic) and physico-chemical (chromatographic retention) properties of a group of 15 pirazolidin-3,5-diones (synthesised in our laboratories) by Cluj and Szeged property indices.

CLUJ AND SZEGED THEORETICAL DESCRIPTORS

The graph-theoretical descriptors⁹⁻¹⁴ CJ , CF and SZ represent the theoretical ground for counting the fragmental property indices. They are derived from the cardinality of the vertex sets defined by:

$$CJ_{i,j,p} = \{v \mid v \in V(G); di(G)_{v,i} < di(G)_{v,j}; \text{ and } \exists w \in W_{v,i}, V(w) \cap V(p) = \{i\}\} \quad (1)$$

$$CF_{i,j,p} = \{v \mid v \in V(G); di(G_p)_{v,i} < di(G_p)_{v,j}; G_p = G - p \quad (2)$$

$$SZ_{i,j} = \{v \mid v \in V(G); di(G)_{v,i} < di(G)_{v,j} \quad (3)$$

In the above relations, $G_p = G - p$ is the spanning subgraph, resulted by deleting the path p joining the vertices i and j (except its endpoints), $di(G)$ and $di(G_p)$ denote the topological distances measured in G and G_p , respectively.

The sets $CJ_{i,j,p}$ and $CF_{i,j,p}$ represent subgraphs (connected or not) in G , referred to the endpoint i and related to j and path p .

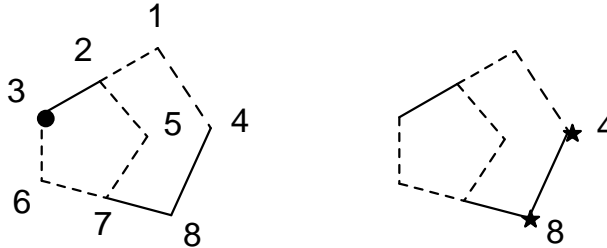
In defining *Cluj indices*, the *path* p plays the central role in selecting the subgraphs (eqs 1 and 2), particularly in cycle-containing graphs, where more than one path could join the pair (i,j) . In such graphs, more than one subgraph (i.e. fragment), referred to i , can be counted. By this reason, the nondiagonal entries $[UM]_{ij}$ in Cluj matrices are defined as the *maximum cardinality* of the sets supplied by eq 1 or 2

$$[UM]_{ij} = \max_p |V_{i,j,p}| \quad (4)$$

where $V_{i,j,p}$ is either $CJ_{i,j,p}$ or $CF_{i,j,p}$ and consists of vertices, v , lying *closer* to the vertex i than to the vertex j . When $p \in Di(G)$, (i.e. the set of all topological distances, or geodesics in G) then $M = CJD_i$ (Cluj-Distance) or CFD_i (Cluj-Fragmental-Distance). When $p \in De(G)$, (i.e. the set of all topological detours, or the longest distances in G) $M = CJDe$ (Cluj-Detour) or $CFDe$ (Cluj-Fragmental-

Detour). The diagonal entries are zero. The Cluj matrices are square arrays, of dimension $N \times N$, usually *unsymmetric* (excepting some symmetric regular graphs).

Figure 1 illustrates the construction of **CJDe** matrix.



Cluj Detour Sets $CJDe_{i,j,p}$; pair (3, 4):

(3, 4) [3, 6, 7, 5, 2, 1, 4]{ 3 } (4, 3) [4, 1, 2, 5, 7, 6, 3]{ 4, 8 }

Cluj-Detour Matrix **UCJDe**

0	1	1	1	1	1	2	1	8
2	0	2	2	2	2	2	3	15
2	1	0	1	1	1	1	1	8
1	1	2	0	2	2	1	1	10
1	1	1	1	0	1	1	1	7
1	1	1	1	1	0	1	2	8
3	2	2	2	2	2	0	2	15
1	2	1	1	1	1	1	0	8
11	9	10	9	10	10	9	11	79

$$IP2(CJDe) = 56$$

$$IE2(CJDe) = 15$$

Figure 1. Construction of Cluj Detour matrix, UCJDe

The entries in the *unsymmetric Szeged distance matrix*, **USZDi**, are supplied by the cardinality of the sets in eq 3. Note that in defining the Szeged fragments, the path joining the vertices i and j is irrelevant. Thus, for each pair (i,j) it results one and only one fragment.

When the distance criterion $di(G)_{v,i} < di(G)_{v,j}$ (eq 3) is changed by the *detour criterion* $de(G)_{v,i} < de(G)_{v,j}$, the cardinality of the sets thus supplied represent entries in the unsymmetric Szeged detour matrix, **USZDe**.

The above definitions hold for any connected graph.

The unsymmetric matrices can be symmetrized, e.g., by the Hadamard product with their transposes

$$SM_p = UM \bullet (UM)^T \tag{5}$$

$$SM_e = SM_p \bullet A \tag{6}$$

The symbol \bullet indicates the Hadamard (pairwise) matrix product (i.e. $[\mathbf{M}_a \bullet \mathbf{M}_b]_{ij} = [\mathbf{M}_a]_{ij} [\mathbf{M}_b]_{ij}$). In eq 6, the Hadamard product between the path-defined matrix \mathbf{SM}_p and the adjacency matrix \mathbf{A} (i.e. the matrix having the non-diagonal entries unity for two adjacent vertices and zero otherwise) provides the corresponding edge-defined matrix, \mathbf{SM}_e , which is a weighted adjacency matrix. For the symmetric matrices, the letter \mathbf{S} is usually missing.

In trees, \mathbf{CJDi} , \mathbf{CJDe} , \mathbf{CFDi} and \mathbf{CFDe} , are identical, due to the uniqueness of the path joining a pair of vertices (i, j) .

The above matrices allow the calculation of indices by relations given for the fragmental property indices.

FRAGMENTAL PROPERTY INDICES

Model Parameters

In physical phenomena, the macroscopic interactions are often interactions of field-type. The field is produced by a scalar function of potential. Let $f(x, y, z)$ be such a scalar function. The field induced by this function can be written as:

$$\vec{\nabla} \cdot f = \left(\frac{\partial}{\partial x} \vec{i} + \frac{\partial}{\partial y} \vec{j} + \frac{\partial}{\partial z} \vec{k} \right) \cdot f(x, y, z) = \frac{\partial f}{\partial x} \vec{i} + \frac{\partial f}{\partial y} \vec{j} + \frac{\partial f}{\partial z} \vec{k} \quad (7)$$

For the potential of type

$$f(x, y, z) = \rho z \quad (8)$$

the associated field can be derived as

$$\begin{aligned} \vec{\nabla} \cdot f &= \frac{\partial f}{\partial x} \vec{i} + \frac{\partial f}{\partial y} \vec{j} + \frac{\partial f}{\partial z} \vec{k} = \frac{\partial(\rho z)}{\partial x} \vec{i} + \frac{\partial(\rho z)}{\partial y} \vec{j} + \frac{\partial(\rho z)}{\partial z} \vec{k} = \\ &= 0\vec{i} + 0\vec{j} + \rho\vec{k} = \rho\vec{k} = \vec{p} \end{aligned} \quad (9)$$

This is the case of the well-known uniform gravitational field:

$$\vec{G} = m\vec{g} \quad (10)$$

with the corresponding potential given by

$$E_p = E_p(z) = mgz \quad (11)$$

where m is the mass of the probe and z is the reference coordinate.

Note that eq 9 is applicable both to the Newtonian (gravitational) interactions and the Coulombian (electrostatic) interactions. In both cases the relation is valid if the mass m (or the charge q) that generates the potential f and associated field $\vec{\nabla} \cdot f$ is far enough ($r \gg z$) so that the approximation $(r+z)^2/r^2 = (r^2 + 2rz + z^2)/r^2 = 1 + 2z/r + (z/r)^2 \cong 1$ is valid.

For the potential of type:

$$f(x, y, z) = \rho/z \quad (12)$$

eq 7 leads to the associated field:

$$\begin{aligned}\vec{\nabla} \cdot f &= \frac{\partial f}{\partial x} \vec{i} + \frac{\partial f}{\partial y} \vec{j} + \frac{\partial f}{\partial z} \vec{k} = \frac{\partial(p/z)}{\partial x} \vec{i} + \frac{\partial(p/z)}{\partial y} \vec{j} + \frac{\partial(p/z)}{\partial z} \vec{k} = \\ &= 0\vec{i} + 0\vec{j} + \frac{-p}{z^2} \vec{k} = -\frac{p}{z^2} \vec{k} = -\frac{p}{z^3} \vec{z} = -\frac{\vec{p}}{z^2}\end{aligned}\quad (13)$$

This is the case of well-known (non-uniform) gravitational field:

$$\vec{G} = \vec{G}(m, r) = -k \frac{m}{r^3} \vec{r} \quad (14)$$

and the associated potential of the form:

$$U = U(m, r) = k \frac{m}{r} \quad (15)$$

where m is the mass of the probe and r is the position relative to the location of the point producing the field.

For the Coulombian field eq 13 becomes:

$$\vec{F}_C = \vec{F}_C(r) = -k \frac{q}{r^3} \vec{r} \quad (16)$$

and the potential associated to the Coulombian field:

$$U = U(q, r) = k \frac{q}{r} \quad (17)$$

Four models were implemented in the view of building the *fragmental property indices*: two of them *topological* (dense topological and rare topological) and two others *geometric* (dense geometric and rare geometric). In these models a *weak dependence on distance* for the potential of the type (8) generating a uniform field (9), and a *strong dependence on distance* for the potential of the type (12) that generates a non-uniform field (13) were considered.

The variables in the models are: *property* Φ (mass M , electronegativity E , cardinality C , partial charge or any other atomic property P), *property descriptor* Ω ($p, d, pd, 1/p, 1/d, p/d, p/d^2, p^2/d^2$) and *superposition* Ψ (S, P, A, G, H).

The expressions for the *property descriptors* are:

$$\Omega.p = p ; d = d ; pd = p \cdot d ; 1/p = \frac{1}{p} ; 1/d = \frac{1}{d} ; p/d = \frac{p}{d} ; p/d^2 = \frac{p}{d^2} ; p^2/d^2 = \frac{p^2}{d^2} \quad (18)$$

where p is any property ($p \in \Phi$) and d is any metric of distance.

The (mathematical) superposition Ψ , given by

$$\Psi: S = \sum_{i=1}^n x_i ; P = \prod_{i=1}^n x_i ; A = S/n ; G = (\text{sgn}(P))^n \cdot \sqrt[n]{\text{abs}(P)} ; H = \left(\sum_{i=1}^n \frac{1}{x_i} \right)^{-1} \quad (19)$$

is applied upon a string of vertex descriptors to give a fragment descriptor. The used symbols are: $S = \text{sum}$; $P = \text{product}$; $A = \text{arithmetic mean}$; $G = \text{geometric mean}$ and $H = \text{harmonic sum}$. The summation is suitable in case of any additive property (mass, volume, partial charges, electric capacities, etc.). The other operators find appropriate justification.

MODEL DESCRIPTION

Let (i,j) be a pair of vertices and $Fr_{i,j}$ any fragment referred to i and related to j .

Dense Topological Model

Let v be a vertex in the fragment $Fr_{i,j}$. The property descriptor applies to the vertex property p_v and topological distance $d_{T_{v,j}}$. The fragmental *property descriptor* PD , resulting by the vertex descriptor superposition, gives the interaction of all the points belonging to the fragment $Fr_{i,j}$ with the point j :

$$PD(Fr_{i,j}) = \Psi_{v \in Fr_{i,j}} (\Omega (d_{T_{v,j}}, p_v)) \quad (20)$$

The j point can be conceived as an *internal probe atom* with no chemical identity.

Rare Topological Model

Within this model, the property descriptor applies to the fragmental property and topological distance $d_{T_{i,j}}$. The fragmental property descriptor models the interaction of the whole fragment $Fr_{i,j}$ with the point j and looks the global property being *concentrated* in the vertex i :

$$PD(Fr_{i,j}) = \Omega (d_{T_{i,j}}, \Psi_{v \in Fr_{i,j}} (p_v)) \quad (21)$$

Dense Geometric Model

The fragmental property descriptor is the vector sum of the vertex descriptor vectors. It applies the property descriptor to the vertex property p_v and the Euclidean distance $d_{E_{v,j}}$ in providing a *point of equivalent (fragmental) property* located at the Euclidean distance $d_{E_{CP,j}}$ (with $d_{E_{CP,j}}$ being the *distance of property*). The vector of the fragmental property has the orientation of this *distance vector*. The model simulates the interactions in non-uniform fields (gravitational, electrostatic, etc):

$$PD(Fr_{i,j}) = \left\| \sum_{v \in Fr_{i,j}} \vec{\Omega}(d_{E_{v,j}}, p_v) \right\|; \vec{\Omega} = \Omega \frac{\vec{d}_{E_{v,j}}}{d_{E_{v,j}}}; P(Fr_{i,j}) = \Psi_{v \in Fr_{i,j}} (p_v);$$

$$d_{E_{CP,j}} = \Omega_p^{-1} (DG(Fr_{i,j}), P(Fr_{i,j})), \quad (22)$$

where $d_{E_{CP,j}}$ is the distance that satisfies: $\Omega (d_{E_{CP,j}}, P(Fr_{i,j})) = PD(Fr_{i,j})$

Rare Geometric Model

The scalar fragmental descriptor applies the property descriptor to the *center of fragment property* and Euclidean distance between this center and the vertex j .

The model simulates the interactions in uniform fields (uniform gravitational, electrostatic, etc):

$$PD(Fr_{i,j}) = \Omega (d_{E_{CP,j}}, \Psi_{v \in Fr_{i,j}} (p_v));$$

$$\begin{aligned}
 CP_i(x_{CP,i,j}, y_{CP,i,j}, z_{CP,i,j}); x_{CP,i,j} &= \sum_{v \in Fr_{i,j}} x_v \cdot p_v / \sum_{v \in Fr_{i,j}} p_v \\
 y_{CP,i,j} &= \sum_{v \in Fr_{i,j}} y_v \cdot p_v / \sum_{v \in Fr_{i,j}} p_v; z_{CP,i,j} = \sum_{v \in Fr_{i,j}} z_v \cdot p_v / \sum_{v \in Fr_{i,j}} p_v
 \end{aligned} \quad (23)$$

Some Particular Fragmental Property Models were discussed elsewhere.¹⁴

Fragmental Property Matrices

The fragmental property matrices are non-symmetric square matrices of order N (i.e. the number of non-hydrogen atoms in the molecule). The non-diagonal entries in such matrices are fragmental properties corresponding to any pair of vertices (i,j) by a chosen model.

In case of Cluj criteria, the fragmentation can supply more than one maximal fragment for the pair (i,j) . In such cases, the matrix entry is the arithmetic mean of the individual values.

Thus, if $i, j \in V(G)$, $i \neq j$ and $P_{i,j} = \{p_{i,j}^1, p_{i,j}^2, \dots, p_{i,j}^k\}$ paths joining i and j , then cf. *CJ* or *CF* definition (eqs 1-3), the fragments $Fr_{i,j}^1, Fr_{i,j}^2, \dots, Fr_{i,j}^k$ are generated.

Let m be the number of maximal fragments among all the k fragments, $1 \leq m \leq k$, and let $\sigma_1, \dots, \sigma_m$ be the index for the maximal fragments.

By applying any of the above models, for all m maximal fragments we obtain m values, e.g.:

$$PD(Fr_{i,j}^{\sigma_1}), PD(Fr_{i,j}^{\sigma_2}), \dots, PD(Fr_{i,j}^{\sigma_m})$$

and consequently, the matrix entry associated to the pair (i,j) is the mean value:

$$PD_{i,j} = \frac{\sum_{t=1}^m PD(Fr_{i,j}^{\sigma_t})}{m} \quad (24)$$

The resulting matrices are in general *unsymmetric* but they can be symmetrized (see eqs 5, 6). The symbols for the fragmental property matrices will be detailed below.

Fragmental Property Indices

Fragmental property indices are calculated at any fragmental property matrices above discussed, by applying four types of index operators: P_- , P_2 , E_- , E_2 according to the relations:

$$\begin{aligned}
 P_-(M) &= \frac{1}{2} \sum \sum [\mathbf{M}]_{i,j} & ; P_2(M) &= \frac{1}{2} \sum \sum [\mathbf{M}]_{i,j} [\mathbf{M}]_{j,i}; \\
 E_-(M) &= \frac{1}{2} \sum \sum [\mathbf{M}]_{i,j} [\mathbf{A}]_{i,j} & ; E_2(M) &= \frac{1}{2} \sum \sum [\mathbf{M}]_{i,j} [\mathbf{M}]_{j,i} [\mathbf{A}]_{i,j}
 \end{aligned} \quad (25)$$

where \mathbf{M} is any property matrix, symmetric or unsymmetric.

Symbolism of the Fragmental Property Matrices and Indices

The name of *fragmental property matrices* is of the general form:

$$\mathbf{ABcDdEffffG} \quad (26)$$

where:

$\mathbf{A} \in \{\mathbf{D}, \mathbf{R}\}$; $\mathbf{D} = \text{Dense}$; $\mathbf{R} = \text{Rare}$;

$\mathbf{B} \in \{\mathbf{T}, \mathbf{G}\}$; $\mathbf{T} = \text{Topological}$; $\mathbf{G} = \text{Geometric}$;

$\mathbf{c} \in \{\mathbf{f}, \mathbf{j}, \mathbf{s}\}$; $\mathbf{f} = \text{CF-type}$; $\mathbf{j} = \text{CJ-type}$; $\mathbf{s} = \text{Sz-type}$;

$\mathbf{Dd} \in \{\mathbf{Di}, \mathbf{De}\}$; $\mathbf{Di} = \text{Distance}$; $\mathbf{De} = \text{Detour}$;

$\mathbf{E} \in \Phi$ (i.e. $\mathbf{E} \in \{\mathbf{M}, \mathbf{E}, \mathbf{C}, \mathbf{P}\}$ where $\mathbf{M} = \text{mass}$; $\mathbf{E} = \text{electronegativity}$; $\mathbf{C} = \text{cardinality}$; $\mathbf{P} = \text{other atomic property - implicitly, partial charge}$; explicitly, a property given by manual input);

$\mathbf{ffff} \in \Omega$ (i.e. $\mathbf{ffff} \in \{_p, _1/p, _d, _1/d, _p.d, _p/d, _p/d2, p2/d2\}$)

$\mathbf{G} \in \Psi$ (i.e. $\mathbf{G} \in \{\mathbf{S}, \mathbf{P}, \mathbf{A}, \mathbf{G}, \mathbf{H}\}$ with the known meaning (see above).

The name of *fragmental property indices* is of the general form:

$$\mathbf{ABcDdEffffGii} \quad (27)$$

where:

$\mathbf{ii} \in \{P_ , P2, E_ , E2\}$ with the known meaning (eq 25).

If an operator, such as $f(x)=1/x$ (inverse operator) or $f(x)=\ln(x)$, is applied the indices are labeled as follows:

$$\begin{aligned} \ln \mathbf{ABcDdEffffGii} &:= \ln(\mathbf{ABcDdEffffGii}); \\ 1/\mathbf{ABcDdEffffGii} &:= \frac{1}{\mathbf{ABcDdEffffGii}} \end{aligned} \quad (28)$$

For example, index $\ln \mathbf{DGfDeM_p_SP_}$ is the logarithm of index $\mathbf{DGfDeM_p_SP_}$ computed on the property matrix $\mathbf{DGfDeM_p_S}$. The model used is dense, geometric, on fragment of type *CF*, with the cutting path being detour. The chosen property is the mass, the descriptor for property is even the property (mass) and the sum operator counts the vertex descriptors.

The fragmental indices were calculated by the aid of **Cluj3Cmd** original 16-bit windows computer programs.

CORRELATING STUDIES

A mathematical model for correlating some biological activities or physical properties with molecular structures can be built up by using *multy linear regression MLR*.

MLR, for n observations and m independent variables is represented by equation

$$Y_i = b_0 + \sum_j^m b_{ij} X_{ij} \quad (29)$$

The regression coefficients b_{ij} can be determined by the least-squares method. Eq (29) can be used for estimating a chosen property in any other sets of chemical structures.

To avoid the chance correlations, it is recommended that the number of descriptors submitted to regression be less than 60 % of the number of observations in the training set.¹⁵

Within this work, biological activities as well as some physical properties of a set of 15 pirazolidin-3,5-diones were modeled by using **FPIF** descriptors.

The set of pirazolidin-3,5-diones

The molecules presented in Figure 2 were synthesized in our laboratory. The molecular structures were input and optimized by HyperChem (HyperCube Inc.) package. Partial charges were calculated by AM1 semiempirical approach.

1. Modeling Biological Activity

Pirazolidin-3,5-diones are known having antiinflammatory activity.¹⁶ They also show some antimicrobial and antifungal activity (on *Staphylococcus aureus*, *Bacillus subtilis*, *Escherichia coli*, *Pseudomonas aeruginosa*, *Candida albicans*, etc.). Table 1. shows the biological activity, in mm inhibition zone.

Table 1. Antimicrobial Activity; Inhibition Zone (mm)

Compound	Gram-positives			Gram-negatives			Fungi
	Staphyl. aureus	Staphyl epider	Bacill subtilis	Esc coli	Prot. vulg.	Pseu. aerug	Cand. albicans
1	0	0	0	0	0	0	0
2	10	10	10	0	0	0	0
3	14	10	13	0	0	10	0
4	12	17	14	0	0	10	10
5	0	0	10	0	0	10	10
6	0	0	10	0	0	10	10
7	12	0	10	0	0	10	0
8	12	0	10	0	0	10	0
9	12	0	10	0	0	10	0
10	12	10	10	0	0	0	10
11	12	13	13	0	0	10	12
12	0	0	12	0	0	10	13
13	0	0	0	0	0	10	12
14	0	0	0	0	0	0	0
15	0	0	0	0	0	0	0

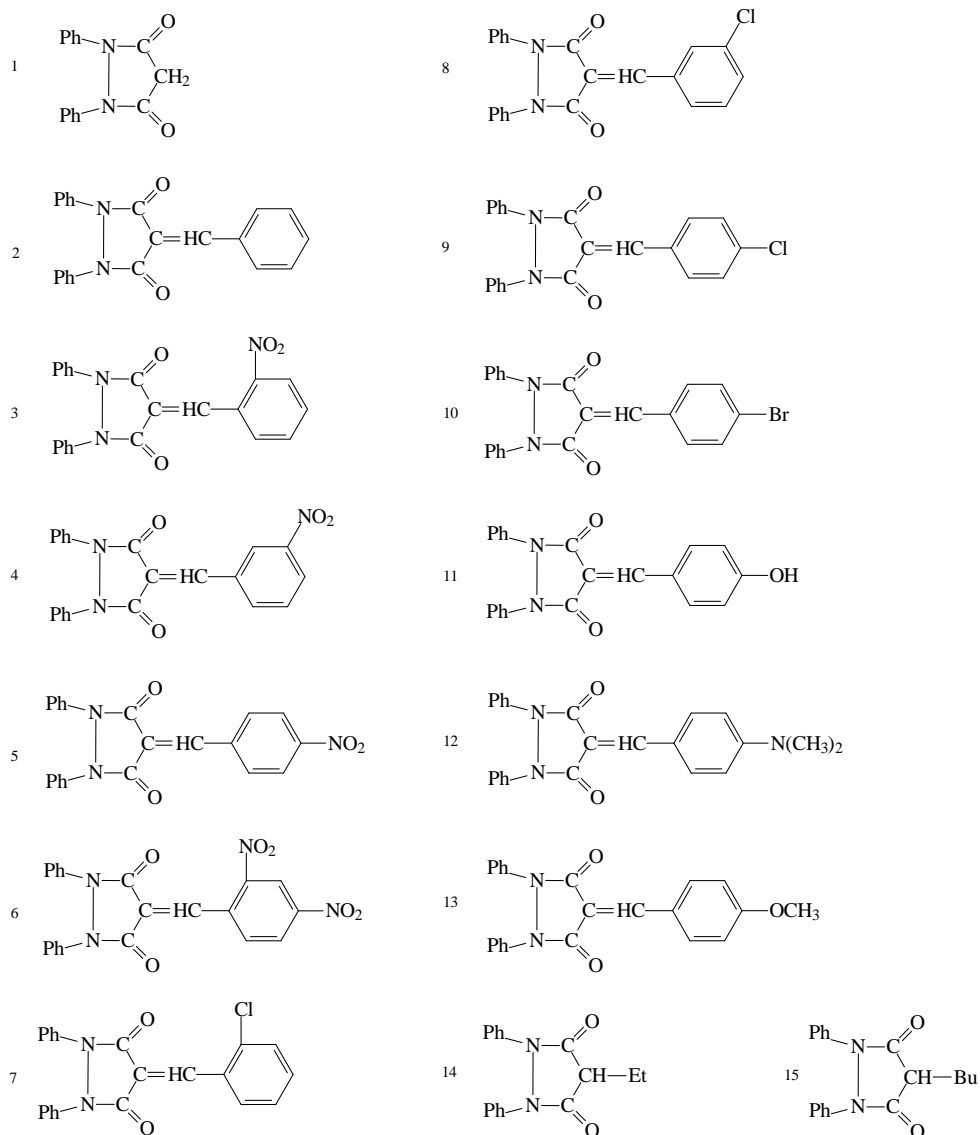


Figure 2. The set of Pirazolidin-3,5-diones

In the following, only two activities are considered for modeling: BA vs *Bacillus subtilis* and BA vs *Candida albicans*.

The activity vs. *Bacillus subtilis*, was estimated, in minovariate regression. The best three regression equations are given below:

$$BA_{\text{calc}} = -147,1950 + 35,4337 * \ln \text{RGjDeE_p/d_HP2} \quad (30)$$

CLUJ AND SZEGED INDICES IN PROPERTY MODELING

$$n = 15; r = 0.8320$$

$$BA_{\text{calc}} = -147,3113 + 35,4626 * \ln \text{RGfDeE_p/d_HP2} \quad (31)$$

$$n = 15; r = 0.8319$$

$$BA_{\text{calc}} = -75,9515 + 35,6724 * \ln \text{RGjDeC_p/d_HP2} \quad (32)$$

$$n = 15; r = 0.8316$$

In *bivariate* regression the model is still improved:

$$BA_{\text{calc}} = 21.0809 - 306.3117 * 1/\text{RGfDeC_p/d_HP2} + 4.4915 * \ln \text{DGjDeP_p_GE_} \quad (33)$$

$$n = 15; r = 0.9857$$

$$BA_{\text{calc}} = 6.2856 - 578.8831 * 1/\text{DGjDeP_p/d2PE_} + 4.8740 * \ln \text{DGjDeP_p*d_GE_} \quad (34)$$

$$n = 15; r = 0.9883$$

$$BA_{\text{calc}} = 4.0166 - 191.7906 * 1/\text{RGjDeC_p/d2HE_} + 4.9157 * \ln \text{DGjDeP_p*d_GE_} \quad (35)$$

$$n = 15; r = 0.9885$$

Figure 3 shows the plots given by eqs 33-35.

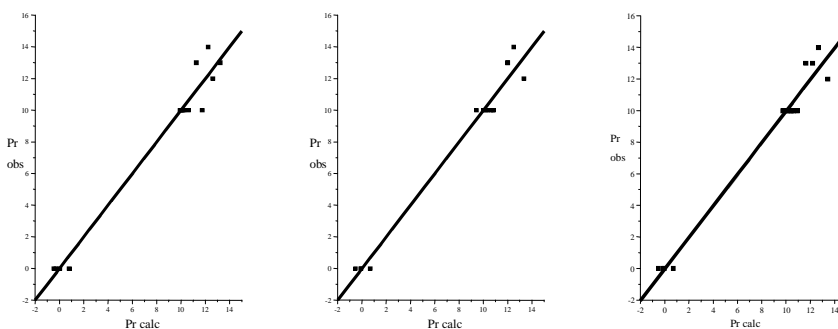


Figure 3. Bivariate regression: Plots BA_{obs} vs. BA_{calc} cf. eqs 33-35.

Table 2 includes the observed inhibitory activity vs. *Bacillus subtilis* and calculated BA by the above equations.

Table 2. Biological Activity BA_{obs} - and BA_{calc} by eqs 33-35.

Comp. No.	BA_{obs}	BA (eq 33)	BA (eq 34)	BA (eq 35)
1		9.9993	9.99972	9.99975
2		10.22805	10.60008	10.60684
3		9.9127	10.19882	10.1479
4		10.58298	10.36314	10.41585
5		10.07425	9.42429	9.72681
6		12.21854	12.49914	12.65926

7		13.21094	12.01476	12.15526
Table 2 (continued)				
8		11.72823	10.77013	10.90124
9		0.01434	0.68207	0.69076
10		0.79884	-0.07073	-0.04351
11		-0.46738	-0.53454	-0.5304
12		12.60716	13.32932	13.42582
13		11.2599	11.98897	11.61886
14		10.13089	10.84914	10.37846
15		-0.29874	-0.1143	-0.15289

As can be seen from eqs 30-35, the inhibiting activity of phtalazines vs *Bacillus subtilis* is controlled by the geometry (G in the symbol of indices) and electronic features of these molecules (E - electronegativity and P - partial charges).

The activity vs. *Candida albicans*, was estimated, in *monovariate* regression, as shown below:

$$BA_{\text{calc}} = -4.3416 + 1.5663 \cdot \ln DTfDeP_p*d_PP2 \quad (36)$$

n = 15; r = 0,9252

$$BA_{\text{calc}} = -4.1732 + 1.5461 \cdot \ln DTjDeP_p*d_PP2 \quad (37)$$

n = 15; r = 0,9235

$$BA_{\text{calc}} = -2.3616 + 1.4733 \cdot \ln DTfDiP_p*d_PP2 \quad (38)$$

n = 15; r = 0,8777

In *bivariate* regression the improvement of correlation was not so sound as in case of *Bacillus subtilis*:

$$BA_{\text{calc}} = 58.0019 + 1.9258 \ln DTfDiP_p*d_PP2 - 14.1524 \cdot \ln RGsDiEp2/d2GP2 \quad (39)$$

n = 15 ; r = 0.9415

$$BA_{\text{calc}} = 39.1986 + 1.9336 \cdot \ln DTfDiP_p*d_PP2 - 18.7211 \cdot \ln RGsDiE_p/d2AP2 \quad (40)$$

n = 15; r = 0.9429

$$BA_{\text{calc}} = 7.0326 + 2.3522 \ln DTjDiP_p*d_PP2 - 42.8766 \cdot RGfDeP_p/d_AP2 \quad (41)$$

n = 15; r = 0.9523

Figure 4 shows the plots given by eqs 39-41.

CLUJ AND SZEGED INDICES IN PROPERTY MODELING

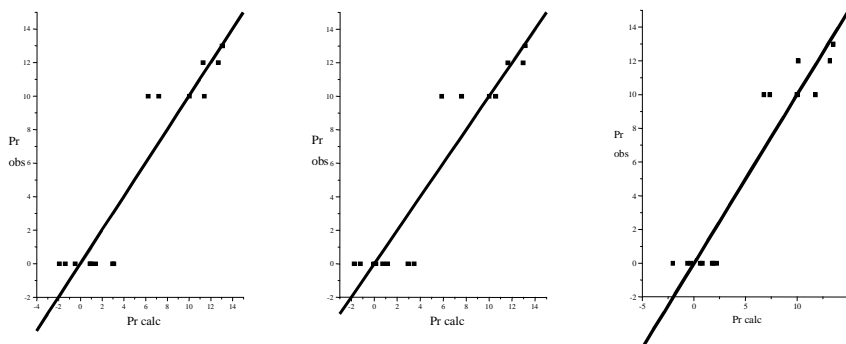


Figure 4. Bivariate regression: plots BA_{obs} vs. BA_{calc} cf. eqs 39-41.

Table 3. Biological Activity BA_{obs} - and BA_{calc} by eqs 39-41.

Comp. No.	BA_{obs}	BA (eq 39)	BA (eq 40)	BA (eq 41)
1		9.99997	10.0001	9.99971
2		3.04322	3.45234	2.19974
3		-0.50416	-0.04724	-2.04358
4		-1.94599	-1.75724	-0.63512
5		11.38851	10.55436	11.786
6		6.21494	5.85683	6.79134
7		1.34103	0.11115	0.59396
8		-1.41583	-1.24372	-0.31398
9		2.93834	2.92499	1.88119
10		0.91587	0.71163	0.8347
11		12.66418	12.95567	13.16947
12		13.03083	13.13947	13.49032
13		11.26882	11.61634	10.11394
14		7.1924	7.60017	7.34929
15		0.86788	1.12515	1.78304

From eqs 36-41, it is suggesting that the antimycotic activity of phtalazines is controlled basically by the topology (T) and geometry (G), on one hand and electronic features (P - partial charges and E - electronegativity) of molecules.

2. Modeling Physico-Chemical Properties

Two physico-chemical properties were considered: the surface tension ε , (in Dyn/cm²) and the chromatographic Rf values.

The **surface tension** ε ,¹⁶ was calculated by eq

$$\varepsilon=(P_i/M_v)^4 \quad (42)$$

where P_i is the parachor and M_v represents the molar volume. The values for ϵ are included in Table 4, along with FPIF descriptors showing the best scores in monivariate regression. The best mono- and bivariate QSPRs are listed below:

$$\epsilon = -65.7844 + 1.9019 \cdot \text{DTjDeE}_p/d2PE2 \quad (43)$$

n = 15; r = 0.8500

$$\epsilon = 2597 - 0.2155 \cdot \text{DTfDeE}_p/d2PP2 - 39,3342 \cdot 1/RTjDeP_p/d_GP2 \quad (44)$$

n = 15; r = 0,9299

The models are basically topological (see eqs 43-44). However, the results are far from those required in predicting studies.

The **TLC Rf values** were studied in the following. These values could give information about the global charge distribution as well as the steric feature of molecules.

Four solvent systems were considered for modeling Rf. The best scored regression equations are listed and plotted below:

Monivariate regression:

Solvent system 1

$$Rf_{\text{calc}} = -22.0579 - 220.8479 \cdot 1/RGfDeP_p/d_HP_ \quad (45)$$

n = 15; r = 0.9683

Solvent system 2

$$Rf_{\text{calc}} = 69.6434 - 231.0150 \cdot 1/RTsDiPp2/d2HP2 \quad (46)$$

n = 15; r = 0.8251

Solvent system 3

$$Rf_{\text{calc}} = 6.6979 - 151.3253 \cdot 1/RGfDeP_p/d_HP_ \quad (47)$$

n = 15; r = 0.8896;

Solvent system 4

$$Rf_{\text{calc}} = 9.5721 - 181.2313 \cdot 1/RGfDeP_p/d_HP_ \quad (48)$$

n = 15; r = 0.8856

The plot supplied by eq 45 is shown in Figure 5.

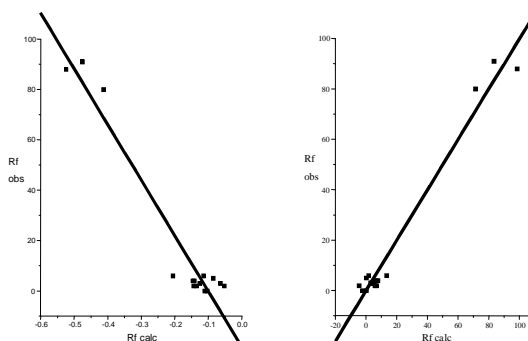


Figure 5. Mono- and bivariate regressions: solvent system 1, plots Rf_{obs} vs. Rf_{calc} cf. eqs 45 and 49.

Bivariate regression: the best scored regression equations are presented.

Solvent system 1

$$Rf_{\text{calc}} = -26.7898 - 261.2937 \cdot 1/RGfDeP_p/d_HP_ + 0.01356 \cdot DGjDeP_p_SP_ \quad (49)$$

n = 15; r = 0.9866

Solvent system 2

$$Rf_{\text{calc}} = 66.0139 + 0.0005 \cdot 1/RTsDiPp2/d2HP2 - 0.0213 \cdot RTjDeP_1/p_AE2 \quad (50)$$

n = 15; r = 0.9361

Solvent system 3

$$Rf_{\text{calc}} = 63.5664 + 14909.1133 \cdot \ln RGjDeP_p/d_HP_ - 38.3984 \cdot RTfDePp2/d2PP2 \quad (51)$$

n = 15; r = 0.9575

Solvent system 4

$$Rf_{\text{calc}} = 15.9934 + 2.8441 \cdot 1/RGfDeP_p/d_HP_ - 162.3196 \cdot 1/RTjDiP_p/d_GP_ \quad (52)$$

n = 15; r = 0.9566

The plot supplied by eq 49 is shown in Figure 5.

As can be seen from eqs 45-52, only the solvent system 1 Rf values are acceptably modeled by FPIF descriptors. The model is geometric (G) and the local property is the partial charge (P), as just expected for this property. Recall that Rf is strongly influenced by the steric and electronic properties of molecules in the mobile phase.

Conclusions

Some biological and physico-chemical properties of a set of pirazolidin-diones (synthesised in our laboratory) were modeled by the aid of FPIF descriptors. These indices take into account the chemical nature of atoms (mass, electronegativity and partial charge), various kinds of interactions between the fragments of molecules as generated by Cluj and Szeged criteria and the 3D geometry of molecular structures as well.

FPIF offer good description for various molecular properties of this class of compounds: the antimicrobial and antifungal activity, surface tension ϵ and TLC Rf index.

Despite a correlational model does not involve a causal relationship between descriptors and a molecular property. However, a look upon the nature of the best scored fragmental property indices can give insight of the type of intra- and/or intermolecular interactions. The results are encouraging in case of modeling

the activity vs *Bacillus subtilis* and *Candida albicans* as well as for the Rf index. They demonstrate the usefulness of our descriptors in modeling biological and physical properties of organic compounds.

Acknowledgement. This work is under financial support of GRANT CNSIS, T 34, 2000.

REFERENCES

1. Balaban, A. T., editor, *From Chemical Topology to Three-Dimensional Geometry*, Plenum Publishing Corporation, New York. (a) Chapter 1 by Balaban, A.T. *From Chemical Graphs to 3D Molecular Modeling*, pp. 1-24. (b) Chapter 2 by Mezey, P. G., *Descriptors of Molecular Shape in 3D*, pp. 25-42. (c) Chapter 3 by Mekenyan, O.; Veith, G. D., *3D Molecular Design: Search for Active Conformers in QSAR*, pp. 43-72. (d) Chapter 4 by Basak, S. C.; Grunwald, G. D.; Niemi, G. J., *Use of Graph-Theoretic and Geometric Molecular Descriptors in Structure-Activity Relationships*, pp. 73-116. (e) Chapter 6 by Randic, M.; Razinger, M., *On Characterization of 3D Molecular Structure*, 1997, pp. 159-236.
2. Devillers, J.; Balaban, A. T., editors, *Topological Indices and Related Descriptors in SAR and QSPR*, Gordon and Breach, Reading, UK, 1999.
3. Diudea, M. V., editor, *QSAR/QSPR Studies by Molecular Descriptors*, Nova Science, Huntington, N.Y. (in press).
4. Katritzky, A. R.; Gordeeva, E. V., *Traditional Topological Indices vs. Electronic, Geometrical and Combined Molecular Descriptors in QSAR/QSPR Research*, J. Chem. Inf. Comput. Sci., 1993, 33, 835-857.
5. Suzuki, T. Ohtaguchi, K.; Koide, K. *Computer-assisted approach to develop a new prediction method of liquid viscosity of organic compounds*, Computers Chem. Engng. 1996, 20, 161-173.
6. Viswanadhan, V. N.; Ghose, A. K.; Singh, U. C.; Wendoloski, J. J. *Prediction of solvation free energies of small organic molecules: additive-constitutive models based on molecular fingerprints and atomic constants*, J. Chem. Inf. Comput. Sci. 1999, 39, 405-412.
7. Basak, S. C.; Gute, B. D.; Ghatak, S. *Prediction of complement-inhibitory activity of benzamidines using topological and geometric parameters*, J. Chem. Inf. Comput. Sci. 1999, 39, 255-260.
8. Raychaudhury, C.; Banerjee, A.; Bag, P.; Roy, S. *Topological Shape and Size of Peptides: identification of potential allele specific helper T cell antigen sites*, J. Chem. Inf. Comput. Sci. 1999, 39, 248-254.
9. Diudea, M. V. *Cluj matrix invariants*, J.Chem.Inf.Comput.Sci. 1997, 37, 300-305.
10. Diudea, M. V. *Cluj Matrix CJ_{ij} : source of various graph descriptors*, Commun. Math. Comput. Chem. (MATCH), 1997, 35, 169-183.
11. Diudea, M., Minailiuc V. O., Katona G. and Gutman I. *Szeged Matrices and Related Numbers*, Commun. Math. Comput. Chem. (MATCH), 1997, 35, 129-143.

CLUJ AND SZEGED INDICES IN PROPERTY MODELING

12. Diudea, M. V., Pârv, B. and Topan, M. I. *Derived Szeged and Cluj Indices*, J. Serb.Chem.Soc., 1997, 62, 267-276.
13. Minailiuc O., Katona G., Diudea, M. V., Strunje, M., Graovac, A. and Gutman, I. *Szeged Fragmental Indices*, Croat. Chem. Acta., 1998, 71, 473-488.
14. 14. Jäntschi, L., Katona, G. and Diudea, M. V. *Modeling Molecular Properties by Cluj Indices*, Commun. Math. Comput. Chem. (MATCH), 2000, 41, 151-188.
15. Topliss, J. G.; Edwards, R. P. *Chance factors in in studies of Quantitative Structure-Activity Relationships*, J. Med. Chem. 1979, 22, 1238.
16. 16. Ardelean, M. Master Dissertation, Babeş-Bolyai Univ., Faculty of Chemistry and Chemical Engineering, 2000.

CORRELATING STUDIES BY CLUJ AND SZEGED INDICES

A.A. KISS, G. TURCU AND M.V. DIUDEA *

*Faculty of Chemistry and Chemical Engineering,
"Babeș-Bolyai" University, 3400 Cluj, Romania*

ABSTRACT. The correlating ability of Cluj and Szeged indices was tested on two sets of poly-chlorinated bipheniles (PCB) and barbiturates. The molecular property was the *vapor pressure*, at 25°C and 100°C, and *log P*, respectively. The results are discussed in comparison with some well known topological indices.

INTRODUCTION

QSPRs (Quantitative Structure-Property Relationships) link in a quantitative manner the physico-chemical properties of chemicals with the molecular structure.¹

Some molecular properties (i.e. those of which numerical value vary with changes in the molecular structure) such as the normal boiling point, critical parameters, viscosity, solubility, retention chromatographic index, are often used for characterizing chemicals in databases. However, a certain property is not always available in tables or other reference sources. It is just the case of newly synthesized compounds. As a consequence, methods of evaluating physico-chemical properties from the structural features of organic molecules become very important.

Monitoring the environmental pollution needs the prediction of toxicity of chemicals in air, waste waters and soil. **QSARs** (Quantitative Structure-Property Relationships) can be used to predict the toxicity accurately, without using more expensive experimental methods.² Drug research and production is also related to the **QSAR** techniques.³

In this work new correlating results by using Cluj and Szeged topological indices are reported, with the aim to demonstrate the capability of our indices to model the molecular properties of organic compounds.

* E-mail: diudea@chem.ubbcluj.ro

The above mentioned indices are calculated on the ground of the Cluj and Szeged matrices,⁴⁻¹⁰ respectively. Before defining these matrices, some graph-theoretical background is needed.

Definitions

Let $G = (V, E)$ be a connected graph, with V being the set of vertices and $E \subset V \times V$ the set of edges.

A walk w is¹¹ an alternating string of vertices and edges, $w_{1,n} = (v_1, e_1, v_2, e_2, \dots, v_{n-1}, e_m, v_n)$, $v_i \in V(G)$, $e_i \in E(G)$, $m \geq n - 1$, such that any subsequent pair of vertices $(v_{i-1}, v_i) \in E(G)$. Revisiting of vertices and edges is allowed. Then $V(w_{1,n}) = \{v_1, v_2, \dots, v_{n-1}, v_n\}$ is the set of vertices of $w_{1,n}$. Similarly, $E(w_{1,n}) = \{e_1, e_2, \dots, e_{m-1}, e_m\}$ is the set of edges of $w_{1,n}$. The length of a walk, $l(w_{1,n}) = |E(w_{1,n})| \geq |V(w_{1,n})| - 1$, equals to the number of its traversed edges. The walk is closed if $v_1 = v_n$ (i.e. its endpoints coincide) and is open otherwise. The set of all walks in G is denoted by $W(G)$.

A path p is a walk having all its vertices and edges distinct: $v_i \neq v_j$, $(v_{i-1}, v_i) \neq (v_{j-1}, v_j)$ for any $1 \leq i < j \leq n$. As a consequence, the revisiting of vertices and edges, as well as branching, is prohibited. The length of a path is $l(p_{1,n}) = |E(p_{1,n})| = |V(p_{1,n})| - 1$. A closed path is a cycle (i.e. circuit). The set of all paths in G is denoted by $P(G)$.

The distance, d_{ij} , between two vertices v_i and v_j is the length of a shortest path joining them, if exists: $d_{ij} = \min l(p_{ij})$; otherwise $d_{ij} = \infty$. A shortest path is often called a geodesic. The eccentricity of a vertex i , ecc_i , is the maximum distance between i and any vertex j of G : $ecc_i = \max d_{ij}$. The radius of a graph, $r(G)$, is the minimum eccentricity among all vertices i in G : $r(G) = \min ecc_i = \min \max d_{ij}$. Conversely, the diameter, $d(G)$, is the maximum eccentricity in G : $d(G) = \max ecc_i = \max \max d_{ij}$. The set of all geodesics (i.e. distances) in G is denoted by $D(G)$.

Cluj Indices

The Cluj Sets, $CJ_{i,j,p}$ collect vertices obeying the relation

$$CJ_{i,j,p} = \{v \mid v \in V(G); d(G)_{v,i} < d(G)_{v,j}; \text{ and } \exists w \in W_{v,i} V(w) \cap V(p) = \{i\}\} \quad (1)$$

where $d(G)$ denotes the topological distance in G and $p \in D(G)$.

$CJ_{i,j,p}$ represent subgraphs (connected or not) in G , related to the endpoint i and referred to j and path p . In Cluj criterion, the path p (joining the vertices i and j) plays the central role in selecting the sets/fragments. In cycle-containing graphs, more than one path could join the pair (i, j) thus resulting more than one fragment related to i . We define the nondiagonal entries $[UCJ]_{ij}$ in the Cluj matrices as

$$[UCJ]_{ij} = \max_p |CJ_{i,j,p}| \tag{2}$$

where $|CJ_{i,j,p}|$ is the cardinality of the set $CJ_{i,j,p}$. The diagonal entries are zero.

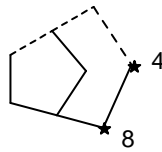
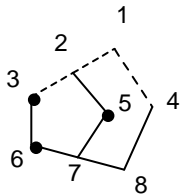
The above definition holds for any connected graph.

The Cluj matrices are square arrays, of dimension $N \times N$, usually *unsymmetric* (excepting some symmetric regular graphs). They can be symmetrized, e.g., by the Hadamard product with their transposes

$$SCJ_p = UCJ \bullet (UCJ)^T \tag{3}$$

$$SCJ_e = SCJ_p \bullet A \tag{4}$$

The symbol \bullet indicates the Hadamard (pairwise) matrix product¹² ($[M_a \bullet M_b]_{ij} = [M_a]_{ij} [M_b]_{ij}$). For the symmetric matrices, the letter **S** is usually missing. In eq 4, the Hadamard product between the path-defined matrix SCJ_p and the adjacency matrix **A** (i.e. the matrix having the non-diagonal entries unity for two adjacent vertices and zero otherwise) provides the corresponding edge-defined matrix, SCJ_e , which is a weighted adjacency matrix. An example of $CJ_{i,j,p}$ set is illustrated in Figure 1.



$$CJ_{3,4,(3,2,1,4)} = \{3, 6, 5\}$$

$$CJ_{4,3,(4,1,2,3)} = \{4, 8\}$$

Cluj Matrix, **UCJ**

0	3	3	4	2	2	2	3	19
5	0	4	4	4	4	3	3	27
3	2	0	<u>3</u>	2	3	3	2	18
3	2	<u>2</u>	0	2	2	2	3	16
3	3	3	4	0	3	3	3	22
2	3	3	3	2	0	2	3	18
3	3	4	4	4	4	0	5	27
3	2	2	4	2	3	3	0	19
22	18	21	26	18	21	18	22	

$$CJ_p = 243$$

$$CJ_e = 103$$

Figure 1. Construction of Cluj matrix, **UCJ**

Cluj indices are calculated from the above matrices, by:

$$CJ_e = \frac{1}{2} \sum \sum [M]_{i,j} [A]_{i,j} ; \quad CJ_e = \sum \sum [UM]_{i,j} [UM]_{j,i} [A]_{i,j} \quad (5)$$

Szeged Indices

Szeged Fragments, $SZ_{i,j}$ representing the entries in the unsymmetric Szeged matrices, USZ , are defined by:^{5,7,8}

$$SZ_{i,j} = \{v \mid v \in V(G); d(G)_{v,i} < d(G)_{v,j}\} \quad (6)$$

and the corresponding indices are calculated cf. eq 5. In any graph, $CJ_e = SZ_e$ and, in general, $CJ_p \neq SZ_p$.

In the view to account for heteroatoms and multiple bonds in molecular graph, we introduced the **Szeged property matrices**:¹⁰

$$[USZP]_{ij} = P_{i,p} \quad (7)$$

$$P_{i,p} = f(P_v) \mid v \in V(G); d(G)_{v,i} < d(G)_{v,j} \quad (8)$$

$$f(P_v) = m \sum_v P_v \quad (9)$$

$$f(P_v) = (\Pi_v P_v)^{1/N} \quad (10)$$

The summation and product in eqs 9 and 10 run over all vertices in graph.

Entries in a Szeged property matrix (see eq 7), in fact properties $P_{i,p}$ of vertex i (with respect to the path p), are defined by a function $f(P_v)$, evaluated on vertices v which obey the Szeged index condition (see eq 6). In other words, the set of such vertices can be viewed as a fragment (i.e., a subgraph). Consequently, $P_{i,p}$ can be viewed as a fragmental property. $P_{i,p}$ is mainly a topological (local) property (e.g., a topological index) but other physico-chemical properties are also considered (e.g., atomic mass or group electronegativities – see below). Two types of $f(P_v)$ are here proposed: an additive and a multiplicative one.

Several cases of the **additive function** (eq 9) are considered:

- $P_v = 1$ (i.e., the cardinality) and the weighting factor $m = 1$ (classical **USZ** matrix).
- $P_v =$ some vertex property; $m = 1$; (property matrix, **USZP**).
- $P_v =$ some vertex property; $m = 1/P(G)$; $P(G)$ is a global property of the graph;
- $P_v = \sum_v A_v$; $m = 1/12$; A_v is the atomic mass and the matrix, **USZA**. The factor m indicates that $f(P_v)$ is a fragmental mass, relative to the carbon atomic mass.

The **multiplicative function** (eq 10) was used for group electronegativities: $P_v = X_v$; (**USZX** matrix). X_v is a local electronegativity, calculated from the Sanderson group electronegativities, for heteroatoms and fragments.¹³

The corresponding **property indices** are calculated cf. eq 5.

Correlating Studies

The mathematical models of a certain property are performed by MLR (Multiple Linear Regression) and/or CNN (Computational Neural Networks). In our case, the model is built by using MLR. Next, it is validated by the *leave-one-out* cross-validation procedure. In the following, the MLR procedure is presented.

MLR, for n observations and m independent variables is represented by

$$Y_i = b_0 + \sum_j^m b_{ij} X_{ij} \quad (11)$$

or, in matrix form as

$$\mathbf{Y} = \mathbf{bX} \quad (12)$$

where \mathbf{Y} is the $n \times 1$ vector of responses, \mathbf{X} is an $n \times (m + 1)$ matrix of independent variables and \mathbf{b} is the $(m + 1) \times 1$ vector of regression coefficients. The regression coefficients can be determined by the least-squares solution of (12)

$$\mathbf{b} = (\mathbf{X}^T \mathbf{X})^{-1} \mathbf{X}^T \mathbf{Y} \quad (13)$$

With \mathbf{b} calculated, eq 12 can be used for estimating the chosen property for other chemical structures.

To avoid the chance correlations, it is recommended that the number of descriptors submitted to regression be less than 60 % of the number of observations in the training set.¹⁴

Set 1. Poly-Chlorinated Bipheniles.

A set of 15 Poly-Chlorinated Bipheniles (PCB - Table 1) was correlated against the vapor pressure (as log), at 25°C and 100°C, respectively. This property is important in connection with the toxicity of this class of compounds.

Statistics of the correlation are given in Tables 2 and 3.

It can be seen that our descriptors are able to model this property at least as well as the Wiener W , and hyper-Wiener indices.¹⁵ The Szeged index weighted with the electronegativity brings some improvement in correlation. However, it is not a strong evidence of the electronegativity contribution since the set is a congeneric one.

The results of the bivariate regression can be used in prediction studies.

Table 2. Correlation of PCB: $\log VP(25^\circ C) = a + bx_1 + cx_2 \dots$

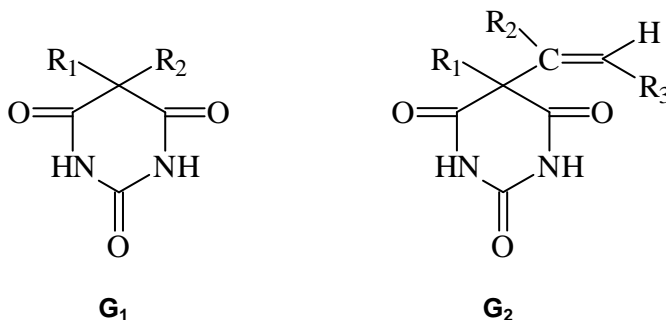
Indices	a	b	c	r	s	F
CJ _e	1.9971	-0.0059	-	0.9649	0.5259	175.82
CJ _p	1.6213	-0.0015	-	0.9704	0.484	209.98
SZ _e	2.0179	-0.0060	-	0.9646	0.528	174.32
W	1.6787	-0.0093	-	0.9630	0.5401	166.03
WW	1.2497	-0.0030	-	0.9703	0.4843	209.67
CJ _e + SZ _p X	-8.5702	-0.0258	0.0287	0.9817	0.397	159.67
CJ _p + SZ _p X	-5.2096	-0.0030	0.0174	0.9810	0.4044	153.65
SZ _e + SZ _p X	-8.4933	-0.0159	0.0287	0.9812	0.4023	155.33

Table 3. Correlation PCB: $\log VP(100^\circ C) = a+bx_1+cx_2 \dots$

Indices	a	b	c	r	s	F
CJ _e	4.0565	-0.0045	-	0.9753	0.3398	156.22
CJ _p	3.7665	-0.0011	-	0.9833	0.2799	234.07
SZ _e	4.067	-0.0045	-	0.9742	0.3471	149.44
SZ _p	2.4867	-0.0003	-	0.9758	0.3362	159.75
W	3.8154	-0.0071	-	0.9744	0.3457	150.67
WW	3.4661	-0.0023	-	0.9819	0.2915	215.18
CJ _e + CJ _p	2.8123	0.0137	-0.0045	0.9934	0.1876	265.92
CJ _p + SZ _e	2.8591	-0.0042	0.0125	0.9936	0.1853	272.61
CJ _p + SZ _p X	-0.8422	-0.0021	0.0117	0.9930	0.1944	247.45
CJ _p + W	3.5364	-0.0044	0.0207	0.9941	0.1791	291.91

Set 2. Barbiturates.

A set of 25 barbiturates¹⁶ (Table 4) was correlated against the logP. This property is important in connection with the drug membrane transport phenomena.



Statistics of data included in Table 4 are given in Table 5. For comparison, the correlation shown by the super-index EATI₁ in monivariate regression was: $r = 0.9293$; $s = 0.232$.¹⁶ It is clear that the Szeged property index SZ_eA (Table 5, entry 4) is far more appropriate in modeling logP. The plot SZ_eA vs logP is shown in Figure 2.

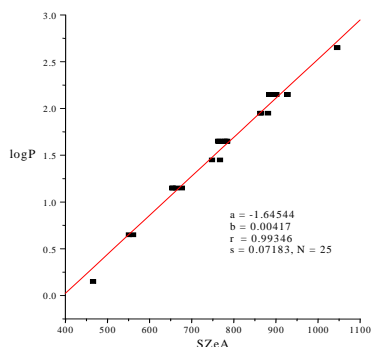
Table 5. Statistics for Data in Table 4: $\log P = a + \sum b_i X_i$

No.	X _i	b	a	r	s	cv (%)	F
1	SZ _p	0.0003	0.0604	0.9085	0.2627	15.924	108.82
2	SZ _e	0.0045	-1.1072	0.9562	0.1840	11.154	245.66
3	SZ _p A	0.0002	-0.1949	0.9541	0.1883	11.415	233.53
4	SZ_eA	0.0041	0.9934	0.9935	0.0718	4.354	1740.58
	Cross Validation		-	0.9913	0.0824	4.999	-

CORRELATING STUDIES BY CLUJ AND SZEGED INDICES

Table 5 (continued)

5	SZ _p X	0.0136	-0.8170	0.8310	0.3498	21.202	51.34
6	SZ _e X	0.1397	-1.6967	0.7075	0.4445	26.941	23.03
7	SZ _p SZ _e	-0.0005 0.0121	-2.9098	0.9872	0.1023	6.202	423.46
8	SZ _p SZ _e A	0.0000 0.0044	-1.7284	0.9938	0.0717	4.351	871.96
11	SZ _e SZ _p X	0.0080 -0.0131	-0.9247	0.9881	0.0991	6.006	452.38
12	SZ _e SZ _e X	0.0066 -0.1021	0.0401	0.9895	0.0931	5.643	513.80
13	SZ _p A SZ _e A	-0.00001 0.00486	-1.8626	0.9943	0.0685	4.157	956.23
	Cross Validation		-	0.9921	0.0721	4.796	-

**Figure 2.** The plot SZ_eA vs logP

On the other hand, the Szeged property indices weighted with electronegativities show lower ability in describing this property (entries 5,6, 11 and 12). No significant improvement was recorded in bivariate regression (entries 7 - 13). The cross-validation test (no significant drop in r-value) indicates the good predicting ability of the equations given in entries 4 and 13.

Concluding, the original descriptors, Cluj and Szeged-property, demonstrated a good ability in modeling some important physico-chemical properties. In the particular case of logP of barbiturates, the recorded results surpass that reported in literature and can be used in predicting studies.

Acknowledgement. This work is under financial support of GRANT CNSIS, T 34, 2000.

REFERENCES

- Free, S. M.; Wilson, J. W. A mathematical contribution to structure-activity studies, *J. Med. Chem.* **1964**, *7*, 395.
- Gao, C.; Govind, R.; Tabak, H. H. Application of the group contribution method for predicting the toxicity of organic chemicals. *Environmental Toxicol. Chem.* **1992**, *11*, 631-636.
- Diudea, M., Ed., QSPR/QSAR studies by molecular descriptors, NOVA SCIENCE Publishers, Inc., Huntington, N. Y., 2000
- Diudea, M.V. Cluj matrix CJ_u : source of various graph descriptors, *Commun. Math. Comput. Chem. (MATCH)*, **1997**, *35*, 169-183.
- Diudea, M.V.; Minailiuc, O.; Katona, G.; Gutman, I. Szeged matrices and related numbers, *Commun. Math. Comput. Chem. (MATCH)*, **1997**, *35*, 129-143.
- Diudea, M.V. Cluj matrix invariants, *J. Chem. Inf. Comput. Sci.* **1997**, *37*, 300-305.
- Diudea, M.V.; Pârv, B.; Topan, M.I. Derived Szeged and Cluj indices, *J. Serb. Chem. Soc.* **1997**, *62*, 267-276.
- Kiss, A.A.; Katona, G.; Diudea, M.V. Szeged and Cluj matrices within the matrix operator $W_{(M_1, M_2, M_3)}$ *Coll. Sci. Papers Fac. Sci. Kragujevac* **1997**, *19*, 95-107.
- Gutman, I.; Diudea, M.V. Defining Cluj matrices and Cluj matrix invariants, *J. Serb. Chem. Soc.* **1998**, *63*, 497-504.
- Minailiuc, O.; Katona, G.; Diudea, M.V.; Strunje, M., Graovac, A.; Gutman, I. Szeged fragmental indices, *Croat. Chem. Acta* **1998**, *71*, 473-488.
- Jäntschi, L.; Katona, G.; Diudea, M. V. Modeling molecular properties by Cluj indices, *Commun. Math. Comput. Chem. (MATCH)*, **2000**, *41*, 151-188.
- Horn, R.A.; Johnson, C.R. *Matrix Analysis*; Cambridge Univ. Press, Cambridge, **1985**.
- Diudea M.V.; Kacso I.E.; Topan M.I. Molecular topology. 18. A Qspr/Qsar study by using new valence group carbon-related electronegativities. *Rev. Roum. Chim.* **1996**, *41*, 141-157.
- Topliss, J. G.; Edwards, R. P. Chance factors in in studies of Quantitative Structure-Activity Relationships. *J. Med. Chem.* **1979**, *22*, 1238.
- Diudea, M.V.; Gutman, I. Wiener-type topological indices, *Croat. Chem. Acta* **1998**, *71*, 21-51.
- Guo, M.; Xu, L.; Hu, C.Y.; Yu, S. M. Study on structure-activity relationship of organic compounds - applications of a new highly discriminating topological index. **1997**, *35*, 185-197.

THE EFFECT OF COPPER, LEAD AND IRON IONS ON THE OXIDATION OF MERCAPTOSUCCINIC ACID BY CHROMATE

ALEXANDRA RUSTOIU-CSAVDARI, IOAN BALDEA

*"Babeș-Bolyai" University, Faculty of Chemistry and Chemical Engineering,
Department of Physical Chemistry, 11 Arany Janos Street,
3400 Cluj-Napoca, E-mail: arustoiu@chem.ubbcluj.ro*

ABSTRACT. The effect of copper, lead and iron ions on the oxidation of mercaptosuccinic acid (thiomalic acid or TMA) by chromate in acidic media has been investigated in order to draw a conclusion about its potential use in kinetic analysis. Similar studies have been carried out for the oxidation of mercaptoacetic acid (thioglycolic acid or TGA), but only in the presence of lead. All ions increase the overall reaction rate: the Fe(II)-Fe(III) couple *via* an induction mechanism, while the Cu(I)-Cu(II) and Pb(II)-Pb(IV) couples *via* catalytic cycles. Reaction mechanisms have been proposed for all cases and "saturation" at high ion concentration has been explained. The effect of five other metal ions on both TMA and TGA oxidation has also been checked. Finally, the possible applications of both indicator reactions among kinetic methods of analysis are discussed and some recommendations are made.

Introduction

The reactions between some thiols and chromate in acidic media have been recently used as indicator reactions in kinetic methods of analysis. For example, the oxidation of thiosulfate has been proposed to determine Cu(II) [1,2], while the reactions of mercaptosuccinic acid (thiomalic acid or TMA) and mercaptoacetic acid (thioglycolic acid or TGA) may be used to determine both Cu(II) [3] and Pb(II) [4,5] in water samples. On the other hand, the oxidations of cysteine [6] and ethanethiol [7] are far too slow to be employed in such a way. All these methods rely on the catalytic effect of the metal ions in order to determine their concentration. Reaction rate (or some parameter related to it) against catalyst concentration graphs are used in calibration.

In order to elaborate a sensitive and selective catalytic method of analysis, the mechanism and kinetics of both catalyzed and uncatalyzed reaction paths have to be known. Therefore, the aim of this work was to elucidate the influence of

copper, lead and iron ions on the reaction between thiomalic acid and chromate. The oxidation of thioglycolic acid (TGA) was investigated in more detail only in the presence of lead, since the effect of copper and iron is already known [8]. Experimental results for the reaction of TGA in the presence of Cu and Fe were compared with published ones.

Experimental

Reagents and solutions: Analytical grade reagents provided by *Reactivul* (Bucharest, Romania), *Reanal* (Budapest, Hungary), *Merck* (Darmstadt), *Fluka* (Buchs, Switzerland) and *Panreac* (Barcelona, Spain) were used without further purification. All solutions were prepared in demineralized and four times distilled water.

Stock solutions of 0.1 M perchloric acid as well as of 5×10^{-3} M $K_2Cr_2O_7$ were used to prepare the working solutions of 5×10^{-3} M and 2.64×10^{-4} M respectively. The 10^{-2} M working solutions of thiomalic and thioglycolic acids were prepared on a daily basis. Aqueous 10^{-2} M stock solutions of copper sulfate, iron nitrate and lead nitrate were prepared by dissolving the appropriate weighted amount in volumetric flasks of 100 ml. When necessary, 10^{-3} M and 10^{-4} M working solutions were prepared by means of dilution. Ionic strength was adjusted with 2.18 M sodium perchlorate.

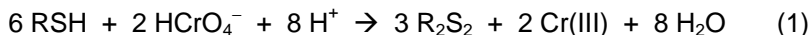
The acids were standardized by the usual procedures. Concentration of each salt was determined by titrating the acid generated when 2 ml stock solution passed through a column of C-100H cationite resin (*Virolyte*, Victoria, Romania).

Instrumentation and procedure: A Jasco V-530 UV/VIS (*Jasco*, Japan) spectrophotometer with temperature controlled cell holders was employed to monitor the extent of the reaction. Temperature was kept constant with the aid of a Lauda-M12 (*Lauda*, Germany) precision circulation bath at 20.0 ± 0.1 °C. All solutions were thermostated prior to use and during the experiments in the same water-bath. Quartz cells of 5 cm path length were used at 345 nm. Data acquisition was performed automatically by means of a DTK personal computer.

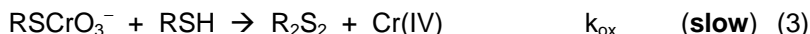
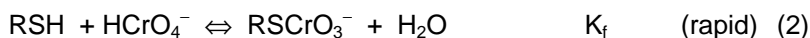
During all experiments, the colored species Cr(VI) was the limiting component. The reaction was initiated directly in the cell, by the rapid injection of 4 ml of the chromate solution into a mixture of 12 ml containing all the other reagents. Simultaneously, the automated data acquisition was started and values of the absorbance were recorded, depending on the needs of experiments, every 1 to 5 sec. The mixing time of reagents did not exceed 0.5 sec. The order of adding the solutions into the cell prior the addition of chromate, did not affect the results. Each kinetic run was carried out for approximately four half-lives. The final value of the absorbance, A_∞ , was considered to be the smallest achieved value after 8 to 10 half-lives. Three to five replicate runs were carried out under identical experimental conditions.

Results and discussions

The uncatalyzed oxidation of TMA [9], TGA [10] thiosulfate [11] as well as of other nine biological and non-biological thiols [12] by chromate in acidic media has already been investigated. When the substrate is in excess, a disulfide is the main reaction product in all cases:



RSH stands for the thiol, while R_2S_2 stands for $\text{S}_2(\text{CH}(\text{COOH})-\text{CH}_2-\text{COOH})_2$ in the case of TMA and for $\text{S}_2(\text{CH}_2-\text{COOH})_2$ in the case of TGA, respectively. The reaction starts with a rapid equilibrium to form a relatively stable thioester RSCrO_3^- . This will further yield the products in some rate determining steps.



RSCrO_3^- stands for $\text{HOOC}-\text{CH}_2-\text{CH}(\text{COOH})-\text{SCrO}_3^-$ in the case of TMA and for $\text{HOOC}-\text{CH}_2-\text{SCrO}_3^-$ in the case of TGA, respectively. The rates of processes (2) and (3) are described by the following laws:

$$\text{rate}_f = \{k_f^0 + k_f^H [H^+]\} [\text{RSH}] [\text{HCrO}_4^-] \quad (4)$$

and
$$\text{rate}_{\text{ox}} = \{k_{\text{ox}}^0 + k_{\text{ox}}^H [H^+]\} [\text{RSH}] [\text{HCrO}_4^-] \quad (5)$$

respectively. k_f^0 and k_{ox}^0 stand for second order rate coefficients of the uncatalyzed paths of reactions (2) and (3) respectively, while k_f^H and k_{ox}^H stand for third order, H^+ catalyzed paths of the same processes. Their values, along with the equilibrium constant K_f of reaction (2), are given in Table 1 for both TMA [9] and TGA [10].

Table 1

Individual rate coefficients - oxidation of TMA and TGA by chromate at 25.0 ± 0.1 °C.
Literature data.

Parameter	Substrate	
	TMA	TGA
k_f^0 ($\text{M}^{-1}\text{s}^{-1}$)	44.1 ± 0.3	66.3 ± 1.2
k_f^H ($\text{M}^{-2}\text{s}^{-1}$)	$(1.92 \pm 0.01) \times 10^2$	$(2.47 \pm 0.05) \times 10^3$
K_f (M^{-1})	$(1.48 \pm 0.07) \times 10^3$	$(1.10 \pm 0.15) \times 10^3$
k_{ox}^0 ($\text{M}^{-1}\text{s}^{-1}$)	23.8 ± 0.03	11.7 ± 0.70
k_{ox}^H ($\text{M}^{-2}\text{s}^{-1}$)	$(2.03 \pm 0.13) \times 10^2$	$(4.33 \pm 0.06) \times 10^2$
Ionic strength (M)	0.5	0.2

It may be concluded from Table 1 that only the formation of the thioester of thiomalic acid occurs somewhat slower than that of thioglycolic acid. Otherwise, the rates of TMA and TGA oxidation are comparable under identical experimental conditions.

The effect of Fe(II)-Fe(III) and Cu(I)-Cu(II) redox couples on the oxidation of TGA by chromate in acidic media was previously reported by Bâldea [8]. He observed that the reaction rate increased in the presence of small amounts of either iron or copper ions. However, concentrations of 10^{-6} mole/l copper bring about the same effect as a one order of magnitude higher iron ion content. Bâldea explained the rate enhancement by iron *via* an induction mechanism: Fe(II) reduces Cr(VI) to Cr(V) which is a better and faster oxidant of the substrate than HCrO_4^- itself. On the other hand, a catalytic cycle was proposed for copper. Under excess of RSH, Cu(II) traps the substrate as a ligand in Cu(II)-complexes, in ratios 1:1 and 1:2 copper-ligand. These react more easily with chromate to yield the main reaction product. The released Cu(I) will regenerate the catalyst by oxidation with Cr(VI) to form Cu(II) and Cr(V).

According to the rate law (5), under the excess of thiol and constant hydrogen ion concentration, the slow stage (3) obeys a first order rate law with respect to the colored Cr(VI) species. Hence, it can be written as follows:

$$r = - \frac{d[\text{RSCrO}_3^-]}{dt} = k_{\text{obsd}} [\text{Cr(VI)}] \quad (6)$$

where k_{obsd} is a pseudo-first-order rate constant. First order kinetics is proved by the linear dependence, in terms of absorbance, of the semilogarithmic plots of the equation below.

$$\ln(A - A_\infty) = \ln(A_0 - A_\infty) - k_{\text{obsd}} t \quad (7)$$

A , A_0 and A_∞ stand for the absorbance at any reaction time t , initial absorbance and the value of A at completion, respectively.

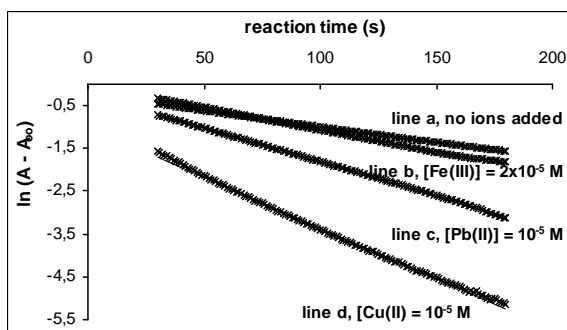


Fig. 1. Oxidation of TMA: semilogarithmic plots to determine k_{obsd} in the absence (line a) and presence (lines b,c and d) of metallic ions; 20.0 ± 0.1 °C, 10^{-3} M TMA, 2.2×10^{-4} M HClO_4 , 6.6×10^{-5} M Cr(VI), ionic strength of 0.15 M.

Figure 1 refers to the oxidation of thiomalic acid. It shows that points lie on lines for more than 90 % of reaction completion, both in the absence (line *a*) and in the presence (lines *b*, *c* and *d*) of small amounts of iron, lead or copper ions. This proves that pseudo-first order kinetics is preserved in the presence of the metal ions. The slopes give the values of the rate coefficients k_{obsd} . The higher slopes of lines *b*, *c* and *d* as compared to the one of line *a*, reveal a rate enhancement by even very small amounts of the above listed ions. Similar conclusions were drawn for the oxidation of thioglycolic acid in the presence of small amounts of lead.

The dependence of k_{obsd} versus total copper, lead and iron concentration is presented in Figure 2 for the oxidation of TMA. It is obvious that in the range of small ion concentrations k_{obsd} may be expressed as:

$$k_{obsd} = k_0 + k_{ion}[ion] \quad (8)$$

where k_0 and k_{ion} stand for the contributions of a pseudo-first and a -second order reaction path, respectively. Under the same experimental conditions, but an ionic strength of 0.2 M, similar results were obtained for TGA. However, preliminary experiments proved that the ionic strength does not affect reaction rates of neither TMA or TGA oxidation.

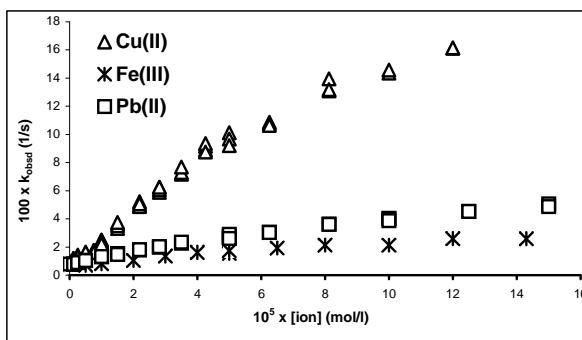


Fig. 2. Oxidation of TMA: the dependence k_{obsd} vs total ion concentration. Experimental conditions of Figure 1.

The values we found for k_0 and k_{ion} are given in Table 2 for both substrates. For TGA computed values on the base of literature data [8] are also given. It may be observed that although the overall reaction rates of TMA and TGA oxidation are comparable, the latter occurs somewhat slower under the same experimental circumstances, regardless of the absence or presence of any metallic ions. Further, for all metal species, k_{obsd} levels off towards higher concentrations. Therefore, the following dependence was assumed:

$$k_{ion} = k_{obsd} - k_0 = \frac{a[ion]}{1+b[ion]} \quad (9)$$

where **a** and **b** are some constants. The equation above can also be written in its linear form:

$$\frac{1}{k_{ion}} = \frac{b}{a} + \frac{1}{a} * \frac{1}{[ion]} \quad (10)$$

Table 2

k_0 and k_{ion} values for TMA and TGA oxidation at 20.0 ± 0.1 °C, 10^{-3} M RSH, 2.2×10^{-4} M $HClO_4$, 6.6×10^{-5} M Cr(VI), ionic strength of 0.15 M (TMA) and 0.2 M (TGA).

Parameter	Substrate		
	TMA	TGA	
k_0 (s^{-1})	$(7.85 \pm 0.54) \times 10^{-3}$	$(4.25 \pm 0.16) \times 10^{-3}$	* 6.63×10^{-2}
k_{ion} ($M^{-1}s^{-1}$)	Pb: $(4.44 \pm 0.23) \times 10^2$	Pb: $(3.85 \pm 0.19) \times 10^2$	* ---
	Cu: $(1.96 \pm 0.06) \times 10^3$	Cu: $(2.39 \pm 0.24) \times 10^2$	* Cu: 2.82×10^4
	Fe: $(2.09 \pm 0.75) \times 10^2$	Fe: 1.80×10^2	* Fe: 2.55×10^3

* Computed values on the base of literature data [8] at 25.0 ± 0.1 °C, 4×10^{-3} M TGA, 1×10^{-2} M H^+ , 4×10^{-4} M Cr(VI), ionic strength of 0.2 M.

According to relationship (10), the plot of $1/k_{ion}$ vs $1/[ion]$ should give a straight line. From its slope and intercept, the values of **a** and **b** may be obtained.

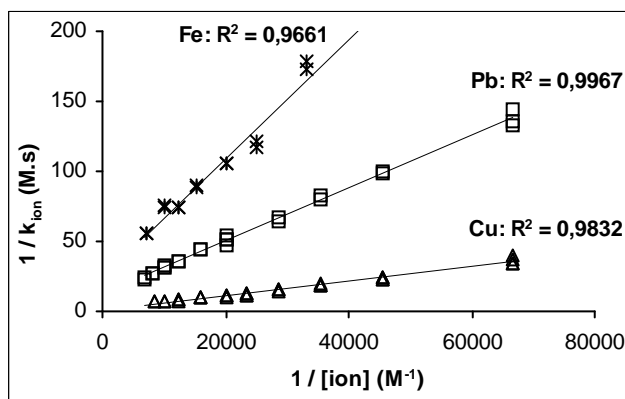


Fig. 3. Oxidation of TMA: the dependence of the inverse of k_{ion} on the inverse of the total ion concentration.

Figure 3 presents the plots of equation (10) for the oxidation of TMA. For all the studied ions, points lie on lines with good or satisfactory correlation coefficients. Similar results were obtained for the oxidation of TGA. The constants **a** and **b** are given in Table 3 for both substrates, along with the values obtained on the base of literature data [8] for TGA.

Table 3

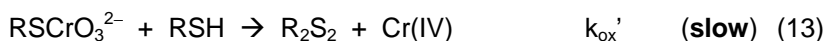
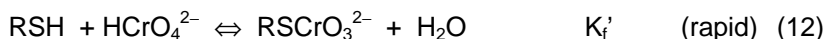
The constants **a** and **b** for TMA and TGA oxidation. Experimental conditions of Table 2.

Parameter	Substrate					
	TMA			TGA		
	Cu	Pb	Fe	Cu	Pb	Fe
a ($M^{-2}s^{-1}$)	1965	542	227	488 * 64350	480 * ---	315 * 3235
b (M^{-1})	2413	7113	5033	6946 * 303730	2139 * ---	20268 * 15872

* Computed values on the base of literature data [8].

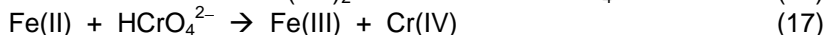
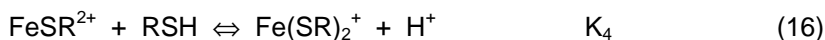
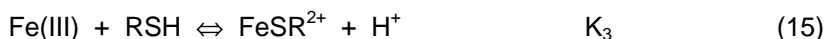
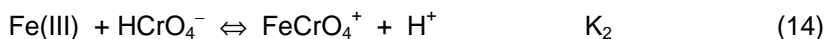
Based on Figures 2 and 3 as well as on data in Tables 2 and 3, it may be concluded that the effect of Cu(I)-Cu(II) and Fe(II)-Fe(III) redox couples on the oxidation of TMA by Cr(VI) is similar to that on the oxidation of TGA. Moreover, our findings for TGA oxidation are in agreement with those published by Baldea. Therefore, a rate enhancement *via* an induction mechanism for iron and *via* a catalytic cycle for copper may be assumed for the reaction of thiomalic acid.

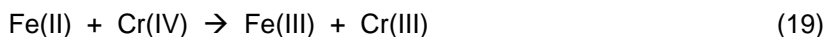
Hence, the following sequence of steps is believed to concur processes (2) and (3) in the presence of iron:



In step (11) Fe(II) reduces chromate to Cr(V) in $HCrO_4^{2-}$. This is a better oxidant of the substrate than Cr(VI). An equilibrium has been considered for process (11) because the standard reduction potentials of the Cr(VI)/Cr(V) and Fe(III)/Fe(II) redox couples are comparable [8]. Equilibrium (12), in which $HCrO_4^{2-}$ combines with an TMA molecule to form a Cr(V)-S bonding, has been assumed by analogy with process (2) and the general tendency of all $H_nMO_4^-$ type acids to form poly- or heteropoly-compounds. Step (13), which yields the main reaction product, is slow within the sequence (11)-(13), but faster than step (3). Thus, the overall reaction rate (6) will increase. Steps (11)-(13) are consistent with an induction mechanism.

Parallel to processes (2)-(3) and (11)-(13), the reactions below may also occur. These are consistent with rate a enhancement *via* a catalytic cycle [13].



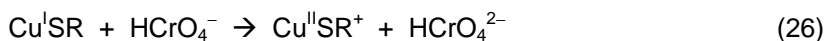
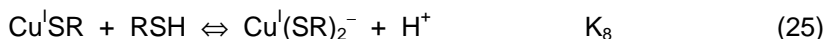
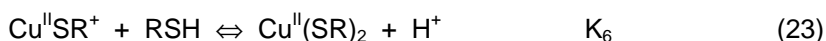


All processes are faster than (3) or (13). Some regenerate Fe(II) or yield Cr(IV), which further may oxidize the substrate. The species RS• stands for a thiyl radical. The concentration of FeCrO_4^+ from equilibrium (14), which will cause an inhibitory effect, is extremely low ($K_2 = 1.4$ [14]) under the employed experimental conditions (both $[\text{HCrO}_4^-]$ and $[\text{Fe}(\text{III})]$ are small). Although the oxidation of Fe(II) by Cr(V) in step (17) is considered to be rate determining in the overall process of Fe(II) oxidation by Cr(VI) [14], within this context it is considered to proceed fast.

Under the excess of RSH and higher iron concentrations, equilibria (15) and (16) are shifted to the right; so that more Fe(III) is trapped in some complexes and less will be able to follow the sequence (11)-(13). Therefore, the contributions in the total reaction rate of the inductive and catalytic paths are modified. This explains the curvature of the k_{obsd} vs total iron concentration in Figure 2.

The above inductive mechanism was proposed by Baldea [8] for the oxidation of thioglycolic acid, by taking into account the individual mechanisms of the TGA-Cr(VI), TGA-Fe(III) and Fe(II)-Cr(VI) reactions.

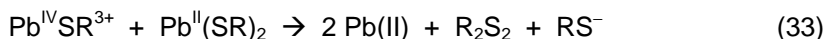
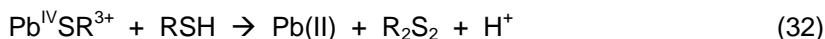
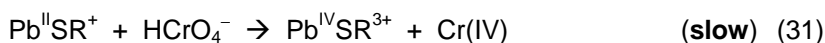
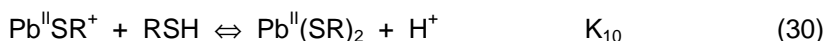
The reaction mechanism of thiomalic acid oxidation by chromate in the presence of copper ions relies on the formation of some copper-thiol complexes [15,16]. Thus, the sequence of steps below is considered to occur in parallel with processes (2) and (3):



Rapid equilibria (22)-(25) yield the above mentioned complexes. When RSH is in excess, Cu(I)-thiol complexes will be mainly formed in Cu:RSH ratios of 1:1 and 1:2 [15,16]. Process (27) is similar to (18). It is (27) rate determining, but still much faster than step (3), (13) or (18). The catalytic cycle is closed and Cu(II) is regenerated by means of reaction (28). It may be compared with the similar process for iron in step (11). Instead, because the standard reduction potential of the Cu(II)/Cu(I) couple is far below the one of Cr(VI)/Cr(V) [8], process (28) is far

from equilibrium. This is why, a catalytic cycle and not an induction mechanism was proposed to explain the rate enhancement by copper ions. Cr(V) obtained in (26) or (28) may further be involved in steps like (12) and (13). However, these will have a negligible contribution to the overall reaction rate because (27) is faster than (13), k_{obsd} values for copper laying higher in Figure 2 than those for iron. The sequence above is completed by fast steps (20) and (21). The tendency to level off, of the k_{obsd} vs [Cu] plot in Figure 2, is explained in a similar way to that of iron: in excess of RSH and higher copper content more chelate complex $\text{Cu}^{\text{I}}(\text{SR})_2^-$ will form. It is more stable against oxidation by chromate, hence it will remove part of copper from the catalytic cycle.

Because the oxidation of thiomalic acid in the presence of lead resembles that in the presence of copper (significantly higher reaction rate as compared to that of iron, curvature of the k_{obsd} versus total ion concentration plots in Figure 2), a similar catalytic cycle has been assumed to explain the rate enhancement. Thus, the following reaction path was assumed to occur in parallel with (2) and (3):



Mchrotra [17] and Begley [18] proved that Pb(II) can form lead-thiol complexes in Pb:RSH ratios of 1:2. Přebil [19] also mentions that some thiols, such as thioglycolic acid, bind lead. Therefore, rapid equilibria (29) and (30) were assumed. Rate determining would be the two-equivalent electron transfer within the lead-thiol complex, that is step (31). This may be slow within the cycle (29)-(33), but it is faster than (3), (13) or (18) and slower than (27) (see the plots in Figure 2). Regeneration of the catalyst may also occur rapidly in (33), which could also involve a two-equivalent process with the formation of RS^+ . RS^+ reacts immediately with RS^- to yield R_2S_2 . Process (33) is similar to (27) and (18). The sequence is completed by reactions (20) and (21). An analog catalytic cycle has been assumed for the oxidation of thioglycolic acid in the presence of lead.

Another slow electron transfer process - slower than (31) - involves $\text{Pb}^{\text{II}}(\text{SR})_2$ and chromate. We suppose, by similarity with copper, that the complex $\text{Pb}^{\text{II}}(\text{SR})_2$ is more resistant to oxidation by chromate than $\text{Pb}^{\text{II}}\text{SR}^+$. Hence, at higher ion concentrations more lead will be bound in this form and thus removed from further catalytic action. This could explain the shape of the k_{obsd} vs [Pb] plot in Figure 2.

The curvature of the k_{obsd} plots can be also explained, for all studied ions, on the base of equation (9) and the values of constants **a** and **b** given in Table 3. At small ion concentrations (of the order of magnitude of 10^{-6} M), the second term of the sum $(1 + b[\text{ion}])$ is negligible; hence rate enhancement depends linearly on [ion]. When the latter is increased, its significance in the sum will also increase and the plots of k_{obsd} will level off.

The weaker effects of iron and copper on TGA oxidation are probably due to the fact that TGA is indicated as masking agent for iron in acidic media [19] as well as for copper in alkaline [20] or weak acid media [19]. With iron an intensely red complex is formed, while the complexes of copper may be colorless – in alkaline – or red – in weak acid media. This is consistent with our experimental observations: values of absorbance (including A_{∞}) were somewhat higher when kinetic runs were carried out in the presence of iron or copper.

Both Figure 2 and Table 2 reveal the fact that, under the same experimental conditions, copper achieves the best rate enhancement of TMA oxidation. Lead and iron follow it. On the other hand, lead ions affect the most significantly the rate of TGA oxidation. Their catalytic effect is even stronger than that of copper ions, while rate enhancement by iron is barely sensed. These findings led to the conclusion that the $\text{Cu}^{\text{I}}(\text{SR})_2^-$ complex of TGA is more stable against oxidation by chromate than the complex of TMA. The same is applicable for the $\text{Pb}^{\text{II}}(\text{SR})_2$ complexes, although rate enhancements by lead are almost identical for both substrates.

Thus, from analytical point of view, the use of TMA oxidation in kinetic determination of Cu(II) is rather indicated than that of TGA oxidation, provided the effects of lead and iron can be suppressed. This was already achieved in the presence of pyrophosphate [3,19]. If only the effect of iron ions is masked, for example with the aid of 1,10-phenanthroline [19], both substrate oxidations are recommended as indicator reactions for the joint analysis of Cu(II)-Pb(II) mixtures. However, the concentration of lead in the reaction mixture should not exceed 5×10^{-4} M. Otherwise, precipitates will form with the thiols.

The effect of several other ions on the oxidation of TMA and TGA by chromate has been investigated, under the same experimental condition as employed for copper, lead and iron. Comments on the obtained results, along with the concentration limits C_{lim} at which their presence in the reaction mixture is sensed *via* kinetic measurements, are given in Table 4.

Table 4

Effect of various metal ions on the rates of TMA and TGA oxidation.

Experimental conditions are the same as listed for Figure 1.

Ion	C_{lim} (M)	Comments
Cd(II)	10^{-4}	Increases rate for both TMA and TGA; If $[\text{Cd}(\text{II})] > 5 \times 10^{-4}$ M, precipitates will form.
Ni(II)	5×10^{-4}	Increases rate for TMA
	10^{-4}	Increases rate for TGA
Co(II)	10^{-3}	Decreases slightly the rate for TMA
		Increases significantly the rate for TGA
Zn(II)	5×10^{-4}	Increases rate for both TMA and TGA
Mn(II)	---	Does not affect reaction rates

Oxidation of the two substrates behaves similarly in the presence of all, but Co(II), ions listed above. However, these species affect reaction rates only when

present in a relatively high concentration. Thus, it is unlikely that any kinetic method will be developed for their analysis, on the base of indicator reaction (1).

REFERENCES

1. A. Rustoiu - Csavdari, I. Bâldea, *Proceedings of the 2nd International Conference of the Chemical Societies of the South-Eastern European Countries On Chemical Sciences for Sustainable Development*, Chalkidiki, Greece, **2000**, PO 658.
2. A. Rustoiu - Csavdari, I. Bâldea, L. Copolovici, D. Mhai, *Lucrările celei de a XI-a Conferință Internațională de Chimie și Inginerie Chimică*, București, România, **1999**.
3. D. Mihai, *Kinetic Determination of Cu(II) by its Catalytic Effect on the Oxidation Reaction of Mercaptosuccinic Acid by Chromate (Advanced Studies Thesis)*, Babeș-Bolyai University, Cluj-Napoca, Romania, **2000**; A. Rustoiu - Csavdari, I. Bâldea, D. Mihai, *unpublished work*.
4. A. Rustoiu - Csavdari, I. Bâldea, C. Călin, *Proceedings of the 6th International Symposium On Kinetics in Analytical Chemistry, KAC'98*, Kassandra, Greece, **1998**, p. 39.
5. A. Rustoiu - Csavdari, I. Bâldea, M. Stan, *Chem. Bull. "Politehnica" Univ. (Timișoara)*, **1998**, 43(57), 143.
6. I. Bâldea, G. Niac, *Studia Univ. Babeș-Bolyai, Chem.*, **1986**, 31(2), 41.
7. G. Niac, S. Schön, I. Bâldea, *Studia Univ. Babeș-Bolyai, Chem.*, **1986**, 31(2), 31.
8. I. Bâldea, *Studia Univ. Babeș-Bolyai, Chem.*, **1989**, 34(1), 80.
9. I. Bâldea, *Studia Univ. Babeș-Bolyai, Chem.*, **1994**, 39(1-2), 138.
10. I. Bâldea, *Studia Univ. Babeș-Bolyai, Chem.*, **1987**, 32(2), 42.
11. I. Bâldea, G. Niac, *Inorg. Chem.*, **1968**, 7, 1232; I. Bâldea, G. Niac, *Inorg. Chem.*, **1970**, 9, 110.
12. J. F. Perez - Benito, N. Saiz, E. Amat, *J. Mol. Catal., A-Chem.*, **1998**, 135, 1.
13. D. L. Leussing, I. M. Kolthoff, *J. Amer. Chem. Soc.*, **1953**, 75, 3904, D. L. Leussing, L. Newman, *J. Amer. Chem. Soc.*, **1955**, 78, 552.
14. J. H. Espenson, E. L. King, *J. Amer. Chem. Soc.*, **1963**, 85, 3328.
15. A. McAuley, *Coordin. Chem. Rev.*, **1970**, 5, 245.
16. I. M. Klotz, G. H. Czertinski, A. A. Fies, *J. Amer. Chem. Soc.*, **1958**, 80, 2920.
17. R. C. Mchotra, *J. Organometallic Research*, **1986**, 283, 185.
18. M. G. Begley, C. Gaffney, P. G. Harrison, A. Steel, *J. Organometallic Research*, **1985**, 289, 281.
19. R. Pribil, *Applied Complexonometry*, Pergamon Press, Oxford, **1982**, pgs. 72, 113 and 149.
20. R. Pribil, V. Vesely, *Talanta*, **1961**, 8, 880.

THE HYDROGEN PEROXIDE – IODIDE REACTION IN KINETIC ANALYSIS. AN ATTEMPT FOR MULTICOMPONENT CALIBRATION

ALEXANDRA RUSTOIU-CSAVDARI, IOAN BÂLDEA, LUCIAN COPOLOVICI,
DANA MIHAI

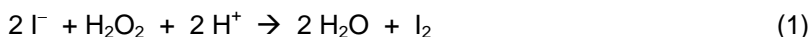
*"Babeș-Bolyai" University, Faculty of Chemistry and Chemical Engineering,
Department of Physical Chemistry, 11 Arany Janos Street, 3400 Cluj-Napoca
E-mail: arustoiu@chem.ubbcluj.ro*

ABSTRACT. The applications of the Landolt-type hydrogen peroxide – iodide reaction has been extended to other species than those mentioned in the literature, such as vanadium, copper and iron. Detection of the incubation time was carried out visually. Reaction conditions towards Mo(VI) and V(V) were optimized and calibration lines t_0/t versus catalyst concentration were drawn. Further, the most often cited interferents, that is Cu(II) and Fe(III), were added to the reaction mixture and the joint behavior of V(V)-Cu(II), Cu(II)-Fe(III) and Mo(VI)-Cu(II)-Fe(III) matrixes have been studied. Their joint catalytic effect was proved to be neither additive nor synergistic. Bi-component and tri-component calibration models based on a $t_0/t = f\{[ion1],[ion2]\}$ response surface or on a family of such surfaces respectively, were proposed. Results of visual and potentiometric detection of the reaction end-point were compared. The two methods have comparable performances.

Introduction

In recent years, kinetic or catalytic methods have opened a completely new area of research in analytical chemistry [1]. Within these, the analytical applications of Landolt reactions among chronometrical methods are obvious. Since the reaction time t decreases in the presence of a catalyst, it can be related to the catalyst concentration by means of $1/t$ or t_0/t versus analyte concentration calibration graphs. t_0 and t correspond to the absence and presence of the catalyst, respectively.

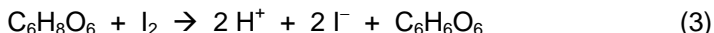
The slow oxidation of iodide by hydrogen peroxide in acidic medium to form iodine



was studied by many scientists [2], but the first to elucidate its mechanism and to give some kinetic parameters were Liebhafsky and Mohammed [3]. The following law can describe the reaction rate:

$$r = \frac{d[H_2O_2]}{dt} = k_2[H_2O_2][I^-] + k_4[H_2O_2][I^-][H^+] \quad (2)$$

To serve the purpose of kinetic analysis, the hydrogen peroxide-iodide reaction can be easily transformed into a Landolt-type system by adding some trap for iodine (ascorbic acid [4,5] or thiosulfate [38]) to the reaction mixture. In the case of ascorbic acid for example, the iodine produced by reaction (1) will instantaneously be reduced back to iodide and dehydroascorbic acid will be released:



Therefore, as long as the ascorbic acid is not completely consumed, iodine does not accumulate. When it is totally consumed, I_2 is suddenly accumulated and the Landolt-effect [4,5] occurs. This phenomenon can easily be observed, even visually, because the mixture turns suddenly from colorless to yellow (which is typical for iodine), blue (in the presence of starch) or violet (in the presence of variamine blue). Yet, one may use any other indicator of the occurrence of the Landolt-effect. Its time lapse, also called "reaction time" t or "incubation time", depends on the concentration of the single reactants as well as on the concentration of any catalyst present in the mixture. Svehla [4], proved a linear dependence of t on the $C_6H_8O_6$ concentration as well as an exponential correlation with the I^- concentration. He also explained the linear dependence of $1/t$ and t_0/t on the catalyst concentration, on the base of reaction kinetics and mechanism.

Reaction (1) is catalyzed by many metal ions in their higher oxidation states and was proposed as possible indicator reaction in kinetic analysis for the determination of Zr, Hf, Th, Ta, Mo, W and Fe by Yatsimirskii [6]. Mottola [8] added Pb and Ag to the list. Methods to determine some non-metallic catalysts, such as $Cr_2O_7^{2-}$ and PO_4^{3-} [9], were also reported.

Yet, in spite of the long list of metal ions above, the majority of catalytic methods based on the hydrogen peroxide – iodide Landolt-type reaction were developed to determine molybdenum [10-27], tungsten [26-29] or their mixtures [33-37]. However, analysis of iron [30], hafnium and zirconium [31] or joint determination of molybdenum–iron [32,38,39], molybdenum–copper [38,39] mixtures were also mentioned. The end-point of the reaction was detected visually [10,17-18,28,38-39], spectrophotometrically [15,34-37], potentiometrically [11-14,20,32-33], thermometrically [22] or amperometrically [19]. A large variety of samples were analyzed, such as water, food, vegetal material, minerals and steel.

Many of the methods are highly sensitive; detection limits as low as 0.7 $\mu\text{g/l}$ [15] were reported. The most significant interferences for the determination of molybdenum are copper and iron, hence EDTA [14,20,29,32,38-39] is commonly used to remove their effect. Analysis of Mo(VI) is sometimes interfered by vanadium and tungsten [18] as well. Improvement of selectivity was also achieved either by removing the interferences during the pretreatment of samples [18,22-23] or by incorporating a cation-exchange resin column into the system [21]. Other scientists [27] preferred a mathematical correction of their calibration model.

During the 1970's, researchers were enthusiastic because of the simplicity of the principle and experimental device. By just using some temperature controlled vessels and a stopwatch (the so-called "clock method"), they were able to visualize the end-point of the reaction and develop some fairly sensitive kinetic methods [10]. However, during the years to come more performant and accurate apparatus replaced this tedious "monitoring" procedure. Nowadays, efforts concentrate rather on miniaturization [12-13,15] and automatization [9,13,15,21,25-26] of processes: samples can be as tiny as 100 μl [12] and sampling rates can reach up to 120 every hour [25].

Bi-component analysis, although it does not require pre-separation, it still needs two distinct experiments to determine the concentration of both analytes. One corresponds to the cumulative effect of both ions, while the other only to the effect of one of them. The catalytic effect of the second ion is removed by masking it. Thus, Mo(VI)-Fe(III) and Mo(VI)-W(VI) mixtures were analyzed by masking Fe(III) with EDTA [32] and Mo(VI) with citric acid [35], respectively. These procedures, however, rely on the additive joint effect of the catalysts. Recent methods not only deal with synergistic effects [36,37] by compensating the deviation from additivity within the calibration model *via* a synergistic catalytic coefficient, but also give the composition of the matrix by means of just one experiment.

The first purpose of this paper is to undertake the simple experimental device of the 1970's and extend the application of the hydrogen peroxide – iodide Landolt-type reaction to other bi- and tri-component mixtures, such as Cu(II)-Fe(III) and Mo(VI)-Cu(II)-Fe(III) as well as to other species, such as V(V) and its mixtures with Cu(II). The Mo(VI)-Cu(II) and Mo(VI)-Fe(III) couples exhibit an additive catalytic effect [38] for narrow concentration ranges. Hence, the second purpose was to enlarge the Cu(II) and Fe(III) concentration ranges to values where the joint effect of the catalyst is neither additive nor synergistic. Some attempts were also made to elaborate a suitable calibration model for Mo(VI)-Cu(II)-Fe(III) and V(V)-Cu(II) mixtures by obtaining the appropriate calibration surfaces or family of surfaces. Copper and iron were chosen as components of the mixtures because they are the most interferents in determination of molybdenum. Results of these simple kinetic experiments are verified by potentiometric runs for the case of Mo(VI) and some of its mixtures with Cu(II) and Fe(III).

Experimental

Reagents and Solutions

Analytical grade reagents provided by *Reactivul* (Bucharest, Romania), *Reanal* (Budapest, Hungary) and *Merck* (Darmstadt, Germany) were used without further purification. All solutions were prepared in twice distilled water produced by a VDB-3A glass device.

A stock solution of sulfuric acid was used as source of hydrogen ions. Ammonium molybdate $(\text{NH}_4)_6\text{Mo}_7\text{O}_{24}$, ammonium meta-vanadate NH_4VO_3 , copper sulfate $\text{CuSO}_4 \cdot 5\text{H}_2\text{O}$ and iron chloride FeCl_3 were used as sources for Mo(VI), V(V), Cu(II) and Fe(III) ions, respectively. Aqueous stock solutions of 10^{-2} mol.dm⁻³

of all salts were prepared by dissolving the appropriate amount in volumetric flasks of various volumes, according to the needs of the experiments. Working solutions were obtained by adequate dilution of stock solutions. The Cu(II) concentration was determined by titration of the acid gained when 2 ml stock solution passed through a column of C-100H cationite resin (*Virolyte*, Victoria, Romania). The Fe(III) content of the acidulated iron chloride solution was determined by titration of the iodine obtained when 2 ml stock solution were mixed with KI and H₂SO₄. The acidity of this solution was also established. The solutions of hydrogen peroxide ascorbic acid or sodium ascorbate were freshly prepared before each set of experiments. The H₂SO₄ and H₂O₂ solutions were standardized by usual procedures. An aqueous 1 % wg. starch solution was used as color indicator for iodine.

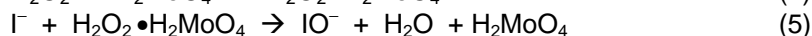
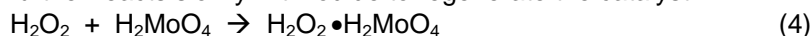
Experimental device. Procedure

Experiments were carried out at constant temperature of 293 ± 0.1 K. Two solutions were prepared for each experiment, so that after mixing the total volume was of 20 ml. The oxidant solution **A**, of 15 ml volume, contained H₂O₂, Na₂C₆H₆O₆ or C₆H₈O₆, H₂SO₄, starch and the catalyst, while the 5 ml of the reductant solution **B** contained only KI. Both were kept at controlled temperature as follows: solution **A** in a double wall glass vessel (which also served as reaction vessel) connected to a WOBSEER U15 precision circulation bath, while solution **B** in a separate vessel kept in the water bath. The reaction vessel was placed on a magnetic stirrer. Solution **B** was injected into solution **A** under stirring and a precision stopwatch was started. Mixing time did not exceed 0.5-1 s. The reaction time *t* for the mixture to turn from colorless to blue, was recorded. Three to five replicate runs were carried out for each set of experimental conditions. Time measurements did not differ to more than ± 1 %.

Potentiometric runs were carried out with an electrochemical cell consisting of two temperature controlled glass vessels. One contained the reaction mixture and a working I⁻ - selective electrode, while the other a saturated calomel reference electrode. The electrodes were connected to a Radelkis multimeter. A bridge salt of saturated potassium nitrate was used to connect the half-cells. The electromotive force was monitored versus time. The "*Raluca Ripan*" Chemical Research Institute of Cluj-Napoca provided the electrodes. The solutions used in potentiometric experiments were prepared in demineralized and four time distilled water.

Results and discussions

The catalytic effect of molybdate on the hydrogen peroxide – iodide reaction is probably due to the rapid formation of peroxy molybdic acid [4,14], that further reacts slowly with iodide to regenerate the catalyst:



Iodine is formed from IO⁻, so that the empirical reaction is the same as expressed in (1). Among the processes above, (5) is slow but much faster than its uncatalysed correspondent. The other steps occur rapidly. Thus, H₂MoO₄ is regenerated during

the entire cycle. Besides, combination of reactions (1) and (3) ensures constant I⁻ concentration in the reaction mixture.

Hence, in the presence of molybdate and under an excess acid concentration (or in buffer solution), the consumption rate of hydrogen peroxide [40] can be described as:

$$r = - \frac{d[H_2O_2]}{dt} = (k_{un} + k_{cat} [Mo(VI)]) [H_2O_2] \quad (6)$$

where k_{un} stands for a pseudo-first order rate coefficient in the absence of the catalyst. On the other hand, k_{cat} stands for a second order rate coefficient of the molybdenum catalyzed reaction path.

Rate equation (6) can be integrated by considering that when reagents are mixed (time $t = 0$) $[H_2O_2] = [H_2O_2]_0$ and at the end of the induction period (time t) $[H_2O_2] = [H_2O_2]_0 - [C_6H_8O_6]_0$ (the subscript indicates initial concentrations). This leads to

$$\frac{1}{t} = \frac{k_{un} + k_{cat} [Mo(VI)]}{\ln \left(\frac{[H_2O_2]_0}{[H_2O_2]_0 - [C_6H_8O_6]_0} \right)} \quad (7)$$

Hence, the ratio t_0/t of reaction times recorded in the absence and presence of catalyst, can be expressed as

$$\frac{t_0}{t} = 1 + \frac{k_{cat} [Mo(VI)]}{k_{un}} \quad (8)$$

It is obvious that linear calibration graphs may be obtained by plotting either $1/t$ or t_0/t against the catalyst concentration. Svehla [10] proved that the t_0/t vs concentration plot is more independent of the individual time values, provided experimental conditions do not vary too much. Based on this as well as on its simplicity, we have chosen equation (18) as the base of calibration graphs for our analytical purposes.

Monocomponent calibration for Mo(VI), Cu(II), Fe(III) and V(V)

Molybdenum

Optimal reaction conditions regarding concentration of reagents were searched for in order to ensure a high sensitivity towards molybdenum, that is a high slope in equation (8). Therefore, kinetic runs were performed at various ascorbic acid, potassium iodide and sulfuric acid concentrations, for both in the absence and presence of 10^{-6} mole.dm⁻³ Mo(VI).

The mineral acid has to be in excess and the concentration of ascorbic acid should be two orders of magnitude smaller than that of hydrogen peroxide. The latter condition ensures less than 10 % reaction extent at the end-point. A small extent of the reaction presents the advantage that the side reactions, such as the decomposition of H₂O₂, will not affect the experimental results.

Because of practical reasons, an initial H₂O₂ concentration of 1.2×10^{-2} mole.dm⁻³ and a temperature of 293 ± 0.1 K were chosen for all experiments.

Experimental $k_{\text{cat}}/k_{\text{un}}$ values (mean of at least three replicate runs) are presented in Table 1 along with the corresponding pH and ionic strength of the reaction mixture.

No precautions were taken to maintain the ionic strength. Its value is practically given by the contributions of KI and the acid. However, these species have always the same initial concentration for each set of measurements and in all cases the ionic strength is high enough to cover any possible contribution due to a water sample to be analyzed [41].

Table 1

Influence of reagent concentrations on the $k_{\text{cat}}/k_{\text{un}}$ ratio at 1.2×10^{-2} mole. dm^{-3} H_2O_2 and 10^{-6} mole. dm^{-3} Mo(VI) at 293 ± 0.1 K.

Reaction conditions (concentrations given in mole. dm^{-3})	Concentration of studied species (mole. dm^{-3})	$10^{-5} \times k_{\text{cat}}/k_{\text{un}}$ ($\text{dm}^3 \cdot \text{mole}^{-1}$)	pH	Ionic strength (mole. dm^{-3})
Effect of $\text{Na}_2\text{C}_6\text{H}_6\text{O}_6$: [H_2SO_4] = 0.1 [KI] = 3×10^{-3} [KI] = 6×10^{-3}	4×10^{-4}	5.80	1.02	0.19
	8×10^{-4}	2.80		
	2×10^{-4}	6.50		0.20
	4×10^{-4}	6.20 *		
	6×10^{-4}	4.10		
Effect of KI : [H_2SO_4] = 0.1 [$\text{Na}_2\text{C}_6\text{H}_6\text{O}_6$] = 4×10^{-4}	3×10^{-3}	6.00	1.02	0.19
	6×10^{-3}	6.20 *		0.20
	12×10^{-3}	6.50		
Effect of H_2SO_4 : [$\text{Na}_2\text{C}_6\text{H}_6\text{O}_6$] = 4×10^{-4} 4 [KI] = 6×10^{-3} [$\text{Na}_2\text{C}_6\text{H}_6\text{O}_6$] = 8×10^{-4} [KI] = 1.2×10^{-3}	0.06	7.60	2.01	0.12
	0.10	6.20 *	1.02	0.20
	0.12	0.80	0.96	0.24
	0.16	1.70	0.85	0.32

* Labeled values in the third column correspond to identical reaction conditions.

Table 2

Results of kinetic runs. Calibration for Mo(VI).
 1.2×10^{-2} mole.dm⁻³ H₂O₂, 6×10^{-3} mole.dm⁻³ KI, 6×10^{-2} mole.dm⁻³ H₂SO₄,
 4×10^{-4} mole.dm⁻³ Na₂C₆H₆O₆ and ionic strength of 0.12 mole.dm⁻³ at 293 ± 0.17 K.

$10^7 \times [\text{Mo(VI)}] \text{ (mole.dm}^{-3}\text{)}$	$t \text{ (s)}$	Average t_0/t
0.0 (the blank run)	10 recordings average $t_0 = 372 \text{ s}$	1.000
2.0	327, 328, 329	1.135
4.0	288, 290, 291	1.287
6.0	260, 261, 260	1.429
8.0	239, 237, 238	1.562
10.0	223, 220, 222	1.679

It may be observed from Table 1 that all concentration values of the reagents are rather small; more concentrate solutions would lead to a much too rapid process for an accurate detection of the end-point with the employed device.

According to rate laws (2) and (6), the iodide content of the reaction mixture should not affect reaction times t , that is values of $k_{\text{cat}}/k_{\text{un}}$. The same conclusion can be drawn from Table 1; the slight differences are probably due to the slight changes in pH and ionic strength of the mixture. Results in Table 1 also show that regardless the iodide content, lower ascorbic acid concentrations induce a better sensitivity. Lower concentrations of the "scavenger" for iodine also correspond to smaller extents of the reaction. Further, as expected from the expressions of k_{un} and k_{cat} , the acid brings about the most significant changes. It is obvious that the best experimental conditions, giving the highest sensitivity for molybdenum, imply the following reagent concentrations: 1.2×10^{-2} mole.dm⁻³ H₂O₂, 6×10^{-3} mole.dm⁻³ KI, 6×10^{-2} mole.dm⁻³ H₂SO₄ and 4×10^{-4} mole.dm⁻³ Na₂C₆H₆O₆ (see Table 1).

Individual reaction time t and mean t_0/t values obtained under these circumstances are presented in Table 2. One may observe that replicate runs give repeatable results. A concentration range of Mo(VI) up to 10^{-6} mole.dm⁻³ was covered. The following calibration line t_0/t vs catalyst concentration was obtained:

$$t_0/t = (1.01 \pm 0.02) + (6.81 \pm 0.26) \times 10^5 x [\text{Mo(VI)}] \quad (R=0.999) \quad (9)$$

Its correlation coefficient is very good and for all points RSD is less than 2 %. The statistically computed intercept, corresponding to the absence of the catalyst, approaches very well the theoretical value of unity in equation (8). The detection limit was estimated according to IUPAC recommendations [42] and is of 2.5×10^{-8} mole.dm⁻³ ($2.4 \mu\text{g.dm}^{-3}$) Mo(VI).

Vanadium

The same principle was applied to find the optimal experimental conditions for catalysis by V(V). It was found that only ascorbic acid, that is the reaction extent, affects significantly the sensitivity towards vanadium. Reaction conditions,

at 293 ± 0.1 K, to ensure its highest value are: 1×10^{-2} mole.dm⁻³ H₂O₂, 5×10^{-3} mole.dm⁻³ KI, 0.125 mole.dm⁻³ H₂SO₄ and 8.5×10^{-4} mole.dm⁻³ C₆H₈O₆. Individual reaction time t and t_0/t values recorded under these circumstances are presented in Table 3. Again, replicate runs are repeatable.

Table 3

Results of kinetic runs. Calibration for V(V).
 1×10^{-2} mole.dm⁻³ H₂O₂, 5×10^{-3} mole.dm⁻³ KI, 0.125 mole.dm⁻³ H₂SO₄,
 8.5×10^{-4} mole.dm⁻³ C₆H₈O₆ and ionic strength of 0.15 mole.dm⁻³ at 293 ± 0.17 K.

$10^5 \times [V(V)]$ (mole.dm ⁻³)	0.00	1.25	2.50	5.00	7.50	10.00	12.50
t_0/t	0.998	1.172	1.383	1.732	2.175	2.432	3.049
	1.000	1.175	1.378	1.725	2.186	2.474	3.070
	1.002	1.173	1.381	1.738	2.209	2.400	2.965

The covered concentration range is $1.25 \times 10^{-5} \div 1.25 \times 10^{-4}$ mole.dm⁻³ V(V).
 The equation of the obtained calibration line is:

$$t_0/t = (0.98 \pm 0.08) + (1.57 \pm 0.12) \times 10^4 \times [V(V)] \quad (R=0.996) \quad (10)$$

A good correlation coefficient and agreement between the computed and the theoretical intercepts can be noticed again. The detection limit is of 2.1×10^{-6} mole.dm⁻³ (0.1 mg.dm⁻³) V(V).

Copper and iron

Because one of our goals was the determination of molybdenum and vanadium in the presence of interferents, no attempts were made to find experimental conditions that give best selectivity towards copper and iron. Therefore, optimal conditions for analysis of Mo(VI) and V(V) were taken over. Table 4 presents the values of t_0/t for both Cu(II) and Fe(III). Experiments for Cu(II) were performed in both conditions for Mo(VI) and V(V); while covered concentration ranges covered up to 10^{-5} mole.dm⁻³ and 10^{-4} mole.dm⁻³ Cu(II), respectively. Kinetic runs for Fe(III) were performed only under the optimal circumstances for molybdenum. The covered range was up to 10^{-5} mole.dm⁻³.

Table 4

Results of kinetic runs. Calibration for Cu(II) and Fe(III).

Calibration for Cu(II). Optimal experimental conditions of Mo(VI) – Table 2						
$10^6 \times [\text{Cu(II)}]$ (mole.dm ⁻³)	0.00	2.00	4.00	6.00	8.00	10.00
t_0/t	1.002 1.000 0.998	1.420 1.419	1.828 1.851	1.909 1.925	2.079 2.064	2.371 2.394
Calibration for Cu(II). Optimal experimental conditions of V(V) – Table 3						
$10^5 \times [\text{Cu(II)}]$ (mole.dm ⁻³)	0.00	1.25	2.50	5.00	7.50	10.00
t_0/t	1.002 1.000 0.998	1.061 1.049 1.027	1.038 1.029 1.034	1.054 1.050 1.048	1.056 1.066 1.060	1.071 1.070 1.073
Calibration for Fe(III). Optimal experimental conditions of Mo(VI) – Table 2						
$10^6 \times [\text{Fe(III)}]$ (mole.dm ⁻³)	0.00	2.00	4.00	6.00	8.00	10.00
t_0/t	1.002 1.000 0.998	1.476 1.481	2.348 2.348	2.750 2.784	3.448 3.500	6.365 6.197

The following calibration lines were obtained for copper:

$$t_0/t = (1.05 \pm 0.08) + (1.35 \pm 0.13) \times 10^5 [\text{Cu(II)}] \quad (R=0.995) \quad (11)$$

$$\text{and } t_0/t = (1.00 \pm 0.01) + (6.90 \pm 2.55) \times 10^2 [\text{Cu(II)}] \quad (R=0.966) \quad (12)$$

under optimal circumstances for Mo(VI) and V(V), respectively. Because of the steeper slope in equation (11), it is obvious that favorable conditions for the catalysis by Mo(VI) are also more convenient for the catalysis by Cu(II). Even though the studied concentration range is some orders of magnitude smaller than that in the case of V(V), the slope is much higher. Hence the detection limits of the two sets of experimental conditions will also differ considerably: 3×10^{-7} mole.dm⁻³ ($20 \mu\text{g.dm}^{-3}$) and 7.4×10^{-6} mole.dm⁻³ (0.5 mg.dm^{-3}) Cu(II) according to equations (11) and (12), respectively.

The calibration line for iron is:

$$t_0/t = (0.93 \pm 0.17) + (3.26 \pm 0.28) \times 10^5 [\text{Fe(III)}] \quad (R=0.996) \quad (13)$$

Its detection limit is of 5.6×10^{-7} mole.dm⁻³ ($31 \mu\text{g.dm}^{-3}$) Fe(III).

The slopes of calibration lines (11) and (13), corresponding to catalysis by Cu(II) and Fe(III) respectively, are smaller but still comparable to that in equation (9), corresponding to catalysis by Mo(VI) under identical experimental circumstances. This can explain the strong interference by the two ions in the determination of molybdenum.

Bi-component calibration. Vanadium – copper mixtures

In order to study the joint catalytic effect of the vanadium – copper couple, the ions were added together to the reaction mixture. In the presence of constant Cu(II) concentration, the content of V(V) was increased stepwise.

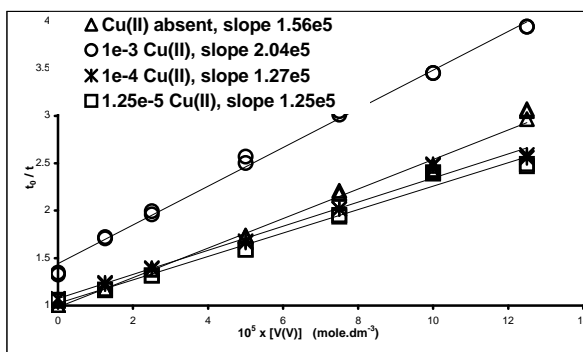


Fig. 1. t_0/t vs V(V) concentration for various Cu(II) contents. Other experimental conditions are the same as listed for Table 3.

Figure 1 presents experimental t_0/t values plotted against $[V(V)]$, for various Cu(II) contents. Although the lines corresponding to 1.25×10^{-5} and 10^{-4} mole. dm^{-3} Cu(II) have practically equal slopes, they lay under the line of "pure" vanadium. On the other hand, a very high content of copper, as compared to that of vanadium, seems to enhance the catalytic effect of the later. This phenomenon may also be due to the fact that Cu(II) promotes the side reaction of H_2O_2 decomposition, so that its contribution to the overall H_2O_2 consumption rate will be more significant. Still, because the extent of process (1) is of 8 %, the linearity of the plot is maintained. To restate, it is obvious that the cumulative catalytic effect of the V(V)-Cu(II) couple is neither additive (lines in Figure 1 are not parallel) nor synergistic.

Therefore, a tri-dimensional $t_0/t = f \{[V(V)], [Cu(II)]\}$ representation to generate a calibration surface is required for this bi-component matrix. Figure 2 presents the surface of t_0/t values recorded for both stepwise increased vanadium and copper contents. Because t_0/t did not vary significantly for small concentration steps, the surfaces are described by rather few points and are therefore quite "edgy". Figure 2a shows the case of equivalent covered concentration ranges, of up to 10^{-4} mole. dm^{-3} . However, the Cu(II) content was extended to values of two orders of magnitude higher (till 2.5×10^{-3} mole. dm^{-3}) than that of V(V). This is why, in Figure 2b where all experimental results are presented, a logarithmic concentration scale was chosen for Cu(II). Both Figures 1 and 2b prove that as long as the contents in vanadium and copper are comparable, no dramatic changes of the incubation times occur. But as soon as $[Cu(II)]$ exceeds 5×10^{-4} mole. dm^{-3} , the rate of hydrogen peroxide decomposition increases abruptly. As already mentioned, this is probably due to side reactions.

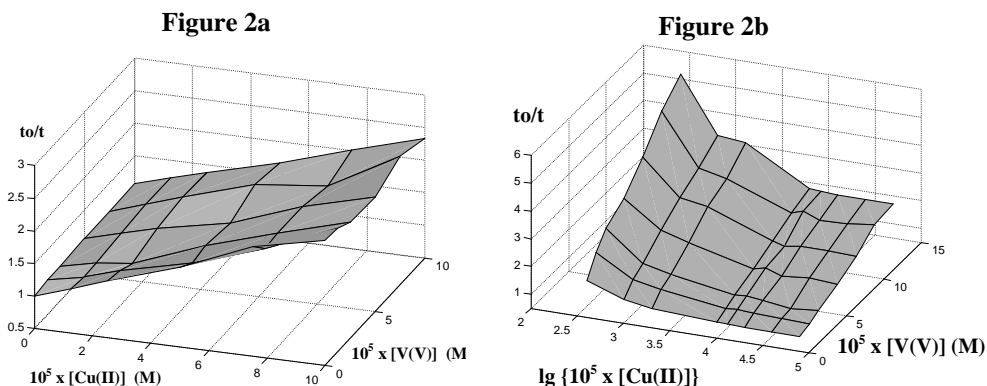


Fig. 2. $t_0/t = f \{[\text{V(V)}], [\text{Cu(II)}]\}$ response surfaces for the V(V)-Cu(II) mixture. a) equivalent concentration ranges; b) non- equivalent concentration ranges. Other experimental conditions the same as listed for Table 3.

The supplementary catalytic effect of copper can be suppressed by masking it with EDTA. Table 5 presents average t_0/t values, recorded both in the absence (column A) and presence (columns B and C) of 10^{-5} mole. dm^{-3} Cu(II) and 10^{-3} mole. dm^{-3} EDTA. It is obvious that values in Column C are practically equal to those corresponding to catalysis by only V(V).

To perform a bi-component V(V)-Cu(II) analysis, two distinct kinetic runs are required. The first experiment, carried out in the presence of EDTA, will generate a t_0/t consistent with catalysis by only vanadium. From calibration line (10), its exact concentration can be calculated. The second experiment will lead to a t_0/t value consistent with catalysis by both ions. By cutting the appropriate surface in Figure 2 with a plane, drawn parallel to the XOY plane at the t_0/t value of the unknown sample, a concentration level curve will be obtained. This corresponds to all V(V)-Cu(II) concentration couples that generate the cumulative t_0/t in the second experiment. With the already known V(V) concentration, that of Cu(II) can be easily determined. Figure 3 presents five examples of such level curves at arbitrary taken t_0/t values.

Table 5

Kinetic runs in the presence of EDTA; 10^{-5} mole. dm^{-3} Cu(II) (columns B and C); 10^{-3} mole. dm^{-3} EDTA (column C). Experimental conditions as listed for Table 3.

$10^5 \times [\text{V(V)}]$ (mole. dm^{-3})	t_0/t		
	A	B	C
0.75	1.100	1.145	1.085
2.50	1.375	1.935	1.378
7.50	2.129	2.460	2.139
12.50	2.860	3.287	2.849

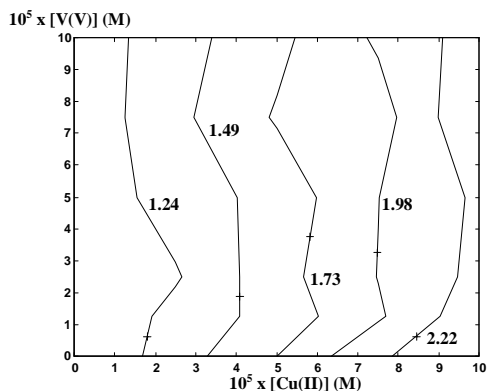


Fig. 3. Examples of concentration level curves corresponding to the surface in Figure 2a.

Tri-component calibration. Molybdenum – copper – iron mixtures

In order to study the joint catalytic effect of the molybdenum – copper – iron mixture, the ions were added together to the reaction mixture. Their concentration was increased stepwise and $t_0/t = f \{[Cu(II), Fe(III)]\}$ values were recorded, first in the absence of molybdenum and then in the presence of it.

Figure 4 presents the t_0/t values plotted against $[Cu(II)]$ for various $Fe(III)$ contents, in the absence of molybdenum. Because of some parallel lines, it is obvious that the cumulative catalytic effect of $Cu(II)$ - $Fe(III)$ couple is additive only for concentrations under 4×10^{-6} mole. dm^{-3} for both ions. Beyond this value their joint effect is neither additive nor synergistic. The same conclusion may be drawn also from Figure 5, that is the response surface $t_0/t = f \{[Cu(II), Fe(III)]\}$ in the absence of $Mo(VI)$.

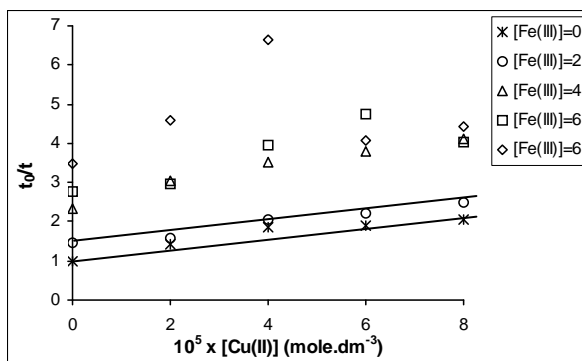


Fig. 4. t_0/t vs $Cu(II)$ concentration for various $Fe(III)$ contents given in 10^{-6} mole. dm^{-3} . Molybdenum is absent. Other experimental conditions are the same as listed for

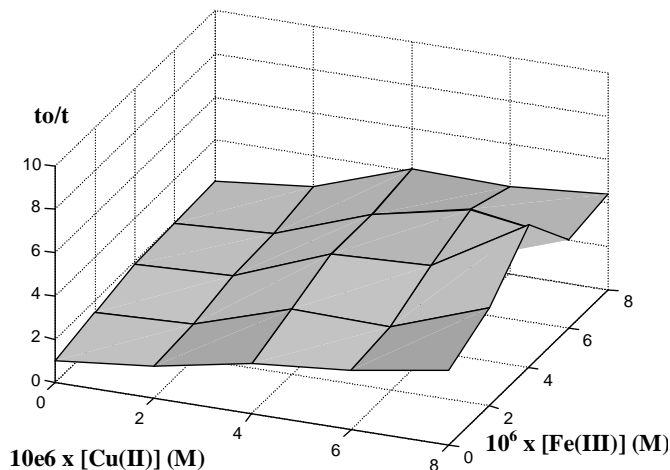


Fig. 5. $t_0/t = f \{[\text{Cu(II)}], [\text{Fe(III)}]\}$ response surface in the absence of molybdenum. Other experimental conditions the same as listed for Table 2.

By increasing the Mo(VI) content of the mixture, a family of calibration surfaces was obtained. Their superposition is presented in Figure 6 and stands for the tri-component Mo(VI)-Cu(II)-Fe(III) calibration. Again, because t_0/t did not vary significantly for small concentration steps, each surface is described by only 25 points and has therefore quite sharp edges and angles.

The picture in Figure 6 shows that even though higher t_0/t values are sensed for higher catalyst concentrations, the surfaces lay on top of each other forming a multi-layer body, only for both copper and iron concentrations smaller than $4 \times 10^{-6} \text{ mole.dm}^{-3}$, regardless of the amount of molybdenum present in the mixture. This is probably due to the additive catalytic effect, applying only for narrow concentration ranges, of the Cu(II)-Fe(III) as well as of the Mo(VI)-Cu(II) and Mo(VI)-Fe(III) [38] couples. Moreover, high Cu(II) and Fe(III) contents will favorably influence the side reaction of H_2O_2 decomposition; so that, because it is catalyzed by Fe(III) and promoted by Cu(II), it may significantly affect the overall reaction rate (6). These phenomena may all contribute to the fact that when higher catalyst amounts are present in the sample, the same t_0/t is measured for totally different concentration triplets and the surfaces will cut each other as it may be observed from Figure 6.

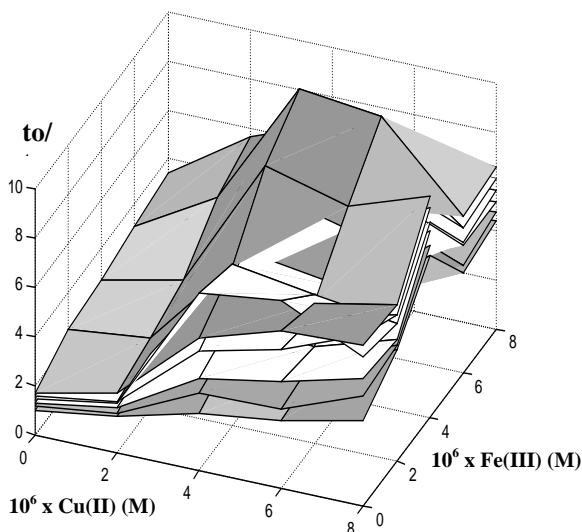


Fig. 6. Tri-component calibration. The family of $t_0/t = f\{[Cu(II)], [Fe(III)]\}$ response surfaces for 2×10^{-7} , 4×10^{-7} , 6×10^{-7} , 8×10^{-7} and 10×10^{-7} mole. dm^{-3} Mo(VI). Other experimental conditions are the same as listed for Table 2.

The calibration model to be elaborated is based on the t_0/t measurements for known triplets of [Mo(VI)], [Cu(II)] and [Fe(III)]. Its purpose is to function in a reversed way: it will have to give some information about the unknown ion concentrations for a measured t_0/t value of an unknown sample.

The concentration of Mo(VI), like in the case of V(V), can be obtained by means of a distinct experiment. If EDTA is added to the reaction mixture, it will mask the cationic catalysts. Hence, the measured t_0/t value will depend only on the Mo(VI) content of the sample. By using the calibration line of equation (9), its concentration can be determined.

In order to gain some information about the Cu(II) and Fe(III) contents, a $t_0/t = f\{[Cu(II)], [Fe(III)]\}$ surface for the exact found [Mo(VI)] is needed. Again, the intersection of this surface with a plane, drawn parallel to the XOY plane at the t_0/t value of the unknown sample, will generate some level curves. These correspond to the Cu(II)–Fe(III) concentration couples to generate the experimentally determined t_0/t , for a certain Mo(VI) content. Figure 7 presents 15 examples of such curves obtained in the absence of Mo(VI), by cutting the surface in Figure 5 with the same number of arbitrary chosen planes. As it may be observed, the exact concentrations of Cu(II) and Fe(III) may not be established, the curves will indicate only a range of values (a minimum and a maximum).

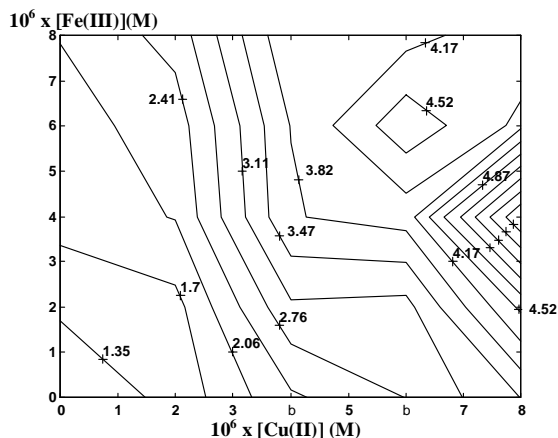


Fig. 7. Examples of concentration level curves corresponding to the surface in Figure 5.

In order to construct an appropriate $t_0/t = f \{[Cu(II),Fe(III)]\}$ calibration surface at any Mo(VI) concentration within the range of concentrations of up to 10^{-6} mole.dm⁻³, we employed an artificial neural network (ANN) [43,44]. The surface has to be much smoother than those in Figures 5 and 6, thus described by much more points.

To resume, the proposed calibration model would consist of both the calibration line (9), and a $t_0/t = f \{[Cu(II),Fe(III)]\}$ surface generated by an ANN. In order to elaborate such a model, an artificial neural network was trained by using 115 sets of experimental data $t_0/t = f \{Mo(VI),[Cu(II)],[Fe(III)]\}$. Its characteristics are listed in Table 6. A Levenberg–Marquardt learning algorithm [45] was employed for 60 epochs till the sum squared error reached a satisfactory predetermined value. Testing was performed with 10 sets of data.

To evaluate the prediction capacity of the network, calculated data Y were plotted against experimental data X, for both the training and the testing set of values. The equations of the obtained lines are:

$$Y = 0.117 + 0.974 X \quad (R = 0.987) \quad (14)$$

and $Y = 0.079 + 0.980 X \quad (R = 0.985) \quad (15)$

respectively. Both have rather good correlation coefficients, intercepts close to zero and slopes close to unity (ideal values). Thus, the simulation capacity of the ANN is expected to be rather good.

The trained network was further used to generate, by means of simulation, the replicate of the $t_0/t = f \{[Cu(II),Fe(III)]\}$ surface in Figure 5. The obtained result is presented in Figure 8.

Table 6

Characteristics of the artificial neural network

Parameter	Value
Input nodes	3
Output nodes	1
Hidden layers	1
Hidden nodes	7
Input layer transfer function	Identity
Hidden layer transfer function	Sigmoid: $f(x) = 1/(1 + e^{-x})$
Output layer transfer function	Sigmoid: $f(x) = 1/(1 + e^{-x})$
Bias	Variable
Learning rate	Variable

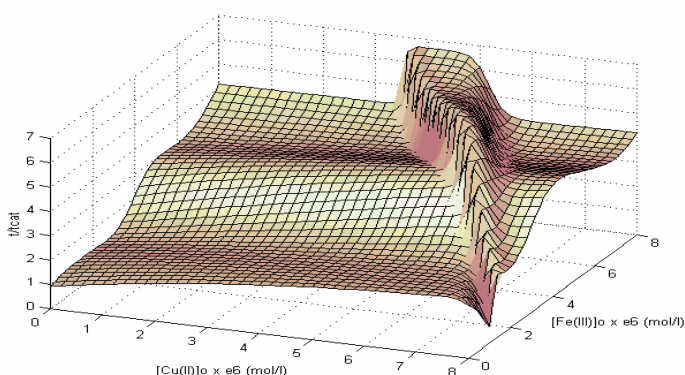


Fig. 8. ANN generated $t_0/t = f\{[Cu(II), Fe(III)]\}$ calibration surface in the absence of molybdenum. The chosen concentration step is of 2×10^{-7} mole.dm⁻³.

It is obvious that the two surfaces, the experimental one in Figure 5 and the simulated one in Figure 8, do not match. The latter exhibits a steep increase exactly in the region of concentrations where the response surfaces in Figure 6 cut each other. Only for Cu(II) and Fe(III) concentrations smaller than 4×10^{-6} mole.dm⁻³, do simulated data approximate measured ones.

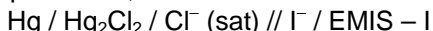
As a result, because in a certain range of catalyst concentrations their cumulative effect is completely nonlinear and completely different sets of inputs correspond to the same output, none of the surfaces obtained by means of simulation by this ANN are suitable in the proposed calibration model. However, in a more narrow concentration range of copper and iron, where experimental response surfaces lay one on the top of each other, an artificial neural network could be employed in calibration. In this case an other ANN, with different

characteristics, has to be trained, tested and used for generating the required $t_0/t = f\{[Cu(II), Fe(III)]\}$ surfaces. Unfortunately, there is not enough available experimental data, for $[Cu(II)]$ and $[Fe(III)]$ less than $4 \times 10^{-6} \text{ mole.dm}^{-3}$, to do so.

Potentiometric detection of the end-point

Because visual detection of the reaction's end-point is a monotonous and tedious process, the accuracy of the results may be questioned. Therefore, potentiometric verification of the calibration line (19) for molybdenum was performed. Moreover, some results for Mo(VI)-Cu(II) and Mo(VI)-Fe(III) couples were also compared. It is worth mentioning that the water to prepare these solutions was more pure (contained no ionic residuals) than that used for previous experiments, so that results may be affected. In order to have a basis for comparison potentiometric measurements were doubled by visual detection, under identical reaction conditions and by using the same reagent solutions.

During these experiments, the electromotive force of the



electrochemical cell was monitored versus time. Typical kinetic runs are presented in Figure 9 for both the absence (the blank) and the presence of $10^{-6} \text{ mole.dm}^{-3}$ Mo(VI). The plots have the shape of titration curves. For the simplicity of computing, the end-point of the reaction was considered to correspond to the inflection point of the curve. The time at which it occurred, was considered to be the searched for incubation time.

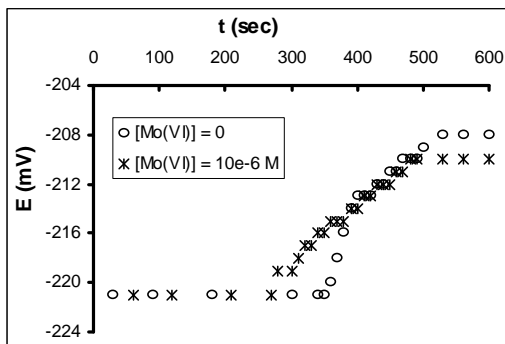


Fig. 9. Typical potentiometric kinetic runs. Experimental conditions as listed for Table 2.

Values of the individual t_0/t ratios for potentiometric detection of the reaction time t were plotted against the values obtained by visual detection. Some selected results are presented in Figure 10. It is obvious that the kinetic runs are repeatable and the two methods give comparable results.

The equations of the obtained calibration lines are:

$$t_0/t = (0.97 \pm 0.05) + (4.04 \pm 0.83) \times 10^5 x [\text{Mo(VI)}] \quad (R=0.990) \quad (16)$$

and $t_0/t = (0.99 \pm 0.03) + (3.77 \pm 0.46) \times 10^5 x [\text{Mo(VI)}] \quad (R=0.992) \quad (17)$

for potentiometric and visual detection of incubation time, respectively. The lines have good and comparable correlation coefficients. Their intercepts and slopes are also in good agreement. However, both slopes are somewhat smaller than 6.81×10^5 in equation (9). This is due to the fact that the water used to prepare the reagent solutions was more pure in these cases. It was demineralized as well as four times distilled, while the water used in previous experiments was only twice distilled. We suspect that it also contained some residual amounts of ions with catalytic activity towards the indicator reaction. This fact was confirmed by other kinetic experiments in our laboratory, too.

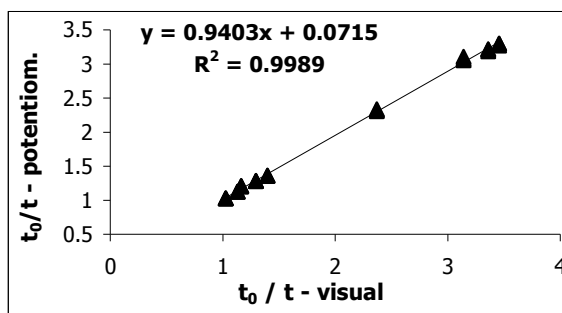


Fig. 10. Potentiometric versus visual detection of the end-point.

By taking into account the experimental data in Figure 10 as well as the calibration equations (16) and (17), it may be concluded that the two methods have comparable performances.

Acknowledgments. The authors thankfully acknowledge Dr. Ing. Nagy Zoltan for developing the necessary ANN software as well as for the financial support of the CNCSIS – Romanian Ministry of Education, Grant No 46174/27.11.1997, codes no 10 and Grant No 32575/1999, code no 40/113.

REFERENCES

1. J.-M. M e r m e t, M. O t t o, H.M. Widmer (eds.), *Analytical Chemistry*, Wiley-VCH, Weinheim, Chap. 6, **1998**, pg. 227-252.
2. A. A. N o y e s, W. O. S c o t t, *Z. Phys. Chem.*, **1895**, *18*, 118; G. B r e d l g, J. H. W a l t o n, *Z. Elektrochem.*, **1903**, *9*, 114; J. H. W a l t o n, *Z. Phys. Chem.*, **1904**, *47*, 184; K., O k a b e, *J. Chem. Soc. Japan*, **1940**, *61*, 1235; M. A. G a r b a l l o, *Anales Assoc. Qcim., Arg.*, **1948**, *36*, 150; M. K a t a o k a, Y. Y o s h i z a w a, T. K a m b a r a, *Bunseki Kagaku*, **1982**, *31*, E171.
3. H. L i e b h a f s k y, A. M o h a m m e d, *J. Amer. Chem. Soc.*, **1933**, *55*, 3977.

4. G. Svehla, L. Erdey, *Mikrochem J.*, **1963**, 7, 206.
5. G. Svehla, *Analyst*, **1969**, 94, 1120.
6. K. B. Yatsimirskii, *A kemai analízis kinetikus módszerei*, Akadémiai Kiadó, Budapest, **1966**, pg. 71-83.
7. K. B. Yatsimirskii, MTP, *International Review of Science, Physical Chemistry Series One*, Vol. 12, *Analytical Chemistry*, part 1, University Park Press, Baltimore, London, **1973**, pg. 193-217.
8. H. A. Mottola, *Kinetic Aspects of Analytical Chemistry* (Vol. 96 of the series "Chemical Analysis"), John Wiley & Sons, New York, **1988**, Chapter 2, pg. 24-52.
9. H. Müller, *CRC Crit. Rev. Anal. Chem.*, **1982**, 13, 313.
10. G. Svehla, L. Erdey, *Mikrochem. J.*, **1963**, 7, 221.
11. H. Weisz, H. Ludwig, *Anal. Chim. Acta*, **1975**, 75, 181.
12. H. Müller, P. Nennung, S. Artmann, *2nd Symp. Anal Solid State Mater.*, Karl-Marx Stadt, Germany, **1978**; H. Müller, *CRC Crit. Rev. Anal. Chem.*, **1982**, 13, 313.
13. B. F. Quinn, P. H. Woods, *Analyst*, **1979**, 104, 552.
14. M. Kataoka, K. Nishimura, T. Kambara, *Talanta*, **1983**, 30, 941.
15. Z. Fang, S. Xu, *Anal. Chim. Acta*, **1983**, 145, 143.
16. J. A. Amberson, G. Svehla, *Anal. Chim. Acta*, **1985**, 178, 255.
17. H. Dacka-Seliga, *Chem. Anal. (Warsaw)*, **1985**, 30, 881.
18. J. T. Kennedy, G. Svehla, *Fresenius' Z. Anal. Chem.*, **1986**, 324, 19.
19. M. Trojanowicz, A. Hulanicki, W. Matuszewski, M. Palys, A. Fuksiwicz, T. Hulanicka-Michalak, S. Raszewski, J. Szylter, W. Augustyniak, *Anal. Chim. Acta*, **1986**, 188, 165.
20. Z. Yu, Y. Li, *Fenxi Huaxue*, **1987**, 15, 841; H. A. Mottola, D. Pérez-Bendito, H. B. Mark, Jr., *Anal. Chem.*, **1990**, 62, 441R.
21. L. C. R. Pessenda, A. O. Jacintho, E. A. G. Zagatto, *Anal. Chim. Acta*, **1988**, 214, 239.
22. R. M. Villanueva, I. D. Martinez, G. Ramis, M. C. Garcia, *Thermochim. Acta*, **1990**, 158, 215.
23. C. Zhuang, S. Fu, *Fenxi Ceshi Tongbao*, **1990**, 9, 39; H. A. Mottola, D. Pérez-Bendito, *Anal. Chem.*, **1992**, 64, 407R.
24. D. Liu, A. Zhang, *Yingyang Xuebao*, **1991**, 13, 68; *Chem. Abstr.*, **1991**, 115, 269443u.
25. J. C. Andrade, S. P. Eiras, R. E. Burns, *Analyst*, **1993**, 118, 213; J. C. Andrade, S. P. Eiras, R. E. Burns, *Anal. Chim. Acta*, **1991**, 255, 149.
26. T. Yamane, Y. Aruga, T. Ogawa, *Monatsh. Chem.*, **1994**, 125, 20; *Chem. Abstr.*, **1994**, 121, 220560q.
27. E. N. V. M. Carrilho, F. J. Krug, E. A. G. Zagatto, *Talanta*, **1995**, 42, 2021.
28. R. N. Voevutskaya, V. K. Pavlova, A. T. Pilipenko, *Zh. Analit. Khim.*, **1979**, 34, 1299.
29. M. Kataoka, K. Nishimura, T. Kambara, *Bunseki Kagaku*, **1983**, 32, 516; *Analytical Abstracts*, Royal Society of Chemistry, Silver Platter International N.V., Cambridge, UK, 1980-1998/09, Accession Number 4605B00205.

30. M. Kataoka, Y. Yoshizawa, T. Kambara, *Bunseki Kagaku*, **1982**, 31, E171; D. Pérez-Bendito, M. Silva, *Kinetic Methods in Analytical Chemistry*, Ellis Horwood Limited, Chichester, **1988**, pg. 49.
31. I. I. Alekseeva, V. V. Borisova, A. V. Shuginina, L. T. Yuranova, *Zh. Analit. Khim.*, **1981**, 36, 108.
32. Q. Cai, R. Yang, *Fenxi Huaxue*, **1988**, 16, 1021, *Analytical Abstracts*, Royal Society of Chemistry, Silver Platter International N.V., Cambridge, UK, 1980-1998/09, Accession Number 5107B00107.
33. A. Altinata, B. Pekin, *Anal. Lett.*, **1973**, 6, 667.
34. R. H. He, J. H. Wang, *Mikrochim. Acta*, **1996**, 124, 195.
35. R. Liu, D. Liu, A. Sun, G. Liu, *Analyst*, **1995**, 120, 565.
36. J. Wang, R. He, *Talanta*, **1996**, 43, 391.
37. C. Wiese, G. Schwedt, *Fresenius' J. Anal. Chem.*, **1997**, 358, 718.
38. I. Bâldea, C. Călin, *Rev. Chim.*, **1998**, 49, 665.
39. A. Rustoiu–Csavdari, I. Bâldea, C. Călin, *Proceedings of the 6th Internat. Symp. On Kinetics in Anal. Chem., KAC'98*, Kassandra, Greece, **1998**, p. 39; A. Rustoiu–Csavdari, I. Bâldea, L. Copolovici, D. Mihai, *a XI-a Conferinta Internationala de Chimie si Inginerie Chimica*, București, România, **1999**.
40. C. H. Bamford, C. F. H. Tipper (eds.), *Comprehensive Chemical Kinetics*, Elsevier, Amsterdam, Vol.6, **1972**, pg. 406.
41. G. Niac, V. Voiculescu, I. Bâldea, M. Preda, *Formule, tabele, probleme de chimie fizică*, Ed. Dacia, Cluj-Napoca, **1984**, pg. 264.
42. Analytical Method Committee, *Analyst*, **1987**, 112, 199.
43. F. Despaigne, D. L. Massart, *Analyst*, **1998**, 123, 323.
44. A. Rustoiu–Csavdari, L. Copolovici, Z. Nagy, *Proceedings of the 14th International Congress of Chemical and Process Engineering* (on CD-ROM), Praha, Czech Republic, **2000**, 1447.
45. M. T. Hagan, M. Menhaj, *IEEE Transactions on neural Networks*, **1994**, 5, 989.

SPECTROPHOTOMETRIC AND PAPER ELECTROPHORETIC STUDIES OF THE COPPER (II) POLYOXOTUNGSTOBISMUTHATE COMPLEXES

DAN RUSU,^a CRISTINA ROȘU, MARIANA RUSU, GHEORGHE MARCU^b

^aPharmacy Department, Iuliu Hațieganu University, 13 Emil Isac, 3400-Cluj-Napoca, Romania

^bChemistry Department, Babes-Bolyai University, 11 Arany Janos, 3400-Cluj-Napoca, Romania

ABSTRACT. The starting point of this study is represented by the trilacunar structure of the polyoxotungstate anion $[\text{BiW}_9\text{O}_{33}]^{9-}$ having the capacity of functioning as the coordinating ligand for the copper Cu^{2+} cation, and the formation of the complex polyoxotungstate anions of the type $[\text{Cu}_3(\text{BiW}_9\text{O}_{33})_2]^{12-}$ and $[\text{Cu}_4(\text{BiW}_9\text{O}_{33})_2]^{10-}$. The pH range of the complexes' formation was established and the stability constants were calculated by the electrophoresis method. By applying the molar ratio method to spectrophotometry, the molar ratio of polyoxometalate ligands and Cu^{2+} cations have been found to have the values of 2:3 and 2:4, respectively.

INTRODUCTION

The lacunar polyoxometalates generally react readily with any potential addenda or with a wide variety of octahedrally coordinating metal ions to refill the vacant sites. This produces complexes that are hybrids between polyoxometalate species and coordination complexes.[1] We reported a lot of works to polyoxometalate complexes containing metallic cations, especially those wherein that atoms act as a bridge connecting two lacunar units.[2-9]

This paper presents the results of our work on the formation in solution of Cu^{2+} polyoxometalates with $\text{BiW}_9\text{O}_{33}^{9-}$ as ligand by the paper electrophoresis method, which permits the identification of the formed polyoxometalates in very limited pH ranges, thus enabling them to separate in the electric field due to the various electrophoretic mobilities of the existing ionic species.[10]

One of the widely used methods in establishing the stoichiometry of the formation reactions of the complex combinations is the method of the molar ratio variation applied to the spectrophotometric study.[11,12] This method has also

been applied to the systems Cu^{2+} - $\text{BiW}_9\text{O}_{33}^{9-}$ in order to establish the values of the combination ratio between Cu^{2+} ion and the polyoxometalate ligand.

EXPERIMENTAL PART

1. Solution Preparation

The experiments were carried out on a $\text{Na}_9\text{BiW}_9\text{O}_{33}$ polyoxometalate in aqueous medium; the polyoxometalate was prepared according to Krebs [13] at the concentration of 10^{-2} - 5×10^{-2} mole·l⁻¹ in the ligand and at pH values ranging from 1.5 to 8.5. The aqueous solutions of $\text{Cu}(\text{SO}_4)_2$ were obtained out of the $\text{Cu}(\text{SO}_4)_2 \cdot 5\text{H}_2\text{O}$ in distilled water.

2. Spectrophotometric study

A set of solutions was prepared, containing Cu^{2+} and $\text{BiW}_9\text{O}_{33}^{9-}$, and having a 10^{-2} mole·l⁻¹ concentration in various molar ratios. The pHs of the solutions were adjusted to the values of 6.5 and 4 with NaOH 10^{-1} mole·l⁻¹ and HCl 10^{-1} mole·l⁻¹, respectively, with the purpose of being within the optimal pH of the formation of Cu^{2+} polyoxometalates.

The absorbances of these solutions were measured with a SPECORD UV-Vis spectrophotometer, using 1 cm wide glassy cuvettes at a wavelength of 824.13 nm and 780 nm, respectively.

3. Electrophoretic Study.

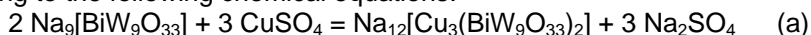
This study was carried out on an ordinary electrophoresis apparatus, at usual voltage, cooled with water. The $\text{Cu}(\text{SO}_4)_2$ solution, of 10^{-4} mole·l⁻¹ concentration was deposited with a microdropper in the center of a Karl-Schneider Schull chromatographic paper impregnated in the ligand solutions having 10^{-4} - 10^{-2} mole·l⁻¹ concentration, with different pH values (1.5 to 8.5). The pHs were adjusted with HCl and NaOH solutions and their values were measured with a OK-102 Radelkis pH-meter. The ionic strength was maintained at constant value by a corresponding addition of NaClO_4 10^{-1} mole·l⁻¹.

Experiments were performed at a difference in voltage of 360 V, at a temperature of 15 ± 2 °C, for 3600 s. The formed polyoxometalates were identified by their green color, the Cu^{2+} ion was identified by developing with rubeanic acid and the noncomplexed ligand by reducing W^{6+} with UV rays to "blue tungsten".

Besides the solutions containing the metallic cation, an electrically neutral glucose drop was added, towards which the shifts of the ionic species after electromigration were adjusted. The R_f values of the formed polyoxometalates were determined by the ascending paper chromatography, relating the shift of the formed chemical species to the front of the saturated NaCl as eluent.

RESULTS AND DISCUSSION

If a solution that contains Cu^{2+} ions is rapidly added to a solution of sodium salt of $[\text{BiW}_9\text{O}_{33}]^{9-}$ polyoxometalate anions, the following reactions take place, according to the following chemical equations:





We observe that the green colour of the obtained solutions appears immediately. The colour intensity doesn't change, even on standing 24 hours.

The spectrophotometric study concerned with the formation of the polyoxometalate complexes having Cu^{2+} as central ion has been carried out by the molar ratios method.

By representing graphically the absorbances of the solutions that contain the two compounds, the copper sulfate and the sodium salt of the polyoxometalate ligand, versus different molar ratios combination, we obtain three straight lines which cross each other in two points which correspond to the molar ratio of 3:2 and 4:2 respectively (Fig.1).

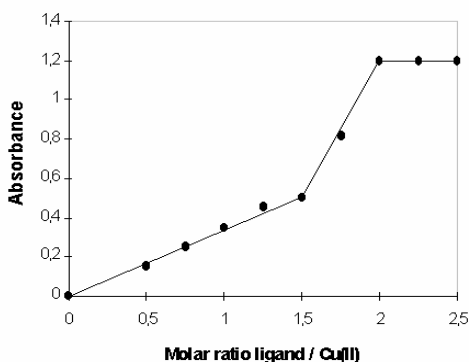


Fig. 1. Dependence of the absorbance versus various molar ratios of components: Cu^{2+} - $\text{BiW}_9\text{O}_{33}^{9-}$.

According to the reaction stoichiometry, the molar ratios Cu^{2+} :ligand=3:2 and 4:2 respectively, the values of the equivalence points that were calculated theoretically concord with the values obtained experimentally.

In order to establish the pH-range of the $[\text{Cu}_3(\text{BiW}_9\text{O}_{33})_2]^{12-}$ and $[\text{Cu}_4(\text{BiW}_9\text{O}_{33})_2]^{10-}$ heteropolyanion formation, we started from the premise that the reactions (a) and (b) of the polyoxoanion species' formations may be considered as reactions with formation of complex combinations according with the following equations:



In order to establish the optimal conditions of the formation of Cu_3L_2 and Cu_4L_2 polyoxometalates, where $\text{L}=\text{BiW}_9\text{O}_{33}^{9-}$, a study has been accomplished on their formation by the chemical reactions (a') and (b') in solutions of 10^{-2} mole.l⁻¹ concentrations, using the electrophoresis method.

Thus, considering that the studied reactions occur according to the equations (a') and (b') they have the following equilibrium constants:

$$K_1 = \frac{[\text{Cu}_3\text{L}_2]}{[\text{Cu}^{2+}]^3 \cdot [\text{L}]^2} \quad (1)$$

$$K_2 = \frac{[\text{Cu}_4\text{L}_2]}{[\text{Cu}_3\text{L}_2] \cdot [\text{Cu}^{2+}]} \quad (1')$$

The Kunkel and Tiselius [14] method has been applied to estimate the sum of the electrophoretic mobilities of the formed ions which is given by the relations:

$$M_1 = \frac{\mu_{\text{Cu}^{2+}} \cdot [\text{Cu}^{2+}] + \mu_{\text{Cu}_3\text{L}_2} \cdot [\text{Cu}_3\text{L}_2]}{[\text{Cu}^{2+}] + [\text{Cu}_3\text{L}_2]} \quad (2)$$

$$M_2 = \frac{\mu_{\text{Cu}_3\text{L}_2} \cdot [\text{Cu}_3\text{L}_2] + \mu_{\text{Cu}_4\text{L}_2} \cdot [\text{Cu}_4\text{L}_2]}{[\text{Cu}_3\text{L}_2] + [\text{Cu}_4\text{L}_2]} \quad (2')$$

where: M_1, M_2 = the sum of the electrophoretic mobilities;

$L = \text{Na}_9[\text{BiW}_9\text{O}_{33}]$;

$\mu_{\text{Cu}^{2+}}, \mu_{\text{Cu}_3\text{L}_2}, \mu_{\text{Cu}_4\text{L}_2}$ = the electrophoretic mobilities of Cu^{2+} , Cu_3L_2 and

Cu_4L_2 ions;

$[\text{Cu}^{2+}], [\text{Cu}_3\text{L}_2], [\text{Cu}_4\text{L}_2]$ = the mole concentrations of the Cu^{2+} , $[\text{Cu}_3\text{L}_2]$ and $[\text{Cu}_4\text{L}_2]$ ionic species.

The sum of the electrophoretic mobilities of the formed ions, which are pH-dependent, was graphically represented in order to obtain the stability range and the optimal pH of the formation of the polyoxometalates. As a result of the electrophoretic study on the formation reactions of the polyoxometalates, values ranging from 3.5 to 5.5 for the first complex, and from 5.5 to 7 for the second were found. Subsequently, the values of the stability constants were calculated according to the above-mentioned method in a two step chemical reaction, as follows: 3.615 and 1.879 for $\text{Na}_{12}[\text{Cu}_3(\text{BiW}_9\text{O}_{33})_2]$ and $\text{Na}_{10}[\text{Cu}_4(\text{BiW}_9\text{O}_{33})_2]$ respectively; the values of the equilibrium constants being of 0.97×10^2 and 0.5×10^2 respectively.

The electrophoretic study on the $\text{Na}_{12}[\text{Cu}_3(\text{BiW}_9\text{O}_{33})_2]$ and $\text{Na}_{10}[\text{Cu}_4(\text{BiW}_9\text{O}_{33})_2]$ polyoxometalates informs us about the optimum pH of formation, 4.5 and 6.25 for these compounds, about the relative stability of these compounds as well as about their purity. These compounds are unitary and not mixtures of polyoxometalates.

The displacement in centimeters of the formed polyoxometalates was observed experimentally, thus allowing the calculation of the electrophoretic mobilities (μ), the determination of the R_f values and the calculation of the real μ_d mobilities of the formed species by means of the Kunkel-Tiselius [14] relation (3):

$$\mu_d = d \cdot \frac{1}{V \cdot t \cdot R_f} \cdot \left(\frac{l'}{l} \right)^2 \quad (3)$$

where: μ_d = the sum of the experimentally determined electrophoretic mobilities;

d = the migration of the ionic species in cm;

V = the difference of potential;

t = the time of electromigration;

l = the length of the chromatographic paper (38,5 cm);

$$\frac{l'}{l} = 1.69; \text{ the porosity factor of the chromatographic paper ;}$$

$$R_f = 0.99 \text{ for } \text{Na}_{12}[\text{Cu}_3(\text{BiW}_9\text{O}_{33})_2] \text{ and } 0.98 \text{ for } \text{Na}_{10}[\text{Cu}_4(\text{BiW}_9\text{O}_{33})_2]$$

The variation of the sum of the electrophoretic mobilities depending on the pH is plotted in Fig. 2.

It may be observed that $\mu = \mu_{\text{Cu}^{2+}}$ for the minimal μ value in case the formation of the polyoxometalate Cu_3L_2 has not proceeded yet, and $[\text{Cu}_3\text{L}_2]=0$, while $\mu = \mu_{\text{Cu}_3\text{L}_2}$ for the maximal μ value in case Cu^{2+} is partially consumed in reaction (a'); it also becomes obvious that $\mu = \mu_{\text{Cu}_3\text{L}_2}$ for the minimal μ value in case the formation of the polyoxometalate Cu_4L_2 has not proceeded yet and $[\text{Cu}_4\text{L}_2]=0$, while $\mu = \mu_{\text{Cu}_3\text{L}_2}$ for the maximal μ value in case Cu^{2+} is completely consumed in reaction (b'), μ being equal to $\mu_{\text{Cu}_4\text{L}_2}$.

The optimal formation ranges of the complexes were determined from the electrophoretic curves and correspond to the pH range within which the sum of the electrophoretic mobilities is: $\mu_{\text{formation}} \geq 90\%$. The optimal pH formation ranges of the formed polyoxometalates given by the $\mu_{90\%}$ values are 3.5 - 5.5 for Cu_3L_2 and 5.5 - 7 for Cu_4L_2 , respectively. The values $\mu_{\text{Cu}^{2+}}$, $\mu_{\text{Cu}_3\text{L}_2}$, and $\mu_{\text{Cu}_4\text{L}_2}$ were obtained from the curves presented in Fig.2. By introducing them into relations (4) and (4'), the equilibrium constants K_1 and K_2 were determined.

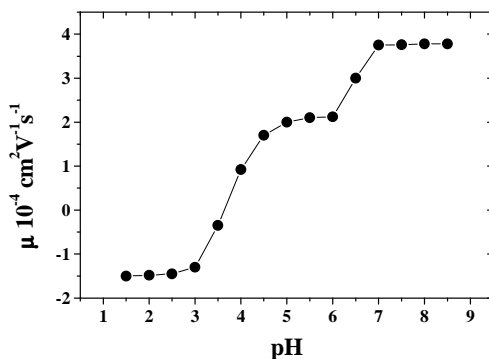


Fig.2. Dependence of μ_d electrophoretic mobilities versus pH values for the systems Cu^{2+} - $[\text{BiW}_9\text{O}_{33}]^{9-}$.

In order to study the formation (equilibrium) constants of the complexes, the Consden, Gordon and Martin equation is applied to the studied systems: [15]

$$\log \frac{M_1 - \mu_{\text{Cu}^{2+}}}{\mu_{\text{Cu}_3\text{L}_2} - M_1} = \log K_1 + \log C \quad (4)$$

$$\log \frac{M_2 - \mu_{Cu_3L_2}}{\mu_{Cu_4L_2} - M_2} = \log K_2 + \log C \quad (4')$$

where: C= the concentration of the ligand solution;

K_1, K_2 = the equilibrium constants.

The equilibrium constants will further be used in the determination of the β stability constants, according to relation (5).

$$\log \beta = \log K + \log c \quad (5)$$

where: β = the stability constant;

K= the equilibrium constant;

c= the optimal concentration of the ligand solution.

Furthermore, a graphic representation of $\log [M_1 - \mu_{Cu^{2+}} / \mu_{Cu_3L_2} - M_1]$ and $\log [M_2 - \mu_{Cu_3L_2} / \mu_{Cu_4L_2} - M_2]$, respectively vs. the various ligand concentrations (Fig. 3 and 4) is presented. By extrapolating the straights presented in Fig. 3 and 4, we obtained the optimal ligand concentration which is later on introduced into relation (5) in the purpose of determining the stability constants.

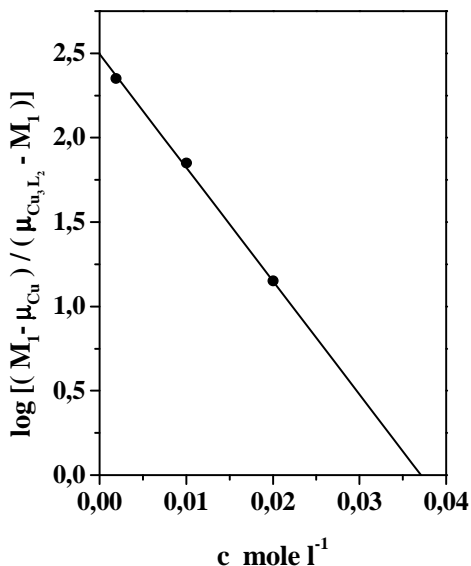


Fig. 3. Dependence of $\log M_1 - \mu_{Cu^{2+}} / \mu_{Cu_3L_2} - M_1$ vs. various ligand concentrations.

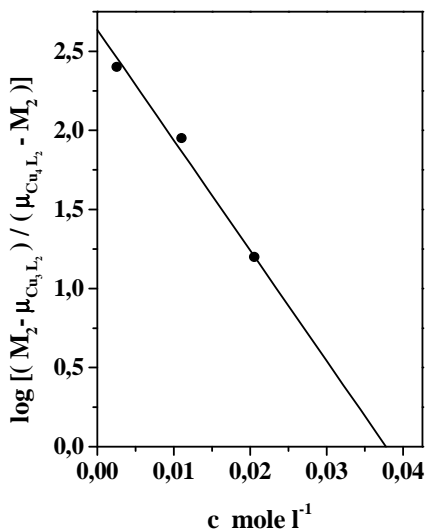


Fig. 4. Dependence of $\log \frac{M_2 - \mu_{Cu_3L_2}}{\mu_{Cu_3L_2} - M_2}$ vs. various ligand concentrations.

Acknowledged. This work was performed under Grant from the National Agency for Science, Technology and Innovation, which is gratefully acknowledged.

CONCLUSIONS

The spectrophotometric study and the method of molar ratios variation has established the formation, in both cases, of the complexes with the molar ratio Cu^{2+} :polyoxometalate ligands of 3:2 and 4:2 respectively.

As a result of the electrophoretic study on the Cu^{2+} - $[BiW_9O_{33}]^{9-}$ system by the paper electrophoresis method there is clear-cut evidence of the formation, in the two steps, of a single pure complex polyoxometalate species.

The formation pH range of the Cu_3L_2 and Cu_4L_2 complexes are to be found between 3.5-5.5 and 5.5-7 respectively. The optimal pH values are 4.5 and 6.25 for Cu_3L_2 and Cu_4L_2 respectively.

The similar values of the stability constants point out to the formation of some stable polyoxometalate complexes.

REFERENCES

1. L. C. BAKER, J. S. FIGGIS, *J. Am. Chem. Soc.*, 1970, 92, 3794.
2. G. MARCU, M. RUSU, A. BOTAR, *Rev. Roum. Chim.*, 1974, 19, 827.
3. G. MARCU, M. RUSU, *Rev. Roum. Chim.*, 1976, 21, 385.
4. G. MARCU, M. RUSU, L. OCHEȘEL, *Rev. Roum. Chim.*, 1973, 22, 849.
5. G. MARCU, M. RUSU, L. OCHEȘEL, *Stud. Univ. Babeș-Bolyai, Chem.*, 1977, 22, 68.
6. M. RUSU, G. MARCU, *Stud. Univ. Babeș-Bolyai, Chem.*, 1978, 23, 12.
7. G. MARCU, M. RUSU, A. BOTAR, *Stud. Univ. Babeș-Bolyai, Chem.*, 1986, 31, 76.
8. C. RAȚIU, M. RUSU, A. BOTAR, *Stud. Univ. Babeș-Bolyai, Chem.*, 1993, 38,99.
9. M. RUSU, E. TOMA, A. BOTAR, *Stud. Univ. Babeș-Bolyai, Chem.*, 1994, 39, 104.
10. G. HERVÉ, *Ann. Chim. (France)*, 1971, 6, 219.
11. C. TOURNÉ, G. TOURNÉ, S. A. MALIK, T. J. R. WEAKLEY, *J. Inorg. Nucl. Chem.*, 1970, 32, 3875.
12. BOTAR, R. RIPAN, *Rev. Roumaine Chim.*, 1970, 15, 1577.
13. KREBS, R. Klein, *Mol. Engineering.*, 1993, 3, 43.
14. H. G. KUNKEL, A. TISELIUS, *J. Gen. Physiol.*, 1951, 35, 89.
15. R. CONSDEN, A. H. GORDON, A. P. MARTIN, *J. Biochim.*, 1946, 40, 33.

WATERS SAMPLING OF WASTE WATERS

ADRIAN MARIUS HAIDUC*, ANCA GABRIELA HAIDUC*
AND IOVANCA HAIDUC**

* *Lehigh University, Department of Analytical Chemistry, Bethlehem, PA, SUA*

** *Universitatea Babeș-Bolyai Cluj, Napoca, Facultatea de
Chimie si Inginerie Chimică, Romania*

1. Introduction

The selection of sampling procedures is the basis of environmental study because any sample must be representative of the environment from which they are taken. In water sampling we must know all problems associated with sampling contamination from sampling equipment; sorption and leaching of contaminants by sampling tool materials; replication; frequency of sampling; nature of samples and problems associated with sample collection.

Perhaps the most critical element in environmental analysis is the sampling and analysis plan. Recently, some guidelines about the quality control in sampling for water analysis were reported [1].

Sampling plan objectives after Barcelo [2] are:

1. Definition of objectives Aims of the measurements
2. Select target analytes and analytical methods
3. Determine sampling locations
4. Fix number of increments and method of sampling
5. Select methods for sample preservation and pre-treatment
6. Prepare final plan.

A general book on this topics was republished in 1996 by Keith as Editor [3].

2. Types of samples

The two basic types of water and wastewater samples are: discrete and composite samples. In fig. 1 are illustrated the types of samples .

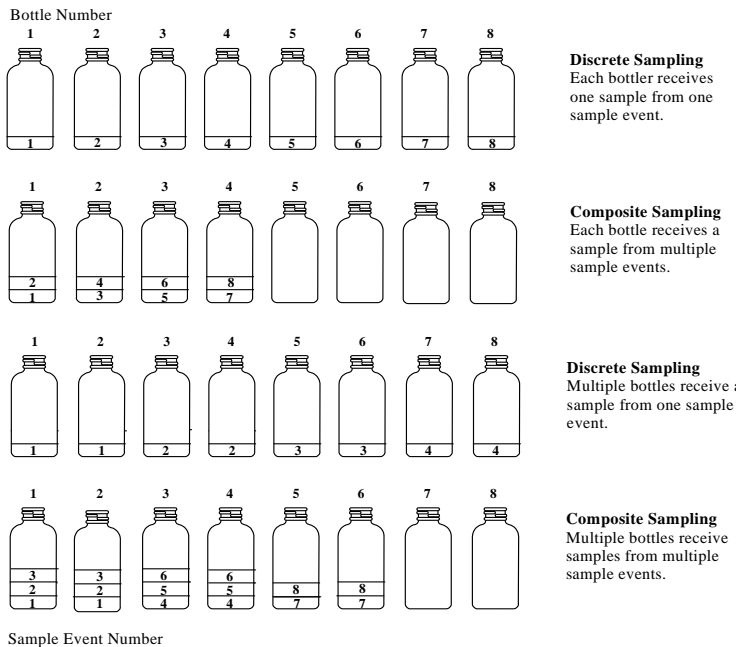


Figure 1. Types of water and wastewater samples

A *discrete sample* , also known as a *grab sample* , is an individual sample collected in less than 15 min. *Discrete sample* are recommended when the quality of the discharge is essentially constant.

A *composite sample*, consist of series of smaller samples collected over time and deposited into the same container. They are useful in calculating the average concentration and pollutant loading during the sampling period. Depending on the collection method, can be produced : a *time composite sample*; a *flow- proportional composite sample*, a *sequential composite sample*.

A single grab sample or a half-dozen grab sample over a 24-h period give representative sample only if the streams essentially constant-flow, spatially homogeneous in composition at any time and varying in composition gradually over an extended period of time. A modest series of grab samples may give a fair approximation of stream characteristics. Industrial wastewaters rarely meet the requirements for this idealised model

Particularly for a river ,the most practical river sampling program is accomplished from a boat at known sampling location. The sort of sample collected is almost always a *manual grab* or a series of manual grab sample composites prior to analysis.

There are various techniques for choosing appropriate locations. One technique especially appropriate for sampling rivers for chemical constituents is the *spatial gradient technique*.

3. Manual and Automatic Sampling

Discrete and composite sampling can be collected *manually or automatically*. The sample should be collected in a container which is compatible with both the analyte being determined and the sample matrix. USEPA has published requirements for selecting the right type of containers (Table 1) [4].

According to the 1980s, manual sampling lost ground to automatic samplers with many advantages: rapidity, improved accuracy and reduce costs associated with manual collection.

The two basic types of automatic samplers are *portable and permanent samplers*.

The sample delivery system is a pump designed to transfer the sample from the liquid source to the bottles for storage. At the beginning was used vacuum pumping but now the most commonly used are peristaltic pumps and bladder pumps [5].

Sample volume inaccuracy in peristaltic pump samplers was solved with introduction of liquid detectors [6]. The detector used a thin piezoelectric film sensor. The piezoelectric film does not contact the water or wastewater to be sampled and does not depend on the conductivity, pH, or other characteristics of the water.

According to the EPA more than 100 models of portable automatic sample collection devices existed. All of the portable samplers offer units that operate on ac and dc, weigh less than 20 kg empty, offer sampling intervals from 1 min to at least 4 h, are capable of flow-proportional or timed-interval sampling, have no metal parts in contact with the sample, operate over temperature range from -30 to 50°C and purge the sample line before and after sampling.

Table 1.

Partial list of Parameters and Required Containers

Parameter	Container type
Acidity	Plastic(P), Glass(G)
Alkalinity	P, G
BOD	P, G
COD	P, G
Chlorinated hydrocarbons	G, Teflon-lined cap
Chlorine, total residual	P, G
Coliform, faecal and total	P, G
Colour	P, G
Cyanide	P, G
Fluoride	P
Nitrate	P, G
Metals	Polyethylene
Oil and grease	G, G
OD	G, G
Temperature	P, G

An ideal sampler after Newburn [7] should have include the following:

1. ac and dc operation with adequate dry battery energy for 120 h of operation at 1-h sampling intervals
2. suitability for suspension in a standard manhole and accessibility for inspection and sample removal
3. total weight including batteries under 18 kg
4. sample collection intervals from 10 min to 4 h
5. capability for flow-proportional and time-composite samples
6. capability for collecting a single 9.5 L sample or collecting 400-mL discrete samples in a minimum of 24 containers
7. capability for multiplexing repeated aliquots into discrete bottles
8. a single intake hose having a minimum ID of 0.64 cm
9. intake-hose liquid velocity adjustable from 0.61 to 3 m/s
10. explosion-proof materials and electronics
11. no metal parts in contact with waste souse or samples
12. an integral sample container compartment capable of maintaining samples from 4 to 6 °C for a period of 24 h in ambient temperature ranging from -30 to 50°C
13. purge cycle before and after each collection interval
14. interchangeability between glass and plastic bottles, particularly indiscreet samplers
15. sampler exterior surface light in colour to reflect sunlight

4. Preserving Sample integrity

The main purpose of sampling project is to collect a sample that truly represents the source at the time of collection. It will be necessarily to preserve the integrity of the sample during and after sampling.

Ideally, the samples should be completely analysed immediately after collection. However, immediate analysis may not be done according to permit requirements, regulations and consist of refrigeration, chemical fixation or both. First step is to select the right automatic sampler (sample bottles and sample tubing. Harris and Keffer [8] concluded that vacuum sampler produced higher BOD and COD and solid concentration than sampler using peristaltic pumps. Vacuum samplers produced higher values than manual flow-weighted grab samples. In conclusion high-vacuum, high liquid intake velocity samplers were more effective in capturing solid than peristaltic pump samplers. Thomas and Eads [9] study about contamination of successive samples in portable sampling systems showed that a vacuum sampler produced more cross-contamination than peristaltic pump sampler. For a good recovery of VOC was recommended moderate speed peristaltic pumps [10].

The basic difference between one sampler over another is in liquid intake velocity and the wetted surface area of the liquid transport system. For toxic pollutants, the sample should contact only Teflon, glass and medical-grade silicone rubber if a peristaltic pump is being used in the sample transport system.

The type of contaminates contributed to water sample by material used in sampling tools are shown in table 2.

Contamination can be minimised by stream cleaning. If the water are transported through soldered pipes the most common contaminants are tin and lead [12]. Adsorption of metals at low concentration on container walls is determined by metal concentration, pH of the sample, length of contact with the container, sample and container composition [13, 14]. Sorption of dilute halogenated hydrocarbon mixture in water by various plastics and PVC was studied [15, 16]. Many samples start changing physically, chemically or biologically almost instantaneously. Sample preservation must be done immediately after collection. At the moment the sample is removed, the chemical processes that affect the sample may deviate from what occurs in situ. In process of collection, the sample is often exposed to ambient light and its temperature most likely has changed. Consequently, photochemical reactions may take place, and the temperature-dependent kinetics of other types of reactions will be altered. The presence of oxygen may initiate oxidation of some chemical species.

The vessel may contribute to the process by adsorbing certain components of the sample. This adsorption permits additional loss of volatile compounds or introduces extraneous compounds into the sample. Complete stability of the sample through preservation cannot be totally achieved for every constituent in a sample, nor can all constituents be stabilised with the same degree of success. The most common change that preservation technique attempt to minimise are *physical changes* such as *adsorption volatilisation*, *diffusion* and *precipitation*, and *chemical changes* including air oxidation, *photochemical changes* and *microbiological degradation*.

Table 2.**Contaminates of Water Samples from Materials Used in Sampling Device.**

Material	Contaminants
PVC - threaded joints	Chloroform
PVC - cemented joints	Methyl ethyl ketone, toluene, acetone, methylene chloride, benzene, ethyl acetate, tetrahydrofuran, cyclohexanone, three organic Sn compounds, and vinyl chloride
Teflon(polytetrafluoroethylene)	Nothing detectable
Polypropylene or polyethylene	Plasticizers and phthalates
FRE(Fiberglas-reinforced epoxy material)	Nothing detectable
Stainless steel	Cr, Fe, Ni, and Mo
Glass	B and Si

Table 3 illustrate a partial list of Preservatives and maximum holding time in water analysis.

Table 3.**A Partial List of Preservatives and Maximum Holding Time**

Parameters	Preservative	Maximum Holding Time
Acidity and Alkalinity	4°C	14 days
BOD	4°C	48 h
COD	4°C; H ₂ SO ₄ to pH<2	28 days
Chlorinated hydrocarbons	4°C	7 days until extraction
Coliform, faecal and total	4°C	6 h
Oil and grease	4°C, H ₂ SO ₄ or HCl to pH<2	28 days
VOCs	4°C	14 days
SVOC, pesticides, dioxins	4°C	7 days until extraction
Metals	2 ml HNO ₃ 50% to pH<2	6 months
Cyanide	2 ml NaOH 50% to pH<12	14 days
Sulfide	4°C, 1 ml Zn(Ac) ₂ , 1 ml NaOH 50% to pH<9	7 days
Fluoride	4°C	28 days

Rapid cooling down to 4°C reduces microbiological activity and the potential for volatilisation of dissolved gases and organic substances contained in the sample [17].

Some parameters, such as temperature, pH, DO, and residual chlorine cannot be preserved. They must be measured on-site during sampling. Proper preservation requires a co-ordination of activities between the field crew and the laboratory staff.

Holding time is defined by ASTM as “*the time during which a water sample can be stored after collection and preservation without significantly affecting the accuracy of analysis*” [18]. In fact, evidence suggests that holding times can be extended for some parameters [19]. The maximum time that a sample can be held before compromising the integrity of the analysis is dictated by the matrix (e.g. surface, ground or wastewater), the properties and concentration of the substance being determined, and preservation technique employed.

Oak Ridge National Laboratory (USA) conducted holding time studies [20, 21] for 17 VOCs and four explosives in three water types (distilled, ground and surface water) and three soil matrices. With respect to VOCs in water preservation with sodium bisulphate provides considerable stability (>28 days) and is considerably safer than hydrochloric acid.

A concept called **practical reporting time** (PRT) was introduced, which provides a technically valid approach for assessing the data usability of samples analysed after the regulatory holding time has expired [22].

The PRT is defined as the day when there is a probability of 15% that the measured analyte will be below the CC. A critical concentration (CC) is determined on the first day of the holding time study; the CC is the concentration below which

there is only a 5% chance, due to measurement error, that a measure concentration will be observed.

5. Replication

The number of replications is determined by the purpose of samplings: a) determination of chemical composition of water body and b) sampling for the purpose of monitoring.

Table 4.

Chemical Results from Various Water Sampling Techniques

Number of Sub-samples		Ca mg/L	Mg mg/L	Sr µg/L	P µg/L	Pb µg/L
Replicated 10 Times						
Three aliquots	1-L	53(4.5)	30(8.3)	130(20)	20.4(5.1)	2.4(0.5)
1 aliquot/three	1-L	29.7(5.0)	11.8(3.8)	64(20)	72(30)	13(4)
$\chi^2, P<$		0.02	0.05	0.001	0.001	0.01
Three 2-L samples		55(10.0)	56.2(10.0)	155(25)	100(25)	5(3.0)
Three 5-L samples		40(11.0)	22(10.0)	120(21)	110(25)	10(3.1)
Three 20-L samples		30(3.0)	12(2.1)	75(10)	75(10)	15(2.4)
Three 30-L samples		31(2.8)	14(2.1)	70(10)	80(8)	18(2.1)

Note: The depth sampled was from the surface to 2,5 m below the surface. The numbers in parentheses denote the standard deviation.

The percent coefficient of variations are dependent of the number of aliquots analysed and is always lower when more aliquots per litter are analysed than when one sub-sample is analysed [23]. Table 3 containing results from various sampling techniques.

6. Nature of Samples

Type of water body (e.g. lakes, rivers, oceans, streams or aquifer) and physical state of sample (e.q. snow, ice, rain, fog or dew) have problem associated with sample collection.

The chemical composition of a following liquid, like a river, may vary with accordance to the changes in a number of parameters such as temperature, flow rate, distance from the source among others; none of them can be controlled during sampling. The full information may be available after a large number of samples have been taken and analysed.

Surface waters include a wide range of different types of waters: *surface run off, ditches, creeks, rivers, lakes, estuaries, seas, industrial areas, effluents, piped water.*

There is no single way or devise that is adequate to sample such a variety of situations. An overview of the different details was published [3, 24].

In many water bodies, the stratum from which the sample is gathered is very important from the standpoint of chemical composition. Data presented in table.4. illustrate this point [25].

Most of the variability is reasonable consistent within the deeps sampled. Position of sample collection is also important in the collection of ice and snow [26, 27]. Ideally snow should be sampled at the time of snowfall ,because its composition changes on standing. The oceans present sampling problems because the chemical composition is far more variable than any composition in freshwater bodies [28]

Table 5.

Variation in Chemical Composition in Relation to Sampling Strata in a 33-m Drinking Water Well

Strata m	Mo $\times 10^{-2} \mu\text{g/L}$	V $\times 10^{-4} \mu\text{g/L}$	Bi $\times 10^{-2} \mu\text{g/L}$	Hg $\mu\text{g/L}$	Be $\times 10^{-2} \mu\text{g/L}$
19 - 21	15(2.5)	0.8(0.2)	8.5(1.7)	1.6(0.4)	0.7(0.2)
24 - 26	10(2.0)	30(4.0)	4.5(1.0)	18.3(1.7)	18(3.0)
29 - 31	28(3.5)	1115(97.3)	18.2(2.0)	3.0(0.5)	11(1.0)

Note: The numbers in parentheses denote the standard deviation.

A general recommendation is that samples from a stream, should be collected 30 cm below the surface and similar distance above the bottom. If systematic sampling takes place in a lake or reservoir then locations in the lake should be planned, generally by dividing the surface in squares or grids and sampling in each on of these imaginary squares.

Water samples collected from the wells follow a protocol that consists of purging water standing in the well prior to the sampling. Usually the water is purged till the pH and conductivity remain constant. Various protocols of groundwater residue sampling were described [29] . The description of multilevel samplers and the pipe diameters, between 38 to 50 mm are given. The distance to the water table should also be defined when groundwater monitoring is performed. In general, when ground or well water monitoring is performed it is very important to know the history of the cultivated field, crops and chemicals used in the land which is above the wells.

Industrial wastewaters are never pure solutions. Substantial suspended particulate are present and rarely are these suspension stable. Sampling of such sedimentary materials used two categories: *bottom grab sampling and core sampling*. Abundant variants and devices of each type are available.

For the sampling of wastewater discharges the three major sampling techniques are available: *grab sampling, composite sampling and continual sampling*. A continuous sampler, should give the most nearly representative sample of a wastewater flow. This statement is especially true for those proportional to stream flow. Such samples, however, generally require large collection containers and present a more challenging routine maintenance problem that the somewhat simpler automatic composite samplers.

WATERS SAMPLING OF WASTE WATERS

Groundwater is one of the most important natural resources, and has a very complex matrix. Although each aquifer represents a different water quality all groundwater has two unique properties for natural water system:

1. the movement of groundwater through the aquifer precludes the transport of chemicals by particulate. Only the substances soluble in the groundwater matrix are mobile within the aquifer.

2. Groundwater is nearly oxygen free and dissolved ions tend to be in their most reduced state.

Groundwater sample cannot contain any particulate matter, and must be protected from air at all times if the sample is to be truly representative.

Techniques for proper groundwater sampling must include the following [30]:

- purge-volume test
- consistent sampling protocol
- anaerobic sampling and sample handling conditions
- filtration of all samples

One of the least consistent elements of groundwater sampling is the time between the purging of the well and the sample removal from the well. Various methods for determining the necessary extent of well purging have been recommended [29-32]. The US Geological Survey recommended pumping the well until temperature, pH, and specific conductance are constant. The USEPA recommends removal of three well-casing volumes prior to sampling. The position of well water sampling should be as close as possible to the point of well purging. From sampling to sampling the sampling point within the well water column must be the same.

In the next review we will present techniques for extraction of the trace analytes (organic compounds and metals) from various water samples.

REFERENCES

1. WRC Guide to Analytical Quality Control for Water Analysis, 1944, WRC, Medmenham, UK.
2. Barcelo D, Henion M. C., *Anal. Chim. Acta*, 1977, 338, 3-18.
3. "Principles of Environmental Sampling", L.H.Keith Ed.ACS, Washington, D.C , 2nd ed., 1996.
4. Required Containers, Preservation Techniques, and Holding Times, Code of Federal Regulations, Title 40, Part.136, 1984, 49FR 43260.
5. Dick E. M, "Automatic Water and Wastewater Sampling" ch. 13 in Principle of Environmental Sampling" ed. by L.H. Keith ACS, Washington DC 1996.
6. Stefanides E. J., *Des .News*, 1991, July 22.
7. Newburn L. H., "Modern Sampling Equipment" ch.12 in "Principle of Environmental Sampling" ed. by L.H.Keith, ACS, Washington DC , 1996.
8. Harris D. J.; Keffer W. J., *Wastewater Sampling Methodologies and Flow Measurements Techniques*, USEPA 907-974-005, Kansas City, 1974.
9. Thomas R. B.; Eads R. E., *Water Resour.Res.*, 1983, 19, 436-440.
10. Ho J. S. Y., *J. Amer. Water Works. Assoc.*, 1983, 75, 583-586.

11. Barkley J. J., Peil K. M.; Highfill J. W.; Water Pollution Sampler Evaluation: Army Medical Bioengineering Research and Development Lab. MD 1975 ; AD/A-009-079.
12. Cowgill U. M., *Int.Rev.Gesamten Hydrobiol.*, 1980, 65, 379-409.
13. Miller G. D.; Proc.Nat.Symp.Aquifer Restor.Ground Water Monit., 1982, 236.
14. Masee R., Maessen F. J. M. J., DeGoeij J. J. M.; *Anal. Chim. Acta* ; 1980, 127, 181-193.
15. Barcelona M. J., Helfrich J. A., Garske E. E., *Anal. Chem.*, 1985 ,57, 460-464.
16. Barcelona M. J., Helfrich J. A., Garske E.E., *Anal.Chem.*, 1985, 57, 2752-2757.
17. Barcelo D., Hennion M. C., *Anal. Chim. Acta*, 1997, 338, 3-18.
18. Standard Practice for Estimating of Holding Time for Water Samples Containing Organic Constituents, ASTM Philadelphia, PA, 1987, ASTM D4515-85.
19. Friedman L. C., Shroeder L. J., Brooks M. G., *Environ. Sci. Technol.*, 1986, 20, 826-832.
20. Maskarinec M. P., Bayne C. K., Johnson L. H., Holladay S. K., Jenkins R. A., Stability of VO in Environmental Water Sample, ORNL, Oak Ridge, TN, 1989, ORN/TM-11300.
21. Maskarinec M. P., Bayne C. K., Johnson L. H., Holladay S. K., Jenkins R. A., Tomkins B. A., Stability of Explosives in Environmental Water, ORNL, Oak Ridge, TN, 1991; ORNT/TM-11770.
22. Bayne C. K., Schmoyer D. D., Jenkins R. A., A Practical Reporting Times for Environmental Samples ; ORNL, Oak Ridge, TN, 1993, ORNL/TM-12316.
23. McBean E. A., Rovers F.A., *Ground Water Monit.Rev.* 1985, 5 , 61-64.
24. Pio C.A., Hall A. "Instrumental Analysis of Pollutants" ch.1. Elsevier, London, UK, 1993.
25. Cowgill U. M. "Sampling Waters. The Impact of Sample Variability on Planning and Confidence Level" ch.18 in "Principles of Environmental Sampling" 2nd. ed. Ed. by L.H.Keith ACS, Washington DC, 1996.
26. Cowgill U. M., *Arch. Hydrobiol.*, 1970, 68, 1-95.
27. Cowgill U. M., *Arch. Hydrobiol.*, 1976, 78, 279-309
28. Bryden G., Mobey W., Robine K., *Ground Water Monit. Rev.*, 1986, 6, 67-72.
29. Nash R. G., Leslie A. R., ACS 465, Groundwater Residue Sampling Design, 1991, ch 12, 15-30.
30. Smith S. J.; Steele P. D.; Malley J. M.; Bryant A. Mark Groundwater Sampling " ch. 22. in " Principles of Environmental Samplig" Ed by L.H.Keith. ACS Washington DC, 2nd.ed. 1996.
31. Guidelines for Collection and Field Analysis of Ground Water Samples for Selected Unstable Constituents, US Geological Survey, Washington DC, 1976, Book 1, ch.D-2.
32. Schuller R. M.; Gibb J. P.; Griffin R. A.; *Ground Water Monit. Rev.*, 1981, 1, 46-50.

HEATS OF FORMATION OF MEDIUM-RING STRAINED CYCLO- AND POLYCYCLOALKANES: COMPARISON OF AB INITIO GROUP EQUIVALENT SCHEMES WITH THE PM3 AND MMX METHODS

LILIANA CRĂCIUN^{a,b} and JAMES E. JACKSON^a

^a Michigan State University, Department of Chemistry,
East Lansing MI 48824-1322, USA

^b Babes-Bolyai University, Department of Organic Chemistry,
11 Arany Janos Str., 3400 Cluj-Napoca, Romania

ABSTRACT. Optimized structures and energies were calculated for 57 small- and medium-ring strained polycyclic aliphatic hydrocarbons using ab initio HF/3-21G, HF/6-31G* and HF/6-31G** as well as P (semiempirical) and MMX (force field) methods. Best fit CH₂, CH and C group increments relating ab initio total energies to heats of formation were derived from the experimentally known ΔH_f . The ab initio increments deviate little from those previously reported by Wiberg and by Ibrahim and Schleyer, yielding the expected conclusion that the intrinsically isodesmic group increment approach extends efficiently to small- and medium-ring strained systems. For the present data set, the standard deviation between experimental and calculated heats of formation, from ab initio total energies and group increments, is 1.81 kcal/mol for the RHF/6-31G*/RHF/6-31G* calculation, and 1.74 kcal/mol for RHF/6-31G**/RHF/6-31G**, respectively. Less successful results are obtained from the HF/3-21G, PM3 and MMX data. As expected, systems with fused small rings are especially problematic for the latter methods.

INTRODUCTION

In the course of a study of hybridization and ¹³C-¹H NMR coupling constants,¹ we recently obtained RHF/6-31G*/RHF/6-31G* wavefunctions and ab initio total energies for a large number of small- and medium-ring strained polycyclic hydrocarbons. Roughly half of this number have had experimental heats of formation reported. It was of interest to examine the performance of the Wiberg² and Ibrahim/Schleyer³ (IS) hydrocarbon group increments in calculating heats of formation from ab initio energies for these compounds, as most previous work has focused on unstrained or small-ring systems. This

paper provides such an analysis for 57 hydrocarbons, of which several were beyond the range of practical computational tools when the above papers appeared. The new best fits for the CH₂, CH and C fragments deviate little from those previously reported, yielding the expected conclusion that the intrinsically isodesmic group increment approach extends effectively to medium-ring strained systems.

RESULTS AND DISCUSSION

The heat of formation of a compound is a useful characteristic, traditionally determined from combustion measurements. However, the accumulation of computational data at a consistent level for a wide variety of molecules and their correlation with experimental results allow an evaluation of their heats of formation from ab initio energies, as well. The ability to produce reliable estimates depends upon the computational method that is chosen. Molecular mechanics (MM) or semiempirical methods are not as generally useful, since the former method needs good experimental data, not always available, for parametrization,⁴ while the latter approximates minimal basis-set calculations which frequently handle strained small-ring compounds unevenly.⁵

Conversion of ab initio calculated energies to heats of formation is commonly done by the use of isodesmic comparisons with closely related compounds of known thermochemistry, such that errors due to inadequacies of basis set or electron correlation treatment largely cancel out.⁶ An isodesmic reaction is defined as a hypothetical thermoneutral process in which the number of formal bonds of each type is identical on both sides of the reaction. By appropriately choosing the components of the isodesmic reaction, the unknown heat of formation can be calculated from the corresponding energy differences. The absolute errors are likely to be comparable and can be assumed to cancel in calculation of the energy differences between related molecules. Isodesmic comparisons can provide a test of the reliability of the computational method by comparing the computed results with known experimental values.

The heat of formation of a compound may be estimated from tabulated data pertaining to individual structural fragments. Procedures have been developed for estimating thermodynamic characteristics by summing the contributions of the constituent groups. As was pointed out by Wiberg², such group equivalent schemes can be viewed as a subset of isodesmic reactions in which the substitution levels of all C sites are maintained constant. Thus, Wiberg² and subsequently, Ibrahim and Schleyer³, empirically determined sets of group and atom equivalents, which, when subtracted from a compound's ab initio energy, yield its heat of formation, $\Delta H_f(\text{calcd})$. Accordingly, $\Delta H_f(\text{calcd})$ is expressed as the difference between the molecule's total energy and the summed increments of the component groups, as shown by the following relation:

$$\Delta H_f(\text{calcd}) = 627.5 \left(E_T - \sum_i n_i E_i \right) \quad (1)$$

where E_T is the ab initio total energy, n represents the number of atoms or groups of each sort, and E is the corresponding atom or group equivalent. Following these reports, simplified schemes with reduced number of parameters have been proposed,⁷ and individualized atom or group parameters were developed for particular classes of compounds.⁸ Bond/group equivalents have also been derived for alkanes from density functional calculations.⁹ In a series of recent articles, Allinger *et al.*¹⁰ outlined an alternative method which combines bond energy with group increments, while it includes terms to explicitly account for statistical mechanical effects of populating a molecule's higher energy conformations and low-lying vibrational states, as well as its translational and rotational motions.

The present study confirms that group equivalent-based heats of formation can be calculated with an accuracy close to that from experiments (see Table 1 and Figure 1). The wide variety of small- and medium-ring strained hydrocarbons used in this work provide a stringent test of the method. Heats of formation may also be estimated for species where experimental values are not available or difficult to obtain. In addition, strain energies have been calculated for all the compounds recorded in Table 1.¹¹ The experimental heats of formation, $\Delta H_f(\text{exp})$, and calculated RHF/3-21G¹², RHF/6-31G*¹³ and RHF/6-31G**¹³ ab initio total energies for the compounds considered in this study are listed in Table 1. All quantum-chemical calculations (ab initio and semiempirical) were carried out using the SPARTAN program (version 5.0, Wavefunction Inc., Irvine, CA) running on a SGI Indigo2 workstation and include full geometry optimization. Three gaussian basis sets were used in the ab initio calculations; the resulting enthalpies of formation become more accurate with the use of systematically improved basis sets and point to the necessity of inclusion of d -type functions (basis sets 6-31G* and 6-31G**) in the basis set for more accurate predictions. The calculated values refer only to the lowest energy conformation, although in several cases the compounds exist as a Boltzmann distribution of different conformational isomers with somewhat different energies.

A least squares fit¹⁴ of experimental vs. calculated heats of formation using equation 1 with the increments for CH₂, CH and C groups as adjustable parameters, yielded $\Delta H_f(\text{calcd})$ values at the 3-21G, 6-31G* and 6-31G** basis set levels as listed in Table 1, along with the group increments in Table 2. For a range of $\Delta H_f(\text{exp})$ from -60 to +150 kcal/mol, the standard deviation of experimental vs. calculated heats of formation is 1.81 kcal/mol for the RHF/6-31G**//RHF/6-31G* calculation and 1.74 kcal/mol for RHF/6-31G**//RHF/6-31G**, respectively, (see Table 2).

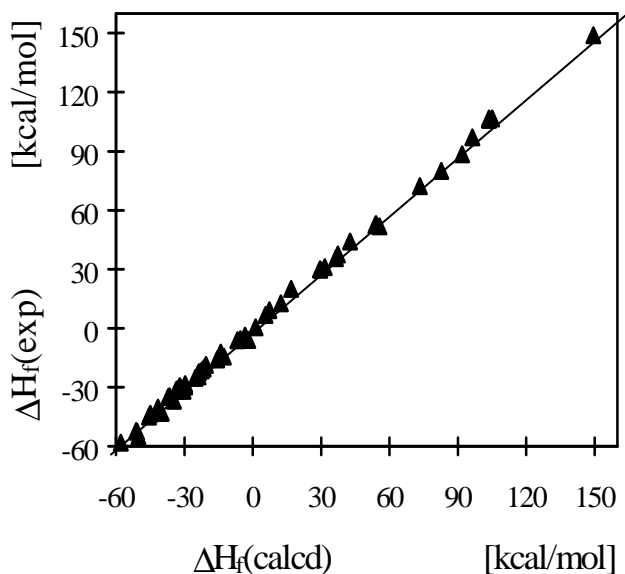


Figure 1. Plot of experimental heats of formation, $\Delta H_f(\text{exp})$, vs. calculated values, $\Delta H_f(\text{calcd})$, from the HF/6-31G* group equivalents evaluated in this work, for the compounds in Table 1. Slope 1.00 was taken for the correlation line.

The thermochemical measurements recently reported for a variety of spirocyclopropanated cyclopropane and cyclobutane derivatives¹⁵ allowed to establish unambiguously an equivalent for the quaternary carbon atom, which was not available from the work of Ibrahim and Schleyer³, while Wiberg's^{2a} value for this parameter is based only on neopentane and spiro-pentane. The equivalents derived in this work for the CH₂, CH and C fragments (see Table 2) are essentially unchanged from those previously reported, supporting the consensus that errors due to incompleteness in basis set correlation treatment, and vibrational contributions scale linearly with the numbers of each group. They are absorbed in the group parameters, to yield calculated heats of formation of accuracy comparable to experimental measurements. The

improved 6-31G** basis set gives $\Delta H_f(\text{calcd})$ basically unchanged from the 6-31G* values, which appears to be the minimal basis set necessary to appropriately describe systems incorporating small strained rings. The $\Delta H_f(\text{calcd})$ values derived for the 3-21G basis set show large errors especially in the case of cyclopropane derivatives, where the flexibility afforded by inclusion of polarization functions into the basis set is essential for a proper description of these compounds.

Analogous values for the semiempirical PM3 method¹⁶ are included in Table 1 for comparison. In general, it can be stated that the ab initio calculations are more reliable whereas semiempirical calculations are faster in terms of computer time. The semiempirical PM3 method is claimed to reliably estimate energies, however, in this work the resulting semiempirical heats of formation show unacceptably large errors; the standard deviation for the best linear fit between PM3 calculated and experimental heats of formation for the compounds listed in Table 1 is 8.0 kcal/mol. Unlike ab initio methods where self-consistency is achieved by iterative procedures and complex calculations with fewer assumptions, the accuracy of empirical methods is limited to the accuracy of the data used in parameterization, whereby parameters are included in the protocol to adjust the results to match experimental data. Semiempirical methods should be applied with care when employed in prediction of properties or compounds not used in the parameterization, where frequent comparison of calculated and experimental results is imperative.

The MMX method, derived from Allinger's¹⁷ MM2 force field, was also employed to compute heats of formation for the compounds included in Table 1.¹⁸ Usually, MM reproduces well the thermodynamic properties of hydrocarbons; e.g., the new MM4 force field applied to 56 alkanes and cycloalkanes, excluding small rings, calculates ΔH_f with a standard deviation of 0.4 kcal/mol vs. experimental values.¹⁹ However, the MMX results in Table 1 show that although most compounds have MMX $\Delta H_f(\text{calcd})$ within experimental accuracy, in some cases there are large discrepancies between experiment and calculation (5 compounds in Table 1 have MMX $\Delta H_f(\text{calcd})$ in error vs. $\Delta H_f(\text{exp})$ with more than 10 kcal/mol). Thus, the performance of the MMX method (the best linear fit

of $\Delta H_f(\text{exp})$ vs. $\Delta H_f(\text{calcd})$ gives a s.d. of 4.2 kcal/mol for the compounds listed in Table 1), although much better than that of PM3 or HF/3-21G models, is not entirely consistent, leaving the ab initio HF/6-31G* or HF/6-31G** group equivalent schemes as the most reliable when compared to experiment.

CONCLUSIONS

The estimates of the enthalpies of formation using the 6-31G* or 6-31G** basis sets are in fair agreement with experimental measurements. As expected, the equivalents at the unpolarized 3-21G basis set cannot be used safely for strained compounds since polarization functions are known to be needed to properly describe small ring carbocyclics. These calculations can be used when experimental results for heats of formation are unavailable, or as an independent check when an experimental result of a particular heat of formation is in question.

REFERENCES

1. L. Craciun and J. E. Jackson, *J. Phys. Chem. A*, 1998, 102, 3738.
2. (a) K. B. Wiberg, *J. Comput. Chem.*, 1984, 5, 197. (b) K. B. Wiberg, *J. Org. Chem.*, 1985, 50, 5285.
3. M. R. Ibrahim and P. v. R. Schleyer, *J. Comput. Chem.*, 1985, 6, 157.
4. U. Burkert and N. L. Allinger, *Molecular Mechanics*, ACS Monograph 177, 1982.
5. M. J. S. Dewar and W. Thiel, *J. Am. Chem. Soc.*, 1977, 99, 4907.
6. (a) W. J. Hehre, R. Ditchfield, L. Radom and J. A. Pople, *J. Am. Chem. Soc.*, 1970, 92, 4796, and subsequent papers. (b) For an example of the use of homodesmotic reactions to calculate the heats of formation of 15 representative strained and unstrained medium-sized hydrocarbons, see: R. L. Disch, J. M. Schulman, M. L. Sabio, *J. Am. Chem. Soc.*, 1985, 107, 1904.
7. (a) Z. Yala, *J. Mol. Struct.: THEOCHEM.*, 1990, 207, 217. (b) E. A. Castro, *J. Mol. Struct.: THEOCHEM.*, 1994, 304, 93. (c) W. C. Herndon, *Chem. Phys. Lett.*, 1995, 234, 82. (d) D. W. Smith, *J. Chem. Soc., Faraday Trans.*, 1996, 92, 1141.
8. (a) J. M. Schulman, R. C. Peck and R. L. Disch, *J. Am. Chem. Soc.*, 1989, 111, 5675. (b) D. A. Armitage and C. W. Bird, *Tetrahedron Lett.*, 1993, 34, 5811.
9. N. L. Allinger, K. Sakakibara and J. Labanowski, *J. Phys. Chem.*, 1995, 99, 9603.

HEATS OF FORMATION OF MEDIUM-RING STRAINED CYCLO- AND OLYCYCLOALKANES

10. (a) N. L. Allinger, L. R. Schmitz, I. Motoc, C. Bender and J. K. Labanowski, *J. Phys. Org. Chem.*, 1990, 3, 732. (b) N. L. Allinger, L. R. Schmitz, I. Motoc, C. Bender and J. K. Labanowski, *J. Am. Chem. Soc.*, 1992, 114, 2880. (c) N. L. Allinger, L. R. Schmitz, I. Motoc, C. Bender and J. K. Labanowski, *J. Comput. Chem.*, 1992, 13, 838. (d) L. R. Schmitz, I. Motoc, C. Bender, J. K. Labanowski and N. L. Allinger, *J. Phys. Org. Chem.*, 1992, 5, 225. (e) R. Liu and N. L. Allinger, *J. Phys. Org. Chem.*, 1993, 6, 551.
11. Strain energy is the difference between the experimental (calculated) heat of formation of a compound and that of a hypothetically "strainless" model, calculated here from Benson's group equivalents (see S. W. Benson, *Thermochemical Kinetics*; John Wiley: New York, 1976).
12. J. S. Binkley, J. A. Pople and W. J. Hehre, *J. Am. Chem. Soc.*, 1980, 102, 939.
13. P. C. Hariharan and J. A. Pople, *Chem. Phys. Lett.*, 1972, 66, 217.
14. The analysis was done with Microsoft Excel version 5.0 employing the function LINEST, which uses the "least-squares" method to calculate simple or multiple linear regressions that best fit the input data.
15. H.-D. Beckhaus, C. Ruchardt, S. I. Kozhushkov, V. N. Belov, S. P. Verevkin and A. de Meijere, *J. Am. Chem. Soc.*, 1995, 117, 11854.
16. J. J. P. Stewart, *J. Comput. Chem.*, 1989, 10, 209.
17. N. L. Allinger, *J. Am. Chem. Soc.*, 1977, 99, 8127.
18. The MMX calculations were done using the interactive molecular modeling program PCMODEL, version 4.0 (Serena Software, Bloomington, IN).
19. N. L. Allinger, K. Chen and J.-H. Lii, *J. Comput. Chem.*, 1996, 17, 642.

HEATS OF FORMATION OF MEDIUM-RING STRAINED CYCLO- AND OLYCYCLOALKANES

Table 1 (continued)

1	2	3	4	5	6	7			
Bicyclo[3.1.0]hexane (C ₅)	9.2±0.1 (32.8)	8.6	8.1	-231.70454	13.1	-233.00107	7.2 (30.8)	-233.01709	6.8 (30.4)
Tetracyclo[4.1.0]heptane (C ₇)	88.4±0.4 (104.8)	106.0	107.6	-268.07893	110.1	-269.60362	92.0 (108.4)	-269.61814	91.2 (107.6)
Quadracycane (C ₈)	80±1 (96.4)	93.4	86.3	-268.10560	93.3	-269.61822	82.9 (99.3)	-269.63239	82.2 (98.6)
<i>trans</i> -Tricyclo[4.1.0]heptane (C ₇)	35.7±0.4 ^a (58.2)	53.4	41.2	-269.31988	47.4	-270.83630	36.5 (59.0)	-270.85294	36.0 (58.5)
Northicycane (C ₈)	20±1 (42.5)	19.5	26.0	-269.36544	18.8	-270.86771	16.8 (39.3)	-270.88387	16.5 (39.0)
Dispiro[2.1.2]heptane (C ₇)	72.3±0.8 ^m (96.1)	76.0	70.9	-269.24060	78.9	-270.77646	74.1 (97.9)	-270.79359	73.8 (97.6)
<i>cis</i> -Bicyclo[4.1.0]heptane (C ₇)	0.5±0.5 (29.1)	1.2	1.2	-270.52345	8.2	-272.03677	1.2 (29.8)	-272.05566	0.9 (29.5)
Bicyclo[2.2.1]heptane* (norbornane) (C ₇)	12.4±0.7 (16.2)	-12.8	-13.7	-270.56656	-18.9	-272.06120	-14.1 (42.7)	-272.07947	-14.0 (42.6)
Cubane* (C ₈)	149±1 (164.2)	148.9	113.8	-305.69590	143.3	-307.39391	149.5 (164.7)	-307.40775	149.3 (164.5)
Dispiro[2.0.2]octane (C ₈)	53.0±0.2 ⁱ (81.7)	56.6	46.9	-308.08974	55.0	-309.83304	54.9 (83.6)	-309.85298	54.8 (83.5)
Dispiro[2.1.2]octane (D _{2h})	52.4±0.3 ⁱ (81.1)	69.4	46.2	-308.08928	55.3	-309.83354	54.6 (83.3)	-309.85351	54.5 (83.2)
<i>cis</i> -Bicyclo[5.1.0]decane (C ₇)	-3.8±0.7 ⁿ (29.7)	-4.1	-3.0	-309.34119	4.0	-311.070361	-3.4 (30.1)	-311.09228	-3.8 (29.7)
<i>cis</i> -Bicyclo[4.2.0]decane (C ₇)	-6.1±1.0 ⁿ (27.4)	-5.7	-15.8	-309.35566	-5.1	-311.07577	-6.8 (26.7)	-311.09724	-6.9 (26.6)
<i>trans</i> -Bicyclo[3.3.0]decane (C ₈)	15.9±0.6 ⁿ (17.6)	-15.7	-18.8	-309.37442	-16.9	-311.08985	-15.7 (17.8)	-311.11112	-15.6 (17.9)
<i>cis</i> -Bicyclo[3.3.0]decane (C ₈)	22.3±0.5 ⁿ (11.2)	-22.5	-31.6	-309.38836	-25.6	-311.10261	-23.7 (9.8)	-311.12391	-23.7 (9.8)
Bicyclo[2.2.2]octane* (D _{3h})	23.7±0.3 ⁱ (9.8)	-22.7	-27.8	-309.39262	-28.3	-311.10360	-24.3 (9.2)	-311.12465	-24.1 (9.4)
Homocubane (C ₈)	97±2 (117.2)	95.1	75.4	-344.59538	87.9	-346.50449	96.5 (116.7)	-346.52095	96.6 (116.8)
Trispiro[2.0.2.1.1]nonane (C ₇)	106.6±0.2 ⁱ (134.8)	108.0	98.7	-345.66021	108.3	-347.63524	104.8 (133.0)	-347.65581	104.9 (133.1)

Table 1 (continued)

1	2	3	4	5	6	7		
Trispro[2.0.2.0]nonane (C_{20})	105.9±0.3 ^b (134.1)	109.2	99.5	-345.65931	108.9 (133.1)	104.9 (133.1)	-347.65566 (133.2)	105.0 (133.2)
cis-Bicyclo[6.1.0]nonane (C_7)	5.5±0.2 (33.0)	-7.7	-6.5	-348.15494	2.3	-5.6 (32.9)	-350.09996 (32.5)	-6.0 (32.5)
trans-Bicyclo[6.1.0]nonane (C_7)	6.0±0.3 (32.5)	-5.7	-3.0	-348.14956	5.7	-2.1 (36.4)	-350.09437 (36.4)	-2.5 (36.0)
cis-Bicyclo[4.3.0]nonane (C_7)	30.0±0.5 (8.5)	-28.8	-36.0	-348.21288	-34.1	-31.8 (6.7)	-350.16598 (6.7)	-31.8 (6.7)
Bicyclo[3.3.1]nonane (C_{20})	30.5±0.6 ^a (8.0)	-30.5	-35.0	-348.21210	-33.6	-31.8 (6.7)	-350.14164 (6.7)	-31.6 (6.9)
trans-Bicyclo[4.3.0]nonane (C_7)	-31.0±0.5 (7.5)	-26.5	-34.8	-348.21330	-34.3	-33.0 (5.5)	-350.14361 (5.5)	-32.9 (5.6)
endo-Tricyclo[5.2.1.0 ^{2,4}]decane (C_7)	-14.4±0.9 ^a (22.9)	-12.5	-20.1	-385.85945	-19.4	-12.7 (24.6)	-387.99314 (24.6)	-12.4 (24.9)
Probadamantane (C_7)	20.5±0.6 (16.8)	-20.7	-25.1	-385.87380	-28.4	-21.5 (15.8)	-388.00723 (15.8)	-21.1 (16.2)
all-cis-Tricyclo[5.2.1.0 ^{2,4}]decane (C_7)	24.5±0.9 ^a (12.8)	-22.1	-35.0	-385.87574	-29.6	-23.7 (13.6)	-388.01069 (13.6)	-23.5 (13.8)
Adamantane (T_d)	-31.8±0.3 (5.5)	-31.5	-34.6	-385.89338	-40.6	-33.6 (3.7)	-388.02648 (3.7)	-33.1 (4.2)
Bicyclo[3.3.2]decane (C_7)	25.3±1.7 ^a (18.1)	-25.2	-28.3	-387.00849	-24.4	-25.2 (18.2)	-389.15735 (18.3)	-25.1 (18.3)
cis-Bicyclo[5.3.0]decane (C_7)	-31.1±1.2 ^a (12.3)	-31.2	-38.3	-387.02301	-33.5	-33.5 (9.9)	-389.17060 (9.9)	-33.5 (9.9)
trans-Bicyclo[5.3.0]decane (C_7)	-31.4±1.4 ^a (12.0)	-32.5	-37.7	-387.02141	-32.5	-32.2 (11.2)	-389.16843 (11.2)	-32.1 (11.3)
Spiro[4.5]decane (C_7)	-34.7±0.5 ^a (9.4)	-36.8	-42.3	-387.03267	-48.7	-36.4 (7.7)	-389.17506 (7.7)	-36.0 (8.1)
cis-Decalin (C_2)	40.4±0.5 (3.0)	-41.0	-42.7	-387.03893	-43.5	-41.7 (1.7)	-389.18357 (1.7)	-41.6 (1.8)
trans-Decalin (C_{2h})	43.5±0.5 (0.1)	-43.8	-44.5	-387.04355	-46.4	-45.1 (1.7)	-389.21624 (1.7)	-45.0 (1.6)
Bicyclo[3.3.3]undecane (manxane) (D_{3h})	21.3±0.5 ^a (27.1)	-24.3	-30.3	-425.81199	-19.6	-22.4 (26.0)	-428.17907 (26.0)	-22.4 (26.0)
Spiro[5.5]undecane (C_2)	45.0±0.6 ^a (4.0)	-46.3	-47.3	-425.85744	-57.3	-45.3 (3.7)	-428.24535 (3.7)	-44.9 (4.1)

Table 1 (continued)

1	2	3	4	5	6	7	
Tetra[pi]2.0.2.0.2.0. 2.0]bicycane (D_{2h})	106.6±0.5 ^a (144.2)	116.2	100.2	-460.94764	102.1	-463.56650 106.6 (144.2)	-463.59392 106.8 (144.4)
Bicyclohexyl (C_{2h})	-52.2±0.7 (1.1)	-52.0	-54.0	-464.67579	-52.7	-467.25114 (2.0)	-467.28436 (2.1)
Congressane (diamantane) (D_{3d})	-34.9±0.6 ^b (10.0)	-34.3	-38.5	-538.87130	-50.5	-541.84810 (7.8)	-541.87788 (8.9)
trans-anti-trans-Perhy- droanthracene (C_2)	-52.7±1.5 ^b (4.4)	-52.0	-53.1	-541.15806	-53.4	-544.15840 (6.3)	-544.19452 (6.7)
trans-cisoid-trans-Per- hydroanthracene (C_2)	-58.1±0.9 (-1.0)	-58.1	-57.9	-541.16868	-60.1	-544.17001 (-1.0)	-544.20612 (-0.6)

^a Heats of formation at 298 K in kcal/mol; total energies in hartrees, 1 H = 627.5 kcal/mol. All structures were fully optimized using Spartan 4.0 (Wavefunction Inc., Irvine, CA). The compounds included in the original Wiberg's regression analysis for deriving group equivalents (ref. 2) are marked with asterisk (*).

^b Symmetry of lowest energy conformation. ^c From NIST Standard Reference Database 25, Structures and Properties, version 2.02, January 1994, by Lias, S. G.; Liebman, J. F.; Levin, R. D.; Kalfali, S. S. A., unless otherwise noted. ^d Strain energy, from experimental \square H, and Benson's group equivalents (Benson, S. W., *Thermochemical Kinetics*, John Wiley: New York, 1976). ^e This work; calculated from group equivalents analysis (see Table 2). ^f Heat of formation based on estimated heat of vaporization or sublimation from vapor pressure measurements. Cox, J. D., Plicher, G., *Thermochemistry of Organic and Organometallic Compounds*, Academic Press: New York, 1970. ^g Estimated from its heat of hydrogenation to cyclopentane. Rolf, W. R.; Klarner, F.-G.; Lemmartz, H.-W., *J. Am. Chem. Soc.*, 1982, 104, 5679. ^h Estimated from its heat of hydrogenation to cyclohexane. See ref. h. ⁱ Beckthaus, H.-D.; Richardt, C.; Kozhushkov, S. I.; Belov, V. N.; Verevkin, S. P.; de Meijere, A., *J. Am. Chem. Soc.*, 1995, 117, 11854. ^j Estimated from its heat of isomerization to 1,3,5-cycloheptatriene. Christl, M.; Brun, E.; Rolf, W. R.; Lemmartz, H.-W., *Tetrahedron*, 1989, 45, 2905. ^k Pimenova, S. M.; Fogel, L.; Kozina Galchenko, G. L., *Russ. J. Gen. Chem.*, 1974, 44, 1383. ^l Boyd, R. H.; Sanwal, S. N.; Shary-Tehrany, S.; McNally, D., *J. Phys. Chem.*, 1971, 75, 1264. ^m Lukyanova, V. A.; Pimenova, S. M.; Kolesov, V. P.; Kuznetsova, T. S.; Kokoreva, O. V.; Kozhushkov, S. I.; Zefirov, N. S., *Russ. J. Phys. Chem.*, 1993, 67, 1023. ⁿ Chang, S.-J.; McNally, D.; Shary-Tehrany, S.; Hickey, S. M. J.; Boyd, R. H., *J. Am. Chem. Soc.*, 1970, 92, 3109. ^o Parker, W.; Steele, W. V.; Watt, I., *J. Chem. Thermodyn.*, 1977, 9, 307. ^p Clark, T.; Knox, T.; Mackle, H.; McKervey, M. A., *J. Chem. Soc., Chem. Commun.*, 1975, 666. ^q Estimated from its heat of isomerization to cis-bicyclo[5.3.0]decane reported in Allinger, N. L.; Zalkow, V., *J. Am. Chem. Soc.*, 1961, 83, 1144. ^r Pedley, J. B.; Naylor, R. D.; Kirby, S. P., *Thermochemical Data of Organic Compounds*, 2nd Ed., Chapman and Hall: London, 1986. ^s Parker, W.; Steele, W. V.; Stirling, W.; Watt, I., *J. Chem. Thermodyn.*, 1975, 7, 795. ^t From its heat of combustion reported in Westrum, E. F.; McKervey, M. A.; Andrews, J. T. S.; Fort, R. C.; Clark, T.; Knox, T., *J. Chem. Thermodyn.*, 1978, 10, 959, (considered the most reliable), and its heat of sublimation reported in Clark, T.; Knox, T.; Mackle, H.; McKelvey, M. A.; Rooney, J. J., *J. Am. Chem. Soc.*, 1975, 97, 3835. In a private communication (1978), McKervey reports a redetermination of the gas-phase heat of formation of diamantane of -34.6±0.6 kcal/mol. ^u Margrave, J. L.; Frisch, R. G.; Clarke, R. L.; Johnson, W. S., *J. Am. Chem. Soc.*, 1963, 85, 546.

EXTRACTION OF ZIRCONIUM(IV) WITH TRITOLYLPHOSPHATE

MARIA CURTUI^a, LOREDANA SORAN^b

*a. Chemistry Department "Babeș-Bolyai" University,
R-3400 Cluj-Napoca, Romania*

b. "Raluca Ripan" Institute of Chemistry

ABSTRACT. Solvent extraction of zirconium(IV) from chloride aqueous media by tritolylphosphate (TTP) has been investigated. The effect of certain variable such as acidity, the concentration of the extractant and the concentration of chloride anion have been examined. Based on slope analysis applied to the distribution data, a possible mechanism for the extraction of Zr(IV) has been proposed.

INTRODUCTION

During recent years we reported a lot of works on the extraction of some actinide and lanthanide with acidic and neutral organophosphorus extractants [1-5]. We have studied the separation of uranium(VI) and thorium(IV) from zirconium(IV), lanthanum(III), cerium(III) and other trivalent and divalent metals by solvent extraction and thin layer chromatography[6-8].

This work deal with the extraction of zirconium(IV) from acidic aqueous solutions with tritolylphosphate in benzene, in order to establish the extraction mechanism.

EXPERIMENTAL

Reagent and equipment

Zirconium chloride, tritolylphosphate and Arsenazo III were supplied by Aldrich and Ventron AG Germany. All the other reagents used were of analytical grade.

A Spekol C. Zeiss Jena (DDR) spectrophotometer was used for the determination of zirconium(IV). The acidity of the aqueous phase was determined by titration with NaOH.

Operating procedure

The partition experiment were carried out by equilibrating equal volumes (10 ml) of organic and aqueous phases in 100 ml separation funnels. Preliminary test

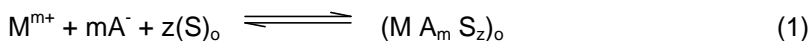
showed that the distribution equilibrium is attained in 4 min. at room temperature (20-23°C). After the phases were separated the zirconium content in the aqueous phase was determined photometrically with Arsenazo III [9].

RESULTS AND DISCUSSION

The extraction of zirconium(IV) with tritolylphosphate (TTP) in benzene was studied. The dependence of the distribution ratio on the aqueous layer acidity, the concentration of chloride anion and the concentration of the extractant in the organic phase was investigated.

Treatment of data

The extraction equilibrium of metal ion M^{m+} with an neutral organophilic extractant S can be described by the following equation:



where A^- is the counter anion present in the aqueous phase and "o" indicates the organic phase.

The extraction equilibrium constant is given by the relation:

$$K = \frac{[MA_m S_z]_o}{[M^{m+}][A^-]^m [S]_o^z} \quad (2)$$

Defining the distribution ratio D as the ratio between the total concentration of the metal in the organic phase and the total concentration of the metal in the aqueous phase it follows that:

$$K = D \cdot \frac{1}{[A^-]^m [S]_o^z} \quad (3)$$

After some simple transformations one obtains:

$$\log D = \log K + m \log [A^-] + z \log [S]_o \quad (4)$$

Equation (4) can give information concerning the nature of the species involved in the extraction process. It should be mentioned that K and D are not thermodynamic constants since they ignore activity coefficient. They can serve only for comparing various extraction systems under similar conditions.

Zr(IV) – TTP – benzene system

The effect of HCl concentration on the extraction of Zr(IV) with TTP in benzene was investigated. The results illustrated in Table 1 indicate an increase of distribution ratio; the maximum value of D is obtained at 1.0 – 1.5M HCl. If the

EXTRACTION OF ZIRCONIUM(IV) WITH TRITOLYLPHOSPHATE

concentration of the hydrochloric acid is greater than 1.5M the extraction of Zr(IV) decrease. This trend in the extraction behaviour of Zr(IV) has been reported by other workers too [10].

Table 1.

The effect of HCl concentration of Zr(IV) with 0.5M TTP in benzene

C_{HCl}	Distribution ratio (D)
0.10	0.50
0.50	0.85
1.00	1.41
1.50	1.53
2.00	0.85
2.50	0.72
3.00	0.54
4.00	0.20

Maintaining constant the concentration of HCl (1M) the influence of TTP on the distribution ratio of Zr(VI) was studied. The data obtained illustrate that the extraction increase with the increasing of extractant concentration. The plot of $\log D$ against to $\log [TTP]$ was determined (Fig. 1, curve 2). The slope of 2 for the linear portion of the curve indicate that two TTP molecules are involved in the formation of the extracted species in the organic phase (Eq. 4, $z = 2$).

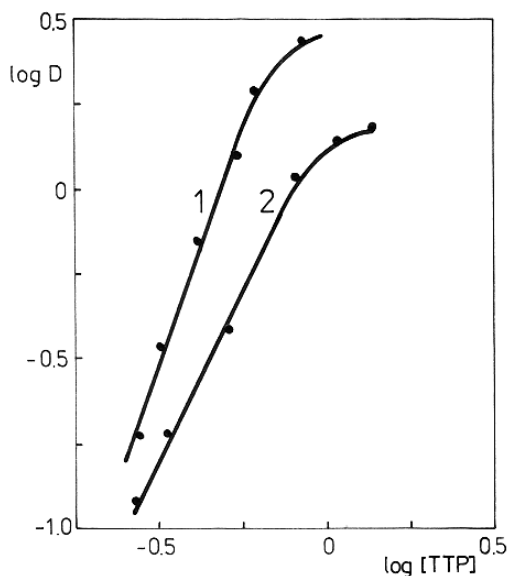


Fig. 1. The dependence of zirconium(IV) extraction with TTP concentration
 $C_{HCl} = 1M$; $C_{Zr} = 0.001M$

The distribution ratio was also determined for different concentrations of chloride ion in the aqueous phase. The variation of $\log D$ versus $\log [Cl^-]$, at constant acidity (1M) of the aqueous phase, is illustrated in Figure 2, curve 1. The slope 3.7 of the straight line obtained suggest that four chloride anions are involved in the extraction process (Eq. 4, $m = 4$). At lower acidity of the aqueous phase (<1M) the slope value of 2 shows that only 2 chloride anion participate in the formation of the extracted species.

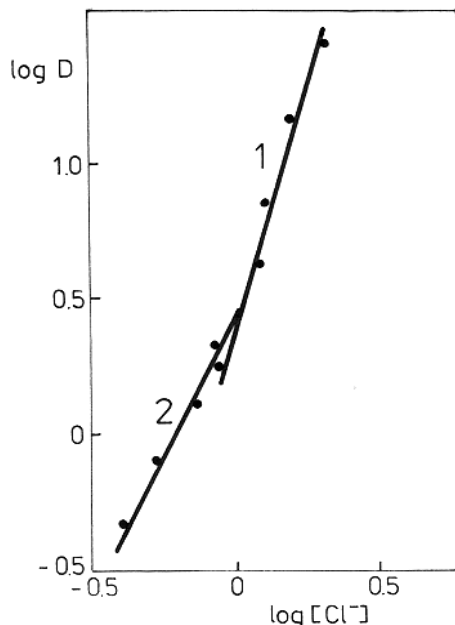
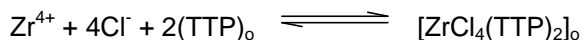


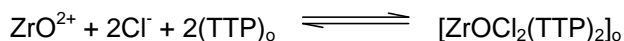
Fig. 2. The dependence of zirconium(IV) extraction with chloride ion concentration. $C_{Zr} = 0.001\text{ M}$; $C_{TTP} = 0.5\text{ M}$

Final remarks

The data presented above show that the extraction of zirconium(IV) is strongly affected by the acidity of the aqueous phase. This can be understood taking into account that the acidity plays an important role in the existence of many chemical forms of Zr(IV) in aqueous phase. At high acidity zirconium(IV) exist as Zr^{4+} ion. In this case the extraction of metal can be described by the equation:



At moderate acidity (<2M) ZrO^{2+} species is dominating in aqueous solutions and extraction process may be represented by the following equation:



EXTRACTION OF ZIRCONIUM(IV) WITH TRITOLYLPHOSPHATE

The decrease of extraction at higher acidities might be due to the formation of the less extractable acido-complex of zirconium in aqueous phase [11]

REFERENCES

1. M. CURTUI, I. HAIDUC, *J. Radioanal. Nucl. Chem.*, 1993, 176, 233.
2. M. CURTUI, I. HAIDUC, *J. Radioanal. Nucl. Chem.*, 1992, 164, 91.
3. M. CURTUI, I. HAIDUC, *J. Radioanal. Nucl. Chem.*, 1994, 186, 273.
4. M. CURTUI, I. HAIDUC, *J. Inorg. Nucl. Chem.*, 1981, 43, 1076.
5. G. MARCU, M. CURTUI, I. HAIDUC, *J. Inorg. Nucl. Chem.*, 1977, 39, 1415.
6. T. HODISAN, M. CURTUI, I. HAIDUC, *J. Radioanal. Nucl. Chem.*, 1998, 238, 129.
7. T. HODISAN, M. CURTUI, S. COBZAC, C. CIMPOIU, I. HAIDUC, *J. Radioanal. Nucl. Chem.*, 1998, 238, 179.
8. I. HAIDUC, M. CURTUI, *Studia Univ. "Babeş-Bolyai", Chemia*, 1974, 19, 71.
9. S. B. SAVIN, *Talanta*, 1961, 8, 673.
10. S. N. SIGH, S. SUJATHA, G.R. MISHRA, *J. Radioanal. Nucl. Chem.*, 1990, 146, 427.
11. F. A. COTTON, G. WILKINSON, *Advanced Inorganic Chemistry*, Fifth Ed., John Wiley and Sons, New York, 1988, p. 779.

INTERACTION OF PROCAINE WITH BIOMEMBRANES

JÁNOS ZSAKÓ, MARIA TOMOAI-COTIȘEL
and AURORA MOCANU

*Physical Chemistry Department, Faculty of Chemistry and Chemical Engineering,
"Babeș-Bolyai" University of Cluj-Napoca, 3400 Cluj-Napoca, Romania*

ABSTRACT. Compression isotherms of stearic acid (SA), dipalmitoyl phosphatidylcholine (DPPC), distearoyl phosphatidylcholine (DSPC) and of cholesterol (C) monolayers, as well as of mixed DPPC and C films have been recorded both in the absence and the presence of procaine. The penetration of procaine molecular species from the aqueous subphase into the lipid monolayers has been studied. By using Gibbs' equation, penetration numbers were derived from compression isotherms. Results are discussed in terms of molecular conformations, hydrophilic and hydrophobic interactions, allowing an insight into the molecular mechanism of procaine binding and penetration into the insoluble lipid monolayers studied.

Keywords. *Compression isotherms; lipid monolayers; procaine binding; procaine penetration*

INTRODUCTION

Studies concerning the interaction between anesthetics and natural membranes revealed a direct correlation between the efficiency of local anesthetics and their penetration into the lipid monolayers [1]. Investigations performed by using different experimental techniques showed some anesthetics to increase the fluidity of lipid bilayers [2], to decrease the order in hydrocarbon chains [3,4], to lower the temperature of the gel to liquid crystal phase transition [5,6], to extend the surface area of both monolayer films maintained at constant surface pressure [7,8] and of erythrocyte membranes [7,9] and to increase the surface pressure of lipid films maintained at constant area [1,10-12]. The molecular origin of the effects observed is presumed to be the weakening of the packing of the lipids due to the anesthetic molecules inserted [8]. The penetration has been evidenced by the energies of interaction of anesthetics with phospholipid monolayers spread at the air/water interface [1].

The major part of the experiments was performed by using monolayer membranes of lipids [1,8,11, 12]. The reason for using these model systems is the evidence of a direct correlation between the anesthetic efficiency and the oil/water partition coefficients of anesthetics [1]. Further, the monolayer represents the half of a lipid bilayer, the latter one determining the structure of the biomembrane [30]. The study of monolayers allows us to obtain direct information, at the molecular level, concerning the conformation and packing of molecules having biological significance in natural biomembranes under conditions near to the "*in vivo*" ones. Monomolecular films called also monolayers provide a convenient structural framework for experimental research and allow a quantitative treatment of the physico-chemical interactions between the film forming molecules, between the latter ones and the various subphase components (drugs, electrolytes, soluble proteins etc.). Monolayers spread at the air/water interface are sufficiently stable and suitable for experimental research.

Previously, we studied the influence of procaine (P), dissolved in the bulk subphase, upon stearic acid (SA) monolayers, spread at the air/water interface, by recording surface pressure (π , mN/m) *versus* mean molecular area (A, nm²/molecule) isotherms, by using acidic, unbuffered and alkaline aqueous subphases [13-20]. Besides SA, also L- α -distearoyl phosphatidylcholine (DSPC), L- α -dipalmitoyl phosphatidylcholine (DPPC) and cholesterol (C) monolayers, as well as mixed DPPC and C containing monolayers have been used as membrane models [21-23].

In this paper we present the maximum binding and the maximum penetration of procaine into various lipid monolayers as a function of the subphase pH, and of the lipid nature, as well as a function of the compactness of the lipid monolayers in the absence and in the presence of cholesterol. The surface solution thermodynamics will be employed to describe the binding and the penetration of procaine into lipid monolayers and we will show that our biophysical approach can be simultaneously fitted to multiple sets of data (e.g., binding at various subphase pH values and at different lipid layers in the absence and in the presence of cholesterol). Finally, we will compare the maximum penetration numbers of procaine into different lipid monolayers at the saturation of lipid layers with procaine molecular species.

The primary purpose of this study is to determine the maximum of procaine penetration into various lipid layers and to evidence the role of electrostatic effects in binding of anesthetics to lipid membranes and the role of cholesterol on the procaine penetration into lipid layers. A secondary purpose is to establish the pH conditions where the most of procaine is bound to the lipid monolayer membranes showing an enhanced stability of the lipid monolayer membranes.

RESULTS AND DISCUSSIONS

In our studies the π vs. A compression isotherms have been recorded by using the Wilhelmy method SA has been spread on different aqueous subphases: viz. having pH 2 generated by HCl, bidistilled water with pH 5.6, which will be referred to as unbuffered subphase and phosphate buffer solution with pH 8.

Compression isotherms have been recorded both in the absence of P and by dissolving P in the aqueous subphase ensuring a P concentration of 10⁻³ M or 10⁻² M. Since both film forming materials SA and P may participate in protolytic

equilibria, it is interesting to see the fraction α of different molecular species as function of pH. In these calculations the surface acidity constant of SA, equal to $pK=5.63$ [24], as well as the acidity constants of the double protonated PH_2^{2+} and the single protonated PH^+ , equal to $pK=1.95$ and 8.87 , respectively [25], have been used. Results are presented in Fig.1.

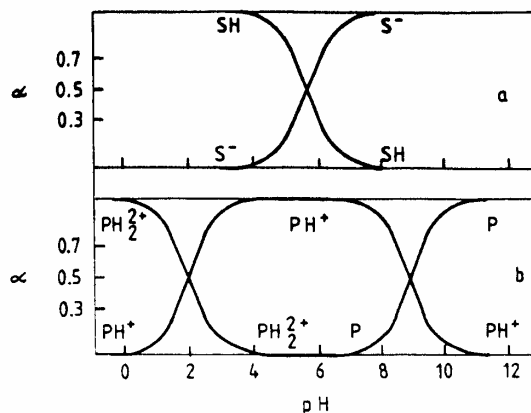


Figure 1. Fraction of molecular species as function of pH; a – for stearic acid (SA or SH); b – for procaine (P).

As seen from Fig.1 at pH 2 the SA film is completely unionized. On unbuffered water of pH 5.6 besides the neutral SA molecules an important amount of stearate anions is present. At pH 8 stearic acid is completely ionized and gives a charged film.

Procaine is a tertiary amine compound (anesthetic), containing also a primary amine group bound to the aromatic ring and may exist as neutral molecules (P), monocations (PH^+) or dications (PH_2^{2+}). At pH 2, the PH_2^{2+} amounts to 47%, the remaining part of 53% being PH^+ . On pure unbuffered water the only species is PH^+ . At pH 8 the predominant species is PH^+ , but one has also 12% of neutral molecules.

The effect of the subphase procaine upon the compression isotherms can be seen from Fig. 2. Obviously, procaine molecular species (P) have an expanding effect upon the SA monolayer, i.e. at a given π , value A is higher in the presence of P, which shows the penetration of P molecules into the SA monolayer, in substantial agreement with literature data on simplified membrane models [26-28]. In the same time an important increase of the collapse pressure is observed, i.e. in the presence of P the lipid monolayer becomes more stable.

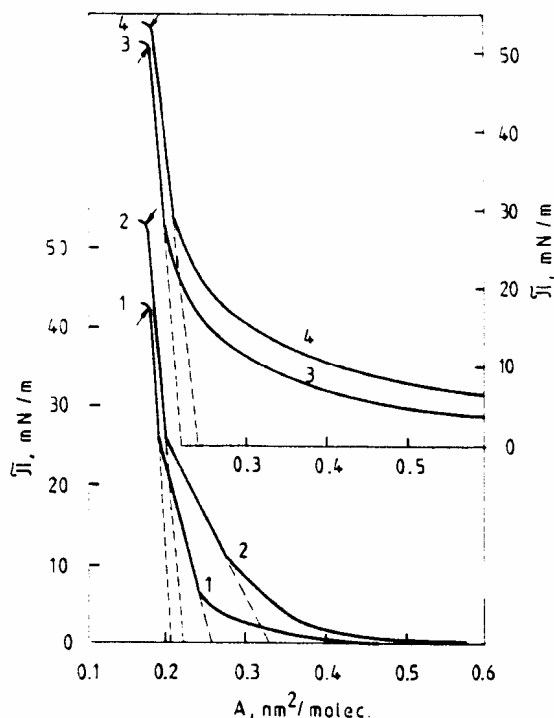


Figure 2. Compression isotherms of SA monolayers; curves (1) and (2) – unbuffered subphase of pH 5.6 and pH 5.2, respectively; curves (3) and (4) for pH 8; (1) and (3) for $[P] = 0$; (2) and (4) for $[P] = 10^{-3}$ M.

Let us introduce some notations. The water will be considered as being component 1, the soluble surfactant as component 2 and the insoluble surfactant as component 3. The number of molecules of these components at the air/water interface will be denoted as N_1 , N_2 and N_3 , respectively. The mean molecular area of the insoluble surfactant will be denoted with A_3 . Nevertheless, this magnitude is correlated to A_t , the whole area of the interface, according to the relation

$$A_3 = A_t / N_3 \quad (1)$$

By denoting the partial molecular areas (cross-section areas), *i.e.* the actual area necessities of the molecules, by \bar{A}_1 , \bar{A}_2 and \bar{A}_3 , one has

$$A_t = N_1 \bar{A}_1 + N_2 \bar{A}_2 + N_3 \bar{A}_3 \quad (2)$$

Since the procaine substrate has an expanding effect upon the SA monolayers, it is useful to define an area increment $\Delta A = A_3 - A_{30}$, representing the difference between the mean molecular area of the insoluble surfactant (A_3), at a given surface pressure π in the presence of component 2, and the mean molecular area of component 3, at the same surface pressure π , but in the absence of the

soluble surfactant 2 (A_{30}). Since in the absence of the soluble surfactant, the interface is a binary system, instead of Eq.(2) one has

$$A_t' = N_1' \bar{A}_1 + N_3' \bar{A}_3 \quad (3)$$

and the significance of A_{30} will be:

$$A_{30} = (N_1' \bar{A}_1 + N_3' \bar{A}_3) / N_3' \quad (4)$$

By constructing the area increment (ΔA) vs. π curves given in Fig. 3, one may observe that at compression ΔA and consequently the P penetration increases, but at the highest π values ΔA vanishes, *i.e.* the penetrated P is squeezed out from the monolayer, probably by forming a monolayer of procaine cations, leading to the stabilization of the SA monolayer, and to its enhanced collapse pressure.

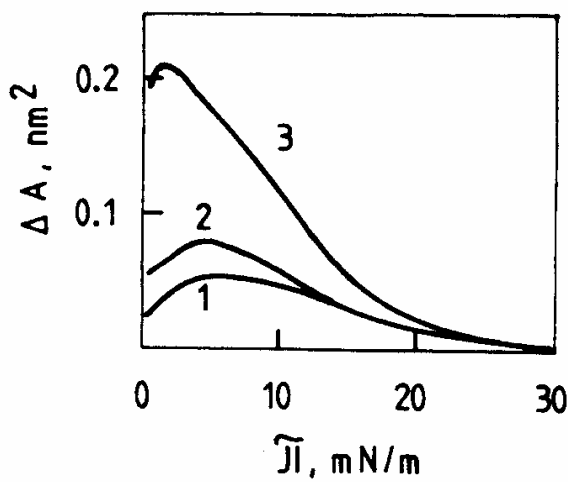


Figure 3. Molecular area increment (ΔA) due to the subphase P: curve (1) pH 2; (2) for pH 5.2; (3) for pH 8

One may see further that the expanding effect of P increases with increasing pH and becomes very important in alkaline media.

The penetration of P into the SA monolayer can be characterized by the penetration number n_p , which can be defined as the number of drug molecules (N_2) divided by the number of SA molecules (N_3)

$$n_p = N_2 / N_3 \quad (5)$$

It can be shown [14], that the penetration number may be correlated to the area increment ΔA , *viz.*

$$n_p = \Delta A / (A_{30} - \bar{A}_3 + \bar{A}_2) \quad (6)$$

Since the SA molecules are vertically oriented in the interface even at low surface pressures, for \bar{A}_3 , the cross sectional area of the COOH group may be

taken, $\bar{A}_3 = 0.18 \text{ nm}^2$. Concerning the area requirement \bar{A}_2 of procaine, molecular model calculations have been performed for different conformations of the molecule [14] and the results were compared to the adsorption data for pure procaine monolayers [20, 29]. Eq. (6) describes very well the experimental n_p vs. A_3 curves if for the variation of A_2 one presumes that at the spreading of the SA monolayer the P

molecules are adsorbed at the interface in a horizontal, lying down position ($A_2 = 1.50 \text{ nm}^2/\text{molecule}$). At compression of the procaine monolayer the P molecules gradually adopt a vertical position and this process is completely achieved ($A_2 = 0.40 \text{ nm}^2/\text{molecule}$) at π about 26 mN/m, that corresponds to the liquid condensed to solid phase transition of the SA pure monolayer.

Penetration number values have been derived from the compression isotherms, by using Gibbs' equation. The adsorption of the subphase component 2 at the air/water interface in the presence of an insoluble lipid monolayer forming component 3, obeys the following relation:

$$\Gamma_2 = \frac{1}{kT} \left(\frac{\partial \pi}{\partial \ln c_2} \right)_{T, A_3} \quad (7)$$

at constant T and for constant mean molecular area A_3 of the insoluble surfactant. The penetration number n_p is equal to:

$$n_p = \frac{A_3 - \bar{A}_3}{kT} \left(\frac{\partial \pi}{\partial \ln c_2} \right)_{T, A_3} \quad (8)$$

where \bar{A}_3 stands for the partial molecular area of component 3. By taking in Eq.(8) for \bar{A}_3 the collapse area A_{3c} of SA, n_p values were calculated as function of A_3 .

The n_p vs. A_3 curves allowed us to have an insight into the conformational changes of P during the compression of the SA monolayer. Upon compression of the SA monolayer spread on subphases of pH = 2, n_p increases at the beginning and it attains a maximum value at about 10 mN/m. Further on, it begins to decrease, indicating a squeezing out of the P molecules from the SA monolayer.

Penetration number values increase with increasing pH, especially in the alkaline region, as seen from the maximum n_p values given in Table 1 for 10^{-3} M and 10^{-2} M of P solutions.

This is due to the protolytic equilibria in which participate both P and SA. Increasing pH entails gradual deprotonation of PH_2^{2+} into PH^+ and P and consequently increases the surface activity of the soluble surfactant. On the other hand the deprotonation of the SA molecules makes easier the penetration of the P cations into the negatively charged SA monolayer.

Table 1.

Influence of pH upon the maximum penetration number values of P into SA monolayers

Subphase	Maximum n_p	
	$c_2 = 10^{-3}$ M	$c_2 = 10^{-2}$ M
pH 2	0.040	0.051
Unbuffered	0.059	0.089
pH 8	0.113	0.130

We have performed a similar study by using, instead of SA, L- α -dipalmitoyl phosphatidyl choline (DPPC) and L- α -distearoyl phosphatidylcholine (DSPC) as insoluble film forming surfactant. The subphase was a solution of procaine in twice distilled water, the pH being of 5.6. The maximum penetration numbers are given in Table 2.

Table 2.

Maximum penetration number values of P into SA, DSPC and DPPC monolayers

Insoluble surfactant	Maximum n_p	
	$c_2 = 10^{-3}$ M	$c_2 = 10^{-2}$ M
SA	0.059	0.089
DSPC	0.075	0.091
DPPC	0.127	0.170

As seen, at the same P concentration n_p increases in the order SA < DSPC < DPPC. The effect of the insoluble monolayer to enhance the P adsorption is due to the hydrophobic interactions between the molecules of both surfactants, but it is strongly influenced also by the compactness of the film.

The hydrophobic moiety of the P molecule is of small dimensions and, consequently, in its interaction with the long hydrocarbon chains of the insoluble surfactants no important differences may arise. Thus, the different behaviour might be assigned to the hydrophobic interactions between the molecules of the insoluble surfactant. The attracting forces between the neighbouring molecules will be the most important in the case of SA, having a small polar group and a single saturated hydrocarbon chain and thus SA will give the most compact film, being the most disadvantageous for the P penetration.

DSPC and DPPC have identical polar headgroups and two saturated hydrocarbon chains each one. These chains are longer with DSPC as compared to DPPC and therefore the former gives more compact films than the latter. Both films are however looser than the SA one and consequently the above order of penetration numbers is quite reasonable.

As lipid membrane models also cholesterol (C) monolayers and mixed monolayers containing C and DPPC in the molar ratio 1:1 have been used. The pure C monolayer at the air/water interface is very condensed even at low surface pressures, characterized by close packing of vertically oriented molecules.

The maximum n_p values observed at 10^{-2} and 10^{-3} M subphase P concentration are presented for C, DPPC, and mixed C and DPPC (1:1) films.

Results are compared with the arithmetical mean of n_p values for C and DPPC films, noted $(C + DPPC) / 2$, given in the last column of Table 3.

Table 3.

Maximum penetration number values of P into C, DPPC, and mixed C and DPPC monolayers

[P], M	Maximum n_p for			
	C Experimental	C and DPPC Experimental	DPPC Experimental	(C + DPPC)/2 Calculated
10^{-2}	0.032	0.058	0.170	0.101
10^{-3}	0.023	0.031	0.127	0.077

The n_p values reveal that procaine has affinity to the DPPC domain interfaces that are probably dominated by lipid chain conformations in substantial agreement with epifluorescent microscopy data [23].

It is interesting to observe that the maximum n_p values of the mixed monolayer are much more closer to the n_p values for C monolayers, than the ones obtained with DPPC. Due to the hydrophobic interactions between the air phase hydrocarbon moieties of C and DPPC, the mixed monolayer is almost as condensed as the pure C one. Thus, cholesterol being a membrane stabilizer in the same time it is found to diminish the membrane permeability and the adsorption of procaine on lipid monolayers. It is also shown that cholesterol appears to squeeze out procaine from the interfaces, especially near the collapse of lipid monolayers. These results are in substantial agreement with findings on the general model study of anesthetics, like halothane and cocaine-derivatives, and lipid membrane interactions [28].

CONCLUSIONS

Our results show that the compression isotherms of insoluble monolayers are a very useful tool in investigating membrane models. It allows to observe the insertion and penetration of soluble surfactants from the subphase into the insoluble lipid monolayer and to have an insight into the molecular mechanism of this penetration, which may play an important part in the physiological effects of anesthetics. In the same time one may observe the effect of cholesterol upon the compactness of phospholipid monolayers and upon the membrane permeability.

REFERENCES

1. F. A. Villalonga and E. W. Phillips, *J. Pharm. Sci.*, 1979, 68, 314.
2. J. R. Trudell, W. I. Hubbell and E. N. Cohen, *Fed. Proc.*, 1972, 31, 549.
3. G. I. Turner and N. Oldfield, *Nature*, 1979, 277, 669.
4. Y. Boulanger, S. Schreier and I. C. P. Smith, *Biochemistry*, 1981, 20, 6824.
5. I. Ueda, C. Tashiro and K. Arakawa, *Anesthesiology*, 1977, 45, 327.
6. J. M. Vanderkool, R. Landsberg, H. Selick and G. G. McDonald, *Biochim. Biophys. Acta*, 1977, 464, 1.

7. P. Seeman, *Pharmacol. Rev.*, 1972, 24(4), 583.
8. A. Seelig, *Biochim. Biophys. Acta*, 1987, 899, 196.
9. J. R. Trudell, *Biochim. Biophys. Acta*, 1977, 570, 509.
10. J. Chr. Skou, *J. Pharm. Pharmacol.*, 1961, 13, 204.
11. A. M. Shanes and N. I. Gershfeld, *J. Gen. Physiol.*, 1960, 44, 345.
12. F. A. Villalonga and E. W. Phillips, *J. Pharm. Sci.*, 1980, 69, 102.
13. M. Tomoaia-Cotișel, E. Chifu, A. Mocanu, J. Zsakó, M. Sălăjan and P. T. Frangopol, *Rev. Roum. Biochim.*, 1988, 25, 227.
14. M. Tomoaia-Cotișel, J. Zsakó, E. Chifu, P. T. Frangopol, W. A. P. Luck and E. Osawa, *Rev. Roum. Biochim.*, 1989, 26, 305.
15. E. Chifu, M. Tomoaia-Cotișel, A. Mocanu, P.T. Frangopol, *Seminars Biophysics*, IAP Press, Bucharest, 1990, vol. 6, p. 117.
16. J. Zsakó, M. Tomoaia-Cotișel, E. Chifu, I. Albu, A. Mocanu and P. T. Frangopol, *Rev. Roumaine Chim.*, 1990, 35, 867.
17. E. Chifu, M. Tomoaia-Cotișel, J. Zsakó, I. Albu, A. Mocanu and P. T. Frangopol, *Rev. Roumaine Chim.*, 1990, 35, 879.
18. J. Zsakó, M. Tomoaia-Cotișel, E. Chifu, A. Mocanu and P. T. Frangopol, *Biochim. Biophys. Acta*, 1990, 1024, 227.
19. M. Tomoaia-Cotișel, E. Chifu, J. Zsakó, P. T. Frangopol, P. J. Quinn and A. Mocanu, *Studia Univ. Babeș-Bolyai Chem.*, 1993, 38, 81.
20. M. Tomoaia-Cotișel, J. Zsakó, E. Chifu, A. Mocanu, P. T. Frangopol and P. J. Quinn, *J. Roumanian Colloid and Surface Chem. Assoc.*, 1997, 2(3-4), 30.
21. J. Zsakó, M. Tomoaia-Cotișel, E. Chifu, A. Mocanu and P. T. Frangopol, *Gazz. Chim. Ital.*, 1994, 124, 5.
22. J. Zsakó, E. Chifu, M. Tomoaia-Cotișel, A. Mocanu, P. T. Frangopol *Rev. Roumaine Chim.*, 1994, 39, 777.
23. B. Asgharian, D. A. Cadenhead, M. Tomoaia-Cotisel, *Langmuir*, 1993, 9, 228.
24. M. Tomoaia-Cotișel, J. Zsakó, M. Lupea and E. Chifu, *J. Colloid Interface Sci.*, 1987, 117, 464.
25. J. Zsakó, M. Tomoaia-Cotișel, I. Albu, A. Mocanu, E. Chifu and P. T. Frangopol, *Rev. Roumaine Biochim.*, 1991, 28, 33.
26. H. Matsuki, K. Shimada, S. Kaneshina, M. Yamanaka, H. Kamaya and I. Ueda, *Langmuir*, 1997, 13, 6115.
27. S. Desai, T. Hadlock, C. Messam, R. Chafetz, G. Strichartz, *J. Pharmacol. Exp. Ther.*, 1994, 271(1), 220.
28. K. Jorgensen, J. H. Ipsen, O.G. Mouritsen, M. J. Zuckermann, *Chem. Phys. Lipids*, 1993, 65(3), 205.
29. M. Tomoaia-Cotișel and D. A. Cadenhead, *Langmuir*, 1991, 7, 964.
30. M. Tomoaia-Cotișel and I. W. Levin, *J. Phys. Chem. B*, 1997, 101, 8477.

SPECTROSCOPIC STUDIES OF SOME METALLIC BIS-DITHIOPHOSPHONATES, $M(\text{DTP})_2$, AND OF SOME ADDUCTS

RODICA MICU-SEMENIUC^A, IONEL HAIDUC^A, RADU SEMENIUC^A AND
ONUȚ COZAR^B

a) "Babeș-Bolyai" University, Department of Chemistry,

b) "Babeș-Bolyai" University, Department of Physics,
3400 Cluj-Napoca, Romania

ABSTRACT. Metallic bis-[4-methoxyphenyl-O-methyl]-dithiophosphonate complexes ($M^{\text{II}}=\text{Fe, Ni, Cu, Zn, Cd, Hg, Sn}$) and the adducts with tertiary amines of Fe(II) and Ni(II) dithiophosphonates were prepared and investigated by UV-VIS, IR and EPR spectroscopies. The electronic spectra show the changes in coordination sphere of Fe(II) and Ni(II)-bis(4-methoxyphenyl-O-methyl-dithiophosphonates) by formation of the adducts. The characteristic frequencies of the PS_2 group confirm different coordination types of dithiophosphonate anion. EPR spectrum presents hyperfine and superhyperfine structure, suggesting a distorted D_{4h} symmetry.

Introduction

For several years we have studied the chemistry of transition metal phosphorodithioates, particularly the ability of nickel(II) phosphorodithioate to form adducts with various donor ligands. Amine adducts of nickel(II) phosphorodithioates of the general formula $\text{Ni}[\text{S}_2\text{P}(\text{OR})_2]_2 \cdot \text{B}$, where R=alkyl, phenyl, 1- and 2-naphtyl and B=mono- and di-amines were investigated¹⁻⁶. We were also interested in coordination behaviour of some phosphonodithioates, such as $M[\text{S}_2(\text{OR})(\text{C}_6\text{H}_4\text{-O-CH}_3\text{-}p)]_n$, where $M=\text{VO}^{2+}$, $n=2$, R=-CH₃, -C₂H₅, -ⁱC₃H₇, -ⁿC₃H₇, -ⁿC₄H₉, -ⁱC₄H₉, -^sC₄H₉⁷, M=Cr³⁺, $n=3$, R=-CH₃, -C₂H₅, -ⁿC₃H₇, -ⁱC₃H₇⁸ and $\text{Cr}[\text{S}_2\text{P}(\text{OCH}_3)(\text{C}_6\text{H}_4\text{-O-CH}_2\text{-CH}_3\text{-}p)]_3$ and $\text{Cu}[\text{S}_2\text{P}(\text{OCH}_3)(\text{C}_6\text{H}_4\text{-O-CH}_2\text{-CH}_3\text{-}p)]_9$.

In the present paper we report the preparation and investigation of some metallic O-methyl-p-anisil-dithiophosphonates (dtp) of general formulae $M(\text{dtp})_2$ (where $M^{\text{II}}=\text{Fe, Ni, Cu, Zn, Cd, Hg, Sn}$) and some of Ni(dtp)₂ and Fe(dtp)₂ adducts with tertiary amines, in order to follow the influence of different metallic ions and amines on the coordination behaviour of the O-methyl-p-anisil-dithiophosphonate ion.

Results and Discussion

Our compounds (table 1 and 5) were obtained with good yields, varying between 40 and 90%. It can be observed that the yields of simple metallic dithiophosphonate are greater than those of the corresponding adducts. Some of the compounds studied have sharp melting points, while the others do not present such behaviour, or undergo decomposition after melting (adducts with pyridine and picolines, $\text{Hg}(\text{dtp})_2$, etc).

The compounds are relatively stable on storage; the relatively low melting points (table 1) suggest monomeric molecular structures, while the compounds without melting points may have a polymeric or, at least, a dimeric structure.

In order to gain some insight into the thermal behaviour of compounds, thermogravimetric curves were recorded for selected compounds, considered as representatives from this point of view. Since the thermolysis curves were not recorded in an inert atmosphere, the presence of oxygen should be taken into account in the interpretation of data. Small endothermal effects, without weight loss are observed on all curves at melting temperature. The next thermal process is a weight loss accompanied by an exothermal effect, at temperatures immediately above the melting points, which corresponds to the elimination of the tertiary amines. This process takes place in two steps: the first molecule of pyridine and picolines is eliminated at 160° ($\text{Ni}(\text{dtp})_2(\text{pic})_2$), 165° ($\text{Ni}(\text{dtp})_2(4\text{-pic})_2$) and the second one at 190° , 180° , 200° respectively. The adducts of the type $\text{Fe}(\text{dtp})_2\text{-B}_2$ ($\text{B}=\text{pyridine}$, 3-, 4-picoline) have the same behaviour; the loss of the tertiary amine takes place in an overlapping process, between $130\text{-}200^\circ$.

The loss of coordinated amines is followed by the combustion of the organic groups, with the py_2 , 150° ($\text{Ni}(\text{dtp})_2(3\text{-pic})_2$) thermal effects partially overlapping with one another. After the combustion of the organic components of the molecules, the inorganic residue exhibits some minor exothermal effects between $550\text{-}700^\circ$, probably due to some polymorphic transformations. Such a thermal behaviour of our complexes resembles the one observed in other similar compounds^{6,10}.

Table 1

Elemental Analysis and Some Properties of Compounds

Compound	Colour	Mp ° (dc)	Elemental Analysis (found/calc.)			
			% M	% P	% S	% N
NH ₄ dip	white					
Fe(dtp) ₂	reddish-brown	293 dark-brown	10.35/10.70	11.53/11.88	23.95/24.52	-
Fe(dtp) ₂ .py ₂	white-yellow	147-150	8.35/8.21	8.85/9.11	18.32/18.82	3.84/4.11
Fe(dtp) ₂ ·(2,2'-dipy)	cherry-red	145	8.40/8.23	8.83/9.14	18.24/18.87	3.97/4.13
Fe(dtp) ₂ ·(o-phen) ₂	red	120 brown	6.52/6.32	7.23/7.03	14.22/14.51	6.21/6.35
Ni(dtp) ₂	violet	178	11.35/11.18	12.15/11.81	23.95/24.39	-
Ni(dtp) ₂ .py ₂	green	148-151	8.35/8.60	9.30/9.08	18.38/18.74	3.82/4.10
Ni(dtp) ₂ ·(3-pic) ₂	green	138-140	7.90/8.86	8.50/8.72	17.70/18.01	3.80/3.94
Ni(dtp) ₂ ·(4-pic) ₂	green	150-152	8.15/8.26	8.90/8.72	17.65/18.01	3.75/3.94
Ni(dtp) ₂ ·(2,2'-dipy)	green	130	8.70/8.62	9.37/9.10	18.70/18.80	4.02/3.97
Ni(2,2'-dipy) ₃ ·(dtp) ₂	pink	56-60 (90)	5.68/5.91	6.38/6.24	12.55/12.90	-
Ni(dtp) ₂ ·(o-phen)	green	145	8.54/8.33	8.95/8.79	18.46/18.16	3.82/3.97
Ni(o-phen) ₃ ·(dtp) ₂	pink	177-180 (185)	5.35/5.14	6.01/5.82	11.75/12.02	-
Cu(dtp) ₂	beige-yellow	190 orange	12.35/12.00	11.25/11.70	23.75/24.17	-
Zn(dtp) ₂	white	140	12.66/12.30	11.33/11.66	23.80/24.08	-
Cd(dtp) ₂	white	155-157*	19.19/19.43	11.00/10.71	21.82/22.13	-
Hg(dtp) ₂	yellow-greenish	100-101 117-120 orange	29.75/30.09	9.75/9.30	18.88/19.20	-
Sn(dtp) ₂	yellow	>200 beige	20.50/20.29	10.88/10.60	22.00/21.89	-

* 195⁰ re-solidifies; 225⁰ greenish; 245-255⁰ re-melts

Electronic Spectra

The changes in iron(II) and nickel(II) coordination induced by adding the amine ligands are clearly shown by the features of the electronic spectra. The electronic transitions in the spectra of the adducts are strongly dependent on the nature of the amine ligands.

Electronic spectra for $\text{Fe}(\text{dtp})_2$ and its adducts were recorded and spectral data were listed in table 2.

For $\text{Fe}(\text{dtp})_2$ the recorded spectrum is only qualitative because of the insolubility of this compound in solvents without donor properties. The spectrum was recorded on a freshly-prepared solution by the reaction of metallic iron with *O*-methyl-*p*-anisil dithiophosphonic acid, before the precipitations should have become quantitative. In the electronic spectrum, two bands are resolved, located at 19 300 and 16 400 cm^{-1} .

The data in table 2 certify the formation of complex combinations: in the UV domain two bands appear located between 43 000 and 34 000 cm^{-1} , which represent intraligand transitions and have high values of molar extinction coefficient. These bands will be shifted towards lower values in complexes as compared to the free dithiophosphonate ion, thus certifying the structural modifications which occur by the shift of the negative charge density towards the central ion through coordination.

Table 2.

Electronic Spectra of $\text{Fe}(\text{dtp})_2$ Adducts

Compound	c (mol/L)	Bands (cm^{-1})	ϵ ($\text{l} \cdot \text{mol}^{-1} \cdot \text{cm}^{-1}$)	Transitions
$\text{NH}_4 \text{ dtp}$	$7.9 \cdot 10^{-6}$	42 640 41 773	$1.15 \cdot 10^4$ $1.27 \cdot 10^4$	$n-\pi^*$ (L)
$\text{Fe}(\text{dtp})_2 \cdot \text{py}_2$	$3 \cdot 10^{-6}$	40 325 35 800 18 400 16 500	$6.8 \cdot 10^4$ $6.1 \cdot 10^4$ $5 \cdot 10^3$ $2 \cdot 10^2$	$n-\pi^*$ (L) $t_{2g}(\text{Fe})-\pi^*(\text{L})$
$\text{Fe}(\text{dtp})_2 \cdot \text{dipy}$	$9 \cdot 10^{-6}$	38 462 37 981 21 792 19 948	$5.29 \cdot 10^4$ $5.38 \cdot 10^4$ $5.1 \cdot 10^3$ $5.9 \cdot 10^3$	$n-\pi^*$ (L) $t_{2g}(\text{Fe})-\pi^*(\text{L})$
$\text{Fe}(\text{dtp})_2 \cdot (\text{o-phen})_2$	$9 \cdot 10^{-6}$	41 827 34 616 22 915 21 792 20 509	$9.23 \cdot 10^4$ $2.1 \cdot 10^4$ $3.67 \cdot 10^3$ $4.44 \cdot 10^3$ $4.91 \cdot 10^3$	$n-\pi^*$ (L) $t_{2g}(\text{Fe})-\pi^*(\text{L})$

In the visible range, bands appear between 22 300-16 900 cm^{-1} , bands whose molar extinction coefficients have lower values; yet, these values are not low enough to be associated with *d-d* transitions, they are due to metal-ligand transitions ($t_{2g}(\text{Fe})-\pi^*(\text{L})$). The values of these transitions decrease from the *o*-phenanthroline adduct to the one with pyridine. The presence of these bands in the spectra represents another proof of the formation of complex combination as they

are responsible for the colour of the compounds. One may notice that the values of the $t_{2g}-\pi^*$ transitions increase from the pyridine adduct to the one with o-phenantroline, which corresponds to the peculiar structures of organic ligands.

The electronic spectrum of $\text{Cu}(\text{dtp})_2$ exhibits the following bands in UV: 41 900 cm^{-1} and 38 000 cm^{-1} ($n-\pi^*$), 29 070 cm^{-1} ($\pi-\pi^*$), all of them being intraligand transitions. There are also some bands in visible: 23 800 cm^{-1} ($t_{2g}-\pi^*(L)$), 21 690 cm^{-1} and 15 105 cm^{-1} (${}^2B_{1g} \rightarrow {}^2E_g$ and ${}^2B_{1g} \rightarrow {}^2A_{1g}$ respectively). Similar bands are observed also for other $\text{Cu}(\text{II})$ -dithiophosphonates¹¹; their positions indicate a distorted square-planar geometry around the copper atom involved in the CuS_4 chromophore.

The electronic transitions in the spectra of $\text{Ni}(\text{dtp})_2$ adducts are dependent on the nature of the amine ligands (table 3). $\text{Ni}(\text{dtp})_2$ exhibits two bands in the visible region situated at 14 400 cm^{-1} (${}^1A_{1g} \rightarrow {}^1B_{1g}$) and at 18 600 cm^{-1} (${}^1A_{1g} \rightarrow {}^1B_{2g}$), usually values for NiS_4 chromophores¹².

The assignment of transitions is in accordance with a (more or less distorted) O_h symmetry¹³. The Lever's method¹⁴ was used to calculate the crystalline field splitting parameter (10 Dq), the Racah parameter (B) and the nephelauxetic parameter β (table 3). The calculated values of 10 Dq depend on the type of chromophore (higher for NiN_6 than for NiS_4N_2 , i.e. 9 380 cm^{-1} and 9 420 cm^{-1} for $\text{Ni}(\text{dipy})_3(\text{dtp})_2$ and $\text{Ni}(\text{o-phen})_3(\text{dtp})_2$ respectively). The covalent contribution of the dithiophosphonic ligand is reflected by the values of the β nephelauxetic parameter; this parameter is lower when the sulphur atoms are coordinated and slightly higher when only nitrogen atoms are coordinated to the nickel atom (table 3).

Table 3.**Electronic Spectra of $\text{Ni}(\text{dtp})_2$ Adducts**

Compound	ν_2 (cm^{-1}) ${}^3A_{2g}(F) \rightarrow {}^3T_{1g}(F)$	ν_3 (cm^{-1}) ${}^3A_{2g}(F) \rightarrow {}^3T_{1g}(P)$	B (cm^{-1})	β	$\nu_1 = 10Dq$ (cm^{-1}) ${}^3A_{2g}(F) \rightarrow {}^3T_{2g}(F)$
$\text{Ni}(\text{dtp})_2 \cdot \text{py}_2$	13 800	22 140	664	0.63	8 630
$\text{Ni}(\text{dtp})_2 \cdot (3\text{-pic})_2$	13 650	21 700	620	0.59	8 060
$\text{Ni}(\text{dtp})_2 \cdot (4\text{-pic})_2$	13 750	22 200	660	0.63	8 580
$\text{Ni}(\text{dtp})_2 \cdot \text{dipy}$	13 900	22 300	669	0.64	8 690
$\text{Ni}(\text{dipy})_3(\text{dtp})_2$	15 000	24 050	721	0.68	9 380
$\text{Ni}(\text{dtp})_2 \cdot \text{o-phen}$	14 000	22 700	681	0.65	8 850
$\text{Ni}(\text{o-phen})_3(\text{dtp})_2$	15 100	24 150	724	0.69	9 420

EPR Spectrum of $\text{Cu}(\text{dtp})_2$

The powder EPR spectrum of $\text{Cu}(\text{II})$ -bis[4-methoxyphenyl-O-methyl]-dithiophosphonate at room temperature is typical for square planar CuS_4 species (figure 1). The shape of the spectra shows the presence of hyperfine and superhyperfine structure.

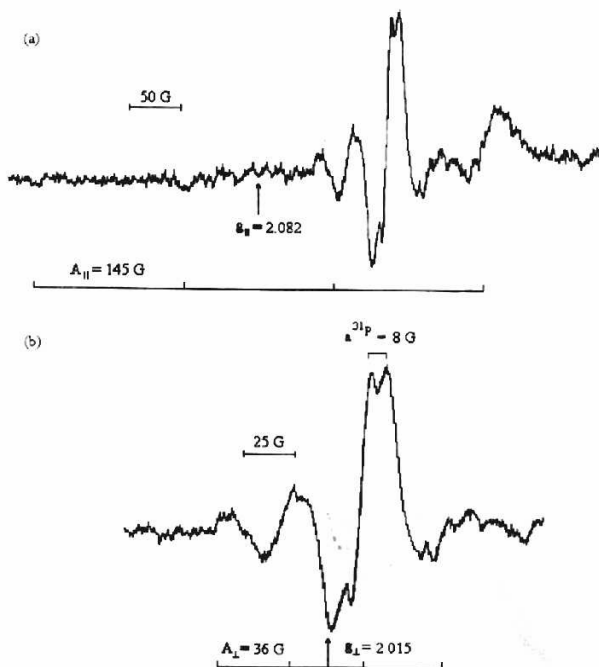


Figure 1. EPR spectrum of Cu(dtp)₂

The spin Hamiltonian used for the studied complex is:

$$H = \beta [g_{\parallel} B_z S_z + g_{\perp} (B_x S_x + B_y S_y)] + A_{\parallel} S_z I_z + A_{\perp} (S_x I_x + S_y I_y) + S \sum_{n=1}^2 a^n I_p$$

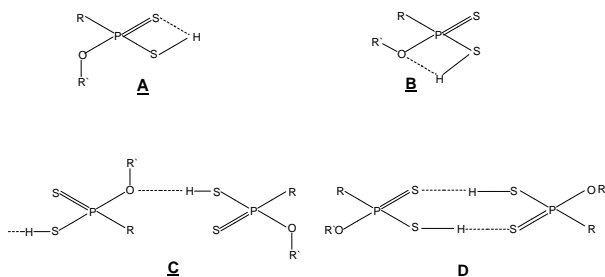
where g_{\parallel} and g_{\perp} are the principal values of the g tensor, β is the Bohr magneton, B_x , B_y and B_z are the components of the external magnetic field, S_x , S_y and S_z are the components of the electron magnetic moments S , I_x , I_y and I_z are the components of the nuclear spin moment of $^{63,65}\text{Cu}$ and I_p - the nuclear spin moment of ^{31}P and $a^{31}\text{P}$ the superhyperfine tensor.

Using the experimental EPR parameters (figure 1) and optical spectral data we have estimated, according to Kivelson and Neiman¹⁵ the covalency degree of the σ in plane bonding ($\alpha^2=0.52$) and the delocalisation degree of the paramagnetic electron in $3s$ orbital of phosphorous atoms ($c_s^2=0.002$). Both values are typical for distorted CuS_4 chromophores⁹.

Infrared Spectra

The interpretation of IR spectrum of O-methyl-*p*-anisildithiophosphonic acid was based on the literature data¹⁶⁻²¹ concerning phosphoro- and phosphonodithionate acids. Thus, two bands in ν_{SH} region, situated at 2 593 and 2 526 cm^{-1} were observed, corresponding to A, respectively to B isomers.

SPECTROSCOPIC STUDIES OF SOME METALLIC BIS-DITHIOPHOSPHONATES



The intramolecular hydrogen bond in both A and B structures was responsible for splitting of ν_{SH} band. The difference between the two bands in our spectrum and that of the literature²¹ can be correlated with influence of organic radical directly bonded to the phosphorous atoms ($-\text{C}_6\text{H}_4-\text{O}-\text{CH}_3$ comparatively to $-\text{CH}_3$). The bands at 593 cm^{-1} and 526 cm^{-1} were assigned to $\nu_{P=S}$ and ν_{P-S} respectively. The smaller value of $\nu_{P=S}$ related to $\nu_{P=S}$ (620 cm^{-1}) in 4-methoxyphenyl-thionophosphine sulfide can be a consequences of the involmnet of SH group to hydrogen bonding (structures A-D).

The infrared spectra can provide useful information concerning the coordination of the PS_2 groups. The IR absorption bands containing the highest PS_2 contributions, namely $\nu_a(\text{PS}_2)$ and $\nu_s(\text{PS}_2)$ are listed in table 4. The combinations with other normal modes (especially ν_{P-O} and ν_{P-C}) have some influence upon the behaviour of these bands. The attributions were made accroding to the literature data²² and by comparison with NH_4dtp spectrum (table 4).

Table 4.

Infrared Spectra of Compounds

Compound	$\nu_a(\text{PS}_2)$	$\nu_s(\text{PS}_2)$	$\Delta\nu$	Coordination type of the PS_2 group
NH_4dtp	627	556	71	ionic
$\text{Fe}(\text{dtp})_2$	627 653	531 546	96 107	anisobidentate bridge
$\text{Fe}(\text{dtp})_2\cdot\text{py}_2$	633	533	100	anisobidentate
$\text{Fe}(\text{dtp})_2\cdot\text{dipy}$	633	543	90	anisobidentate
$\text{Fe}(\text{dtp})_2\cdot(\text{o-phen})_2$	643	520	123	monodentate
$\text{Ni}(\text{dtp})_2$	620	552	68	isobidentate
$\text{Ni}(\text{dtp})_2\cdot\text{py}_2$	628	550	78	iso-anisobidentate
$\text{Ni}(\text{dtp})_2\cdot(3\text{-pic})_2$	628	550	78	iso-anisobidentate
$\text{Ni}(\text{dtp})_2\cdot(4\text{-pic})_2$	628	543	85	iso-anisobidentate
$\text{Ni}(\text{dtp})_2\cdot\text{dipy}$	635	546	89	anisobidentate
$\text{Ni}(\text{dipy})_3\cdot(\text{dtp})_2$	629	559	70	ionic
$\text{Ni}(\text{dtp})_2\cdot\text{o-phen}$	632	542	90	anisobidentate
$\text{Ni}(\text{o-phen})_3\cdot(\text{dtp})_2$	622	553	69	ionic
$\text{Cu}(\text{dtp})_2$	647	534	113	bridge
$\text{Zn}(\text{dtp})_2$	621	540	81	iso-anisobidentate
$\text{Cd}(\text{dtp})_2$	622 642	521 541	101 101	anisobidentate bimetallic triconnective bridge
$\text{Hg}(\text{dtp})_2$	634	536	98	anisobidentate
$\text{Sn}(\text{dtp})_2$	610 655	525 539	85 116	iso-anisobidentate bridge

On analysing the data in the table 4 and the reference in the literature²² according to which the mode of coordination of the PS₂ group can be established in keeping with the values of the $\Delta\nu = \nu_a(\text{PS}_2) - \nu_s(\text{PS}_2)$ difference, i.e.:

$$60 < \Delta\nu < 70 \text{ cm}^{-1} \text{ (isobidentate coordination)}$$

$$\text{and } 90 < \Delta\nu < 100 \text{ cm}^{-1} \text{ (anisobidentate coordination),}$$

we find that:

a) The O-methyl-*p*-anisildithiophosphonic anion may be *ionically bonded* in compounds having the formula Ni(dtp)₂·B₃ (B=dipyridil (dipy) and ortho-phenantroline (o-phen)), for which the ν_a and $\nu_s(\text{PS}_2)$ and $\Delta\nu$ values are close to the once found in the IR spectrum of NH₄dtp.

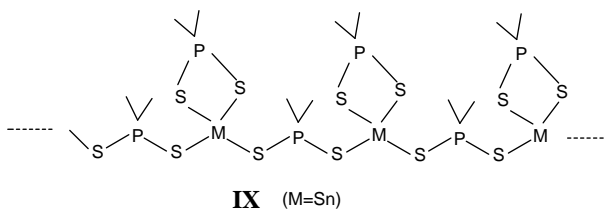
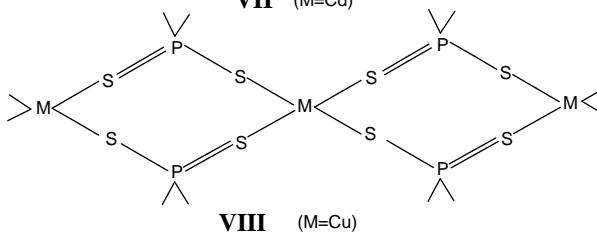
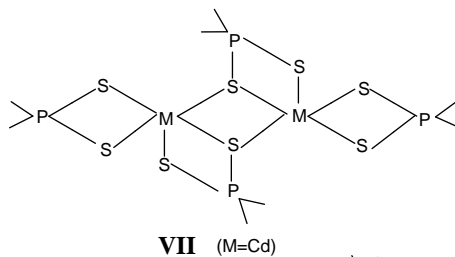
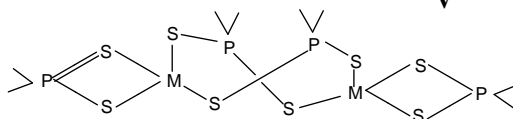
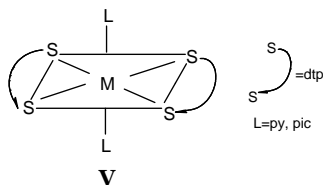
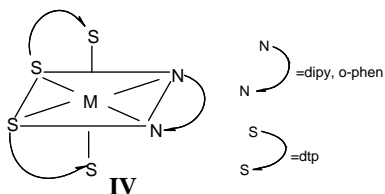
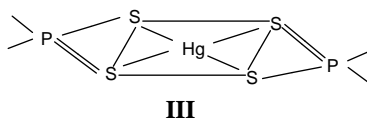
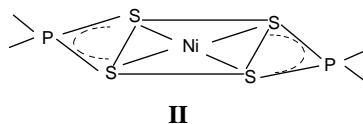
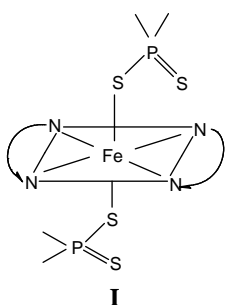
b) The phosphonodithioate anion may achieve a *monodentate coordination* (structure I) like in the case of Fe(dtp)₂(o-phen)₂ when the double character of the P=S bond is strengthened, while the P-S bond is weakened, which leads to an increase of the ν_a frequency and to the decrease of the ν_s frequency as related to the corresponding values for NH₄dtp compound. In fact ν_a becomes $\nu_{\text{P=S}}$, while $\nu_s - \nu_{\text{P-S}}$; $\Delta\nu$ assumes the highest value (table 4).

c) *The bidentate coordination* of the ⁻S₂P(OCH₃)(C₆H₄OCH₃) ion may be of two types: *isobidentate* (structure II) which is found in Ni(dtp)₂; both frequencies ν_a and ν_s will shift to lower values as related to those of NH₄dtp, as a consequence of sulphur coordination to the central atom. *Anisobidentate* coordination takes place without delocalisation of the π system of electrons over the whole PS₂ group (structure III), with a $\Delta\nu$ difference located within the ~90-100 cm⁻¹ interval. This occurs in Hg(dtp)₂ and in the Fe(dtp)₂·B (B=2py, dipy) or the Ni(dtp)₂·B (B=dipy, o-phen) adducts (structure IV). There are compounds in which the ν_a and $\nu_s(\text{PS}_2)$ frequencies assume intermediary values, between those specific to isobidentate and anisobidentate coordinations, as is the case with the Ni(dtp)₂·B₂ (B=py, 3- and 4-pic) adducts (structure V) and for Zn(dtp)₂.

In the case of bidentate coordination of the anion, the frequencies characteristic of the PS₂ group vibrations will undergo the following changes: ν_a shifts to higher values, while ν_s - to lower once compared to the values of the frequencies characteristic of the parent compound, Fe(dtp)₂, respectively Ni(dtp)₂. Such shifts can be explained by the fact that, as a consequence of the coordination of tertiary amines. The density of negative charge around the central ion increases, which induces a weakening of the metal-sulphur bond and, concomitantly, the strengthening of the phosphorous-sulphur bond.

d) For the M(dtp)₂ (M^{II}=Fe, Cu, Cd, Sn) compounds, there are two pairs of bands in the range of ν_{PS_2} (700-500 cm⁻¹) which may be attributed to different types of dithiophosphonate ions coordination; they correspond to structures VI-VIII. In order to discriminate these structures one can appeal to the $\Delta\nu$ values and thermal behaviour of the compounds. Thus for Fe(dtp)₂, $\Delta\nu=96 \text{ cm}^{-1}$ suggests the PS₂ group bound by chelation, while $\Delta\nu=107 \text{ cm}^{-1}$ can be correlated with bridge coordination. Since the compound is decomposed generating a black waxy oil product only over 300° (table 1), it means that this compound is at least dimeric, taking a VI type structure. For Cd(dtp)₂ the two values of $\Delta\nu$ are equal (table 4), but the ν_a and ν_s values undergo such shifts that the structure of the compound can be associated with a model in which a sulphur atom of two PS₂ group is bonded bimetallic triconnective²³ (structure VII).

SPECTROSCOPIC STUDIES OF SOME METALLIC BIS-DITHIOPHOSPHONATES



For $\text{Cu}(\text{dtp})_2$, $\Delta\nu=113 \text{ cm}^{-1}$ suggests a bridged-bonded dithiophosphonate anion as in the structure VIII, which fits with no melting point of these substance. For $\text{Sn}(\text{dtp})_2$, there are two values for $\Delta\nu$ (table 4): one of them suggests a bidentate anion and the other - a bridged one, like in structure IX; this compound have no melting point also. The last two compounds undergo changes of colour by increasing of the temperature (table 4), so a polymeric structure is expected.

However, it is hard to assume, relying only on data provided by IR spectra whether the bridge achived is iso- or anisobidentate.

Experimental

Reagents and Procedures

The reagents used here were analytical grade purity.

4-Methoxy-phenylthiophosphine sulfide was obtained by Lecher's method²³ and used for preparation of *O*-methyl-*p*-anisildithiophosphonic acid: 4g disulfide was refluxated, under stirring with 100 mL anhydrous methanol for 30 minutes. The acid was separated by vacuum distillation as an incolour viscous liquid. Yield: 88.6%: acidic constant, k_a , is $1.4 \cdot 10^{-4} \text{ mol/l}$. Other acids were obtained by the same procedure with different alcohols, ROH (R=-C₂H₅, *n*- and *i*-C₃H₇, *n*-, *i*-, *sec*- and *t*-C₄H₉; -CH₂-CH₂OPh, -CH₂-CH₂OMe, -CH₂Ph, -C₅H₁₁, -C₆H₁₁, α - and β -C₁₀H₇, but here we report only *O*-methyl derivative and some coordination properties of it.

Ammonium O-methyl-p-anisil-dithiophosphonate was obtained by refluxing 4g methoxy-phenyl-thiophosphine sulfide in 50 mL anhydrous benzene and the stoichiometric amount (0.5 mL) of anhydrous methanol, at 40-60°, under stirring, for 30 minutes. In the benzenic solution of *O*-methyl-*p*-anisil-dithiophosphonic acid thus obtained, was bubbled a current of dry ammonia. The bulky, white precipitate resulted was filtered, washed with benzene and dried in vacuum. Elemental analysis: %P found(calc) 12.15(12.35): %S found(calc) 22.25(22.50); $\text{Mp}^{\circ}=152\text{-}158$ (with decomposition), $\eta\%=70$.

Table 5.

Synthesis and Yields of Compounds

Compound	$\text{MX}_2 \cdot n\text{H}_2\text{O}$ solvent (mL)	(g)	NH_4dtp solvent (mL)	(g)	$\text{M}(\text{dtp})_2$ (g) solvent (mL)	Base (g) solvent (mL)	Yield (%)
$\text{Fe}(\text{dtp})_2^{\text{a}}$	$(\text{NH}_4)_2 \cdot \text{Fe}(\text{SO}_4)_2 \cdot 6\text{H}_2\text{O}$ (0.4) water (20)		water	(0.5) (25)	-	-	60
$\text{Fe}(\text{dtp})_2\text{py}_2^{\text{b}}$	$(\text{NH}_4)_2 \cdot \text{FeSO}_4 \cdot 6\text{H}_2\text{O}$ (0.4) water (20)		water	(0.5) (25)	-	py (0.2) MeOH (10)	62
$\text{Fe}(\text{dtp})_2\text{2,2' dipy}^{\text{b}}$	$(\text{NH}_4)_2 \cdot \text{FeSO}_4 \cdot 6\text{H}_2\text{O}$ (0.4) water (20)		water	(0.5) (25)	-	dipy (0.154) MeOH (20)	51
$\text{Fe}(\text{dtp})_2\text{o-phen}^{\text{b}}$	$(\text{NH}_4)_2 \cdot \text{FeSO}_4 \cdot 6\text{H}_2\text{O}$ (0.4)		water	(0.5) (25)	-	o-phen (0.36) MeOH (25)	40

SPECTROSCOPIC STUDIES OF SOME METALLIC BIS-DITHIOPHOSPHONATES

	(20)				
--	------	--	--	--	--

Table 5.

Synthesis and Yields of Compounds

Compound	$MX_2 \cdot nH_2O$ solvent	(g) (mL)	NH_4dtp (g) solvent (mL)	$M(dtp)_2$ (g) solvent mL	Base (g) solvent (mL)	Yield (%)
$Ni(dtp)_2^c$	$NiCl_2 \cdot 6H_2O$ MeOH	(4.75) (20)	(10.04) MeOH (20)	-	-	78
$Ni(dtp)_2 \cdot py_2$	-	-	-	$Ni(dtp)_2$ (0.52) acetone (50)	py (0.2) acetone (10)	86
$Ni(dtp)_2 \cdot (3-pic)_2$	-	-	-	$Ni(dtp)_2$ (0.52) acetone (50)	3-pic (0.2) acetone (10)	40
$Ni(dtp)_2 \cdot (4-pic)_2$	-	-	-	$Ni(dtp)_2$ (0.52) acetone (50)	4-pic (0.2) acetone (10)	60
$Ni(dtp)_2 \cdot dipy$	-	-	-	$Ni(dtp)_2$ (0.52) acetone (50)	dipy (0.156) acetone (20)	41
$Ni(dipy)_3 \cdot (dtp)_2$	-	-	-	$Ni(dtp)_2$ (0.52) acetone (50)	dipy (0.465) acetone (30)	62
$Ni(dtp)_2 \cdot o\text{-phen}$	-	-	-	$Ni(dtp)_2$ (0.52) acetone (50)	o-phen (0.18) acetone (10)	45
$Ni(o\text{-phen})_3 \cdot (dtp)_2$	-	-	-	$Ni(dtp)_2$ (0.52) acetone (50)	o-phen (0.54) acetone (30)	80
$Cu(dtp)_2^d$	$CuSO_4 \cdot 5H_2O$ water	(0.25) (20)	(0.25) water (20)	-	-	61
$Zn(dtp)_2^e$	$ZnSO_4 \cdot 7H_2O$ water	(0.29) (20)	(0.5) water (15)	-	-	70
$Cd(dtp)_2$	$Cd(NO_3)_2 \cdot 4H_2O$ water	(0.308) (20)	(0.5) water (10)	-	-	75
$Hg(dtp)_2$	HgI_2 MeOH	(0.455) (20)	(0.5) MeOH:H ₂ O 1:1 (20)	-	-	30
$Sn(dtp)_2$	$SnCl_2 \cdot 2H_2O$ slightly acidulated water	(0.23) (30)	(0.5) water (25)	-	-	67

a) Iron (II) O-methyl-*p*-anisildithiophosphonate was also obtained by another method, namely, the reaction between $Hdtp$ and iron powder: 0.4g *p*-anisildithiophosphine sulfide in 20 mL anhydrous methanol with an excess of iron powder were refluxed for 90 minutes. A brown-greenish solution was obtained, from which a brown-reedish compound, $Fe[S_2P(OCH_3)(C_6H_4OCH_3)]_2$ was separated on cooling. The precipitate was filtered, washed with methanol (5-7 mL) and ether (5-7 mL) and was dried in air. Elemental analysis: %Fe found(calc): 10.50(10.70); %P found(calc): 11.52(11.88); %S found(calc): 24.13(24.52); $\eta=50\%$. It does not present melting point, it decomposes up to 300°.

b) Iron (II) O-methyl-*p*-anisilphosphonodithioate adducts can not be obtained directly from $Fe(dtp)_2$ due to its insolubility in usually solvents. However,

these adducts were prepared also by following method: the solutions obtained in a, were separated by decantation over the methanolic solutions containing the amounts of tertiary amines listed in table 5. Under stirring the corresponding adducts precipitated. The precipitates were filtered, washed with 2 mL methanol and 3 mL ether, then were dried in air.

c) Nickel (II) O-methyl-*p*-anisildithiophosphonate can be obtained also by reaction of 4g *p*-anisil-thionophosphine sulfide in 20 mL anhydrous methanol and an excess of nickel powder. It was refluxed, under stirring, during 90-120 minutes. The violet precipitate of $\text{Ni}[\text{S}_2\text{P}(\text{OCH}_3)(\text{C}_6\text{H}_4\text{OCH}_3)]_2$ was separated, filtered washed with methanol (5-10 mL) and ether (5-10 mL). The same product was obtained by the reaction of HdtP with other nickel salts.

d) NH_4dtp solution was added to the CuSO_4 solution (table 5), drop by drop, under continuous stirring for 30 minutes.

e) $\text{Zn}(\text{dtp})_2$ can be obtained also by the methods described at a and c.

The metallic compounds and their adducts were obtained according to the known procedure¹⁻⁸ and are listed in table 5.

The compounds were analysed by classical methods²⁵ and the results were listed in table 1.

Thermolysis curves were recorded using a MOM Erdelyi-Paulik derigratograph. Electronic spectra were recorded in methanol, chloroform or methylene chloride with a JASCO V-530 UV-VIS apparatus, infrared spectra - in KBr pellets, with a FT-IR JASCO-615 instrument and the powder EPR spectrum was recorded at 9.4 GHz (X band) using a standard JEOL-JES-3B equipment with a magnetic field modulation of 100 kHz.

REFERENCES

1. R. Micu-Semeniuc, L. Silaghi-Dumitrescu and I. Haiduc, *Ionrg. Chim. Acta*, **17**, 5(1976).
2. R. Micu-Semeniuc, L. Silaghi-Dumitrescu and I. Haiduc, *Ionrg. Chim. Acta*, **33**, 281(1979).
3. R. Micu-Semeniuc, L. Silaghi-Dumitrescu, N. Chirilă and I. Haiduc, *Rev. Roumaine Chim.*, **25**, 1025(1980).
4. R. Micu-Semeniuc, C. Opreș and I. Haiduc, *Rev. Roumaine Chim.*, **25**, 1489(1980).
5. R. Micu-Semeniuc, F. Vesa and I. Haiduc, *Studia Univ. "Babeș-Bolyai", Chemia*, **25**, 43(1980).
6. Haiduc, R. Micu-Semeniuc and L. Silaghi-Dumitrescu, *Synth. React. Inorg. Met.-Org. Chem.*, **23**, 1629(1993).
7. O. Cozar, R. Micu-Semeniuc, V. Zramirovski and I. Haiduc, *Rev. Roumaine Phys.*, **33**, 1131(1988).
8. O. Cozar, R. Micu-Semeniuc, L. David, C. Bălan and I. Haiduc, *Studia Univ. "Babeș-Bolyai", Physica*, in press.

9. Haiduc, L. David, O. Cozar, R. Micu-Semeniuc, G. Mezei and M. Armean, *J. Mol. Struct.*, **482-483**, 153(1999).
10. R. N. Mukherjee, V. S. Vijava and P. K. Gogoi, *Thermochim. Acta*, **57**, 387(1982).
11. U. N. Tripathi, R. Bohra, G. Grivastava and R. C. Mehrotra, *Polyhedron*, **11**, 1187(1992).
12. J. D. Lebeda and R. A. Palmer, *Inorg. Chem.*, **10**, 2708(1971); **11**, 484(1972).
13. C. K. Joergensen, *Acta Chem. Scand.*, **16**, 2017(1962).
14. B. P. Lever, *J. Chem. Educ.*, **45**, 711(1968).
15. T. Kivelson and R. Neiman, *J. Chem. Phys.*, **29**, 35(1961).
16. R. A. Buldakova and R. R. Sagydullin, *Izv. Akad. Nauk SSSR, ser Khim.*, **1968**, 672.
17. R. R. Shagydullin, I. P. Lipatova, O. A. Raevskii, L.I. Vachugova, R. A. Cherkasov, P. G. Kharitov and S. A. Samartseva, *Izv. Akad. Nauk SSSR, ser Khim*, **1973**, 541.
18. T. P. Ereemeeva and I. A. Varashina, *Izv. Akad. Nauk SSSR, ser Khim*, **1976**, 1267.
19. R. R. Shagydullin, L. I. Vachugova and L. V. Avukunova, *Izv. Akad. Nauk SSSR, ser Khim*, **1979**, 2820.
20. R. A. Bulkacova and R. R. Shagydullin, *Izv. Akad. Nauk SSSR, ser Khim*, **1979**, 363.
21. R. Grecu, R. Constantinescu, I. Silaghi-Dumitrescu and I. Haiduc, *J. Mol. Struct.*, **218**, 111(1990).
22. Haiduc, I. Silaghi-Dumitrescu, R. Grecu, R. Constantinescu and L. Silaghi-Dumitrescu, *J. Mol. Struct.*, **114**, 467(1984).
23. M. J. Cox and E. R. T. Tiekink, *Rev. Inorg. Chem.*, **17**, 1(1997).
24. H. Z. Lecher, R. A. Greenwood, K. C. Whithouse and T. H. Chas, *J. Amer. Chem. Soc.*, **78**, 5018(1956).
25. Gh. Macarovic, "Analiza chimică cantitativă anorganică", Editura Acad. RSR, 1979.

SPECTROSCOPIC STUDIES OF SOME METALLIC BIS-DITHIOPHOSPHONATES, $M(\text{DTP})_2$, AND OF SOME ADDUCTS

RODICA MICU-SEMENIUC^A, IONEL HAIDUC^A, RADU SEMENIUC^A AND
ONUC COZAR^B

a) "Babeș-Bolyai" University, Department of Chemistry,

b) "Babeș-Bolyai" University, Department of Physics,
3400 Cluj-Napoca, Romania

ABSTRACT. Metallic bis-[4-methoxyphenyl-O-methyl]-dithiophosphonate complexes ($M^{II}=\text{Fe, Ni, Cu, Zn, Cd, Hg, Sn}$) and the adducts with tertiary amines of Fe(II) and Ni(II) dithiophosphonates were prepared and investigated by UV-VIS, IR and EPR spectroscopies. The electronic spectra show the changes in coordination sphere of Fe(II) and Ni(II)-bis(4-methoxyphenyl-O-methyl-dithiophosphonates) by formation of the adducts. The characteristic frequencies of the PS_2 group confirm different coordination types of dithiophosphonate anion. EPR spectrum presents hyperfine and superhyperfine structure, suggesting a distorted D_{4h} symmetry.

Introduction

For several years we have studied the chemistry of transition metal phosphorodithioates, particularly the ability of nickel(II) phosphorodithioate to form adducts with various donor ligands. Amine adducts of nickel(II) phosphorodithioates of the general formula $\text{Ni}[\text{S}_2\text{P}(\text{OR})_2]_2 \cdot \text{B}$, where R=alkyl, phenyl, 1- and 2-naphtyl and B=mono- and di-amines were investigated¹⁻⁶. We were also interested in coordination behaviour of some phosphonodithioates, such as $M[\text{S}_2(\text{OR})(\text{C}_6\text{H}_4\text{-O-CH}_3\text{-}p)]_n$, where $M=\text{VO}^{2+}$, $n=2$, R=-CH₃, -C₂H₅, -ⁱC₃H₇, -ⁿC₃H₇, -ⁿC₄H₉, -ⁱC₄H₉, -^sC₄H₉⁷, $M=\text{Cr}^{3+}$, $n=3$, R=-CH₃, -C₂H₅, -ⁿC₃H₇, -ⁱC₃H₇⁸ and $\text{Cr}[\text{S}_2\text{P}(\text{OCH}_3)(\text{C}_6\text{H}_4\text{-O-CH}_2\text{-CH}_3\text{-}p)]_3$ and $\text{Cu}[\text{S}_2\text{P}(\text{OCH}_3)(\text{C}_6\text{H}_4\text{-O-CH}_2\text{-CH}_3\text{-}p)]_9$.

In the present paper we report the preparation and investigation of some metallic O-methyl-p-anisil-dithiophosphonates (dtp) of general formulae $M(\text{dtp})_2$ (where $M^{II}=\text{Fe, Ni, Cu, Zn, Cd, Hg, Sn}$) and some of $\text{Ni}(\text{dtp})_2$ and $\text{Fe}(\text{dtp})_2$ adducts with tertiary amines, in order to follow the influence of different metallic ions and amines on the coordination behaviour of the O-methyl-p-anisil-dithiophosphonate ion.

Results and Discussion

Our compounds (table 1 and 5) were obtained with good yields, varying between 40 and 90%. It can be observed that the yields of simple metallic dithiophosphonate are greater than those of the corresponding adducts. Some of the compounds studied have sharp melting points, while the others do not present such behaviour, or undergo decomposition after melting (adducts with pyridine and picolines, $\text{Hg}(\text{dtp})_2$, etc).

The compounds are relatively stable on storage; the relatively low melting points (table 1) suggest monomeric molecular structures, while the compounds without melting points may have a polymeric or, at least, a dimeric structure.

In order to gain some insight into the thermal behaviour of compounds, thermogravimetric curves were recorded for selected compounds, considered as representatives from this point of view. Since the thermolysis curves were not recorded in an inert atmosphere, the presence of oxygen should be taken into account in the interpretation of data. Small endothermal effects, without weight loss are observed on all curves at melting temperature. The next thermal process is a weight loss accompanied by an exothermal effect, at temperatures immediately above the melting points, which corresponds to the elimination of the tertiary amines. This process takes place in two steps: the first molecule of pyridine and picolines is eliminated at 160° ($\text{Ni}(\text{dtp})_2 \cdot \text{pic}_2$), 165° ($\text{Ni}(\text{dtp})_2(4\text{-pic})_2$) and the second one at 190° , 180° , 200° respectively. The adducts of the type $\text{Fe}(\text{dtp})_2 \cdot \text{B}_2$ ($\text{B}=\text{pyridine}$, 3-, 4-picoline) have the same behaviour; the loss of the tertiary amine takes place in an overlapping process, between $130\text{-}200^\circ$.

The loss of coordinated amines is followed by the combustion of the organic groups, with the py_2 , 150° ($\text{Ni}(\text{dtp})_2(3\text{-})$ thermal effects partially overlapping with one another. After the combustion of the organic components of the molecules, the inorganic residue exhibits some minor exothermal effects between $550\text{-}700^\circ$, probably due to some polymorphic transformations. Such a thermal behaviour of our complexes resembles the one observed in other similar compounds^{6,10}.

Table 1

Elemental Analysis and Some Properties of Compounds

Compound	Colour	Mp ° (dc)	Elemental Analysis (found/calc.)			
			% M	% P	% S	% N
NH ₄ dip	white					
Fe(dtp) ₂	reddish-brown	293 dark-brown	10.35/10.70	11.53/11.88	23.95/24.52	-
Fe(dtp) ₂ .py ₂	white-yellow	147-150	8.35/8.21	8.85/9.11	18.32/18.82	3.84/4.11
Fe(dtp) ₂ .(2,2'-dipy)	cherry-red	145	8.40/8.23	8.83/9.14	18.24/18.87	3.97/4.13
Fe(dtp) ₂ .(o-phen) ₂	red	120 brown	6.52/6.32	7.23/7.03	14.22/14.51	6.21/6.35
Ni(dtp) ₂	violet	178	11.35/11.18	12.15/11.81	23.95/24.39	-
Ni(dtp) ₂ .py ₂	green	148-151	8.35/8.60	9.30/9.08	18.38/18.74	3.82/4.10
Ni(dtp) ₂ .(3-pic) ₂	green	138-140	7.90/8.86	8.50/8.72	17.70/18.01	3.80/3.94
Ni(dtp) ₂ .(4-pic) ₂	green	150-152	8.15/8.26	8.90/8.72	17.65/18.01	3.75/3.94
Ni(dtp) ₂ .(2,2'-dipy)	green	130	8.70/8.62	9.37/9.10	18.70/18.80	4.02/3.97
Ni(2,2'-dipy) ₃ .(dtp) ₂	pink	56-60 (90)	5.68/5.91	6.38/6.24	12.55/12.90	-
Ni(dtp) ₂ .(o-phen)	green	145	8.54/8.33	8.95/8.79	18.46/18.16	3.82/3.97
Ni(o-phen) ₃ .(dtp) ₂	pink	177-180 (185)	5.35/5.14	6.01/5.82	11.75/12.02	-
Cu(dtp) ₂	beige-yellow	190 orange	12.35/12.00	11.25/11.70	23.75/24.17	-
Zn(dtp) ₂	white	140	12.66/12.30	11.33/11.66	23.80/24.08	-
Cd(dtp) ₂	white	155-157*	19.19/19.43	11.00/10.71	21.82/22.13	-
Hg(dtp) ₂	yellow-greenish	100-101 117-120 orange	29.75/30.09	9.75/9.30	18.88/19.20	-
Sn(dtp) ₂	yellow	>200 beige	20.50/20.29	10.88/10.60	22.00/21.89	-

* 195^o re-solidifies; 225^o greenish; 245-255^o re-melts

Electronic Spectra

The changes in iron(II) and nickel(II) coordination induced by adding the amine ligands are clearly shown by the features of the electronic spectra. The electronic transitions in the spectra of the adducts are strongly dependent on the nature of the amine ligands.

Electronic spectra for $\text{Fe}(\text{dtp})_2$ and its adducts were recorded and spectral data were listed in table 2.

For $\text{Fe}(\text{dtp})_2$ the recorded spectrum is only qualitative because of the insolubility of this compound in solvents without donor properties. The spectrum was recorded on a freshly-prepared solution by the reaction of metallic iron with *O*-methyl-*p*-anisil dithiophosphonic acid, before the precipitations should have become quantitative. In the electronic spectrum, two bands are resolved, located at 19 300 and 16 400 cm^{-1} .

The data in table 2 certify the formation of complex combinations: in the UV domain two bands appear located between 43 000 and 34 000 cm^{-1} , which represent intraligand transitions and have high values of molar extinction coefficient. These bands will be shifted towards lower values in complexes as compared to the free dithiophosphonate ion, thus certifying the structural modifications which occur by the shift of the negative charge density towards the central ion through coordination.

Table 2.

Electronic Spectra of $\text{Fe}(\text{dtp})_2$ Adducts

Compound	c (mol/L)	Bands (cm^{-1})	ε ($\text{l} \cdot \text{mol}^{-1} \cdot \text{cm}^{-1}$) ¹⁾	Transitions
$\text{NH}_4 \text{ dtp}$	$7.9 \cdot 10^{-6}$	42 640 41 773	$1.15 \cdot 10^4$ $1.27 \cdot 10^4$	$n-\pi^*$ (L)
$\text{Fe}(\text{dtp})_2 \cdot \text{py}_2$	$3 \cdot 10^{-6}$	40 325 35 800 18 400 16 500	$6.8 \cdot 10^4$ $6.1 \cdot 10^4$ $5 \cdot 10^3$ $2 \cdot 10^2$	$n-\pi^*$ (L) $t_{2g}(\text{Fe})-\pi^*(\text{L})$
$\text{Fe}(\text{dtp})_2 \cdot \text{dipy}$	$9 \cdot 10^{-6}$	38 462 37 981 21 792 19 948	$5.29 \cdot 10^4$ $5.38 \cdot 10^4$ $5.1 \cdot 10^3$ $5.9 \cdot 10^3$	$n-\pi^*$ (L) $t_{2g}(\text{Fe})-\pi^*(\text{L})$
$\text{Fe}(\text{dtp})_2 \cdot (\text{o-phen})_2$	$9 \cdot 10^{-6}$	41 827 34 616 22 915 21 792 20 509	$9.23 \cdot 10^4$ $2.1 \cdot 10^4$ $3.67 \cdot 10^3$ $4.44 \cdot 10^3$ $4.91 \cdot 10^3$	$n-\pi^*$ (L) $t_{2g}(\text{Fe})-\pi^*(\text{L})$

In the visible range, bands appear between 22 300-16 900 cm^{-1} , bands whose molar extinction coefficients have lower values; yet, these values are not low enough to be associated with *d-d* transitions, they are due to metal-ligand transitions ($t_{2g}(\text{Fe})-\pi^*(\text{L})$). The values of these transitions decrease from the *o*-phenanthroline adduct to the one with pyridine. The presence of these bands in the spectra represents another proof of the formation of complex combination as they

are responsible for the colour of the compounds. One may notice that the values of the $t_{2g}-\pi^*$ transitions increase from the pyridine adduct to the one with o-phenantroline, which corresponds to the peculiar structures of organic ligands.

The electronic spectrum of $\text{Cu}(\text{dtp})_2$ exhibits the following bands in UV: 41 900 cm^{-1} and 38 000 cm^{-1} ($n-\pi^*$), 29 070 cm^{-1} ($\pi-\pi^*$), all of them being intraligand transitions. There are also some bands in visible: 23 800 cm^{-1} ($t_{2g}-\pi^*(L)$), 21 690 cm^{-1} and 15 105 cm^{-1} (${}^2B_{1g}\rightarrow{}^2E_g$ and ${}^2B_{1g}\rightarrow{}^2A_{1g}$ respectively). Similar bands are observed also for other $\text{Cu}(\text{II})$ -dithiophosphonates¹¹; their positions indicate a distorted square-planar geometry around the copper atom involved in the CuS_4 chromophore.

The electronic transitions in the spectra of $\text{Ni}(\text{dtp})_2$ adducts are dependent on the nature of the amine ligands (table 3). $\text{Ni}(\text{dtp})_2$ exhibits two bands in the visible region situated at 14 400 cm^{-1} (${}^1A_{1g}\rightarrow{}^1B_{1g}$) and at 18 600 cm^{-1} (${}^1A_{1g}\rightarrow{}^1B_{2g}$), usually values for NiS_4 chromophores¹².

The assignment of transitions is in accordance with a (more or less distorted) O_h symmetry¹³. The Lever's method¹⁴ was used to calculate the crystalline field splitting parameter (10 Dq), the Racah parameter (B) and the nephelauxetic parameter β (table 3). The calculated values of 10 Dq depend on the type of chromophore (higher for NiN_6 than for NiS_4N_2 , i.e. 9 380 cm^{-1} and 9 420 cm^{-1} for $\text{Ni}(\text{dipy})_3\cdot(\text{dtp})_2$ and $\text{Ni}(\text{o-phen})_3\cdot(\text{dtp})_2$ respectively). The covalent contribution of the dithiophosphonic ligand is reflected by the values of the β nephelauxetic parameter; this parameter is lower when the sulphur atoms are coordinated and slightly higher when only nitrogen atoms are coordinated to the nickel atom (table 3).

Table 3.**Electronic Spectra of $\text{Ni}(\text{dtp})_2$ Adducts**

Compound	ν_2 (cm^{-1})	ν_3 (cm^{-1})	B (cm^{-1})	β	$\nu_1 = 10Dq$ (cm^{-1})
	${}^3A_{2g}(F)\rightarrow{}^3T_{1g}(F)$	${}^3A_{2g}(F)\rightarrow{}^3T_{1g}(P)$			${}^3A_{2g}(F)\rightarrow{}^3T_{2g}(F)$
$\text{Ni}(\text{dtp})_2\cdot\text{py}_2$	13 800	22 140	664	0.63	8 630
$\text{Ni}(\text{dtp})_2\cdot(3\text{-pic})_2$	13 650	21 700	620	0.59	8 060
$\text{Ni}(\text{dtp})_2\cdot(4\text{-pic})_2$	13 750	22 200	660	0.63	8 580
$\text{Ni}(\text{dtp})_2\cdot\text{dipy}$	13 900	22 300	669	0.64	8 690
$\text{Ni}(\text{dipy})_3\cdot(\text{dtp})_2$	15 000	24 050	721	0.68	9 380
$\text{Ni}(\text{dtp})_2\cdot\text{o-phen}$	14 000	22 700	681	0.65	8 850
$\text{Ni}(\text{o-phen})_3\cdot(\text{dtp})_2$	15 100	24 150	724	0.69	9 420

EPR Spectrum of $\text{Cu}(\text{dtp})_2$

The powder EPR spectrum of $\text{Cu}(\text{II})$ -bis[4-methoxyphenyl-O-methyl]-dithiophosphonate at room temperature is typical for square planar CuS_4 species (figure 1). The shape of the spectra shows the presence of hyperfine and superhyperfine structure.

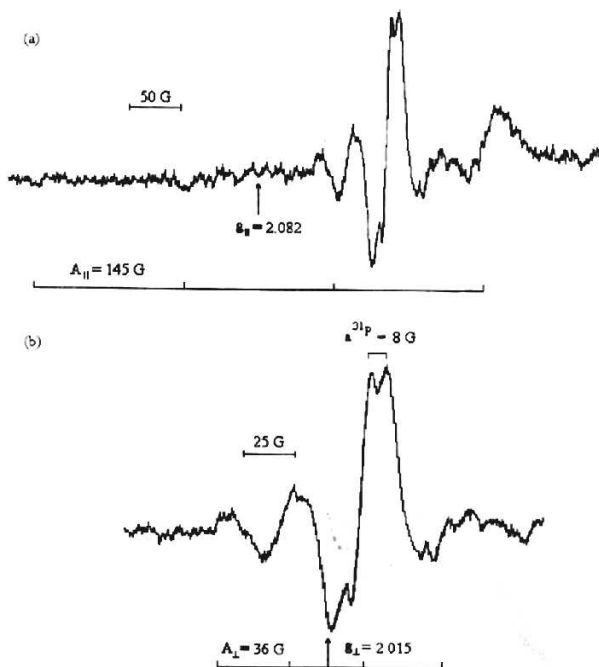


Figure 1. EPR spectrum of $\text{Cu}(\text{dtp})_2$

The spin Hamiltonian used for the studied complex is:

$$H = \beta [g_{\parallel} B_z S_z + g_{\perp} (B_x S_x + B_y S_y)] + A_{\parallel} S_z I_z + A_{\perp} (S_x I_x + S_y I_y) + S \sum_{n=1}^2 a^{31\text{P}} I_p$$

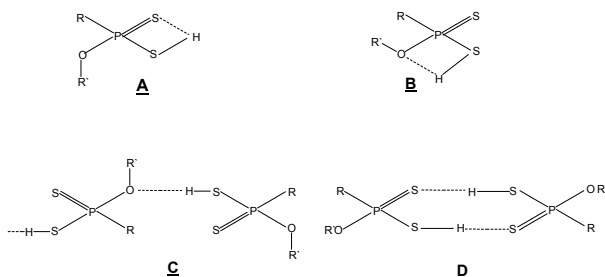
where g_{\parallel} and g_{\perp} are the principal values of the g tensor, β is the Bohr magneton, B_x , B_y and B_z are the components of the external magnetic field, S_x , S_y and S_z are the components of the electron magnetic moments S , I_x , I_y and I_z are the components of the nuclear spin moment of $^{63,65}\text{Cu}$ and I_p - the nuclear spin moment of ^{31}P and $a^{31\text{P}}$ the superhyperfine tensor.

Using the experimental EPR parameters (figure 1) and optical spectral data we have estimated, according to Kivelson and Neiman¹⁵ the covalency degree of the σ in plane bonding ($\alpha^2=0.52$) and the delocalisation degree of the paramagnetic electron in $3s$ orbital of phosphorous atoms ($c_s^2=0.002$). Both values are typical for distorted CuS_4 chromophores⁹.

Infrared Spectra

The interpretation of IR spectrum of *O*-methyl-*p*-anisildithiophosphonic acid was based on the literature data¹⁶⁻²¹ concerning phosphoro- and phosphonodithionate acids. Thus, two bands in ν_{SH} region, situated at 2 593 and 2 526 cm^{-1} were observed, corresponding to A, respectively to B isomers.

SPECTROSCOPIC STUDIES OF SOME METALLIC BIS-DITHIOPHOSPHONATES



The intramolecular hydrogen bond in both A and B structures was responsible for splitting of ν_{SH} band. The difference between the two bands in our spectrum and that of the literature²¹ can be correlated with influence of organic radical directly bonded to the phosphorous atoms ($-\text{C}_6\text{H}_4\text{-O-CH}_3$ comparatively to $-\text{CH}_3$). The bands at 593 cm^{-1} and 526 cm^{-1} were assigned to $\nu_{P=S}$ and ν_{P-S} respectively. The smaller value of $\nu_{P=S}$ related to $\nu_{P=S}(620\text{ cm}^{-1})$ in 4-methoxyphenyl-thionophosphine sulfide can be a consequences of the involmnet of SH group to hydrogen bonding (structures A-D).

The infrared spectra can provide useful information concerning the coordination of the PS_2 groups. The IR absorption bands containing the highest PS_2 contributions, namely $\nu_a(\text{PS}_2)$ and $\nu_s(\text{PS}_2)$ are listed in table 4. The combinations with other normal modes (especially ν_{P-O} and ν_{P-C}) have some influence upon the behaviour of these bands. The atributions were made accroding to the literature data²² and by comparison with NH_4dtp spectrum (table 4).

Table 4.

Infrared Spectra of Compounds

Compound	$\nu_a(\text{PS}_2)$	$\nu_s(\text{PS}_2)$	$\Delta\nu$	Coordination type of the PS_2 group
NH_4dtp	627	556	71	ionic
$\text{Fe}(\text{dtp})_2$	627 653	531 546	96 107	anisobidentate bridge
$\text{Fe}(\text{dtp})_2 \cdot \text{py}_2$	633	533	100	anisobidentate
$\text{Fe}(\text{dtp})_2 \cdot \text{dipy}$	633	543	90	anisobidentate
$\text{Fe}(\text{dtp})_2 \cdot (\text{o-phen})_2$	643	520	123	monodentate
$\text{Ni}(\text{dtp})_2$	620	552	68	isobidentate
$\text{Ni}(\text{dtp})_2 \cdot \text{py}_2$	628	550	78	iso-anisobidentate
$\text{Ni}(\text{dtp})_2 \cdot (3\text{-pic})_2$	628	550	78	iso-anisobidentate
$\text{Ni}(\text{dtp})_2 \cdot (4\text{-pic})_2$	628	543	85	iso-anisobidentate
$\text{Ni}(\text{dtp})_2 \cdot \text{dipy}$	635	546	89	anisobidentate
$\text{Ni}(\text{dipy})_3 \cdot (\text{dtp})_2$	629	559	70	ionic
$\text{Ni}(\text{dtp})_2 \cdot \text{o-phen}$	632	542	90	anisobidentate
$\text{Ni}(\text{o-phen})_3 \cdot (\text{dtp})_2$	622	553	69	ionic
$\text{Cu}(\text{dtp})_2$	647	534	113	bridge
$\text{Zn}(\text{dtp})_2$	621	540	81	iso-anisobidentate
$\text{Cd}(\text{dtp})_2$	622 642	521 541	101 101	anisobidentate bimetallic triconnective bridge
$\text{Hg}(\text{dtp})_2$	634	536	98	anisobidentate
$\text{Sn}(\text{dtp})_2$	610 655	525 539	85 116	iso-anisobidentate bridge

On analysing the data in the table 4 and the reference in the literature²² according to which the mode of coordination of the PS₂ group can be established in keeping with the values of the $\Delta\nu = \nu_a(\text{PS}_2) - \nu_s(\text{PS}_2)$ difference, i.e.:

$$60 < \Delta\nu < 70 \text{ cm}^{-1} \text{ (isobidentate coordination)}$$

$$\text{and } 90 < \Delta\nu < 100 \text{ cm}^{-1} \text{ (anisobidentate coordination),}$$

we find that:

a) The O-methyl-*p*-anisildithiophosphonic anion may be *ionically bonded* in compounds having the formula Ni(dtp)₂·B₃ (B=dipyridil (dipy) and ortho-phenantroline (o-phen)), for which the ν_a and $\nu_s(\text{PS}_2)$ and $\Delta\nu$ values are close to the once found in the IR spectrum of NH₄dtp.

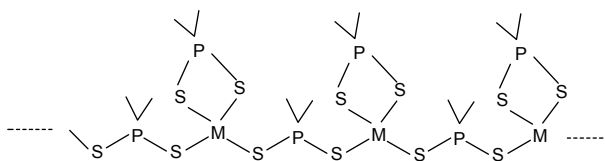
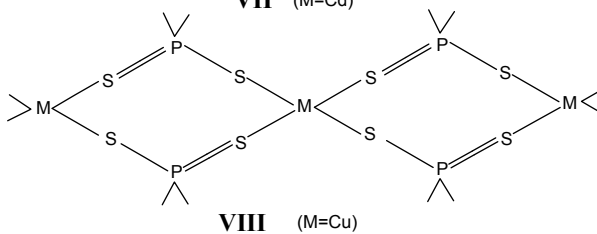
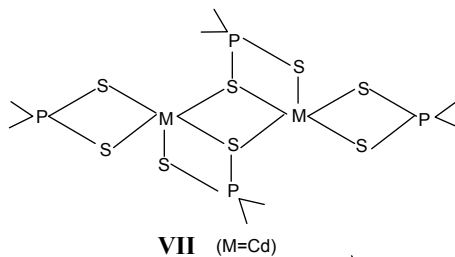
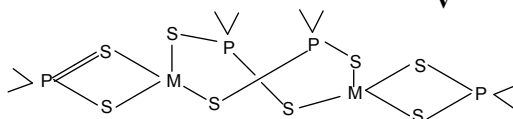
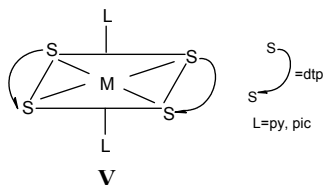
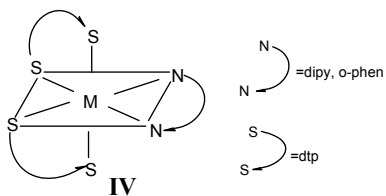
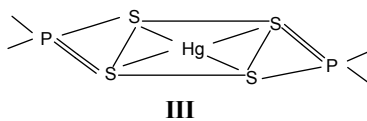
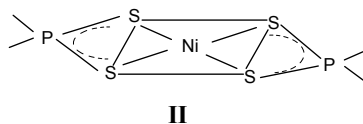
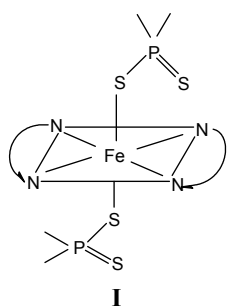
b) The phosphonodithioate anion may achieve a *monodentate coordination* (structure I) like in the case of Fe(dtp)₂(o-phen)₂ when the double character of the P=S bond is strengthened, while the P-S bond is weakened, which leads to an increase of the ν_a frequency and to the decrease of the ν_s frequency as related to the corresponding values for NH₄dtp compound. In fact ν_a becomes $\nu_{\text{P=S}}$, while $\nu_s - \nu_{\text{P-S}}$; $\Delta\nu$ assumes the highest value (table 4).

c) *The bidentate coordination* of the $\text{S}_2\text{P}(\text{OCH}_3)(\text{C}_6\text{H}_4\text{OCH}_3)$ ion may be of two types: *isobidentate* (structure II) which is found in Ni(dtp)₂; both frequencies ν_a and ν_s will shift to lower values as related to those of NH₄dtp, as a consequence of sulphur coordination to the central atom. *Anisobidentate* coordination takes place without delocalisation of the π system of electrons over the whole PS₂ group (structure III), with a $\Delta\nu$ difference located within the ~90-100 cm⁻¹ interval. This occurs in Hg(dtp)₂ and in the Fe(dtp)₂·B (B=2py, dipy) or the Ni(dtp)₂·B (B=dipy, o-phen) adducts (structure IV). There are compounds in which the ν_a and $\nu_s(\text{PS}_2)$ frequencies assume intermediary values, between those specific to isobidentate and anisobidentate coordinations, as is the case with the Ni(dtp)₂·B₂ (B=py, 3- and 4-pic) adducts (structure V) and for Zn(dtp)₂.

In the case of bidentate coordination of the anion, the frequencies characteristic of the PS₂ group vibrations will undergo the following changes: ν_a shifts to higher values, while ν_s - to lower once compared to the values of the frequencies characteristic of the parent compound, Fe(dtp)₂, respectively Ni(dtp)₂. Such shifts can be explained by the fact that, as a consequence of the coordination of tertiary amines. The density of negative charge around the central ion increases, which induces a weakening of the metal-sulphur bond and, concomitantly, the strengthening of the phosphorous-sulphur bond.

d) For the M(dtp)₂ (M^{II}=Fe, Cu, Cd, Sn) compounds, there are two pairs of bands in the range of ν_{PS_2} (700-500 cm⁻¹) which may be attributed to different types of dithiophosphonate ions coordination; they correspond to structures VI-VIII. In order to discriminate these structures one can appeal to the $\Delta\nu$ values and thermal behaviour of the compounds. Thus for Fe(dtp)₂, $\Delta\nu=96 \text{ cm}^{-1}$ suggests the PS₂ group bound by chelation, while $\Delta\nu=107 \text{ cm}^{-1}$ can be correlated with bridge coordination. Since the compound is decomposed generating a black waxy oil product only over 300° (table 1), it means that this compound is at least dimeric, taking a VI type structure. For Cd(dtp)₂ the two values of $\Delta\nu$ are equal (table 4), but the ν_a and ν_s values undergo such shifts that the structure of the compound can be associated with a model in which a sulphur atom of two PS₂ group is bonded bimetallic triconnective²³ (structure VII).

SPECTROSCOPIC STUDIES OF SOME METALLIC BIS-DITHIOPHOSPHONATES



For $\text{Cu}(\text{dtp})_2$, $\Delta\nu=113 \text{ cm}^{-1}$ suggests a bridged-bonded dithiophosphonate anion as in the structure VIII, which fits with no melting point of these substance. For $\text{Sn}(\text{dtp})_2$, there are two values for $\Delta\nu$ (table 4): one of them suggests a bidentate anion and the other - a bridged one, like in structure IX; this compound have no melting point also. The last two compounds undergo changes of colour by increasing of the temperature (table 4), so a polymeric structure is expected.

However, it is hard to assume, relying only on data provided by IR spectra whether the bridge achived is iso- or anisobidentate.

Experimental

Reagents and Procedures

The reagents used here were analytical grade purity.

4-Methoxy-phenylthiophosphine sulfide was obtained by Lecher's method²³ and used for preparation of *O*-methyl-*p*-anisildithiophosphonic acid: 4g disulfide was refluxated, under stirring with 100 mL anhydrous methanol for 30 minutes. The acid was separated by vacuum distillation as an incolour viscous liquid. Yield: 88.6%: acidic constant, k_a , is $1.4 \cdot 10^{-4} \text{ mol/l}$. Other acids were obtained by the same procedure with different alcohols, ROH (R= $-\text{C}_2\text{H}_5$, *n*- and *i*- C_3H_7 , *n*-, *i*-, *sec*- and *t*- C_4H_9 ; $-\text{CH}_2-\text{CH}_2\text{OPh}$, $-\text{CH}_2-\text{CH}_2-\text{OMe}$, $-\text{CH}_2\text{Ph}$, $-\text{C}_5\text{H}_{11}$, $-\text{C}_6\text{H}_{11}$, α - and β - C_{10}H_7 , but here we report only *O*-methyl derivative and some coordination properties of it.

Ammonium O-methyl-p-anisil-dithiophosphonte was obtained by refluxing 4g methoxy-phenyl-thionophosphine sulfide in 50 mL anhydrous benzene and the stoichiometric amount (0.5 mL) of anhydrous methanol, at 40-60°, under stirring, for 30 minutes. In the benzenic solution of *O*-methyl-*p*-anisil-dithiophosphonic acid thus obtained, was bubbled a current of dry ammonia. The bulky, white precipitate resulted was filtered, washed with benzene and dried in vacuum. Elemental analysis: %P found(calc) 12.15(12.35): %S found(calc) 22.25(22.50); $\text{Mp}^\circ=152-158$ (with decomposition), $\eta\%=70$.

Table 5.

Synthesis and Yields of Compounds

Compound	$\text{MX}_2 \cdot n\text{H}_2\text{O}$ solvent (mL)	(g)	NH_4dtp solvent (mL)	(g)	$\text{M}(\text{dtp})_2$ solvent (mL)	(g)	Base solvent (mL)	(g)	Yield (%)
$\text{Fe}(\text{dtp})_2^a$	$(\text{NH}_4)_2 \cdot \text{Fe}(\text{SO}_4)_2 \cdot 6\text{H}_2\text{O}$ (0.4) water (20)		water (25)	(0.5)	-		-		60
$\text{Fe}(\text{dtp})_2 \cdot \text{py}_2^b$	$(\text{NH}_4)_2 \cdot \text{FeSO}_4 \cdot 6\text{H}_2\text{O}$ (0.4) water (20)		water (25)	(0.5)	-	py MeOH (0.2) (10)			62
$\text{Fe}(\text{dtp})_2 \cdot 2,2'\text{-dipy}^b$	$(\text{NH}_4)_2 \cdot \text{FeSO}_4 \cdot 6\text{H}_2\text{O}$ (0.4) water (20)		water (25)	(0.5)	-	dipy MeOH (0.154) (20)			51
$\text{Fe}(\text{dtp})_2 \cdot \text{o-phen}^b$	$(\text{NH}_4)_2 \cdot \text{FeSO}_4 \cdot 6\text{H}_2\text{O}$ (0.4) (20)		water (25)	(0.5)	-	o-phen MeOH (0.36) (25)			40

Table 5.

Synthesis and Yields of Compounds

Compound	MX ₂ · nH ₂ O (g) solvent (mL)	NH ₄ dtp (g) solvent (mL)	M(dtp) ₂ (g) solvent (mL)	Base (g) solvent (mL)	Yield (%)
Ni(dtp) ₂ ^c	NiCl ₂ · 6H ₂ O (4.75) MeOH (20)	(10.04) MeOH (20)	-	-	78
Ni(dtp) ₂ ·py ₂	-	-	Ni(dtp) ₂ (0.52) acetone (50)	py (0.2) acetone (10)	86
Ni(dtp) ₂ ·(3-pic) ₂	-	-	Ni(dtp) ₂ (0.52) acetone (50)	3-pic (0.2) acetone (10)	40
Ni(dtp) ₂ ·(4-pic) ₂	-	-	Ni(dtp) ₂ (0.52) acetone (50)	4-pic (0.2) acetone (10)	60
Ni(dtp) ₂ ·dipy	-	-	Ni(dtp) ₂ (0.52) acetone (50)	dipy (0.156) acetone (20)	41
Ni(dipy) ₃ ·(dtp) ₂	-	-	Ni(dtp) ₂ (0.52) acetone (50)	dipy (0.465) acetone (30)	62
Ni(dtp) ₂ ·o-phen	-	-	Ni(dtp) ₂ (0.52) acetone (50)	o-phen (0.18) acetone (10)	45
Ni(o-phen) ₃ ·(dtp) ₂	-	-	Ni(dtp) ₂ (0.52) acetone (50)	o-phen (0.54) acetone (30)	80
Cu(dtp) ₂ ^d	CuSO ₄ · 5H ₂ O (0.25) water (20)	(0.25) water (20)	-	-	61
Zn(dtp) ₂ ^e	ZnSO ₄ · 7H ₂ O (0.29) water (20)	(0.5) water (15)	-	-	70
Cd(dtp) ₂	Cd(NO ₃) ₂ · 4H ₂ O (0.308) water (20)	(0.5) water (10)	-	-	75
Hg(dtp) ₂	HgI ₂ (0.455) MeOH (20)	(0.5) MeOH:H ₂ O 1:1 (20)	-	-	30
Sn(dtp) ₂	SnCl ₂ · 2H ₂ O (0.23) slightly acidulated water (30)	(0.5) water (25)	-	-	67

a) Iron (II) O-methyl-*p*-anisildithiophosphonate was also obtained by another method, namely, the reaction between Hdtp and iron powder: 0.4g *p*-anisildithiophosphine sulfide in 20 mL anhydrous methanol with an excess of iron powder were refluxed for 90 minutes. A brown-greenish solution was obtained, from which a brown-reedish compound, Fe[S₂P(OCH₃)(C₆H₄OCH₃)₂] was separated on cooling. The precipitate was filtered, washed with methanol (5-7 mL) and ether (5-7 mL) and was dried in air. Elemental analysis: %Fe found(calc): 10.50(10.70); %P found(calc): 11.52(11.88); %S found(calc): 24.13(24.52); η=50%. It does not present melting point, it decomposes up to 300°.

b) Iron (II) O-methyl-*p*-anisilphosphonodithioate adducts can not be obtained directly from Fe(dtp)₂ due to its insolubility in usually solvents. However, these adducts were prepared also by following method: the solutions obtained in a,

were separated by decantation over the methanolic solutions containing the amounts of tertiary amines listed in table 5. Under stirring the corresponding adducts precipitated. The precipitates were filtered, washed with 2 mL methanol and 3 mL ether, then were dried in air.

c) Nickel (II) O-methyl-*p*-anisildithiophosphonate can be obtained also by reaction of 4g *p*-anisil-thionophosphine sulfide in 20 mL anhydrous methanol and an excess of nickel powder. It was refluxed, under stirring, during 90-120 minutes. The violet precipitate of $Ni[S_2P(OCH_3)(C_6H_4OCH_3)]_2$ was separated, filtered washed with methanol (5-10 mL) and ether (5-10 mL). The same product was obtained by the reaction of Hdtp with other nickel salts.

d) NH_4dtp solution was added to the $CuSO_4$ solution (table 5), drop by drop, under continuous stirring for 30 minutes.

e) $Zn(dtp)_2$ can be obtained also by the methods described at a and c.

The metallic compounds and their adducts were obtained according to the known procedure¹⁻⁸ and are listed in table 5.

The compounds were analysed by classical methods²⁵ and the results were listed in table 1.

Thermolysis curves were recorded using a MOM Erdelyi-Paulik derigratograph. Electronic spectra were recorded in methanol, chloroform or methylene chloride with a JASCO V-530 UV-VIS apparatus, infrared spectra - in KBr pellets, with a FT-IR JASCO-615 instrument and the powder EPR spectrum was recorded at 9.4 GHz (X band) using a standard JEOL-JES-3B equipment with a magnetic field modulation of 100 kHz.

REFERENCES

1. R. Micu-Semeniuc, L. Silaghi-Dumitrescu and I. Haiduc, *Ionrg. Chim. Acta*, **17**, 5(1976).
2. R. Micu-Semeniuc, L. Silaghi-Dumitrescu and I. Haiduc, *Ionrg. Chim. Acta*, **33**, 281(1979).
3. R. Micu-Semeniuc, L. Silaghi-Dumitrescu, N. Chirilă and I. Haiduc, *Rev. Roumaine Chim.*, **25**, 1025(1980).
4. R. Micu-Semeniuc, C. Opreș and I. Haiduc, *Rev. Roumaine Chim.*, **25**, 1489(1980).
5. R. Micu-Semeniuc, F. Vesa and I. Haiduc, *Studia Univ. "Babeș-Bolyai", Chemia*, **25**, 43(1980).
6. Haiduc, R. Micu-Semeniuc and L. Silaghi-Dumitrescu, *Synth. React. Inorg. Met.-Org. Chem.*, **23**, 1629(1993).
7. O. Cozar, R. Micu-Semeniuc, V. Zramirovski and I. Haiduc, *Rev. Roumaine Phys.*, **33**, 1131(1988).
8. O. Cozar, R. Micu-Semeniuc, L. David, C. Bălan and I. Haiduc, *Studia Univ. "Babeș-Bolyai", Physica*, in press.

SPECTROSCOPIC STUDIES OF SOME METALLIC BIS-DITHIOPHOSPHONATES

9. Haiduc, L. David, O. Cozar, R. Micu-Semeniuc, G. Mezei and M. Armean, *J. Mol. Struct.*, **482-483**, 153(1999).
10. R. N. Mukherjee, V. S. Vijava and P. K. Gogoi, *Thermochim. Acta*, **57**, 387(1982).
11. U. N. Tripathi, R. Bohra, G. Grivastava and R. C. Mehrotra, *Polyhedron*, **11**, 1187(1992).
12. J. D. Lebeda and R. A. Palmer, *Inorg. Chem.*, **10**, 2708(1971); **11**, 484(1972).
13. C. K. Joergensen, *Acta Chem. Scand.*, **16**, 2017(1962).
14. B. P. Lever, *J. Chem. Educ.*, **45**, 711(1968).
15. T. Kivelson and R. Neiman, *J. Chem. Phys.*, **29**, 35(1961).
16. R. A. Buldakova and R. R. Sagydullin, *Izv. Akad. Nauk SSSR, ser Khim.*, **1968**, 672.
17. R. R. Shagydullin, I. P. Lipatova, O. A. Raevskii, L.I. Vachugova, R. A. Cherkasov, P. G. Kharitov and S. A. Samartseva, *Izv. Akad. Nauk SSSR, ser Khim*, **1973**, 541.
18. T. P. Ereemeeva and I. A. Varashina, *Izv. Akad. Nauk SSSR, ser Khim*, **1976**, 1267.
19. R. R. Shagydullin, L. I. Vachugova and L. V. Avukunova, *Izv. Akad. Nauk SSSR, ser Khim*, **1979**, 2820.
20. R. A. Bulkacova and R. R. Shagydullin, *Izv. Akad. Nauk SSSR, ser Khim*, **1979**, 363.
21. R. Grecu, R. Constantinescu, I. Silaghi-Dumitrescu and I. Haiduc, *J. Mol. Struct.*, **218**, 111(1990).
22. Haiduc, I. Silaghi-Dumitrescu, R. Grecu, R. Constantinescu and L. Silaghi-Dumitrescu, *J. Mol. Struct.*, **114**, 467(1984).
23. M. J. Cox and E. R. T. Tiekink, *Rev. Inorg. Chem.*, **17**, 1(1997).
24. H. Z. Lecher, R. A. Greenwood, K. C. Whithouse and T. H. Chas, *J. Amer. Chem. Soc.*, **78**, 5018(1956).
25. Gh. Macarovic, "Analiza chimică cantitativă anorganică", Editura Acad. RSR, 1979.

MEDIATED ANODIC OXIDATION OF TOLUENE WITH THE Ce(IV)/Ce(III) SYSTEM IN SULPHURIC ACID MEDIUM

LIVIU ONICIU, CLAUDIA G. MUREȘANU¹, CRISTINA G. BUCȘA²

*Faculty of Chemistry and Chemical Engineering "Babeș-Bolyai" University of Cluj,
11 Arany Janos Str., 3400-Cluj-Napoca, Romania;*

ABSTRACT. The Ce(IV)/Ce(III) couple was used as a mediator to oxidize an emulsion of toluene in aqueous H₂SO₄ medium, on graphite electrode using a divided electrochemical cell. The only oxidation product that could be identified, was benzaldehyde. The influence of several parameters upon benzaldehyde formation was investigated. The best yield for benzaldehyde formation, under the conditions employed was about 36%. Cyclic voltammetry was used to study the Ce(IV)/Ce(III) couple. Diffusion coefficients, reaction orders with respect to Ce (IV) and Ce(III) as well as the rate constants for Ce(IV) reduction and Ce(III) oxidation were determined. Ce (IV) regeneration on graphite electrode in H₂SO₄ medium using a divided cell was investigated. Good yields over 80% were obtained working under best conditions we found.

Keywords: cerium, toluene, benzaldehyde, voltammetry, mediated electrosynthesis.

In recent years the anodic oxidation of aromatic hydrocarbons aroused considerable interest. Substituted toluenes were oxidized up to 80-90% in an organic medium¹⁻⁵, while the degree of transformation for toluene did not exceed 20%^{1,6-8}. The main disadvantage of direct electrochemical oxidation of these organic compounds is its low selectivity. In aqueous medium where the oxidation potentials of toluene and substituted toluenes are higher than that of the solvent, mediated electrosynthesis gave better results than direct electrochemical oxidation. This procedure proved to be highly selective for the oxidation of toluene and substituted toluenes to the corresponding aldehydes. The Ce(IV)/Ce(III) couple has been the target of several studies of mediated electrochemical oxidation⁹⁻¹³. That is because of its high selectivity for partial oxidation of organic compounds

¹ muresanu@chem.ubbcluj.ro

² gbucsa@chem.ubbcluj.ro

accompanied by the possibility of electrochemical regeneration of Ce(IV) in various acidic media, with high current efficiencies^{9,13-18}. The best results for mediated electrooxidation are mentioned for p-chlorotoluene in HClO₄, between 80 and 90%¹⁰, and for p-methoxytoluene in HNO₃, about 63%, in the presence of phase transfer reagents¹³.

Mediated electrooxidation of toluene by Ce(IV)/Ce(III), in aqueous H₂SO₄, was less studied¹², that is why we have chosen this to the subject of our present paper. We report here also the results of voltammetric investigations and Ce(IV) regeneration in aqueous H₂SO₄ medium, on graphite electrode.

EXPERIMENTAL

Voltammetric measurements were performed in an undivided glass cell, using either a stationary or a rotating disc graphite electrode (*rde*) (diameter 4 mm), a 3,6 cm² Pt foil counter electrode and SCE reference electrode separated from the working electrode by a Luggin capillary. The electrodes were connected to a potentiostat controlled by PC. Current - potential data were stored directly on the computer memory. Ce(IV) regeneration was conducted in a divided cell of H-type, where compartments were separated by a large glass frit. A 6,84 cm² graphite bar was introduced in the anode compartment of volume 50 cm³ fitted with a magnetic stirrer bar. The cathode, a Pt strip, was always immersed in an aqueous H₂SO₄ solution. The instrumentation employed included a stabilized power supply, a voltmeter and a miliampermeter. During a run, current and cell potential readings were taken every 10 min. The Ce(IV) formed by electrolysis was monitored by titration. The samples taken at intervals were shaken with a measured volume of 0.01 mol/dm³ KI solution, followed by the titration of the formed iodine with Na₂S₂O₃.

The mediated electrosynthesis was carried out in the same cell, with the same instrumentation as Ce(IV) regeneration. Experiments were performed under methane gas atmosphere, to avoid further oxidation of benzaldehyde. After neutralizing the samples with NaOH, the content of benzaldehyde was estimated volumetrically. The method we employed recommends the transformation of benzaldehyde into the corresponding oxime, followed by titration with NaOH¹⁹. The content of benzaldehyde determined with this titration technique was in satisfactory agreement with that obtained by gas-chromatograph (*gc*) analysis (Table 1)

Table 1
Comparison between benzaldehyde content of samples analyzed by *gc* and by titration.

	Benzaldehyde %			
Titration	25.5	29.6	27.5	31.6
Gc	24	27.3	29.1	30.4

All chemicals came from commercial sources and were used without further purification. Solutions were prepared in twice distilled water. All measurements, unless otherwise stated, were made at room temperature, $18 \pm 2^\circ\text{C}$.

RESULTS AND DISCUSSIONS

Voltammetry

Cyclic voltammograms recorded on stationary graphite electrode (Fig. 1.) in aqueous H_2SO_4 exhibited a well formed anodic peak at $1,25\text{V}/\text{SCE}$ and a corresponding cathodic peak at $1,19\text{V}/\text{SCE}$, while oxygen evolution becomes important at about $1,5\text{V}/\text{SCE}$. Increasing the potential sweep rate, ν , between 10^{-2} and $15 \cdot 10^{-2}\text{V}/\text{s}$, when the $[\text{Ce}(\text{IV})/\text{Ce}(\text{III})]$ ratio was unity, no shift of peak potential was observed neither for the anodic, nor for the cathodic peak. The separation of peak potentials, $\Delta\varepsilon$, varied between 60 and 70 mV, but peak current ratio was higher than one and slightly increased from 1,25 to 1,43, when ν was varied between the limits mentioned above. That is why the $\text{Ce}(\text{IV})/\text{Ce}(\text{III})$ system should be considered just quasireversible. Voltammetric investigations with the *rde* were also performed, but no influence of electrode rotation speed upon half-wave potentials could be observed.

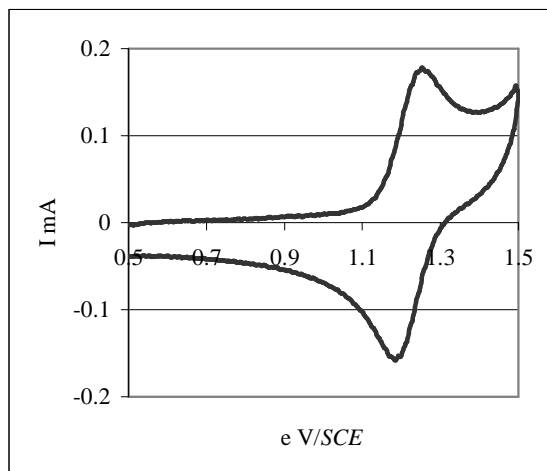


Figure 1. Cyclic voltammogram of the $\text{Ce}(\text{IV})/\text{Ce}(\text{III})$ system in $0,5 \text{ mol}/\text{dm}^3 \text{H}_2\text{SO}_4$ on stationary graphite electrode

Linear plots $I_v = f(\nu^{1/2})$ for the stationary electrode and $I_L = f(\omega^{1/2})$ for the *rde* (Fig. 2.) served to determine the diffusion coefficients for $\text{Ce}(\text{IV})$ and $\text{Ce}(\text{III})$ in aqueous $0,5 \text{ mol}/\text{dm}^3 \text{H}_2\text{SO}_4$: at the stationary electrode $D = (9,68 \pm 0,06) \cdot 10^{-5} \text{cm}^2 \cdot \text{s}^{-1}$ for $\text{Ce}(\text{III})$ and $D = (6,36 \pm 0,21) \cdot 10^{-5} \text{cm}^2 \cdot \text{s}^{-1}$ for $\text{Ce}(\text{IV})$; at the rotating disc electrode $D = (1,72 \pm 0,29) \cdot 10^{-6} \text{cm}^2 \cdot \text{s}^{-1}$ for $\text{Ce}(\text{III})$ and $D = (1,37 \pm 0,33) \cdot 10^{-6} \text{cm}^2 \cdot \text{s}^{-1}$ for $\text{Ce}(\text{IV})$.

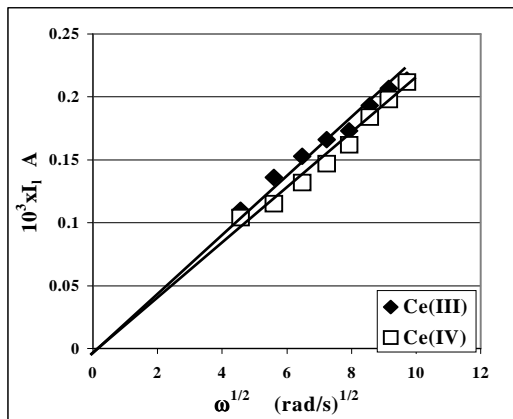
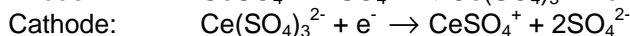
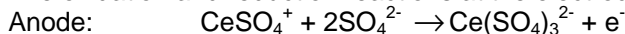


Figure 2. Levich linear plots for the Ce(IV)/Ce(III) couple at graphite electrode in 0.5 mol/dm³ H₂SO₄

Peak currents and limiting currents, used for the determination of diffusion coefficients, don't occur at the same potential, that means the diffusion coefficients in our experiments were not determined at the same potential. This may be a possible explanation for the differences noticed between the values of diffusion coefficients obtained from stationary electrode and from rotating disc electrode data.

The oxidation and reduction reactions at the electrode are probably:



because in H₂SO₄ medium Ce(IV), as well as Ce(III) may form many sulphatocomplexes²⁰⁻²³ like: CeSO₄²⁺, Ce(SO₄)₂, Ce(SO₄)₂³⁻ or CeSO₄⁺, Ce(SO₄)₂⁻, Ce(SO₄)₃³⁻, respectively. The dominant species, in 0,5 mol/dm³ H₂SO₄, or solutions of higher concentration, is the voluminous Ce(SO₄)₃²⁻ sulphatocomplex. Ce(III) has a less pronounced tendency to form sulphatocomplexes than Ce(IV), this may account for the slight higher values of diffusion coefficients in the case of Ce(III).

Diffusion coefficients of cerium, we obtained from *rde* experiments, are smaller than those obtained, by the same method in HClO₄ or HNO₃ medium^{16, 24}, because sulphato- complexes of cerium are stronger than other anions.

Voltammograms of *rde* experiments were used to find reaction orders with respect to Ce(IV) and Ce(III) from $I = f(\omega^{1/2})$ plots at different potentials. The orders were determined according to a procedure recommended in literature²⁵ by means of equation²⁴:

$$\mu = \frac{\log I_2/I_1}{\log [I_{L,1}/(I_{L,1} - I_1)] - \log [I_{L,2}/(I_{L,2} - I_2)]}$$

where: I_1 and I_2 are the currents recorded at the same potential for different square roots of angular velocity: $\omega_1^{1/2}$ and $\omega_2^{1/2}$

$I_{L,1}$ and $I_{L,2}$ are the limiting currents corresponding to $\omega_1^{1/2}$ and $\omega_2^{1/2}$
 Rate constants, for the oxidation of Ce(III) and the reduction of Ce(IV) respectively
 were calculated from the intercepts of these plots.

Linear $1/I=f(1/\omega^{1/2})$ plots for the relation

$$\frac{1}{I} = \frac{1}{z \cdot F \cdot A \cdot k \cdot C} + \frac{1,61 \cdot v^{1/6}}{z \cdot F \cdot D^{2/3} \cdot A \cdot C} \cdot \frac{1}{\omega^{1/2}}$$

were obtained. The mean values obtained for the reaction orders were:
 $\bar{\mu} = 1.12 \pm 0.11$ for Ce(IV) and $\bar{\mu} = 0.5 \pm 0.025$ for Ce(III), while the rate constants were:
 $10^3 \cdot k_{red} = 2,68 \pm 0.05$ cm/s and $10^3 \cdot k_{ox} = 1.6 \pm 0.05$ cm/s

A possible explanation for the small reaction order with respect to Ce(III) is the adsorption of inactive Ce(III) sulphatocomplex, like $Ce(SO_4)_2$ or solvent molecules on the electrode.

Ce(IV) regeneration at graphite electrode in aqueous H_2SO_4 medium

In order to approach to conditions of mediated anodic oxidation the electrolysis was carried out when 10^{-2} mol/dm³ Ce(IV) was also initially present.

By increasing the current density from 0,2 to 1,6 mA/cm² the degree of Ce(IV) formation increased till it reached a maximum value at about 1,2 mA/cm² (Fig. 3)

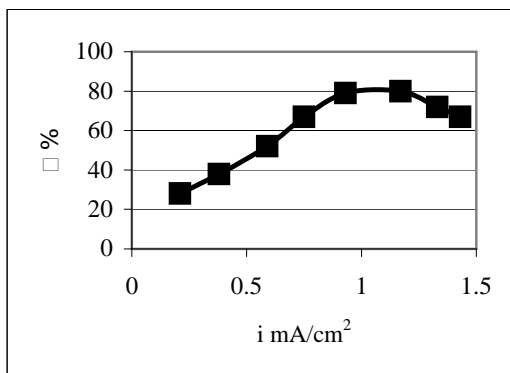


Figure 3. The influence of current density upon the conversion of Ce(III) to Ce(IV);
 $[H_2SO_4] = 1 \text{ mol/dm}^3$; $[Ce(IV)]/[Ce(III)] = 2$, $t = 20^\circ C$

To achieve sustained electrolysis, experiments had to be performed at a cell potential, where both Ce(III) oxidation and oxygen evolution is possible. As expected, the conversion of Ce(III) to Ce(IV) decreased at higher current densities due to the increasing significance of the oxygen evolution reaction.

Sulphuric acid concentration exerted a positive effect on Ce(IV) regeneration till about 1 mol/dm³ (Fig. 4.).

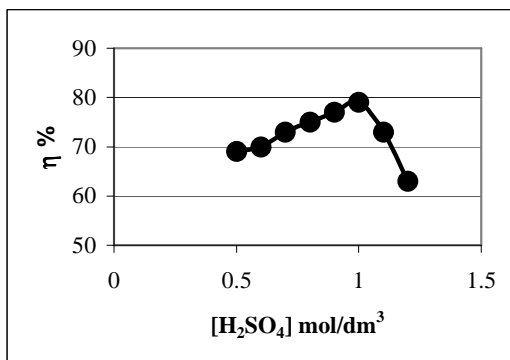


Figure 4. The influence of H₂SO₄ concentration upon the conversion of Ce(III) to Ce(IV); $i = 0.97 \text{ mA/cm}^2$; $[\text{Ce(IV)}]/[\text{Ce(III)}] = 2$; $t = 20^\circ\text{C}$

As mentioned above, at higher concentrations of H₂SO₄, voluminous sulphatocomplexes of Ce(IV) and Ce(III) are dominant. The low mobility and the small diffusion coefficients of these species caused the decrease of Ce(IV) formation at concentrations over 1 mol/dm³ H₂SO₄.

When [Ce(III)] was increased at constant Ce(IV) concentration, the best results were obtained for a [Ce(IV)/Ce(III)] equal to one (Fig. 5).

The presence of toluene exerted a negative influence on the regeneration process as it results from Table 2.

Table 2.

The influence of toluene concentration upon Ce(IV) regeneration process; $[\text{Ce(IV)/Ce(III)}] = 10^{-2} \text{ mol/dm}^3$, $i = 0,965 \text{ mA/cm}^2$, $[\text{H}_2\text{SO}_4] = 1 \text{ mol/dm}^3$, $t = 20^\circ\text{C}$

[Toluene] mol/dm ³	0,1	0,5	0,75
η% without toluene		79	
η%with toluene	61	60	58

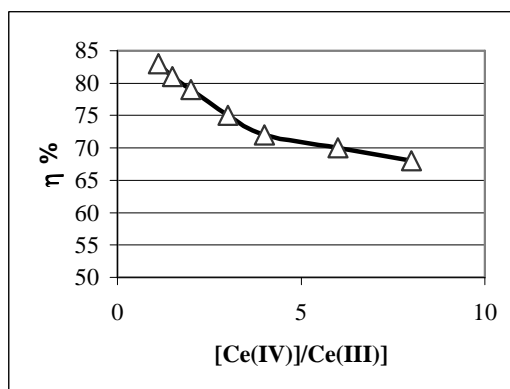


Figure 5. The influence of [Ce(IV)]/[Ce(III)] ratio upon the conversion of Ce(III) to Ce(IV); $i = 0.97 \text{ mA/cm}^2$; $[\text{H}_2\text{SO}_4] = 1 \text{ mol/dm}^3$; $t = 20^\circ\text{C}$

Mediated electrosynthesis of benzaldehyde

Due to low solubility of toluene in the aqueous medium the experiments were carried out in a two-phase system, under vigorous stirring. In this case the oxidation of toluene by Ce(IV) occurs at the boundary between the two phases and homogeneously in the aqueous solution. The role of the second phase is to maintain a saturation of the aqueous solution by the toluene and also to extract the product.

As mentioned earlier in this paper the only product was benzaldehyde. The formation of benzyl alcohol and benzoic acid was not observed. The amount of formed benzaldehyde increased with the content of mixtures in toluene up to 0,023 mole toluene/50ml mixture. Further increase of the content in toluene had no significant influence upon benzaldehyde formation (Table 3.)

Table 3.

The influence of initial amount of toluene upon mediated electrosynthesis of benzaldehyde [Ce(IV)/Ce(III)] = 10^{-2} mol/dm³; [H₂SO₄] = 1 mol/dm³; V_{mixture} = 50ml; i = 0,965 mA/cm²; t = 20⁰C

Toluene	mmole	8	12	23	47	71
Benzaldehyde	mmole	2,3	3,3	6,1	6,1	6,2
η	%	28,75	27,50	26,53	12,97	8,73

This behaviour is probably due to low saturation of the aqueous phase with toluene and to the slow chemical reaction between Ce(IV) and toluene.

To improve the solubility of toluene in the aqueous phase n-propanol was added to the reaction mixture. An increase in the material yield of benzaldehyde was observed till the content of n-propanol reached 30% (Table 4.).

To increase the solubility of toluene we tested also nonionic surfactant like polyoxiethylenelauryl ether, with the commercial designation Brij 35. The surfactant had positive influence upon the formation of benzaldehyde, but the results did not surpass that one obtained in the presence of n-propanol (Table 4.).

Better results were achieved at higher rates of the chemical reaction between Ce(IV) and toluene, obtained by increasing temperature. Best yields for the formation of benzaldehyde were observed at 60⁰C in a mixture containing 0,023 moles of toluene in the presence of surfactant (Table 4.).

Table 4.

Influence of additions (n-propanol and surfactant) and temperature upon mediated electrosynthesis of benzaldehyde; [Ce(IV)/Ce(III)] = 10^{-2} mol/dm³; [H₂SO₄] = 1 mol/dm³; V_{mixture} = 50 ml, i = 0,965 mA/cm², t = 20⁰C; 0,023 moles of toluene; reaction time 10 h.

n-propanol	%	10	20	30	40
Benzaldehyde	mmole	6,4	6,7	7,1	7
10 ³ surfactant	mol/dm ³	0,5	0,7	1	2
Benzaldehyde	mmole	6,8	6,9	7	6,9
Temperature	K	293	313	323	333
Benzaldehyde	mmole	6,1	6,8	7,5	8,4

CONCLUSIONS

- (i) The Ce(IV)/Ce(III) redox couple exhibits a quasi-reversible behaviour at a graphite electrode in H₂SO₄ medium.
- (ii) The smaller values of the diffusion coefficients of Ce(IV) and Ce(III), compared to other acidic media, are due to the voluminous ceric and cerous sulphatocomplexes present in H₂SO₄ solutions.
- (iii) The electrode kinetics of the Ce(IV)/Ce(III) couple is rapid in aqueous sulphuric acid medium. The reaction order less than unity found with respect to Ce(III) is probably caused by the adsorption of voluminous, inactive cerous sulphate complexes or solvent molecules at the electrode.
- (iv) Ceric sulphate was successfully regenerated electrochemically working under optimum conditions we found: [Ce(IV)/Ce(III)] = 1, [H₂SO₄] = 1 mol/dm³, i = 1,2 mA/cm²
- (v) The mediated electrooxidation of toluene with the Ce(IV)/Ce(III) mediator yields no other products but benzaldehyde. Because of the slow chemical reaction between mediator and toluene, even best yields in benzaldehyde are not encouraging, although they are better than those mentioned for direct anodic oxidation of toluene in organic solvents¹.

SYMBOLS

ε	potential
ω	angular velocity
A	electrode area
I_v	peak current
I_L	limiting current
z	number of exchanged electrons
F	Faraday constant
k	rate constant of electron transfer
ν	kinematic viscosity
C	concentration
μ	reaction order
η	material yield

REFERENCES

1. Wendt H., Bitterlich S., Lodowicks E., Liu Z.: *Electrochimica Acta*, **1992**, 37(11), 1959.
2. Kryuchkova E. I., Solomin A. V., Usanovich M. I.: *Elektrokhimiya*, **1972**, 8(1), 116.

MEDIATED ANODIC OXIDATION OF TOLUENE

3. Usanovich M., Solomin A. V., Kryuchkova E. I.: *Elektrokhimiya*, **1970**, 6(6), 894.
4. Nishiguchi I., Hiroshuna T.: *J.Org.Chem.*, **1985**, 50(4), 539.
5. Pysh E. S., Yang B. E.: *J.Amer.Chem.Soc.*, **1963**, 85(14), 2124.
6. Usanovich M., Solomin A. V., Kryuchkova E. I.: *Elektrokhimiya*, **1971**, 7(6), 915.
7. Parker V. P., Burgert B. E.: *Tetrahedron Lett.*, **1968**, 20, 2411.
8. Ross S. D., Finkelstein M., Petersen R. C.: *J.Org.Chem* **1970**, 35(3), 781.
9. Ramaswamy R., Venkatachalapathy M. S., Udupa H. V. K.: *Bull.Chem.Soc.Jpn* **1962**, 35, 214.
10. Kramer K., Robertson P. M., Ibl N.: *J.Appl.Electrochem.* **1986**, 10, 29.
11. Abdelhedi R., Bougerra M. L.: *Electrochimica Acta* **1990**, 35(1), 273.
12. Wendt H., Blitterlich S., Krüger K.: *Dechema-Monographien* **1992**, 125, 613.
13. Pletcher D., Valdes E. M.: *Electrochimica Acta*, 1988, 33(4), 509.
14. Been J., Oloman C. W.: *J.Appl.Electrochem.*, **1993**, 23, 1301.
15. Bishop E., Cofré P.: *Analyst(London)* **1981**, 106, 316.
16. Pletcher D., Valdes E. M.: *Electrochimica Acta* **1988**, 33(4), 499.
17. Randle T. H., Kuhn A. T.: *Aust.J.Chem.* **1989**, 42, 229.
18. Randle T. H., Kuhn A. T.: *Aust.J.Chem.* **1989**, 42, 1527.
19. Heinz Becker, Werner Berger & al: *Organicum*, 15th ed., p. 425. VEB Deutscher Verlag der Wissenschaften, Berlin 1978.
20. Hardwick T. J., Robertson E.: *Can. J. Chem.* **1951**, 29, 828.
21. Bondareva T. N., Brkovskii V. F., Velikanova T. V.: *Zh. Neorgan. Khim.* **1965**, 10(1), 127.
22. Blatz L. A.: *J. Phys. Chem.* **1962**, 66, 160.
23. Newton T. W., Archand G. M.: *J. Am. Chem. Soc.* **1953**, 75, 2449.
24. Pekar F., Beran P.: *J. Electroanal. Chem.* **1976**, 69, 1.
25. Müller L.: *Z. Phys. Chem.* **1969**, 214, 185.

ANALYTICAL APPLICATIONS OF ION MOBILITY SPECTROMETRY

VICTOR BOCOȘ-BINȚIȚAN^{1*}, EMIL CORDOȘ^{1,2},
MUȘATA BOCOȘ-BINȚIȚAN²

¹ - *Research Institute for Analytical Instrumentation Cluj-Napoca*

² - *"Babeș-Bolyai" University of Cluj-Napoca*

ABSTRACT. Ion Mobility Spectrometry is, first at all, a vapors' identification technique by measuring their ionic mobilities in the gaseous phase and at atmospheric pressure, under the influence of a weak electric field. The applications of Ion Mobility Spectrometry (IMS) could be separated into the use of IMS instrument as stand-alone spectrometer and its use in hyphenated technologies (as a detector following chromatographic techniques or as a separator before a mass spectrometer). By using the IMS technology a wide range of chemical compounds (both organic and inorganic) at trace detection levels can be detected, but the most spectacular applications of the Ion Mobility Spectrometry are the military/security ones (chemical warfare agents, explosives and illicit drugs). However, there is an increasing trend towards the civilian applications, like the industrial process monitoring and the detection of the pollutants. This paper's goal is to summarize the applications of Ion Mobility Spectrometry, which is definitely one of the most powerful trace detection techniques available today.

1. Introduction

In Ion Mobility Spectrometry (IMS), a powerful and promising trace detection technique that appeared in 1970 [1,2], the two main steps that occur are ionization of a gas (or vapors), followed by separation of ionic species resulted in a drift tube, under the driving influence of an electric field with low intensity (under 300 V/cm), at or near atmospheric pressure [3,4,5].

It can be emphasized that because of the versatility of Ion Mobility Spectrometry, detectors based on its principle promise to satisfy a wide range of practical applications, from explosives, chemical warfare agents and drugs detection to monitoring air pollutants [3,4]. Many IMS applications are not laboratory applications but field applications, who have totally different specifications. For instance, IMS has become attractive as a field technique due to its physical and mechanical simplicity of instrumentation and also to its low cost electronics, comparing with other bulk and complex systems (such as vacuum pumps used in mass spectrometers).

Using an ion mobility spectrometer one can made some separations very easily, but the other are impossible; for example, some anesthetic gases were

* Corresponding author

separated (even the isomers), but hexane can't be separated from carbon dioxide (because none of them is "seen" in IMS).

It is worthy to say that Ion Mobility Spectrometry is practically the backbone of defense systems against chemical warfare agents in all NATO armies, that it helps real-time detection of explosives and illicit drugs and that, last but not least, it contributes to industrial hygiene standards observance and to environment protection [3,4].

Usually the IMS spectrometer can be used as a chemical analyzer only if the target analyte has very different ionization characteristics as compared with the other sample components, because of the competitive charge exchange in the ionization region of the ion mobility spectrometer cell. Currently the IMS technology has not predictive or interpretative properties when mixtures which contain compounds with similar ionization parameters have to be analyzed [4,6].

The advantages of Ion Mobility Spectrometry are:

- ☺ analytical flexibility, because it can be applied to analyze both organic and inorganic vapors, and also can be monitored both positive and negative ions.
- ☺ very fast response (the drift times are in the millisecond range, up to several dozens ms); so, a complete analysis cycle will take only several seconds, and consequently we can speak here about real-time response
- ☺ very good sensitivity, in the parts-per-billion (ppb) and even parts-per-trillion (ppt) range without any preconcentration
- ☺ good selectivity; it can be improved by using dopants and/or different ionization sources
- ☺ the analysis is done at (or near) atmospheric pressure, and not in vacuum like in mass spectrometry
- ☺ the instrumentation is very robust and can be easily miniaturized [3].

Of course, IMS has a number of major disadvantages:

- ☹ the theoretical concepts concerning ion mobility spectrometry were not yet perfectly defined
- ☹ there are not comprehensive models for the response characteristics
- ☹ the dynamic range is quite limited, which in turn don't encourage the quantitation.

2. Coupling IMS with other analytical techniques

Hyphenated analytical techniques are now more and more used because of their great advantages. In the most common case, the first step is a separation one, and the second gives spectral information about separated substances [4].

The molecular ions generated in the IMS instrument can be injected directly into a quadrupole mass spectrometer. It is very important to say at this point that in almost all the cases the identification of the ions generated in the IMS spectrometer is performed by using mass spectrometry [3,4]. So, the IMS/MS tandem is a very powerful analytical tool, widely used to analyze/ identify the ions that are formed by atmospheric pressure chemical ionization [4,7]. Since the analytical applications of IMS will certainly reflect also the effects due to contaminants/matrix of the sample, only the use of the IMS/MS tandem can prove with a high degree of confidence if a given IMS response is generated by the target analyte [7].

The ion mobility spectrometer can be used also as an interface between a gas chromatograph and a mass spectrometer, and so it is obtained a complex analytical chain: GC/IMS/MS. In this particular situation, the sample analyzed by IMS is just a specific GC peak, and using mass spectrometry the identification of ions is made.

It is interesting to note that the first use of an ion mobility spectrometer was in a GC/IMS chain, when some disadvantages due to chemical ionization were reduced [8,9]. In such a chain, the chromatographic column serves as sample introduction system for IMS spectrometer, and this will avoid the competitive charge exchange between 2 or many chemical compounds (of course, only if we don't have some GC peak co-elution) and also will avoid sample overloading.

The possibilities for using ion mobility spectrometer as a chromatographic detector are:

- ☺ the tandem IMS spectrometer - gas chromatograph (GC/IMS) [10,11]
- ☺ the tandem IMS spectrometer - liquid chromatograph (LC/IMS) [12,13]
- ☺ the tandem IMS spectrometer - supercritical fluid chromatograph (SFC/IMS) [14].

3. Detection of vapors using IMS

3.1. Basic concepts

Since its appearance in 1970, IMS spectrometer was quickly seen as an useful sensor for trace vapor analysis and it is not at all surprising that the military used this new technology to detect chemical warfare agents [4]. However, IMS instruments were evaluated as environmental sensors or used in the industrial processes control only since 1980 [15].

It is important to emphasize here that by neglecting the IMS spectrometers used by armed forces to detect and monitor chemical warfare compounds, the number of IMS units used as field monitoring instruments is still low. The good news is that the situation tends to a change, due to several reasons:

- ☺ IMS instrumentation is better and cheaper
- ☺ the need to protect the environment is continuously increasing
- ☺ threshold values in the regulations are lower, and consequently the old analytical techniques can't help the user [3,4].

As any other analytical technique, the usefulness of IMS for a particular application is to be judged on an individual basis; the factors that must be considered include detection limits, response time, matrix interferences, the cost and the portability.

3.2. Applicability fields of IMS technology

Ion mobility spectrometer can be set to detect a great diversity of chemicals, both organic and inorganic. This device has been considered for a long time as an ideal detector for organic vapors monitoring, but it can also be used to detect many inorganic gases. In the bibliographic reference [3] can be found an exhaustive list (with about 170 bibliographic references) of practical applications of Ion Mobility Spectrometry.

There are many applications, but with a minimum systematization these can be classified as follows:

- ⇒ alkanes, alkenes (at extremely low water vapor levels) [16]
- ⇒ organophosphoric compounds: insecticides (of type Malathion, Parathion, Dichlorvos) [17] and chemical warfare agents (nerve gases like Tabun, Sarin, Soman, VX and others) [18]
- ⇒ organic compounds with nitro functional group: explosives (nitroglycerin, TNT, EGDN, ammonium nitrate, RDX, PETN, etc.) [19,20]
- ⇒ isocyanates: MDI, TDI [21]
- ⇒ metalcarbonyls: nickel tetracarbonyl [22]
- ⇒ inorganic compounds: halogens (Cl_2 , Br_2 , I_2) [23]; acid gases (HCN, HCl, HF, HI, HNO_3) [24], ammonia [25], phosgene [7,26], $\text{NO}_2/\text{N}_2\text{O}_4$, ClO_2 [27]
- ⇒ organic amines, aliphatic and aromatic: aniline [28], diethylamine, triethylamine [29]
- ⇒ aromatics: benzene, toluene, xylenes, ethylbenzene [30], PAHs (polycyclic aromatic hydrocarbons) [31]
- ⇒ solvents: furan, cyclohexanone, phenols, alcohols $>\text{C}_3$, acrylonitrile, DMF, DMSO [32,33]
- ⇒ chlorinated solvents: dichloromethane, Me bromide, Me chloride, CHCl_3 , CCl_4 , $\text{C}_2\text{H}_4\text{Cl}_2$, CH_3I [34]
- ⇒ freons and CFCs (chlorofluorinated hydrocarbons) [35]
- ⇒ anesthetics (Halothane, Enflurane, Isoflurane, Desflurane, Methoxy-flurane) [36]
- ⇒ chlorinated alkenes: vinyl chloride, allyl chloride, tetrachloroethylene [37]
- ⇒ aldehydes and ketones [33,38]
- ⇒ organic acids & their esters [39]
- ⇒ chlorinated pesticides [40]
- ⇒ propellants/rocket fuels: hydrazine, monomethylhydrazine, dimethylhydrazine, N_2O_4 [41]
- ⇒ drugs: analgesics; illicit drugs (cocaine, heroine, amphetamines, ephedrine, THC from cannabis) [42,43]
- ⇒ water and soil monitoring: PAHs and VOCs in water [44]; amines and chlorinated solvents in waste water; pesticides in soils
- ⇒ applications in semiconductor industry: arsine, diborane, NF_3 , PCl_3 ; contamination of Si wafers and their QC; N-methylpyrrolidone [45]
- ⇒ chlorinated phenols (used as wood preservatives) [46]
- ⇒ perfumes, flavors and aromatic oils [47]
- ⇒ some "exotic" applications: wood species characterization [48]; exobiology studies [49]; pheromone detection; monitoring the degree of freshness of fish or other organic matters (by monitoring aliphatic amines); micro-organisms detection, in particular detection of biological warfare agents (using pyrolysis or enzymatic techniques) [50,51]; nicotine detection in cigarette factories [52].

3.3. Industrial and environmental applications

These categories of applications use two classes of IMS spectrometers:

1. Fixed-point monitors, used to detect, monitor and measure the concentration of an analyte (or a chemical class of compounds). The

ANALYTICAL APPLICATIONS OF ION MOBILITY SPECTROMETRY

measurements are performed continuously, and the instrument keep the same location; this way will result a concentration vs. time profile.

- Hand-held portable instruments, which are used especially to detect gas/vapor leaks. These instruments will generate concentration vs. location profiles.

A very suggestive example for industrial hygiene applications is the list from the company *ETG (Environmental Technology Group) Inc.* [3] and presented here in Table 1.

Table 1.

Application groups of the IMS in industrial hygiene and air monitoring

<i>Compound</i>	<i>M.D.L. [ppm]</i>	<i>Compound</i>	<i>M.D.L. [ppm]</i>
ACID AND STACK GASES/VAPORS:			
HCN	0.1	Phosgene COCl ₂	0.1
HCl	0.1	HNO ₃	0.1
HF	0.1	NH ₃	0.1
HI	0.1	NO ₂	0.1
HALOGENS:			
Chlorine Cl ₂	0.1	Iodine I ₂	0.005
Bromine Br ₂	0.1		
ORGANIC AMINES:			
Aliphatic amines	0.005	Aniline	0.005
Aromatic amines	0.005	Methylenedianiline	0.010
ISOCYANATES:			
TDI	0.005	NDI	0.005
1,6-Diisocyatohexane	0.1	H12MDI	0.1
TDA	0.005	TXMDI	0.1
SOLVENTS:			
Alcohols	0.1	Phenols	0.1
Furans	0.1	Ketones	0.01
Ethers	0.1	Esters	0.01
Acetonitrile	0.01	Acrylonitrile	0.01
Cyclohexanone	0.01	Toluidine	0.1
Chlorinated solvents	1.0		
GASES IN THE SEMICONDUCTOR INDUSTRY:			
NF ₃	0.1	PCl ₃	0.1
OTHER CHEMICALS:			
Aldehydes	0.1	Vinyl acetate	0.1

Nitrobenzene	0.005	PCBs	0.1
H ₂ S	1.0	Mercaptans	0.1

where M.D.L. is the Minimum Detectable Limit.

Major applications (industrial and environmental) deal with many toxic compounds and industrial emissions that are dangerous to people or environment [15].

3.4. Drugs, explosives and chemical warfare agents detection

Currently there is a considerable current of interest for the detection of illicit drugs, explosives and chemical warfare agents. In fact, IMS systems were and still are intensively used as screening devices for persons and baggages/goods.

Concerning the IMS detection of illicit drugs (and explosives), a serious problem is the "collection" of enough molecules to obtain a response, because most drugs and explosives have very low vapor pressures. As a matter of fact, the key word is here the preconcentration sampling [53-55].

A typical military application is field detection of the chemical warfare agents. IMS spectrometers are extremely sensitive in the positive operation mode to organophosphoric compounds (nerve agents); in the negative mode, IMS instruments detect easily blister agents (like mustard gas) [56,57].

4. Laboratory applications of IMS

4.1. Ionic mobility measurement

The reduced mobility K_0 of an ion represents a qualitative parameter useful for its identification, quite like is the retention time in gas chromatography.

It is interesting to note that the use of some "reference ions" (from compounds called *calibrants*) with well known mobilities would lead to obtain sets of "universal" reduced mobilities. Until now, such a standard compound fully accepted does not exist yet, but 2,4-lutidine (proposed by Karpas, having $K_0 = 1,95 \text{ cm}^2/\text{Vs}$ [58]), DMF (dimethylformamide) and nonanone in the positive mode of operation, and bromide ions, phenol, trinitrotoluene and methylsalicylate [7] in the negative mode of operation appear to be serious candidates.

The methodology used to measure the reduced mobilities is quite simple: instrumental and operational parameters are set, the sample is introduced and finally drift times are measured. Of course, mass spectrometric identification of IMS product ions is the unique procedure that can certify the assignment of a product ion peak [29,59].

4.2. Studies of ions' structure

Isomers separation and identification using IMS was observed very soon (in 1974), in a study concerning mono- and di-halogenated nitrobenzenes [60].

Some typical examples for isomers detection are:

1. the isomers of aliphatic amines [58]
2. anilines [61]
3. diamines and aminoalcohols [62]
4. geometric isomers E/Z [63].

Collision section measurements. Using IMS studies on isomers or on homologous series of compounds one can obtain structural information, and specifically one can calculate the transversal collision integral Ω_D of the ion-molecule pair [64].

Large atomic clusters and biomolecule studies. As well as reduced mobilities information, drift tube studies can also supply valuable information about the kinetics of ion-molecule reactions and about the equilibria involved in these processes [65,66].

5. Future trends in IMS

In the last two decades Ion Mobility Spectrometry has developed in an explosive manner, so that it is now a powerful and quite less expensive tool for the detection and quantitation of a very large number of chemical compounds at trace levels, directly or after a chromatographic pre-separation. Currently IMS is extensively used to monitor directly several chemical categories, such as chemical warfare agents, explosives and illicit drugs [3,4].

Latest significant trends in Ion Mobility Spectrometry regarding its applications are:

- use of selective techniques for sampling and dynamic range broadening
- use and implementation of new signal processing techniques for IMS signal, such as Fourier transform and neural networks
- the emerging of biological applications
- manufacturing of portable GC/IMS and IMS/MS instrumentation
- use on a larger scale of the non-radioactive ionization sources.

An increasing interest is currently directed towards atmospheric pollutants monitoring, but also towards analyzing directly, with little if any sample preparation, liquid and even solid samples.

Although IMS could be seen today as a mature technology, it still remains in many fields and application niches a brand new technique. Its low detection limits, speed and simplicity of the instrumentation reserve to IMS a strategic place in analytical chemistry between the universal non-specific detectors (like ECD and FID detectors) and more powerful qualitative techniques (like mass spectrometry).

BIBLIOGRAPHY

- [1] Karasek, F.W., Res. Dev. 1970, 21(3), 34.
- [2] Cohen, M.J.; Karasek, F.W., J. Chromatogr. Sci. 1970, 8(6), 330.
- [3] Bocoş-Binţinţan, V., "Spectrometria de mobilitate ionică", Editura Presa Universitară Clujeană, Cluj-Napoca, 1998.
- [4] Eiceman, G.A.; Karpas, Z., "Ion Mobility Spectrometry", CRC Press, Boca Raton, FL, 1994.
- [5] Carr, T.W. (Ed.), "Plasma Chromatography", Plenum Press, New York, 1984.
- [6] Siegel, M.W., "Atmospheric pressure ionization", in "Plasma Chromatography", Plenum Press, New York, 1984, 95.
- [7] Bocoş-Binţinţan, V., "Studies on phosgene and chlorine by ion mobility spectrometry and mass spectrometry", PhD Thesis, "Babeş-Bolyai" University, 2000.

- [8] Rokushika, S.; Hatano, H.; Hill, H.H., Jr., *Anal. Chem.* 1987, 59, 8.
- [9] Campbell, D.N.; Vora, K.N.; Davis, R.C., U.S. Patent 4.597.299: "Ion gate sample gas inlet control for gas chromatograph analyzer", July 1, 1986.
- [10] Shumate, C.; Hill, H.H., Jr., *Anal. Chem.* 1989, 61, 601.
- [11] StLouis, R.H.; Siems, W.F.; Hill, H.H., Jr., *J. Chromatogr.* 1989, 479, 221.
- [12] McMinn, D.G.; Kinzer, J.; Shumate, C.B.; Siems, W.F.; Hill, H.H., Jr., *J. Microcolumn Sep.* 1990, 2, 188.
- [13] Geniec, J.; Mack, L.L.; Nakamae, K.; Gupta, C.; Kumar, V.; Dole, M., *Biomed. Mass Spectrom.* 1984, 11, 259.
- [14] Tarver, E.; Hill, H.H., Jr., "ECD-like response after supercritical fluid chromatography", West ACS Conf., Los Angeles, 1988.
- [15] Roehl, J., *Appl. Spectrosc. Rev.* 1991, 26, 1.
- [16] Bell, S.E.; Ewing, R.G.; Eiceman, G.A.; Karpas, Z., *J. Am. Soc. Mass Spectrom.* 1994, 5(3), 177.
- [17] Eiceman, G.A.; Wang, Y.F.; Garcia-Gonzales, L.; Harden, C.S.; Shoff, D.B., *Anal. Chim. Acta* 1995, 306(1), 21.
- [18] Adler, J.; Doering, H.-R., *Zfl.-Mitt.* 1990, 154, 75.
- [19] Christophorou, L.G.; McCorkle, D.L.; Sauers, I., *Anal. Chim. Acta* 1982, 135(2), 179.
- [20] Cohen, M.J.; Wernlund, R.F.; Stimac, R.M., *J. Inst. Nucl. Mater. Manage.* 1984, 13, 220.
- [21] Brokenshire, J.L.; Dharmarajan, V.; Coyne, L.B.; Keller, J., *J. Cell. Plast.* 1990, 29, 123.
- [22] Wernlund, R.F.; Cohen, M.J., *Res. Dev.* 1975, 26(7), 32.
- [23] Karpas, Z.; Pollevooy, Y.; Melloul, S., *Anal. Chim. Acta* 1991, 249(2), 503.
- [24] Bacon, A.T.; Reategui, J.A., U.S. Patent 5.095.206: "Method and apparatus for improving the specificity of an ion mobility spectrometer utilizing sulfur dioxide dopant chemistry", Mar. 10, 1992.
- [25] Przybylko, A.R.M.; Thomas, C.L.P.; Anstice, P.J.; Fielden, P.R.; Brokenshire, J.L.; Irons, F., *Anal. Chim. Acta* 1995, 311(1), 77.
- [26] Adler, J.; Doering, H.-R., *Zfl.-Mitt.* 1990, 154, 97.
- [27] Bacon, A.T.; Getz, R.C., U.S. Patent 5.283.199: "Chlorine dioxide monitor based on ion mobility spectrometry with selective dopant chemistry", Feb. 1, 1994.
- [28] Karasek, F.W.; Kim, S.H.; Rokushika, S., *Anal. Chem.* 1978, 50(14), 2013.
- [29] Karpas, Z., *Anal. Chem.* 1989, 61(7), 684.
- [30] Lubman, D.M., *Anal. Chem.* 1984, 56(8), 1298.
- [31] Eiceman, G.A.; Anderson, G.K.; Danen, W.C.; Ferris, M.J.; Tiee, J.J., *Anal. Lett.* 1988, 21(4), 539.
- [32] Karasek, F.W.; Cohen, M.J.; Carroll, D.I., *J. Chromatogr. Sci.* 1971, 9(7), 390.
- [33] Karasek, F.W.; Kilpatrick, W.D.; Cohen, M.J., *Anal. Chem.* 1971, 43, 1441.
- [34] Baim, M.A.; Hill, H.H., Jr., *J. High Resolut. Chromatogr. Chromatogr. Commun.* 1983, 6(1), 4.
- [35] Cram, S.P.; Chesler, S.N., *J. Chromatogr. Sci.* 1973, 11(8), 391.
- [36] Sacristan, E., U.S. Patent 5.455.417: "Ion mobility method and device for gas analysis", Oct. 3, 1995.
- [37] Simpson, G.; Klasmeier, M.; Hill, H.H., Jr.; Atkinson, D.; Radolovich, G.; Lopez-Avila, V.; Jones, T.L., *J. High Resolut. Chromatogr.* 1996, 19(6), 301.
- [38] Benezra, S.A., *J. Chromatogr. Sci.* 1976, 14(3), 122.
- [39] Kim, S.H.; Karasek, F.W., *J. Chromatogr. Sci.* 1982, 234(1), 13.
- [40] Louis, R.S.H.; Hill, H.H., Jr., *J. High Resolut. Chromatogr.* 1990, 13(9), 628.
- [41] Eiceman, G.A.; Salazar, M.R.; Rodriguez, M.R.; Limero, T.; Beck, S.W.; Cross, J.H.; Young, R.; James, J.T., *Anal. Chem.* 1993, 65(13), 1696.

ANALYTICAL APPLICATIONS OF ION MOBILITY SPECTROMETRY

- [42] Lawrence, A.H.; Elias, L., *Bull. Narc.* 1985, 37(1), 3.
- [43] Lawrence, A.H., *Anal. Chem.* 1986, 58(6), 1269.
- [44] Vandiver, V.J.; Leasure, C.S.; Eiceman, G.A., *Int. J. Mass Spectrom. Ion Processes* 1985, 66(2), 223.
- [45] Budde, K.J.; Holzapfel, W.J., *Proc.-Electrochem. Soc.* 1992, 92-7, 271.
- [46] Jones, D.; Brenton, A.G.; Games, D.E.; Brittain, A.H.; Taylor, S.; Kennedy, D.; Smith, P., *Rapid Commun. Mass Spectrom.* 1993, 7(6), 561.
- [47] Karasek, F.W.; Keller, R.A., *J. Chromatogr. Sci.* 1972, 10(10), 626.
- [48] Lawrence, A.H., *J. Pulp. Pap. Sci.* 1989, 15(5), J196.
- [49] Kojiro, D.R.; Cohen, M.J.; Stimac, R.M.; Wernlund, R.F.; Humphry, D.E.; Takeuchi, N., *Anal. Chem.* 1991, 63(20), 2295.
- [50] Smith, G.B.; Eiceman, G.A.; Walsh, M.K.; Critz, S.A.; Andazola, E.; Ortega, E.; Cadena, F., *Field Anal. Chem. Technol.* 1997, 1(4), 213.
- [51] Dworzanski, J.P.; McClennen, W.H.; Cole, P.A.; Thornton, S.N.; Meuzelaar, H.L.C.; Arnold, N.S.; Snyder, A.P., *Field Anal. Chem. Technol.* 1997, 1(5), 295.
- [52] Eiceman, G.A.; Sowa, S.; Lin, S.; Bell, S.E., *J. Hazard. Mater.* 1995, 43(1-2), 13.
- [53] Garofolo, F.; Marziali, F.; Migliozi, V.; Stama, A., *Rapid Commun. Mass Spectrom.* 1996, 10(11), 1321.
- [54] Rodacy, P., SANDIA Natl. Lab. Report 1993, SAND-92-0229.
- [55] Karasek, F.W.; Kim, S.H., *Anal. Chem.* 1975, 47(7), 1166.
- [56] Doering, H.-R.; Hartmann, E., U.S. Patent 5,510,268: "Method and device for detecting substances in an ambient substance, in particular for detecting chemical warfare agents", Apr. 23, 1996.
- [57] Allinson, G.; McLeod, C.W., *J. Forensic Sci.* 1997, 42(2), 312.
- [58] Karpas, Z.; Stimac, R.M.; Rappoport, Z., *Int. J. Mass Spectrom. Ion Processes* 1988, 83, 163.
- [59] Karpas, Z.; Cohen, M.J.; Stimac, R.M.; Wernlund, R.F., *Int. J. Mass Spectrom. Ion Processes* 1986, 74, 153.
- [60] Karasek, F.W.; Kane, D.M., *Anal. Chem.* 1974, 46(6), 780.
- [61] Karpas, Z.; Berant, Z.; Stimac, R.M., *Struct. Chem.* 1990, 1, 201.
- [62] Karpas, Z., *Struct. Chem.* 1992, 3, 139.
- [63] Carr, T.W., *J. Chromatogr. Sci.* 1977, 15(2), 85.
- [64] Karpas, Z.; Berant, Z., *J. Phys. Chem.* 1989, 893, 3021.
- [65] Clemmer, D.E.; Jarrold, M.F., *J. Mass Spectrom.* 1997, 32(6), 577.
- [66] Giles, K.; Grimsrud, E.P., *J. Phys. Chem.* 1992, 96(16), 6680.

ION MOBILITY SPECTROMETRY - THEORY AND INSTRUMENTATION

VICTOR BOCOȘ-BINȚINȚAN¹

¹ - Research Institute for Analytical Instrumentation Cluj-Napoca

ABSTRACT. The main aspects concerning a new, powerful and very promising trace analysis technique - Ion Mobility Spectrometry (IMS) - are reviewed. Ion Mobility Spectrometry is based upon the separation of ions, which occurs because of their mobility differences in a relatively low intensity electrical field. Ions are obtained by the ionization of the neutral chemical species in the gaseous phase, at atmospheric pressure, by very fast and complex collisional charge exchanges and ion-molecule reactions. Included are sections which deal with the IMS principle, its theoretical basis, atmospheric pressure ionization processes, response characteristics and the corresponding instrumentation. Ion Mobility Spectrometry is definitely a technology with a very promising future, in spite of the current lack of information.

1. Introduction

Ion Mobility Spectrometry (*IMS*) is a modern analytical technique used especially to detect ultra-traces of chemical compounds in the air and so far less known worldwide. This technology emerged in 1970 [1,2] and rapidly developed, especially in the last decade. IMS succeeded very soon to pass from the laboratory toward field applications (in industry processes control and environmental pollution control, for instance).

The resurrection of IMS -after a period of slight stagnation in the 1980s- is due mainly to the real-time response, to its amazing detection limits and also to several practical considerations concerning the instrumentation (great simplicity compared with the complex instruments used in mass spectrometry, reliability, ruggedness and miniaturization). We have also to underline here another serious advantage of IMS: it is an analytical technique which fits perfectly to field applications and to process applications.

Ion Mobility Spectrometry is based upon the separation of ions (obtained by the ionization of the neutral chemical species in the gaseous phase, at atmospheric pressure, by collisional charge exchanges and ion-molecule reactions),

which occurs because of their mobility differences in a relatively low intensity electrical field.

It can be stated today that Ion Mobility Spectrometry is practically the backbone of defense systems against chemical warfare agents in many NATO countries, that it helps real-time detection of explosives and illicit drugs and that, last but not least, it contributes to industrial hygiene standards observance and to environment protection.

The development of this technique after its discovery in 1970 was not at all simple or straightforward. The initial enthusiasm due to the extremely low detection limits (at part-per-billion levels), versatility and very fast response fell down when disadvantages were also made evident: low selectivity, relatively low resolution and severe memory effects. However, the biggest part of all these drawbacks were surpassed by major improvements in the instrumentation design, but also by application of knowledge due to the better understanding of the ionic mobility theory and of the processes involved in atmospheric pressure chemical ionization.

This paper aims to demonstrate the advantages of Ion Mobility Spectrometry. It is quite sure so far that IMS will be soon an usual and widely accepted analytical technique, especially in several particular niches. In fact, it is obvious that the latest trends in IMS field (including the commercial market) predict a very interesting evolution, of course if the IMS experts and users will focus upon solving the problems remained unclear.

2. Theoretical basis of IMS

2.1. Principle of IMS

When an ion (at atmospheric pressure and in gaseous phase) is placed in a constant electric field, it will be accelerated until collides a neutral molecule, then it is re-accelerated and suffers another collision, and so forth. This chaotic sequence of accelerations/collisions at molecular level is translated, at the macroscopic level, in a constant speed of the ion. The ratio between the ion speed and the electric field intensity is called "*ionic mobility*", and the analytical technique that uses ions' separation upon different mobilities was consequently named ***ion mobility spectrometry*** [3,4].

Ion mobility spectrometry is actually ruled by two distinct processes:

- a) the ionization in the gaseous phase, at atmospheric pressure, by collisional charge transfer and ion-molecule reactions;
- b) the separation of the resulted ions due to their different mobilities in a neutral gas (usually purified air or nitrogen are used), in a relatively small electric field (up to 300 V/cm).

In the last two decades Ion Mobility Spectrometry developed practically in an explosive manner, so that IMS is now a powerful and quite less expensive tool for the detection and even quantitation of a very large number of chemical compounds at trace levels (directly or after a chromatographic pre-separation). It is worthy to mention that currently IMS is extensively used to monitor directly several chemical categories, such as chemical warfare agents, explosives and illicit drugs [3,4].

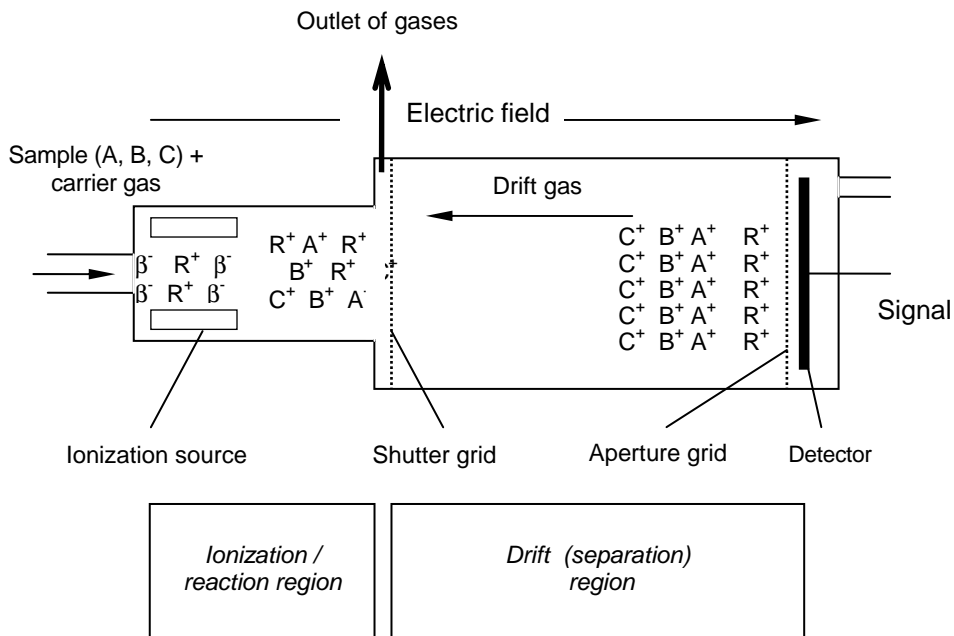


Fig. 1. Schematic of an ion mobility spectrometer

As a conclusion, Ion Mobility Spectrometry is, first at all, a vapors' identification technique by measuring their ionic mobilities in the gaseous phase.

In IMS, chemical separation and detection are accomplished by:

1. Ionization of a gas (or vapors).
2. Separation of ionic species resulted in a drift tube, under the driving influence of an electric field with low intensity, at (or near) atmospheric pressure.
3. Conversion of ionic clouds in ionic current at the detector (placed at the end of the drift tube), after traveling down the drift tube.
4. Signal processing, in order to extract the useful analytical information (qualitative and quantitative) [4,5].

A typical ion mobility spectrometer is illustrated schematically in Figure 1. After their separation inside the drift tube the ions strike the detector, resulting a so-called "ion mobility spectrum", named also "plasmagram" or pure and simple "signature" (Figure 2). In Figure 2, R^+ represent the RIP (reactant ions peak) and A^+ , B^+ and C^+ are product ions peaks (PIP).

The IMS information is contained in the IMS signal, which represents the variation of ionic current in time, averaged for a number of scans (Figure 2). The ion cloud formed in the reaction region varies continuously, together with the concentration of chemical compounds which enter the instrument. The ions with suitable polarity are sent, due to the electric field, to the drift tube. Meanwhile, the shutter grid (made by closely spaced, parallel metallic wires) is periodically pulsed

open so that the ions are allowed to pass into the drift region, where they suffer collisions with the neutral drift gas molecules and consequently their separation occurs. Finally, at the end of the drift tube the ion clouds will be converted into ion currents (with very low intensity, of the order of picoamperes pA) by a Faraday plate (the detector).

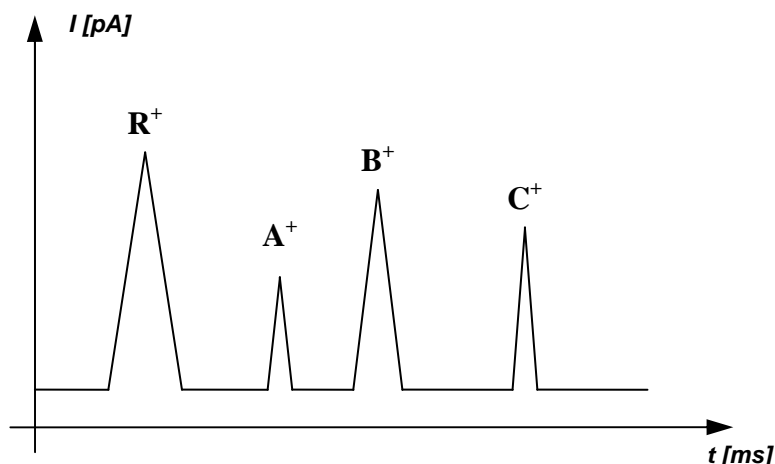


Fig. 2. A typical ion mobility spectrum (plasmagram; signature)

Ion Mobility Spectrometry has a number of similarities with several analytical techniques: electrophoresis, chromatography and mass spectrometry (time-of-flight MS and chemical ionization MS). The resemblance of Ion Mobility Spectrometry with MS-TOF is quite evident, because both analytical techniques rely on ions separation in a drift tube, and the resemblance with CI-MS could be seen in the ionization processes (which imply ion-molecule reactions with generation of the primary reactant ions, then formation of secondary product ions) [3]. It is now usual to say that in IMS the ions are subject of the time-of-flight measurements at atmospheric pressure.

Ion Mobility Spectrometry has several advantages:

- analytical flexibility, because it can be applied to analyze both organic and inorganic vapors, and also either positive or negative ions can be monitored
- very fast response (the drift times are in the millisecond range, up to several dozens ms); so, a complete analysis cycle will take only several seconds, and consequently we can speak here about real-time response
- very good sensitivity, in the parts-per-billion (ppb) and even parts-per-trillion (ppt) range without any preconcentration
- good selectivity; it can be improved by using dopants and/or different ionization sources

- the analysis is done at (or near) atmospheric pressure, and not in vacuum like in mass spectrometry
- the instrumentation is very robust and can be easily miniaturized.

Of course, IMS has a number of major drawbacks:

- the theoretical concepts concerning ion mobility spectrometry were not yet perfectly defined
- there are not comprehensive models for the response characteristics
- the dynamic range is quite limited, which in turn don't encourage the quantitation.

2.2. Theory of ionic mobility

In this section the theory of gaseous ions, with emphasis on most important characteristics for IMS [6,7,8] is shortly reviewed. The main applications of the IMS theory include: the effects of temperature variation, the effects of electric field intensity and drift gas pressure [6], the effect due to the drift gas change [9,10], the behavior of the multiple charged ions, mass-mobility correlations [11,12,13], the correlation with vapor diffusion coefficients, peak width and shape analysis [14,15], and IMS resolution [16].

The essential theoretical relations which govern in IMS are the following:

- *drift rate equation*: The average rate of an ion moving in a neutral drift gas is called *drift rate*, v_d , and is proportional to the electric field E , if E is not too large:

$$v_d = KxE = l_d/t_d \quad (2.1).$$

This proportionality constant K is exactly *ionic mobility*, l_d is the drift length, and t_d is the drift time of an ion.

- *reduced mobility equation*: The mobility $K=l_d/t_d$ could be normalized (reduced), to eliminate the effects of pressure and temperature:

$$K_0 = (273/T)(P/760)K \quad (2.2)$$

where K_0 is the reduced mobility, T is the absolute temperature of the drift gas, and P is the atmospheric pressure.

- *low field condition*: At that electric fields normally used in IMS at atmospheric pressure, the mobility K is independent on E . A semiquantitative criterion for low field operation (at room temperature) could be written as follows:

$$\frac{E}{N} \left\langle \left(\frac{m}{m+M} \right)^{1/2} \cdot \frac{d^2}{z} \right. \quad (2.3)$$

where m represents ion mass, M is the mass of neutral molecules (of the drift gas), d is the sum of ion and neutral molecule radii (in Angstroms), and z is the charge of the ion. The parameter E/N is measured in Townsends (Td): $1 \text{ Td} = 10^{-17} \text{ Vxcm}^2$. It is important to note here that in IMS the typical values for E/N ratio are 1...2 Td.

- *relationship between ionic mobility and diffusion coefficient*: This equation has many names: Einstein equation, Nernst-Einstein equation or Nernst-Townsend-Einstein equation:

$$K = qD/kT \quad (2.4)$$

where $q=ze$ is the electrical charge of an ion, and k is the Boltzmann constant. This equation is very useful in connecting the results obtained in IMS with those obtained about air diffusion of uncharged vapors. It also gives a connection between the measured transit times and shapes and widths of the detected ionic pulses, which means an additional information about the studied ion.

- *Mason-Schamp equation*: Because the collisions between particles are controlled by forces occurring between them, the mobility should clearly depend on the force between ion and neutral molecule. Because in fact the collisions between particles are controlled by their interaction forces, the mobility will depend finally on the force between ion and neutral molecule. This kind of dependence appears as an integral of diffusional collision, or the average collision section, Ω_D :

$$K = \frac{3}{16} \cdot \frac{q}{N} \cdot \left(\frac{1}{m} + \frac{1}{M} \right)^{1/2} \cdot \left(\frac{2\pi}{kT} \right)^{1/2} \cdot \frac{1}{\Omega_D} \quad (2.5)$$

Mason-Schamp equation

where q is the electric charge of the ion, N is the drift gas density, m is the mass of the ion, M is the mass of drift gas molecule, k is the constant of Boltzmann, and T is the temperature.

The whole dependence of ionic mobility on ion-molecule interaction is included in the collision integral Ω_D . Because of the fact that Ion Mobility Spectrometry wants to use the measured ionic mobility to characterize a specific ion, it is important to know in detail how Ω_D (and consequently the mobility) depends on ion-neutral molecule forces.

The detailed theoretical approaches show that mobility depends in a well-defined way on ion-neutral interactions. An ion mobility spectrum contains information about these ion-molecule interactions, and this information can help to interpret that spectrum. In addition, not only the measured mobilities can be used successfully to study the ion-molecule potentials, but also the independent cognition of these potentials could be used to check the mobility measured. The relationship between ion-molecule forces and mobility is very well represented by the temperature dependence of ionic mobility.

The mobility definition equation underlines as well an inverse relationship between K and N (drift gas density). So, an increase of N will lead to an increase of the collision number, to a lower drift rate and to a lower mobility. The variation of E (electric field) and of N (the drift gas density) produce similar effects, and the mobility depends in fact on the variable E/N .

Another useful parameter that can be easily modified in IMS is the neutral drift gas itself. In this way, making experiments with different drift gases may be a good test of the agreement between results and theory and also may offer some valuable additional information about ion-molecule interactions. Moreover, using another drift gas or a mixture of gases in the drift cell is a good opportunity to test if a studied ion changes its chemical identity by forming clusters or complex ions. To calculate how mobility changes with the drift gas, the masses and polarizabilities of neutral molecules are needed.

The values of the reduced mobility K_0 for different drift gases were already compared, and it was found that generally K_0 changed with the drift gas polarizability. For example, using drift gases with a large polarizability, the attractive forces between the product ions and the induced dipole moment will increase, we will have a greater number of collisions and finally a lower mobility.

Usually the ions produced in the IMS spectrometer are single charged, but it can be expected that larger, bulky ions (for example, those formed by large biomolecules) will have many electrical charges. The additional charge leads to an increase of the interaction energy between ion and neutral molecule, and also will increase the collision probability. However, the diffusion coefficient decreases with charge increase if K is a constant, according to the Einstein equation. So, the mobility could be greater or lower, but for large ions the effect will be very probable a slight increase of ionic mobility due to the multiple charge.

The equation (2.5) is very important, because it shows us that drift time t_d (which is proportional with K^{-1}) depends on mass and size of the ion:

$$K^{-1} \sim \mu^{1/2} \cdot \Omega_D \quad (2.6)$$

, where μ is the reduced mass ($1/\mu = 1/m + 1/M$), and the size is measured by Ω_D .

For a series of small ions in the same drift gas, Ω_D is almost a constant, and hence the mobility is controlled by reduced mass μ . For heavy ions, the reduced mass μ is practically equal with drift gas molecule mass, and the separation property is the ion size (reflected by Ω_D).

Of course, for those ions that are between the above two extreme categories (and that form the majority of ions), the mobility is function both of ion mass and size/conformation of that ion. For instance, the analysis of mass-mobility correlations [11] has indicated a dispersion of about $\pm 20\%$ for the compounds that were not structurally related, but only of $\pm 2\%$ in a homologous series of aromatics. We can clearly observe that mass measurement using IMS is indeed a very inaccurate process.

The Einstein equation (2.4) suggests the existence of the relationship between drift times and diffusion coefficients, so that the diffusion coefficients could be seen as equivalent mobilities.

Concerning the shape and width of the ionic pulse, it should be emphasized that the main characteristics of an ionic pulse reaching the detector are imposed by four factors:

1. initial width and initial shape of the pulse which enters drift region
2. pulse broadening by coulombian mutual repulsion between ions
3. diffusional broadening, as ionic pulse travels in the drift tube
4. ion-molecule reactions with drift gas and/or with impurities.

Resolution R measures the ability of an instrument to distinguish between two very closed peaks. In IMS, resolution is given by the equation:

$$R = t_d / (2 \cdot T_{1/2}) \quad (2.7)$$

where t_d represents drift time, and $T_{1/2}$ is the temporal broadening at 1/2 of peak height.

From an experimental point of view, the parameter $T_{1/2}$ and also peak shape are governed by many factors:

- 1) shape and width of the initial pulse
- 2) diffusional broadening
- 3) coulombian repulsion
- 4) capacitive coupling between ionic pulse and detector
- 5) gradients of the electric field
- 6) gradients of the temperature
- 7) emptying of the gate (shutter grid) and dynamic drains
- 8) pressure variations
- 9) ion-molecule reactions inside the drift tube.

Experimental data suggested several trends concerning IMS resolution, which can be easily explained only when the initial width of ionic pulse, t_0 , was introduced in the equation of resolution:

1. Resolution increases with drift time t_d .
2. Resolution depends on electric field E .
3. In most cases, a lower drift potential generates a better resolution.
4. There is a linear relationship between R and $T^{1/2}$.

At high initial width of ionic pulse, the peak's shape is gaussian, having $T_{1/2}$ proportional with $t_d^{1/2}$.

The values of H_{TT} (theoretical plate height) for IMS are several orders of magnitude lower than H_{TT} in gas chromatography. The mass resolution ($R=M/\Delta M$) is in IMS only about 10...50, comparing with values of 400...70000 in mass spectrometry. All these considerations let us to the conclusion that Ion Mobility Spectrometry has modest resolutions comparing with mass spectrometry, and also that its separation power is lower than in chromatography.

In conclusion, the mobility of ionic species is connected with collision processes which occur in the drift tube. In the theoretical analyses of IMS, the reaction region and the drift region are usually treated separately, being supposed that in the reaction tube separation of the ions don't occurs, and that in the drift tube we don't have any ion-molecule reactions.

The most important ideas concerning the theory of ionic mobility are:

- (1) The information contained in the ion mobility spectrum can be extracted by measuring the drift time and peaks' area.
- (2) The mobility K depends on environmental variables; K is inversely proportional with pressure in the IMS cell.
- (3) The reduced mobility K_0 depends also on average transversal collision section Ω_D , which has a very complex form.
- (4) Theoretical treatment of small ions and of macro-ions is quite different.
- (5) Changing the neutral drift gas has a great effect on ionic mobilities.

3. Ionization processes in IMS

The first step in a measurement involving IMS consists in ionization of neutral molecules present in the vapor sample. These ionization processes occur in gaseous phase, at atmospheric pressure, by a series of very fast ion-molecule reactions

between neutral molecules of analyte and the reactant ions. Therefore, it is easy to understand that ionization is a crucial event in IMS.

The ionization involves proton transfer (or electron transfer, for the negative mode of operation) reactions between reactant ions and neutral analytes, and the final ions that result by these processes are called "product ions".

Atmospheric pressure chemical ionization which occurs in IMS differs from other type of ionization processes by two essential characteristics:

1. A gentle energetic of product ions formation, which implies the absence of any fragmentation of the molecules ionized (even if there are few exceptions, such as the butylacetates for example).
2. The available charge is competitively and preferentially distributed between the different types of neutral molecules co-existing in the vapor sample, as a function of their proton affinities (for the positive ions) or electron affinities (for the negative species) [4].

In IMS the reactant ions' composition depends on composition of the gas in the reaction region and may be easily altered by temperature, humidity and dopants adding [17,18,19]. The complex nature of reactant species, as well as the very complex equilibria between them is not at all a disadvantage for IMS analyses, if the gas that enters the reaction region (usual air) has a constant composition and is purified [20-23].

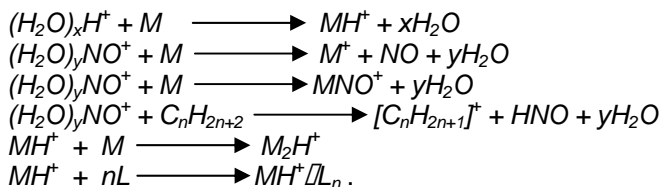
On the other hand, this complexity of the reactant ions mixture was leading to the impossibility to effect physico-chemical studies using exclusively IMS, and exactly this absence of such studies has obstructed the development of a predictive & interpretative model of this atmospheric pressure ionization chemistry. However, the increasing number of studies (conducted especially in the last two decades) is definitely a positive aspect concerning the ionization chemistry elucidation in the ion mobility spectrometer.

The results of main reactions leading to the positive and negative reactant ions, with emphasis on ionization processes that occur using the radioactive source with β isotope ^{63}Ni (which is by far the most common ionization source in IMS) [24,25] are summarized as follows:

<i>Positive reactant ions:</i>	<i>Negative reactant ions:</i>
$(\text{H}_2\text{O})_x\text{H}^+$; $(\text{H}_2\text{O})_y\text{NO}^+$; $(\text{H}_2\text{O})_z\text{NH}_4^+$	$(\text{H}_2\text{O})_x\text{O}_2^-$; $(\text{H}_2\text{O})_y\text{O}^-$; $(\text{H}_2\text{O})_z\text{O}_4^-$
predominant species: $(\text{H}_2\text{O})_x\text{H}^+$	predominant species: $(\text{H}_2\text{O})_x\text{O}_2^-$

Product ions are formed in the reaction region, mainly by collisional charge transfer reactions between the reactant ions and analyte neutral molecules from the sample. They could be also generated by attachment reaction of a reactant ion to the neutral species. At the first sight, product ions formation seems to be quite simple, at least from a qualitative point of view. However, all the efforts undertaken to study product ions generation using IMS coupled to mass spectrometry (IMS/MS) did not lead to a comprehensive quantitative model so far.

There are several main processes that generate positive product ions: proton transfer reactions, charge transfer reactions, electrophilic addition reactions, hydride ion transfer, dimer formation, cluster formation [26,27]. These processes are summarized below:



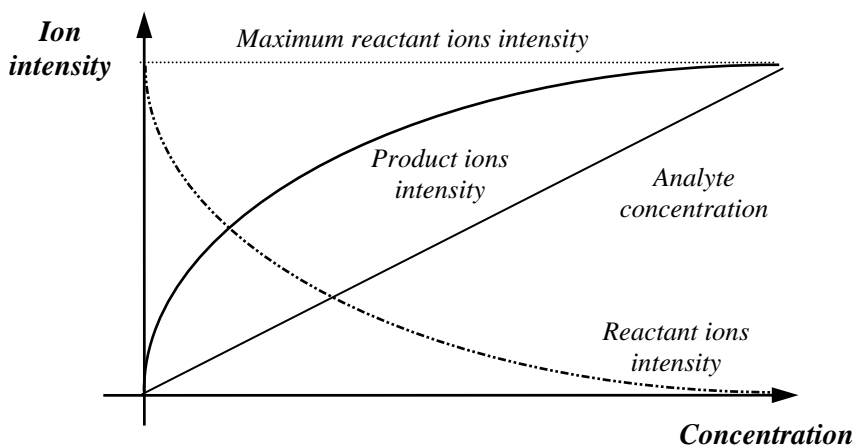
The negative product ions are generated by: associative electron capture, dissociative electron capture, proton extraction processes, as follows:



We shall remind here that in the radioactive ionization source -which is by far the most used source used in IMS- the distribution of available charge is done in a competitive way. The consequence is that the apparition of an ion should lead, because of the charge conservation, to a decrease in intensity of another ion (or ions).

In a first approximation, the charge seems to be distributed proportionally with the concentration of each component in the sample and with its proton (or electron) relative affinity.

The charge will distribute virtually to any compound present in the vapor sample, and this is exactly the cause of the IMS extraordinary versatility. However, because most of drift tubes used currently have a low resolution, they can't be used to separate complex mixtures of ions.



The IMS response could be shortly defined as the intensity change of the product ions with the change of analyte's concentration (as seen in Figure 3).

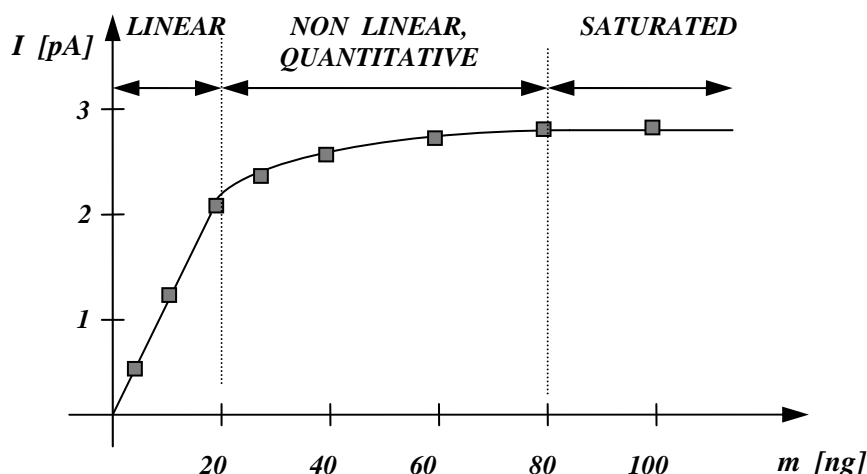


Fig. 3. Typical quantitative IMS response

Fig. 4. The dependence of reactant and product ions intensity upon concentration of the analyte in the vapor sample

This particular kind of response is bound on concentration profiles of reactant and product ions correlated with sample concentration; Figure 4 illustrates well the variation of both reactant and product ion peaks' intensity with analyte concentration.

There were many attempts to control the separation/resolution in IMS, and one of these attempts is based exactly on changing ions' selectivity by modifying the atmospheric pressure ionization chemistry. More specifically, this change of the selectivity implies to continuously add a chemical compound called *dopant* (at a constant concentration level, usually in the parts-per-million range) into the carrier gas flow [4,22,28]. Even water could be seen as a dopant, but the "real" dopants most used in IMS are acetone, carbon tetrachloride and ammonia.

Depending on the origin of the reactant ions, the competitive charge exchange would be an advantage or a disadvantage for a given application. The critic parameters are here the complexity of the sample, sample composition and the relative ionization properties of the target analyte comparing with those of the other compounds present in that sample.

If the target analyte has a greater proton/electron affinity than any other sample component, then it will present a strong IMS response on the expense of the rest of compounds. If all the compounds have approximately the same

proton/electron affinity, then the resulting IMS spectrum will contain all the product ions generated by these compounds. Finally, if the proton/electron affinity of our target analyte is much lower than the affinities of all other components, the detection by IMS becomes very problematic, because it is quite sure that this analyte will not catch the charge; in that case, one should take into consideration a pre-separation of the sample (using gas chromatography, for example) or the use of an alternative ionization chemistry (with a dopant).

Nowadays Ion Mobility Spectrometry can be successfully used to the identification of chemical vapors, and even to their quantitation in a complex matrix. Unfortunately IMS poses a number of problems, so that it is an analytical tool often difficult to use. As a matter of fact, because of these drawbacks IMS is not a real challenge for mass spectrometry or other usual laboratory analytical techniques [29-32]. It must specify here that an absolute identification of the ions can be made only by coupling the IMS spectrometer to a quadrupole mass spectrometer, using a micrometric circular aperture driven in the detector plate of the ion mobility spectrometer (IMS/MS).

Many IMS applications are not laboratory applications but field applications, which do have totally different specifications. For instance, IMS has become attractive as a field technique due to its physico-mechanical simplicity of instrumentation and also to its low cost electronics, comparing with other bulk and complex systems (such as vacuum pumps used in mass spectrometers).

Using an ion mobility spectrometer one can make some separations very easily, but the other are impossible. For example, some anesthetic gases were separated (even if they were isomers !), but hexane can't be separated from carbon dioxide (because none of them is "seen" in IMS).

We can expect that the IMS spectrometer can be used as a chemical analyzer only if the target analyte has very different ionization characteristics as compared with the other sample components. At this stage of knowledge, the IMS technology has not predictive or interpretative properties when it analyzes mixtures which contain compounds with similar ionization parameters.

4. The instrumentation: ion mobility spectrometer

The diagram of an ion mobility spectrometer is presented in Figure 5.

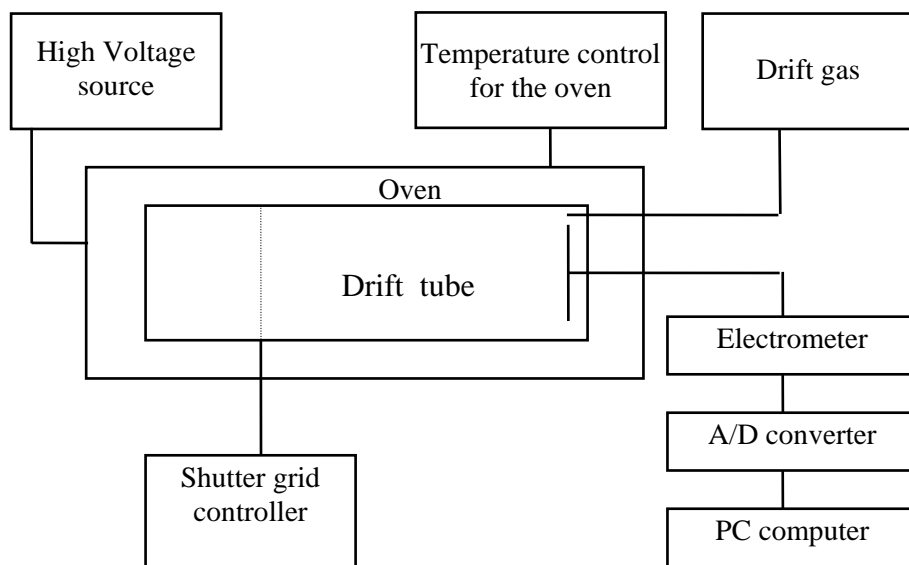


Fig. 5. Schematic diagram of an IMS spectrometer

The essential parts of an IMS spectrometer are the following:

- 1) a sample inlet system
- 2) an ionization source
- 3) a reaction region
- 4) an ion gate (shutter grid)
- 5) a drift region
- 6) a detector (ion collector).

The ancillary equipment necessary for an IMS spectrometer includes:

- 1) a high voltage source, which creates the electric field along the drift tube
- 2) a gate controller
- 3) a drift (and carrier) gas source
- 4) temperature control instrumentation
- 5) a fast electrometer
- 6) data collecting and processing devices, which usually include a computer.

Figures 6 and 7 depict these components of the IMS spectrometer for the two main different configurations of the IMS cell - stacked ring design and compact (ceramic tube) design.

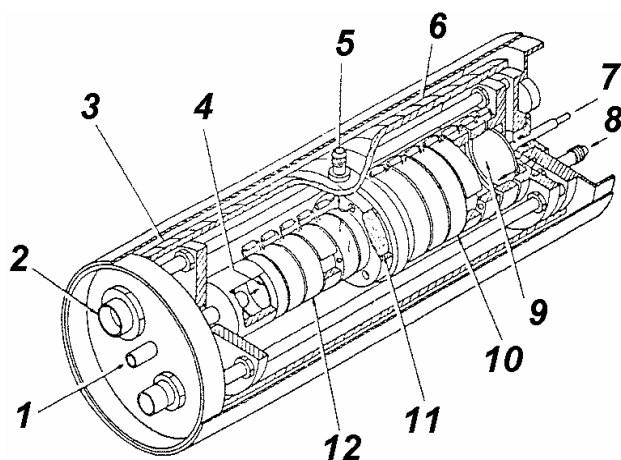


Fig. 6. IMS cell with stacked rings

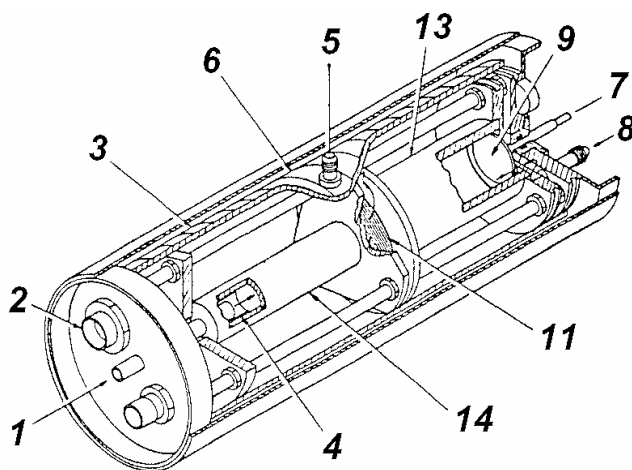


Fig. 7. IMS cell with ceramic tube

The corresponding legend for Figures 6 and 7 is:

- | | |
|--------------------------------|--|
| 1 = Carrier gas + sample inlet | 8 = Drift gas inlet |
| 2 = High voltage connectors | 9 = Faraday plate (detector) |
| 3 = Heating strips | 10 = Drift region |
| 4 = Ionization source | 11 = Shutter grid |
| 5 = Gas exit | 12 = Reaction region |
| 6 = Sealed and heated housing | 13 = Ceramic drift tube + resistive coating |
| 7 = Electrometer | 14 = Ceramic reaction tube + resistive coating |

There are many methods for the introduction of sample vapors into the ionization/reaction region of an IMS spectrometer. Among these are: metal wire sample introduction [33]; syringe injection [34]; exponential dilution flask [35]; permeation tubes [36]; diffusion tubes [36,37]; thermal desorption ovens [38]; laser desorption [39]; sample introduction into the instrument (directly or via a membrane) [40,41]; introduction of the effluent from a chromatographic column (gas, liquid or supercritical) [42,43].

It must be underlined that if the main role of these sample introduction systems is to vaporize and/or carry the vapors into the ionization source, a secondary role is to control the size of the sample, to avoid instrument's overloading.

Sample inlet systems could be classified, according to the initial form of the sample, as follows [3]:

A. *Gaseous samples*: direct introduction (with or without preheating); syringe injection; exponential dilution flask; permeation tubes; diffusion tubes; introduction from gas chromatographic columns; membrane systems.

B. *Liquid samples*: mobile metallic wire systems; syringe injection; electrospra & coronaspray systems; introduction from liquid chromatographic columns.

C. *Solid samples*: thermal desorption ovens; laser desorption.

Membrane-based sample introduction systems are currently mounted on the majority of IMS spectrometers operated at ambient temperature [44,45,46]. The final conclusion concerning these sample introduction systems is that membrane inlets are not useful for the heated IMS cells (where cluster formation is minimized); moreover, a membrane inlet will affect negatively detection limits. However, because membrane inlets are very effective in maintaining a constant low level of water vapors concentration inside the IMS cells operated at ambient temperature (20°C...35°C), they are now the most used systems for portable and hand-held IMS spectrometers.

Vapors ionization is the initial event in the IMS spectrometer, and will define the species that are observed in the mobility spectrum. The ionization of different molecules could be made in many ways:

1. Radioactive ionization [1,2,47], which is by far the most used method in IMS
2. Photoionization [48-50]
3. Laser ionization [51-53]
4. Surface ionization [54,55]
5. Electrospray and coronaspray ionization [56-58].

The IMS cell is the heart of an ion mobility spectrometer. It contains the drift tube (with reaction region and drift region), the grids (ion gates), the detector and optionally a heating system.

Drift tubes could be classified according to the manner of drift field generation, or according to the gas flow through the cell. There are many types of drift tubes [18,33,59-61]:

- stacked ring drift tube (the classical and still most used IMS drift tube)

- compact drift tube - ceramic tube with resistive internal coating
- unidirectional drift tube
- non-conventional drift tubes.

Ion mobility spectrometers contain entrance grids (called also shutter grids) [12,62] and aperture grids (located very close near detector plate) [63].

Shutter grids introduce (inject) periodically the ions from reaction region into drift region. They are pulsed open and closed by a specialized electronic circuit (grid controller); sometimes the opening time can be set by the operator (between 0.1 and 1 milliseconds). The usual opening time is 0.2 ms.

The aperture grid dramatically reduces the capacitive response of the detector when ion clouds are approaching (capacitive decoupling). Without an aperture grid, the ion cloud is coulombically detected before it really strikes the detector plate; the result is the peak broadening and consequently a serious loss in resolution.

In ion mobility spectrometry a gas source (for drift and carrier gases) [3,64,65] is needed. These gases have many functions:

1. To introduce the sample inside ionization/reaction region (carrier gas).
2. To continuously supply neutral molecules for ion-molecule collisions (carrier gas; in the unidirectional IMS cells this function is accomplished by drift gas).
3. To clean the drift tube by continuous purging, avoiding its contamination and memory effects (drift gas).
4. To supply molecules for reactant ions formation.

Usually as carrier and drift gases are used purified air or purified nitrogen. Their purification is done by filtering through molecular sieve cartridges (13X molecular sieve), which retain the impurities and also maintain a very low water vapor level (several ppm). Activated charcoal is also used to retain the organic impurities.

Drift gas may differ from carrier gas. For example, one can use air as carrier gas and nitrogen, air, or sulfur hexafluoride as drift gas. The restrictive condition is the following: drift gas must be chemically inert toward product ions injected into drift region. This requirement is necessary to avoid any ion-molecule reaction in the drift region.

For portable IMS spectrometers the most convenient gas source is in fact a closed loop which filters the air using molecular sieves, coupled with a membrane inlet. Fixed point and laboratory/desktop ion mobility spectrometers can be supplied with compressed air (from air cylinders or from a compressor), after drying and purification.

To collect and process ion mobility spectra one can use many methods: single scan, signal averaging, second gate moving, Fourier transform method [4,66-68]. Currently, the most used is signal averaging method.

Ion mobility spectrometers have been used successfully in many applications involving vapors detection: industrial hygiene, quality control in semiconductor industry, drugs and explosive detection and chemical warfare agents detection.

There is a rule of paramount importance: when all reactant ions were consumed (so the reactant ion peak disappeared from the spectrum), any possibility to

quantitatively interpret the IMS response was also lost. Consequently, to have quantitative information from the IMS spectra an excessive consumption of reactant ions (also called saturation; see Figure 4) must be avoided, and the reactant ion peak must be observed in the spectrum.

Although there are still many unknown aspects, there is a continuously increasing amount of experimental data and studies which assess the quantitative performances of the IMS spectrometers. Several basic considerations regarding the response of ion mobility spectrometers [4,5] are:

- detection limits are very low (in the range 10^{-15} ... 10^{-12} mol/s)
- precision is good (in accordance with some studies, the relative standard deviation RSD of a modern IMS instrument is between 5% and 25%)
- stability of the IMS response is excellent over very long periods of time
- the response sensitivity and linear range
- separation efficiency (in IMS, the number of theoretical plates is several thousands)
- resolution (to have an IMS separation, two ions must have at least a difference of 3% in their reduced mobilities K_0).

Ion Mobility Spectrometry has suffered tremendous progress after the appearance, in the late 1980s, of hand-held portable, small, lightweight and relatively low cost IMS spectrometers issued from the military research & development programs. The problems related to chemical warfare agents detection lead to a large number of very valuable studies and to a great development of IMS instrumentation, but IMS units used in environmental applications appeared only after 20 years from IMS invention. There are several IMS instrumentation manufacturers, most of them being located in USA and Canada: *Graseby Dynamics Ltd.* (United Kingdom); *Bruker GmbH* (Germany); *PCP Inc.* (USA); *Ion Track Instruments Inc.* (USA); *Barringer Research Ltd.* (Canada/USA); *Molecular Analytics Inc.* (USA); *Environmental Technologies Group Inc.* (USA); *CPAD Technologies Inc.* (Canada) and *FemtoScan Corporation* (USA).

Commercial IMS instruments could be classified according to their size and specific applications [3] in: laboratory instruments - stationary or desktop (transportable in a vehicle), fixed-point field instruments and hand-held portable instruments.

5. Conclusions

Most important trends in the evolution of Ion Mobility Spectrometry are the following:

- continuous simplification and miniaturization of the IMS cells
- use of selective techniques for sampling
- implementation of new signal processing techniques for IMS signal (such as neural networks) [69]

- use of new designs of the IMS cells, such as non-conventional field control
- building of portable heated IMS cells
- manufacturing of portable GC/IMS and IMS/MS instrumentation
- use on a larger scale of the non-radioactive ionization sources [70]
- ultraminiaturization of the IMS instrumentation [71].

As a final conclusion, we can say that after 1980 Ion Mobility Spectrometry has developed very fast and passed the boundary from an "exotic" laboratory technique to a simple technique for ultra-trace analysis, alone or coupled with another analytical technique (like mass spectrometry or chromatography).

BIBLIOGRAPHY

1. Karasek, F.W., *Res. Dev.* 1970, 21(3), 34.
2. Cohen, M.J.; Karasek, F.W., *J. Chromatogr. Sci.* 1970, 8(6), 330.
3. Bocoș-Bințințan, V., *"Spectrometria de mobilitate ionică"*, Editura Presa Universitară Clujeană, Cluj-Napoca, 1998.
4. Eiceman, G.A.; Karpas, Z., *"Ion Mobility Spectrometry"*, CRC Press, Boca Raton, FL, 1994.
5. Carr, T.W. (Ed.), *"Plasma Chromatography"*, Plenum Press, New York, 1984.
6. McDaniel, E.W.; Mason, E.A., *"The mobility and diffusion of ions in gases"*, John Wiley, New York, 1973.
7. McDaniel, E.W., *"Collision Phenomena in Ionized Gases"*, John Wiley, New York, 1964.
8. Revercomb, H.E.; Mason, E.A., *Anal. Chem.* 1975, 47, 970.
9. Biondi, M.A.; Chanin, L.M., *Phys. Rev.* 1961, 122, 843.
10. Kolaitis, L.; Lubman, D.M., *Anal. Chem.* 1986, 58, 1993.
11. Griffin, G.W.; Dzidic, I.; Carroll, D.I.; Stillwell, R.N.; Horning, E.C., *Anal. Chem.* 1973, 45, 1204.
12. Tyndall, A.M., *"The Mobility of Positive Ions in Gases"*, Cambridge University Press, London, 1938.
13. Kim, S.H., *Ph.D. Dissertation*, University of Waterloo, Ontario, Canada, 1977.
14. Graham, E.; James, D.R.; Keever, W.C.; Gatland, I.R.; Albritton, D.L.; McDaniel, E.W., *J. Chem. Phys.* 1973, 59, 4648.
15. Crank, J., *"The Mathematics of Diffusion"*, Oxford University Press, London, 1956.
16. Rokushika, S.; Hatano, H.; Baim, M.A.; Hill, H.H., Jr., *Anal. Chem.* 1985, 57, 1902.
17. Kim, S.H.; Karasek, F.W.; Rokushika, S., *Anal. Chem.* 1978, 50, 152.
18. Eiceman, G.A.; Leasure, C.S.; Vandiver, V.J.; Rico, G., *Anal. Chim. Acta* 1985, 175, 135.
19. Sumner, J.; Nicol, G.; Kebarle, P., *Anal. Chem.* 1988, 60, 1300.
20. Carr, T.W., *Anal. Chem.* 1979, 51, 705.
21. Siegel, M.W.; Fite, W.L., *J. Phys. Chem.* 1976, 80, 2871.
22. Lawrence, A.H.; Neudorfl, P., *Anal. Chem.* 1988, 60(2), 104.

23. Eiceman, G.A.; Shoff, D.B.; Harden, C.S.; Snyder, A.P.; Martinez, P.M.; Fleischer, M.E.; Watkins, M.L., *Anal. Chem.* 1989, 61(10), 1093.
24. Siegel, M.W., "Atmospheric pressure ionization", in "Plasma Chromatography", Plenum Press, New York, 95, 1984.
25. Weast, R.C., Ed., "CRC Handbook of Chemistry and Physics", CRC Press, Boca Raton, FL, B-264, 1972.
26. Harrison, A.G., "Chemical Ionization Mass Spectrometry", CRC Press, Boca Raton, FL, 1983.
27. Dressler, M., "Selective Gas Chromatographic Detectors", Elsevier, New York, 217, 1986.
28. Proctor, C.J.; Todd, J.F.J., *Anal. Chem.* 1984, 56, 1794.
29. Vandiver, V.J.; Leasure, C.S.; Eiceman, G.A., *Int. J. Mass Spectrom. Ion Processes* 1985, 66(2), 223.
30. Eiceman, G.A.; Shoff, D.B.; Blyth, D.A.; Snyder, A.P., *Anal. Chem.* 1990, 62(14), 1374.
31. Kim, S.H.; Betty, K.R.; Karasek, F.W., *Anal. Chem.* 1978, 50, 2006.
32. Preston, J.M.; Rajadhyax, L., *Anal. Chem.* 1988, 60, 31.
33. Spangler, G.E.; Cohen, M.J., "Instrument design and description", in "Plasma Chromatography", Plenum Press, New York, 1, 1984.
34. Metro, M.M.; Keller, R.A., *J. Chromatogr. Sci.* 1973, 11(10), 520.
35. Spangler, G.E.; Lawless, P.A., *Anal. Chem.* 1978, 50(7), 884.
36. O'Keefe, A.E.; Ortman, G.C., *Anal. Chem.* 1966, 38, 760.
37. Grob, R.L., Ed., "Modern Practice of Gas Chromatography", John Wiley & Sons, New York, 194, 1977.
38. Nanji, A.A.; Lawrence, A.H.; Mikhael, N.Z., *J. Toxicol. Clin. Toxicol.* 1987, 25(6), 501.
39. Huang, S.D.; Kolaitis, L.; Lubman, D.M., *Appl. Spectrosc.* 1987, 41(8), 1371.
40. Roehl, J.E., *Opt. Eng.* 1985, 24, 985.
41. Spangler, G.E.; Collins, C.I., *Anal. Chem.* 1975, 47, 393.
42. Eatherton, R.L.; Morrissey, M.A.; Siems, W.F.; Hill, H.H., Jr., *J. High Resolut. Chromatogr. Chromatogr. Commun.* 1986, 9, 154.
43. McMinn, D.G.; Kinzer, J.; Shumate, C.B.; Siems, W.F.; Hill, H.H., Jr., *J. Microcolumn Sep.* 1990, 2, 188.
44. Spangler, G.E.; Carrico, J.P., *Int. J. Mass Spectrom. Ion Phys.* 1983, 52, 267.
45. Eiceman, G.A.; Snyder, A.P.; Blyth, D.A., *Int. J. Environ. Anal. Chem.* 1990, 38(3), 415.
46. Spangler, G.E., U.S. Patent 4.311.669: "Membrane interface for ion mobility detector cells", Jan. 19, 1982.
47. Poole, C.F.; Zlatkis, A., "Electron Capture, Theory and Practice in Chromatography", Elsevier/North-Holland, Amsterdam, 1981, 13.
48. Baim, M.A.; Eatherton, R.L.; Hill, H.H., Jr., *Anal. Chem.* 1983, 55, 1761.
49. Eatherton, R.L., *Ph.D. Thesis*, Washington State University, Pullman, WA, 1987.
50. Leasure, C.S.; Fleischer, M.E.; Anderson, G.K.; Eiceman, G.A., *Anal. Chem.* 1986, 58, 2142.
51. Lubman, D.M.; Kronick, M.N., *Anal. Chem.* 1982, 54, 1546.
52. Lubman, D.M.; Kronick, M.N., *Anal. Chem.* 1983, 55, 1486.

53. Eiceman, G.A.; Vandiver, V.T.; Leasure, C.S.; Anderson, G.K.; Ttee, T.T.; Danen, W.C., *Anal. Chem.* 1986, 58, 1690.
54. Wohltzer, H., *U.S. Patent US 581398 AO*, 03.08.1984.
55. Vora, K.N.; Campbell, D.N.; Davis, R.C.; Spangler, G.E.; Reategui, J.A., *U.S. Patent 5.053.343: "Selective ionization of gas constituents using electrolytic reactions"*, Oct. 1, 1991.
56. Geniec, J.; Mack, L.L.; Nakamae, K.; Gupta, C.; Kumar, V.; Dole, M., *Biomed. Mass Spectrom.* 1984, 11, 259.
57. Yamashita, M.; Fenn, J.B., *J. Phys. Chem.* 1984, 88, 4451.
58. Dole, M.; Gupta, C.V.; Mack, L.L.; Nakamae, K., *Polym. Prepr.* 1977, 18, 188.
59. Carrico, J.P.; Sickenberger, D.W.; Spangler, G.E.; Vora, K.N., *J. Phys. E: Sci. Instrum.* 1983, 16, 1058.
60. Browning, D.R.; Sima, G.R.; Schmidt, J.C.; Sickenberger, D.W., *U.S. Patent 4.390.784: "One piece ion accelerator for ion mobility detector cells"*, June 28, 1983.
61. Blanchard, W., *Int. J. Mass Spectrom. Ion Processes* 1989, 95, 199.
62. Bradbury, N.E.; Nielson, R.A., *Phys. Rev.* 1936, 49, 388.
63. Eiceman, G.A.; Vandiver, V.J.; Chen, T.; Rico-Martinez, G., *Anal. Instrum.* 1989, 18, 227.
64. Davies, J.H.; Jackson, R.A.; Kuja, F.J., *U.S. Patent 5.552.600: "Pressure stabilized ion mobility spectrometer"*, Sep. 3, 1996.
65. Bradshaw, R.F.D., *U.S. Patent 5.475.217: "Ion mobility spectrometry equipment"*, Dec. 15, 1995.
66. Baim, M.A.; Schuetze, F.J.; Frame, J.M.; Hill, H.H., Jr., *Am. Lab.* 1987, 14, 59.
67. Knorr, F.J.; Eatherton, R.L.; Siems, W.F.; Hill, H.H., Jr., *Anal. Chem.* 1985, 57, 402.
68. Knorr, F.J.; Eatherton, R.L.; Siems, W.F.; Hill, H.H., Jr., *U.S. Patent 4.633.083: "Chemical analysis by time dispersive ion spectrometer"*, Dec. 30, 1986.
69. Davis, D.; Kroutil, R.T., *Anal. Chim. Acta* 1990, 232(2), 261.
70. Taylor, S.J.; Turner, R.B.; Arnold, P.D., *U.S. Patent 5.6---84.300: "Corona discharge ionization source"*, Nov. 4, 1997.
71. Harden, C.S., *"Hand-held IMS devices - the case for small, fast analytical instruments"*, in *Proceedings of the 5th International Workshop on Ion Mobility Spectrometry*, Jackson, Wyoming, Aug. 20-22, 1996, p. 321.

PILOT ASSESSMENT OF CONTAMINANT ELEMENTS IN SOILS AND CRYPTOGAM PLANTS FROM EMISSIONS FROM AN ORE PROCESSING PLANT, ZLATNA REGION, ROMANIA

ANA-MARIA RUSU¹, KATALIN BARTOK², WILLIAM PURVIS³
and WILLIAM DUBBIN⁴

¹ Department of Chemistry, Babes-Bolyai University, Cluj-Napoca, Romania

² Department of Biology, Babes-Bolyai University, Cluj-Napoca, Romania

³ Department of Botany, The Natural History Museum, London, UK

⁴ Department of Mineralogy, The Natural History Museum, London, UK

ABSTRACT. Soil samples were collected from 7 sampling stations (in duplicate) and associated terricolous lichen (*Cladonia fimbriata* and *Cladonia coniocraea*) and moss (*Bryum argenteum*) samples along an W-E transect from Zlatna plant. *Cladonia* and moss samples were digested with HNO₃ + H₂O₂ mixtures and analyzed for Pb, Zn, Cu using acetylene-air flame atomic absorption spectrometry. Chemical analyses of bulk samples for soil-surface horizons were digested with Lunge mixture and analyzed also with FAAS. Lead and Cu contents decreased more-or-less linearly with increasing distance from the ore-processing plant and soil pH values increased as a function of distance. Soils (surface horizons) are acidic virtually throughout the area. Lichen and moss metal content was significantly higher than soil metal content. Metal concentrations are amongst the highest reported for natural ecosystems, the most serious being for Pb.

INTRODUCTION

Romania is confronted with serious problems of environmental pollution as a consequence of intensive industrialisation. One 'intensely polluted zone' is the Zlatna region of central Transilvania. A copper ore processing plant in the centre of Zlatna town lying in a sheltered valley produces acidic emissions and large amounts of metal particulates, both causing extreme environmental degradation throughout the locality [1]. Forest soils of the area are eroded, acidified and sparsely vegetated: trees are visibly damaged and agriculture in some parts of the area is noticeably affected [2].

The ore used for copper smelting contains a range of trace metals including: Pb, Zn, Cd, Sb, Bi, As, Ag, Au. The smelting process results in a

concentration of these elements and smelter particles ranging from < 5 to 100 µm in diameter, many in the size class commonly referred to as PM10, are released directly to the atmosphere. During oxidation of the Cu sulphide concentrate, S is partitioned into the volatile phase to produce SO₂, which at Zlatna is released directly into the environment - up to 1305 µg/m³ SO₂ /30-minute mean concentration was recorded in the town centre in 1996. Unfortunately, only the old factory is currently functioning and this has a very inefficient filter: the retention of dust being only about 50% efficiency. Emissions are released directly to the atmosphere, via the two chimneys from the smelting and conversion works, both 100 m in height.

This study forms part of an ongoing study into the impact of pollution in Zlatna region. Previous studies have focussed on macrolichen transplants [3, 4] and bioaccumulation of lead by *Acarospora smaragdula* [5]. The purpose of this pilot study is to sample native cryptogamic plants (mosses and lichens) and associated soils along a WE gradient transect in the Ampoi Valley to a site 25 km downwind from the smelter. The present paper compares the contents of Cu, Pb and Zn in lichens (*Cladonia fimbriata* and *Cladonia coniocraea*), mosses (*Bryum argenteum*) and soils. A combination of plant and soil chemical data will enable determination of functional relationships, which may be useful for predicting the response of the ecosystem to future change and which may also facilitate the planning of strategies for managing the ecosystem for multiple land use (e.g. agriculture, silvaculture, etc.).

EXPERIMENTAL

Sampling and sample digestion procedure. Soil samples were collected from 7 sampling stations (in duplicate) and associated terricolous lichen (*Cladonia fimbriata* and *Cladonia coniocraea*) and moss (*Bryum argenteum*) samples. The sampling points are marked (Figure 1).

Approximately 1000 g brown forest soil samples (soil-surface horizons, 10 cm depth) were collected using a trowel and were placed into plastic bags. These samples were air-dried at room temperature prior to grinding in agate mortars, sieving (at -80 mesh) and dissolution. The results represent the average of 2 soil samples/site made in duplicate each one.

The moss and lichen samples were carefully removed by hand from their substrate and covered in tissue paper. These were then stored in plastic flasks prior to drying and cleaning. It was made a mixture of the two *Cladonia* species, and analysed in duplicate for each site.

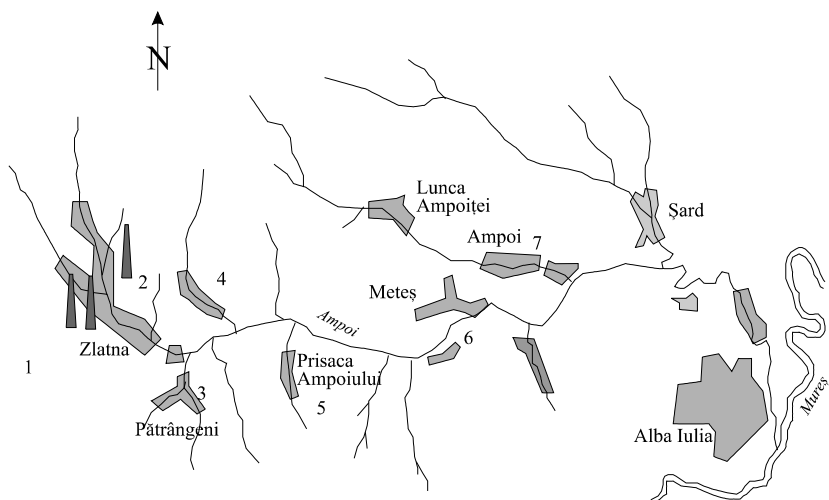


Fig. 1. The sketch map of the Zlatna region and the location of the studied sites.

Dissolution procedure for soil samples. In the acid digestion procedure (Lunge method) [6], 0.2 g of finely ground soil sample was weighed. Ten millilitres of 1:1 HCl were added to the sample and the solution was fumed to near dryness. After cooling, 10 ml of 1:3 HCl:HNO₃ (v/v) (Lunge mixture), was added, and again the acid was fumed off to near dryness. The residue was dissolved in 25 ml 1:4 HCl and heated for approximately 15 min. The sample was then transferred into a 50 ml volumetric flask and diluted to volume with distilled water.

Dissolution procedure for vegetable samples. Samples were hand-cleaned to remove foreign material and oven dried at 108^o C for 8-10 hrs. Each sample was carefully ground in a porcelain mortar. Approximately a 0.5 g portion was digested in a glass vessel using 14 ml HNO₃; this was carried out for over night at room temperature then heated 3 hrs at 120^o C. It was then cooled, 6 ml H₂O₂ added, and reheated to 120^oC until no brown fumes were given off. The resulting sample was cooled and bulked to 50 ml.

Reagent and standard solution. Nitric acid (65% m/v), hydrochloric acid (37% m/v) and H₂O₂ (30% m/v) (Merck, Darmstadt, Germany) were used for the soils, mosses and lichen digestion. The blank sample contained only the reagents used for digestion. All solutions were stored in plastic vials cleaned with acid solution and rinsed with distilled water.

Single element stock solutions of 1000 mg L⁻¹ were prepared by dissolution of high-purity metal (Merck, Darmstadt, Germany) in a minimum volume of HNO₃ (Cu, Pb) or HCl (Zn) and diluted to 1 L.

Instrumentation. Flame atomic absorption measurements were performed on a Perkin-Elmer Model 2100 atomic absorption spectrometer operating with acetylene-air flame and optimised standard operating conditions. Linear curves from monoelement external standards were used for quantification.

Soils pH determination.

Procedure. Weigh 25 g of soil in a clean beaker. Add 25 ml distilled water and stir for 15 minutes. Calibrate the pH meter prior to use by inserting the combination glass electrode in a buffer solution of pH 7.0. Adjust the pH meter to read pH 7.0. Rinse the electrode with distilled water and place it in a buffer solution of pH 4.0 to read pH 4.0. Rinse the electrode again with distilled water and place it in the soil suspension above. Read the pH in the scale of the pH meter.

Soil pH is strongly affected by acid emissions from the Zlatna plant (Table 1).

Table 1.

pH values of the soil samples collected on 16 May 1999.

Sample	Sampling point definition	pH
1a 1b	Site 1 300 m SSW of two smelter chimneys above house	3.93 3.82
2a 2b	Site 2 opposite site 1, 500 m NE from new factory	3.78 3.83
3a 3b	Site 3 P ³ / ₄ trângeni (station)	4.00 4.01
4a 4b	Site 4 opposite Patrangeni forest (300 m below calcareous stone with cross)	4.42 4.46
5a 5b	Site 5 Presaca Ampoiului	4.38 4.25
6a 6b	Site 6 Metes	5.32 5.05
7a 7b	Site 7 Ampoita	4.58 7.17

Down-valley of the plant soils display low pH due to acid deposition. The acidity of the soils decreases with increasing distance from the plant. This is in agreement with the prevailing wind direction and the dispersal (and dilution) of pollutants from the smelter plant (west-east). Soil pH at site 4, is slightly buffered by the local calcareous (limestone) bedrock (Wildflisch Formation), but the soils are still very acidic. Soils at site 7 show a large variation in pH values due to the soils in the area being largely agricultural and recently ploughed.

Results and discussion

The variation in Pb, Cu and Zn concentrations in moss samples collected along the 25 km is represented in Figure 2. Lead concentrations show the greatest variation between sample sites, and also the highest concentrations overall. Zinc is not present in very high concentrations; variation between sites 1,2,4 and 5 is very little. Copper shows a similar degree of variation as lead, but is not present in such high concentrations; it is greater than zinc since the primary ore (chalcopyrite) does not contain much zinc.

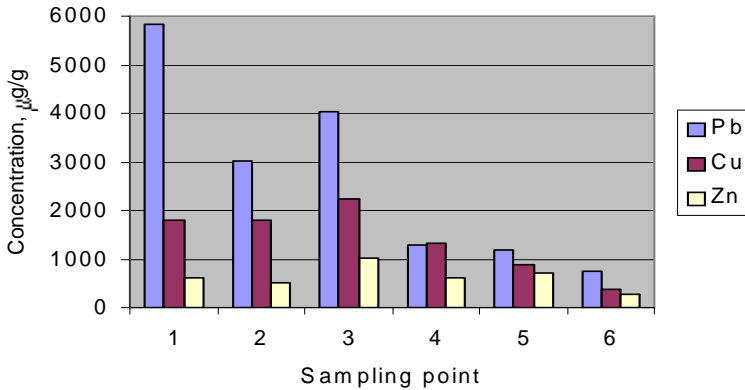


Fig. 2 Pb, Cu and Zn concentration in mosses.

llected along the Ampoi Valley is represented in Figure 3. Lead is once again the greatest concentrations in comparisons with the other studied elements. In sites 1 and 2 *Cladonia fimbriata* and *Cladonia coniocraea* (fruticulous lichens) could not be found at all; this effect is probably due to the fact that SO₂ and the metals are too concentrated in these areas for these lichens to exist.

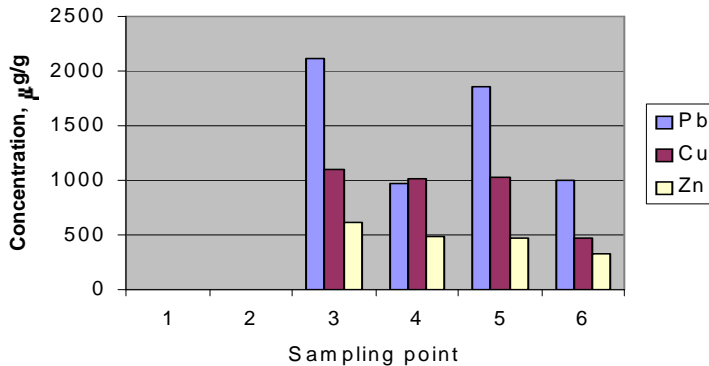


Fig. 3 Pb, Cu and Zn concentration in lichens.

The degree of accumulation of the analysed elements is different for soils, mosses, lichens and oak leaves. In Figure 4 the Cu, Zn and Pb concentrations in the studied samples versus the distance from the polluted source are represented comparatively. It is interesting to compare lichens and mosses data (perennial plants) with oak leaves chemical data (deciduous trees).

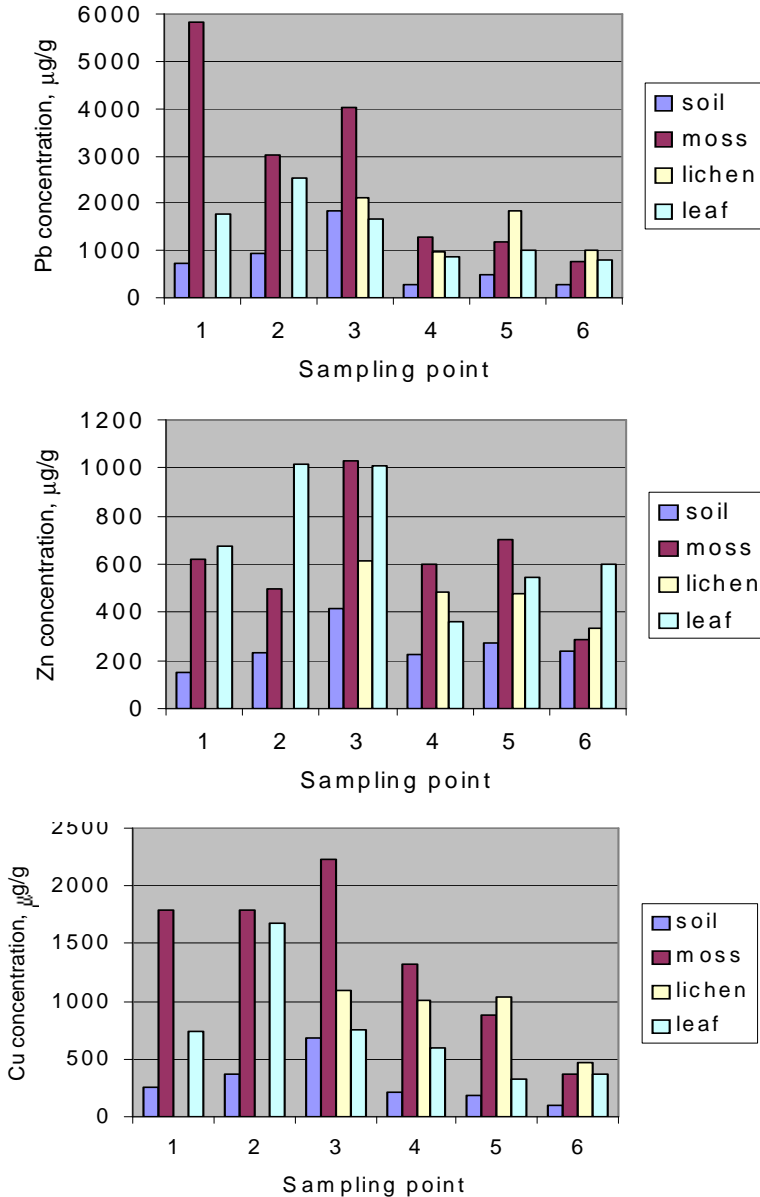


Fig. 4 Pb, Zn and Cu concentration in studied samples

PILOT ASSESSMENT OF CONTAMINANT ELEMENTS

For copper the mosses accumulate the greatest concentrations. The trend of the concentrations for leaves, mosses and soils is such that levels of copper increase up to site 3, at which point they begin to decline as distance from the source increases. This is not the case for lichens: these can only exist from point 3 eastwards, and perhaps their copper levels do not show the same trend as, say mosses, due to their being saturated with copper.

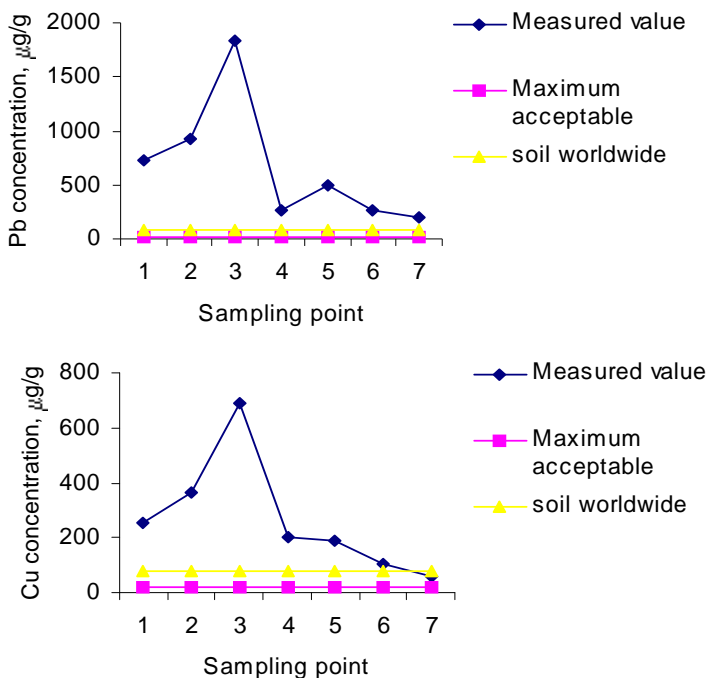
For zinc mosses and leaves show similar levels of concentration, in the lichens this metal decrease with the distance from the pollution source. The general trend is less clear than that of copper.

For lead the relationship of concentrations between each of the sample media is similar to that of copper. The general trend between sites is less clear, but there is some trend of decrease away from the source. Site 3 and 4 interesting as these are on opposite sides of the valley, equidistant from the plant and yet soil Pb values are much lower in 4 than 3. It shows that there is some local variation due to the topographical influences. As the soil pH is higher here (site 4) we would expect, the metals are not mobilised in these acidic conditions.

The soil concentrations are not very high compared to the vegetation samples, but show a trend of increasing towards site 3 and decreasing eastwards.

The fact that soils are much lower in concentration of the studied elements than the biological samples may be due acid rains leaching the lower horizons, and also because soils do not accumulate the metals biologically to the same degree.

The Cu, Zn and Pb concentrations found in soils were compared with the maximum value admitted by Romanian standards and with the soil worldwide (Figure 5).



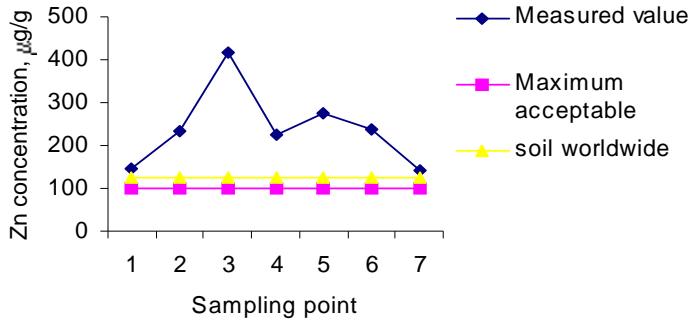


Fig. 5 Pb, Cu and Zn distribution in the sampling points along Ampoi Valley.

These graphs indicate the concentrations of copper, lead and zinc in soils along the transect in the Ampoi Valley. These are compared, in each case, with both the average concentration (worldwide- Pb: range 10 to 84 ppm, Cu: range 6 to 80 ppm, Zn: range 17 to 125 ppm [7]) and the maximum acceptable concentrations of these elements (Official Romanian Standard, 1997- Pb 20ppm, Cu 20ppm, Zn 100ppm). In all situations the element concentrations exceed these maximum levels — by a considerable margin.

Conclusions.

- Our pilot study identified a strong gradient of metal contamination in soils and biota as well as soil acidification along a WE transect from the plant.
- Highest impact of pollution is at site Patrangeni (3), 3.5 km from the plant.
- Local topographic influences may protect certain areas from metal deposition as at site (4) directly opposite the most contaminated site.
- Mosses accumulated higher levels of metals than lichens, leaves and soils.
- Extreme SO₂ contamination in the results in a low macrolichen diversity present in insufficient quantities in the vicinity of the plant to allow bulk chemical analysis by conventional means.
- We conclude that in view of the high soil and biotic metal concentrations which are significantly higher than recommended levels, this suggests there may be important health implications from ingestion of locally contaminated crops.
- We recommend that future biomonitoring studies should focus on utilising moss/lichen transplants using a grid system to minimise problems in obtaining sufficient samples *in situ* for analysis. This is necessary to assess the full extent of contamination.

REFERENCES

1. C. Clepan. Poluarea mediului, Editura Altip, Alba-Iulia, 1999, 62-105.
2. B.J. Williamson, O.W. Purvis, K. Bartok, N. Har, E. Manolache, C.J. Stanley, N.S. Vlad. *Studia Universitatis Babes-Bolyai, Geologia*, 1998, **61**: 87-93.
3. K. Bartok. *Contribuții Botanice (Cluj-Napoca)*, 1982, 101-106.
4. K. Bartok. *Revue Roumaine de Biologie Vegetale*, 1988, **33**: 127-134.
5. O.W. Purvis, B.J. Williamson, K. Bartok, N. Zoltani. *New Phytologist* (2000) **147(3)** [in press].
6. A. Demetrescu, A. Tutoveanu, M. Ionescu. Analiza tehnica a minereurilor. Editura tehnica Bucuresti, 1966, p 133.
7. M.B. McBride, Environmental chemistry of soils. Oxford University Press, Oxford, 1994, p 406.

TRACE ELEMENT MEASUREMENT BY ICP-AES FOR THE ROUTINE MULTI-ELEMENT ANALYSIS OF LICHEN AND SOIL SAMPLES FOR ENVIRONMENTAL POLLUTANT STUDIES

ANA-MARIA RUSU¹, KATALIN BARTOK², VICTOR DIN³,
WILLIAM PURVIS⁴ and WILLIAM DUBBIN³

¹ *Department of Chemistry, Babes-Bolyai University, Cluj-Napoca, Romania*

² *Department of Biology, Babes-Bolyai University, Cluj-Napoca, Romania*

³ *Department of Mineralogy, The Natural History Museum, London, UK*

⁴ *Department of Botany, The Natural History Museum, London, UK*

ABSTRACT. Inductively-coupled plasma atomic emission spectrometry (ICP-AES) is a very important technique for the determination of trace element concentrations in environmental samples. Lichen and soil samples were collected from different polluted sites around Zlatna town, Romania. Contaminant elements in the samples were determined by ICP-AES after extraction from the soils using DTPA and TEA mixture and digestion of the lichens in HNO₃ + H₂O₂ mixture. Copper, Pb, Zn, Ni, Fe, Cd and S were determined in both soils and lichens. Mean and extreme values of the elements determined are listed. A certified reference material, BCR CRM 482 lichen, provided comparative data for the lichen samples. The methods described are rapid and easy to use for environmental pollution studies.

INTRODUCTION

Inductively-coupled plasma atomic emission spectrometry (ICP-AES) is widely recognised as a suitable technique for the determination of trace elements in environmental samples, particular because of its multi-element capability, large dynamic range and effective background correction. The technique is important for the determination of trace metal concentrations in environmental samples [1].

Airborne contaminants are usually measured with specialised instruments but, during the last two decades, lichens have increasingly been used as bioindicators of metal contaminants. Most work on the accumulation of heavy metals by lichens has focused on pollution from smelters, power plants, busy roads, urban sites and rural areas. Puckett [2] pointed out that lichens and bryophytes have certain characteristics which meet several requirements of ideal biological monitors. For example, they are geographically widespread, growing everywhere from rocky coasts to mountain summits, from Polar Regions to the tropics, on rocks, trees, soil, buildings, etc. This allows comparison of the concentrations of pollutant metals from diverse regions; they form a more-or-less constant, perennial body enabling accumulation to occur throughout the year. Puckett also mentioned the ability of lichens and bryophytes to accumulate metals to

concentrations far above their expected physiological needs. Other characteristics that make lichens suitable as biomonitors are their very slow growth rates, their longevity and their rapid uptake and accumulation of cations and metal particulates [3].

The town of Zlatna, in the Apuseni Mountains of Romania, is built around a mineral processing plant and smelter. The plant processes a variety of complex ores (mainly sulphides) for Cu, with Au, Ag, Pb, Zn, S, Bi, Cd and Mo as major by-products. Release of SO₂ and metals via the vapour phase and as fine particles of slag causes acid precipitation and metal contamination for more than 30 km down wind from the smelter [4]. On previous studies in Zlatna area, Bartok and co-workers [5] determined Pb, Mn, Cu and Zn in transplanted macrolichens; Purvis and co-workers [6] used microanalysis techniques for measuring Pb bioaccumulation in *Acarospora smaragdula* collected from the same area.

Environmental analyses are commonly carried out using established classical methods. In this paper, we would like to propose two rapid and easy methods for the determination of pollutant elements in lichen and soil samples using an ICP-AES instrument. The main aim of this work is to present methods for the analysis of environmental samples, which fulfil the following demands:

- (i) many elements can be determined in the same digest
- (ii) the sample preparation is simple and fast
- (iii) the minimum volume of acid is used
- (iv) calibration is preferably made by direct methods, not by the standard addition method, and
- (v) applicable to a large variety of samples.

In addition, an ICP-AES method is described for the determination of trace elements in soil samples after extraction of those elements into DTPA/TEA reagent. Extraction is one of the most frequently used sample pre-treatment techniques applied to the determination of trace metals in environmental samples by ICP-AES. The extraction serves the dual purposes of concentrating the metals of interest and separating them from an interfering matrix. Isolation from the matrix significantly decreases any background signal caused by concomitants and the solids content of the solution. On other hand, the results obtained provide a general overview on air pollution patterns within the investigated area.

EXPERIMENTAL

Survey area. The sample sites are 200 -300m east and west of the factory chimneys, and along an east – west transect which runs from the town, along the Ampoi Valley, to a site 25km downstream. A map of the sites chosen was published in a previous paper [7]. The sites, listed in order of distance from the pollutant source are:

- site 1* in Zlatna town (300m SSW of two smelter chimney)
- site 2* in Zlatna town (opposite to site 1 at 500m NE from new factory)
- site 3* in Patrangeni station (3.5km SW Zlatna)
- site 4* opposite Patrangeni forest (4km WSW Zlatna, 300m below a calcareous stone with cross)
- site 5* in Presaca Ampoiului (9km SW Zlatna)

- site 6 Metes (16km WSW Zlatna)
site 7 Ampoita (25km WSW Zlatna).

Sampling. Soil and associated terricolous lichen, *Cladonia floerkeana* samples were collected from the sites. The soil samples (approximately 200g) were collected from the surface mineral horizon, after removing the organic layer, in locations free of growing plant material. These samples were air-dried, crushed to a fine consistency in agate mortar and sieved through an 80 mesh sieve. Only a small amount of lichen could be collected from some sites and it was not possible to collect any *Cladonia* in Zlatna town (sites 1 and 2) because this species was absent due to high levels of air pollution. *Cladonia floerkeana* was also absent from sites 6 and 7. All samples were collected during October 1998.

Sample preparation methods.

Reagents and standard solutions. Deionised water and, where possible, analytical grade or better reagents were used for all the procedures described.

Nitric acid (65% m/v), hydrochloric acid (37% m/v) and hydrogen peroxide (30% m/v) were used for the lichen digestions.

Soil extraction solution: 0.005M diethylenetriaminepentaacetic acid (DTPA), 0.01M calcium chloride and 0.1M triethanolamine (TEA) adjusted to pH 7.3 with HCl. To prepare 1 litre of this solution 14.92g of reagent grade TEA, 19.67g of DTPA and 1.47g of $\text{CaCl}_2 \cdot 2\text{H}_2\text{O}$ were dissolved in approximately 200mL of deionised water. The pH of this solution was adjusted to 7.3 ± 0.05 with 1M HCl while stirring and it was then diluted to 1.0L with deionised water[8].

Stock multi-element standard solutions were prepared from $10,000 \mu\text{g} \cdot \text{ml}^{-1}$ single element, high purity standards. Working standard solutions were prepared daily by appropriate dilution of the intermediate solutions with deionised water.

Lichen dissolution procedure. Lichen thalli were cleaned carefully under a binocular microscope without washing. Samples were dried at 108°C for 8 hours and ground. Samples of 50mg of dry weight were measured into borosilicate test tubes with reflux bulbs and digested in 3ml HNO_3 (concentrated) at 50°C overnight, then for 3 hours at 120°C , cooled and 1ml 30% H_2O_2 was added. The solutions were reheated to 50°C for half hour, then to 120°C until brown fumes were no longer evolved. The water-clear contents of the test tubes were filtered through Whatman No 42 filter paper and brought to a volume of 15ml with deionised water. The solutions were analysed for Pb, Cu, Zn, Fe, Cd, Ni, Ag, As and S.

Extraction procedure. 10g of the air-dried, sieved soil samples were weighed into 125ml conical flasks and 20ml of the DTPA extraction solution were added. Each flask was sealed with stretchable paraffin film and secured upright on a horizontal shaker with a speed of $120 \text{ cycles min}^{-1}$. After exactly 2 hours of shaking the suspensions were filtered by gravity through Whatman No 42 filter paper. The shaking time is very important because extraction is not complete after 2 hours, the labile and non-labile trace metals fractions will continue to dissolve.

The filtrates were analysed for the trace elements Cu, Ni, Zn, Pb, Fe, Cd and S by ICP- AES.

Instrumentation.

Table 1.

Operating conditions for the ICP.	
Forward power	650 W
Reflected power	3-5W
Integration time	1 second
Plasma argon	0.8 L.min ⁻¹
Auxiliary argon	7.5 L.min ⁻¹
Carrier (nebuliser) argon	0.7 L.min ⁻¹
Sample uptake rate	2.9 mL.min ⁻¹ , free aspirating
Analytical lines, nm	
As: 189.042; Ag: 328.068;	Cd: 228.802; Cu: 324.754;
Fe: 259.940; Ni: 231.604;	Pb: 220.353; Zn: 213.856;
S: 182.037.	

The determination of trace elements by ICP-AES in all of the samples investigated was performed using a model 3410 ARL "Minitorch" sequential spectrometer with pneumatic nebuliser (Meinhard concentric, type TR-30 – K3). The instrument was optimised for routine multi-element analysis by aspirating a solution containing 2µg.ml⁻¹ of each of the elements of interest. All measurements were background corrected. Linear working curves generated from five multi-element external standards were used for quantification. Lichen standard solutions were prepared in the same acid concentration as the samples, whilst blank solutions were prepared by following the steps of the sample dissolution procedure. Also, multi-element soil extract standards were prepared for quantification, every solution containing 2%HNO₃ and 400µg.mL⁻¹ Ca. All measurements were made in duplicate for the samples and standard solutions. The instrument operating parameters are listed in Table 1.

RESULTS AND DISCUSSION

The results obtained for the BCR CRM 482 lichen sample [9,10] are listed in Table 2. The values measured for most elements are higher than the published certified concentrations, except for Zn. The high results for the elements measured were attributed to memory effects from preceding samples rich in those elements. Thus, the data presented in Table 3 show the high levels of contamination in lichens. However, as can be seen the metal concentrations determined by the proposed method are in satisfactory agreement with the certified values.

Table 2.

Measured and certified concentrations of elements ($\mu\text{g}\cdot\text{g}^{-1}$) in BCR CRM 482 lichen sample.

Element	Certified concentration ($\mu\text{g}\cdot\text{g}^{-1}$)	Measured concentration ($\mu\text{g}\cdot\text{g}^{-1}$)
Pb	41.0 \pm 0.2	49.7 \pm 0.9
Cu	7.0 \pm 0.2	7.8 \pm 0.3
Zn	101.0 \pm 3	64.0 \pm 3
Cd	0.56 \pm 0.02	0.60 \pm 0.03
Ni	2.5 \pm 0.07	3.2 \pm 0.05
As	0.85 \pm 0.07	1.28 \pm 0.2

Tables 3 and 4 show the results of our analysis of the lichen and soil samples collected from the area studied. Mean and extreme values of the data are listed. The concentrations of contaminant elements found in lichens and soils show remarkable differences according to the different exposures to air pollution in the Zlatna region. Relative standard deviations given in Tables 3 and 4 indicate spatial or biological variation of the mean values. The variation of the concentrations found within sites differ considerably. In all our results, we are confronted by high statistical variability that indicates regional differences in airborne heavy metal pollution. Besides the pollutant element content of soil, other ecological parameters of the habitats (pH, organic matter content, etc.) governing the uptake of metals have to be taken into account.

Conclusions

The analysis of soils for the evaluation of the contaminants level of an area is very important, as are also assessment of the bioavailability and uptake by organisms. Therefore the analysis of total metal contents in soils alone is not sufficient. Lichens, due to their morphological characteristics, yield reliable data on the distribution and concentration of contaminant elements. In fact, from these data it is possible to assess deposition rates and map variations in concentration across either small or large areas. All can be done at a very low cost when compared to the traditional physicochemical techniques. Certainly, to obtain comparable results (lichen – soil) more emphasis has to be put on standardising sampling and analysis procedures.

The concentrations of pollutant elements measured in the samples studied indicate high levels of pollution in the area of the smelter. Of the pollutants investigated, Pb was the most abundant in both soils and lichens. The smelting process to recover Cu from its ores results in much particulate matter escaping to atmosphere via the chimney of the plant. Significant amount of Pb plus small amount of Cd, Ni and As are released into the environment. Lichen samples exhibited element concentrations higher than that for soil samples. It is normal, because soils are leaching and lichens are leaching too and bioaccumulators same time are.

The proposed method is efficient for determination of elements in soil samples. The main advantage offered by the fast solvent extraction of elements prior to determination are the suppression of interferences and an increase in the sensitivity by

pre-concentration of the analytes. The ability to analyse such contaminated soil samples, with little sample preparation will clearly benefit environmental waste remediation efforts. ICP-AES can be used for multielement analysis of contaminate lichen samples (in this study: Pb, Cu, Zn, Cd, Ni, Fe, Ag, As and S). The accuracy of ICP-AES has been shown to be acceptable for routine environmental soils and lichens work.

Table 3.

Minimum, maximum, mean and relative standard deviation of element contents ($\mu\text{g}\cdot\text{g}^{-1}$) found in *Cladonia floerkeana* at selected sites.

Element	Statistic	Site		
		3	4	5
Pb	minimum	1377.0	317.2	832.1
	maximum	5399.0	354.0	2571.7
	mean	3254.0	331.1	1609.5
	RSD %	62	5	55
Cu	minimum	424.7	169.4	257.7
	maximum	575.1	328.4	387.6
	mean	483.0	245.1	306.3
	RSD %	17	75	23
Zn	minimum	192.8	159.4	195
	maximum	267.4	247.1	191.6
	mean	226.5	198.1	117.2
	RSD %	16	21	76
Cd	minimum	2.6	2.9	2.0
	maximum	4.0	6.4	4.6
	mean	3.3	4.1	3.2
	RSD %	21	39	42
Fe	minimum	934.0	1016.0	1031.6
	maximum	4440.3	1825.2	5948.8
	mean	2908.0	1489.0	3575.0
	RSD %	60	23	69
Ni	minimum	4.0	3.7	7.0
	maximum	6.0	5.6	9.3
	mean	4.8	4.7	8.0
	RSD %	22	18	14
Ag	minimum	5.2	4.1	3.7
	maximum	73.0	5.4	8.3
	mean	35.5	5.0	5.7
	RSD %	96	10	41
As	minimum	16.1	0	10.3
	maximum	46.3	9.3	12.6
	mean	28.0	5.7	14.2
	RSD %	57	88	35
S	minimum	1290.8	1158.5	1192.8
	maximum	2893.1	1640.4	1989.7
	mean	2046.0	1405.0	1575.0
	RSD %	39	74	25

Table 4.

Minimum, maximum, mean and relative standard deviation of element contents of soils ($\mu\text{g}\cdot\text{g}^{-1}$) from selected sites. (not determined: n.d.)

Element	Statistic	Sites						
		1	2	3	4	5	6	7
Pb	minimum	245.5	154.1	114.7	171.1	49.0	32.7	10.6
	maximum	491.2	270.1	399.6	264.1	317.1	113.6	43.1
	mean	411.3	202.0	256.8	232.7	178.9	73.2	26.9
	RSD %	21	28	37	17	87	78	85
Cu	minimum	171.4	74.5	83.0	105.7	23.0	20.6	3.2
	maximum	339.7	282.8	252.2	233.9	118.3	45.8	10.1
	mean	223.3	162.9	152.2	157.1	68.9	32.2	6.7
	RSD %	30	55	39	39	70	56	75
Zn	minimum	9.1	10.8	11.8	47.9	8.3	5.8	1.3
	maximum	39.3	136.2	31.5	73.4	27.3	9.6	19.6
	mean	19.9	64.8	21.9	65.5	15.8	6.7	10.5
	RSD %	50	80	36	18	63	45	123
Cd	minimum	0.18	0.09	0.12	0.61	0.11	0.08	0.12
	maximum	0.50	2.89	0.28	1.33	0.40	0.20	0.59
	mean	0.27	1.33	0.19	1.12	0.22	0.14	0.36
	RSD %	44	96	42	29	77	71	83
Fe	minimum	284.8	30.7	281.2	211.5	53.4	75.7	116.2
	maximum	481.9	113.7	469.5	231.1	522.6	254.0	214.2
	mean	354.5	78.8	374.8	226.7	325.0	164.9	165.6
	RSD %	20	51	19	5	75	76	42
Ni	minimum	0.11	0.14	0.11	0.74	0.13	0.18	1.02
	maximum	0.24	0.65	0.24	1.73	1.02	0.53	1.05
	mean	0.14	0.39	0.16	1.33	0.44	0.36	1.04
	RSD %	36	67	31	32	111	69	2
S	minimum	108.9	50.0	100.8	53.9	38.4	n.d.	n.d.
	maximum	239.3	182.9	131.0	64.4	101.8	n.d.	n.d.
	mean	149.4	116.8	115.5	59.4	89.1	n.d.	n.d.
	RSD %	35	62	9	7	52	n.d.	n.d.

The high concentration of metals in the locality is damaging to soils, plants and human health. Other studies have indicated that high lead concentrations are deleterious to human health: particularly there is concern about the negative effects of lead on children – their mental abilities and growth. Both zinc and copper are bio-toxic in high enough concentrations, weakening the biological activity of vegetation and possibly damaging human health. In order to reduce emissions, the factory needs to improve its production technologies and install fume reduction equipment such as scrubbers and filters. Of course, such action is dictated by economics. Another option to reduce further damage to the environment would be to utilise bio-remediation methods: through widespread use of vegetation with a high affinity for the contaminant metals soil concentrations could be greatly reduced. In order to

reduce human exposure to the pollutants, it is necessary to educate the local population about the potential hazards and to suggest ways in which they could minimise their personal exposure.

Acknowledgements

The authors gratefully acknowledge the financial support provided by grants from the Royal Society Joint Projects with Central/Eastern Europe and the former Soviet Union grant Ref: rc/jp/nov.

REFERENCES

1. M.S. Cresser, L. Ebdon, J.R. Dean, *J. Anal. Atom. Spectr.*, 1989, **4**, 1R.
2. K.J. Puckett, *Lichens, bryophytes and air quality*, Nash III, T.H., Wirth, V.(eds.)Bibliotheca Lichenologica Berlin and Stuttgart: Cramer, 1988, Vol. 30, 231-267.
3. P.W. James, *Air pollution and lichens*, B.W. Ferry, M.S. Baddeley, D.L. Hawksworth, (eds.), London, The Athlone Press, 1973, 143-175.
4. B.J. Williamson, O.W. Purvis, K.Bartok, N. Har, E. Manolache, D. Jones, C. Stanley, N. Vlad, *Studia Univ. Babeş-Bolyai, Geologia*,1996, **XLI**, **1**, 87-93.
5. K. Bartók, A. Nicoara, V. Bercea, T. Osvath, *Rev. Roum. Biol. Biol. Veget.*, 1992, **37(2)**, 135-143.
6. O.W. Purvis, B. Williamson, K. Bartok, N. Zoltani, *New Phytologist* 2000, **147**: 591-599.
7. A.M. Rusu, K. Bartok, B. Dubbin, W. O. Purvis, *Studia Univ. Babeş-Bolyai, Chimia*, 2000, in press.
8. D.E. Baker, M.C. Amaker, Nickel, Copper, Zinc and Cadmium. In A.L.Page *et al.* (eds). *Methods of soil analysis*. Part 2, 2nd edition. American Society of Agronomy, Madison, WI, USA, 1982 p.331 – 333.
9. M. Bettinelli, S. Spezia, G. Bizzarri, 1996, **17**: 133-141
10. P. Quevauvillier, R.Herzig, H. Muntau, *Sci. Total Environ*, 1996, **187**: 143-152.

THE ACID CATALYSED HYDRATION OF 1-ISOPROPYL-4- METHYLENEBICICLO [3.1.0] HEXANE (SABINENE). THE SYNTHESIS OF THE TERPINEN-4-OL

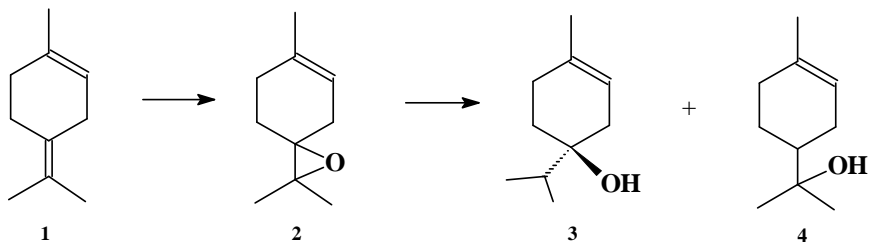
IOAN CRISTEA*, ERIKA KOZMA and ANAMARIA RIȚIU

*Universitatea "Babeș-Bolyai", Facultatea de Chimie și Inginerie Chimică
Catedra de Chimie Organică, Str. Arany Janoš, nr. 11, 3400 Cluj-Napoca,
Romania, Fax:40-64-190818, e-mail: cristea@chem.ubbcluj.ro*

ABSTRACT. The acid catalysed hydration of (+)-sabinene, using various acids in aqueous acetone at 30°C for 50 hours, gave (+)-terpinen-4-ol as a main product (80%), α - and γ -terpinene (about 15%), p-cymene (6-10%) together with trace quantities of unidentified materials.

INTRODUCTION

Terpinen-4-ol (**3**), was identified by Wallach [1], as the one present in majoram oil from *Origanum majorana* L. This alcohol is a constituent of numerous essential oils and occurs in the dextro modification: $[\alpha]_D +17^0$ (homo.). It is used as an important additive in the perfume industry. Because of its importance, several syntheses of this compound has been reported [2-4]. Terpinen-4-ol can be prepared from terpinolene, α -thujene and sabinene. The manufacture of this alcohol utilizes a novel method using a terpinolene (**1**) as a starting material [5-7].

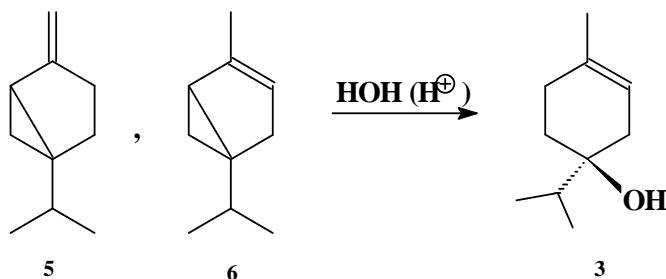


Terpinolene is epoxidized with peracetic acid in methylene chloride to give 94% 4,8-epoxy terpinolene (**2**). Lithium aluminium hydride reduction of the epoxide produces simultaneously terpinen-4-ol (**3**) and α -terpineol (**4**), the former constituting 60% of the alcohol mixture. By this method, only the racemic terpinen-4-ol is obtained.

A modification of this method consists in treating the epoxide with aq. 40% Me_2NH at 140°C, followed by hydrogenation of the exocyclic double bond to give terpinen-4-ol in 50% yield [5]. Another method performed in the synthesis of the terpinen-4-ol starts from sabinene (**5**) and α -thujene (**6**) [3]. The acid catalysed hy-

dration of the two bicyclic olefins affords terpinen-4-ol. A variety of acids can be used, the most notable being sulphuric, benzene sulphonic, formic and oxalic acids. Sabinene is hydrated more rapidly than α -thujene by a factor of 20:8 at 45°C and appears to be the most suitable raw material for the alcohol production. [4].

By hydrogenation and hydroboration, Brown [8] has suggested that sabinene is stabilised by greater conjugation between the double bond and the cyclopropane ring.



Tolstikov [2] has studied the hydration of sabinene (95% purity) in water and 2-5% H_2SO_4 for 50 hours at 25°C to obtain terpinen-4-ol in 65% isolated yield. Norin et al [3] were also prepared terpinen-4-ol in 70% yield (glc analysis), by hydration of sabinene in aqueous dioxane (75%), using perchloric acid as catalyst.

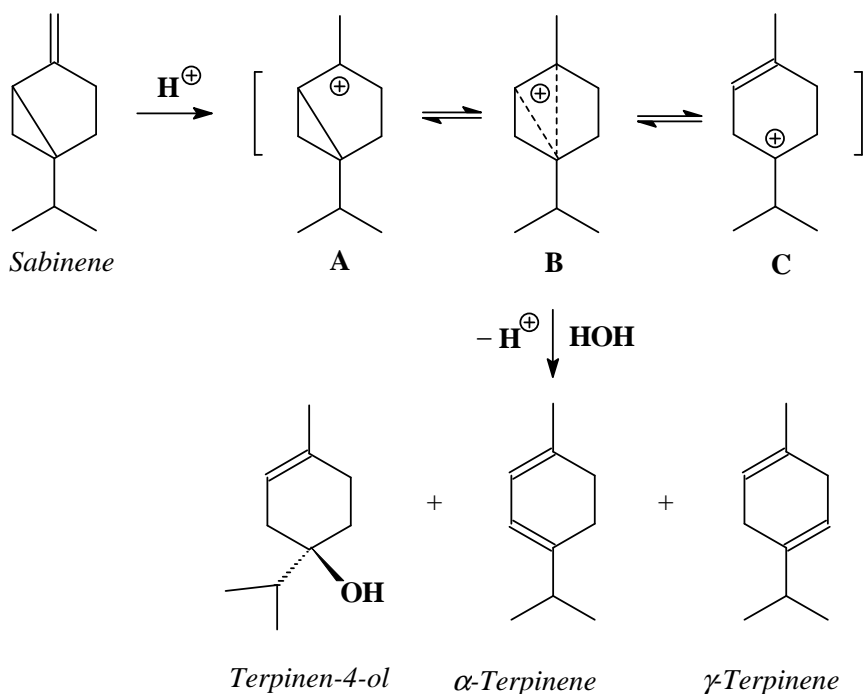
RESULTS AND DISCUSSION

In the present paper, we wish to report some results in the acid catalysed hydration of (+)-sabinene (75% purity). In our investigation, the hydration was performed in aqueous acetone (75%) using various acids: sulphuric acid, HClO_4 , p-TsOH, HPA (heteropoly acids). The reaction was monitored by GC-MS analysis using 20m methylsilicone capillary column. The reaction conditions and product composition are shown in Table 1.

The best results were obtained using sulphuric acid as catalyst. Thus, sabinene (75% purity) reacts in acetone-water solution and 0.02M H_2SO_4 at 30°C for 50 hours to give terpinen-4-ol in 80% yield (determined by GC-MS analysis), 12% γ -terpinene and 6% p-cymene respectively, with a conversion of 95% (see Table 1, run 2).

α -Terpinene was detected in very small amount, only 3%. Increasing the concentration of sulphuric acid (see Table 1, run 5) the yield of the terpinen-4-ol decreased, but increased slowly the yield of γ -terpinene (from 12% to 18%) and α -terpinene. These olefins are probably obtained by the dehydration of the terpinen-4-ol, formed during this reaction.

ACID CATALYSED HYDRATION OF SABINENE



Scheme 1

Table 1.

Reaction conditions for hydration of sabinene^a

Run	Catalyst conc. (M)	GC peak area%		Conversion % ^d		
		terpinen-4-ol	γ -Terpinene	p-cymene	Others ^b	
1	0.01 H ₂ SO ₄	53.3	7.5	3.4	35.8	86
2	0.02 H ₂ SO ₄	76.2	12.4	6.6	24.8	95
3	0.03 H ₂ SO ₄	50.7	16.7	9.5	23.1	84
4	0.05 H ₂ SO ₄	41.4	18.6	10.4	29.6	80
5	0.02 HClO ₄	42.2	14.5	7.8	35.5	81
6	0.04 HClO ₄	46.7	17.6	7.9	27.8	84
7	0.02 pTsOH	31.2	9.4	6.3	53.1	85
8	0.02 W-HPA ^c	32.3	4.2	3.2	60.3	89

^a All experiments were performed in aqueous acetone (75%), at 30^oC, for 50 h.

^b Others consisted of unreacted sabinene and unidentified products.

^c (NH₄)₅H₄[PMo₆V₆O₄₀]

^d Reported to (+)-sabinene 75%

As shown in Scheme 1, three ions in equilibrium (two carbenium ions **A**, **C** and a carbonium ion **B**) can be obtained by the protonation of the sabinene. The

hydration of (+) sabinene takes place with a high retention of configuration at C₁. The terpinen-4-ol produced from optically active sabinene has been shown to retain 80% of the optical activity of the starting material [3]. The stereospecificity in the formation of (+)-terpinen-4-ol is in complete agreement with the carbonium ion **B**, which is the main intermediate in this rearrangement. Thus, there must be extensive charge delocalisation in the rearrangement, and a classical charge-localised ion (**A** or **C**) can be ruled out as a main product-determining intermediate. However, some racemic alcohol is also formed, which thus would suggest that the classical charge-localised ion **C** is also involved in this reaction. Ring opening could also take place to give the ion **C**, which can lose a proton to lead to the observed olefins, but there is no evidence to support this route [9].

The kinetic study of the hydration of sabinene will be the topic of a next paper.

EXPERIMENTAL

Gas chromatography-mass spectroscopy (GC-MS) coupling analyses were performed on a Hewlett-Packard 5890 (GCL)-5972 (MSD) using a HP-5MS 20m x 0.25 x 0.25 μ m capillary. (+)-Sabinene, (+)-terpinen-4-ol and terpinolene were purchased from Aldrich. TLC was performed with Merck Kieselgel 60F 254, using petroleum ether:ether 5:2 as eluent.

Acid-catalysed hydration.

To a stirred solution of (+)-Sabinene (0.1 mol, 75% chemical purity, $[\alpha]_D^{20}=+78^\circ$, $c=1, \text{CHCl}_3$) in 120 ml acetone, 20 ml H₂O (2% H₂SO₄) was dropwise added for 30 min., and the solution was then stirred at 30^oC for 50 hours. The reaction mixture was neutralized with 1M NaHCO₃, then the solvent removed by distillation. The residual liquid was extracted with ether, dried on MgSO₄, filtered and final reaction product was analyzed by GC-MS (see Table 1). The pure terpinen-4-ol was obtained by vacuum distillation at 85-87^oC/14mmHg (59% isolated yield reported to starting material).

Dehydration of terpinen-4-ol.

Terpinen-4-ol (1g) in 30ml benzene and p-toluenesulphonic acid (0,1g) were refluxed for 1 hour, and the water resulted in the reaction was removed using a Dean-Stark trap. The reaction mixture was diluted with water, neutralized with 1M NaHCO₃, extracted with ether, dried on MgSO₄, then analyzed by GC-MS. γ -Terpinene (67%), α -terpinene (25%) and p-cymene (8%) were obtained.

The terpinen-4-ol (1g) was also dehydrated with 30% H₂SO₄ (20ml) at 100^oC for 0,5 hours to give γ -terpinene (52%), α -terpinene (15%) and p-cymene (30%) respectively.

REFERENCES

1. J.Wallach, (a) *Annalen*, 1906, **350**, 168; (b) *Annalen*, 1907, **356**, 206; (c) *Ber.* 1907, **40**, 596.
2. G.A.Tolstikov, L.N.Lishtranova, and M.I.Goryaev, *Zhur.Obshchei Khim.*, 1963, **33**, 683.
3. T.Norin, L.A.Smedman, *Acta Chem.Scandinavica*, 1971, **25**, 2010
4. M.A.Cooper, C.M.Holden, P.Loftus, and D.Whittaker, *J.Chem. Soc. Perkin II*, 1973, 665.
5. J.C.Leffingwell, *Fr.Demande* US 2,003, 498; C.A.1970, **72**, 100934n
6. E.Klein, *Ger.1*, 235, 306; C.A.1967, **67**, 64579m
7. Klein, Farnow, and Rojahn, *Dragoco Report*, 1965, **12**, 99.
8. S.P.Acharya, H.C.Brown, A.Suzuki, S.Nozaawa, and Itoh, *J.Org.Chem.*, 1969, **34**, 3015
9. D.V.Banthorpe and H.S.Davies, *J.Chem.Soc.*, 1968, **B**, 1339

FLAME ATOMIC EMISSION DETERMINATION OF POTASSIUM IN NATURAL WATERS WITH THE METHANE-AIR FLAME AS EXCITATION SOURCE

LADISLAU KÉKEDY-NAGY and EMIL A. CORDOȘ

*Universitatea "Babeș-Bolyai" Facultatea de Chimie și Inginerie Chimică
3400 Cluj-Napoca, Arany J. 11, România*

ABSTRACT. The potassium content of some natural (well and mineral) waters and drinking water (tap) has been determined by flame atomic emission spectrometry using the methane-air flame. Effects of the flame and of instrumental parameters (flame composition, the observation height, the spectral bandpass of the monochromator) on the emission of potassium in methane-air flame was studied and optimized. The best results were obtained using the 766.4 nm potassium line at the observation height of 11 mm, with the flame composition of 1.12 (relative stoichiometric units, RSU) and the slit width of 0.7 mm. The effect of Li, Na, Rb, Cs, Mg, Ca, Sr, Al, Cl⁻, SO₄²⁻, PO₄³⁻ and ClO₄⁻ on the emission of potassium was studied too. The detection limit of $0.3 \pm 0.04 \mu\text{g.l}^{-1}$ was obtained, in the presence of 200 mg.l^{-1} Cs, at a significance level of 0.05 using the two-step Neyman-Pearson criterion. The potassium content of waters has been determined directly using both external calibration curve and standard addition method. The results agree between these two methods.

INTRODUCTION

Flame atomic emission spectrometry (FAES) is a fast, simple, recommended method for the determination of potassium content of different waters. Usually as excitation source, the high temperature C₂H₂-air, C₂H₂-O₂, H₂-O₂ flames are used. The optimal flame conditions for the determination of potassium in these flames were established, the detection limits are of order of $0.1 \mu\text{g.l}^{-1}$ [1-13]. Propane-butane-air (PB-A) and the natural gas-air (NG-A) flames are used in low performance commercial flame-photometers. These flames have a lower temperature than the former ones and from this point of view lie between the hot and cool flames. The methane-air (M-A) flame has similar properties (temperature, burning velocity etc) with the PB-A, NG-A flames [14, 15]. To our best knowledge the behaviour of potassium in the M-A flame was not studied and the determination of potassium content of natural waters using the M-A flame was

not reported. The aim of this work is to study the behaviour of this element in the M-A flame, to optimize instrumental parameters and the determination of potassium in natural waters, respectively.

EXPERIMENTAL

The optimal flame and instrumental parameters were determined, as follows: 1. Determination of the emission spectrum of potassium in the M-A flame; 2. Determination of the optimal values of flame parameters (flame composition, observation height over the burner head (h)) in the flame; 3. Then, the detection limit was determined under optimized conditions. Finally, the potassium content of some natural waters was determined.

INSTRUMENTATION

The instrumental setup was the same as described earlier [16].

CHEMICALS

Stock solutions of K, Na, Li, Rb, Cs (used as ionization suppressor), Ca, Mg, Sr and Al were of 1000 mg.l^{-1} , prepared from RbCl, CsCl, Li_2CO_3 (Merck, Darmstadt, Germany), NaCl, KCl (Reactivul, Bucuresti, Romania), CaCO_3 , SrCO_3 , Al and Mg (Specpure, Johnson Matthey Chemicals Limited, England), HCl, H_2SO_4 , HClO_4 and H_3PO_4 (analytical grade, Merck, Darmstadt, Germany)), respectively. The calibration solutions were obtained by diluting a given volume of stock solution with double distilled water. The diluted solutions were prepared just before measurements. The natural water samples of 350 ml were conserved with 1 ml of conc. HCl (analytical grade, Merck, Darmstadt, Germany).

SAMPLING AND SAMPLE HANDLING

The well water samples were collected in village Săvădisla (county Cluj), located 24 km far north-west from Cluj-Napoca city. The waters were sampled and handled in accordance with the EPA-recommendations [17]. All determinations were carried out within 72 hours after sampling. The mineral waters (commercial available, "Izvorul Minunilor", "Anavie", "Borsec", "Perla Harghitei") were analyzed after the sealed bottles were opened and degassed by shaking. All water samples were diluted properly before measurements. The solutions were prepared just before the measurements.

PROCEDURE

The behaviour of potassium in the M-A flame was studied up to $h = 18 \text{ mm}$ over the burner head in 1 mm steps, at three different flame compositions: 0.88; 1.00; 1.12 (expressed in relative stoichiometric units). Four replicate measurements were made, the mean and the standard deviation, the S/N and the S/B ratios were calculated for each h and flame composition. The homogeneity of the means was tested by the F test at a significance level of 0.05. The sensitivity of the strip chart recorder was different in different spectral domains, in function of the

intensity of the emission lines and the background observed. For a given set of determinations the sensitivity was kept constant.

RESULTS AND DISCUSSION

THE EMISSION SPECTRUM OF POTASSIUM, DETERMINATION OF THE ANALYTICAL EMISSION LINE

First the emission spectrum of potassium was determined by recording the spectrum of the flame alone, then that of the flame in the presence of potassium by nebulizing a solution of 100 mg.l^{-1} potassium in the flame. The composition of the flame was kept constant, 1.12. The investigated spectral range was 200 – 800 nm, the scanning rate of the monochromator being 0.02 nm/sec. Comparing the spectrum using spectral tables there were identified the emission lines with wavelengths of 404.4 nm, 404.7 nm, 766.4 nm and 769.9 nm [18]. These are all atomic lines, the most intensive ones being the doublet of 766.4 nm and 769.9 nm, respectively. The first two lines are superimposed on a high background of the flame, the background at the higher wavelengths is insignificant.

The change of the analytical signal versus h at the wavelengths of 404.4 nm, 766.4 nm and 769.9 nm was studied further. The concentration of the calibration solutions was different, in function of the intensity of potassium emission line under the study, and the background intensity at the given wavelength. The background intensity was measured in the presence of potassium only in the case of the shorter wavelength doublet, at 404.0 nm. The variation of the net emission signal of different potassium lines versus h over the burner head is represented in Fig.1.

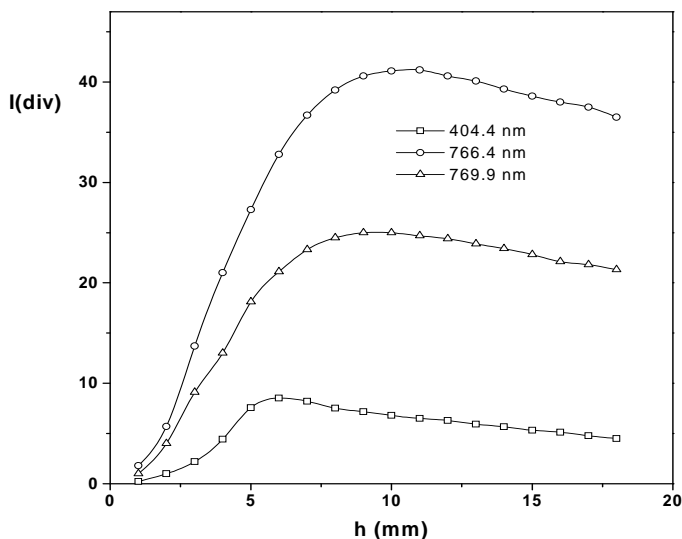


Figure 1. Variation of the net emission signal of different potassium lines versus h .

For the quantitative comparison of the results obtained at different wavelengths only the maximum value of the analytical signal (I) for each line was selected. In order to get comparable data the corrected intensity (I_{corr}) and the relative intensity (I_{rel}) for each line was calculated, taking account of the concentration of the calibration solution, and the sensitivity of the chart recorder used. The reference concentration was of 100 mg.l^{-1} , the sensitivity of 1.10^{-9} A/div and the reference line was the weakest one. The S/B ratio was determined in the same way, the reference concentration being the highest one used. The results are summarized in Table 1.

Table 1

The relative intensities of the emission lines of potassium in the M-A flame

Wavelength (nm)	I (div)	h (mm)	I_{corr}	I_{rel}	S/N	S/B
404.4	33.5	10	67.0	1.00	43.5	2.86
766.4	41.7	11	417.0	6.22	426.9	4170.0
769.9	25	11	250.0	3.73	385.7	2500.0

The 404.4 nm line is weak, more intensive lines are at longer wavelength, the most intensive being that of 766.4 nm. The intensity of these lines varies in the same manner as the translational temperature of the flame, the maximum intensity being at 10-11 mm over the burner head [19].

In conclusion the analytical emission line for potassium in the M-A flame is that of 766.4 nm at $h = 11 \text{ mm}$. The S/B ratio at this wavelength is high too, due to the low value of the background.

DETERMINATION OF THE OPTIMAL VALUES OF THE FLAME COMPOSITION AND THE HEIGHT OF OBSERVATION OVER THE BURNER HEAD

The influence of the flame composition, on h , on the analytical signal and S/N ratio for the most sensitive line was studied, at the concentration level of 10 mg.l^{-1} . The data were processed by using the MicroCal Origin™ Software package, version 5 (MicroCal Software Inc., MA, USA) and plotted as 2D contour map (Fig.2).

The results show, that the maximum intensity is obtained in all cases at the same $h = 11 \text{ mm}$ over the burner head, regardless of the flame composition. The analytical signal decreases with the decrease of the methane content in the flame. The standard deviations of all means are homogeneous, therefore the magnitude of the S/N ratio is decided by the magnitude of the mean. In conclusion, the optimal conditions for the quantitative determination of potassium in the M-A flame are $\lambda = 766.4 \text{ nm}$, $h = 11 \text{ mm}$, flame composition of 1.12.

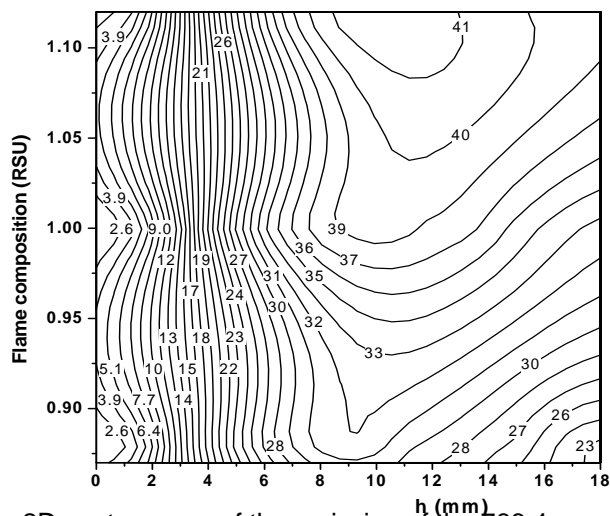


Figure 2. The 2D contour map of the emission of the 766.4 nm potassium line vs. observation height and flame composition. The data labels on the plot indicate the grid matrix values.

THE INFLUENCE OF THE SPECTRAL BANDPASS OF THE MONOCHROMATOR ON THE ANALYTICAL SIGNAL, S/N AND S/B RATIO

The spectral bandwidth of the monochromator, determined by its width of the slit (SW), influences both the amplitude and the fluctuations of the emission signal in different manner. Therefore the optimal slit width for which the S/N ratio is maximum can be determined. The flame and instrumental parameters used were the optimal ones, determined earlier. The influence of the slit over I and S/N ratio was studied in the 0.1-1.5 mm domain in steps of 0.1 mm. The analytical signal exhibits almost a linear variation with the slit width up to 1.5 mm, the I-SW relationship could be approximated best with a second order polinomial function ($I = -1,18 + 28,12 SW + 6,43 SW^2$, $r^2 = 0.999$). The standard deviation of the means is homogeneous up to a width of 0.7 mm, then they differ significantly. The highest value for the S/N ratio was found at a value of the width of 0.7 mm. In conclusion, the width of the slit could be increased up to 0.7 mm without decay of the S/N ratio.

INTERFERENCES

The effect of Li, Na, Rb, Cs, Ca, Sr, Mg, Al, Cl⁻, SO₄²⁻, PO₄³⁻ and ClO₄⁻ ions on the emission signal of potassium of 5 mg.l⁻¹ was investigated, up to a concentration of the interferent of 500 mg.l⁻¹. Some of these elements and ions are potential inorganic interferents, present in natural waters in higher concentration. The optimal experimental conditions were described in a previous paragraph. The background signal was measured at 767.5 nm in the presence of the interferent. The variation of the emission signal of potassium versus the concentration of the interferents is represented in Fig. 3.

The alkaline metals, possessing a lower excitation and ionization energy than that of potassium (Rb, Cs), enhance the emission signal of potassium up to a concentration of 100 mg.l^{-1} , acting as ionization suppressor. Ca enhances the potassium emission signal too, acting as releasing agent. This effect could be attributed to the shift of the chemical equilibrium concerning formation of the more stable CaOH than that of KOH in the flame. Al and PO_4^{3-} decrease significantly the potassium emission. The other interferents do not influence the potassium emission, even at higher concentrations. ClO_4^- do not influence the emission of potassium, fact which suggests the free evaporation of potassium from the condensed phase in the M-A flame.

CALIBRATION, DETERMINATION OF THE DETECTION LIMIT

For the determination of the detection limit the variation of the analytical signal versus concentration was studied. Seven calibration curves were plotted, in the $10 - 10^2 \text{ mg.l}^{-1}$ potassium concentration range. One curve covers only one order of magnitude of concentration. Each calibration curve was established by using six standard solutions. Six replicate measurements were made at each concentration level. There were tested the homogeneity of means and the linearity of the calibration curve, the equation of the regression line, the confidence limits and the coefficient of correlation (r^2), with the least squares method were calculated. The detection limit was calculated using the two-step Neyman-Pearson criteria [20,21]. For the fixed values of $(P_{10})_0 = 0.025$ and $(P_{11})_d = 0.975$ the S/N ratio has the value of 3.92. The results are summarized in Table 2.

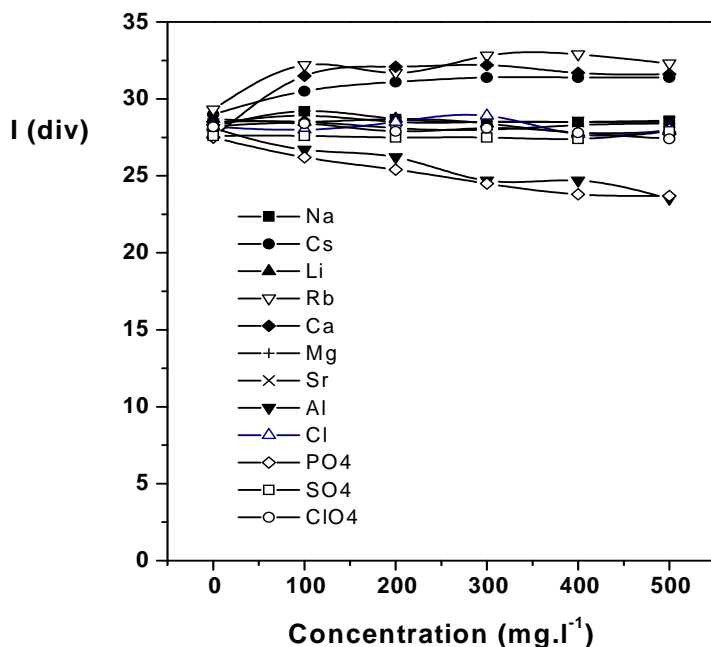


Figure 3. Influence of Li, Na, Rb, Cs, Ca, Sr, Mg, Al, Cl, SO_4^{2-} , PO_4^{3-} and ClO_4^- on the emission of potassium of 5 mg.l^{-1}

Table 2

Calibration curves and detection limits

Nr. eq.	Concentration range potassium (mg.l^{-1})	Slit width (mm)	Equation of the calibration curve	Detection limit (mg.l^{-1})
1	1 – 4	0.1	$I = 16.03 + 5.20C$ $r^2 = 0.9998$	not determined
2	6 - 10	0.1	$I = -2.05C + 9.00C$ $r^2 = 0.9994$	not determined
3 [@]	1 – 10	0.1	$I = -1.7 + 2.47C$ $r^2 = 0.9999$	0.08 ± 0.05
4	0.1 – 1	0.1	$I = -0.5 + 8.56C$ $r^2 = 0.9992$	0.025 ± 0.017
5	0.1 – 1	0.1	$I = 0.6 + 12.14C$ $r^2 = 0.9992$	0.060 ± 0.033
6	0.01 – 0.1	0.1	$I = 0.1 + 35.23C$ $r^2 = 0.9907$	0.006 ± 0.004
7	0.01 – 0.1	0.7	$I = 0.3 + 467.23C$ $r^2 = 0.9997$	0.001 ± 0.0007
8	0.001 – 0.01	0.7	$I = -0.1 + 645.47C$ $r^2 = 0.9933$	0.0003 ± 0.00004

* with Cs added, in final concentration of 200 mg.l^{-1}

@ burner held perpendicular to the optical axis, optical path 8 mm through the flame

In the $1 - 10 \text{ mg.l}^{-1}$ concentration domain no linear relationship exists between concentration (C) and intensity (I). Linear relationship persists only in the $1- 4 \text{ mg.l}^{-1}$ (eq.(1)) and $6-10 \text{ mg.l}^{-1}$ domain, respectively (eq.(2)). The calibration equation (3[@]) plotted in the same concentration range (with burner held perpendicular to the optical axis) could be approximated with the straight line at the chosen significance level. In the lower concentration ranges (eq.(4) - (7)) this phenomenon disappears even in long optical path in the flame. This fact suggests the presence of the line reversal phenomenon as main source of the nonlinear relationship between C and I. In order to enhance the potassium emission, a Cs solution was added to each calibration solution, in the concentration of 200 mg.l^{-1} . The increased slit width allows the signal enhancement and the extension of the usable concentration more than one order of magnitude. The detection limit obtained for each concentration range is also summarized in Table 2. The lowest detection limit, of $0.3 \pm 0.04 \mu\text{g.l}^{-1}$, obtained with the M-A flame is the same order of magnitude with those obtained with the hotter ($\text{C}_2\text{H}_2\text{-air}$, $\text{C}_2\text{H}_2\text{-O}_2$, $\text{H}_2 - \text{O}_2$) flames.

DETERMINATION OF POTASSIUM IN WATER SAMPLES

The potassium content of the water samples was determined by calibration and the standard addition method, the later being used as reference method for the method validation, due to the absence of certified reference material. The

determinations were carried out keeping the burner perpendicular to the optical axis, with the SW of 0.1 mm. The other parameters were the optimal ones. Four parallel measurements ($n=4$) were made everywhere. To minimise the effect of the interferences and to bring the final concentration of the sample within the linear range the samples were properly diluted before measurements. The measuring sample solutions were prepared in 25 ml volumetric flasks. In the case of standard addition method 100 μl of concentrated potassium standard was added to the 25 ml of diluted sample. Three additions of standard were made, in 1 $\text{mg}\cdot\text{l}^{-1}$ concentration steps. The potassium content was determined from the intercept with the abscissa of the regression line. Using the data set, the reproducibility of the standard addition method was tested first. The recoveries found were within 83.2 - 105.3%, the slope of regression lines being close to that obtained by calibration. The results of the two methods (Table 3) agree within the error of determinations for the given water, so the calibration method could be used for potassium quantification.

Table 3Results of analysis of water samples ($n=4$)

Sample		Dilution	Concentration ($\text{mg}\cdot\text{l}^{-1}$, calibration)	Concentration ($\text{mg}\cdot\text{l}^{-1}$, standard addition)
Tap water		1:1	2.0 ± 0.6	2.1 ± 0.7
Mineral water	“Anavie”	1:20	21.0 ± 1.8	20.2 ± 2.1
	“Izvorul Minunilor”	1:20	1.4 ± 0.6	1.9 ± 0.8
	“Perla”	1:20	11.8 ± 1.7	11.9 ± 1.6
	“Borsec”	1:20	15.9 ± 1.7	16.0 ± 1.7
Well water	Nr. 1	1:20	3.9 ± 0.9	3.9 ± 0.8
	Nr. 2	1:20	3.0 ± 0.9	2.2 ± 0.8
	Nr. 3	1:20	6.9 ± 1.1	7.4 ± 0.9
	Nr. 4	1:40	36.4 ± 1.7	37.0 ± 1.6
	Nr. 5	1:20	18.1 ± 1.8	18.9 ± 1.8
	Nr.6	1:100	168 ± 4	169.3 ± 5

The mineral water “Perla” and “Anavie” have different potassium content, originating from other region of the country (as indicated on the label of the bottles). The well water samples no.1, 2 have practically the same potassium content, the wells being sunk very close one to the other (about 20 meters). This suggests that the wells are supplied from the same ground water source. The other samples (no.3-6) have significantly higher potassium content (sample no.6 having a fifty-fold higher potassium content).

The rubidium content of these waters has been determined earlier [16]. In the case of mineral and well waters (samples no.1, 2) the potassium and rubidium content varies in the same manner, the K/Rb concentration-ratio being close (2041 and 2951 for mineral waters, 684 and 545 for well waters, respectively). The high potassium and rubidium content of sample no.6 (the K/Rb concentration-ratio is also high, being of 12923) clearly shows that the well is supplied from an other

ground water source than the others, the wells are sunk in rocks with different geological structure and chemical composition.

In conclusion, the potassium content of natural waters can be determined directly by calibration method in the M-A flame with acceptable precision.

CONCLUSIONS

In the M-A flame potassium exhibits only an atomic spectrum. The most intensive line (the analytical line) is at 766.4 nm. The optimal excitation zone is at 11 mm over the burner head, in fuel rich conditions. The observation height for the maximum intensity is independent of the flame composition. In order to increase the S/N ratio, and lower the detection limit, the width of the slit of the monochromator could be increased till 0.7 mm without decay of the S/N ratio. The calibration curves for the 766.4 nm potassium line are linear in the 4 - 0.001 mg.l⁻¹ concentration range, the detection limit obtained is of 0.3 ± 0.04 µg.l⁻¹ potassium. The ionization of potassium can be suppressed with 200 mg.l⁻¹ of Cs. The potassium content of natural waters can be determined directly with acceptable precision using the calibration method.

REFERENCES

1. P.B.Adams, *Anal.Chem.*, 1961, **33**, 1601.
2. M.G.Reed, A.D.Scott, *Anal.Chem.*, 1961, **33**, 773.
3. R. Henrion, G. Henrion, A. Arndt, *Fresenius'J.Anal.Chem.*, 1993, **345**, 8.
4. J.D. Winefordner, *Spectrochemical methods of analysis*, New York., Wiley Interscience, 1971, p.130.
5. I.Kojima, C.Iida, *Analyst*, 1982, **107**, 1000.
6. V.Otruba, J.Jambor, L.Sommer, *Chem.Listy*, 1983, **77**, 994.
7. C.W.McLeod, P.J.Worsfold, A.G.Cox, *Analyst*, 1984, **109**, 327.
8. G. Schwedt, *LaborPraxis*, 1990, **14**, 620.
9. W.Frenzel, D.Schepers, G.Schulze, *Anal.Chim.Acta*, 1993, **277**, 103.
10. M.Angel de la Fuente, M.Juarez, *Analyst*, 1995, **120**, 107.
11. Z.X.Xu, S.Q.Gong, *Guangpuxue. Yu.Guangpu Fenxi*, 1995, **15**, 81,111.
12. J.L.F.C.Lima, C.D.Matos, M.C.V.F. Vaz, *At.Spectrosc.*, 1996, **17**, 196.
13. S.M.V.Fernandes, A.O.S.S.Rangel, J.L.F.C.Lima, *J.Agric.Food.Chem.*, 1997, **45**, 1269.
14. A.G. Gaydon, H.G. Wolfhardt, *Flames, their Structure, Radiation and Temperature*, Chapman and Hill, New York, 1970.
15. C.S.Mc.Enally, L.D.Pfefferle, R.K.Mohammed, M.D.Smoke, M.B.Colket, *Anal. Chem.*, 1999, **71**, 364.
16. L.Kékedy-Nagy, E.A.Cordoş, *Talanta*, 2000, **52**, 645.

17. *Standard Methods for examination of water and wastewater*, 17th Edition, Ed. L.S.Clesceri, A.E.Greenberg, R.R Trussel, 1-30, 1989 APHA – AWWA – WPCF.
18. R. Mavrodineanu, H. Boiteux, *Flame spectroscopy*, John Wiley, New York, 1965.
19. E. Cordoș, L. Kékedy-Nagy, *Studia*, 1992, **37**, 61.
20. C. Llteanu, I. Rîcă, *Statistical Theory and Methodology of Trace Analysis*, John Wiley, New York, 1980.
21. D.L. Massart, B.G.M. Vandeginste, S.N. Deming, Y. Michotte, L. Kaufman, *Chemometrics: a textbook*, Elsevier, New York, 1988.

FLAME ATOMIC ABSORPTION DETERMINATION OF ZINC IN NATURAL WATERS USING THE METHANE - AIR FLAME

LADISLAU KÉKEDY-NAGY AND EMIL A. CORDOȘ

*Universitatea "Babeș-Bolyai" Facultatea de Chimie și Inginerie Chimică
3400 Cluj-Napoca, Arany J. 11, România*

ABSTRACT. The zinc content of some natural waters (river, well, sea, mineral water) and drinking water (tap) has been determined by flame atomic absorption spectrometry using the methane-air flame. The effect of hollow-cathode lamp current, the flame composition and the observation height in the flame on the absorption of zinc in the methane-air flame was studied at 213.9 nm. The best results were obtained with the lamp current of 3 mA, at the observation height of 7 mm, with the stoichiometric flame. The effect of Na, K, Ca, Mg, Al, ClO_4^- , SO_4^{2-} , and PO_4^{3-} on the absorption of zinc was studied too. The detection limit of $0.006 \pm 0.004 \text{ mg.l}^{-1}$ was obtained at a significance level of 0.05, using the two-step Neyman-Pearson criterion. The zinc content of waters has been determined with the calibration curve and the standard addition method. In the case of low mineralization natural water the results of two methods agree.

INTRODUCTION

Zinc is a widespread element in litho-, hidro- and biosphere. Its mean concentration in Earth crust is of 45 mg.kg^{-1} , in sea and surface water of $10 \text{ }\mu\text{g.l}^{-1}$. Zinc is an essential element of all living organisms, taking part as the inorganic component of more than 100 of vital enzyme [1]. Flame atomic absorption spectrometry (FAAS) is an adequate, sensitive method for the determination of zinc in low concentrations. Usually the high temperature C_2H_2 -air, C_2H_2 - O_2 and C_2H_2 - N_2O flames are used as atomic source. The optimal conditions of the determination of zinc in these flames were established, the detection limits being of order of 10^{-2} - $10^{-4} \text{ mg.l}^{-1}$ [2-16]. The low temperature ($\sim 2000 \text{ K}$) propane-butane-air (PB-A) flame was used in few cases for the determination of zinc, mostly in early stage of the flame atomic absorption spectrometry development [17-19]. The methane-air (M-A) flame has similar properties (temperature, burning velocity etc) with the PB-A flame [20]. To our best knowledge the behaviour of zinc in the M-A flame was not studied, and the detection limits are not known. The aim of this work is to study the behaviour of zinc in the M-A flame, to optimize the flame and instrumental parameters and the determination of zinc in natural waters, respectively.

EXPERIMENTAL

INSTRUMENTATION

The measurements were carried out at 213.9 nm with a single beam HEATH-701 (Heath Co., Benton Harbor, MI, USA) spectrophotometer using a zinc hollow-cathode lamp (NARVA, Germany), a HEATH EU-700 scanning monochromator, a HEATH EU-700-30 type photomultiplier module and a 1P28A (RCA, USA) photomultiplier (-700 V). The photomultiplier signal was recorded with a K-201 (Carl Zeiss Jena) strip chart recorder. The pneumatic nebulizer-spray chamber-burner system was used from an AAS-1 (Carl Zeiss Jena) atomic absorption spectrophotometer. The original slot type burner-head (for C₂H₂-air flame) was replaced with a similar, Mecker type, developed by us for atomic absorption measurements in the M-A flame [21]. In order to increase the nebulization efficiency the original 8 mm glass ball impactor was replaced with an 1 mm cylindrical one, placed at optimal distance of 5 mm from nebulizer head [22]. The air flow-rate was kept constant, 500 L/h, the flow rate of the methane being varied as a function of the gas mixture wanted. As CH₄ source the city gas of 99 % purity was used, from the pipe.

CHEMICALS

Stock standard solutions (1000 mg.l⁻¹) were prepared by dissolving the appropriate amounts of metals (Zn, Mg and Al (Specpure, Johnson Matthey Chemicals Limited, England)) and compound (CaCO₃, Specpure, Johnson Matthey Chemicals Limited, England) in corresponding acid. KCl, NaCl (analytical grade, Reactivul, Bucuresti, Romania), HCl, H₂SO₄, HClO₄ and H₃PO₄ (analytical grade, Merck, Darmstadt, Germany)) were dissolved and diluted in double distilled water, respectively. For further dilutions double distilled water was used in all cases.

SAMPLING AND SAMPLE HANDLING

The river, sea and well waters were sampled and handled in accordance with the EPA-recommendations [23]. All determinations were carried out within 48 hours after sampling. The drinking water (tap water) from the laboratory was acidified and analysed just after sampling. The mineral waters (commercial available, "Anavie", "Borsec", "Perla") were analyzed after the sealed bottles were opened, acidified and degassed by shaking. The samples were diluted 1:1 before measurements. The pH of all the measuring solutions was of 1.5 - 2, in accordance with the literature data [2, 23].

PROCEDURE

The behaviour of zinc in the M-A flame was observed in the flame up to h = 14 mm over the burner head (in 1mm steps), at three different flame compositions: 0.88; 1.00; 1.12 expressed in relative stoichiometric units (RSU). Four replicate measurements were made in each case. The mean, the standard deviation, the S/N was calculated for each h and flame composition investigated. The homogeneity of the means was tested by the F test at a significance level of 0.05. The slitwidth of the monochromator was of 0.050 mm, the sensitivity of the strip chart recorder was different in function of the absorption value measured. For a given set of determinations the sensitivity was kept constant.

RESULTS AND DISCUSSION

OPTIMIZATION OF THE FLAME AND INSTRUMENTAL PARAMETERS

First the effect of the hollow-cathode lamp current (i) on the zinc absorption was studied. The composition of the flame was kept constant, at 1.12 RSU. The concentration of the calibration solution was of 1 mg.l^{-1} . The absorption (A) was measured for different lamp current intensities, between 3 – 10 mA, in 1 mA steps. The variation of the absorption versus the lamp current is represented in Fig.1.

The absorption of zinc is maximal at $i = 3 \text{ mA}$ and decreases with the increase of the lamp current, due to the significant broadening of the lamp emission line with the increase of the current. The $A - i$ relationship could be described best with an exponential decay curve of $A = 0.0464 + 0.02005 \exp(-(i - 3)/2.13)$. In conclusion, then optimal value of the lamp current for the determination of zinc is 3 mA. The low current is advantageous, because the thermal noise of the lamp is low, the reproducibility of the measurements is high and the lifetime of the lamp is also long.

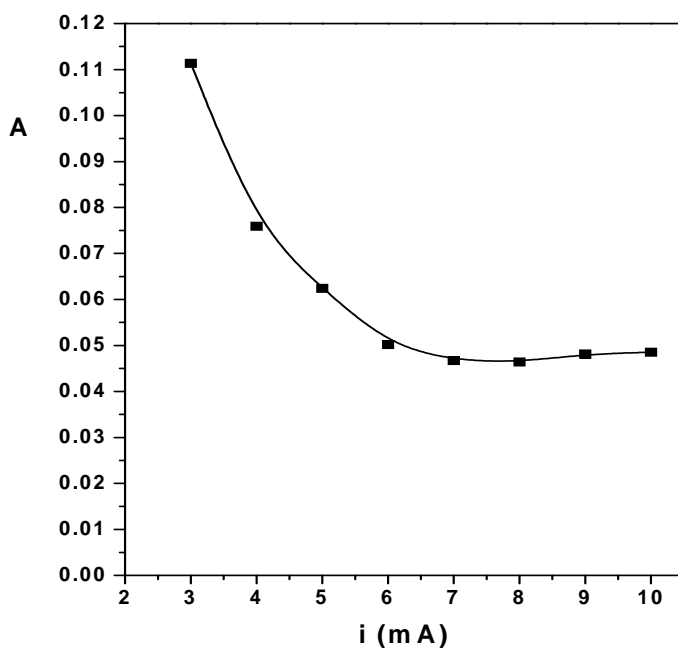


Figure 1. Variation of the absorption of 1 mg.l^{-1} zinc solution versus the hollow-cathode lamp current

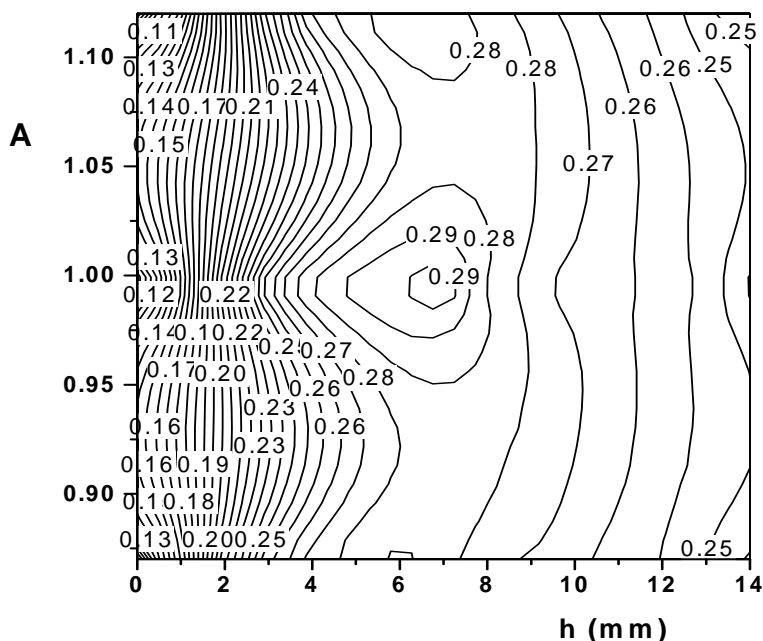


Figure 2. The 2D contour map of the absorption of the 1 mg.l^{-1} zinc vs. observation height and flame composition. The labels on the plot indicate the grid matrix values.

Further, the influence of the flame composition and that of the observation height on the absorption of zinc was investigated using three flame compositions (0.88, 1.00, 1.12 RSU) at the concentration level of 1 mg.l^{-1} of zinc. The lamp current was the optimal one. The data were processed using the MicroCal Origin™ Software package, version 5.0 (MicroCal Software Inc., MA, USA) and plotted as 2D contour map (Fig.2).

The analytical signal depends both on observation height and flame composition. The absorption increases slowly with the increase of the methane content of the flame, being the highest in stoichiometric conditions (1.00 RSU). The maximal absorption was observed at the same height of 7 mm over the burner head, regardless of flame composition. The standard deviation of all means was homogeneous, the magnitude of the S/N ratio being decided by the magnitude of the mean. In conclusion, the optimal conditions for the quantitative determination of zinc in the M-A flame are $h = 7 \text{ mm}$ and flame composition 1.00 RSU.

INTERFERENCES

The effect of Na, K, Ca, Mg, Al, SO_4^{2-} and PO_4^{3-} on the absorption signal of zinc of 1 mg.l^{-1} was investigated up to a 500 fold excess, as possible inorganic interferences, present in natural waters. The effect of HClO_4 was tested too, as matrix modifier. The experimental conditions were the optimal ones, determined previously. The variation of the zinc absorption signal versus the concentration of the interferences is represented in Figure 3.

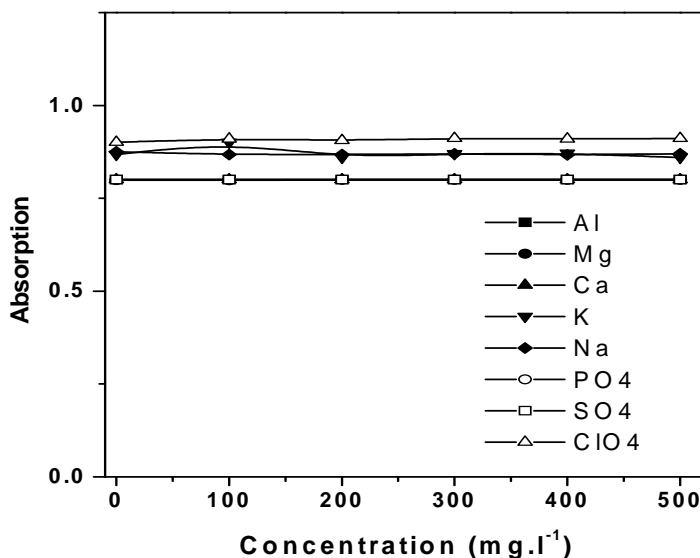


Figure 3. Influence of Na, K, Ca, Mg, Al, SO_4^{2-} , PO_4^{3-} and ClO_4^- on the absorption signal of zinc of 1 mg.l^{-1}

The results show that the studied inorganic ions do not influence the zinc absorption, even in high excess. We can consider that, like in the acetylene flames, zinc is free of interference of these inorganic ions in the methane-air flame. HClO_4 is inefficient, fact which suggests the free evaporation of the analyte from the condensed phase in the flame.

CALIBRATION, DETERMINATION OF THE DETECTION LIMIT

For the determination of the detection limit the variation of the analytical signal versus concentration was studied in the $0.01\text{-}10 \text{ mg.l}^{-1}$ zinc concentration range. Four calibration curves were plotted, one curve covering one order of magnitude of concentration. Each calibration curve was established by using six standard solutions. Six replicate measurements were made at each concentration level. The homogeneity of the means and the linearity of the calibration curve were tested. The equation of the regression line, the confidence limits and the coefficient of correlation (R^2) were calculated with the least squares method. The detection limit was calculated using the two step Neyman-Pearson model [24, 25], for the fixed values of $(P_{10})_0 = 0.025$ and $(P_{11})_d = 0.975$. The results are summarized in Table I.

Table I

Calibration data of zinc determination in the M-A flame

No. Eq	Concentration range (mg.l ⁻¹)	Equation of the calibration curve	Detection limit (mg.l ⁻¹)
1.	10 - 1	$A = 0.1043 * C + 0.0944$ $R^2 = 0.9701$	Not determined
2.	6 - 1	$A = 0.1362 * C + 0.00569$ $R^2 = 0.9990$	0.36 ± 0.20
3 [@]	10 - 1	$A = 0.034 * C + 0.0009$ $R^2 = 0.9994$	0.30 ± 0.17
4.	1 - 0.1	$A = 0.0908 * C - 0.0008$ $R^2 = 0.9995$	0.031 ± 0.02
5.	0.1 - 0.01	$A = 0.4089 * C + 0.0024$ $R^2 = 0.9974$	0.006 ± 0.004

[@] burner held perpendicular to the optical axis, 8 mm optical path in the flame

In the 10 – 1 mg.l⁻¹ concentration domain (eq.(1)) the A – C relationship is not linear in the whole concentration domain, but it can be approximated with a line. The close linearity exists in the 6 – 1 mg.l⁻¹ concentration domain (eq.(2)) only. Holding the burner perpendicular to the optical axis of the spectrophotometer (8 mm optical path in the flame) the linearity can be extended up to 10 mg.l⁻¹ of concentration level (eq.(3[@])). The detection limits obtained for each concentration range are also summarized in Table I. The lowest detection limit of 0.006 ± 0.004 mg.l⁻¹ is low, it is about one order of magnitude higher than that obtained with acetylene flames.

DETERMINATION OF ZINC IN WATER SAMPLES

The zinc content of the water samples was determined by the calibration and by the standard addition method. The later method was used in order to study the presence of interference and/or as reference method due to the absence of certified reference material. The determinations were carried out with optimized flame and instrumental parameters. Four parallel measurements were made in each case. The measuring sample solutions were prepared in 25 ml volumetric flasks, the samples were diluted 1:1. In the case of standard addition method 100 µl of concentrated zinc standard was added to the 25 ml of diluted sample. Three additions of standard were made, in 0.5 mg.l⁻¹ concentration steps. It was calculated the regression line, the zinc content was determined from the intercept with the abscissa of the line. Using the data set, first it was tested the reproducibility of the standard addition method. The recoveries were within 97.7–122.8 % depending on the salt content of the water. The recovery values are close to 100 %, with most samples within the error of determination, so the standard addition method could be considered as the reference method. The results of the determination of zinc content of waters are summarized in Table II.

Table II

Results of analysis of water samples (n = 4)

Water sample		Concentration (mg.l ⁻¹ , by calibration)	Concentration (mg.l ⁻¹ , by standard addition)	Recovery (%)
Tap water		0.024 ± 0.011	0.022 ± 0.010	116.1
River water	Someş	Lower than detection limit	Lower than detection limit	-
Sea water	Black Sea	0.660 ± 0.012	0.575 ± 0.021	102.8
Mineral water	"Anavie"	0.039 ± 0.014	0.030 ± 0.015	91.9
	"Borsec"	0.085 ± 0.014	0.079 ± 0.011	119.7
	"Perla"	0.040 ± 0.014	0.044 ± 0.018	101.1
Well water	Nr. 1	0.048 ± 0.018	0.039 ± 0.020	97.7
	Nr. 2	2.993 ± 0.020	2.259 ± 0.030	122.1
	Nr. 3	0.025 ± 0.018	0.020 ± 0.011	91.9
	Nr. 4	0.295 ± 0.010	0.230 ± 0.015	104.2

The results of the two methods agree for the most of water samples, they are within the errors of the determinations (low salt content waters). Greater differences were obtained for sea water- and well water samples (Nr.2 and Nr.4), having a higher salt content. These differences could be attributed to the nonspecific absorption, due to incomplete evaporation of the sample in the low temperature M-A flame (light scatter) and the lack of the background correction (the spectrophotometer is not equipped with such a device). In these cases the standard addition method offers better results, closer to the real zinc content of waters. For the low salt content waters the calibration method gives acceptable results, for the higher salt content waters the standard addition method is recommended. In conclusion zinc can be determined precisely in natural waters using the M-A flame.

CONCLUSIONS

In the M-A flame zinc exhibits a strong absorption of the resonance line, at the 213.9 nm. The absorption varies with the hollow-cathode lamp current, with the composition of the flame and observation height. The optimal lamp current is of 3 mA, that of observation height over the burner head is 7 mm, in stoichiometric flame (RSU = 1.00). The presence of K, Na, Ca, Mg, Al, SO₄²⁻, and PO₄³⁻ do not effect the absorption of zinc. The absorption-concentration relationship is linear in the 0.01-6 mg.l⁻¹ range, the detection limit is of 0.006 ± 0.004 mg.l⁻¹ of zinc. The zinc content of natural waters can be determined precisely using the calibration or the standard addition method. In conclusion, M-A flame is a suitable for precise atomic absorption determination of zinc in natural waters.

REFERENCES

1. I. Pais, *A mikroelemek jelentősége a mezőgazdasági termelésben. Kutatásuk helyzete a világban*, Kertészeti Egyetem, Budapest, 1984, p.11.
2. G.F. Kirkbright, M. Sargent, *Flame atomic absorption and fluorescence spectroscopy*, Academic Press, London, New York, San Francisco, 1974.
3. H. Armannson, *Anal.Chim.Acta.*, 1979, **110**, 21.
4. S. Olsen, L.C.R. Pessenda, J. Ruzicka, E.H. Hansen, *Analyst*, 1983, **108**, 905.
5. A.S. Attiyat, G.D. Christian, *Talanta*, 1984, **31**, 463.
6. I. Gustavsson, L. Hansson, *Int.J. Environ. Anal. Chem.*, 1984, **17**, 57.
7. P. Koscielniak, *J. Anal. At. Spectrom.*, 1987, **2**, 329.
8. T.V. Rodionova, V.M. Ivanov, *Zh. Anal. Khim.*, 1986, **41**, 2181.
9. V.N. Savitskii, V.I. Peleshenko, V.I. Osadchii, *Zh. Anal. Khim.*, 1987, **42**, 677.
10. A.K. Singh, T.G.S. Kumar, *Microchem. J.*, 1989, **40**, 197.
11. S. Hirata, K. Honda, T. Kumamaru, *Anal. Chim. Acta*, 1989, **221**, 65.
12. Z. Wang, S. Luo, Z. Gong, *Fenxi Huaxue*, 1990, **18**, 859.
13. H. Matusiewicz, R. Sturgeon, V. Luong, K. Moffatt, *Fresenius' J. Anal. Chem.*, 1991, **340**, 35.
14. P. Bermejo-Barrera, R. Dominguez-Gonzalez, R. Soto-Ferreiro, A. Bermejo-Barrera, *Analisis*, 1995, **23**, 135.
15. F. Garcia-Sanchez, A. Navas-Diaz, Arbaizar, *Mikrochim. Acta*, 1995, **118**, 265.
16. G.I. Tszin, E.M. Sedykh, L.N. Bannykh, N.M. Sorokina, Yu.A. Zolotov, *Zh. Anal. Khim.*, 1995, **50**, 76.
17. J. Mohay, Z. Végh, *Fresenius' Z. Anal. Chem.*, 1988, **329**, 856.
18. J.A.F. Gidley, D.T Jones, *Analyst*, 1960, **85**, 249.
19. J.A.F. Gidley, D.T Jones, *Analyst*, 1961, **86**, 271.
20. A.G. Gaydon, H.G. Wolfhardt, *Flames, their Structure, Radiation and Temperature*, Chapman and Hill, New York, 1970.
21. E. Cordoş, L.N. Kékedy, R. Hui, *Patent RSR*, nr. 67867 / 1977.
22. L. Kékedy-Nagy, *Talanta*, 1997, **44**, 1919.
23. L.S. Clesceri, A.E. Greenberg, R.R. Trussel, *Standard Methods for examination of water and wastewater*, 17th Edition, Ed. 1-30, 1989 APHA – AWWA – WPCF.
24. C. Liteanu, I. Rîcă, *Statistical Theory and Methodology of Trace Analysis*, John Wiley, New York, 1980.
25. D.L. Massart, B.G.M. Vandeginste, S.N. Deming, Y. Michotte, L. Kaufman, *Chemometrics: a textbook*, Elsevier, New York, 1988.

INVESTIGATION OF ADSORPTION PRODUCTS OF OXYNE ONTO BLENDE AND SMITHSONITE BY IR SPECTROSCOPY

GABRIELA OPREA and CRISTINA MIHALI

Universitatea de Nord Baia Mare

ABSTRACT. The compounds formed during flotation with oxyne at the surface of smithsonite and blende were studied by IR spectroscopy. By using the potassium bromide pelleting technique the IR spectra were run for blende, smithsonite, oxyne, Zn(II) oxynate, as well as for blende and smithsonite treated with a solution of oxynate. By comparing the obtained spectra the conclusion drawn is that the compound formed at the surface of blende and smithsonite is Zn(II) oxynate.

INTRODUCTION

The solid – liquid interface, however, is more difficult to investigate by IR spectroscopy especially when the liquid is an aqueous solution of reagents, as used in flotation processes.

IR spectroscopic determinations have also been used for surveying the formation of certain species at the surface of minerals during adsorption of various reagents, and there are many reports on this subject [1-10].

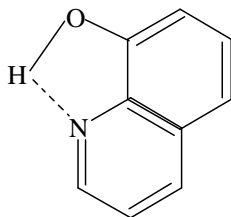
The chelation agents, organic agents acted as precipitants in solution, are lately used in the processes of separation by flotation of ores as well. These reagents are suited to ores containing oxidated minerals and they work as collectors or activators [3-10]

In these investigations and experiments interest in the collector properties exerted by some chelation reagents during the flotation of oxidated minerals [11].

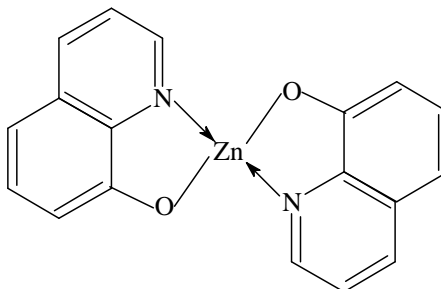
One of this studied reagents, namely 8 – hidroxyquinoline (structure I) or oxyne performs important zinc recoveries in the flotation of smithsonite and blende, and it proves a good collector [12].

In solution, oxyne forms insoluble, stable chelate compounds with many metallic ions, Zn (II) included, and these compounds have (II) type structure.

In the present paper we report some results obtained by an IR spectroscopic investigation, on compounds formed at the surface of smithsonite and blende in the flotation process with oxyne.



Structure I



Structure II

EXPERIMENTAL

The recording of IR spectra was performed by a UR 20, Carl Zeiss Jena, double beam spectrometer; KBr, NaCl, and LiF prisms; resolution 0,6-2000 cm^{-1} ; region 400-5000 cm^{-1} .

We assumed that zinc oxynate was formed at the surface of blende and smithsonite treated with the chelation reagent. This complex is prepared as follows: 150 ml 0,1 mol l^{-1} aqueous $\text{Zn}(\text{CH}_3\text{COO})_2 \cdot 2\text{H}_2\text{O}$ is treated with 75 ml 0,3 mol l^{-1} oxyne in acetic acid 10%; The complex is warmed up and 25 ml oxyne is added, after cooling the pH is established at 9 by NH_4OH , the precipitate it is filtered on crucible G_4 , washed with acetic acid 10% and distilled water, and dried in the drying stove for an hour at 110°C. The preparation method was realised based on personal determinations at different pH values. Thus it was obtained a quantitative precipitation at pH 9, when Zn oxynate contained 18,7% Zn (corresponding to the theoretical composition). By using acetone as a solvent a quantitative precipitation was not possible.

The minerals, blende and smithsonite, was grounded in an agate mortar up to the granulation of approximative $2\mu\text{m}$. A part of the samples was used for the obtaining of IR spectra and another (100 mg) part was treated with 25 ml acetone solution of 10^{-3} mol l^{-1} oxyne at pH 7, stirred for 5 minutes, filtered through a filter crucible, washed and dried in air. Blende and smithsonite flotation recovery is maximum at pH 7 [12]. By using acetic acid as oxyne solvent a maximum recovery can not be obtained [5].

Using the potassium bromide pelleting technique, we recorded the IR spectra in the region 400-1700 cm^{-1} for: oxyne, smithsonite, blende, Zn (II) oxynate, smithsonite and blende treated with acetone solution of oxyne. The pellets contain 10 mg Zn oxynate, 10 mg blende or smithsonite treated with oxyne and 600 mg KBr. Blende contains 57,7 % Zn and smithsonite 49,5 % Zn.

In blende case we also used another method for drawing the IR spectra: 10 mg of blende with the granulation of 45-150 μm is treated with acetone solution of oxyne, filtered and dried in air. The compound formed on the blende surface is extracted 10 ml of CCl_4 or CHCl_3 , under continuing stirring (operation is repeated for 5 times). The extract is dried on KBr support, which is used to prepare the pellets necessary for drawing the IR spectra.

RESULTS AND DISCUSSIONS

The smithsonite – oxyne system

Figure 1 combines the IR spectra for smithsonite (curve a), oxyne (curve b), zinc oxynate (curve c) and smithsonite after treatment with acetone solution of oxyne (curve d). By comparing the spectra we can notice the presence of bands characteristic to the Zn (II) oxynate from 1580; 1505; 1390; 1330; 1280; 1120; 1040; 915; 868 and 680 cm^{-1} in the spectrum of smithsonite treated with oxyne. Therefore on the surface of smithsonite treated with the solution of reagent with chelatant action is formed Zn (II) oxynate.

In the same way was demonstrated the formation of Cu(II) oxynate on the surface of malaquite [7] and that of Pb (II) oxynate on the surface of ceruzite [11].

The intense bands from 1470;735 and 610 cm^{-1} in the spectrum of zinc oxynate are situated at 1465;730 and 620 cm^{-1} , on the smithsonite surface. The band of smithsonit treated with oxyne at 1235 cm^{-1} is shifted against the position in the spectrum of oxyne at 1230 cm^{-1} and against the position of the complex at 1240 cm^{-1} .

Also there can be found some bands at 580 and 465 cm^{-1} which do not appear in the spectra of oxyne and zinc oxynate.

There are, however, numerous bands of oxyne which are absent in the case of smithsonite surface: 1515;1415;1215;1180;742;712;477 cm^{-1} (figure 1b).

The blende – oxyne system

Figure 2 combines the IR spectra for blende (curve a), oxyne (curve b) zinc oxynate (curve c) and blende after treatment with acetone solution of oxyne (curve d), the adsorbion product of acetone on blende extracted with CCl_4 (curve e), and extracted with CHCl_3 (curve f).

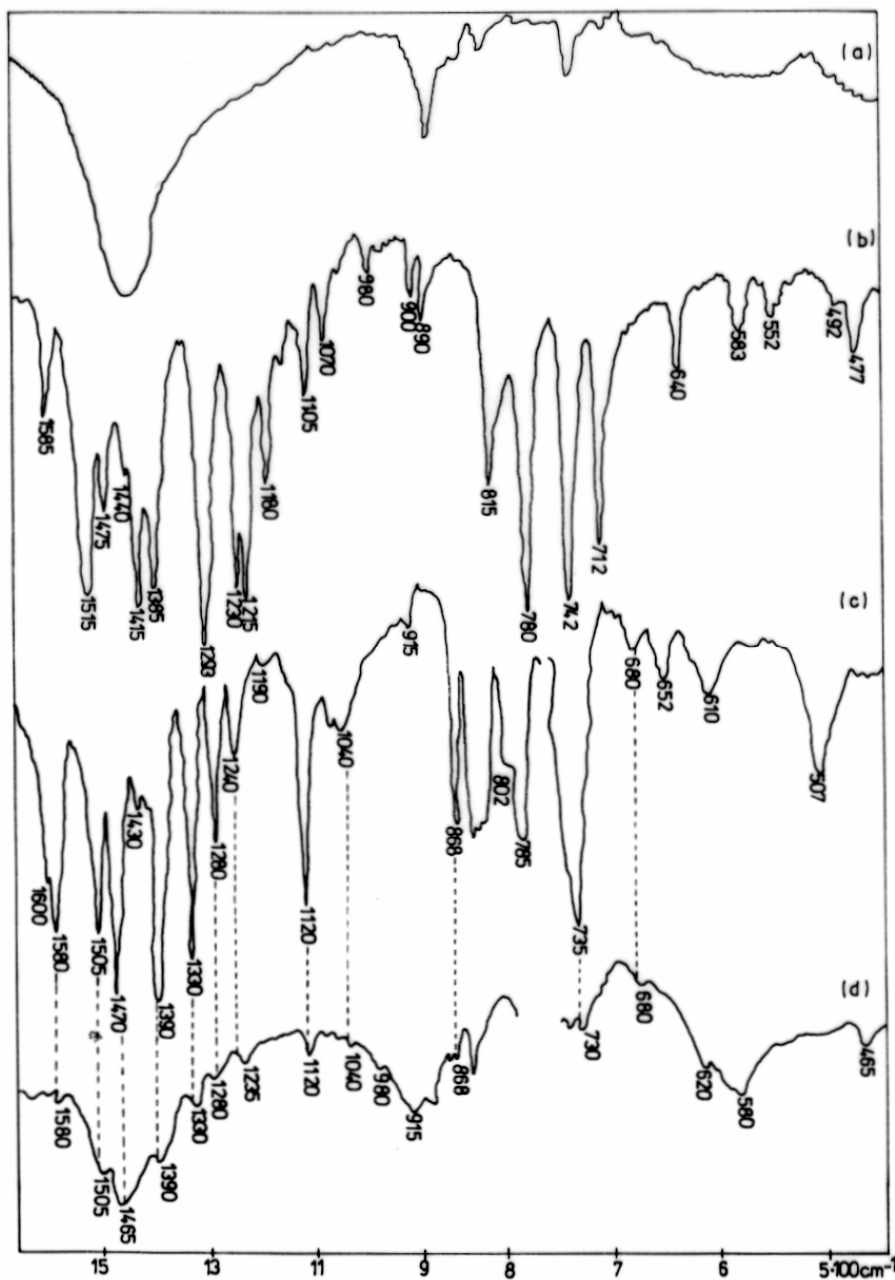


Figure 1. IR spectra indicating the adsorption of oxyne onto smithsonite.
 a) smithsonite in KBr; b) oxyne in KBr; c) zinc oxynate in KBr;
 d) smithsonite after treatment with acetone solution of oxyne

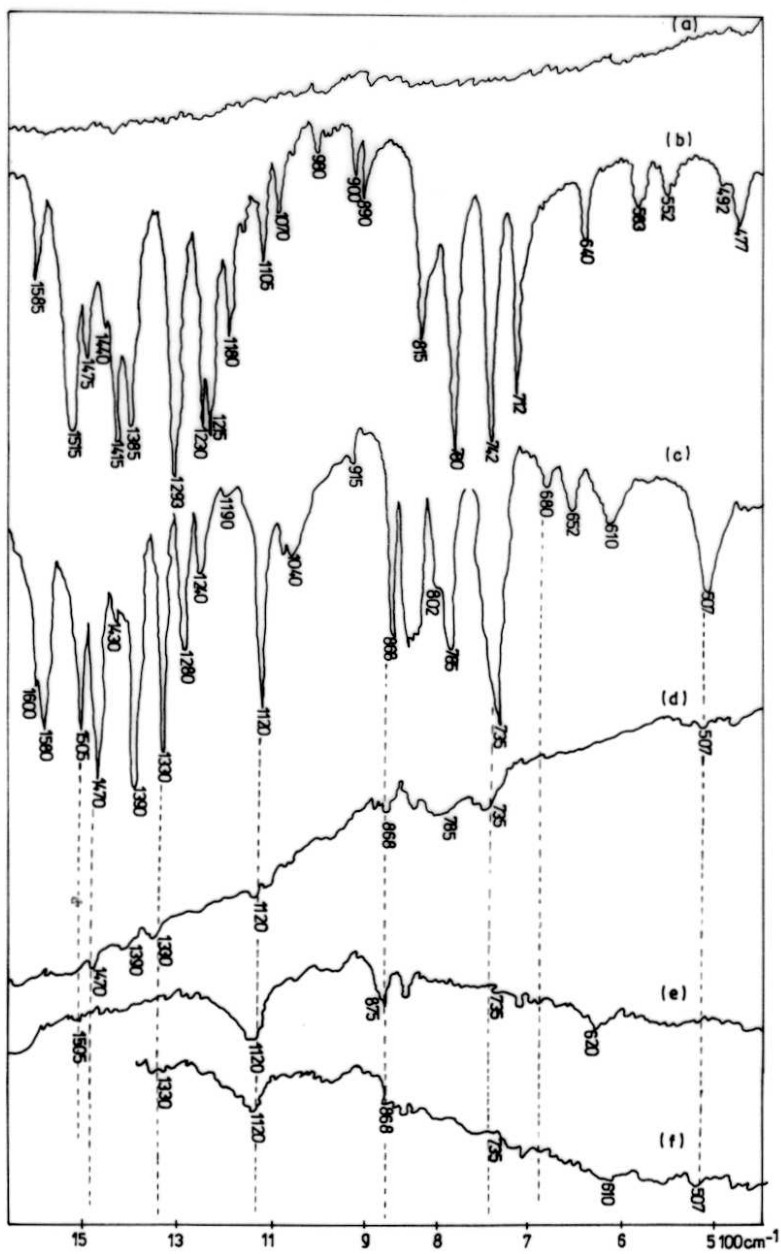


Figure 2. IR spectra indicating the adsorption of oxyne onto blende. a) blende in KBr; b) zinc oxynate; b) oxyne in KBr c) zinc oxynate d) blende after treatment with acetone solution of oxyne; e) adsorption product of oxyne extracted with CCl_4 ; f) adsorption product of oxyne extracted with CHCl_3

By comparing the a, b, c and d spectra (figure 2) we can notice the presence of characteristic bands for zinc oxynate (II) at 1470; 1390; 1330; 1120; 868; 785; 735 cm^{-1} in the spectrum of blende treated with oxyne (curve d). This bands are not very well defined in spectrum from figure 2d.

The spectrum 2e (adsorbition of oxyne on blende extracted with CCl_4) give evidence of a stonger band at 1120 cm^{-1} from zinc (II) oxynate and a undefined band at 1505 cm^{-1} ; we can see that the Zn (II) oxynate band moves from 868 cm^{-1} to 875 cm^{-1} in blende case.

The spectrum 2f (adsorbition of oxyne on blende extracted with CHCl_3) include a well outlined band at 1120 cm^{-1} and undefined bands at 1330; 868; 610 and 507 cm^{-1} of Zn (II) oxynate spectrum.

CONCLUSIONS

The studied IR spectra indicate the presence of characteristic bands from zinc oxynate in the smithsonite an blende spectre treated with oxyne. We can notice that at the smithsonite and blende's surfaces was formed Zn (II) oxynate during flotation using oxyne as collector.

In the case of blende, the IR spectra correspond to adsorbition product of oxyne extracted with CCl_4 or CHCl_3 , have to complete the previous results.

To explain that in some cases appears misplaced bands, that suggest the possible complex formation between the mineral surface and reagents with a different stoichiometric composition than Zn (II) oxynate, may be caused to a smaller concentration of reagents fixed onto mineral surface.

REFERENCES

1. V. M. Lovel, L. A. Gold, N. P. Finkelstein, - International J. Mineral Process, 1, 183, 1974
2. J. Mitlczarsky, P. Novak, J. W. Stojek, A. Pomianowski – 13th International Miner. Process. Congress, Warsawa 61, 1979;
3. S. Raghavan, D. W. Fuerstenau – J. Colloid Interface Sci., 50, 319, 1975;
4. L. Evrard, J. De Cuyper – 11th Internat. Miner. Process, Congress, Cagliari 35, 1975;
5. G. Rinelli, A. M. Marabini, V. Aless – Symposium A. M. Gaudin Flotation, 1, 549, AIME, New York, 1976;
6. G. Barberi, J. L. Cecile – Industrie Minerale – metalurgie, Aout – Septembre, 109, 1979;
7. G. Oprea, E. Chifu – Stud. Univ. Babes Bolyai, 5 Chemia 2/1986, p. 65-68, Cluj Napoca, 1986.
8. G. Oprea – Proceedings of Chemistry and Engineering Chemistry Conference“, vol. II, part I, p. 115-121, Bucuresti, 20-21.10.1995.
9. G. Oprea - Proceedings of International seventh Beijing Conference and Exhibition on Instrumental Analysis, C. Spectroscopy BCEIA, 14-17.10.1997, Shanghai, China, p. 149-150.

10. G. Oprea, C. Varga, A. Mihai, V. Viman – Proceedings of Chemistry and Engineering Chemistry Conference, Bucuresti, 16-18.10.1997, vol. I, p. 6.42 – 6.46.
11. G. Oprea, C. Mihali – Studia Univ. Babes Bolyai, Ser. Chemia, vol. 43(1-2), pag. 116-125,1998, Cluj Napoca.
12. G. Oprea – “Scientific Symposium with International Participation: Technologies for processing of refractory raw materials and for environment protection in areas with extractive industry“, vol. I., p. 127-135, Baia Mare, 17-19 mai 1995.

REAGENTS WITH CHELATANT ACTION FOR Zn (II) AND THE POSSIBILITY OF USING THEM IN FLOTATION

GABRIELA OPREA and CRISTINA MIHALI

Universitatea de Nord Baia Mare

ABSTRACT. In this paper we followed up the data correlation of analytical chemistry of complexation for Zn (II) with chelatants in aqueous solution and the collector power of these reagents in the flotation of the minerals smithsonite and blende that contains this ion.

INTRODUCTION

The problem of scientific base creation for the research and the synthesis of new flotation reagents with some established before properties has constituted the subject of many works [1-3], in which it was proposed a chemical way of approach for solvating this problem. So, the selectivity of the flotation reagents action is considered from the point of view of the chemical nature of the reagent and the electronic structure of the cation that enters in the crystalline network of the floated mineral. For the reagents synthesis the active functional group contained by the reagents is important to be known because its fixation on the mineral must be selective.

It is considered that the fixation of flotation reagents on the mineral surface takes place, in many cases, through chemical bonds, when formed chelat compounds between superficial adsorption center and the reagent atoms. The reagent, which had proved that it is specific to a metallic ions group in solution probably, keeps its selectivity in certain conditions, even in the case of the adsorption at mineral's surface, which contains these metallic ions [3-16].

Unlike the specific action of organic reagents with the metallic ions in solution, in case of minerals, because of the unhomogeneity of surface and of the different unsaturation of the superficial adsorption centers, the quantitative appreciation of adsorption requires experiments. The most results are realized in Hallimond minicells using pure minerals or in laboratory cells using artificial mixtures.

Among the reagents with chelatant action that form in solution chelat compounds with Zn(II), have been studied: 1-(2'-hydroxy-5-'sodiumsulfonate fenylazo) 2 naphthol (Violet solochrome R), 8-hydroxyquinoline (oxyne), 2-hydroxy-benzaldehyde oxime (salicylaldoxime), o-aminobenzoic acid (antranilic acid), 2-quinoline carboxylic acid (quinaldinic acid) and trimetildiaminotetraacetic acid [17].

We followed the collecting action of the mentioned reagent over blende (ZnS) and smithsonite ($ZnCO_3$) to check how both the mineralogic form and the nature of the anion, influence the action of the collectors. The calcite and the magnesite that usually accompanies the utile minerals also in ores should float very little with these reagents. To check this, the reagents with chelatant action were tested in parallel with calcite and magnesite.

The stability of the complex formed between the cations Zn(II), Mg(II) and Ca(II) and the ligands depend on the pH, the modifications resulting from the variation of pH being characterized by the apparent constant of formation, K' .

We have taken in consideration the curves of variation $\log K'$ depending on pH for the following systems: chelatat-Zn(II), chelatat-Ca(II) and chelatat-Mg(II) [3].

EXPERIMENTAL

For the experimental determination we used a microflotation instrument named Hallimond cell [16].

The minerals used smithsonite, blende, calcite and magnezite had the grading between 100-250 μm . One gram of mineral is introduced in the cell and the collector solution with known concentration and pH. The work conditions, kept constant were: the conditioning time (180 seconds), the flotation time (30 seconds), the debit of air (10 l/hour). The floated product is filtrated, dried in the drying stove at 80°C and weighted. The percent of recuperation, %R, for the studied minerals at different pH values and reactant concentrates was calculated. The experiments were orientated towards the determination of the optimum conditions necessary for a good recovery, the concentration of the reagent and the pH domain.

In table 1 are presented for each reagent the amount of the substances weighed (m), the solvent used and the molar concentration(c) of the obtained solution.

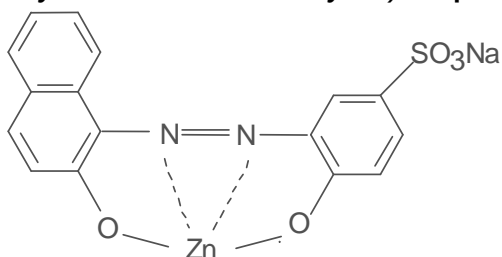
Table 1

The solutions of the reagents prepared in 1l marked balloon.

Nr.	Reagent	m (g)	Solvent	c, mol / l
1.	Violet solochrome R	0,366	water	10^{-3}
2.	Oxyne	0,145	acetone and water	10^{-3}
3.	Salicylaldoxime	0,41	water	3×10^{-3}
4.	Antranilic acid	0,137	water	10^{-3}
5.	Quinaldinic acid	0,173	water	10^{-3}
6.	Trimetildiaminotetraacetic acid	0,0306	NaOH solution	10^{-4}

RESULTS AND DISCUSSIONS

1-(2'-hydroxy-5'-sodiumsulfonate fenylazo)-2 naphthol (Violet solochrome R)



Structure I

This reagent forms with Zn (II) in solution a chelat compound with the structure I [17], which has a maximum stability for the pH between 7,5 – 10, as indicated in figure 1. It can be noticed that the Mg compound has also great stability for pH 11,5-13,5.

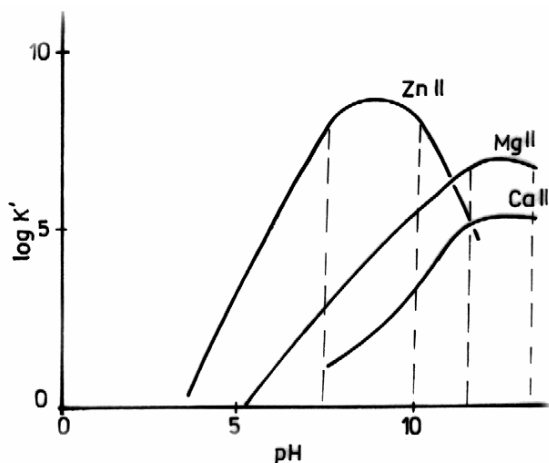


Figure 1
The variation of log K' with the pH for the compounds formed by Violet solochrome R with Zn (II), Ca (II) and Mg (II)

The reagent was utilised also for malachite and cerusite recovery using flotation [3].

For flotation we utilised 10^{-3} mol/l solution in the presence of 0,1 g/l iso-octane at pH between 5,5 and 10,5. The results are presented in Figure 2 which shows that the maximum recuperations of 85% are obtained for blende at pH 8,5 and 84% for smithsonite at pH 10,5. Calcite floats little, 14%, and magnesite 20%.

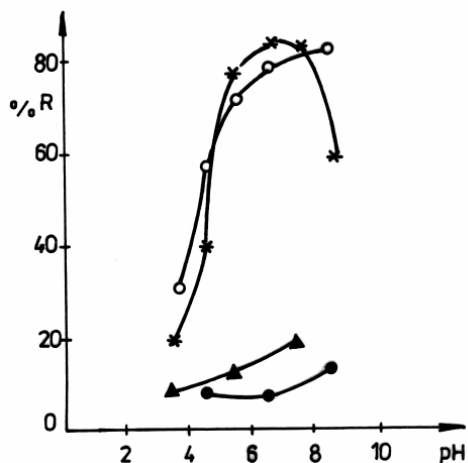
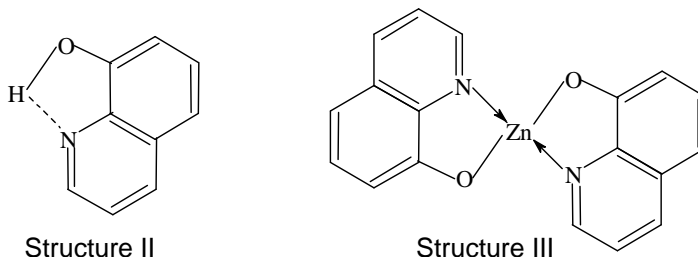


Figure 2
The variation of %R depending on the pH with 0,366 g/l Violet solochrome R and 0,1 g/l iso-octane for: * blende
O smithsonite
● calcite
Δ magnesite

The results are in good concordance with the foresights deduced from the data of analytical chemistry.

8 – Hydroxiquinoline (oxyne)

This reagent presents the structure II and forms with Zn (II) a chelat compound with structure III.



If the precipitation takes place in solution, the Zn oxynate presents the maximum stability for the pH between 4 and 11,5 as indicated in figure 3. The Mg (II) and the Ca (II) oxynate have inferior stability.

In a series of reviews summarized the application of the oxyne is as collector in the flotation of the of zinc and lead oxydes and sulphures [5,12], silicates [8], blende, smithsonite, cerusite galene and copper oxidised ore [3, 14, 16].

During the determinations in the Halimond cell we have maintained constant the concentration of the oxyne, 10^{-3} mol/l, in the presence of 0,1g diesel oil and we have change the pH from 2 to 12.

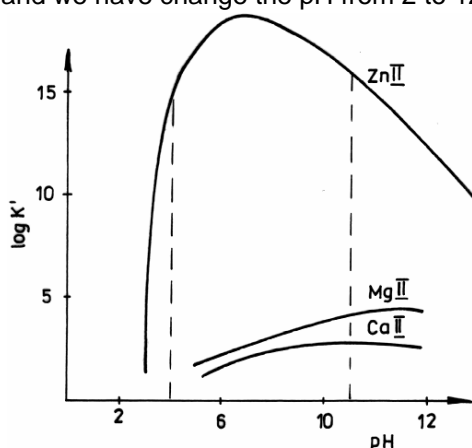


Figure 3
The variation of log K' with the pH for the Zn(II) oxynate, Ca(II) oxynate and Mg(II) oxynate

Figure 4 shows the variation of the recovery percent, %R depending on pH for blende, smithsonite, calcite and magnesite. The maximum recovery of 98% and 100% was obtained for blende with the pH between 5 and 10 and for smithsonite with the pH between 4 and 10. The magnesite and the calcite float little, the maximum recovery being 18%. The blende and the smithsonite float well in a pH-domain where the stability of the chelat compounds formed in the solution is maxim.

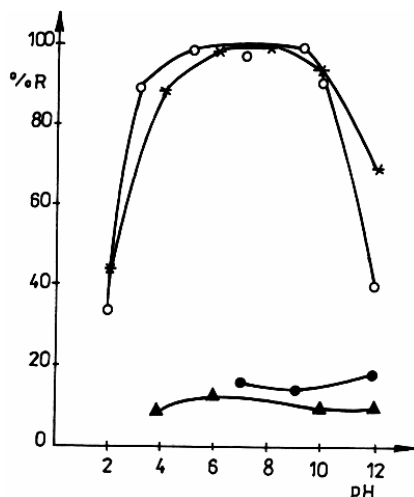


Figure 4

The variation of the recovery percent (%R) depending on the pH with 0,145g/l oxyne and 0,1g/l diesel oil for:

- * blende
- smithsonite
- calcite
- △ magnesite

For smithsonite at pH 7 we have followed the variation %R depending on the concentration of the oxyne solution in the presence and in the absence of diesel oil. The data are presented in Table 2 and in figure 5.

The maximum recovery (100%) is obtained only in the presence of diesel oil and at the minimum concentration of 10^{-3} g/l oxyne. The alone oxyne is only partly effective. We obtained maximum 38% recoveries for smithsonite.

Table 2.

The variation %R of smithsonit with the concentration of oxyne

The concentration oxyne, mol/l $\times 10^{-3}$		0,2	0,5	1	2	3	6	8
%R smithsonite	with 0,1g/l diesel oil	6	90	100	100	98	100	98
	without diesel oil	4	12	18	20	25	38	12

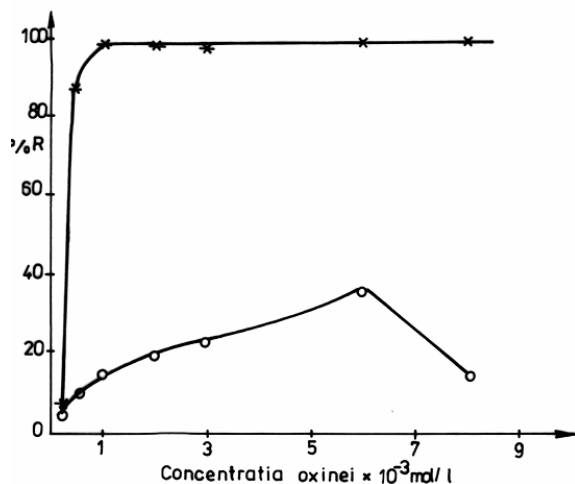


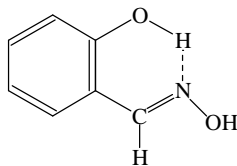
Figure 5

The variation of the recovery percent (%R) depending on the oxyne concentration on pH=7:

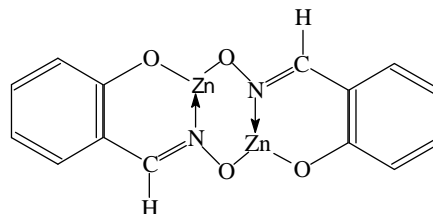
- * with diesel oil
- without diesel oil

Salicylaldoxime

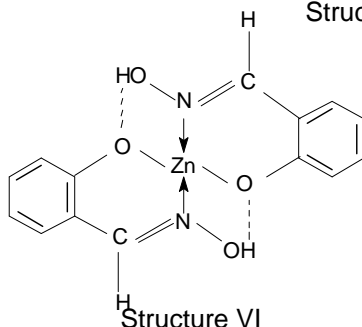
This reagent presents the structure IV and forms chelat compounds having structure V and VI for Zn (II) [9, 11].



Structure IV



Structure V



Structure VI

Salicylaldoxime was utilised as collector for the flotation of the malachite, cerusite, smithsonite [3], casiterite [4], zinc and lead oxydes and sulphures [5].

We worked with 3×10^{-3} mol/l solution (0,41 g/l salicylaldoxyme) and 0,1 g/l isooctane at pH between 5 and 10. The obtained recoveries for blende and smithsonite are little as it is illustrated on Table 3. Calcite and magnesite float little, with recoveries of maxim 15% and 18%.

Table 3

The determination with 0,41 g/l salicylaldoxyme solution and 0,1g/l isooctane

%R	pH					
	5	6	7	8	9	10
Blende	24	28	15	16	7	10
Smithsonite	20	26	10	10	14	10
Calcite	-	-	12	14	15	10
Magnesite	-	8	10	18	14	10

Antranilic acid

In the analytical chemistry the antranilic acid is indicated as precipitation reagent for Zn (II) with which forms a chelatic compound.

The antranilic acid was tested for smithsonite and blende, minerals that contains Zn (II). To check the selectivity we used also calcite and magnesite, minerals that forms the barren gangue in the flotation.

The tested solution contains 0,137 g/l (10^{-3} mol/l) antranilic acid and 0,1 g/l light oil. We worked at pH between 3 and 11. The experimentals results are represented in Figure 6.

It was noticed that the maximum recuperations of 76% for blende and of 70% for smithsonite were obtained at pH 8.

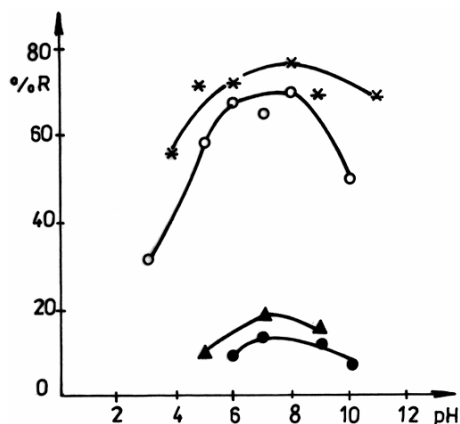


Figure 6

The variation of the recovery percent (%R) depending on pH with 0,137 g/l antranilic acid and 0,1 g/l light oil for:

- * blende
- smithsonite
- calcite
- △ magnesite

Quinaldinic acid

The reagent have chelating action for Zn (II) in solution.

The flotation tested solution have the following composition: 10^{-3} mol/l (0,173 g/l) chinaldinic acid and 0,1 light oil. We worked at pH between 3 and 11. As it is shown in Figure 7, both blende (with recovery of maximum 79%) and smithsonite (76% recovery) float well at pH 8. Calcite floats very little, 12% (at pH 10) and magnesite 18% at pH 9.

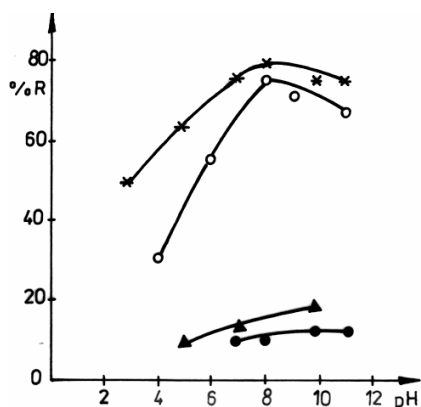


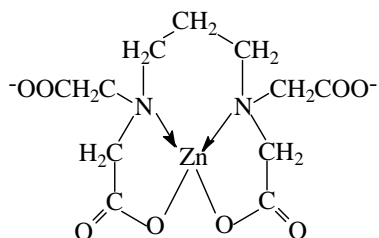
Figure 7

The variation of the recovery percent (%R) depending on pH with 0,173 g/l quinaldinic acid and 0,1 g/l isoocetan for:

- * blende
- smithsonite
- calcite
- △ magnesite

Trimetilendiaminotetraacetic acid

The reagent forms stable chelats with Zn (II) having the structure VII, at pH between 6,5 and 10,3 as it is shown in Figure 8.



Structure VII

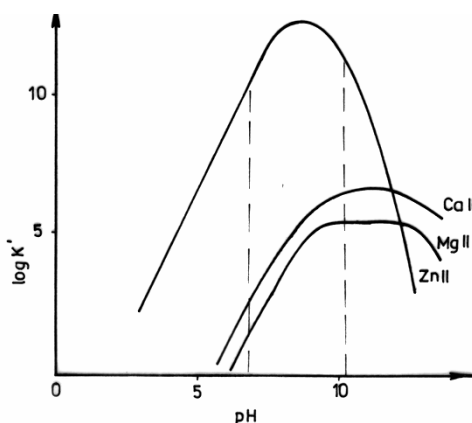


Figure 8

The variation of $\log K'$ depending on the pH for the chelatic compounds formed between the trimethylenediamino-tetraacetic acid and Zn(II), Ca(II) and Mg(II)

This solution don't float the smithsonite and the blende in contradiction with the enough great stability of the Zn (II) chelats in solution.

CONCLUSION

1-(2'-hydroxy-5'-sodiumsulfonate fenylazo)-2 naphtol (Violet solochrome R) in the presence of isoctanol floats well blende and smithsonite, realising maxim 85% separations. The results are in concordance with the foresight deducted from the analytical chemistry data regarding the apparent constant of complexation and the pH domain for the Zn (II) chelats formed in solution.

8 - Hydroxiquinoline (oxyne) floats well blende and smithsonite with maxim recoveries of 100% in a pH domain where the stability of chelatic compounds formed with Zn (II) in solution is maxim. The collector system must contain oxyne and also diesel oil because the oxyne forms with Zn (II) from the mineral's surface insoluble chelats at which, the diesel oil adheres by physical adsorption, realising the mineral's hydrofobisation.

Salicylaldoxime and trimetildiaminotetraacetic acid form stable chelatic compounds with Zn (II) in solution but they don't float the studied minerals.

The quantity of the utilised oxyne is greater than those of salicylaldoxime, but it can be reduced by recovery and recirculation or a better emulsification.

Antranilic acid and quinaldinic acid, in the presence of light oil floats well blende and smithsonite realising recoveries of maximum 76% and 79%, but in solution forms stable complexes with Zn(II).

Calcite and magnesite floats very little with the mentioned reagents and in a different pH domain by the one corresponding of the maxim recovery for blende and smithsonite that permits the separation of the barren gangue from the useful mineral.

For the reagents violet solochrome R, oxyne, antranilic acid and quinaldinic acid the realised recoveries for smithsonite (oxydated mineral of Zn) are comparable with the ones realised for blende (ZnS). This means that choosing a corresponding reagent with chelating action floats both the oxidised and the sulphuric minerals of Zn (II), which have not an identical action as a conventional collector.

The experimental results presented in this paper for smithsonite and blende recovery by flotation are comparable with those reported in the mentioned litterature.

REFERENCES

1. A. V. Glembowski, *Pvetnĭie Metallĭ*, vol. 9, p. 117-121, 1977;
2. V. I. Riaboi, *Obogascenie Rud*, vol. 6, p. 78-84, 1969;
3. J. L. Cecile, Thèse pour obtenir le grand Docteur de specialité, Univ. Orleans, 1978;
4. G. Rinelli, A. M. Marabini, V. Aless, In symposium A. M. Gaudin flotation AIME New-York, N. Y., Vol. 1, p. 549-600, 1976;
5. G. Rinelli, A. M. Marabini, Intern. Min. Process. Congress, London, Vol. 20, p.29 1973;
6. S. Raghavan, D. W., Fuerstenau, J. Coll. & Interf. Sci., Vol. 50, p. 319-330, 1975;
7. H. D. Peterson, M. C. Fuerstenau, J. D. Miller, Trans. of AIME, Vol. 232, p. 388-392 1965;
8. M. Marabini, G. Rinelli, Trans. IMM C 82 Vol. 805, p. 225-228, 1973;
9. M. A. Jarski, E. C. Lingafelter, Acta. Cryst. Vol. 17, p. 1109-1112, 1964;
10. M. C. Fuerstenau, R. W. Harper, J. D. Miller, Trans of AIME, Vol. 247, p. 69-73, 1970;
11. J. L. Cecile, Rapport BRGM nr. 80 SGN 407 MIN, p. 232-235, 1980;
12. L. Usoni, G. Rinelli, A. Marabini, AIME annual meeting, vol. 71 B, p. 10-21, 1971;
13. S. I. Gorlovski, Z. I. Yeropkin, E. M. Kovalov, 8-th Intern. Min. Process. Congress Leningrad, Vol. B3 p. 8, 1968;
14. J. L. Cecile, G. Barberi, *Mineraux et mineraux*, Nancy, p. 26-29, 1978;
15. G. Oprea, Scientific Symposium with International Participation: Technologies for processing of refractory raw materials and for environment protection in areas with extractive industry, vol. I, p. 127-135, Baia Mare, 17-19 May 1995;
16. G. Oprea, C. Mihali – *Studia Univ. Babes Bolyai, Ser. Chemia*, vol. 43(1-2), p. 116-125, 1998, Cluj Napoca;
17. A. Rigbom, *Les complexes en chimie analytique*, Ed. Duond, Paris, 1967.

THERMODYNAMIC EVALUATION OF COAL REACTIVITY

OSSI HOROVITZ¹, ELENA MARIA PICA^{2*}, GAVRIL NIAC²

¹ *Department of Physical Chemistry, University "Babeș-Bolyai", 3400 Cluj- Napoca, România*

² *Department of Chemistry, Technical University, 3400 Cluj-Napoca, România*

ABSTRACT. From empirical formulae for 10 Romanian coals and from their heating values, thermodynamic parameters are evaluated: enthalpies, entropies, heat capacities. With these values, the Gibbs free energies and equilibrium constants for some reactions during coal gasification (including reactions with carbon dioxide, steam, oxygen) are calculated, for temperatures in the 25...1000°C range. The temperature and pressure dependence of the equilibria is discussed by means of zero-affinity plots. Lignites present a much higher thermodynamic reactivity than graphite, that should be exploited in the choice of gasification conditions for coals.

INTRODUCTION

In the study of coal gasification, the reactivity of the coal is a key parameter. Both the kinetic and thermodynamic reactivity are important. Here we try to evaluate the reactivity by means of thermodynamic calculations, i.e., by the calculation of the Gibbs free energy of reaction.

We are concerned here with the reactivity of the *organic coal mass*, i.e., the mass of anhydrous coal less the mineral mass. This latter quantity differs from the ash mass, as a consequence of the processes during heating (water loss from hydrated silicates, the decomposition of carbonates, the combustion of pyrite, volatilization of chlorides). The parameters referred to the organic coal mass can be evaluated from the two phase model of coals [1]. In this way, from the processing of analytical data we determined the empirical formulae of the organic mass, considering the principal elements in their constitution: carbon, hydrogen and oxygen (with neglect of the nitrogen and sulfur content). The higher heating value Q_s^c for the organic mass could also be calculated. The formulae are written as CH_xO_y [2]. These indices are given in Table 1 for 10 coals, on the basis of mean values of the parameters, obtained from representative samples.

Symbols: C_p molar heat capacity under constant pressure; ΔG Gibbs free energy of reaction; H_{298}° standard enthalpy; ΔH_{298}° standard enthalpy of reaction;

ΔH_T° enthalpy of reaction at temperature T , under normal pressure; ΔH_{298}° standard enthalpy; K_p equilibrium constant in partial pressures; K_x equilibrium constant in mole fractions; M molecular mass; p pressure; p_i partial pressure; Q_s^c higher heating value for the organic mass (of the carbonaceous matter); S_{298}° standard entropy; ΔS_{298}° standard entropy of reaction; ΔS_T° entropy of reaction at temperature T , under normal pressure; T temperature; T_e temperature for zero affinity; x, y indices for H and O respectively, in the empirical formulae of coals; ν number of moles; $\Delta \nu$ variation of the number of moles .

EXPERIMENTAL

Starting with proximate and ultimate analysis data on coals from different Romanian coal deposits, in a wide range of incarbonisation degrees, ranging from lignites to bituminous coals (Table 1), we get the values for moisture, ash, volatiles, carbon, hydrogen, sulfur, nitrogen and oxygen contents, as well as the lower and higher heating values. These are the basis for our subsequent calculations. The higher heating values for the organic mass Q_s^c (in kJ.kg^{-1}) are given in Table 1.

RESULTS AND DISCUSSION

The calculation of thermodynamic parameters

In order to make thermodynamic calculations for the reactivity of coals, with respect to the reaction participants, the following parameters are used: standard enthalpies of formation, H_{298}° , standard entropies, S_{298}° and molar heat capacities under constant pressure C_p . For all the involved substances, other than coals, we used the CODATA Key Values [3]. For molar heat capacities we used the temperature dependence equations:

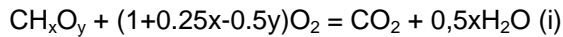
$$C_p = a + bT + cT^2 \quad (1)$$

(for methane) and

$$C_p = a + bT + c'/T^2 \quad (2)$$

for all other compounds [4].

For coals, the *enthalpy of formation* corresponding to the empirical formula is calculated from the higher heating value. The standard enthalpy ΔH_{298}° of the combustion reaction:



is related to the higher heating value of the organic mass Q_s^c by the well-known relation:

$$\Delta H_{298}^\circ = -MQ_s^c/1000 \quad (3)$$

where Q_s^c is obtained by extrapolation of the higher heating value of the anhydrous coal to zero ash content (instead to maceral phase ash content, since no data on SiO_2 content were available [5]). M is the molecular mass of the formula: $M = 12+x+16y$. These values are also given in Table 1. From the combustion reaction, we can calculate the molar enthalpy of formation for the coal:

$$H_{298}^\circ(c) = H_{298}^\circ(\text{CO}_2) + 0.5x H_{298}^\circ(\text{H}_2\text{O},l) - H_{298}^\circ \quad (4)$$

We use the enthalpy of liquid water, since we deal with the upper heating value of coals. The calculated values are given in Table 1; for all the 10 coals the values are negative: the formation of the coals from elements is exothermic, but for bituminous coals the values are only slightly negative.

Table 1.

Composition and thermodynamic characteristics of some coals

No.	Coal	x= H/C	y= O/C	Q_s^C (kJ.kg ⁻¹)	H_{298}^0 (kJ.mol ⁻¹)	$H_{298}^0(C)$ (kJ. mol ⁻¹)	C_p (J. mol ⁻¹ K ⁻¹)	$S_{298}^0(C)$ (J. mol ⁻¹ K ⁻¹)
1	Anina bituminous coal	0.66	0.09	34560	-487.29	-0.54	15.41	18.49
2	Lupeni bituminous coal	0.81	0.14	33660	-506.89	-2.38	17.69	21.23
3	Lonea soft coal	0.91	0.21	31800	-517.61	-5.96	19.82	23.79
4	Țebea brown coal	0.99	0.27	30460	-527.51	-7.49	21.60	25.92
5	Comănești brown coal	0.91	0.27	28640	-493.62	-29.95	20.83	25.00
6	Rovinari lignite	1.00	0.33	27500	-502.74	-33.69	22.70	27.24
7	Ceptura lignite	1.00	0.38	26200	-500.38	-36.05	23.54	28.25
8	Ojasca lignite	1.07	0.35	27030	-504.71	-41.72	23.71	28.45
9	Cămpulung lignite	0.96	0.30	27680	-491.78	-38.93	21.82	26.18
10	Căpeni-Vârghiș lignite	1.02	0.41	25620	-501.85	-37.44	24.24	29.09

The *standard entropy* S_{298}^0 for the coals, as well as the *molar heat capacity* C_p cannot be exactly calculated for complex solid substances such as coal. Values for specific heats can be estimated from Neumann and Kopp-like formulas, such as that proposed by Szadeczky [6], with increments for solids [7-9]. For molar heat capacities (formula CH_xO_y), we find:

$$C_p = 7.56 + 9.6 x + 16.8 y \text{ [J.mol}^{-1}\text{K}^{-1}] \quad (5)$$

The values calculated by this formula are given in Table 1.

The standard entropy can be estimated for organic solids from the Strelkov formula [10]:

$$S_{298}^0 = 1.1 C_p \quad (6)$$

We found it better to use a higher value for the proportionality factor, viz. 1.2 [8,9] and obtained the values given in Table 1. These values are a reasonable good approximation for the entropies, since the reactions that will be considered here show considerable entropy variations, mainly due to gas formation or consumption.

In order to calculate the free energy of reaction at different temperature, we have to calculate the enthalpies and the entropies at these temperatures for all the substances undergoing the reaction. For all the substances except the coals, enthalpies and entropies were exactly calculated:

$$H_T^0 = H_{298}^0 + \int_{298}^T C_p dT; \quad S_T^0 = S_{298}^0 + \int_{298}^T \frac{C_p}{T} dT; \quad (7)$$

with the formulae given above for the temperature dependence of C_p . For the coals, the C_p values were assumed to be constant (Table 1).

The Gibbs free energy of reaction for coal gasification

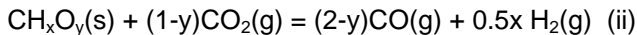
Some basic reactions during coal gasification are:

- Complete combustion (i); its reaction enthalpy is of course negative, the volume variation being determined by the variation of the number of moles of gases, Δv . This is zero for graphite, but positive for coals:

$$\Delta v = 0.25x + 0.5y \quad (8)$$

and increasing with the hydrogen, and still more, with the oxygen content.

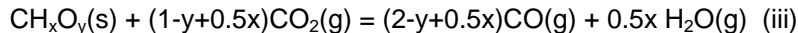
- The Boudouard reaction (gasification with carbon dioxide):



is endothermic under standard conditions and shows a positive volume variation:

$$\Delta v = 1 + 0.5x$$

- A second Boudouard-like reaction could be written for coals:



It is also endothermic at room temperature and with the same volume variation as the previous one.

- The gasification with steam to give H_2 and CO :



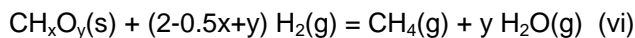
is also an endothermic reaction, with a volume increase: $\Delta v = 1 + 0.5x$

- The analogous reaction, yielding CO_2 :



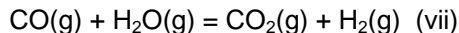
shows the same volume variation as the previous one and is also endothermic.

- The coal hydrogenation reaction, with the hydrogen resulted from other reactions:



is an exothermic reaction, usually with volume decrease: $\Delta v = -1+0.5x$.

- The homogeneous reaction of carbon oxide conversion:



is slightly exothermic and without variation of volume ($\Delta v = 0$).

Of course, not all these reactions are independent; for instance, reaction (iii) is a linear combination of reactions (ii) and (vii) and reaction (v) is simply the sum of reaction (iv) with (vii).

We calculated the molar Gibbs free energies for all these reactions at standard temperature, as well as at temperatures in the range 100 ... 1000°C for the 10 coal types investigated and for graphite:

$$\Delta G_T^\circ = \Delta H_T^\circ - T\Delta S_T^\circ \quad (9)$$

Since the "molar mass" for coals has a purely conventional meaning, it should be more significant to compare the ΔG -values by referring to the mass unity of coal.

Formulas of organic matter of coal per one carbon atom were successfully used by Stephens [11] to calculate equilibrium gas composition for Wyoming coal gasification as well as by Stephens and Miller [12], but the evaluation of indices for H and O was made in a conventional manner.

Table 2 presents these values for the total combustion of the coal. The ΔG -value for graphite is almost temperature independent (reaction with very little entropy variation, $\Delta v = 0$). The values for bituminous coals (1, 2) are more negative than for graphite: the hydrogen content in the fuel increases its heating value. For lignites, the thermal effect is lower than for graphite, a consequence of the higher oxygen content. For the coals, the ΔG value becomes more negative at higher temperatures.

For the Boudouard equilibrium (ii) the free energy is given in Table 3. The values are always lower for coals than for graphite and their temperature variation is less important for lower rank coals. The values for the organic mass of lignites for instance are 4...8 MJ/kg lower than for graphite at the same temperature. Therefore, the zero value of ΔG is reached by coals at significantly lower temperatures as by graphite (with 300...400°C for bituminous coals and with 400-550°C for brown coals and lignites), i.e. their thermodynamic reactivity is higher.

Table 2.

The Gibbs free reaction energy $-\Delta G_T^\circ$ (MJ.kg⁻¹) for coal combustion (i)

T(°C)	C*	1	2	3	4	5	6	7	8	9	10
25	32.86	34.12	33.22	31.42	30.13	28.36	27.25	26.05	26.76	27.42	25.48
100	32.86	34.27	33.41	31.63	30.36	28.58	27.49	26.29	27.02	27.65	25.73
200	32.90	34.47	33.66	31.92	30.67	28.88	27.81	26.63	27.35	27.98	26.07
300	32.92	34.69	33.92	32.21	30.99	29.19	28.14	26.96	27.70	28.28	26.42
400	32.94	34.91	34.18	32.51	31.32	29.50	28.48	27.31	28.05	28.61	26.77
500	32.95	35.14	34.46	32.82	31.65	29.82	28.83	27.66	28.41	28.94	27.13
600	32.96	35.38	34.74	33.14	31.99	30.15	29.18	28.02	28.77	29.28	27.49
700	32.96	35.63	35.03	33.46	32.34	30.48	29.58	28.38	29.14	29.63	27.86
800	32.96	35.88	35.33	33.79	32.70	30.82	29.90	28.76	29.52	29.98	28.24
900	32.96	36.15	35.64	34.13	33.06	31.17	30.27	29.13	29.91	30.34	28.62
1000	32.96	36.42	35.96	34.48	33.43	31.53	30.65	29.51	30.30	30.71	29.01

C* - graphite

Table 3.

The Gibbs free reaction energy ΔG_T° (MJ.kg⁻¹) for the Boudouard reaction (ii)

T(°C)	C*	1	2	3	4	5	6	7	8	9	10
25	10.01	6.08	4.72	3.27	2.11	3.50	2.50	1.78	2.52	3.38	1.36
100	8.90	4.96	3.64	2.25	1.13	2.54	1.57	0.89	1.59	2.43	0.49
200	7.42	3.46	2.17	0.86	-0.19	1.23	0.32	-0.31	0.34	1.15	-0.69
300	5.93	1.93	0.69	-0.54	-1.53	-0.09	-0.95	-1.52	-0.92	-0.14	-1.88
400	4.45	0.40	-0.80	-1.95	-2.89	-1.43	-2.24	-2.75	-2.20	-1.45	-3.08
500	2.97	-1.14	-2.30	-3.37	-4.25	-2.76	-3.53	-3.99	-3.48	-2.77	-4.28
600	1.50	-2.70	-3.82	-4.81	-5.62	-4.12	-4.83	-5.23	-4.78	-4.09	-5.50
700	0.04	-4.26	-5.34	-6.25	-7.00	-5.47	-6.13	-6.48	-6.08	-5.43	-6.72
800	-1.42	-5.83	-6.86	-7.69	-8.38	-6.84	-7.45	-7.74	-7.39	-6.77	-7.96
900	-2.86	-7.40	-8.40	-9.14	-9.77	-8.21	-8.77	-9.00	-8.70	-8.11	-9.19
1000	-4.31	-8.98	-9.93	-10.6	-11.2	-9.58	-10.1	-10.3	-10.0	-9.46	-10.4

C* - graphite

For the other Boudouard-like reaction (iii), the calculated ΔG values are given in Table 4. Here the temperature dependence is greater than for the previous reaction, so the ΔG values are higher for low temperatures and lower for high temperatures. The higher reactivity of coals as compared with graphite is also clearly seen. At high temperatures, this reaction prevails over reaction (ii).

Table 4.

The Gibbs free reaction energy ΔG_T° (MJ.kg⁻¹) for the Boudouard reaction (iii)

T(°C)	C*	1	2	3	4	5	6	7	8	9	10
25	10.01	6.75	5.49	4.07	2.93	4.26	3.28	2.53	3.34	4.16	2.11
100	8.90	5.56	4.32	2.96	1.86	3.21	2.27	1.56	2.32	3.12	1.15
200	7.42	3.96	2.75	1.47	0.42	1.80	0.90	0.25	0.96	1.73	-0.13
300	5.93	2.35	1.17	-0.04	-1.03	0.38	-0.47	-1.06	-0.41	0.33	-1.42
400	4.45	0.72	-0.43	-1.56	-2.49	-1.06	-1.86	-2.39	-1.80	-1.08	-2.71
500	2.97	-0.90	-2.02	-3.08	-3.95	-2.49	-3.24	-3.71	-3.18	-2.48	-4.01
600	1.50	-2.53	-3.63	-4.61	-5.42	-3.93	-4.63	-5.05	-4.57	-3.90	-5.32
700	0.04	-4.17	-5.23	-6.14	-6.89	-5.37	-6.03	-6.38	-5.97	-5.32	-6.62
800	-1.42	-5.82	-6.85	-7.68	-8.37	-6.82	-7.43	-7.72	-7.37	-6.75	-7.94
900	-2.86	-7.46	-8.46	-9.21	-9.84	-8.27	-8.83	-9.06	-8.77	-8.18	-9.25
1000	-4.31	-9.11	-10.1	-10.8	-11.3	-9.73	-10.2	-10.4	-10.2	-9.61	-10.6

C* - graphite

The trends are analogous for coal gasification with steam (reaction iv), as shown in Table 5. The thermodynamic reactivity of coals versus steam is greater at low temperature in comparison with that versus CO₂; from 800°C on, the trend is

THERMODYNAMIC EVALUATION OF COAL REACTIVITY

inverted. The equilibria (iv) are shifted towards coal gasification at temperatures as low as 100°C for lignite (10) as compared to graphite (about 680°C).

Table 5.
The Gibbs free reaction energy ΔG_T° (MJ.kg⁻¹) for the reaction (iv)

T(°C)	C*	1	2	3	4	5	6	7	8	9	10
25	7.62	4.23	3.08	1.89	0.91	2.29	1.45	0.85	1.52	2.26	0.50
100	6.78	3.32	2.18	1.01	0.06	1.46	0.64	0.07	0.71	1.43	-0.28
200	5.63	2.07	0.95	-0.18	-1.10	0.32	-0.47	-1.01	-0.40	0.31	-1.33
300	4.46	0.80	-0.32	-1.39	-2.28	-0.84	-1.60	-2.10	-1.54	-0.84	-2.41
400	3.28	-0.50	-1.60	-2.63	-3.47	-2.01	-2.75	-3.20	-2.68	-2.00	-3.50
500	2.10	-1.82	-2.90	-3.88	-4.69	-3.21	-3.91	-4.33	-3.85	-3.18	-4.60
600	0.92	-3.15	-4.22	-5.15	-5.92	-4.41	-5.08	-5.46	-5.02	-4.37	-5.71
700	-0.27	-4.50	-5.55	-6.43	-7.16	-5.63	-6.27	-6.60	-6.21	-5.57	-6.84
800	-1.46	-5.86	-6.89	-7.72	-8.41	-6.86	-7.47	-7.75	-7.40	-6.79	-7.97
900	-2.66	-7.24	-8.25	-9.02	-9.67	-8.10	-8.67	-8.92	-8.61	-8.01	-9.11
1000	-3.85	-8.62	-9.62	-10.3	-10.9	-9.35	-9.89	-10.1	-9.83	-9.24	-10.3

C* - graphite

The steam gasification with formation of CO₂, reaction (v) (Table 6) shows lower ΔG values than reaction (iv) for temperatures below 800°C, i.e. the formation of CO₂ prevails over the formation of CO. The situation changes at higher temperatures. For almost all lignites, the Gibbs free energy of the reaction is negative already at room temperature, thus the reaction is possible from the thermodynamic point of view (although kinetically too slow to be important).

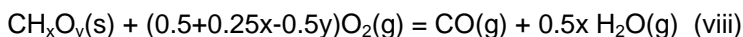
Table 6.
The Gibbs free reaction energy ΔG_T° (MJ.kg⁻¹) for the reaction (v)

T(°C)	C*	1	2	3	4	5	6	7	8	9	10
25	5.24	2.20	1.18	0.13	-0.74	0.63	-0.11	-0.65	-0.01	0.64	-0.96
100	4.65	1.51	0.49	-0.56	-1.41	-0.02	-0.76	-1.27	-0.66	-0.01	-1.58
200	3.83	0.55	-0.48	-1.50	-2.34	-0.93	-1.65	-2.13	-1.56	-0.90	-2.43
300	2.99	-0.46	-1.49	-2.48	-3.30	-1.86	-2.57	-3.02	-2.48	-1.83	-3.31
400	2.12	-1.50	-2.53	-3.49	-4.28	-2.83	-3.51	-3.94	-3.43	-2.79	-4.21
500	1.23	-2.56	-3.60	-4.53	-5.29	-3.82	-4.48	-4.87	-4.41	-3.77	-5.13
600	0.33	-3.66	-4.69	-5.58	-6.32	-4.82	-5.47	-5.83	-5.40	-4.77	-6.07
700	-0.59	-4.77	-5.80	-6.66	-7.37	-5.85	-6.48	-6.80	-6.41	-5.79	-7.03
800	-1.52	-5.91	-6.94	-7.76	-8.44	-6.90	-7.50	-7.79	-7.44	-6.82	-8.00
900	-2.45	-7.06	-8.09	-8.87	-9.52	-7.95	-8.54	-8.79	-8.48	-7.87	-8.99
1000	-3.39	-8.23	-9.25	-10.0	-10.6	-9.03	-9.59	-9.80	-9.53	-8.93	-9.98

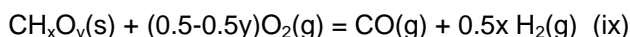
C* - graphite

The coal hydrogenation to methane (vi) presents rather important negative ΔG -values at standard temperature (Table 7). They increase with temperature and become positive for graphite at round 550°C ; for coals the values are much lower and still negative at 1000°C . The brown coal (4), followed by lignite (10), present the highest reactivity toward hydrogen.

For the equilibrium (vii), thermodynamic characteristics are known from literature. We considered also some reactions of incomplete combustion of coals, with formation of carbon monoxide and water:



or of carbon monoxide and hydrogen:



Both are reaction with a volume increase: $\Delta v = 0.5 + 0.25x + 0.5y$ (viii) and $\Delta v = 0.5 + 0.5x + 0.5y$ (ix) respectively. We compared their Gibbs free energies (ΔG) in Table 8 and 9 with those of carbon monoxide formation from elements:

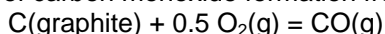


Table 7.

The Gibbs free reaction energy ΔG_T° ($\text{MJ}\cdot\text{kg}^{-1}$) for coal hydrogenation (vi)

T($^{\circ}\text{C}$)	C*	1	2	3	4	5	6	7	8	9	10
25	-4.23	-5.86	-6.37	-6.86	-7.31	-5.97	-6.33	-6.60	-6.10	-5.75	-6.77
100	-3.71	-5.60	-6.18	-6.72	-7.21	-5.84	-6.24	-6.53	-6.03	-5.65	-6.70
200	-2.95	-5.22	-5.89	-6.50	-7.04	-5.65	-6.10	-6.40	-5.91	-5.48	-6.59
300	-2.14	-4.82	-5.57	-6.26	-6.85	-5.43	-5.93	-6.25	-5.77	-5.29	-6.45
400	-1.29	-4.39	-5.25	-6.00	-6.64	-5.20	-5.75	-6.08	-5.62	-5.09	-6.30
500	-0.42	-3.96	-4.91	-5.74	-6.43	-4.96	-5.56	-5.91	-5.47	-4.88	-6.14
600	0.47	-3.53	-4.57	-5.48	-6.22	-4.72	-5.38	-5.74	-5.31	-4.67	-5.98
700	1.38	-3.10	-4.23	-5.21	-6.01	-4.48	-5.19	-5.56	-5.15	-4.46	-5.83
800	2.29	-2.67	-3.90	-4.95	-5.80	-4.25	-5.00	-5.39	-4.99	-4.25	-5.67
900	3.21	-2.25	-3.57	-4.70	-5.60	-4.01	-4.82	-5.23	-4.84	-4.05	-5.52
1000	4.13	-1.83	-3.25	-4.45	-5.40	-3.79	-4.65	-5.07	-4.70	-3.85	-5.37

C* - graphite

Both reactions are exothermic, with ΔG -values becoming more negative with increasing temperature. In the first reaction (viii), coals present more negative ΔG -values than graphite, especially bituminous and brown coals, while for lignites the values get near those for graphite. In the second reaction (ix) the standard ΔG -values are above those for graphite, and their temperature dependence is more pronounced, so that at high temperature, the values for bituminous coals go below those for graphite.

Table 8.

Gibbs free reaction energy $-\Delta G_T^{\circ}$ (MJ.kg⁻¹) for incomplete coal combustion (viii)

T(°C)	C*	1	2	3	4	5	6	7	8	9	10
25	11.43	15.87	16.13	15.61	15.27	13.43	13.18	12.57	12.99	12.93	12.34
100	11.99	16.49	16.75	16.22	15.88	14.03	13.77	13.15	13.59	13.53	12.93
200	12.74	17.31	17.58	17.05	16.70	14.84	14.58	13.95	14.39	14.34	13.72
300	13.49	18.15	18.42	17.88	17.52	15.66	15.39	14.74	15.21	15.15	14.51
400	14.24	19,00	19.28	18.72	18.36	16.48	16.21	15.55	16.03	15.97	15.31
500	14.99	19,85	20.14	19.57	19.20	17.31	17.03	16.36	16.86	16.80	16.12
600	15.72	20.71	21.00	20.43	20.05	18.15	17.87	17.18	17.70	17.64	16.93
700	16.94	21.58	21.88	21.29	20.90	18.99	18.70	18.00	18.54	18.48	17.75
800	17.19	22.46	22.75	22.16	21.76	19.84	19.54	18.83	19.38	19.32	18.57
900	17.91	23.34	23.64	23.03	22.62	20.69	20.39	19.66	20.23	20.17	19.40
1000	18.63	24.23	24.53	23.91	23.49	21.55	21.24	20.50	21.09	21.03	20.23

C* - graphite

Table 9.

The Gibbs free reaction energy $-\Delta G_T^{\circ}$ (MJ.kg⁻¹) for incomplete coal combustion (ix)

T(°C)	C*	1	2	3	4	5	6	7	8	9	10
25	11.43	10.52	9.98	9.21	8.73	7.39	6.92	6.57	6.44	6.75	6.39
100	11.99	11.22	19.69	9.92	9.44	8.08	7.61	7.25	7.13	7.45	7.06
200	12.74	12.15	11.65	10.88	10.39	9.02	8.55	8.17	8.08	8.38	7.97
300	13.49	13.11	12.63	11.85	11.36	9.97	9.50	9.10	9.04	9.33	8.90
400	14.24	14,08	13.62	12.84	12.34	10.92	10.46	10.04	10.01	10.29	9.83
500	14.99	15,05	14.62	13.84	13.33	11.89	11.43	10.99	10.99	11.26	19.78
600	15.72	16.04	15.63	14.84	14.34	12.87	12.40	11.95	11.97	12.24	11.73
700	16.94	17.04	16.65	15.86	15.35	13.86	13.39	12.91	12.97	13.23	12.69
800	17.19	18.04	17.68	16.88	16.36	14.85	14.38	13.89	13.97	14.22	13.66
900	17.91	19.06	18.71	17.91	17.39	15.86	15.38	14.87	14.99	15.23	14.63
1000	18.63	20.08	19.76	18.95	18.42	16.86	16.39	15.85	16.00	16.24	15.61

C* - graphite

Equilibrium constants for some reactions of coal gasification

The equilibrium constant in partial pressures K_p is calculated from ΔG -values:

$$K_p = \exp\left(\frac{-\Delta G_T^{\circ}}{RT}\right) \quad (10)$$

and the K_x constant is obtained by:

$$K_x = K_p \cdot p^{-\Delta v} \quad (11)$$

(Δv - the variation in the number of gases moles).

For reactions with strongly negative ΔG -values (for instance the combustion reactions (i), (viii) or (ix)) the value of the equilibrium constant is enormous and its calculation is of no interest; the reactions are virtually complete. The same is true for the hydrogenation reactions of coals (inasmuch the temperatures are not too high), except the graphite hydrogenation, where over 550°C the equilibrium constant becomes less than 1). It is worth to calculate the equilibrium constants for ΔG values near to zero, when the conversion (obtained from these constants) is neither 1 (as for $\Delta G \ll 0$), nor 0 (as for $\Delta G \gg 0$).

For the homogeneous equilibrium (vii), the equilibrium constants decrease rapidly with increasing temperature. The values K_p for the gasification with CO_2 and hydrogen formation (ii):

$$K_p = \frac{P_{\text{CO}}^{2-y} \cdot P_{\text{H}_2}^{0.5x}}{P_{\text{CO}_2}^{1-y}} \quad (12)$$

and for the reaction (iii):

$$K_p = \frac{P_{\text{CO}}^{2-y+0.5x} \cdot P_{\text{H}_2\text{O}}^{0.5x}}{P_{\text{CO}_2}^{1-y+0.5x}} \quad (13)$$

show a very large range of the values: from 10^{-22} to 10^8 ; they highlight the same regularities concerning the reactivity of coals in the two reactions as the ΔG values.

The equilibrium constants for the reactions of coals with steam (iv) are given by:

$$K_p = \frac{P_{\text{CO}} \cdot P_{\text{H}_2}^{1+0.5x-y}}{P_{\text{H}_2\text{O}}^{1-y}} \quad (14)$$

For the other reaction with steam (v) the equilibrium constants are the product of the K_p -values for reaction (iv) and the corresponding ones for reaction (vii).

Zero-affinity plots for reactions of the coal gasification

For characterizing the thermodynamic reactivity of coal as a function of both temperature and *pressure*, the *zero-affinity plots* were proposed [4,8,13-15]. These curves are plotted in $T - \lg p$ coordinates, and represent the points of zero Gibbs free energy of the reaction, $\Delta G_T^p = 0$, i.e., where the equilibrium constant $K_x = 1$. These plots divide the surface in two areas: one for $\Delta G_T^p > 0$ ($K_x < 1$), the other for $\Delta G_T^p < 0$ and $K_x > 1$; the latter is the domain where reactions go with good conversion. From the thermodynamic point of view, we can use reactions in the domain near the zero-affinity plot on both sides of it.

The pressure for zero affinity depends upon temperature according to the equation:

$$\ln p = \frac{-\Delta G_T^0}{\Delta v RT} \quad (15)$$

THERMODYNAMIC EVALUATION OF COAL REACTIVITY

In the case of reactions with $\Delta v = 0$, only the temperature affects the equilibrium, and there is a constant temperature for zero-affinity:

$$T_z = H_T^\circ / S_T^\circ \quad (16)$$

A reaction of this kind is (vii), with T_z (as mentioned above) about 800°C; the domain $\Delta G < 0$ is the area on the left of the line $T = T_z$ for any pressure. The gasification reactions of coals with carbon dioxide (ii, iii), steam (v, vii) and oxygen (viii, ix) proceed all with an increase of the number of gas moles $\Delta v > 0$. For the reactions (ii), (iii) and (v), the pressures for $K_x = 1$ were calculated; their logarithms are given in Tables 10, 11 and 12 respectively.

Table 10.

Equilibrium pressures $\lg p$ ($K_x = 1$) for the Boudouard reaction (ii)

T(°C)	C*	1	2	3	4	5	6	7	8	9	10
25	-21.0	-11.3	-8.85	-6.41	-4.29	-7.27	-5.34	-3.97	-5.36	-7.11	-3.09
100	-14.9	-7.36	-5.45	-3.52	-1.84	-4.20	-2.68	-1.59	-2.71	-4.09	-0.89
200	-9.82	-4.05	-2.57	-1.07	0.24	-1.61	-0.43	0.43	-0.46	-1.53	0.98
300	-6.49	-1.87	-0.68	0.55	1.62	0.10	1.06	1.77	1.02	0.16	2.22
400	-4.14	-0.33	0.67	1.69	2.59	1.31	2.12	2.72	2.08	1.35	3.10
500	-2.41	0,82	1.67	2.55	3.32	2.21	2.90	3.43	2.86	2.24	3.75
600	-1.08	1.71	2.45	3.22	3.89	2.92	3.52	3.98	3.48	2.94	4.27
700	-0.03	2.42	3.07	3.75	4.35	3.48	4.01	4.42	3.97	3.49	4.68
800	0.83	3.01	3.58	4.19	4.72	3.94	4.42	4.79	4.37	3.95	5.02
900	1.53	3.49	4.00	4.55	5.04	4.33	4.76	5.10	4.71	4.33	5.31
1000	2.12	3.91	4.37	4.86	5.31	4.65	5.05	5.36	5.00	4.66	5.55

C* - graphite

Table 11.

Equilibrium pressures $\lg p$ ($K_x = 1$) for the Boudouard reaction (iii)

T(°C)	C*	1	2	3	4	5	6	7	8	9	10
25	-21.0	-12.5	-10.3	-7.98	-5.95	-8.83	-7.01	-5.64	-7.11	-8.74	-4.78
100	-14.9	-8.24	-6.48	-4.63	-3.01	-5.32	-3.87	-2.77	-3.95	-5.24	-2.09
200	-9.82	-4.64	-3.25	-1.81	-0.54	-2.35	-1.22	-0.36	-1.29	-2.30	0.18
300	-6.49	-2.27	-1.14	0.04	1.08	-0.41	0.52	1.23	0.46	-0.37	1.67
400	-4.14	-0.59	0.36	1.36	2.24	0.97	1.76	2.36	1.45	1.00	2.73
500	-2.41	0,64	1.46	2.33	3.09	1.99	2.67	3.19	2.61	2.01	3.51
600	-1.08	1.61	2.32	3.08	3.75	2.78	3.38	3.84	3.33	2.80	4.12
700	-0.03	2.37	3.01	3.68	4.28	3.41	3.94	4.36	3.90	3.43	4.61
800	0.83	3.00	3.57	4.18	4.71	3.93	4.41	4.78	4.36	3.94	5.01
900	1.53	3.52	4.04	4.59	5.07	4.36	4.79	5.13	4.75	4.37	5.34
1000	2.12	3.96	4.43	4.94	5.38	4.73	5.12	5.43	5.08	4.73	5.62

C* - graphite

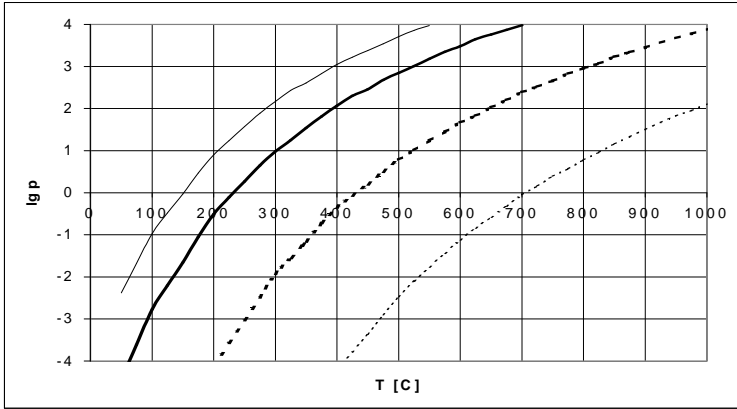


Fig. 1 Zero affinity plots for the Boudouard reaction (ii)

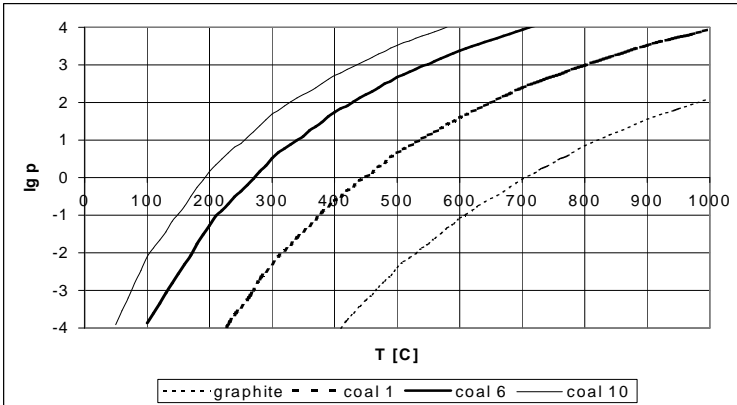


Fig. 2 Zero affinity plots for the Boudouard reaction (iii)

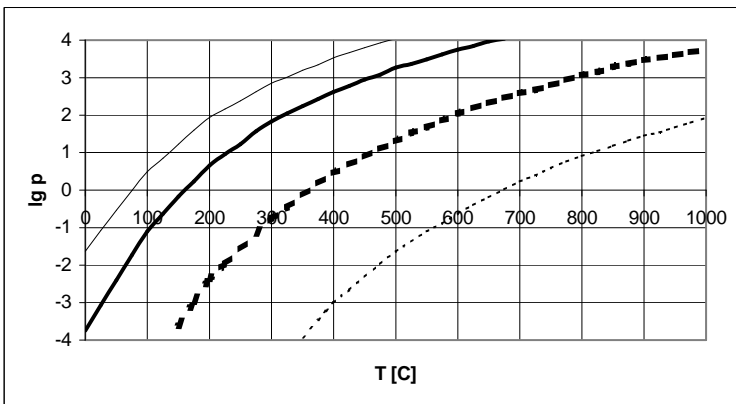


Fig. 3 Zero affinity plots for the steam gasification (iv)

Table 12.Equilibrium pressures $\lg p$ ($K_x = 1$) for coal reactions with steam (iv)

T(°C)	C [*]	1	2	3	4	5	6	7	8	9	10
25	-16.0	-7.86	-5.79	-3.70	-1.85	-4.76	-3.11	-1.90	-3.25	-4.75	-1.13
100	-11.4	-4.93	-3.27	-1.59	-0.10	-2.42	-1.09	-0.12	-1.20	-2.40	0.50
200	-7.46	-2.43	-1.12	0.22	1.40	-0.42	1.63	1.41	0.54	-0.41	1.91
300	-4.88	-0.77	0.31	1.42	2.40	0.90	1.78	2.43	1.70	0.92	2.84
400	-3.06	0.41	1.33	2.28	3.12	1.85	2.60	3.16	2.53	1.86	3.52
500	-1.70	1.30	2.10	2.93	3.67	2.57	3.22	3.72	3.16	2.58	4.03
600	-0.66	2.00	2.70	3.44	4.10	3.13	3.71	4.15	3.65	3.14	4.43
700	0.18	2.56	3.19	3.86	4.45	3.58	4.10	4.51	4.05	3.59	4.76
800	0.86	3.03	3.60	4.20	4.74	3.95	4.43	4.80	4.38	3.96	5.03
900	1.42	3.42	3.94	4.49	4.98	4.27	4.71	5.05	4.66	4.28	5.26
1000	1.89	3.75	4.23	4.74	5.20	4.54	4.94	5.26	4.90	4.55	5.46

C^{*} - graphite

For the two reactions with CO₂: (ii) and (iii), and that with steam (iv) the zero-affinity curves are plotted in Figures 1-3 respectively for graphite, a bituminous coal (1) and two lignites: (6) and (10), in the pressure domain from 10⁻⁴ to 10⁴ bar. The $\Delta G < 0$ area is situated at the right and under the plots. This domain is shifted to the left (lower temperatures) for coals in comparison to graphite, and for lignites as compared to bituminous coals. These reactions are less pressure dependent for lignites in comparison to bituminous coals and graphite: the plots are steeper and only for very high pressures the equilibrium temperature is substantially increased.

CONCLUSIONS

During the first stage of coals gasification in ordinary technical conditions, a thermal decomposition takes place, with loss of volatile components and production of semi-coke. The proper gasification reactions are then reactions of this coke, especially for lignites, meaning an important loss of reactivity, though even the coke has a higher thermodynamic reactivity as graphite [8]. One should take advantage of the high thermodynamic reactivity of lignites, by designing gasogens for low temperature gasification, with the use of the own moisture of the coal, as suggested and experimented by Franke et al. [16] and Block [17], for Rhine-Basin lignite and calculated for Romanian lignites by Niac and Pop [18]. On the other hand, small quantities of inorganic impurities and/or additives can act as catalysts and enhance the reaction rate. For high-rank coals however, this would be of little help, since their equilibrium temperatures are much higher.

REFERENCES

1. G. Niac, *Erdöl, Erdgas, Kohle*, **1995**, 111, 275-280.
2. D.van Krevelen, *Fuel*, **1950**, 29, 269.
3. * * * CODATA Key Values for Thermodynamics, Hemisphere Publ.Corp., New York, 1989.
4. G. Niac, V. Voiculescu, I. Bâldea and M. Preda, *Formule, Tabele, Probleme de Chimie-Fizică*, Cluj-Napoca, **1984**.
5. H. Naşcu, G. Niac and D.I. Comşulea, *Fuel*, **1995**, 74, 119- 123.
6. E. Szadeczky-Kardoss, *A szén petrográfiája*, Budapest, **1956**, p.53.
7. S. Sternberg and F. Daneş, *Termodinamică chimică aplicată*, Bucureşti, **1978**, p.134.
8. G. Niac, *Metalurgia*, **1979**, 31, 551-554;
9. G. Niac and I Focşa, *Mine, Petrol şi Gaze*, **1981**, 435-437.
10. M.H. Karapetyants, *Termodinamica chimică*, Bucureşti, **1953**, p.411.
11. D.R. Stephans, *Thermodynamic equilibria for Wyoming Coal*, **1976**, Lawrence Livermore Laboratory, UCID 17044.
12. D.R. Stephans and D.G. Miller, *Thermodynamic equilibria for Wyoming Coal: New calculations*, **1976**, Lawrence Livermore Laboratory, UCID 17044.
13. V.Voiculescu, G. Niac and L Simoiu, *J.Chem.Educ.*, **1998**, 75, 203-206.
14. V. Voiculescu and G. Niac, *Rev.Chim.*, **1978**, 29 (11), 1026-1030.
15. V. Voiculescu, *Rev.Chim.*, **1985**, 36 (2), 136-140.
16. F.H. Franke, K.I. Klöcher, W. Koch and H. Kreusing, *Brennstoff Wärme-Kraft*, **1979**, 31 (3), 85-89.
17. F.R. Block, *Chem.-Ing.-Techn.*, **1979**, 51 (10), 969-971.
18. G. Niac and I. Pop, *Rev.Chim.*, **1988**, 39, 38-44.

MODELING MOLAR REFRACTION AND CHROMATOGRAPHIC RETENTION BY SZEGED INDICES

LORENTZ JANTSCHI, SIMONA MUREȘAN AND MIRCEA V. DIUDEA

*Facultatea de Chimie si Inginerie Chimica,
Universitatea "Babes-Bolyai" Arany Janos 11, 3400 Cluj, Romania*

ABSTRACT. Modeling the molar refraction and the chromatographic retention by using Szeged topological indices as molecular descriptors, is presented.

INTRODUCTION

Physico-chemical properties, such as the boiling point, molar refraction, critical pressure, viscosity, chromatographic retention, etc. are rather simple experimental available properties of chemical compounds. They are tabulated and may be used e.g., in projecting industrial instalations. Sometimes, it happens that a given compound is toxic, or dangereous or simply not available. In such conditions, it is of interest to have a theoretical tool, say an equation, that can help one in obtaining a desired parameter by structure-related calculations. In this respect, the topological indices (i.e., single numbers encoding the topology of chemical structures) were widely used in the last decade.

In the present paper, we used the Szeged indices as molecular descriptors in modeling the molar refraction and the chromatographic retention of some organo-phosphoruc compounds.

SZEGED TOPOLOGICAL INDICES

Gutman has introduced the *Szeged index*,¹² SZ, as

$$I_{e/p} = \sum_e N_{i,(i,j)} N_{j,(i,j)} \quad (1)$$

where the quantities $N_{i,(i,j)}$ and $N_{j,(i,j)}$ represent the cardinality of the vertex sets lying closer to i and to j , respectively and are defined by

$$N_{i,(i,j)} = |\{v \mid v \in V(G); D_{iv} < D_{jv}\}| \quad (2)$$

$$N_{j,(i,j)} = |\{v \mid v \in V(G); D_{jv} < D_{iv}\}| \quad (3)$$

In the above relations, $V(G)$ denotes the set of vertices in a connected graph and D_{iv} , D_{jv} are the topological distances (i.e., the number of edges on the shortest path) joining the vertices i and j , respectively, with a vertex v . Vertices equidistant to i and j are not counted.

When defined on edge, (i.e., (i,j) is an edge, e), l_e is just the classical Szeged index,¹² in the following symbolized by SZ_e . When defined on path, ((i,j) is a path, p), l_p is the hyper-Szeged index,¹⁴ SZ_p .

The Szeged unsymmetric matrix, SZ_u , was defined by Diudea et al.^{14,18} by analogy to the Cluj matrix,¹⁵⁻¹⁷ CJ_u ,

$$[SZ_u]_{ij} = N_{i,(i,j)} \quad (4)$$

where $N_{i,(i,j)}$ has the meaning given by eq. 2. The diagonal entries are zero.

SZ_u is a square array of dimensions $N \times N$, in general unsymmetric. It allows the calculation of two Szeged indices, by

$$SZ_{e/p} = \sum_{e/p} [SZ_u]_{ij} [SZ_u]_{ji} \quad (5)$$

As an extension to SZ_u , Szeged property matrices¹⁹⁻²¹ have been defined

$$[SZ_u P]_{ij} = P_{i,(i,j)} \quad (6)$$

$$P_{i,(i,j)} = f(P_v) \mid v \in V(G); D_{iv} < D_{jv} \mid \quad (7)$$

$$f(P_v) = m \sum_v P_v; \quad (8)$$

case : (a) $P_v = 1$; $m = 1$ (classical SZ_u matrix)

(b) $P_v = \sum_v A_v$; $m = 1/12$ ($SZ_u A$ matrix)

$$f(P_v) = (\prod_v P_v)^{1/v}; P_v = X_v \text{ (group electronegativity) } (SZ_u X \text{ matrix}) \quad (9)$$

Entries in a Szeged property matrix are defined by a function $f(P_v)$, evaluated on the vertices v which obey the Szeged index condition (see eq 12). The set of such vertices can be viewed as a fragment (i.e., a subgraph) since a molecular graph is always a connected one. Two types of $f(P_v)$ are here proposed: an additive and a multiplicative one. Only two cases of the additive function are here considered:

(a) $P_v = 1$ (i.e., the cardinality) and the factor $m = 1$; it is just the case of classical SZ_u matrix.

(b) $P_v = \sum_v A_v$; $m = 1/12$; A_v is the atomic mass and the matrix is $SZ_u A$. The factor m indicates that $f(P_v)$ is a fragmental mass, relative to the carbon atomic mass.

The multiplicative function was used in calculating group electronegativities, X_v , like EC (Sanderson-type group electronegativities²²) for heteroatoms and fragments.

Indices are calculated on these matrices by the general relation

$$l_{e/p} = \sum_{e/p} [SZ_u P]_{ij} [SZ_u P]_{ji} ; l = SZ; SZA; SZX \quad (10)$$

MODELING THE MOLECULAR REFRACTION

In correlating tests, a multivariable regression equation is used [34]:

$$Y = a + \sum_i b_i X_i \quad (11)$$

where a and b_i are regression coefficients, Y is the modeled property and X_i independent variable (in particular, topological indices). A satisfactory single variable regression is however a happy case. The quality of such an equation is

expressed by the following statistics: r (correlation coefficient), s (standard error), $v(\%)$ (the percent of variance) and F (Fischer ratio).

Molar refraction, MR, is defined as

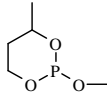
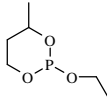
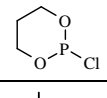
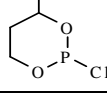
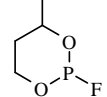
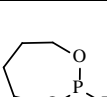
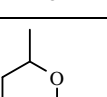
$$MR = \frac{n-1}{n+2} \frac{M}{d} \quad (12)$$

where n is the refraction index, M is the molecular mass and d is the density. It is obvious that Mr is parallel to the molar volume. An electronic dependence is included in the refraction index.

A set of 10 pesticides, cyclic organo-phosphorus compounds (Table 1), was taken in this study. Statistics are presented in Table 2.

Table 1.

Szeged Indices and Molar Refractions for cyclic organo-phosphorus compounds.

NO	Graph	SZ _p	SZ _e	SZ _{pA}	SZ _{eA}	SZ _{pX}	SZ _{eX}	MR
1		481	146	880.403	265.743	50.541	12.615	35.808
2		751	193	1305.576	338.139	58.590	13.165	40.524
3		182	78	473.205	201.288	34.305	11.525	30.030
4		296	108	732.976	2653743	43.281	12.331	34.911
5		296	108	593.069	214.181	64.456	18.480	29.222
6		306	88	606.007	172.535	63.671	18.480	31.636
7		739	186	1278.347	323.139	56.675	12.737	43.005

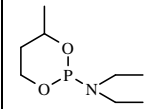
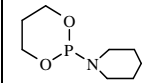
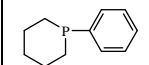
8		1518	290	2488.993	481.722	77.717	14.303	52.029
9		1684	360	2732.333	581.472	79.674	15.691	49.971
10		1684	360	2428.389	517.882	72.630	14.344	58.323

Table 2

Statistics of correlation equations: $Y = a + \sum b_i X_i$, for the set of Table 1

No	X_i	b_i	a	r	s	v(%)	F
1	SZ _p	0.016	27.851	0.9634	2.868	7.074	103.242
2	SZ _e	0.089	23.479	0.9587	3.041	7.500	90.961
3	SZ _p A	0.011	25.855	0.9487	3.381	8.338	72.079
4	SZ _e A	0.066	18.349	0.9370	3.736	9.214	57.575
5	SZ _p X	0.481	11.606	0.6997	7.641	18.846	7.673
6	SZ _e X	-0.467	47.248	0.1135	10.626	26.208	0.104
7	SZ _p	0.019	34.882	0.9727	2.651	6.539	61.604
	SZ _p X	-0.157					
8	SZ _p	0.016	36.821	0.9755	2.516	6.206	68.762
	SZ _e X	-0.631					

From Table 2 one can see that the molar refraction of these compounds is well modeled by two descriptors: one is topological (SZ_p) and another one is electronic (SZ_eX- the index weighted by electronegativity – entry 8, Table 2), the variance of estimation being about 6%. This result is in agreement with the meaning of formula 12.

MODELING THE CHROMATOGRAPHIC RETENTION

The retention chromatographic index, I_{CHR} , is a measure of the interaction between a given compound and two phases: a mobile phase (i.e., the eluent) and a stationary one. This interaction is function of more than one factor, the polarity, lipophilicity and size included. These factors are joined in a "global" molecular property, that is the chromatographic index. It is easily seen that the values of I_{CHR} vary with varying the chromatographic systems, pressure and temperature. This is the reason that, in correlating studies, values I_{CHR} from a single experiment are requested.

A set of 10 herbicides (Table 3) was modeled by the Szeged indices. The statistics are given in Table 4.

Table 3.

 Retention chromatographic index, I_{chr} , and Szeged indices
 for some organo-phosphorus herbicides

No.	Compound	Structure	I_{CHR+}	SZe	SZeA	SZpE	SZeE
1	Acid 3,5-dichlorobenzoic		7.4	236	526.677	79.026	15.956
2	DICAMBA		9.8	340	725.736	110.788	18.614
3	MCPP (MECOPROP)		10.3	441	775.545	118.200	18.373
4	DICHLORPRO P		11.0	441	923.316	124.570	19.535
5	MCPA		11.5	378	670.715	104.590	17.620
6	2,4-D		11.8	378	806.385	110.576	18.810
7	Pentachloro- phenol		12.4	282	1050.444	98.619	18.324
8	2,4,5-T		14.3	453	1121.528	133.206	20.991
9	2,4-DB		14.6	572	1161.483	141.009	20.745
10	BENTAZON		18.5	731	852.472	172.764	24.957

(+) 1995/1996 HP Environmental Solutions Catalog, p. 88.

Table 4Statistics of correlation: $Y = a + \sum b_i X_i$, for the set in Table 3.

No	X_i	b_i	a	r	s	v(%)	F
1	SZ _p X	0.1068	-0.5862	0.8982	1.428	11.743	33.381
2	SZ _e X	1.1797	-10.7168	0.9388	1.118	9.198	57.460
3	SZeX SZeA	1.0678 0.0026	-10.7940	0.9506	1.0776	8.862	32.837

Table 4 shows that the retention chromatographic index depends both on the size (through the mass weighted index, SZ_eX) and electronic characteristics (by SZ_eX). The correlation is satisfactory ($r = 0.951$, $v < 9\%$ - entry 3, Table 4).

Szeged indices have proved here their ability in modeling physico-chemical properties of organo-phosphorus compounds.

Acknowledgement. This work is supported in part by the GRANT CNCSU No. xxxx/1998.

REFERENCES

- Gutman, *Graph Theory Notes New York*, **1994**, 27, 9.
- H. Wiener, *J. Am. Chem. Soc.*, **1947**, 69, 17.
- M.V. Diudea, O.M. Minailiuc, G. Katona, I. Gutman, *Commun. Math. Comput. Chem. (MATCH)*, **1997**, 35, 129-143.
- M.V. Diudea, *J. Chem. Inf. Comput. Sci.*, **1997**, 37, 300-305.
- M.V. Diudea, *Commun. Math. Comput. Chem. (MATCH)*, **1997**, 35, 169-183.
- M.V. Diudea, B. Pârv, M.I. Topan, *J. Serb. Chem. Soc.*, **1997**, 62, 267-276.
- M.V. Diudea, I. Gutman, *Croat. Chem. Acta*, **1998**, 71, 21-51.
- O. Minailiuc, G. Katona, M.V. Diudea, M. Strunje, A. Graovac, I. Gutman *Croat. Chem. Acta*, **1998**, 71, 473-488.
- A.A. Kiss, I. E. Kacso, O. M. Minailiuc, M.V. Diudea, S. Nikolić, I. Gutman *Studia Univ. "Babeș-Bolyai"*, **1997**, 42, 183-192.
- Schirger, M.V. Diudea, *Studia Univ. "Babeș-Bolyai"*, **1997**, 42, 269-280.
- M.V. Diudea, I.E. Kacso, M.I. Topan, *Rev. Roum. Chim.*, **1996**, 41, 141.
- XXXXXXXXXXXX
- A.A. Kiss, I.E. Kacso, O.M. Minailiuc, M.V. Diudea, S. Nikolic, I. Gutman, *Studia Univ. "Babeș-Bolyai"*, 1997, **42**, 000.
- Gutman, *Graph Theory Notes, N.Y.*, 1994, **27**, 9.
- M.V. Diudea, I.E. Kacso, M.I. Topan, *Rev. Roumaine Chim.* 1996, **41**, 141.
- M.V. Diudea, O. Ivanciuc, "Topologie Moleculară", Ed. COMPREX, Cluj, 1995.
- M. Guo, L. Xu, C.Y. Hu, S.M. Yu, *Commun. Math. Comput. Chem. (MATCH)*, 1997, **35**, 185.